Journal of Geophysical Research: Solid Earth

Supporting Information for

Cascading Effects of Extreme Geohazards on Tenerife (Canary Islands)

M. López-Saavedra[1], J. Martí[1], J. L. Rubio[2] and K. Kelfoun[3]

[1]Geosciences Barcelona, CSIC, Lluis Solé Sabaris s/n, 08028 Barcelona, Spain.

[2]Department of Geology, University Autonomous of Barcelona, UAB, Carrer dels Til·lers, 08193 Bellaterra, Spain.

[3]Laboratoire Magmas et Volcans, Université Clermont Auvergne, CNRS, IRD, OPGC, F-63000 Clermont-Ferrand, France.

Contents of this file

Additional Supporting Information (Files uploaded separately)

Introduction

This document contains complementary information about the procedure followed during some of the simulations carried out in this study, which require a more detailed explanation according to what is indicated in Text S1, as well as all the map scenarios and numerical results obtained from these simulations, (figures, summary tables and movies). Results from each event simulation (Pyroclastic Density Currents -PDC-, seismicity, landslide, and tsunami) have also a complementary explanation in Text S2 to S5, detailing their characteristics and where they can be found along this document.

Text S1 contains a more detailed explanation about the procedure used to carry out the seismicity simulations. It explains the methodology used to elaborate the seismic amplification map of Tenerife, necessary as an input file for the seismic model. This map, included as Figure

S1, was obtained by using QGIS 2.14, following the same procedure as the one explained in Núñez (2017), and introduced afterwards in the model developed by the same author, which was designed to be implemented in QGIS 2.14. The information and parameters introduced in the model to carry out the seismic simulations were taken from the work of Núñez (2017) at the beginning of this study, in March 2020.

Text S2, S3, S4 and S5 contain a description of the results obtained for the PDC, seismicity, landslide and tsunami simulations, respectively, and provide instructions to understand the content of the figures and tables exposed here. These simulations and the analysis of their results were carried out from March to September 2020. Information on input parameters for each model were taken from the literature at the beginning of this study, and details about the references, values and procedures used are explained in the main text, in their respective sections.

Results from the PDC simulations are in the form of maps showing the potential extent of the PDC on the Tenerife Island, and they are included as Figures S2 to S15. Results from the seismicity simulations are in the form of maps showing the expected Peak Ground Acceleration (PGA) values in Tenerife for a synthetic earthquake, and are included as Figures S16 to S69. Results from the landslide simulations are in the form of slope stability analysis of the selected cross section, for which a Factor of Safety (FS) of the potentially affected slope is calculated, together with the most probable slip surfaces, and they are include as Figures S70 to S276. All these figures are supported by summary tables (see Text S2 to S4 for more details).

Finally, results from tsunami simulations are in the form of movies and they are attached as Movie S1, called "ms01.avi", and Movie S2, called "ms02.avi". These movies show the propagation with time of the tsunami waves produced by the collision of a sliding block due to a landslide in the Icod Valley, Tenerife, across the Canary Islands, and also show the maximum amplitude reached by these waves. Movie S1 was obtained by introducing a yield strength of 50,000 Pa for the sliding block, while Movie S2 shows the effect of a yield strength for the same block of 100,000 Pa. A brief explanation is shown in Text S5 and captions for both movies are included at the end of this document.

Text S1 – Methodology to elaborate the seismic amplification map of Tenerife

We replied the methodology used by Núñez (2017) to elaborate the seismic amplification map of Tenerife, necessary as input file for the PGA model used in this study. Using the Geographic Information System QGIS, 2.14 version, we grouped the 220 geological units of the geological map GEODE 1:25000 from Tenerife (Bellido-Mulas et al., 2014), introduced as a shapefile, into the 6 synthesis classes (Table A – below –) proposed by Borcherdt (1994). The geological classification was already done by Núñez (2017), and it can be consulted in Table 3.39 of his work, but no seismic amplification map of Tenerife was elaborated then. This new map is shown as Figure S1 of this study. In the legend of this map, the color of each synthesis class is shown, together with the equivalent amplification factor for short periods (Fa).

Once obtained, the seismic amplification map was introduced into the PGA model implemented in QGIS 2.14, together with input parameters from Table 1 (main text), to obtain the results shown as Figures S2 to S15.

Table A. Synthetic Classification of Soils and Rocks According to Their Amplification Capacity.

Type of emplacement		**Geotechnical properties**					
Nº	**Borcherdt (1994)**	**Geotechnical description**	**Vs30 (m/s)**	$\bar{N}$ **(blows/foot)**	$\bar{s}_u$ **(kPa)**	**Minimum thickness (m)**	**F_a**
1	SC-Ia	Hard rocks	Vs30 > 1500				0.86
2	SC-Ib	Medium-resistant rocks	760 < Vs30 ≤ 1500				0.97
3	SC-II	Very dense soils	360 < Vs30 ≤ 760	$\bar{N} > 50$	$\bar{s}_u > 100$	10	1.50
		Soft to firm rocks					
4	SC-III	Hard soils	180 ≤ Vs30 ≤ 360	$15 \leq \bar{N} \leq 50$	$50 \leq \bar{s}_u \leq 100$	5	2.42
		Consistent clays					
5	SC-IVa	Medium-consistent soils	Vs30 < 180	$\bar{N} < 15$	$\bar{s}_u < 50$	3	3.40
		Soils with more than 3 m of soft clay defined as a soil with PI > 20, w ≥ 40 % and s_u < 25 kPa					
6	SC-IVb	Soft soils					2.08
		Soils that require specific geotechnical investigation in situ: 1. Soils prone to liquefaction 2. Quick and highly sensitive clays 3. Highly organic clays 4. Clays with very high plasticity, with H > 8 m and PI > 75 5. Clays with soft-to-medium-hard consistency, with H > 36 m and $\bar{s}_u$ < 50 kPa				3	

Note. Vs30 is the average shear wave speed to a depth of 30 m, N the average resistance according to the SPT (Standard Penetration Test) to a depth of 30 m, PI the Plasticity Index, w the moisture content, s_u the shear and undrained resistance, $\bar{s}_u$ the average shear and undrained resistance to a depth of 30 m, H the power of the soil and Fa the amplification factor for short periods (Núñez, 2017).

Text S2 – Results from PDC simulations.

PDC map scenarios are shown in Figure S2 to S15. Figure S2 to S8 show simulations made with a collapse equivalent height (H_c) of 2,000 m for the different collapse equivalent angles (a_c) tested. Figure S9 to S15 are those results obtained by using H_c = 3,000 m for the different a_c.

Table S1 summarizes the numerical results regarding the maximum length reached and the maximum extension covered by the PDCs, as well as the direction of the maximum length reached on land and the municipalities that they would affect.

Text S3 – Results from PGA simulations.

Expected PGA values maps are shown in Figure S16 to S69. Figure S16 to Figure S42 show expected PGA values for synthetic earthquakes with an epicentre located north of Mt Teide summit. Figure S43 to S69 show expected PGA values for synthetic earthquakes with an epicentre located at the Mt Teide's crater.

Maximum PGA values obtained by each seismic simulation were converted from cm/s^2 to acceleration of gravity values (g). These results are summarized in Table S2 and S3 for an epicentre located north of Mt Teide summit and at the crater, respectively.

Text S4 – Results from landslide simulations.

Results obtained from the slope stability analysis for Model 1 (with alteration zones, Figure 3a from the main text), Model 2 (without alteration zones, Figure 3b from the main text), and Model 1 Bis (the same as Model 1 but considering a caldera collapse) are shown in Figure S70 to S276. In each figure, a semicircular line is indicated, which correspond to the most probable slip surface, and has a related number, which is the FS of this slip surface. The k_h value in the pseudo-static analysis (see the main text for more information) is indicated in the upper right corner of the figure, in red.

Figure S70 to S72 correspond to the slope stability static analysis for Model 1, while Figure S73 to S75 correspond to the slope stability static analysis for Model 2. Figure S76 to S144 show the slope stability pseudo-static analysis for Model 1. Figure S145 to S210 show the slope stability pseudo-static analysis for Model 2. Finally, Figure S211 to S276 show the slope stability pseudo-static analysis for Model 1 Bis.

Table S3 and S4 summarizes the FS values obtained from the slope stability static analysis for Model 1 and Model 2, respectively. Table S6 to S8 summarizes de FS values obtained from the slope stability pseudo-static analysis for Model 1, Model 2 and Model 1 Bis, respectively.

Text S5 – Results from tsunami simulations.

Tsunami simulation videos are included as additional supporting information Movie S1 and S2, called as "ms01.avi" and "ms02.avi", respectively. Movie S1 corresponds to the simulation made for a yield strength of the sliding block of 50,000 Pa, while Movie S2 was obtained by introducing a yield strength of 100,000 Pa.

Videos show the propagation over time across the Canary Islands of the tsunami wave produced by the impact of a sliding block on the ocean after a landslide in the Icod Valley, Tenerife, as well as the maximum amplitude reached by the resulting waves.

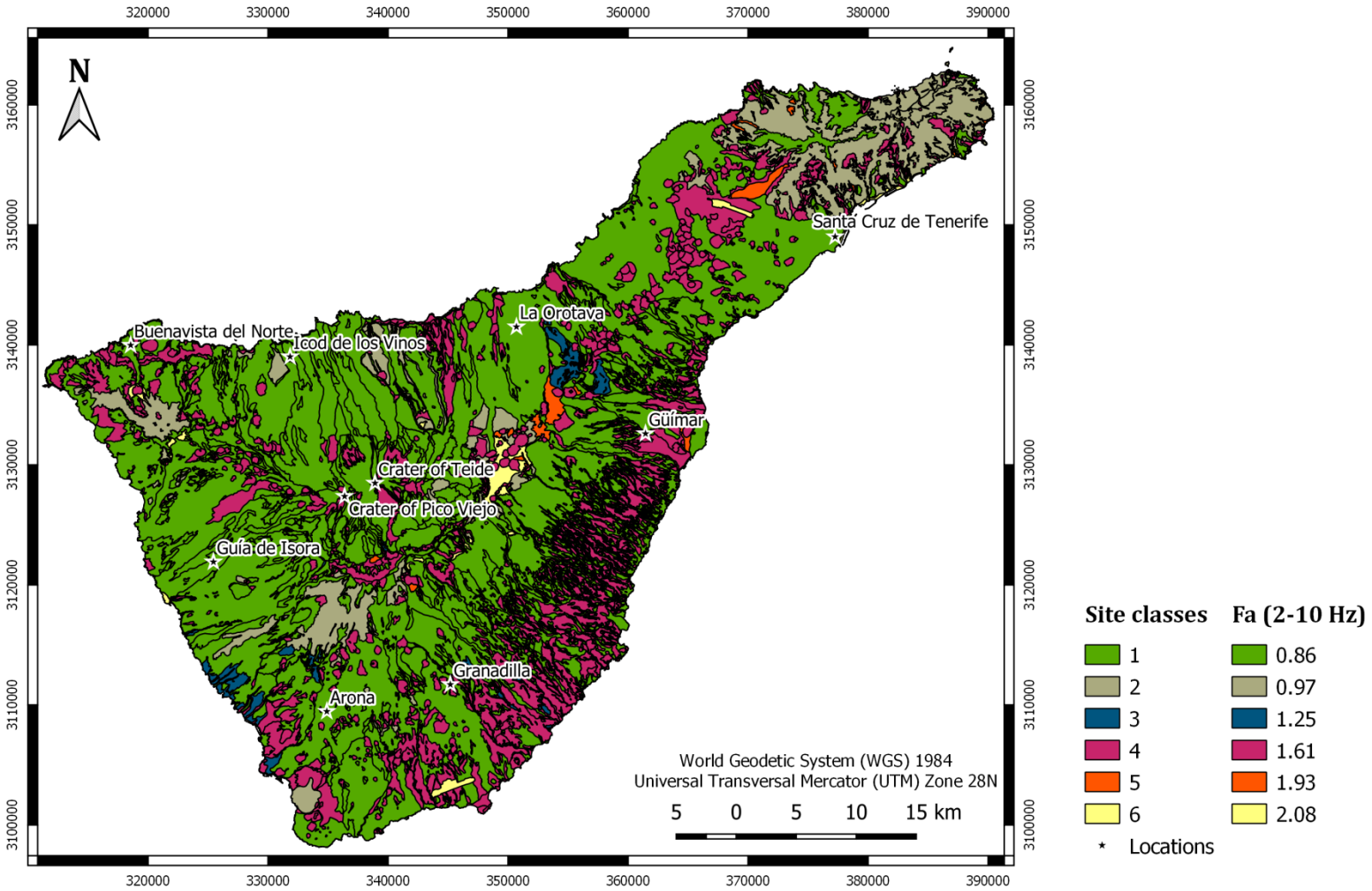

Figure S1. Seismic amplification map of Tenerife (Canary Islands) in terms of the amplification factor (Fa) of Borcherdt (1994) for high frequencies (2-10 Hz).

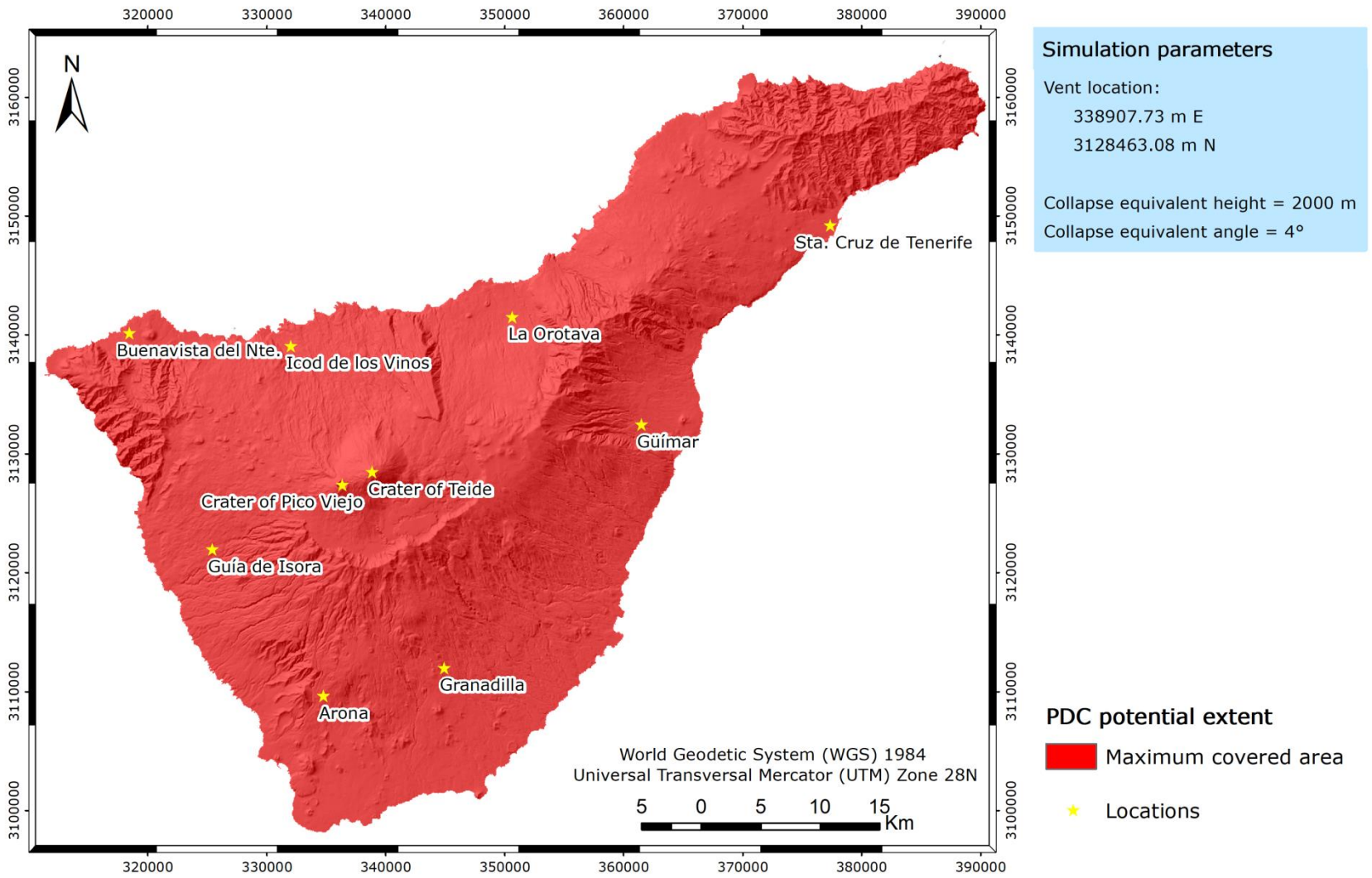

Figure S2. Pyroclastic Density Current (PDC) map scenario considering H_c = 2,000 m and a_c = 4°, for a simulated caldera-forming eruption on Mt Teide, Tenerife (Canary Islands).

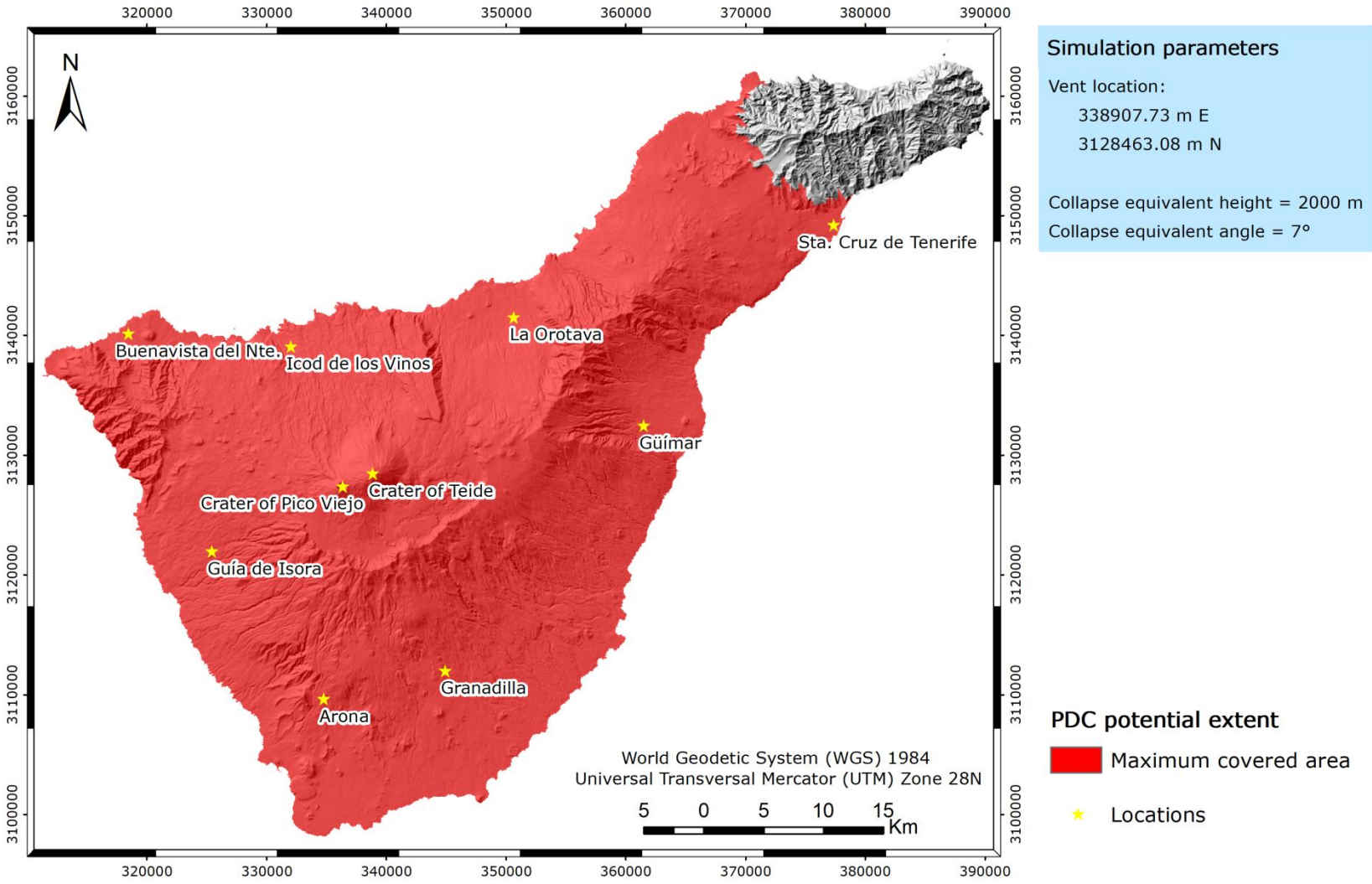

Figure S3. Pyroclastic Density Current (PDC) map scenario considering H_c = 2,000 m and a_c = 7°, for a simulated caldera-forming eruption on Mt Teide, Tenerife (Canary Islands).

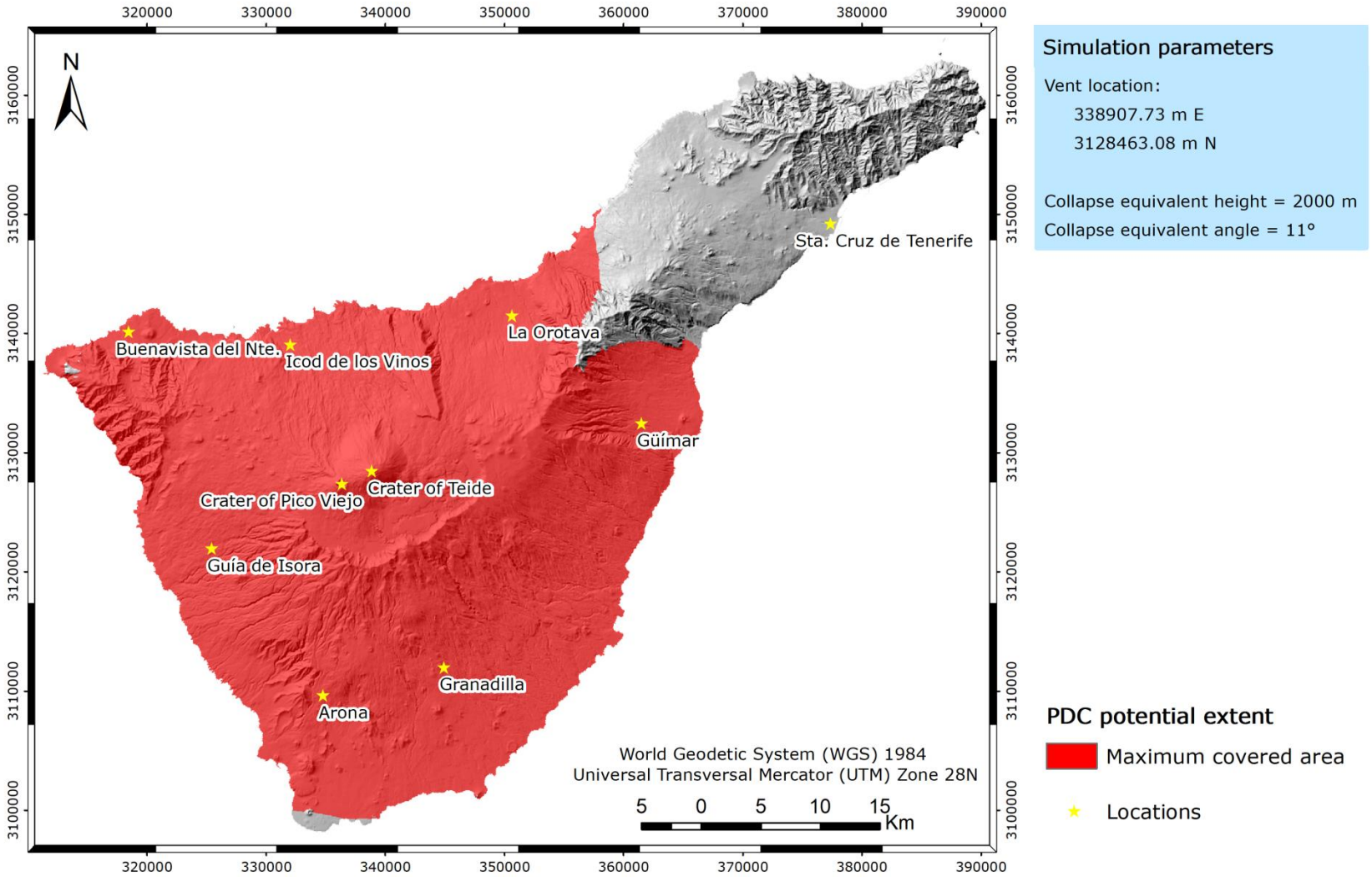

Figure S4. Pyroclastic Density Current (PDC) map scenario considering H_c = 2,000 m and a_c = 11°, for a simulated caldera-forming eruption on Mt Teide, Tenerife (Canary Islands).

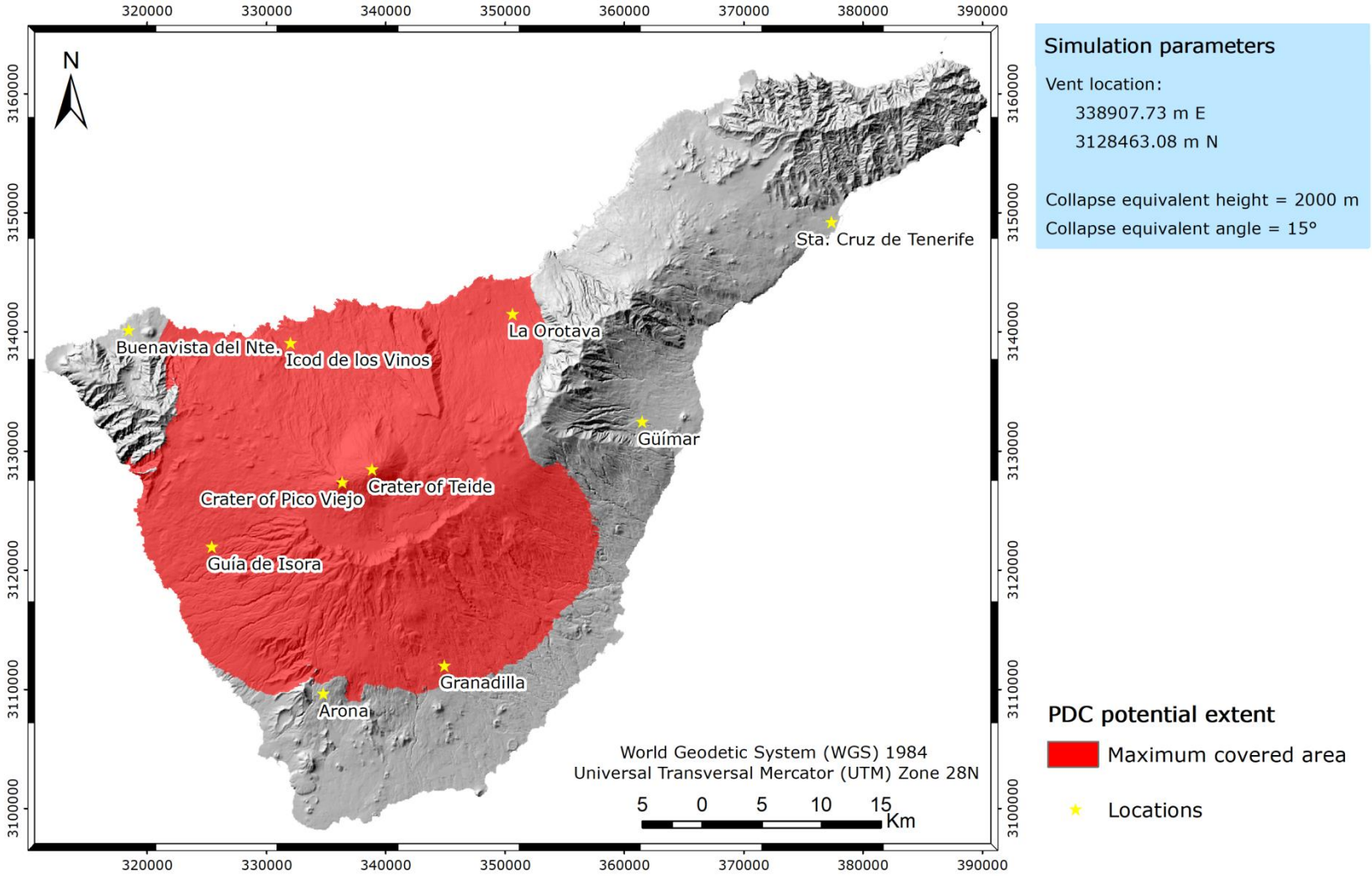

Figure S5. Pyroclastic Density Current (PDC) map scenario considering H_c = 2,000 m and a_c = 15°, for a simulated caldera-forming eruption on Mt Teide, Tenerife (Canary Islands).

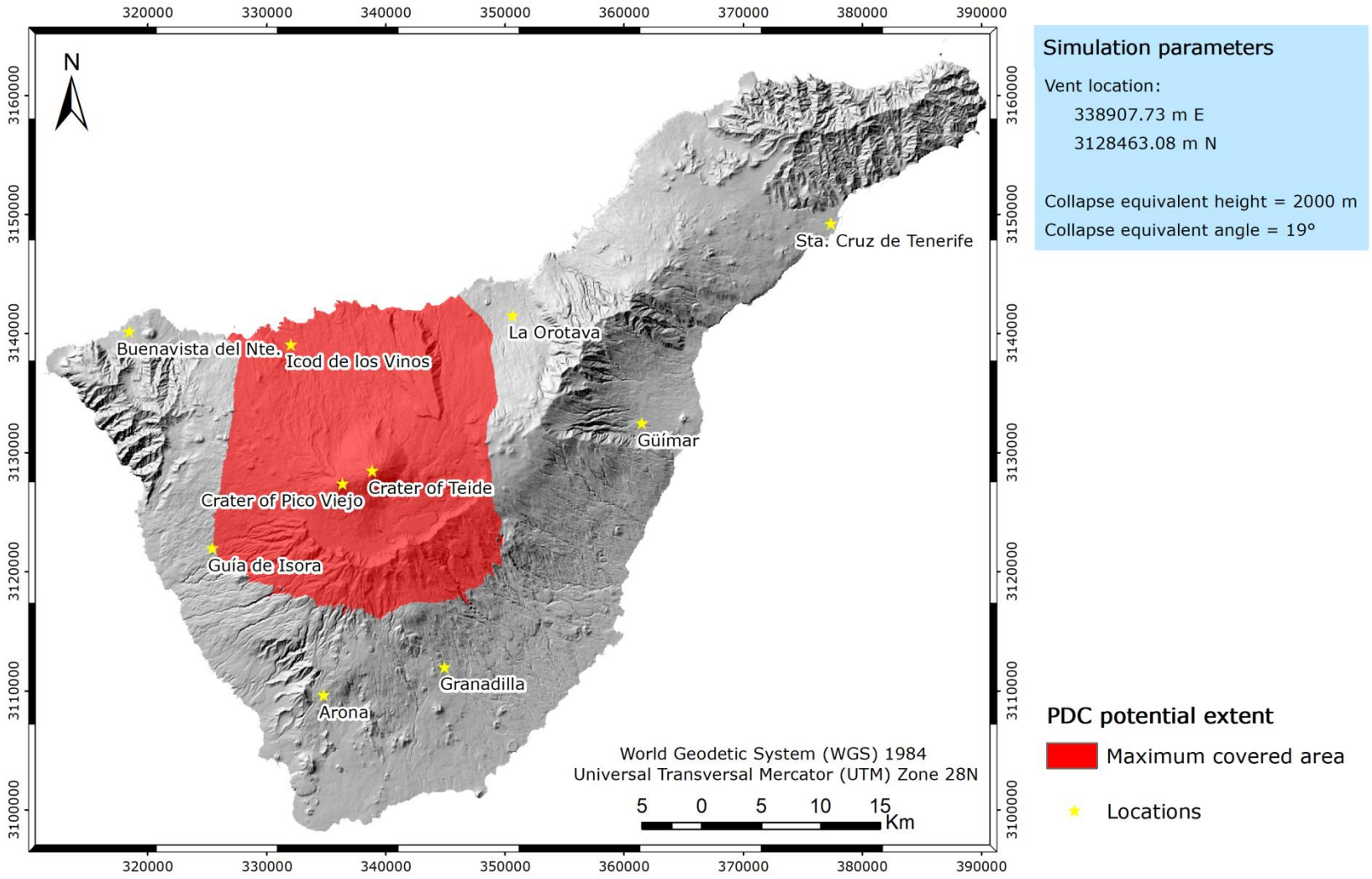

Figure S6. Pyroclastic Density Current (PDC) map scenario considering H_c = 2,000 m and a_c = 19°, for a simulated caldera-forming eruption on Mt Teide, Tenerife (Canary Islands).

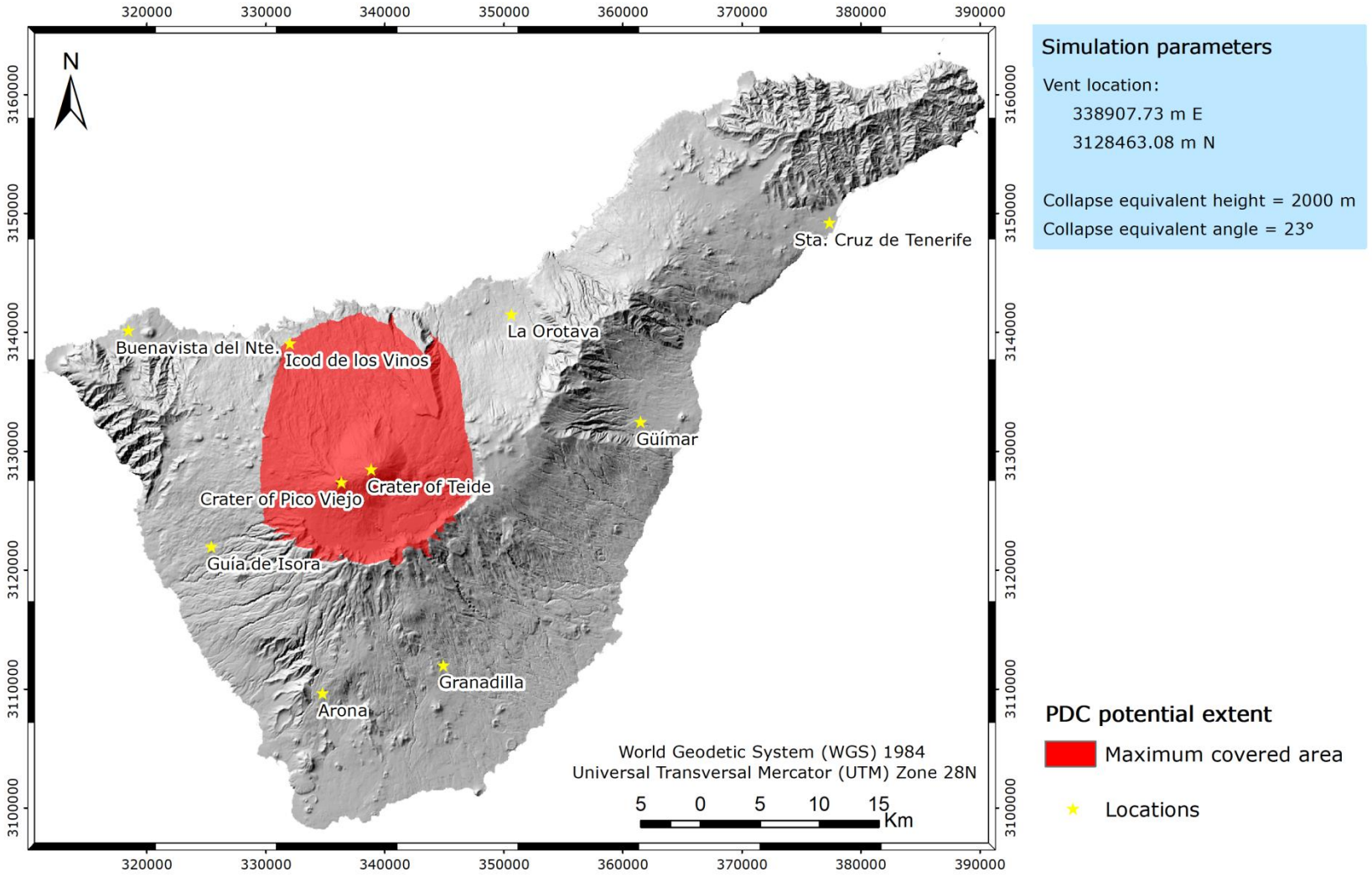

Figure S7. Pyroclastic Density Current (PDC) map scenario considering H_c = 2,000 m and a_c = 23°, for a simulated caldera-forming eruption on Mt Teide, Tenerife (Canary Islands).

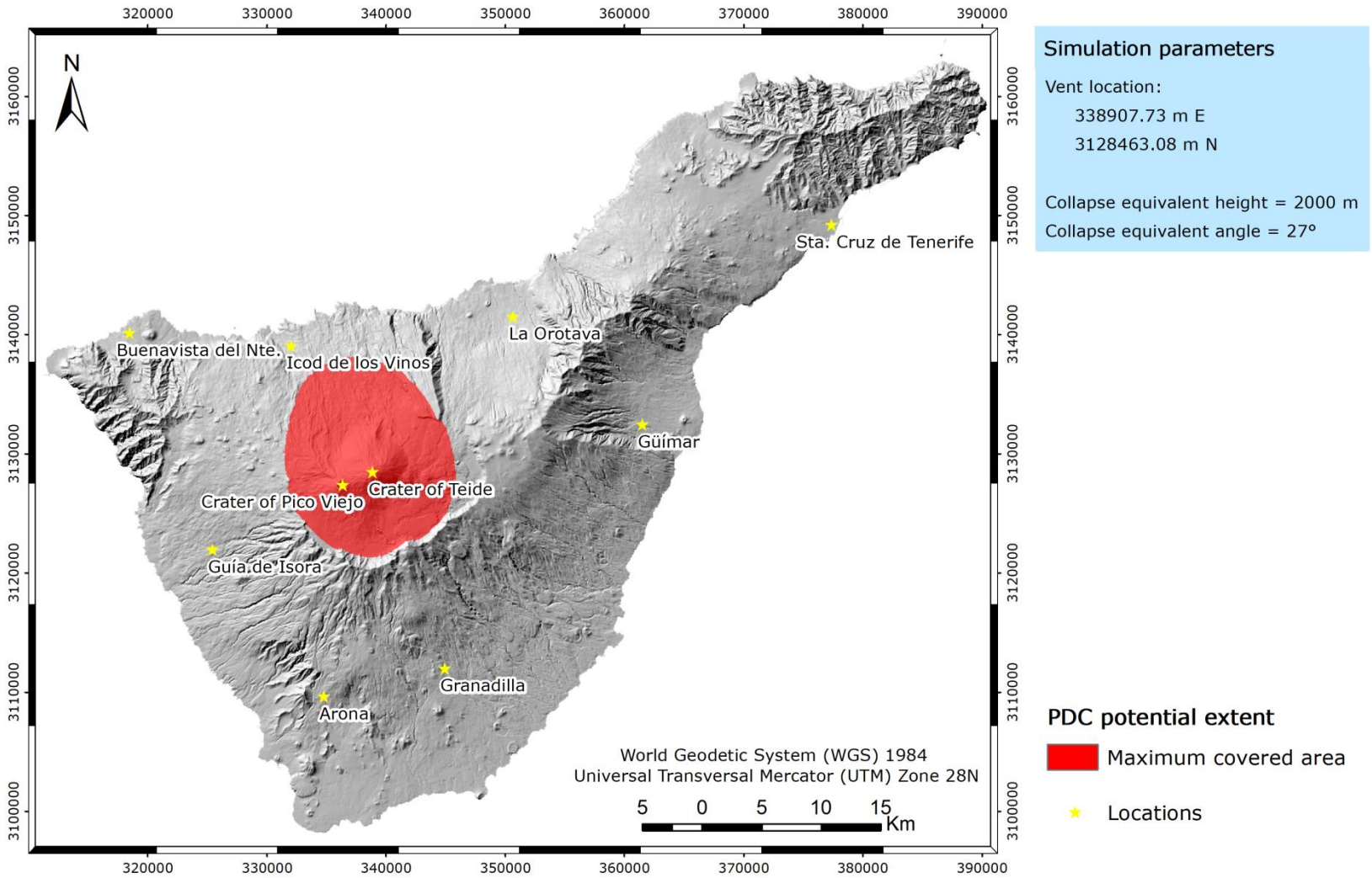

Figure S8. Pyroclastic Density Current (PDC) map scenario considering H_c = 2,000 m and a_c = 27º, for a simulated caldera-forming eruption on Mt Teide, Tenerife (Canary Islands).

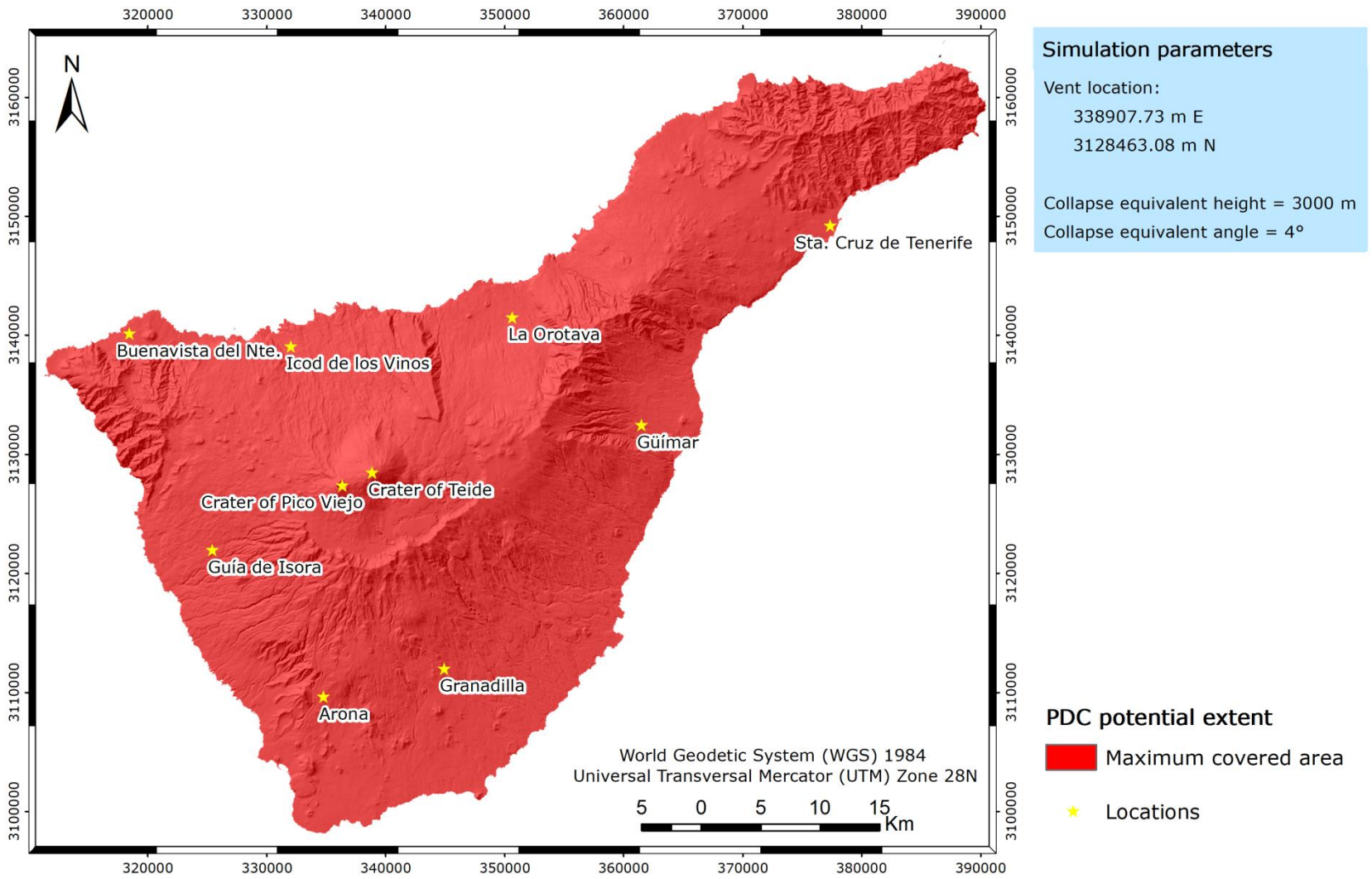

Figure S9. Pyroclastic Density Current (PDC) map scenario considering H_c = 3,000 m and a_c = 4°, for a simulated caldera-forming eruption on Mt Teide, Tenerife (Canary Islands).

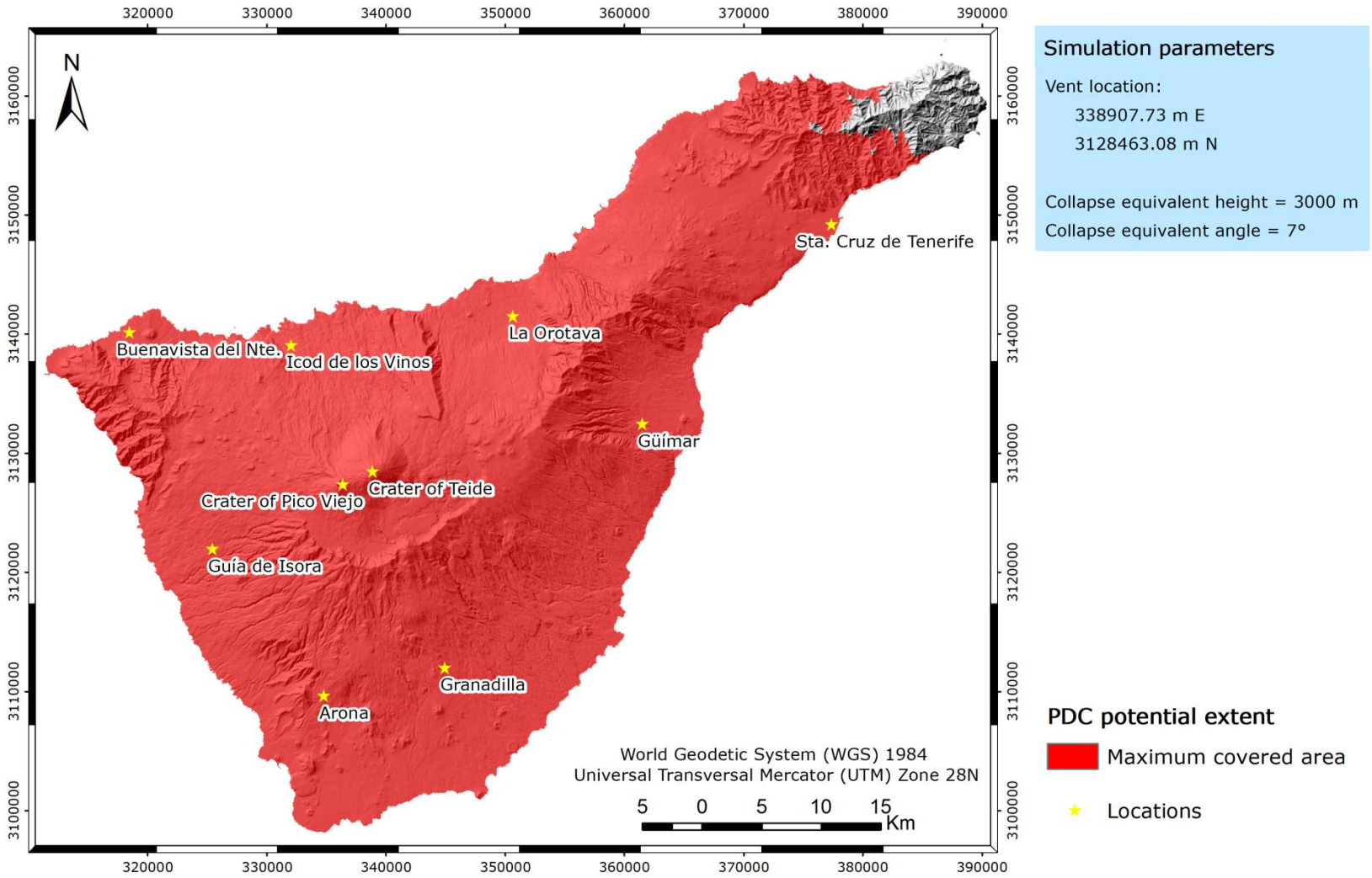

Figure S10. Pyroclastic Density Current (PDC) map scenario considering H_c = 3,000 m and a_c = 7°, for a simulated caldera-forming eruption on Mt Teide, Tenerife (Canary Islands).

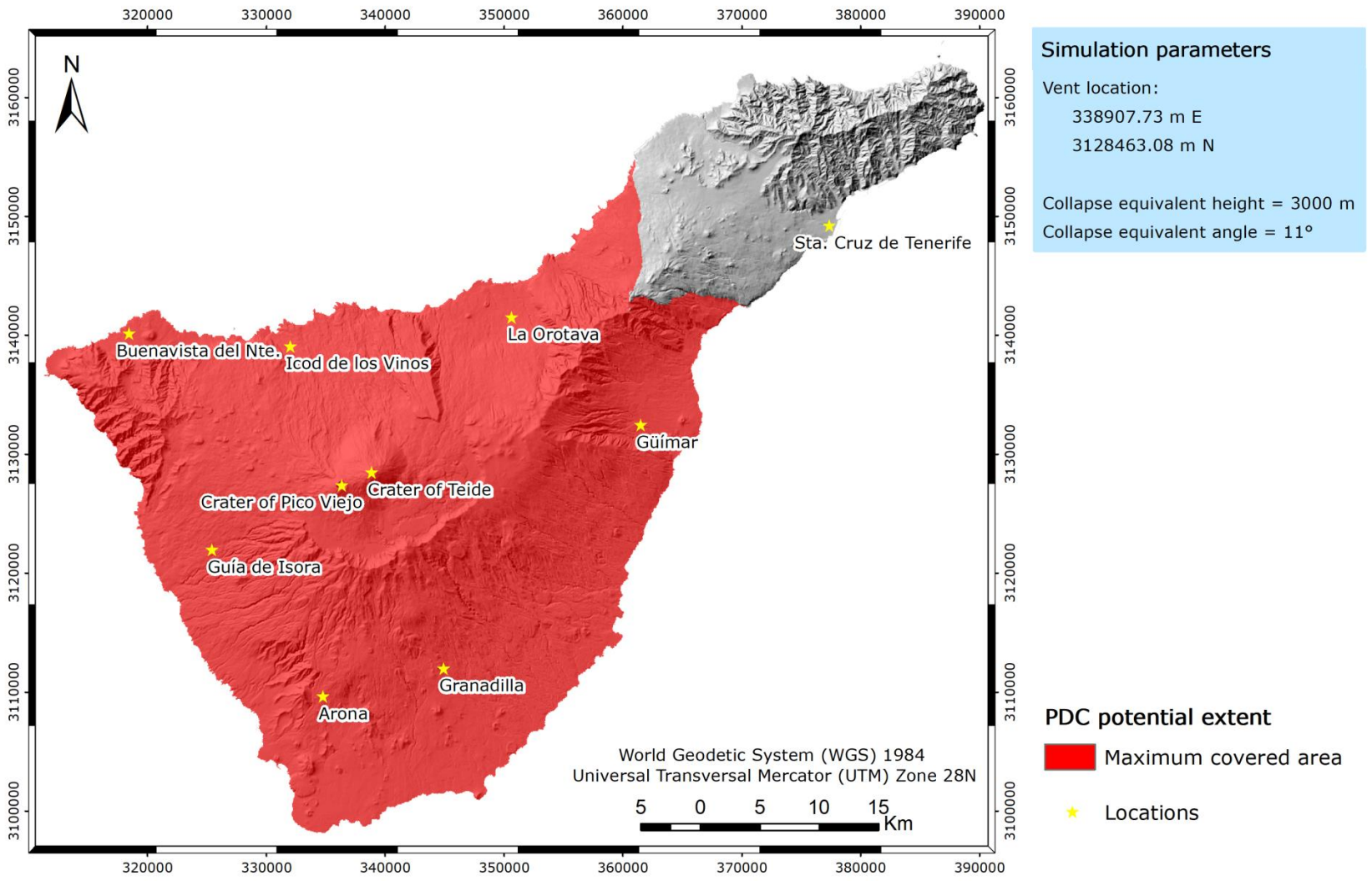

Figure S11. Pyroclastic Density Current (PDC) map scenario considering H_c = 3,000 m and a_c = 11°, for a simulated caldera-forming eruption on Mt Teide, Tenerife (Canary Islands).

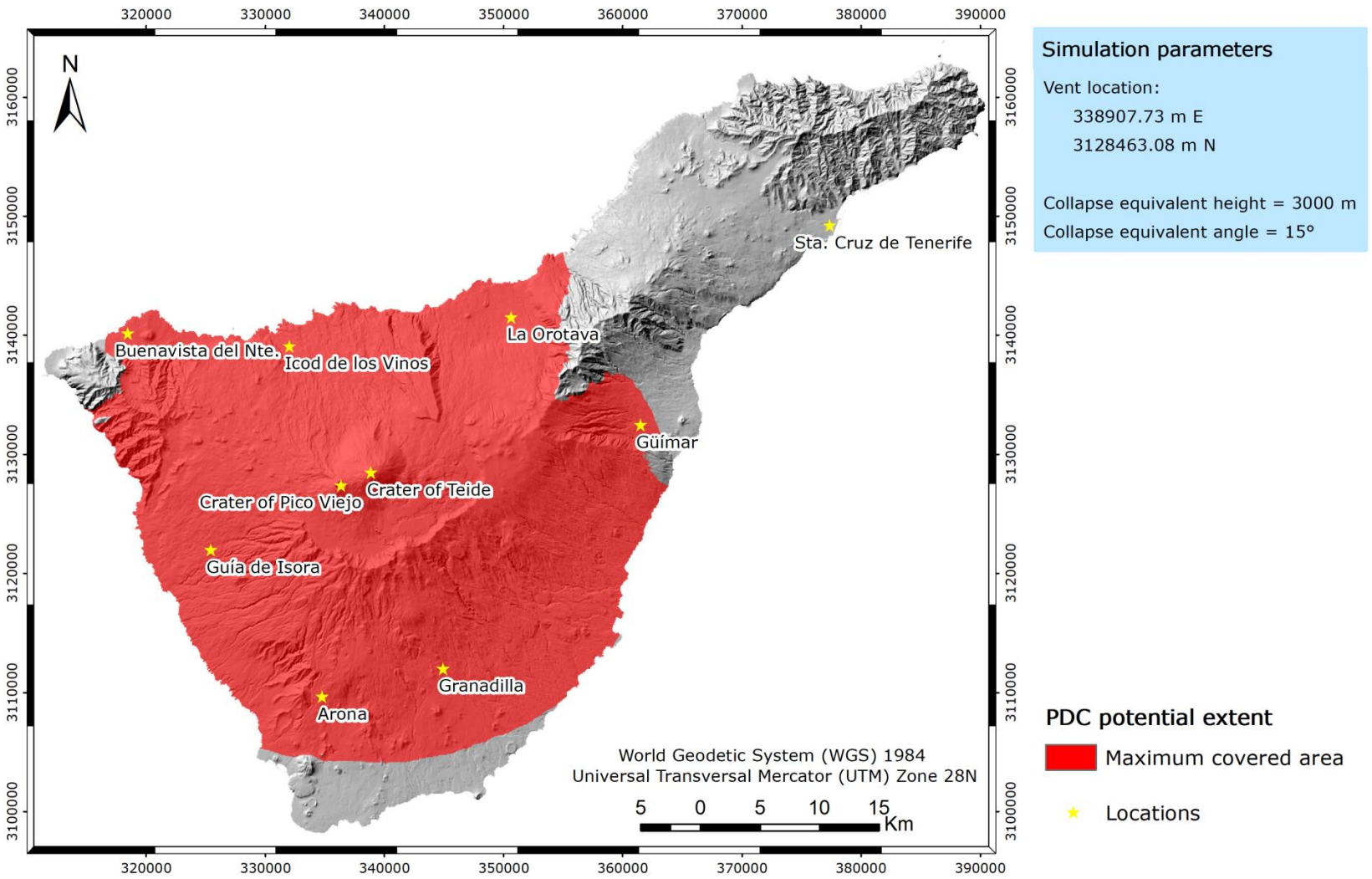

Figure S12. Pyroclastic Density Current (PDC) map scenario considering H_c = 3,000 m and a_c = 15°, for a simulated caldera-forming eruption on Mt Teide, Tenerife (Canary Islands).

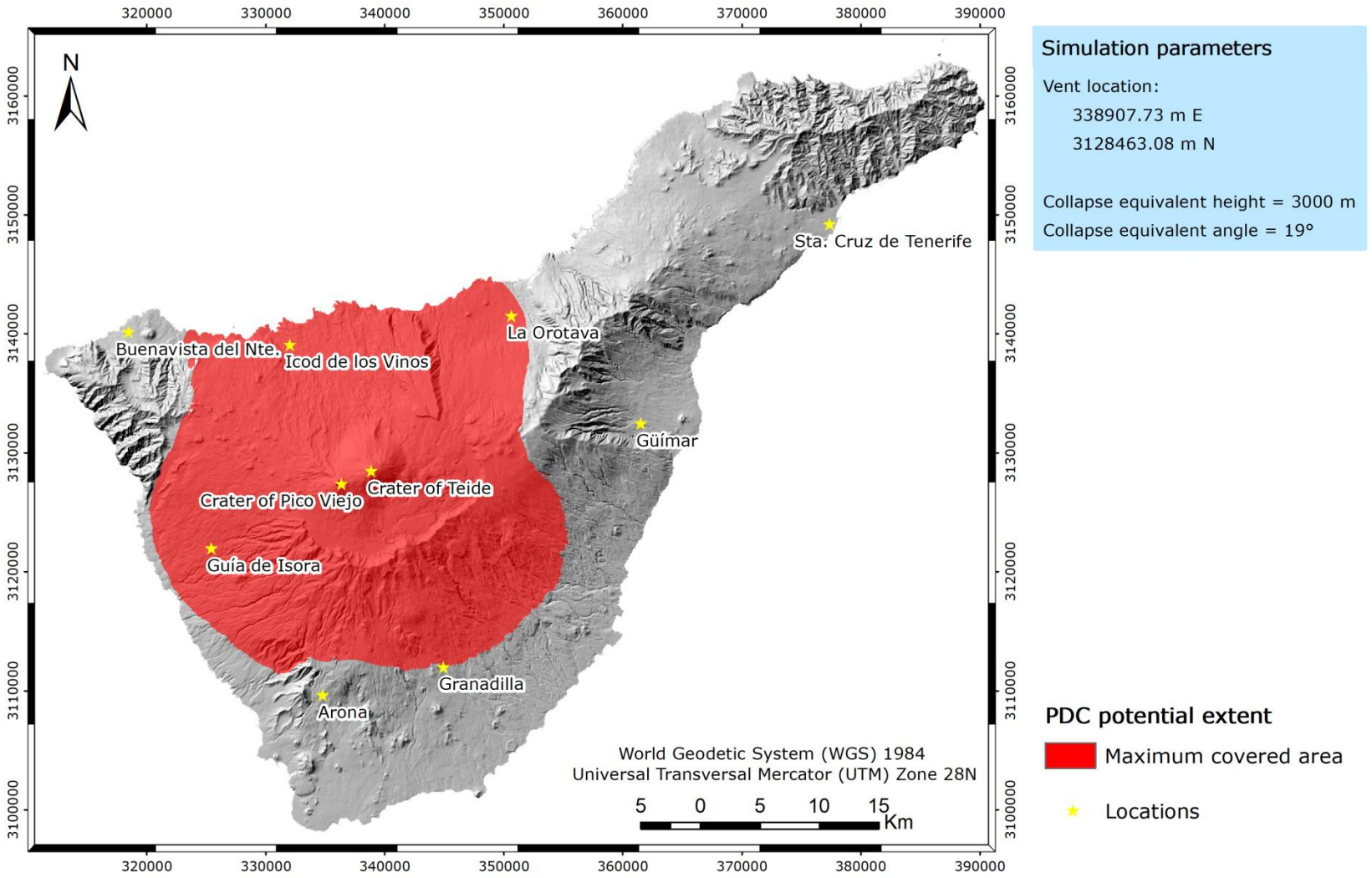

Figure S13. Pyroclastic Density Current (PDC) map scenario considering H_c = 3,000 m and a_c = 19°, for a simulated caldera-forming eruption on Mt Teide, Tenerife (Canary Islands).

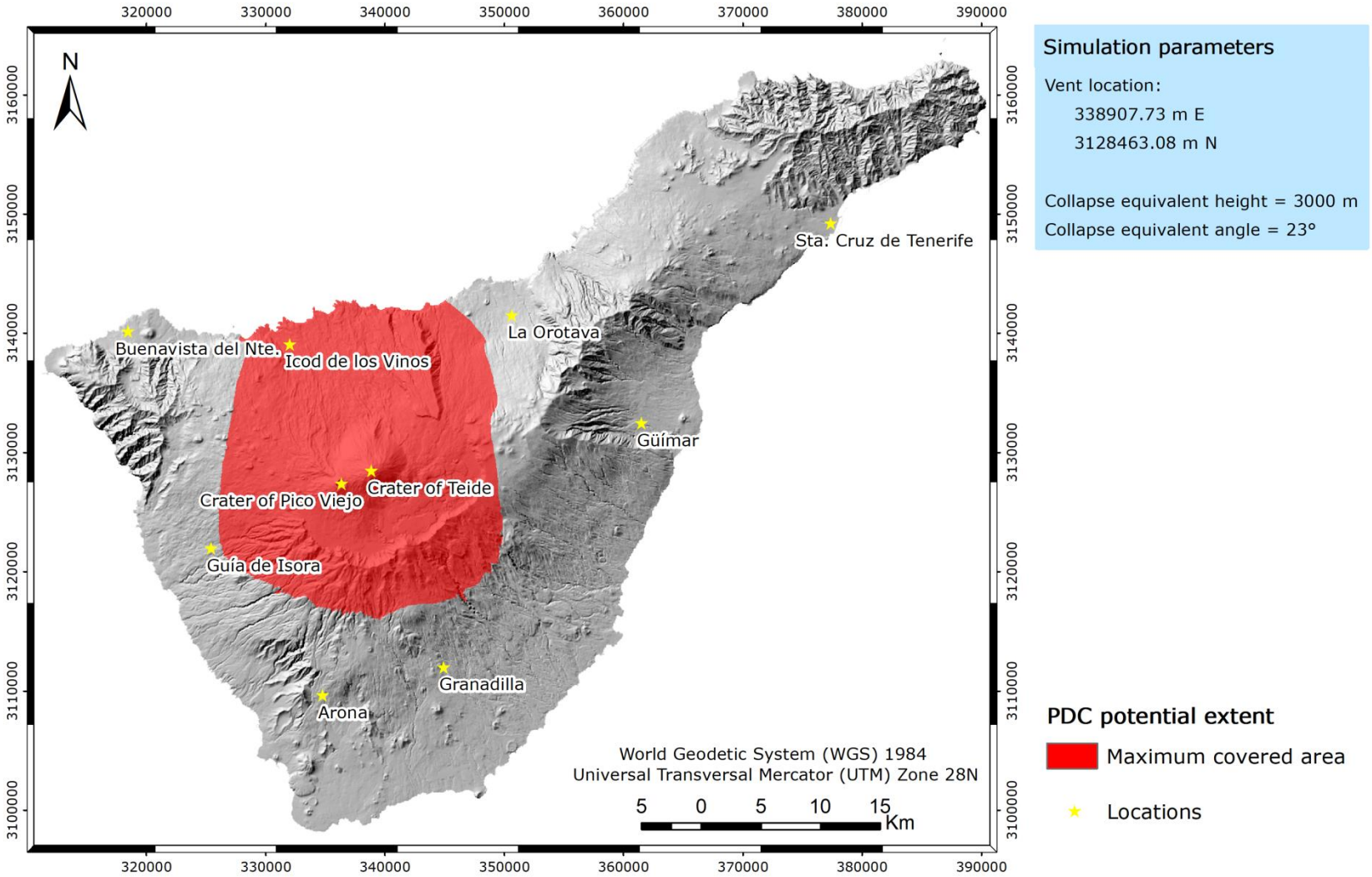

Figure S14. Pyroclastic Density Current (PDC) map scenario considering H_c = 3,000 m and a_c = 23°, for a simulated caldera-forming eruption on Mt Teide, Tenerife (Canary Islands).

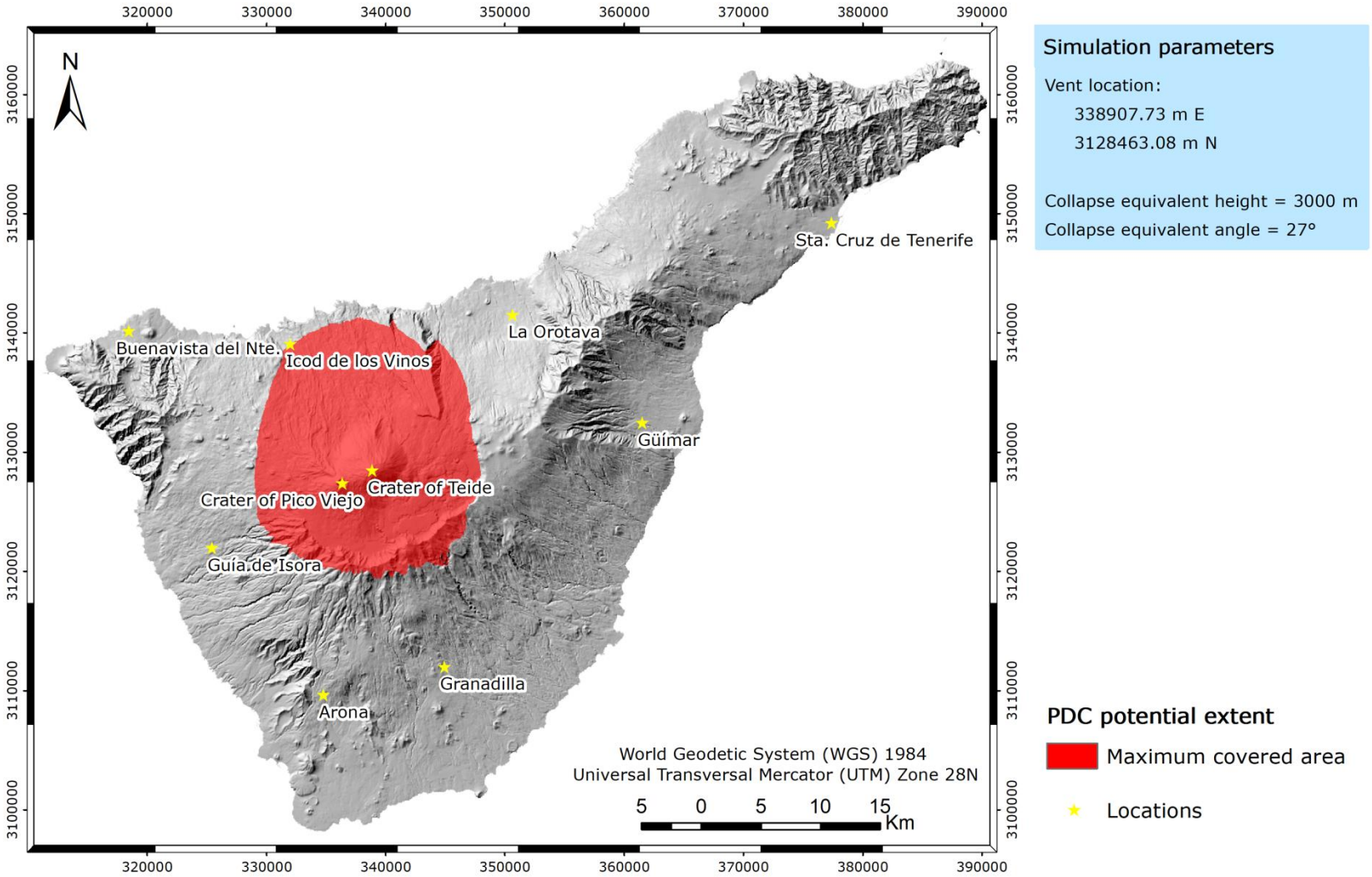

Figure S15. Pyroclastic Density Current (PDC) map scenario considering H_c = 3,000 m and a_c = 27°, for a simulated caldera-forming eruption on Mt Teide, Tenerife (Canary Islands).

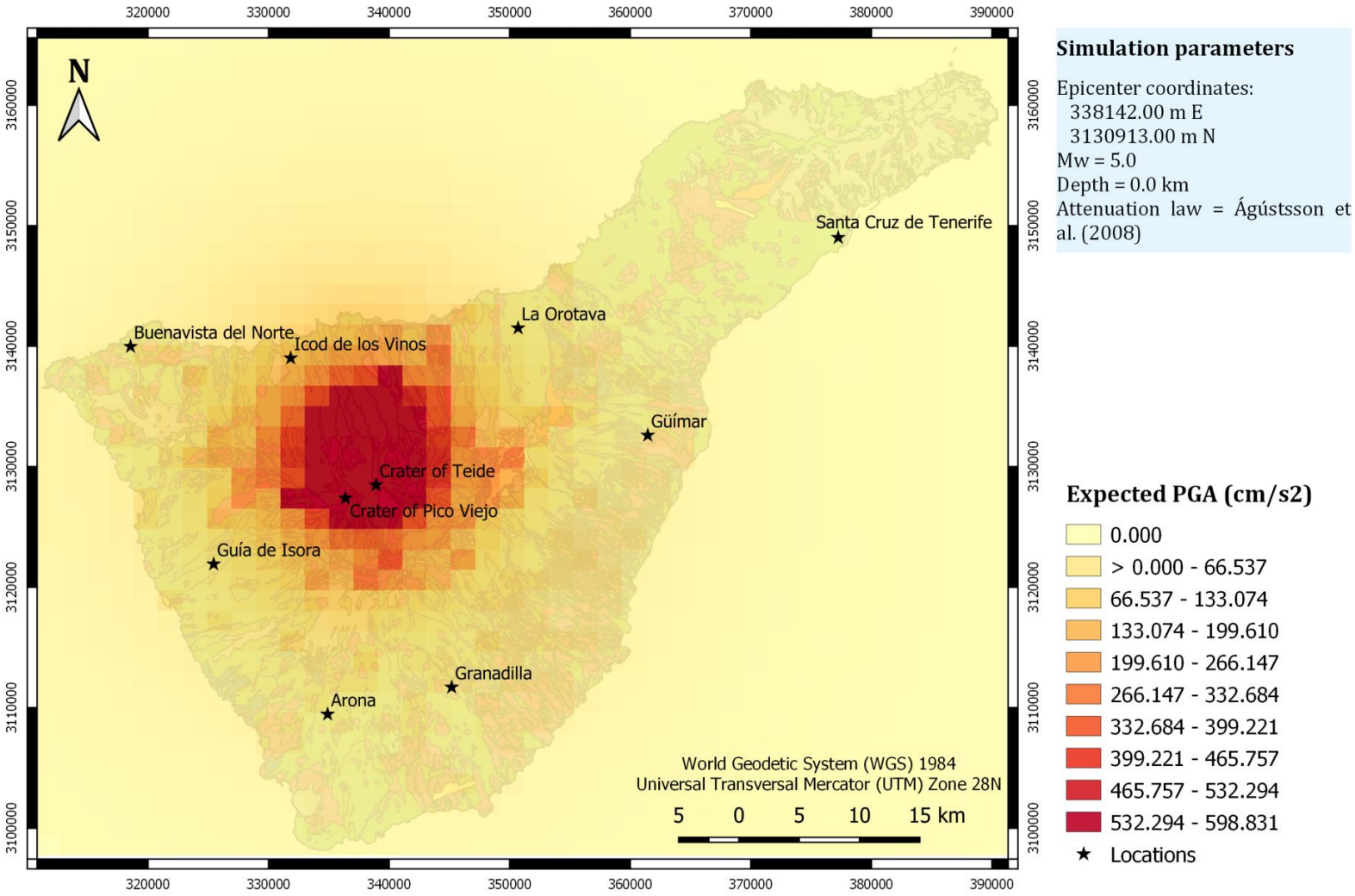

Figure S16. Expected PGA values for a M 5.0 synthetic earthquake located north of the summit of Mt Teide, Tenerife (Canary Islands), at a depth of 0.0 km, after applying the Ágústsson et al. (2008) attenuation law.

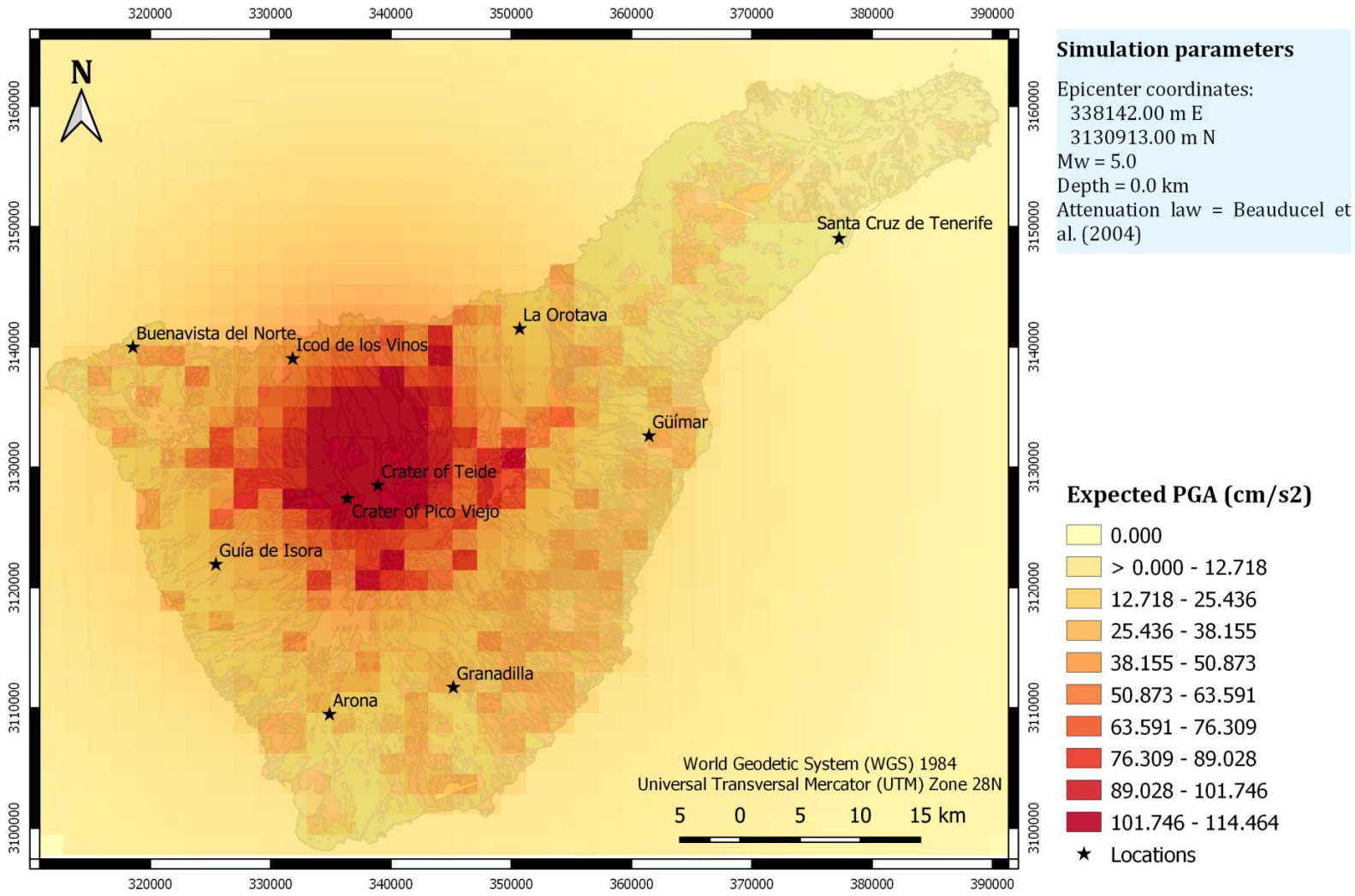

Figure S17. Expected PGA values for a M 5.0 synthetic earthquake located north of the summit of Mt Teide, Tenerife (Canary Islands), at a depth of 0.0 km, after applying the Beauducel et al. (2004) attenuation law.

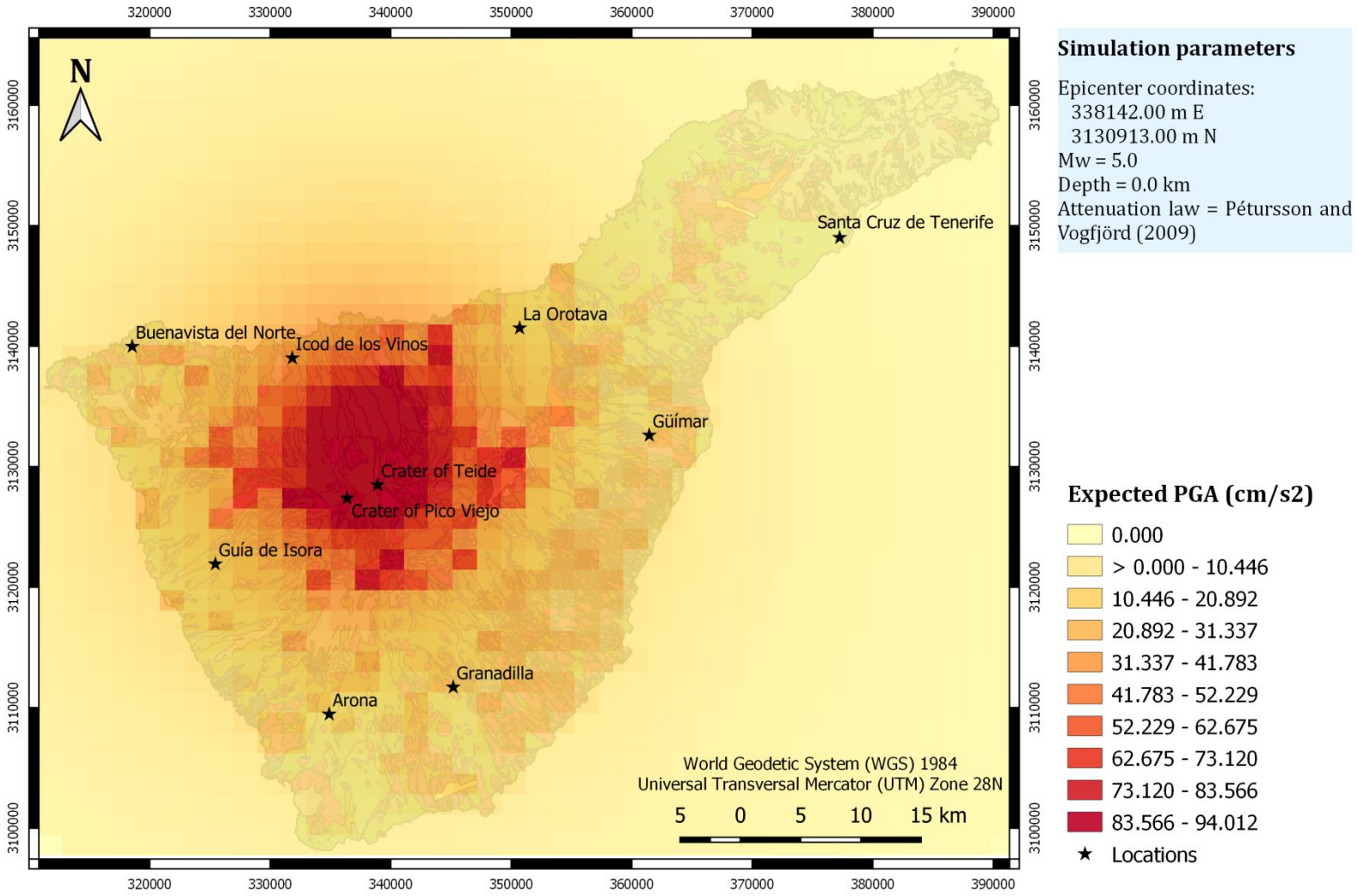

Figure S18. Expected PGA values for a M 5.0 synthetic earthquake located north of the summit of Mt Teide, Tenerife (Canary Islands), at a depth of 0.0 km, after applying the Pétursson and Vogfjörd (2009) attenuation law.

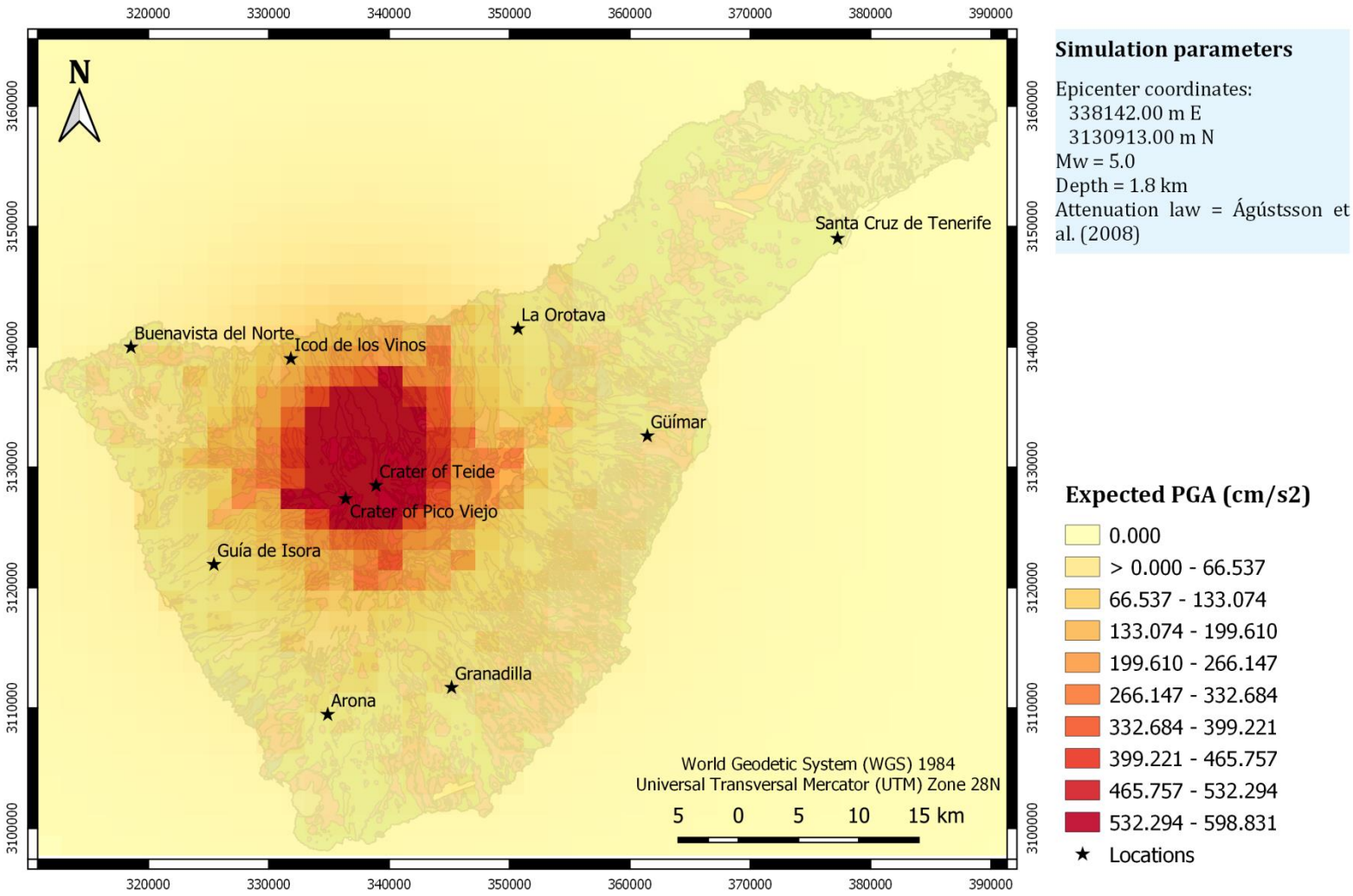

Figure S19. Expected PGA values for a M 5.0 synthetic earthquake located north of the summit of Mt Teide, Tenerife (Canary Islands), at a depth of 1.8 km, after applying the Ágústsson et al. (2008) attenuation law.

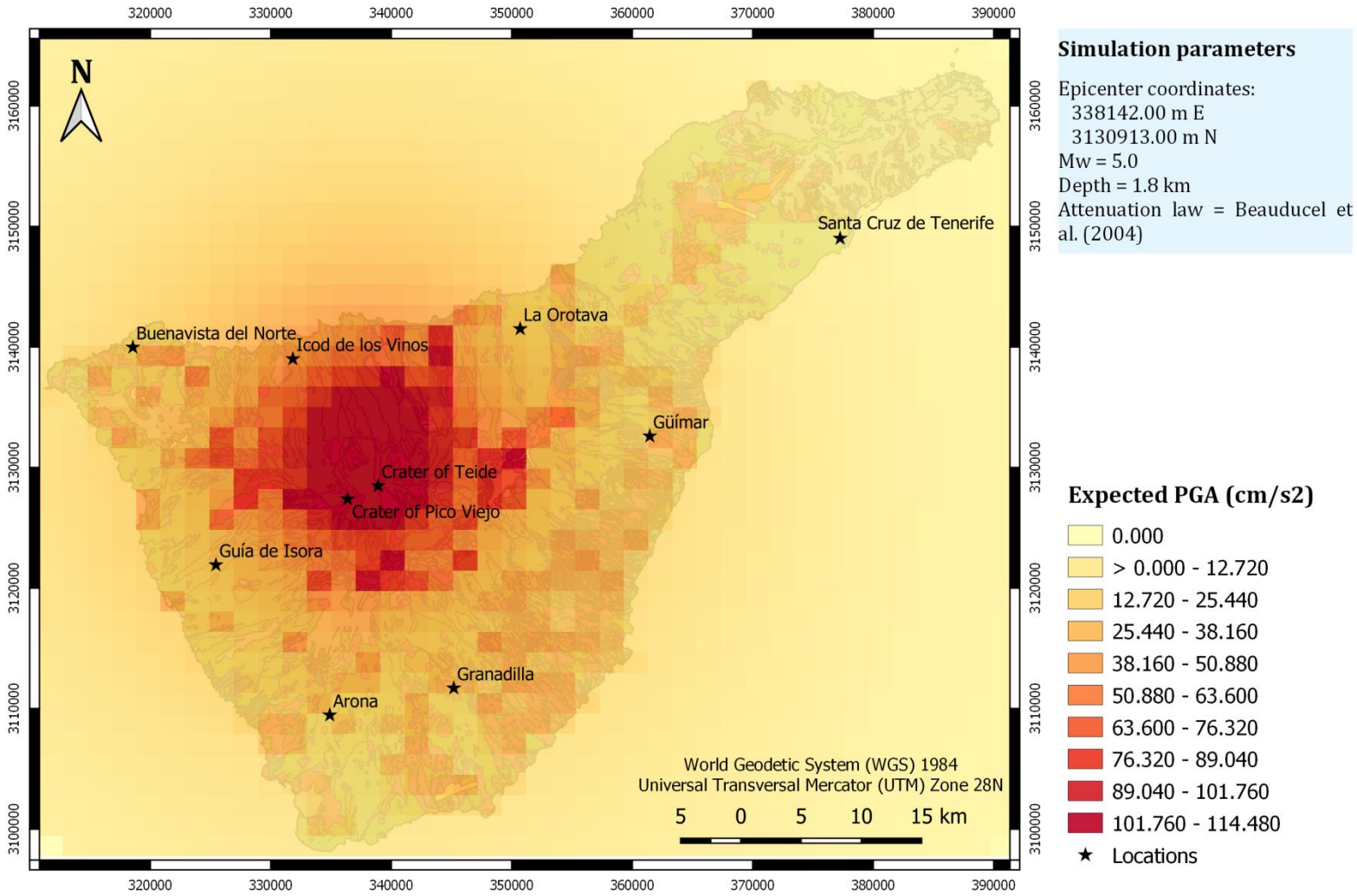

Figure S20. Expected PGA values for a M 5.0 synthetic earthquake located north of the summit of Mt Teide, Tenerife (Canary Islands), at a depth of 1.8 km, after applying the Beauducel et al. (2004) attenuation law.

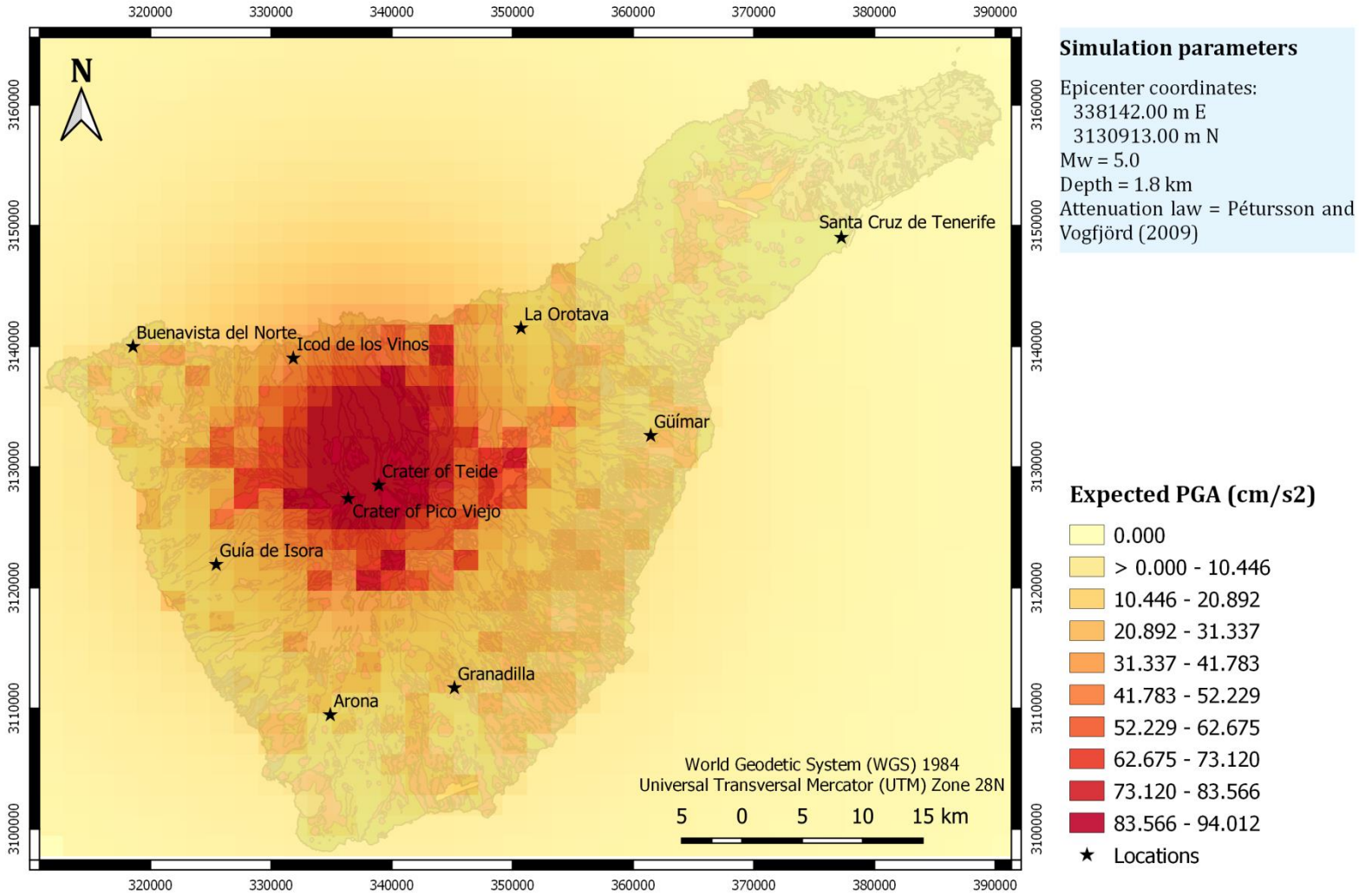

Figure S21. Expected PGA values for a M 5.0 synthetic earthquake located north of the summit of Mt Teide, Tenerife (Canary Islands), at a depth of 1.8 km, after applying the Pétursson and Vogfjörd (2009) attenuation law.

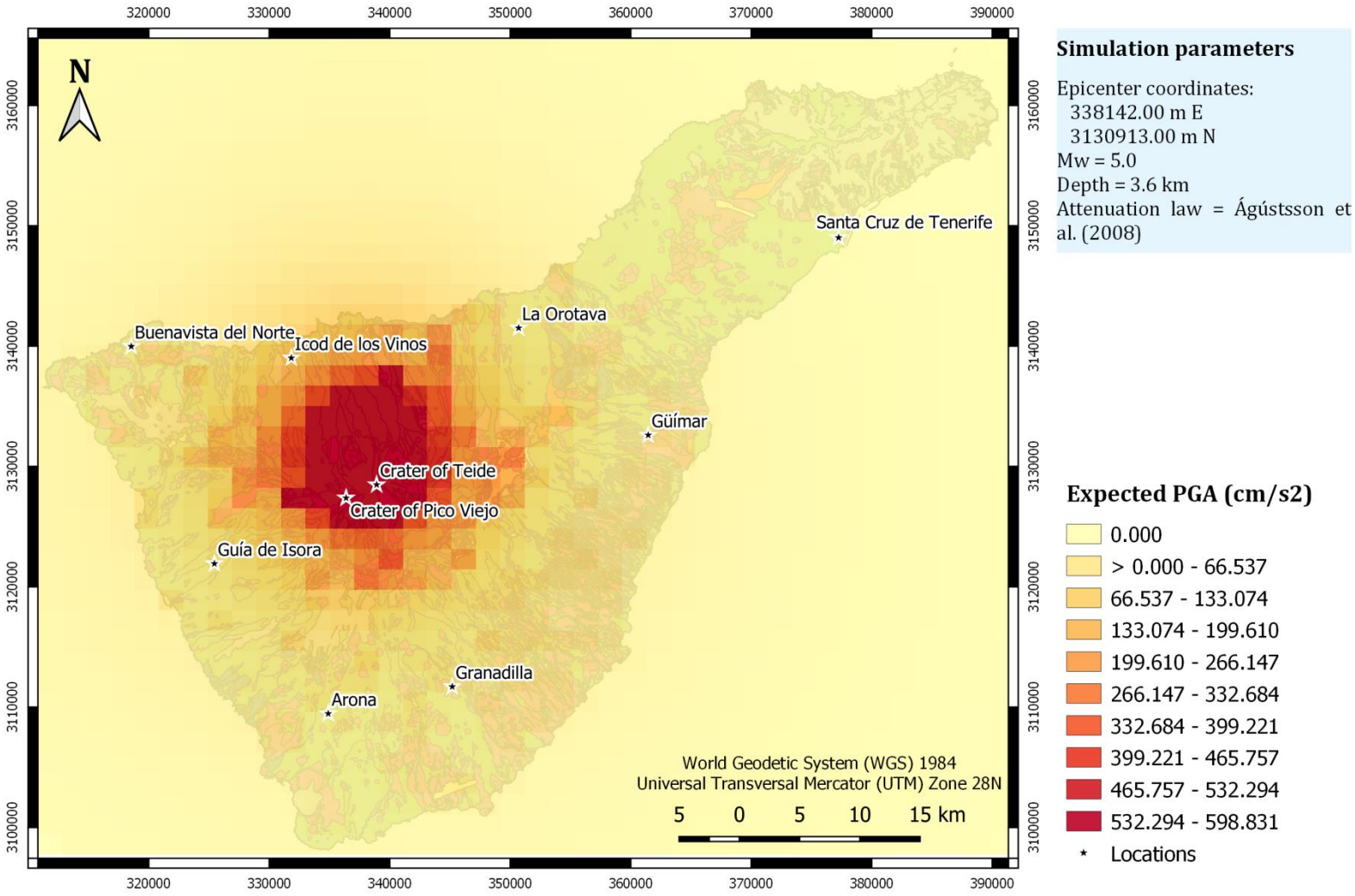

Figure S22. Expected PGA values for a M 5.0 synthetic earthquake located north of the summit of Mt Teide, Tenerife (Canary Islands), at a depth of 3.6 km, after applying the Ágústsson et al. (2008) attenuation law.

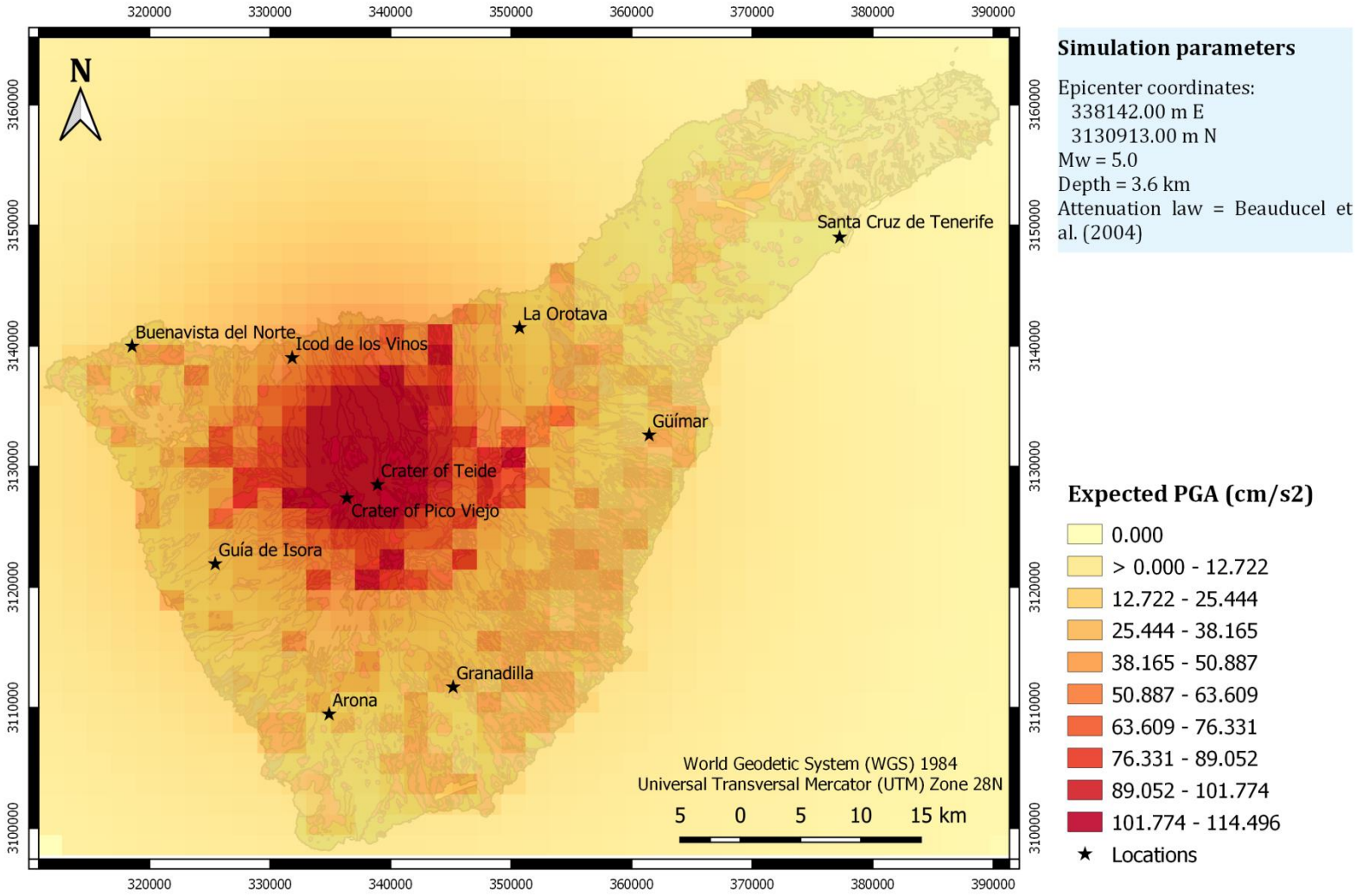

Figure S23. Expected PGA values for a M 5.0 synthetic earthquake located north of the summit of Mt Teide, Tenerife (Canary Islands), at a depth of 3.6 km, after applying the Beauducel et al. (2004) attenuation law.

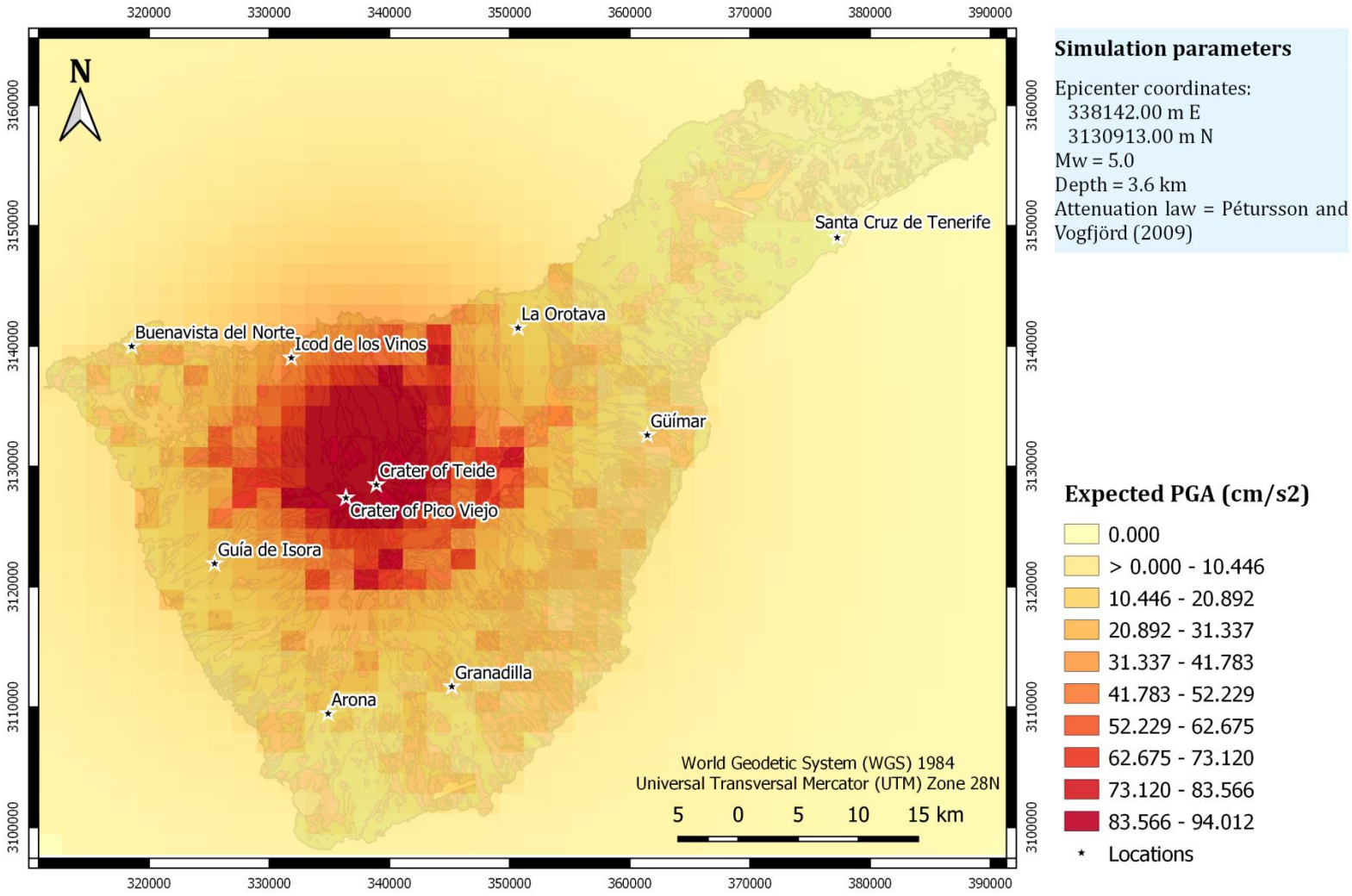

Figure S24. Expected PGA values for a M 5.0 synthetic earthquake located north of the summit of Mt Teide, Tenerife (Canary Islands), at a depth of 3.6 km, after applying the Pétursson and Vogfjörd (2009) attenuation law.

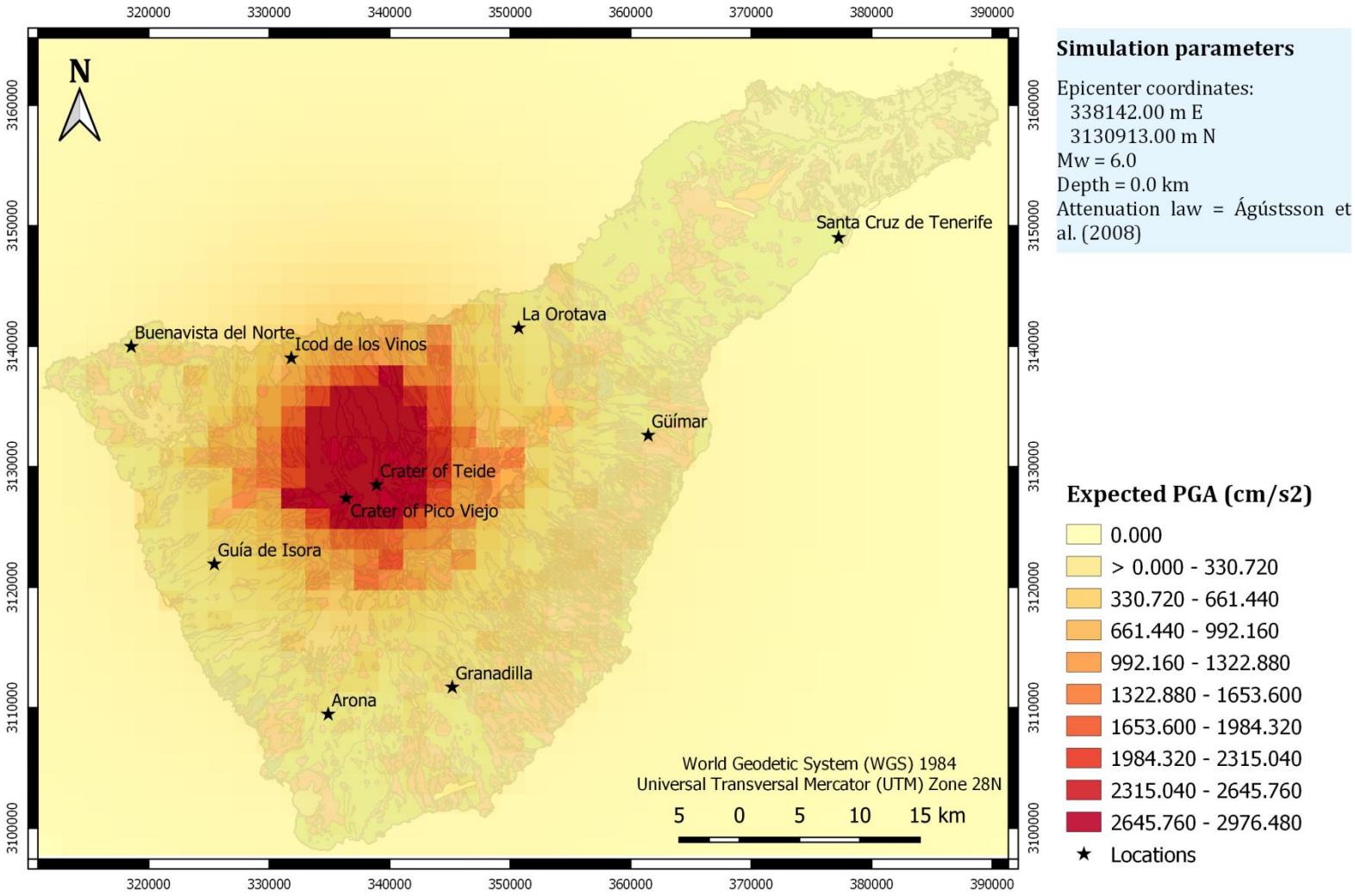

Figure S25. Expected PGA values for a M 6.0 synthetic earthquake located north of the summit of Mt Teide, Tenerife (Canary Islands), at a depth of 0.0 km, after applying the Ágústsson et al. (2008) attenuation law.

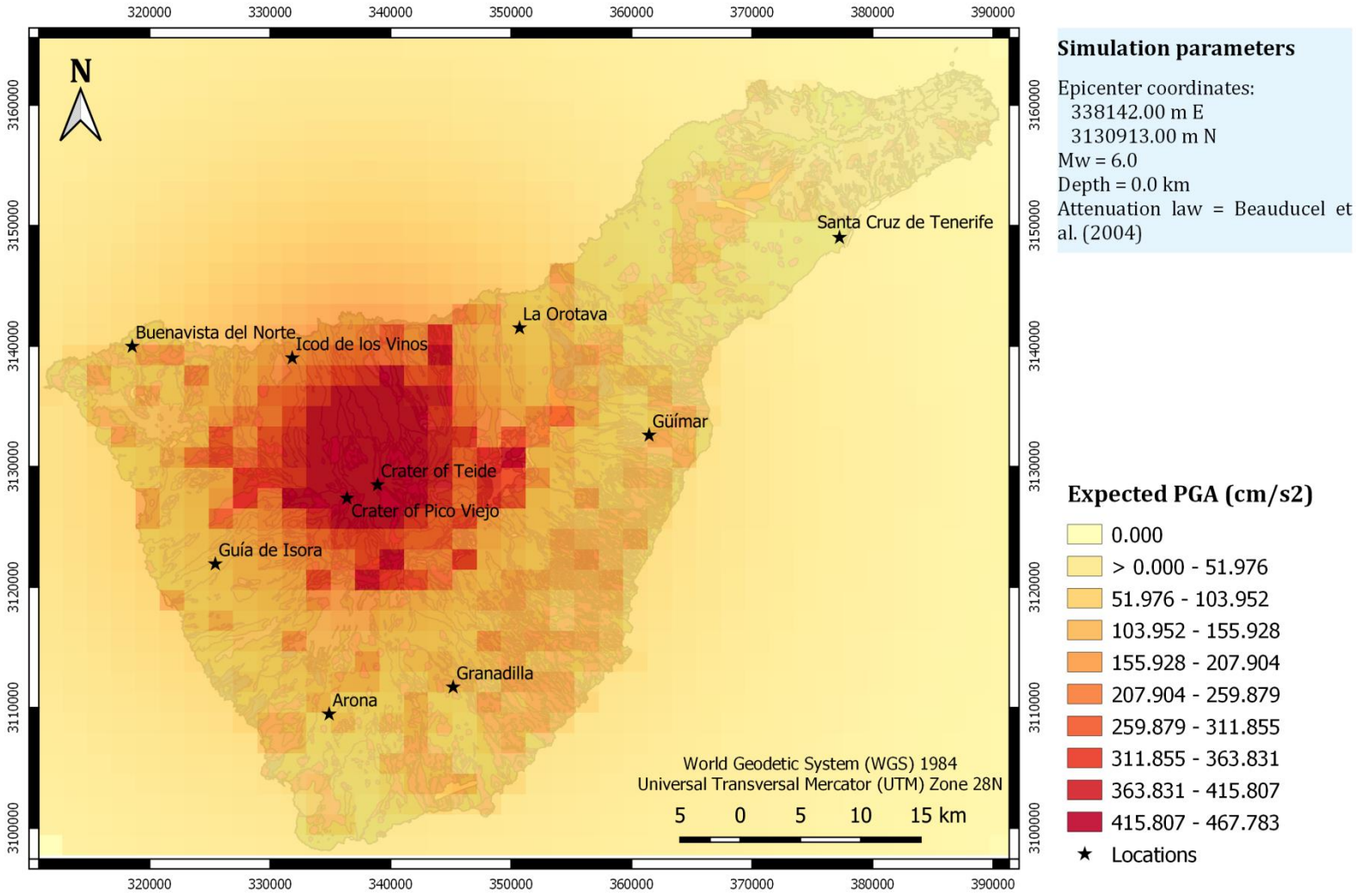

Figure S26. Expected PGA values for a M 6.0 synthetic earthquake located north of the summit of Mt Teide, Tenerife (Canary Islands), at a depth of 0.0 km, after applying the Beauducel et al. (2004) attenuation law.

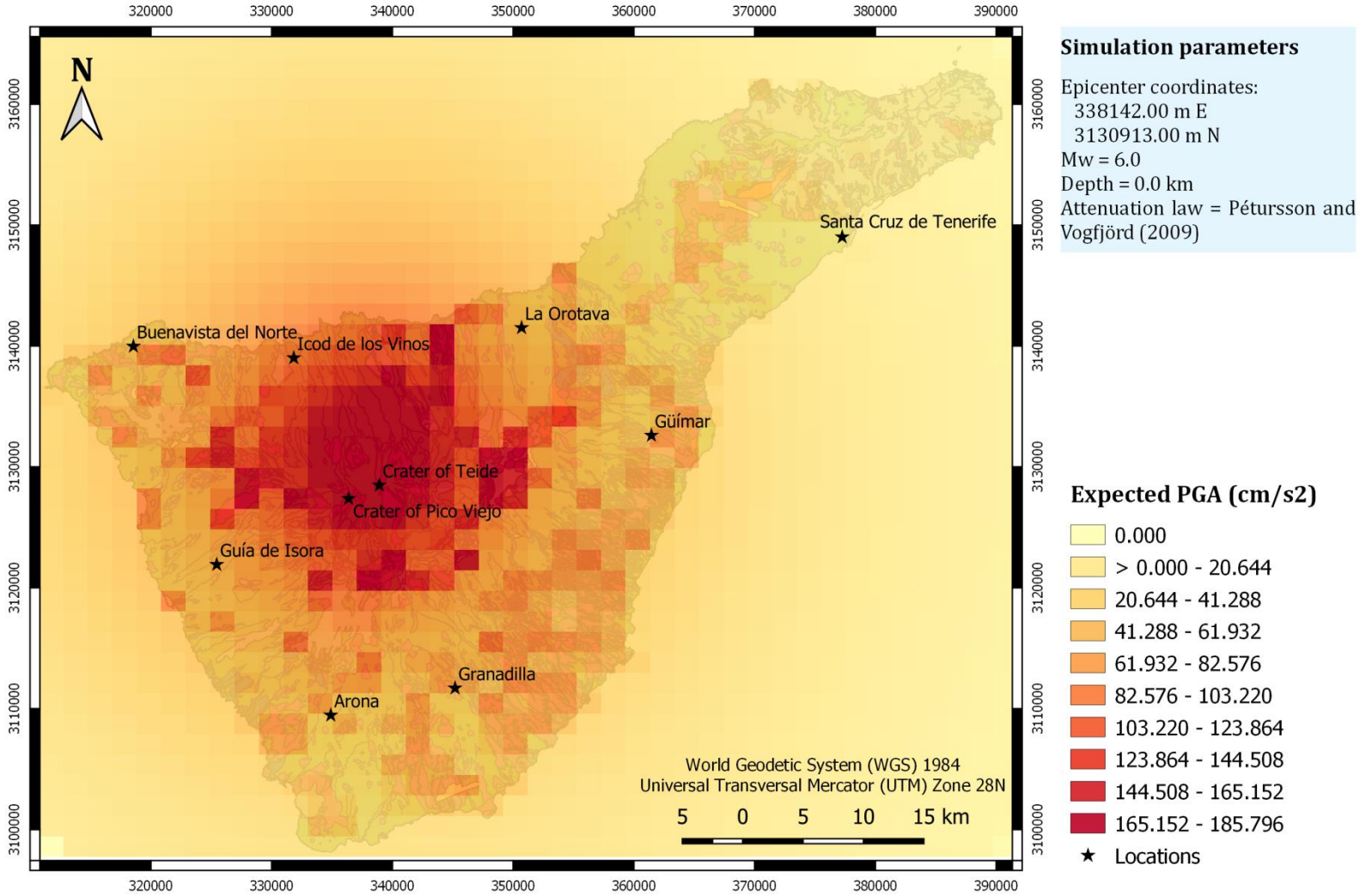

Figure S27. Expected PGA values for a M 6.0 synthetic earthquake located north of the summit of Mt Teide, Tenerife (Canary Islands), at a depth of 0.0 km, after applying the Pétursson and Vogfjörd (2009) attenuation law.

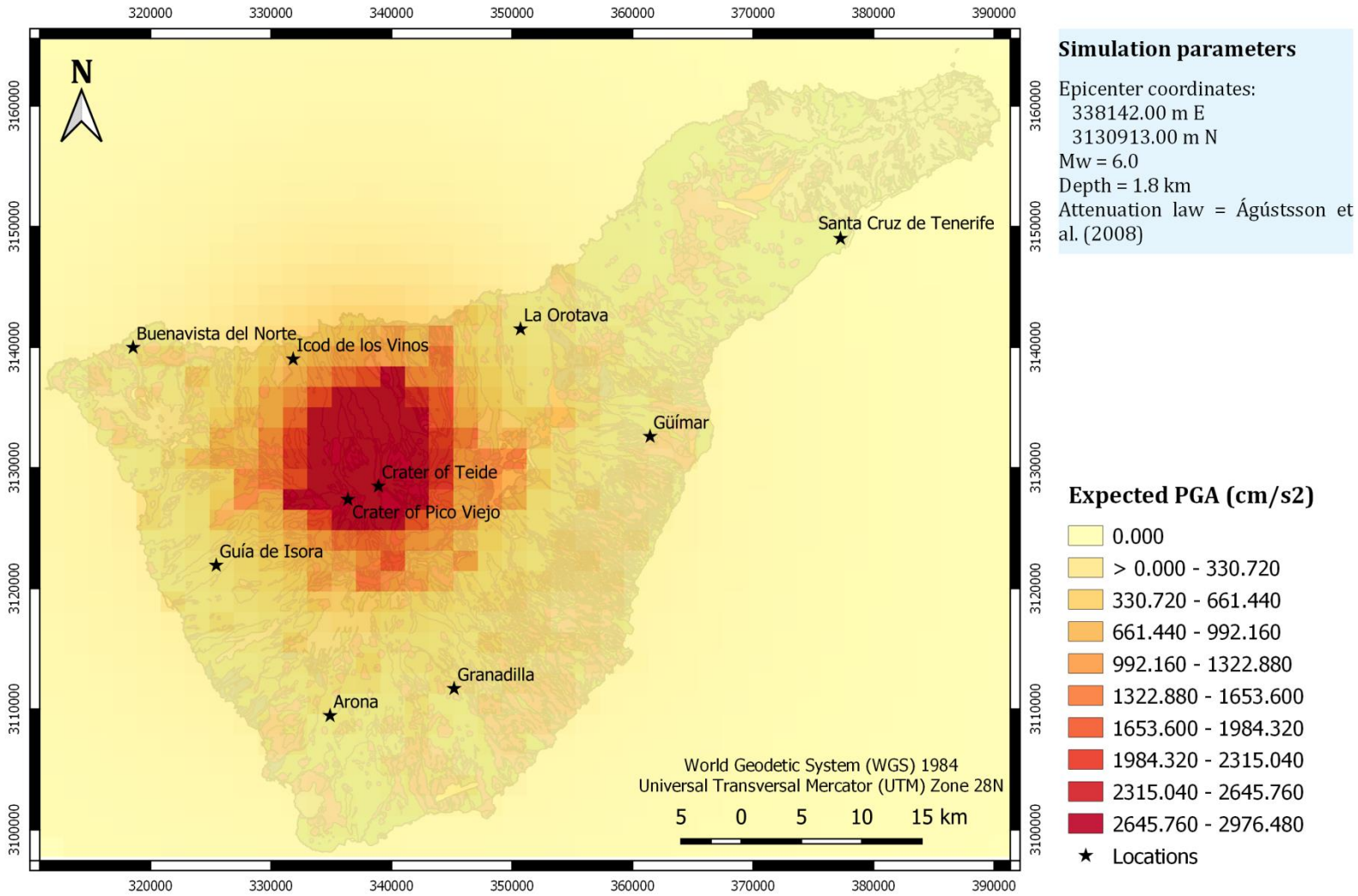

Figure S28. Expected PGA values for a M 6.0 synthetic earthquake located north of the summit of Mt Teide, Tenerife (Canary Islands), at a depth of 1.8 km, after applying the Ágústsson et al. (2008) attenuation law.

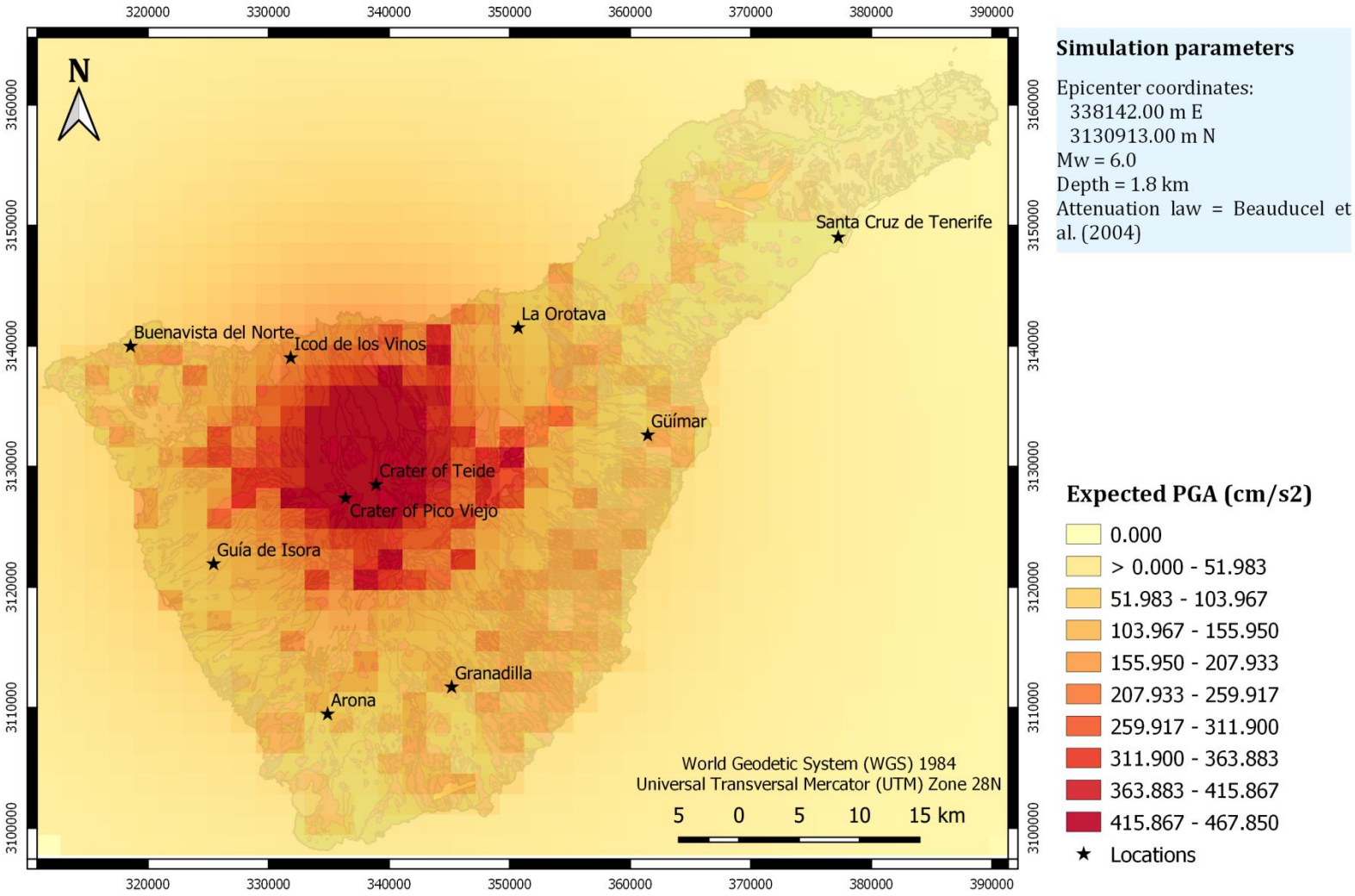

Figure S29. Expected PGA values for a M 6.0 synthetic earthquake located north of the summit of Mt Teide, Tenerife (Canary Islands), at a depth of 1.8 km, after applying the Beauducel et al. (2004) attenuation law.

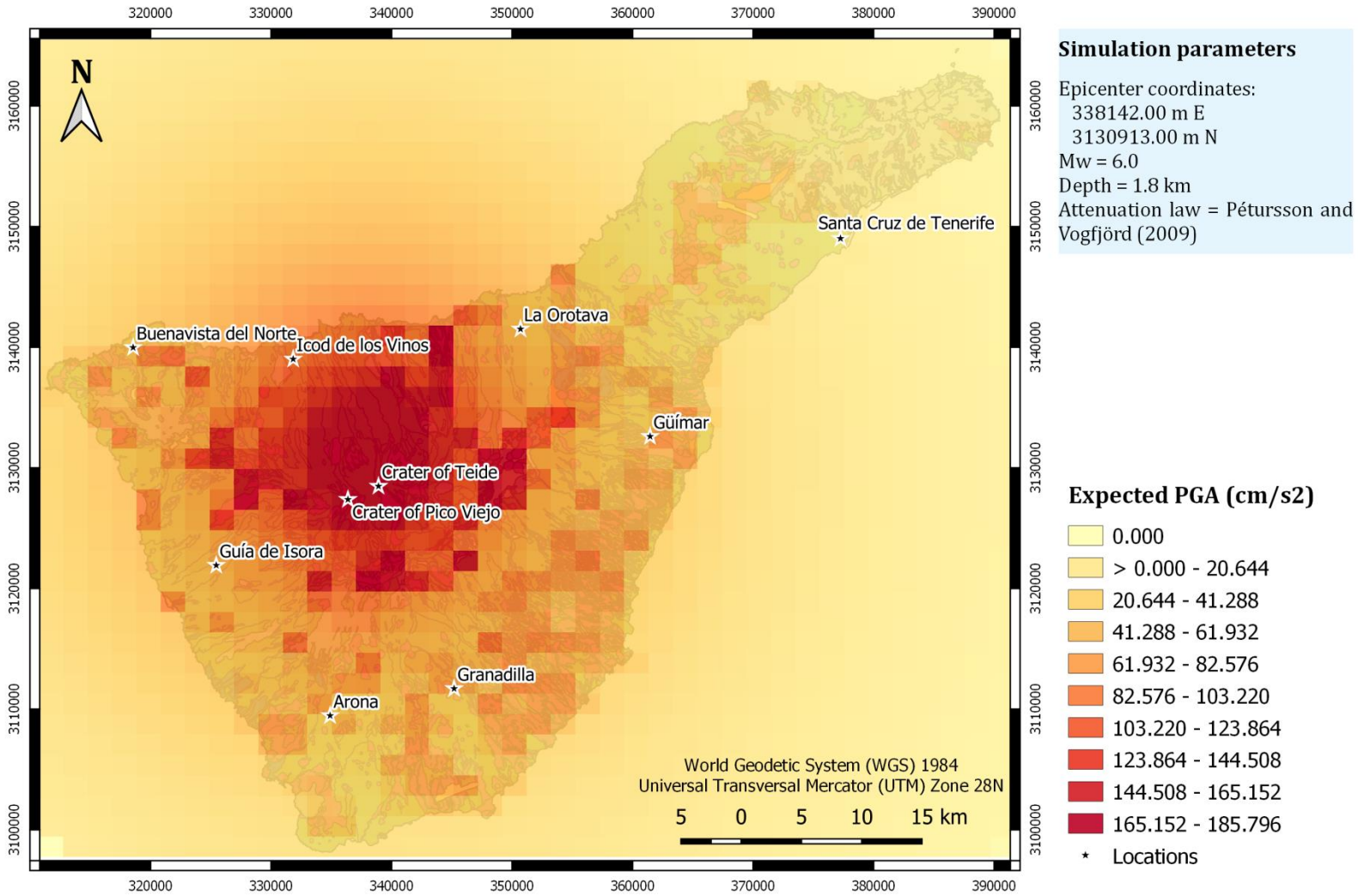

Figure S30. Expected PGA values for a M 6.0 synthetic earthquake located north of the summit of Mt Teide, Tenerife (Canary Islands), at a depth of 1.8 km, after applying the Pétursson and Vogfjörd (2009) attenuation law.

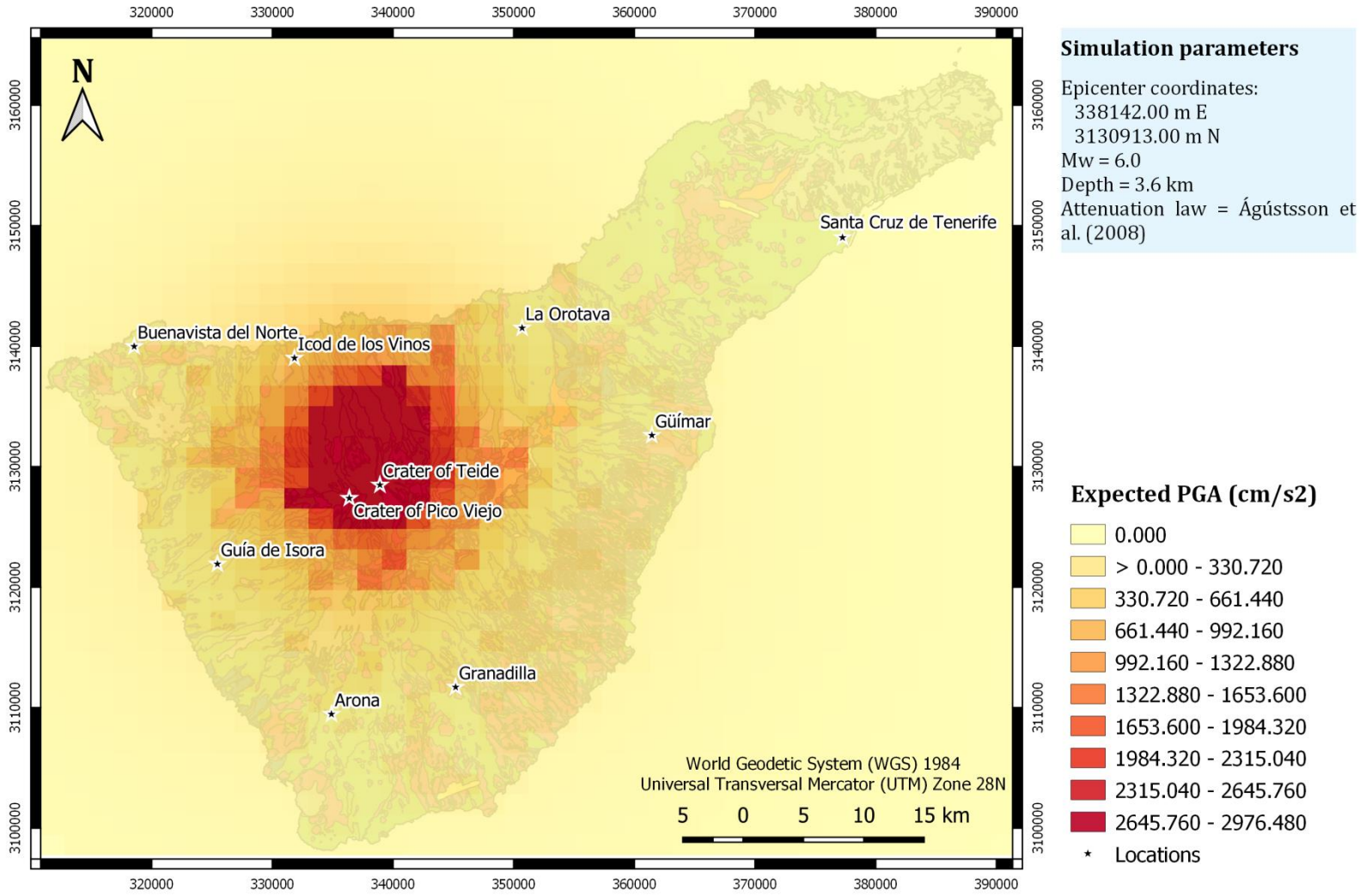

Figure S31. Expected PGA values for a M 6.0 synthetic earthquake located north of the summit of Mt Teide, Tenerife (Canary Islands), at a depth of 3.6 km, after applying the Ágústsson et al. (2008) attenuation law.

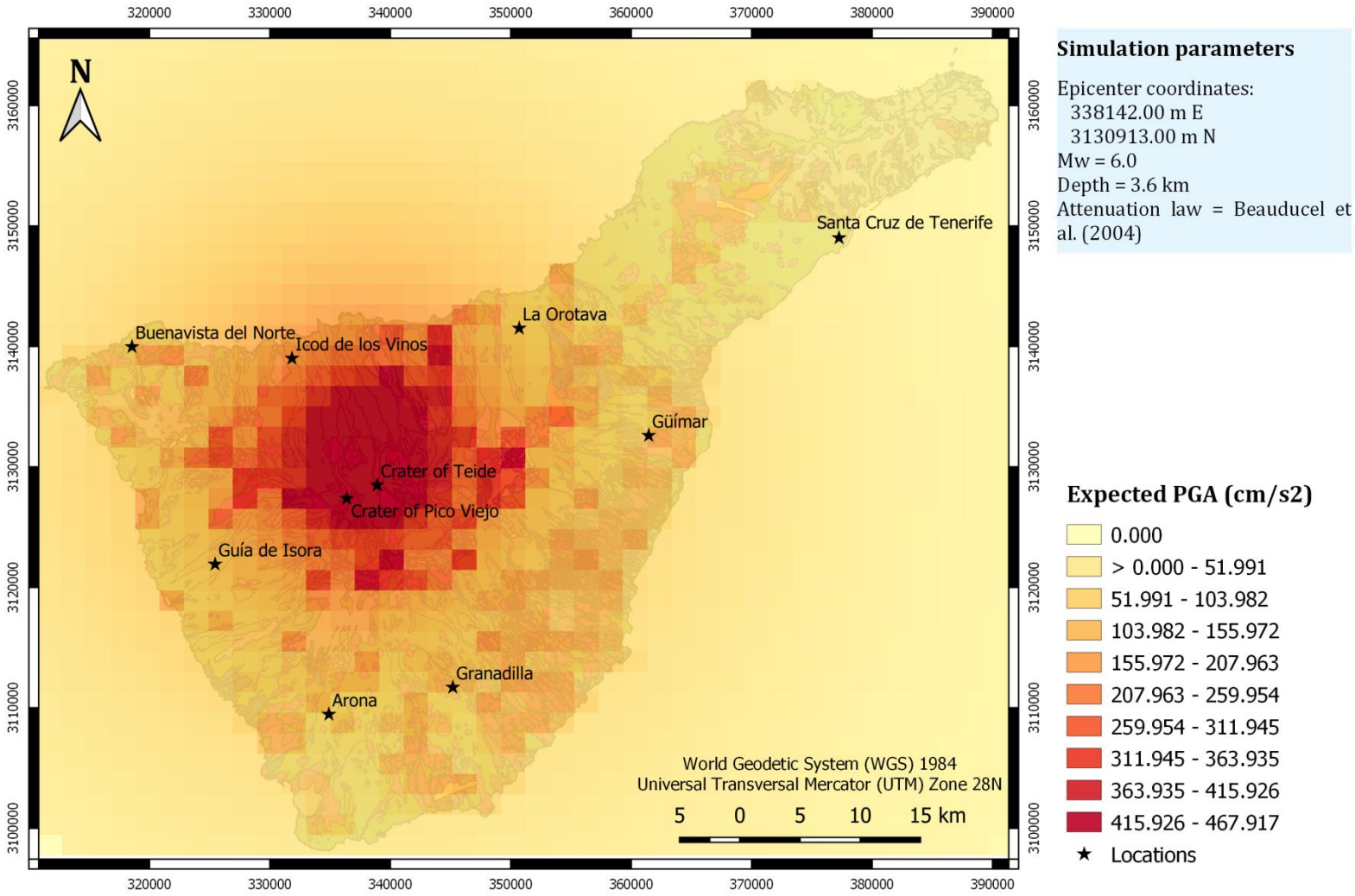

Figure S32. Expected PGA values for a M 6.0 synthetic earthquake located north of the summit of Mt Teide, Tenerife (Canary Islands), at a depth of 3.6 km, after applying the Beauducel et al. (2004) attenuation law.

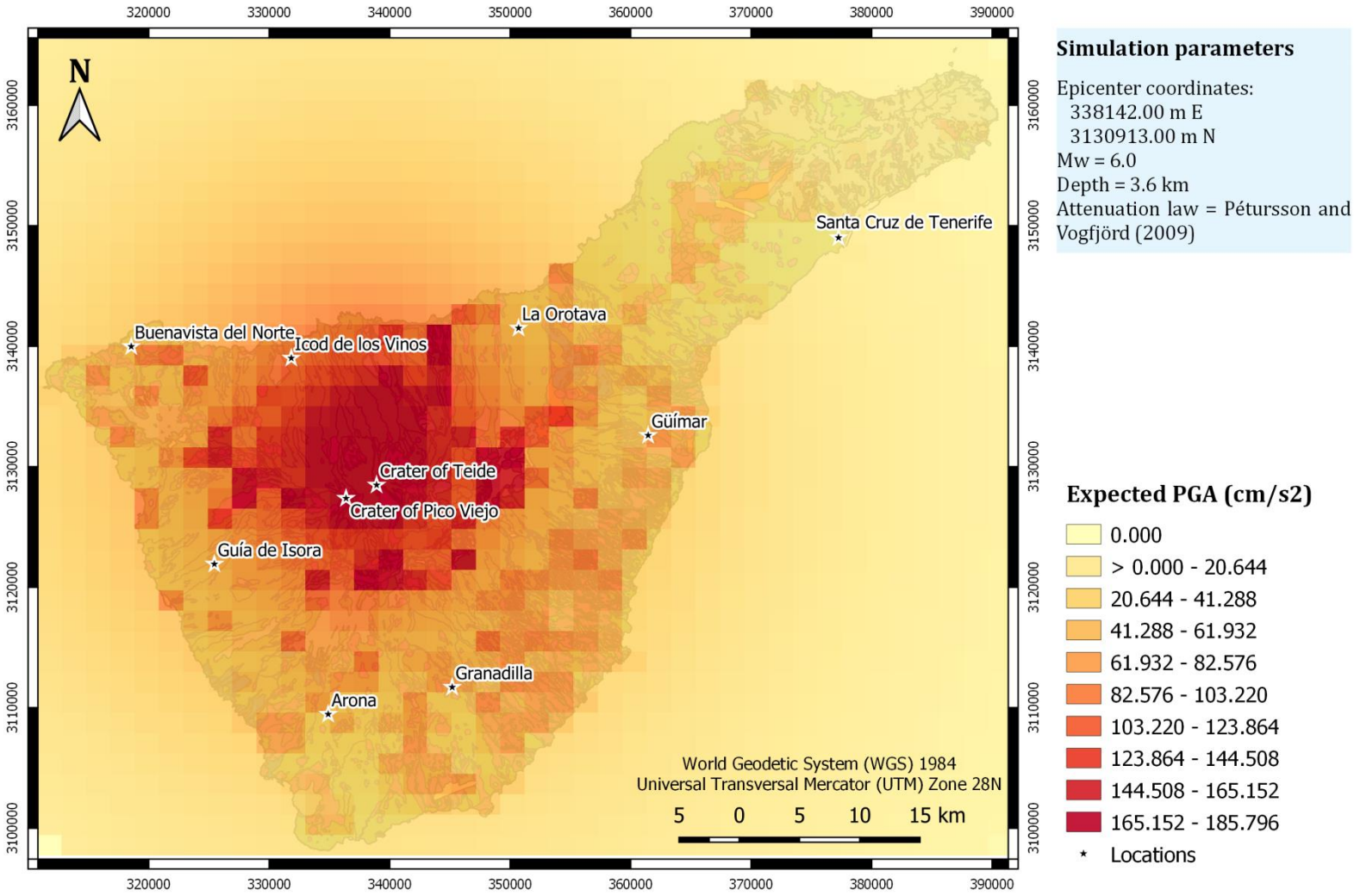

Figure S33. Expected PGA values for a M 6.0 synthetic earthquake located north of the summit of Mt Teide, Tenerife (Canary Islands), at a depth of 3.6 km, after applying the Pétursson and Vogfjörd (2009) attenuation law.

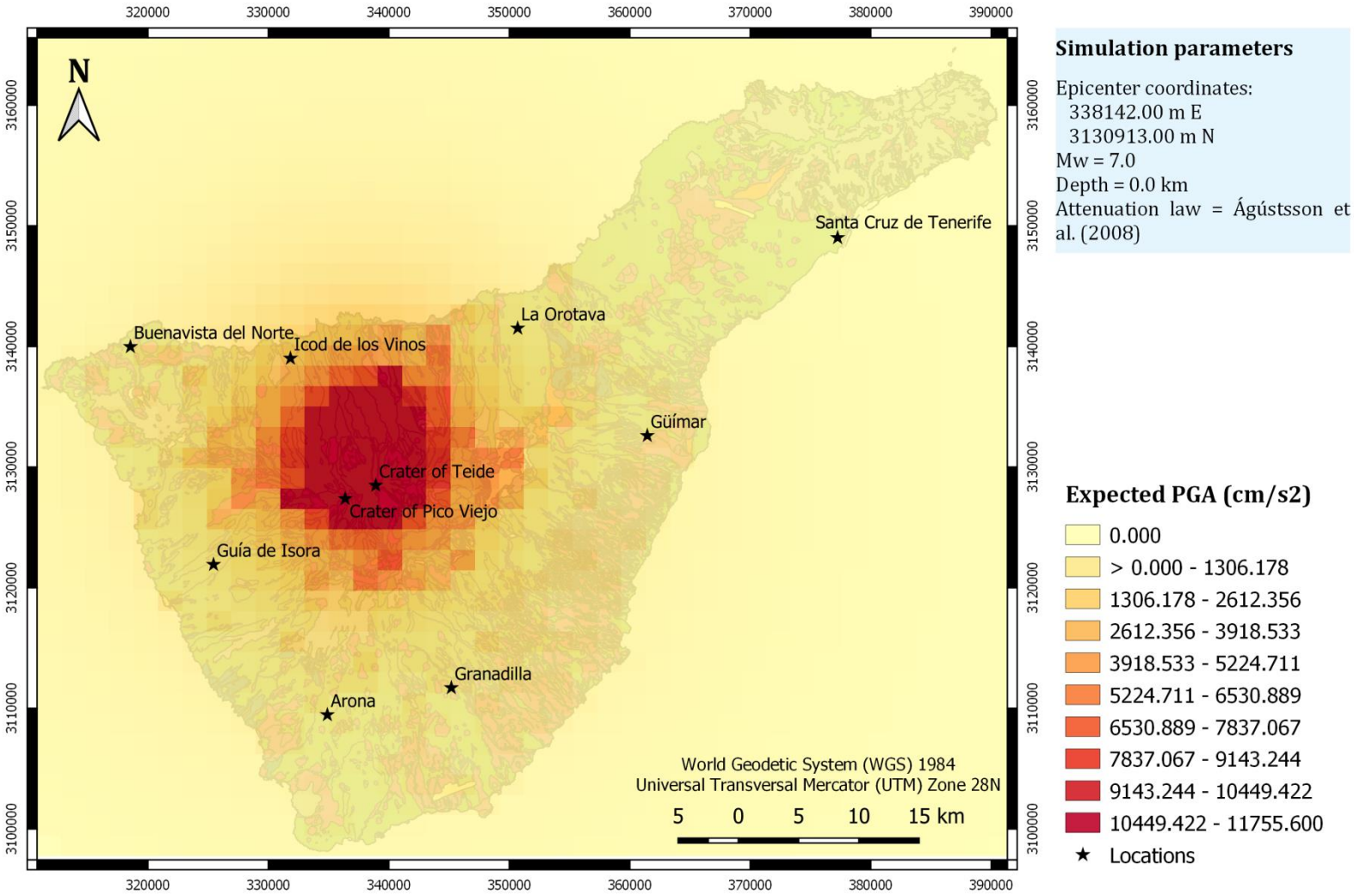

Figure S34. Expected PGA values for a M 7.0 synthetic earthquake located north of the summit of Mt Teide, Tenerife (Canary Islands), at a depth of 0.0 km, after applying the Ágústsson et al. (2008) attenuation law.

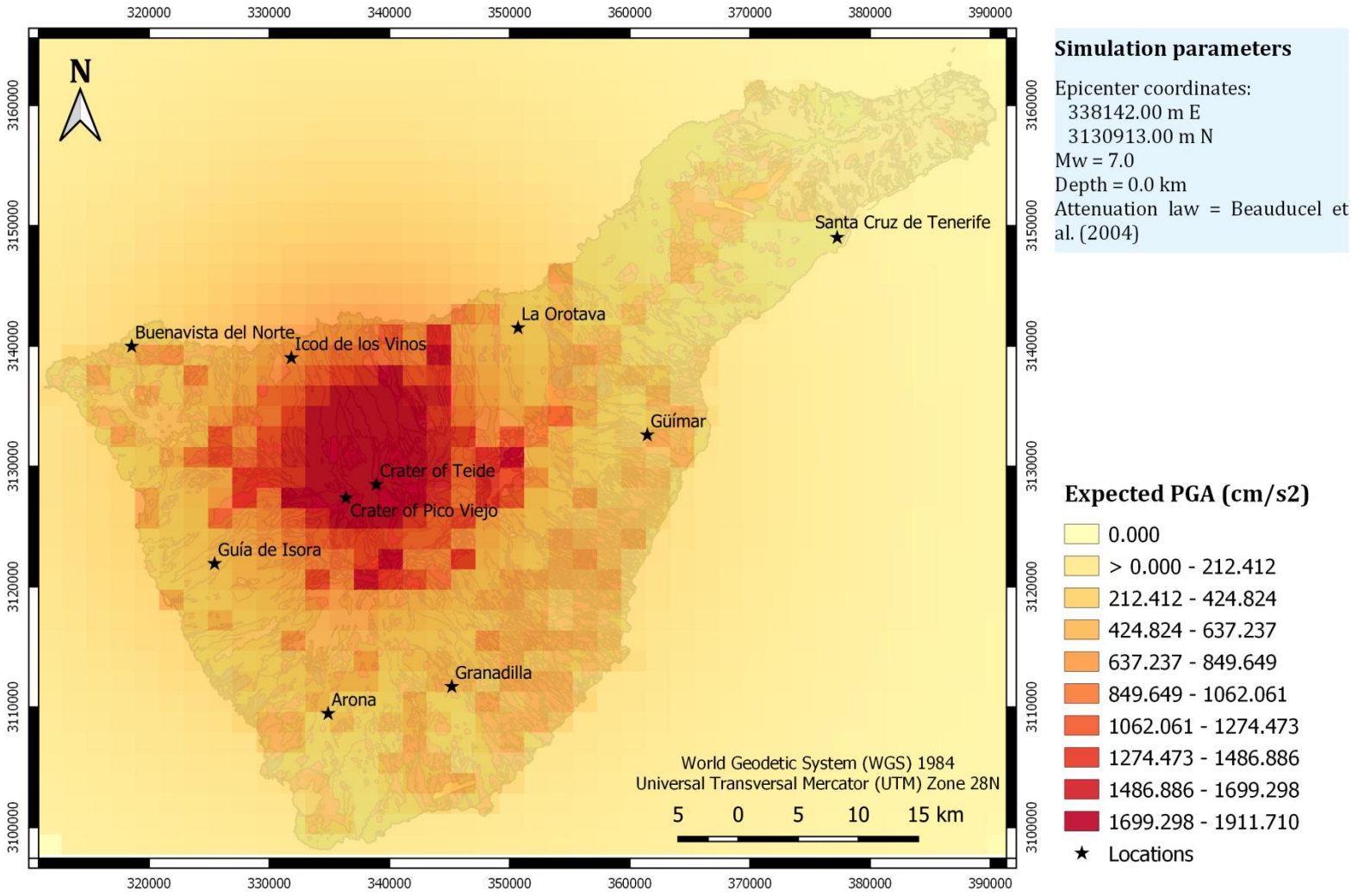

Figure S35. Expected PGA values for a M 7.0 synthetic earthquake located north of the summit of Mt Teide, Tenerife (Canary Islands), at a depth of 0.0 km, after applying the Beauducel et al. (2004) attenuation law.

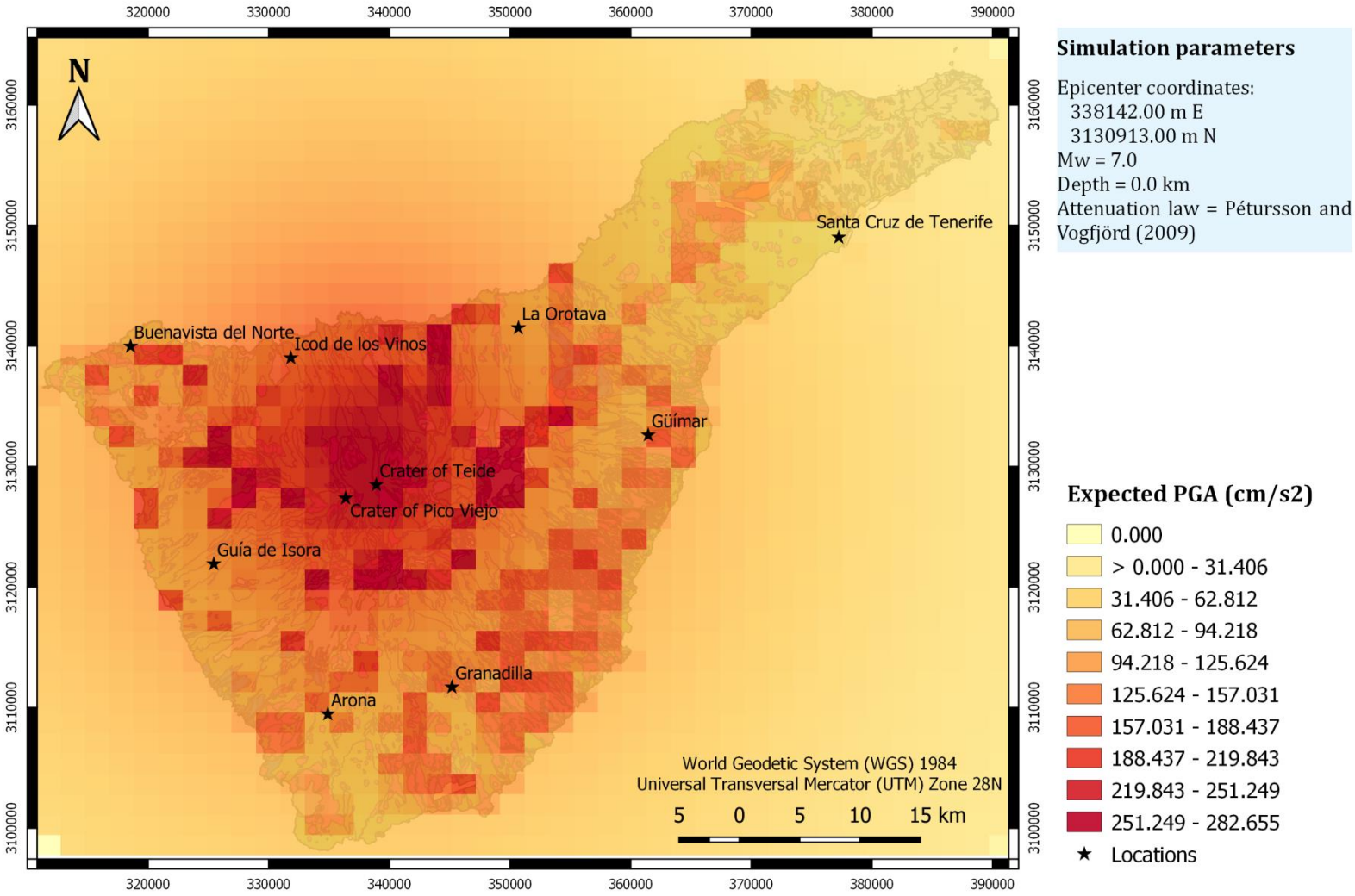

Figure S36. Expected PGA values for a M 7.0 synthetic earthquake located north of the summit of Mt Teide, Tenerife (Canary Islands), at a depth of 0.0 km, after applying the Pétursson and Vogfjörd (2009) attenuation law.

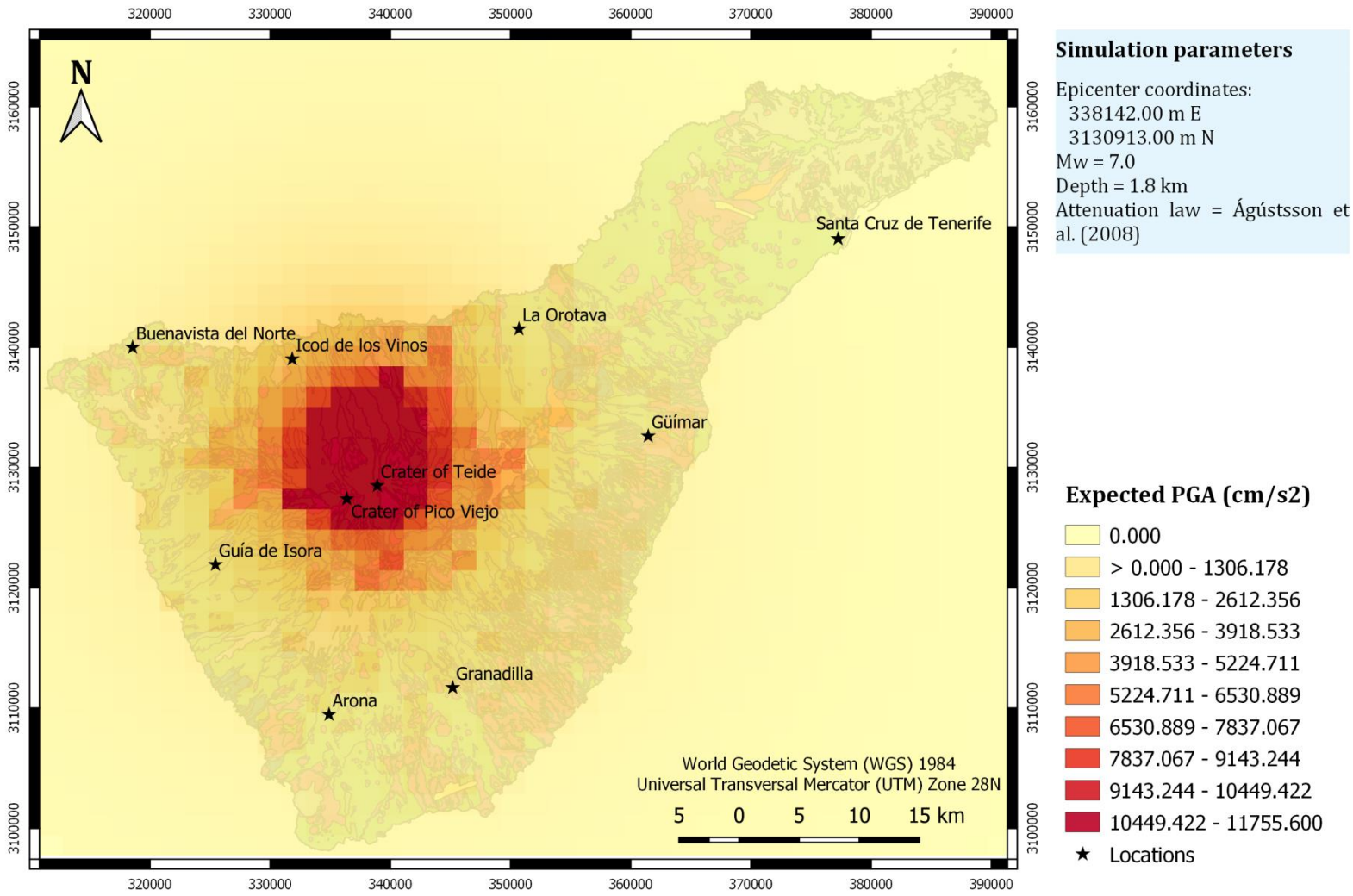

Figure S37. Expected PGA values for a M 7.0 synthetic earthquake located north of the summit of Mt Teide, Tenerife (Canary Islands), at a depth of 1.8 km, after applying the Ágústsson et al. (2008) attenuation law.

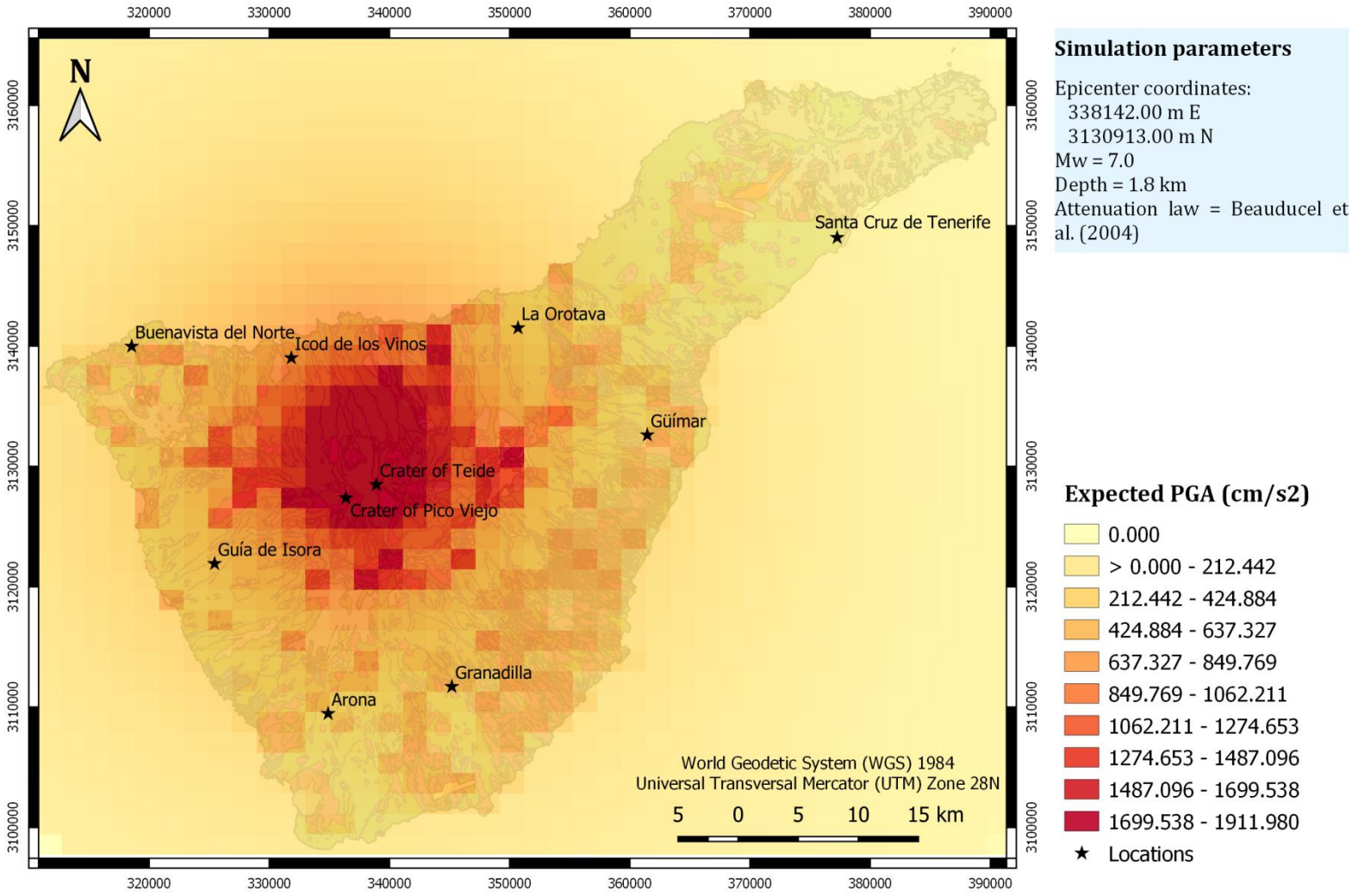

Figure S38. Expected PGA values for a M 7.0 synthetic earthquake located north of the summit of Mt Teide, Tenerife (Canary Islands), at a depth of 1.8 km, after applying the Beauducel et al. (2004) attenuation law.

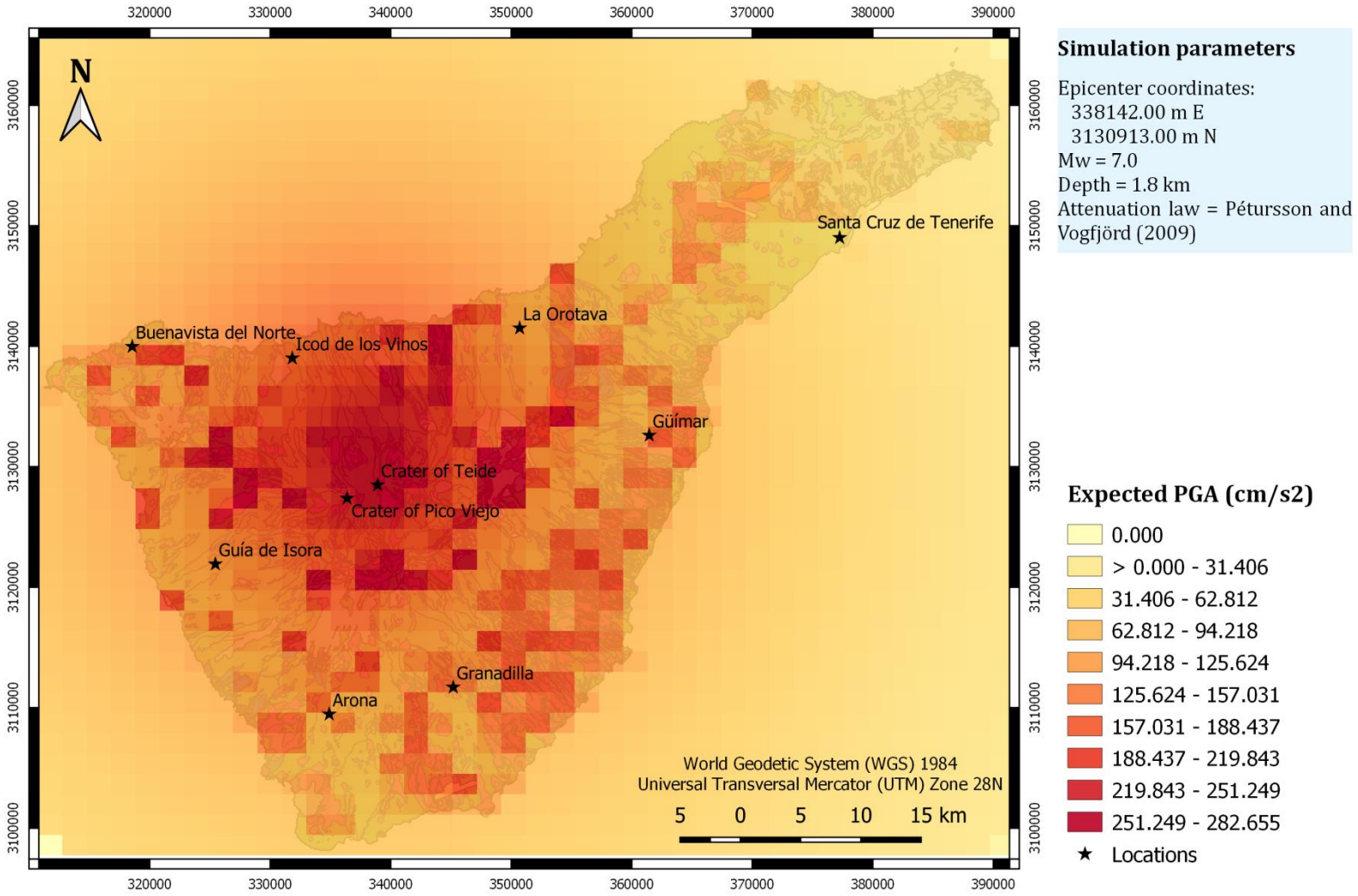

Figure S39. Expected PGA values for a M 7.0 synthetic earthquake located north of the summit of Mt Teide, Tenerife (Canary Islands), at a depth of 1.8 km, after applying the Pétursson and Vogfjörd (2009) attenuation law.

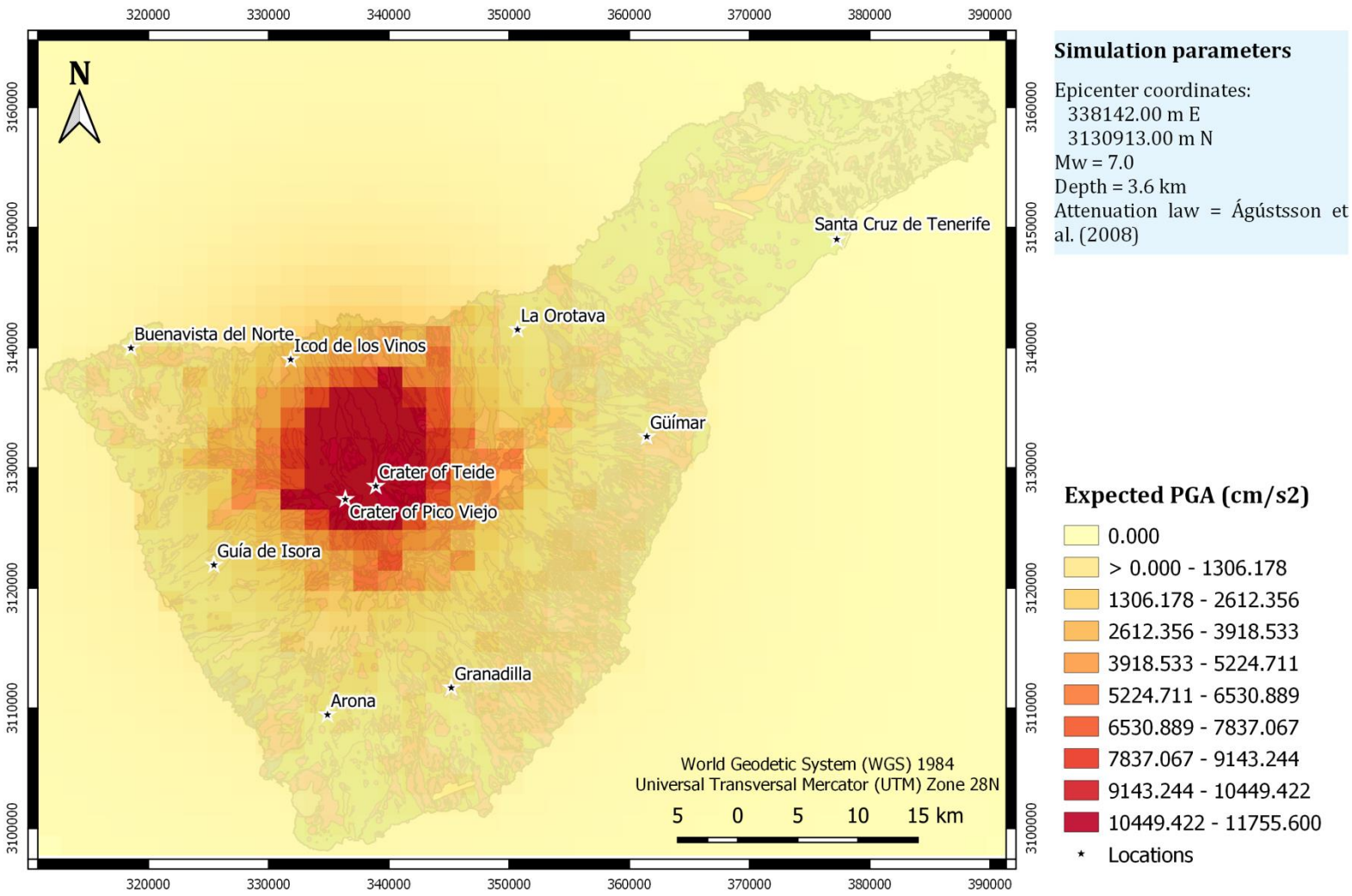

Figure S40. Expected PGA values for a M 7.0 synthetic earthquake located north of the summit of Mt Teide, Tenerife (Canary Islands), at a depth of 3.6 km, after applying the Ágústsson et al. (2008) attenuation law.

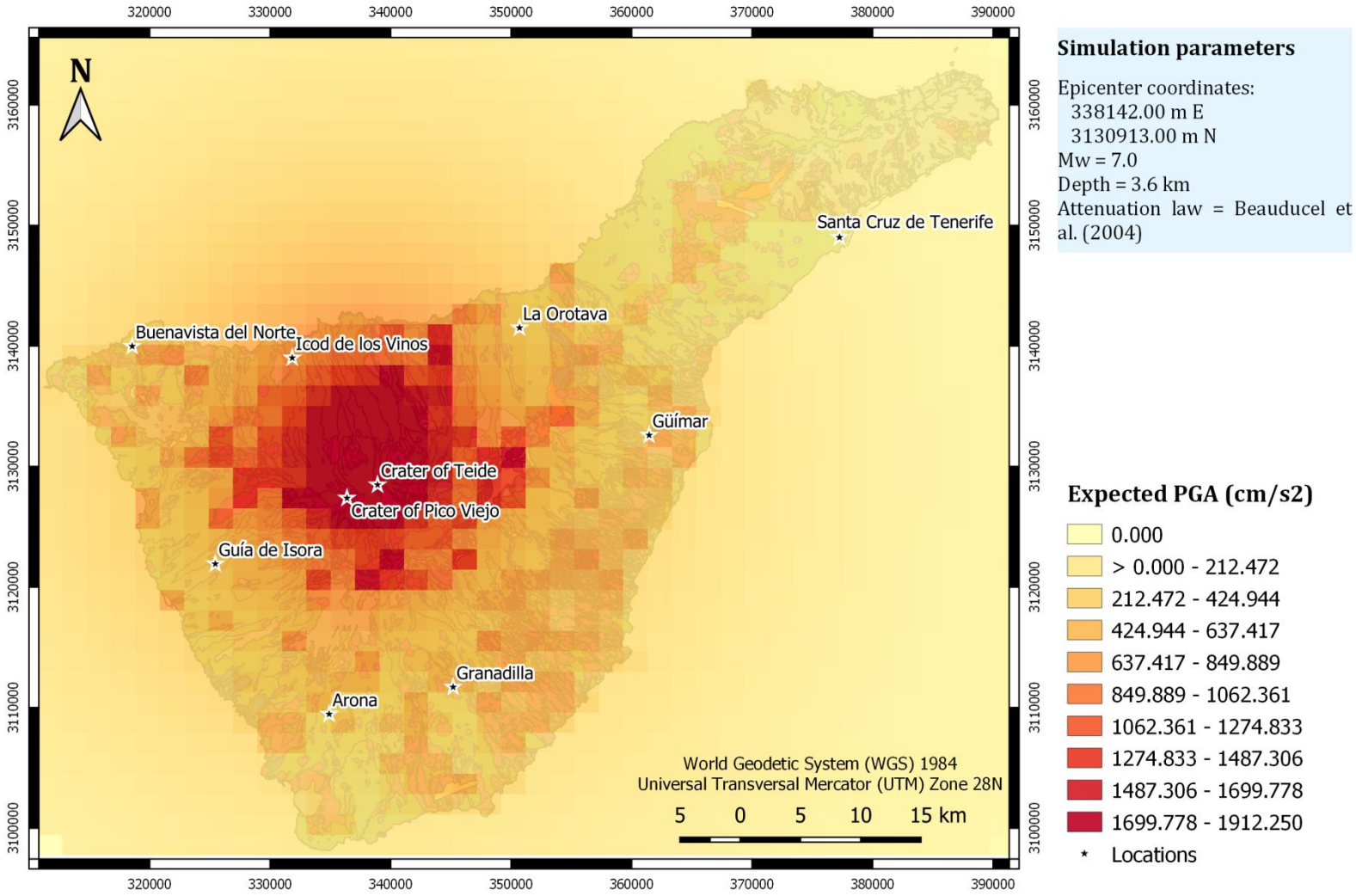

Figure S41. Expected PGA values for a M 7.0 synthetic earthquake located north of the summit of Mt Teide, Tenerife (Canary Islands), at a depth of 3.6 km, after applying the Beauducel et al. (2004) attenuation law.

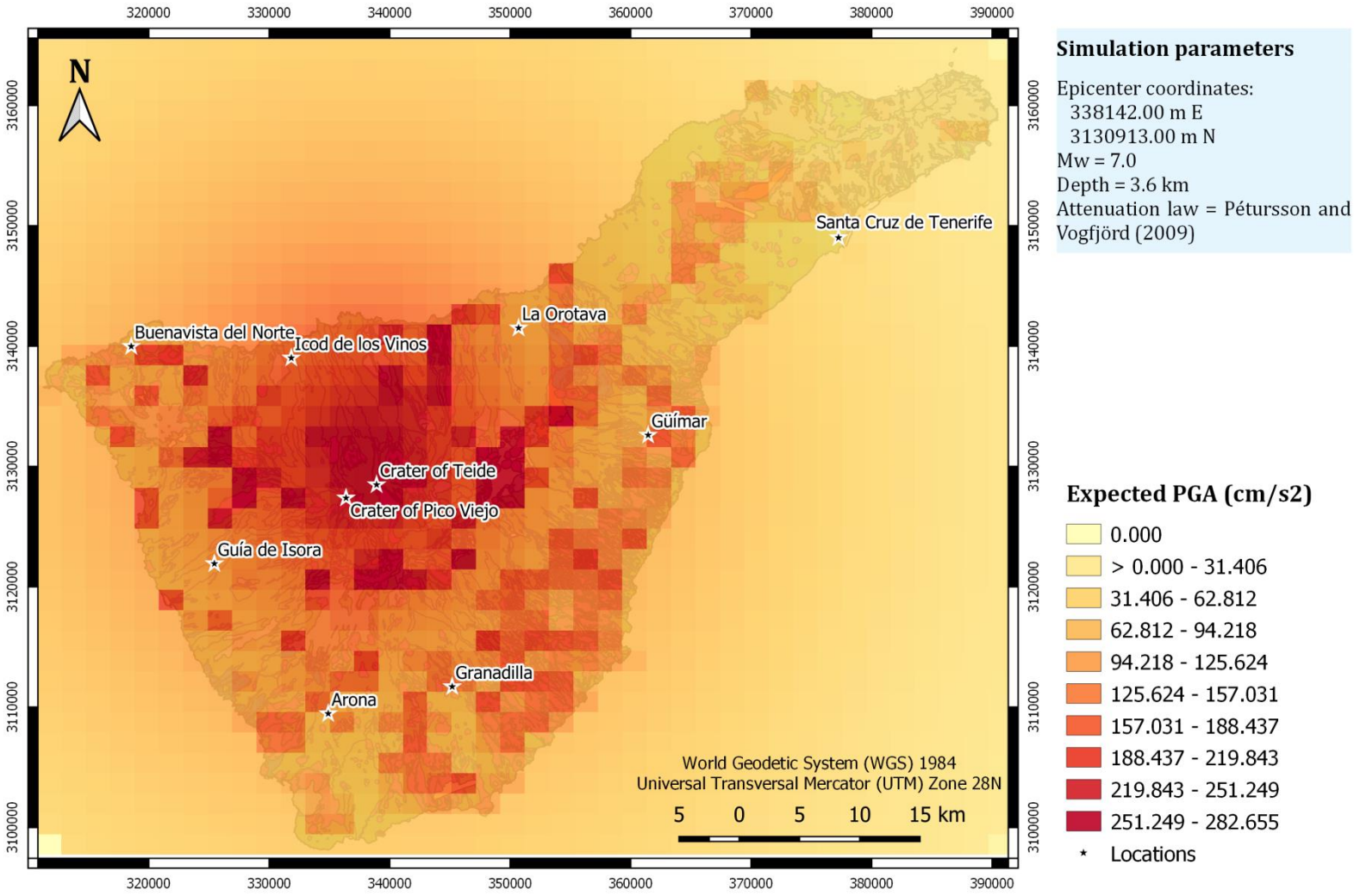

Figure S42. Expected PGA values for a M 7.0 synthetic earthquake located north of the summit of Mt Teide, Tenerife (Canary Islands), at a depth of 3.6 km, after applying the Pétursson and Vogfjörd (2009) attenuation law.

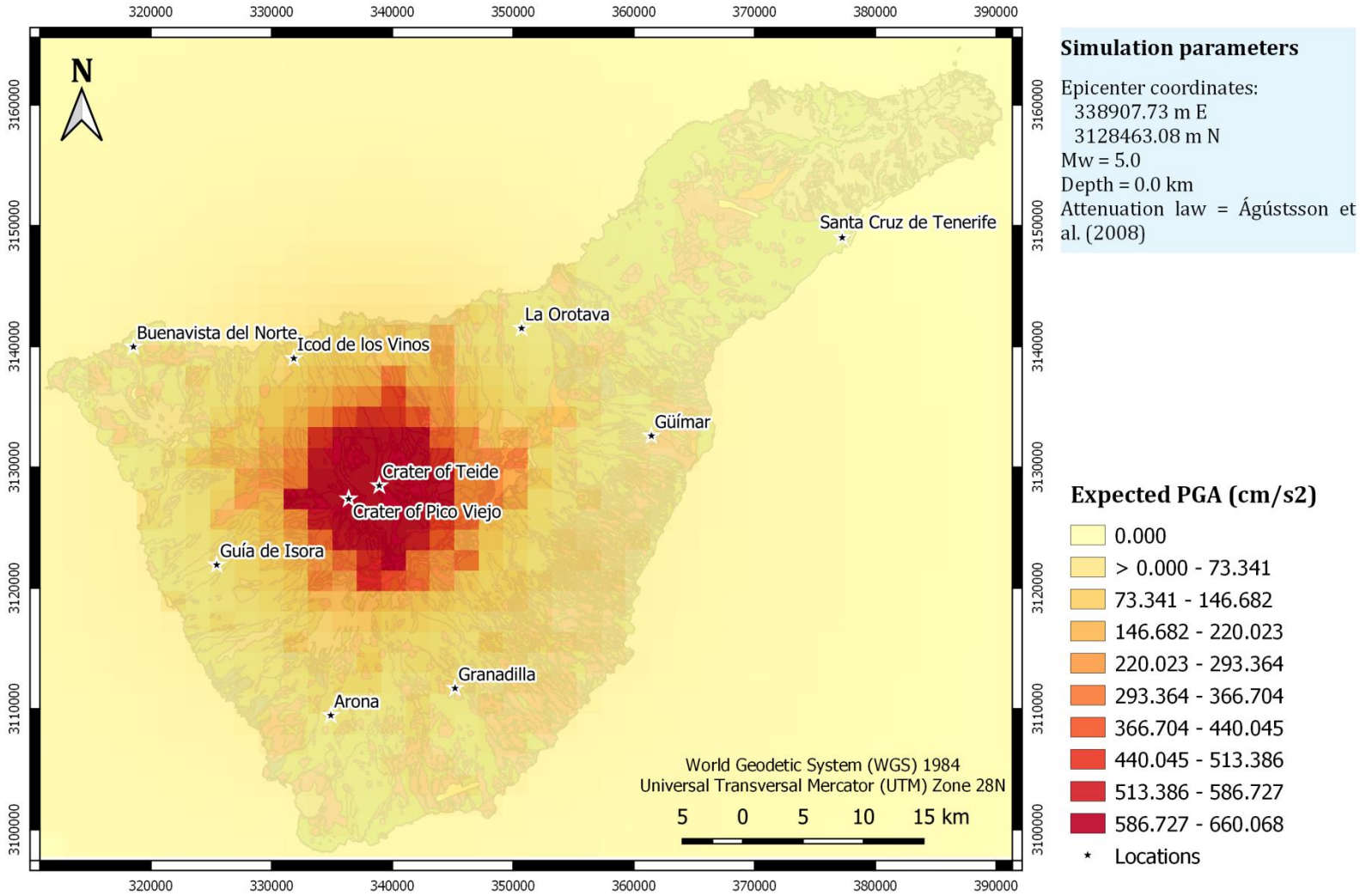

Figure S43. Expected PGA values for a M 5.0 synthetic earthquake located on the crater of Teide, Tenerife (Canary Islands), at a depth of 0.0 km, after applying the Ágústsson et al. (2008) attenuation law.

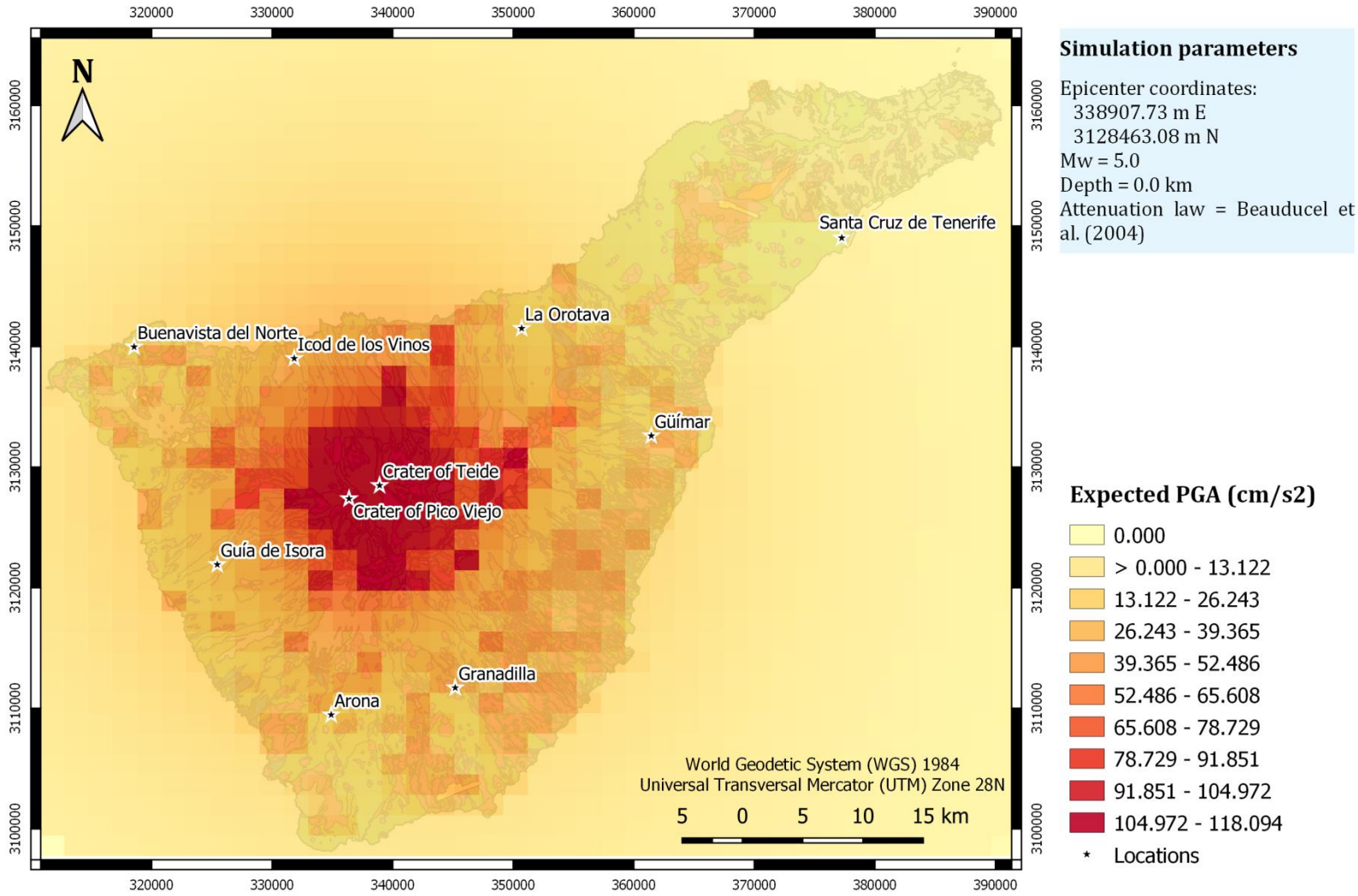

Figure S44. Expected PGA values for a M 5.0 synthetic earthquake located on the crater of Teide, Tenerife (Canary Islands), at a depth of 0.0 km, after applying the Beauducel et al. (2004) attenuation law.

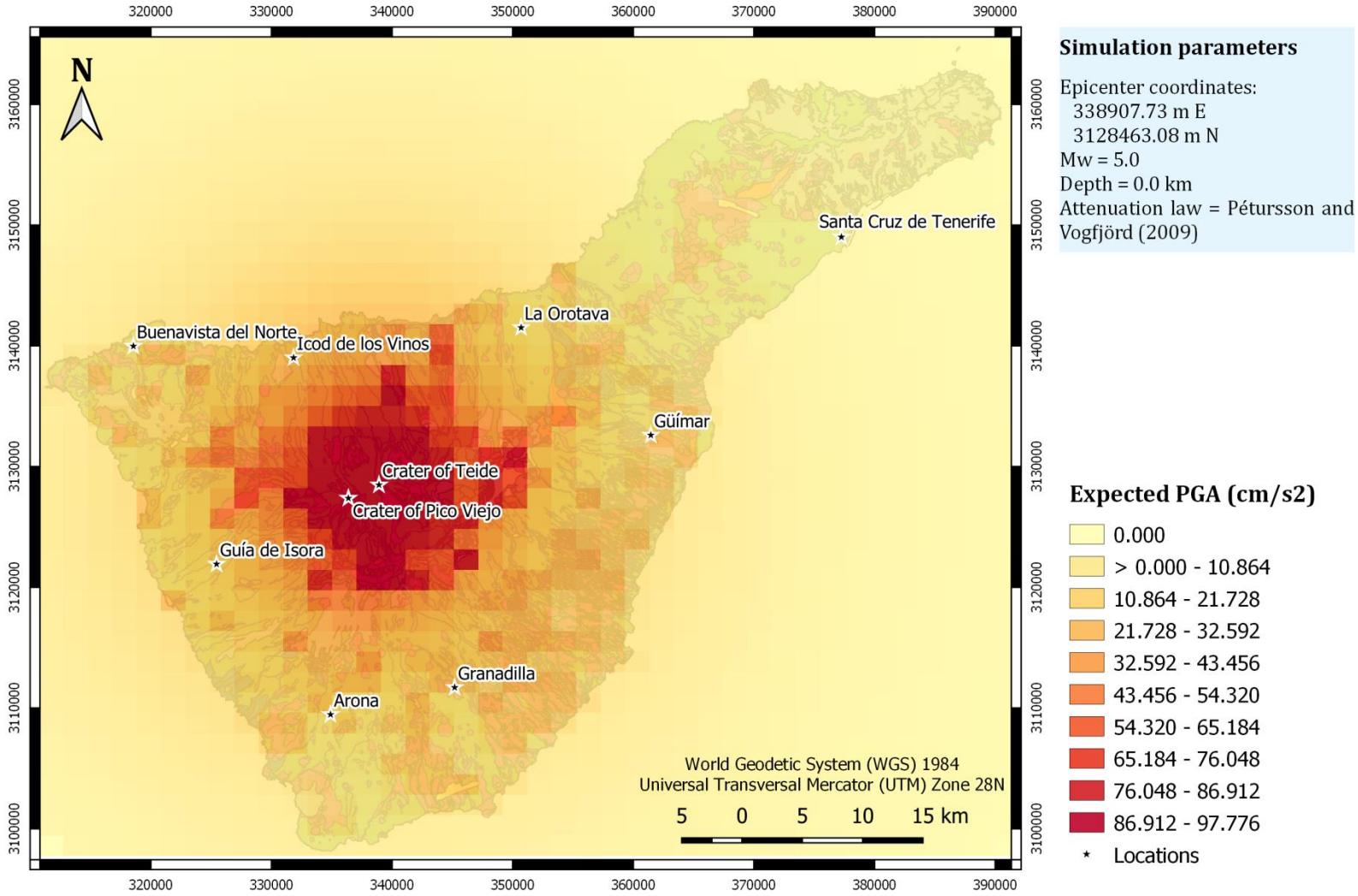

Figure S45. Expected PGA values for a M 5.0 synthetic earthquake located on the crater of Teide, Tenerife (Canary Islands), at a depth of 0.0 km, after applying the Pétursson and Vogfjörd (2009) attenuation law.

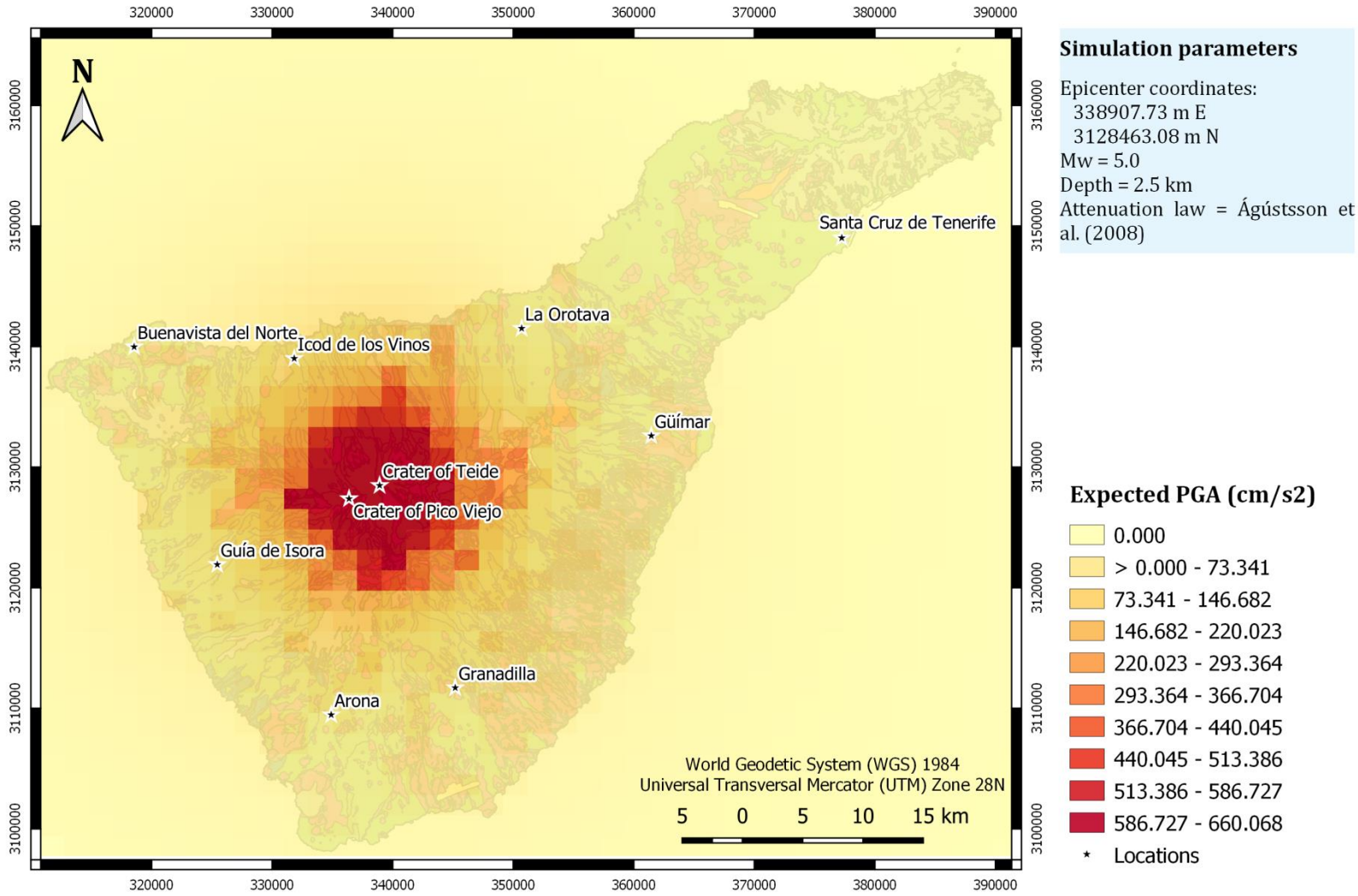

Figure S46. Expected PGA values for a M 5.0 synthetic earthquake located on the crater of Teide, Tenerife (Canary Islands), at a depth of 2.5 km, after applying the Ágústsson et al. (2008) attenuation law.

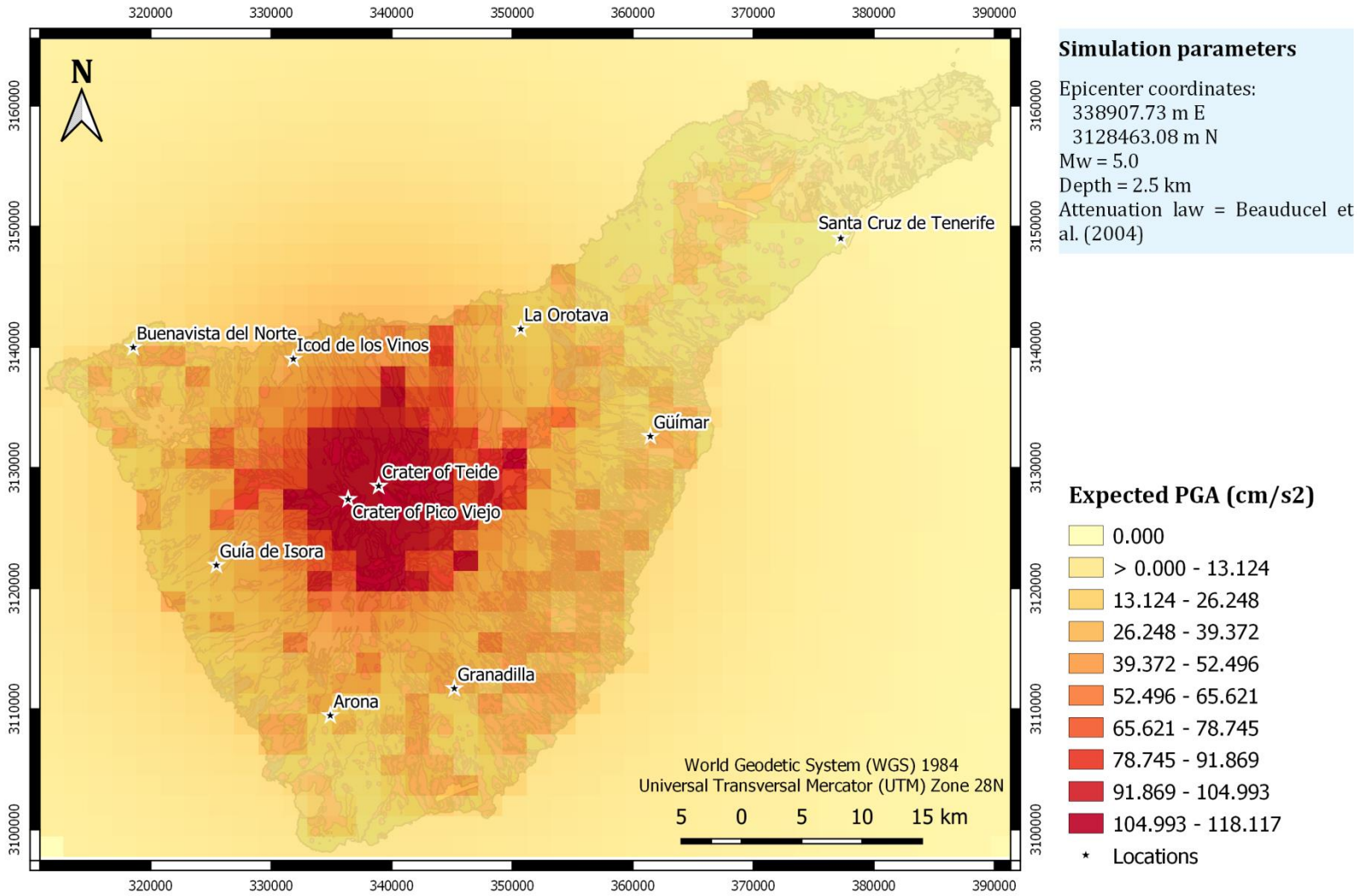

Figure S47. Expected PGA values for a M 5.0 synthetic earthquake located on the crater of Teide, Tenerife (Canary Islands), at a depth of 2.5 km, after applying the Beauducel et al. (2004) attenuation law.

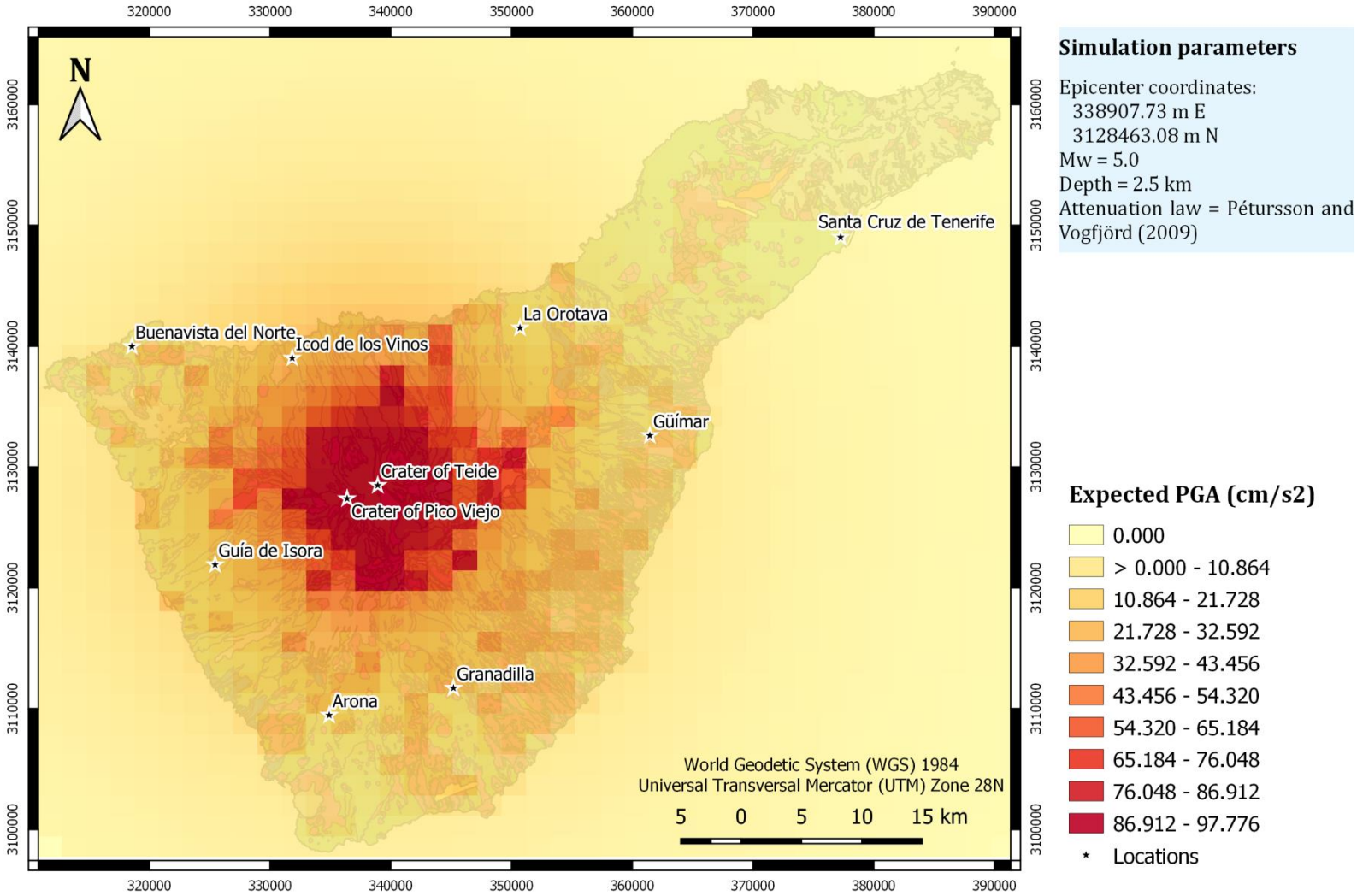

Figure S48. Expected PGA values for a M 5.0 synthetic earthquake located on the crater of Teide, Tenerife (Canary Islands), at a depth of 2.5 km, after applying the Pétursson and Vogfjörd (2009) attenuation law.

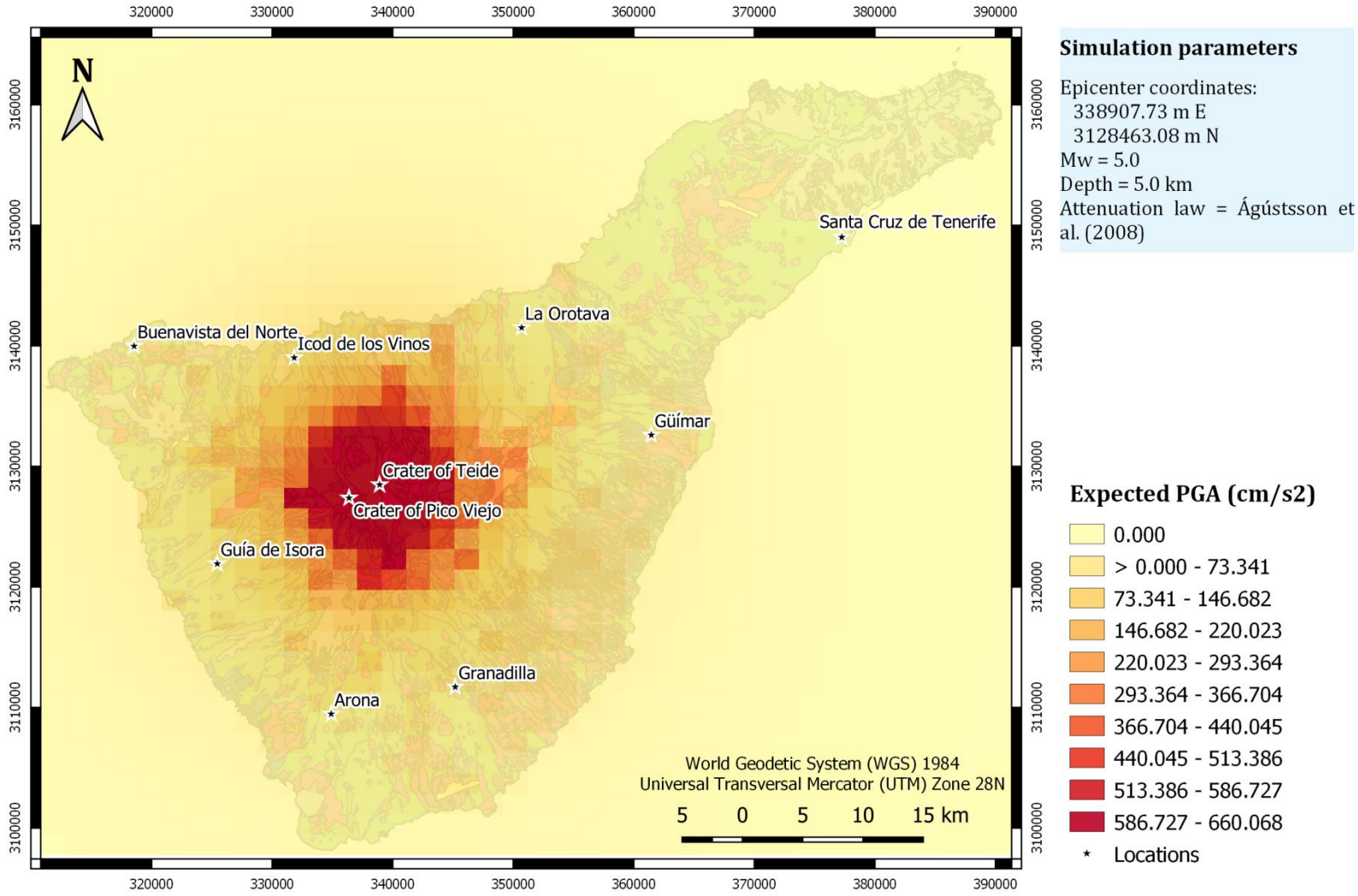

Figure S49. Expected PGA values for a M 5.0 synthetic earthquake located on the crater of Teide, Tenerife (Canary Islands), at a depth of 5.0 km, after applying the Ágústsson et al. (2008) attenuation law.

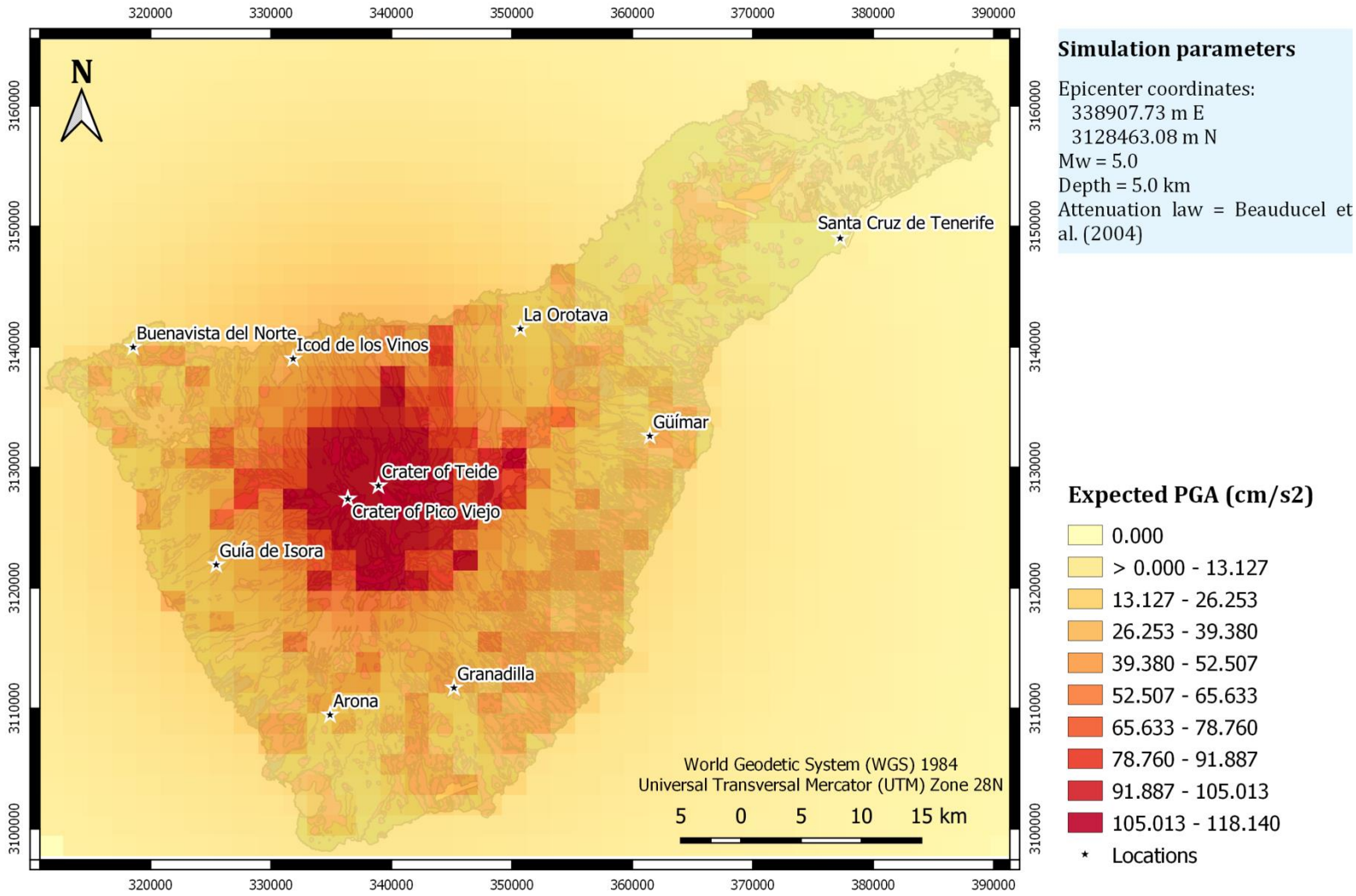

Figure S50. Expected PGA values for a M 5.0 synthetic earthquake located on the crater of Teide, Tenerife (Canary Islands), at a depth of 5.0 km, after applying the Beauducel et al. (2004) attenuation law.

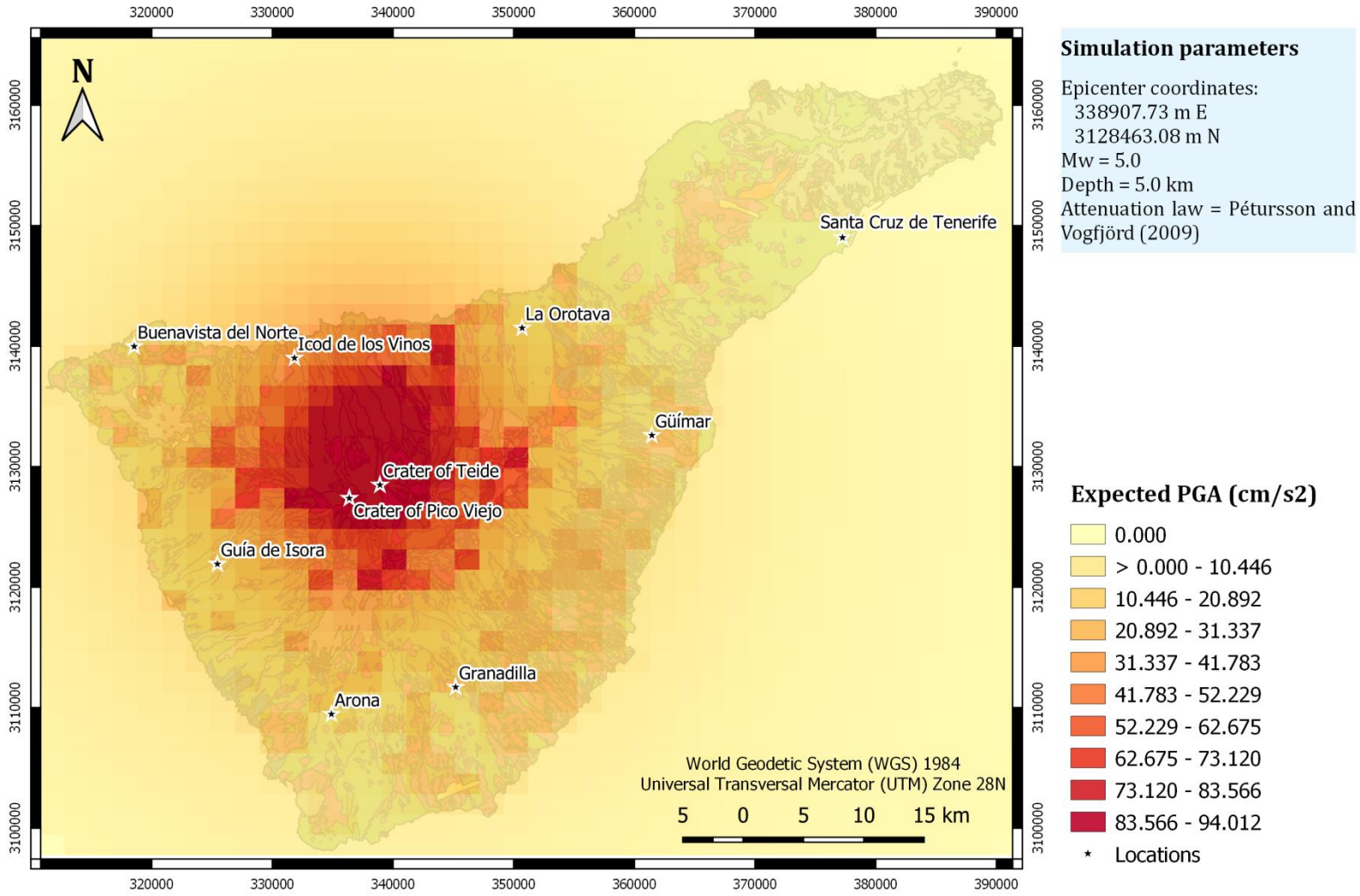

Figure S51. Expected PGA values for a M 5.0 synthetic earthquake located on the crater of Teide, Tenerife (Canary Islands), at a depth of 5.0 km, after applying the Pétursson and Vogfjörd (2009) attenuation law.

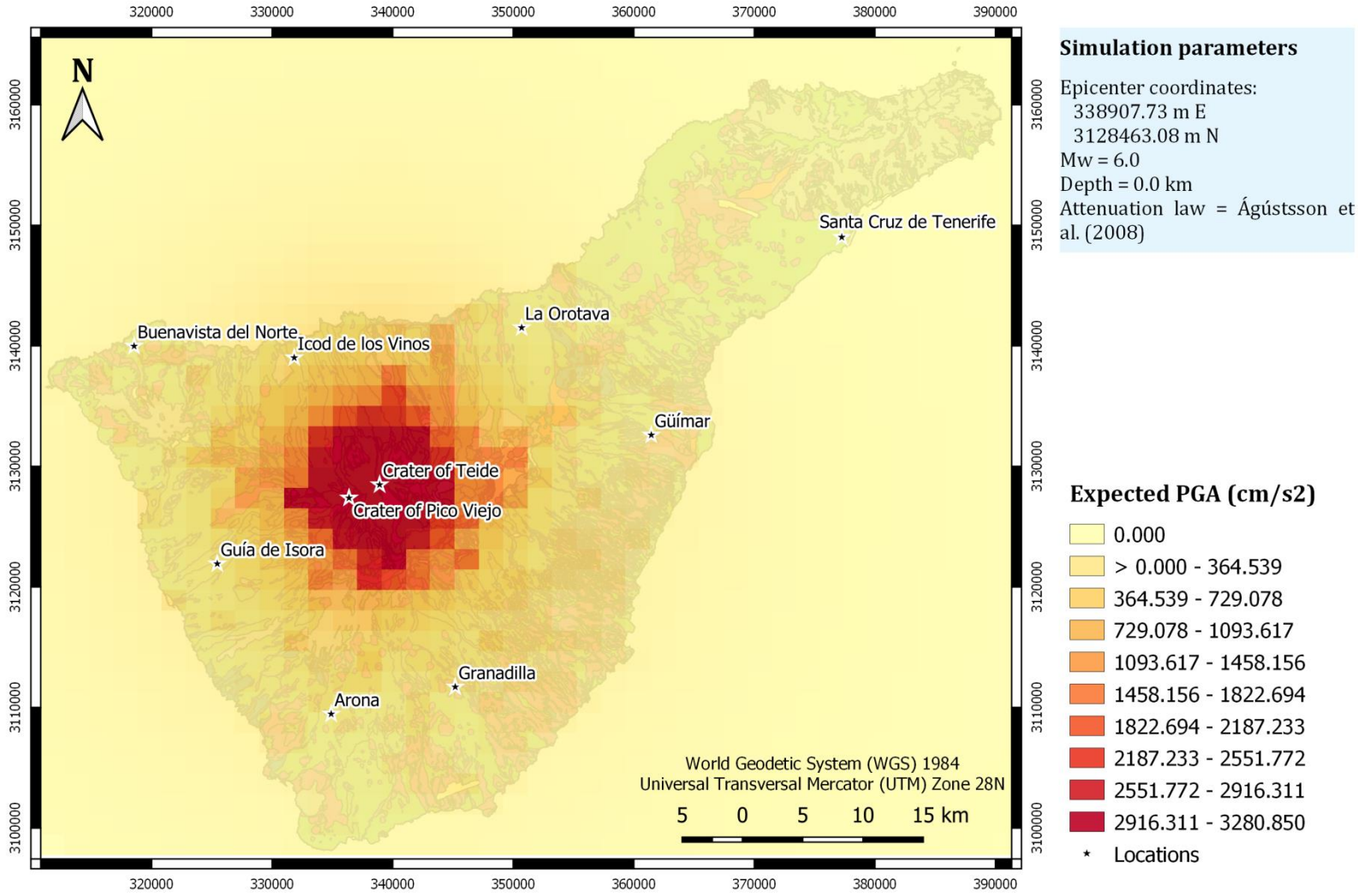

Figure S52. Expected PGA values for a M 6.0 synthetic earthquake located on the crater of Teide, Tenerife (Canary Islands), at a depth of 0.0 km, after applying the Ágústsson et al. (2008) attenuation law.

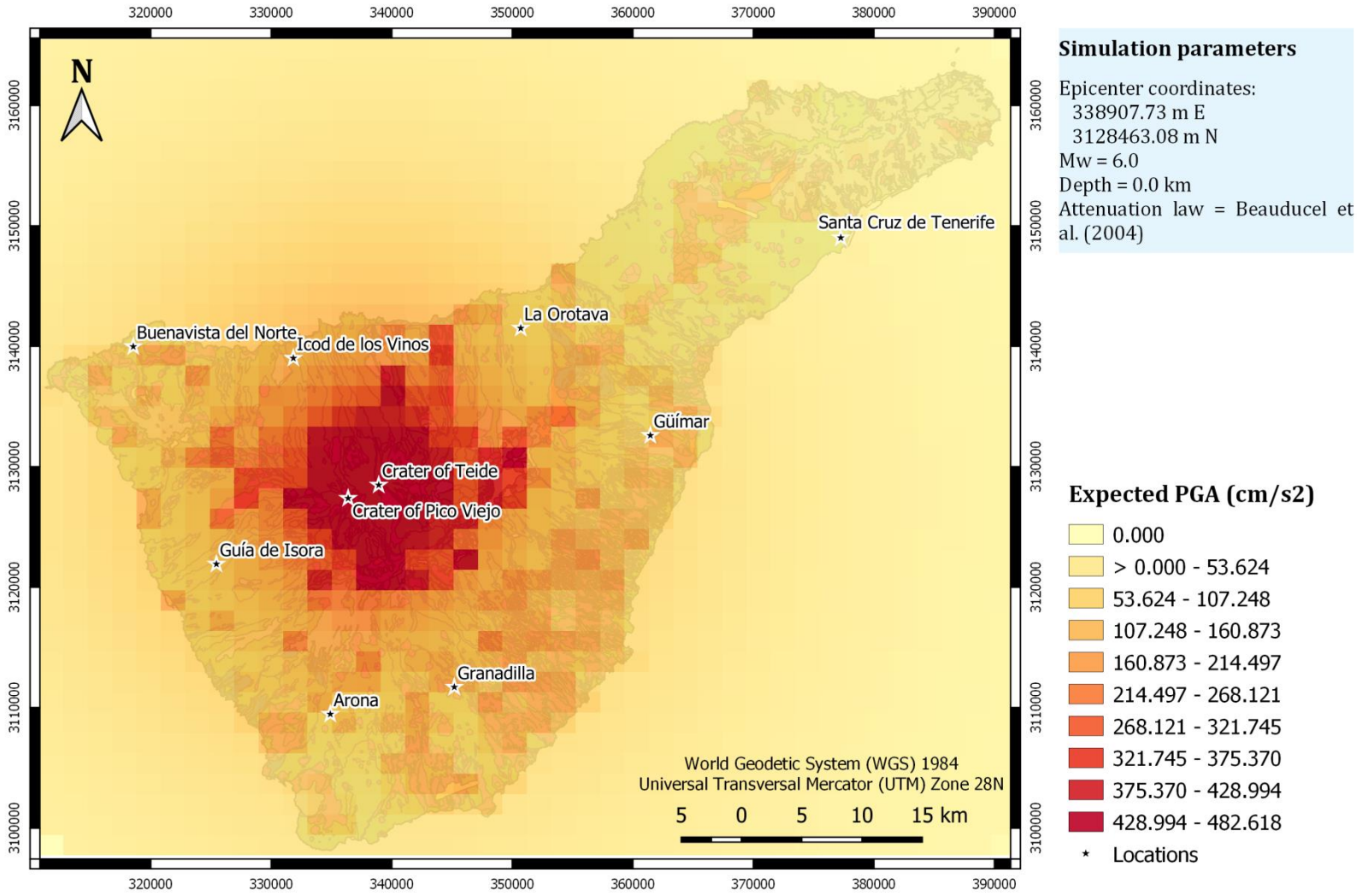

Figure S53. Expected PGA values for a M 6.0 synthetic earthquake located on the crater of Teide, Tenerife (Canary Islands), at a depth of 0.0 km, after applying the Beauducel et al. (2004) attenuation law.

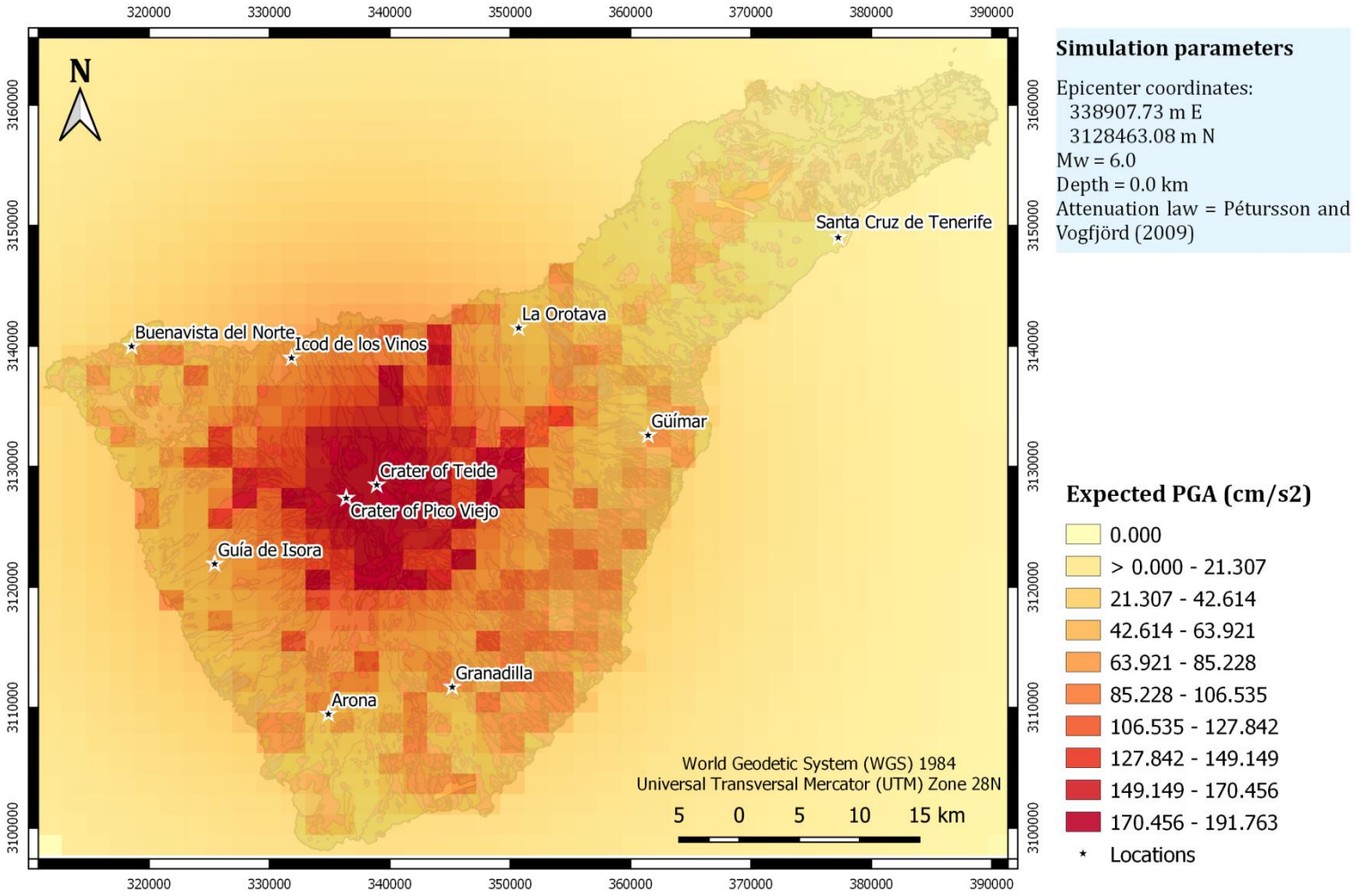

Figure S54. Expected PGA values for a M 6.0 synthetic earthquake located on the crater of Teide, Tenerife (Canary Islands), at a depth of 0.0 km, after applying the Pétursson and Vogfjörd (2009) attenuation law.

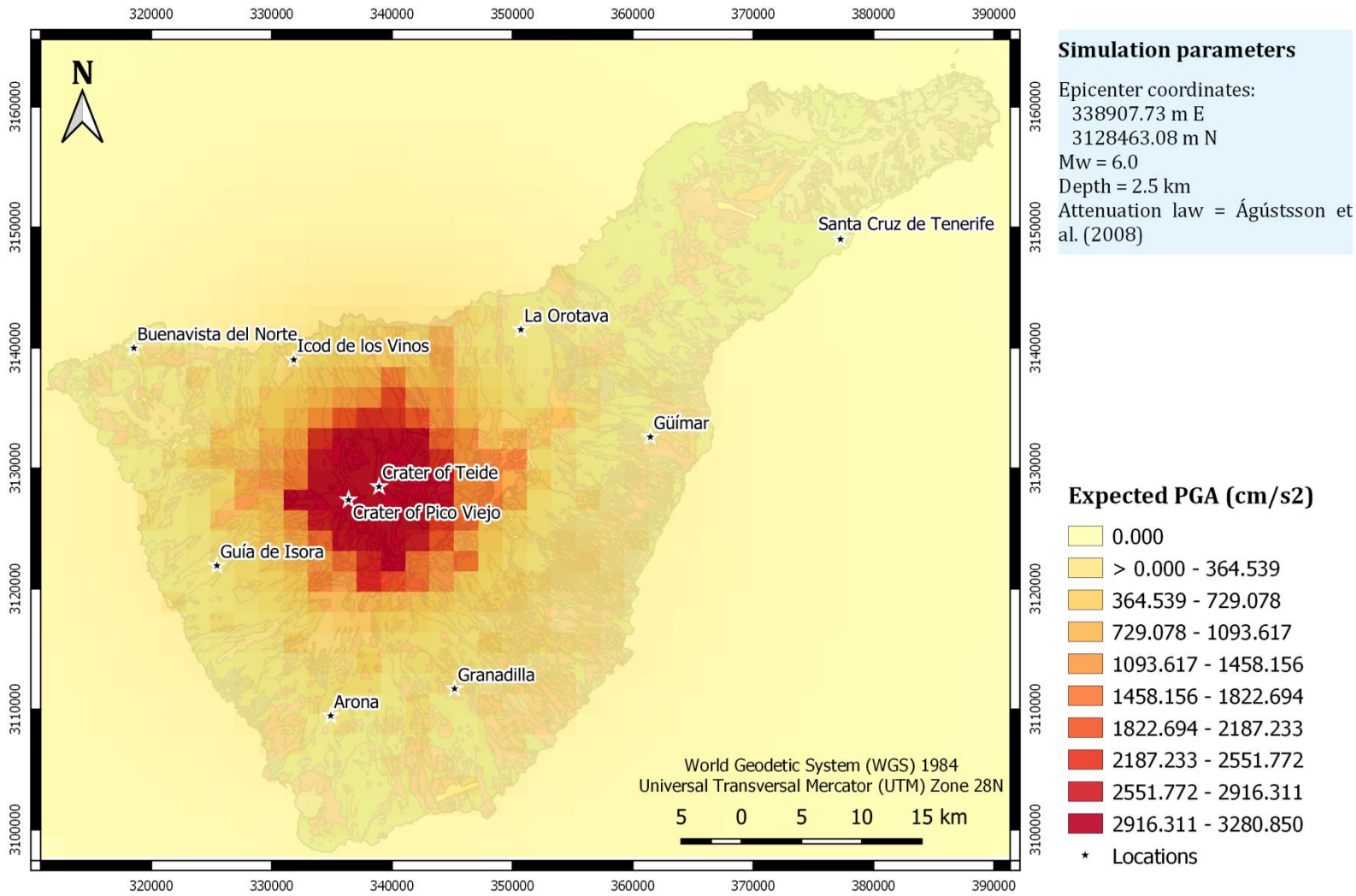

Figure S55. Expected PGA values for a M 6.0 synthetic earthquake located on the crater of Teide, Tenerife (Canary Islands), at a depth of 2.5 km, after applying the Ágústsson et al. (2008) attenuation law.

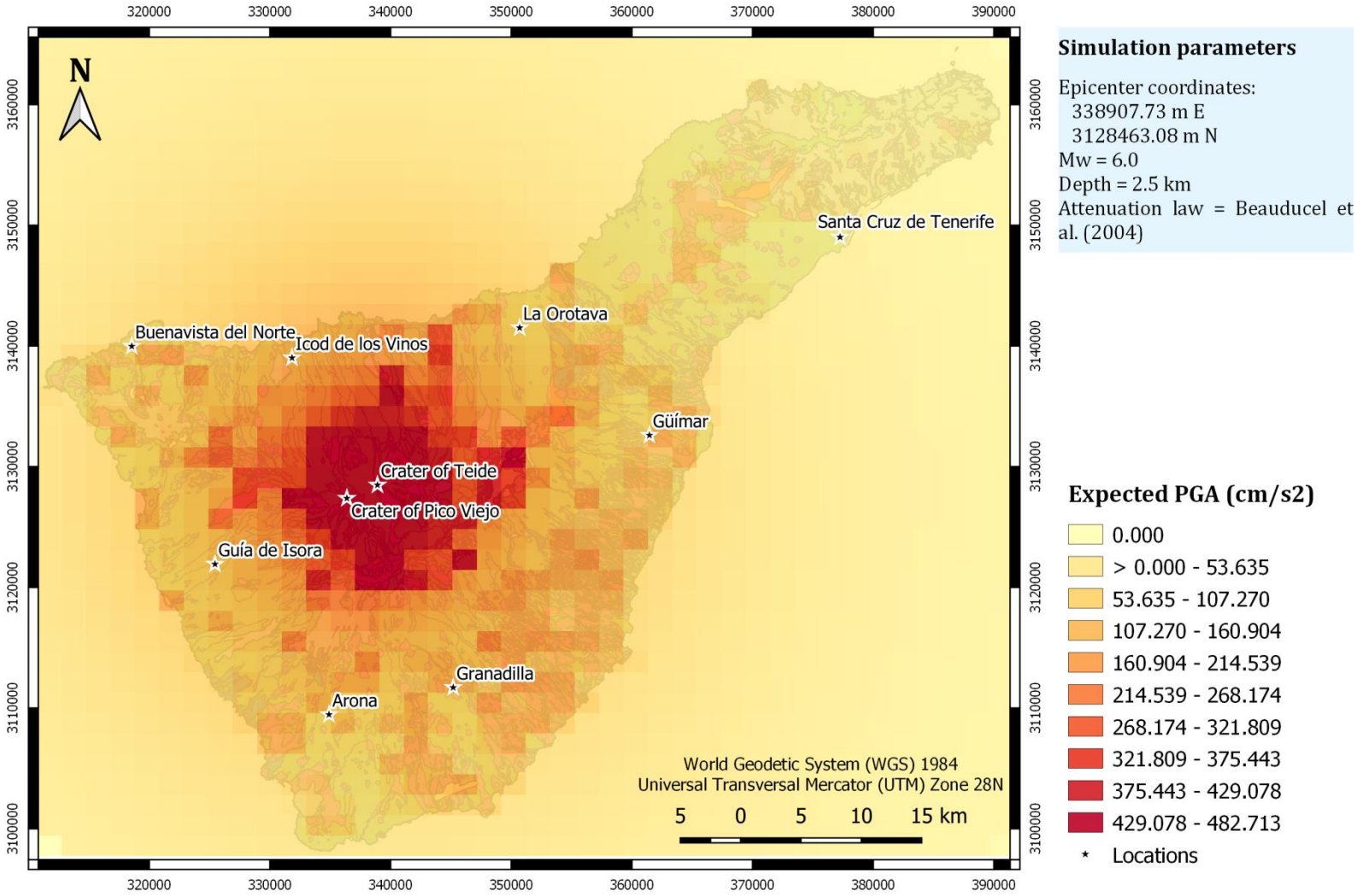

Figure S56. Expected PGA values for a M 6.0 synthetic earthquake located on the crater of Teide, Tenerife (Canary Islands), at a depth of 2.5 km, after applying the Beauducel et al. (2004) attenuation law.

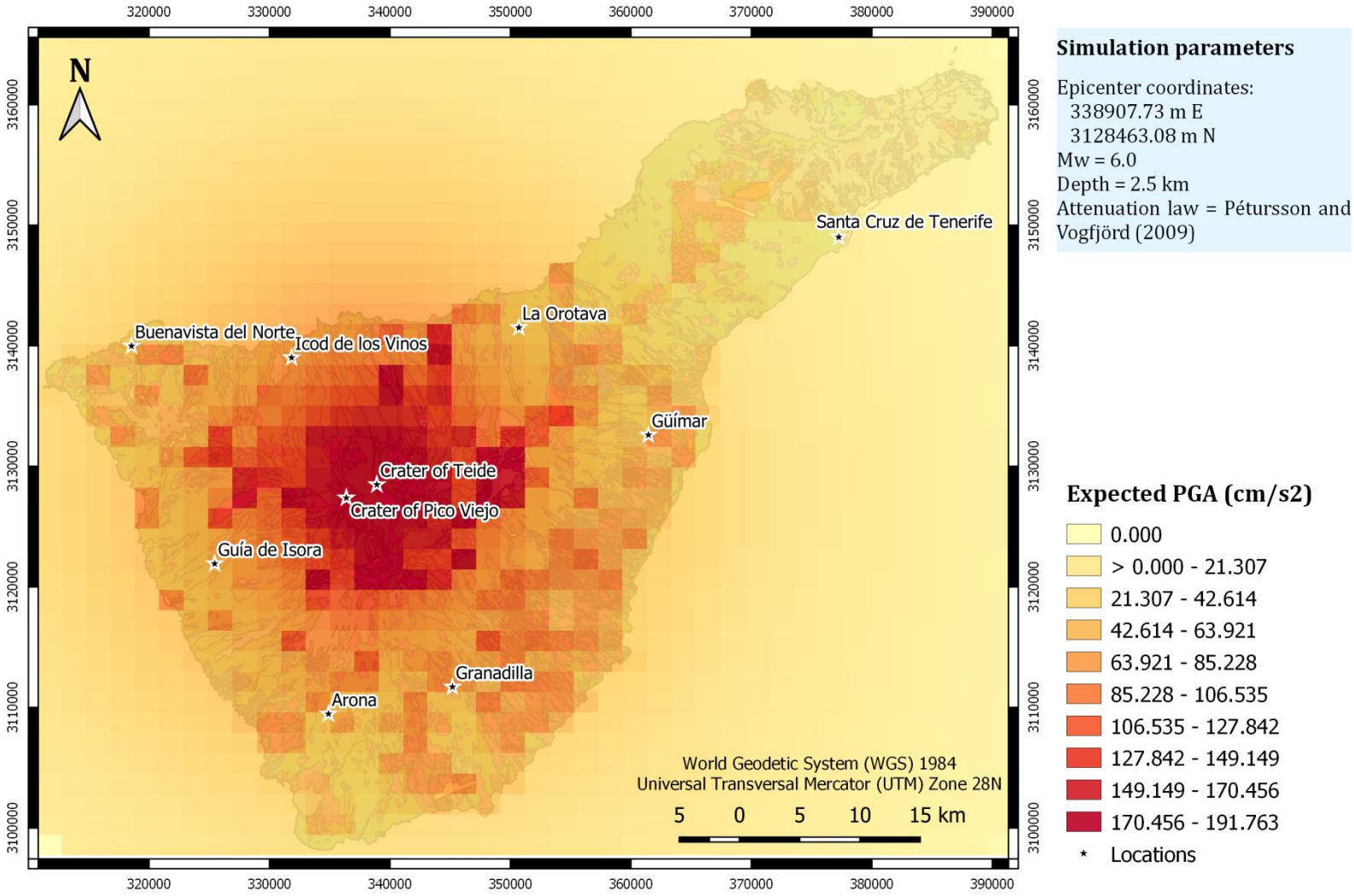

Figure S57. Expected PGA values for a M 6.0 synthetic earthquake located on the crater of Teide, Tenerife (Canary Islands), at a depth of 2.5 km, after applying the Pétursson and Vogfjörd (2009) attenuation law.

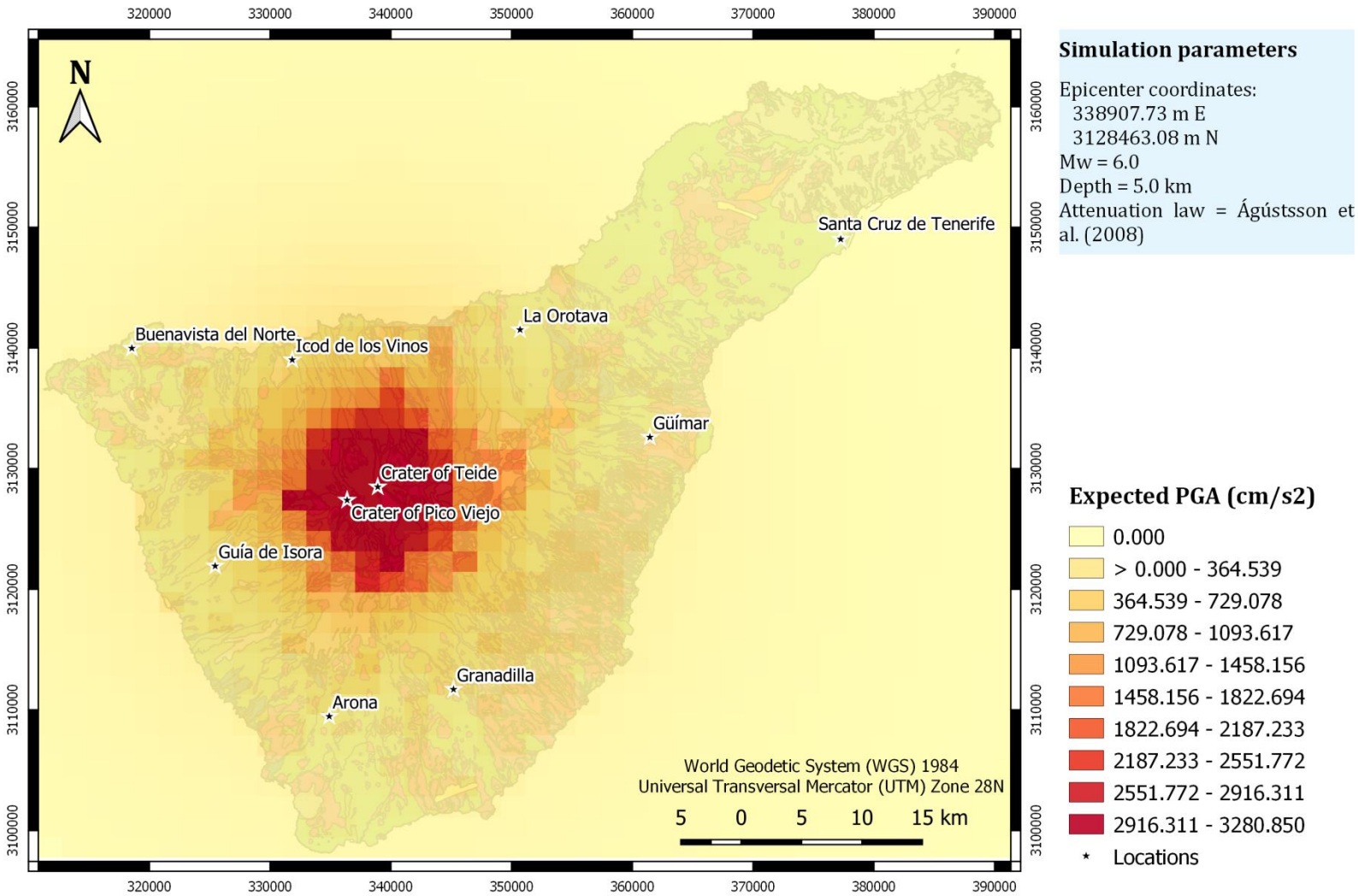

Figure S58. Expected PGA values for a M 6.0 synthetic earthquake located on the crater of Teide, Tenerife (Canary Islands), at a depth of 5.0 km, after applying the Ágústsson et al. (2008) attenuation law.

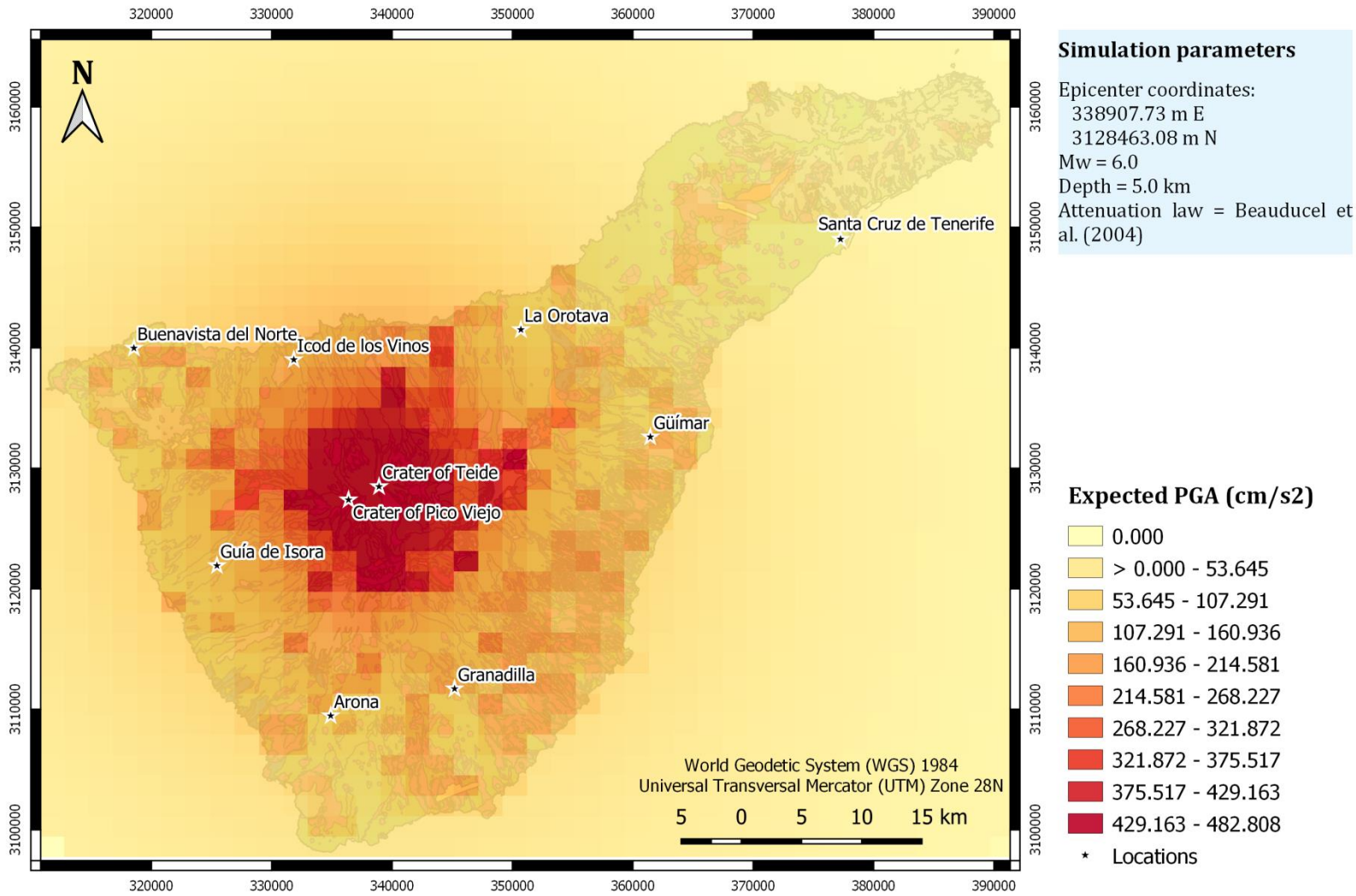

Figure S59. Expected PGA values for a M 6.0 synthetic earthquake located on the crater of Teide, Tenerife (Canary Islands), at a depth of 5.0 km, after applying the Beauducel et al. (2004) attenuation law.

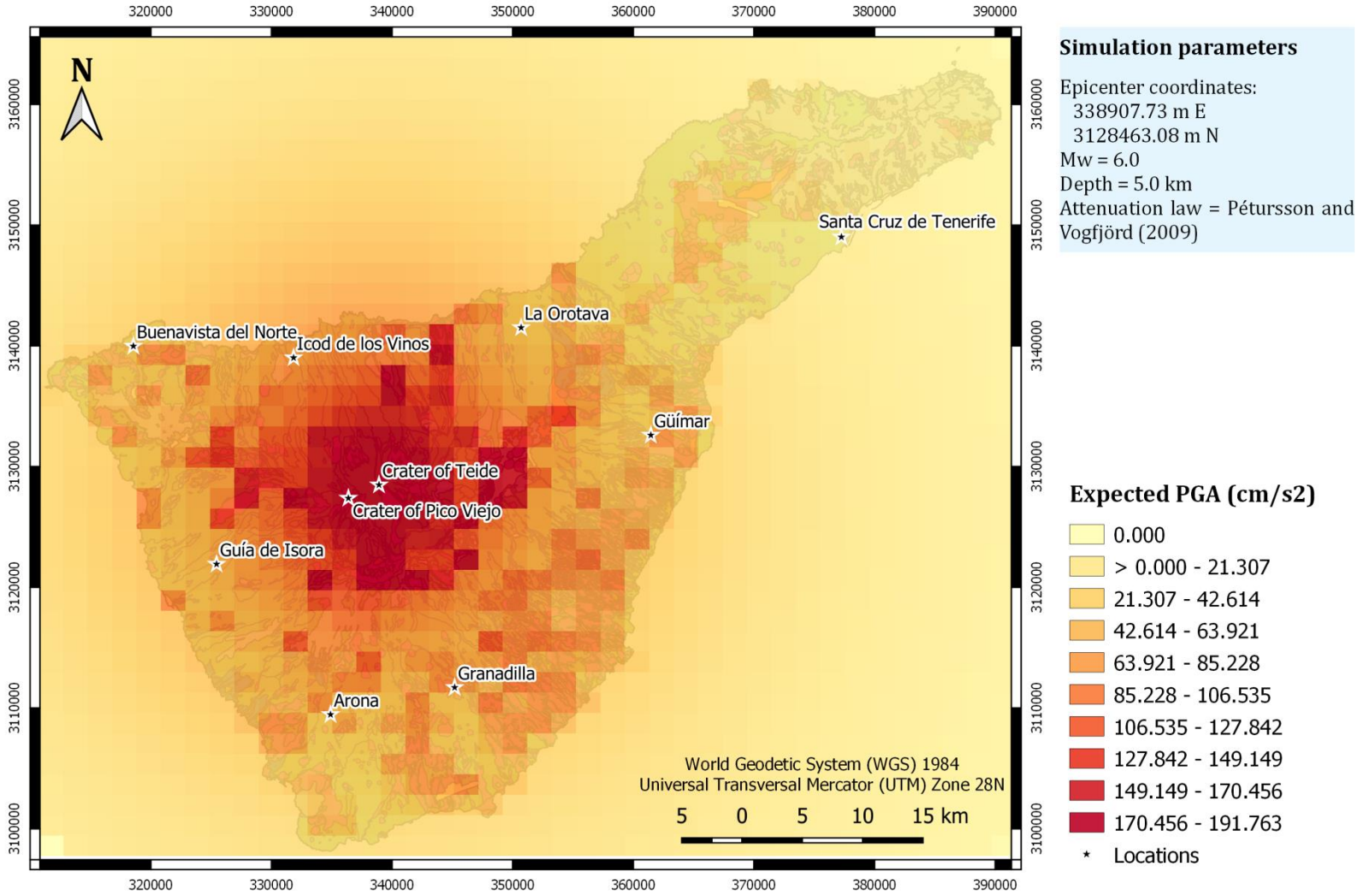

Figure S6o. Expected PGA values for a M 6.0 synthetic earthquake located on the crater of Teide, Tenerife (Canary Islands), at a depth of 5.0 km, after applying the Pétursson and Vogfjörd (2009) attenuation law.

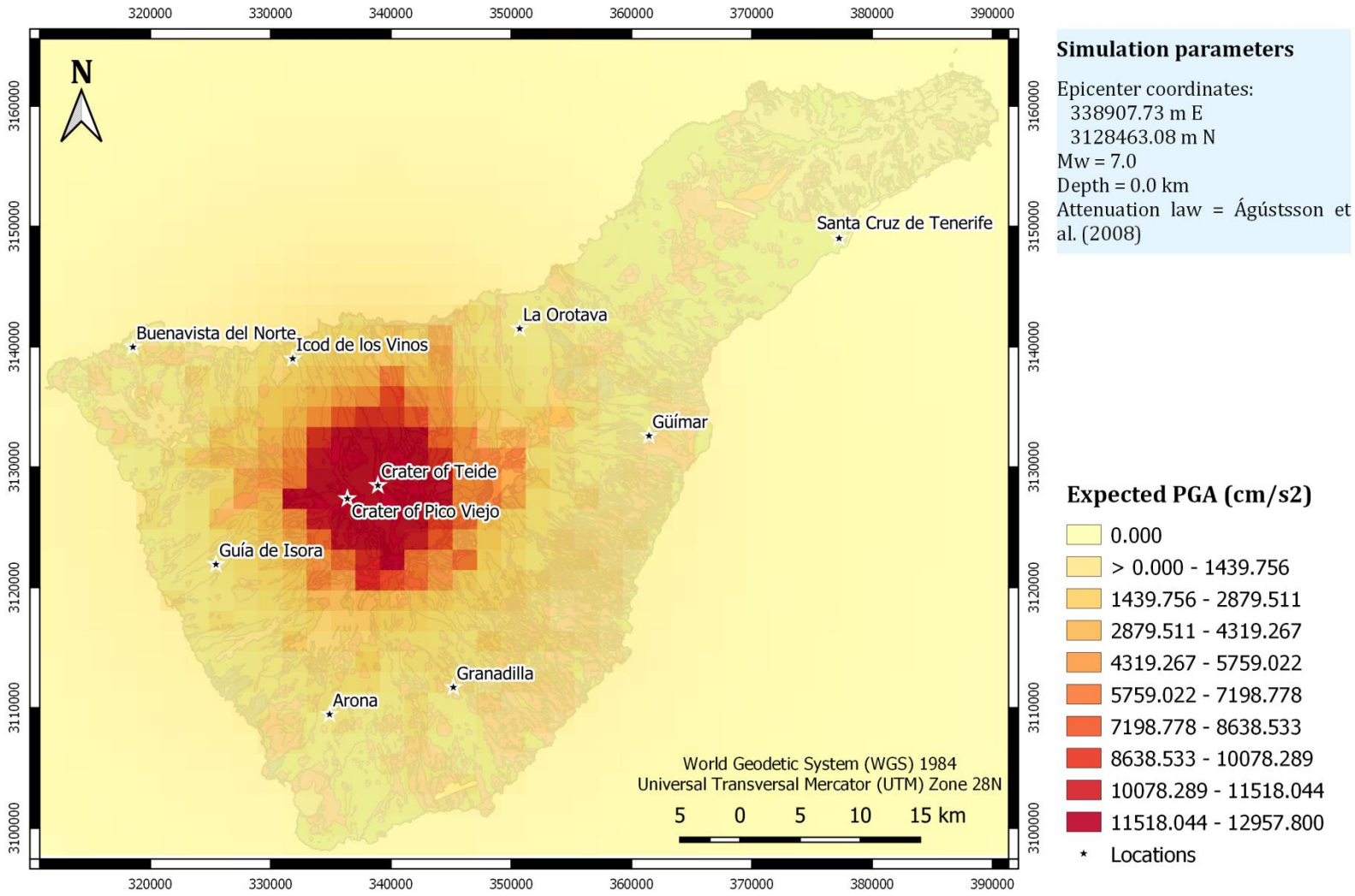

Figure S61. Expected PGA values for a M 7.0 synthetic earthquake located on the crater of Teide, Tenerife (Canary Islands), at a depth of 0.0 km, after applying the Ágústsson et al. (2008) attenuation law.

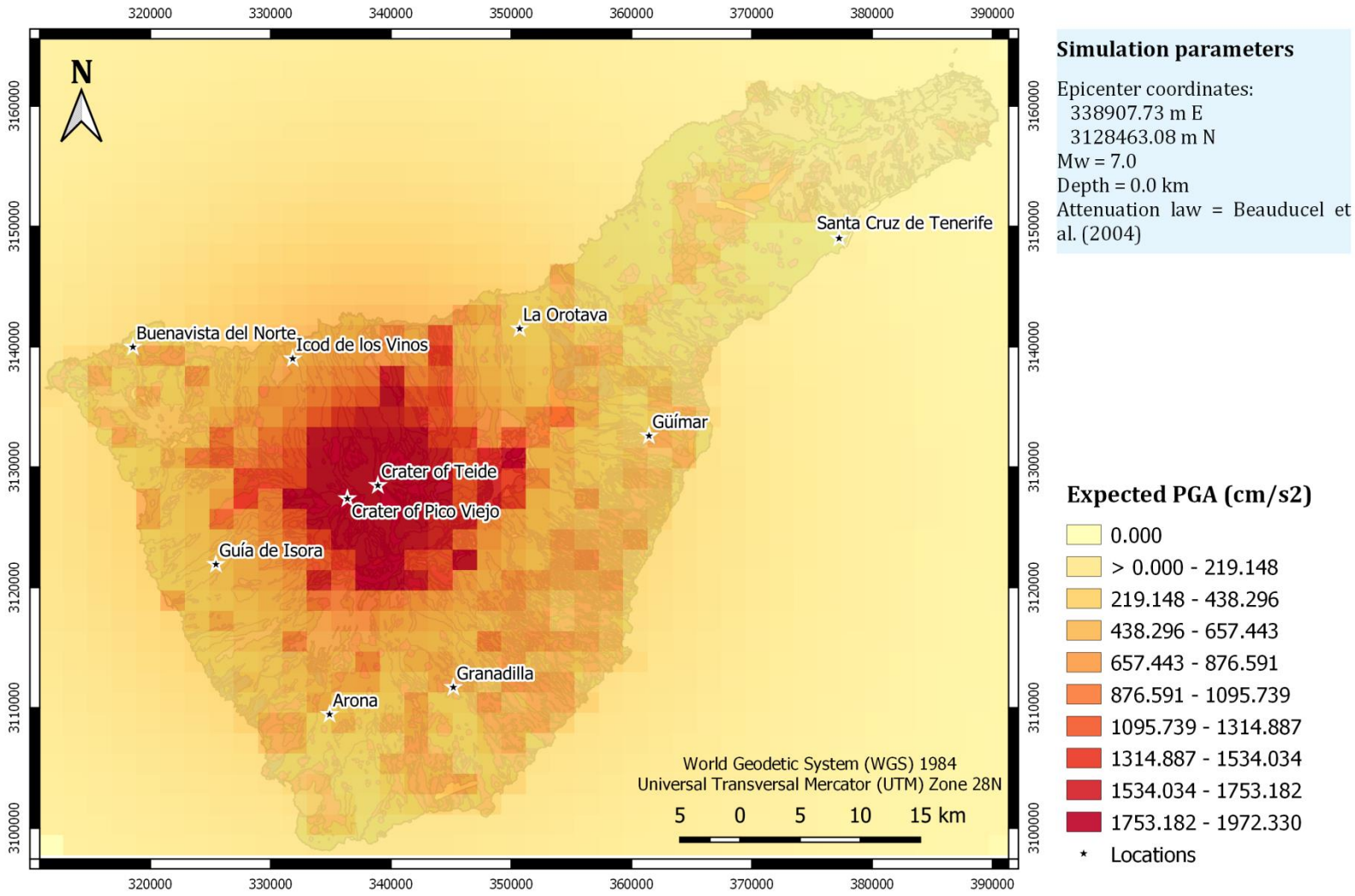

Figure S62. Expected PGA values for a M 7.0 synthetic earthquake located on the crater of Teide, Tenerife (Canary Islands), at a depth of 0.0 km, after applying the Beauducel et al. (2004) attenuation law.

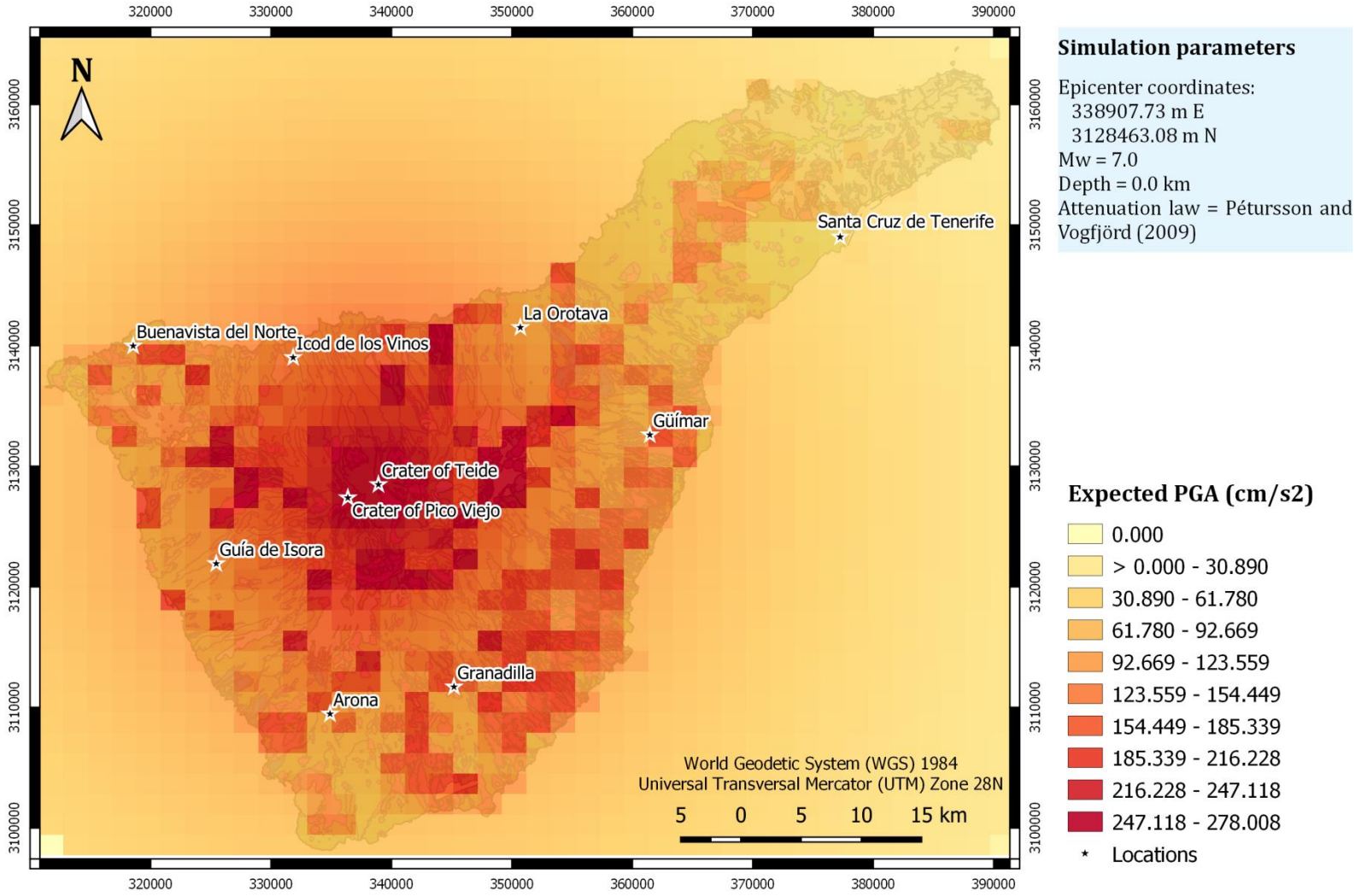

Figure S63. Expected PGA values for a M 7.0 synthetic earthquake located on the crater of Teide, Tenerife (Canary Islands), at a depth of 0.0 km, after applying the Pétursson and Vogfjörd (2009) attenuation law.

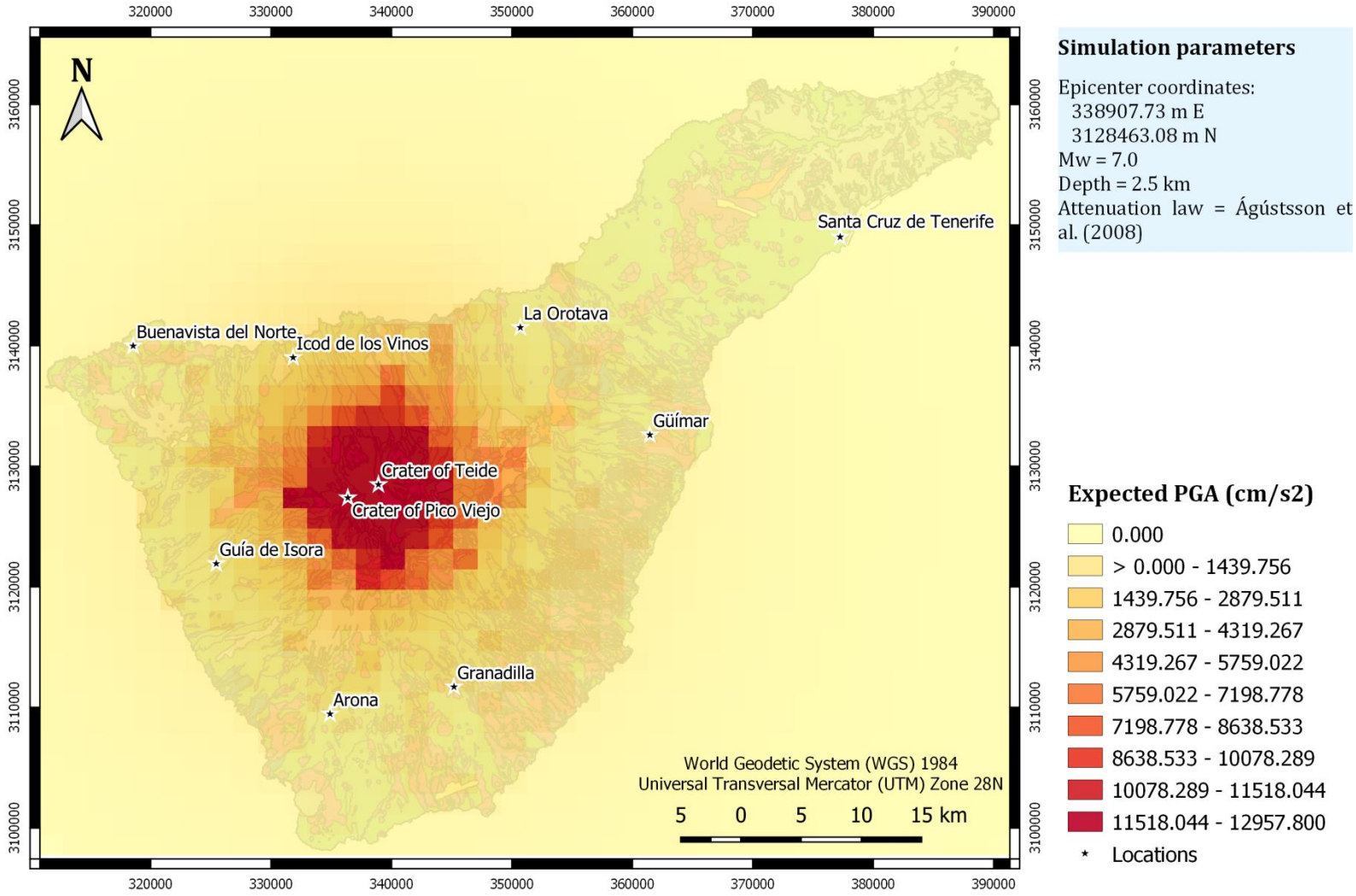

Figure S64. Expected PGA values for a M 7.0 synthetic earthquake located on the crater of Teide, Tenerife (Canary Islands), at a depth of 2.5 km, after applying the Ágústsson et al. (2008) attenuation law.

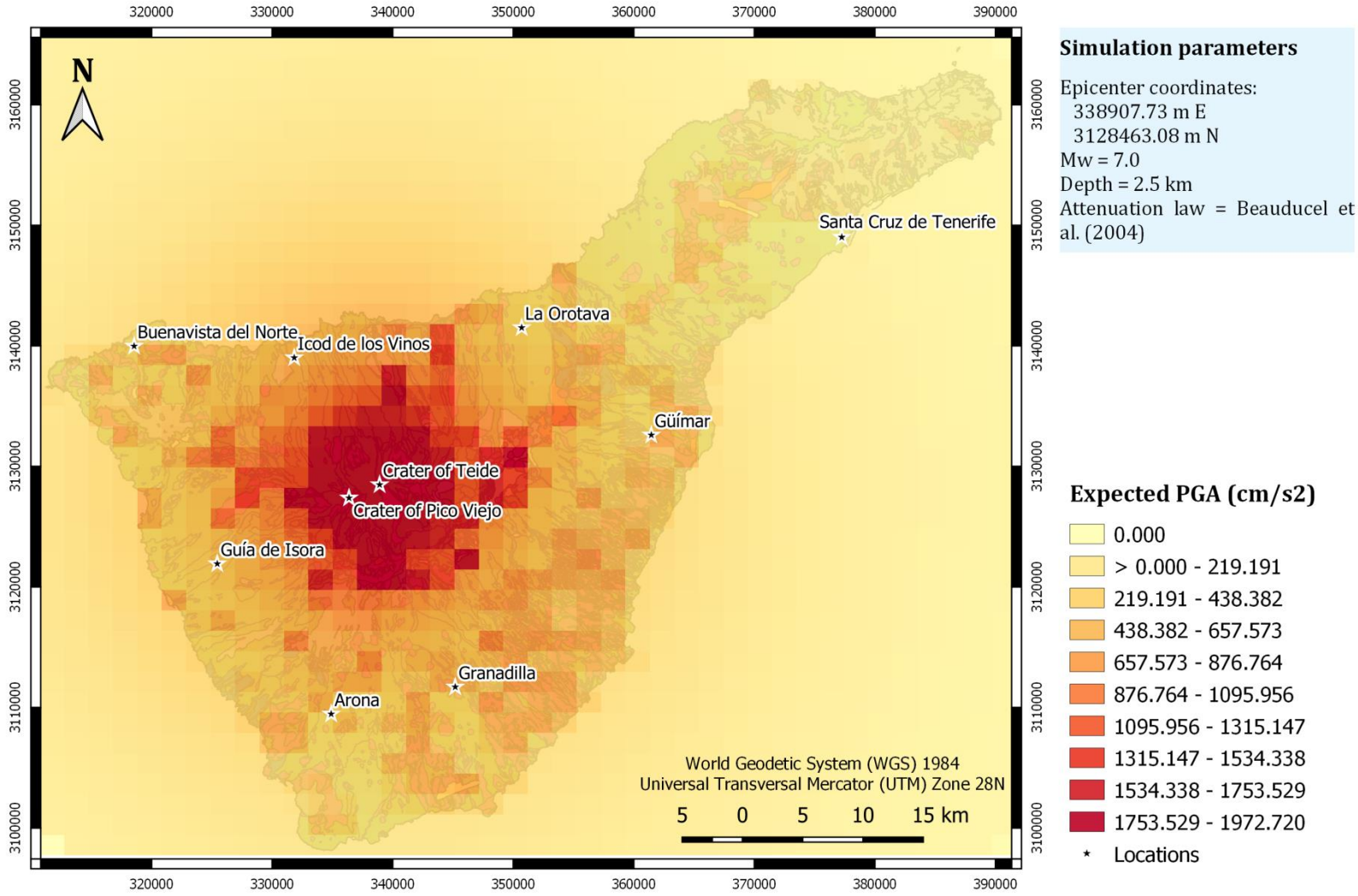

Figure S65. Expected PGA values for a M 7.0 synthetic earthquake located on the crater of Teide, Tenerife (Canary Islands), at a depth of 2.5 km, after applying the Beauducel et al. (2004) attenuation law.

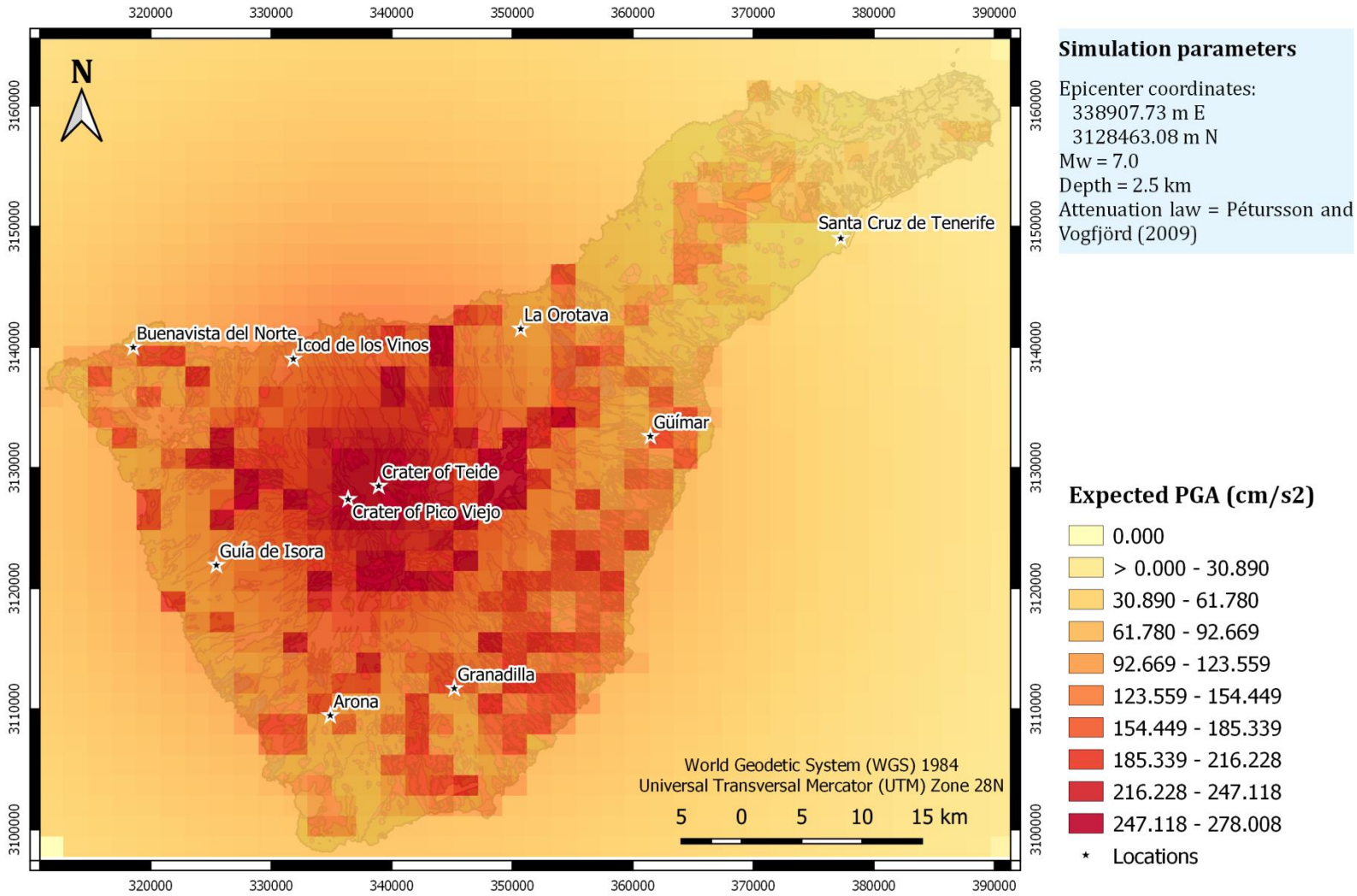

Figure S66. Expected PGA values for a M 7.0 synthetic earthquake located on the crater of Teide, Tenerife (Canary Islands), at a depth of 2.5 km, after applying the Pétursson and Vogfjörd (2009) attenuation law.

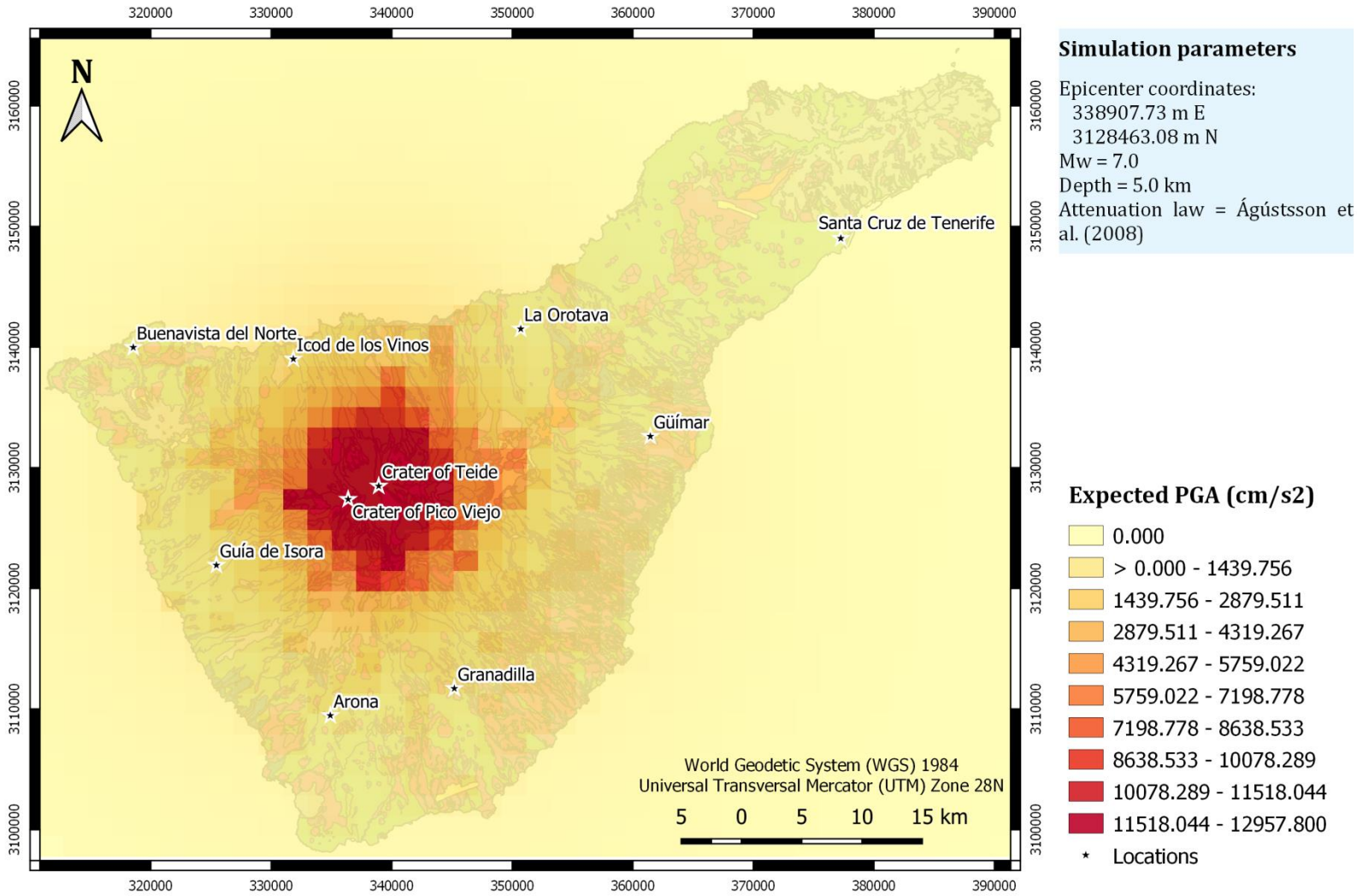

Figure S67. Expected PGA values for a M 7.0 synthetic earthquake located on the crater of Teide, Tenerife (Canary Islands), at a depth of 5.0 km, after applying the Ágústsson et al. (2008) attenuation law.

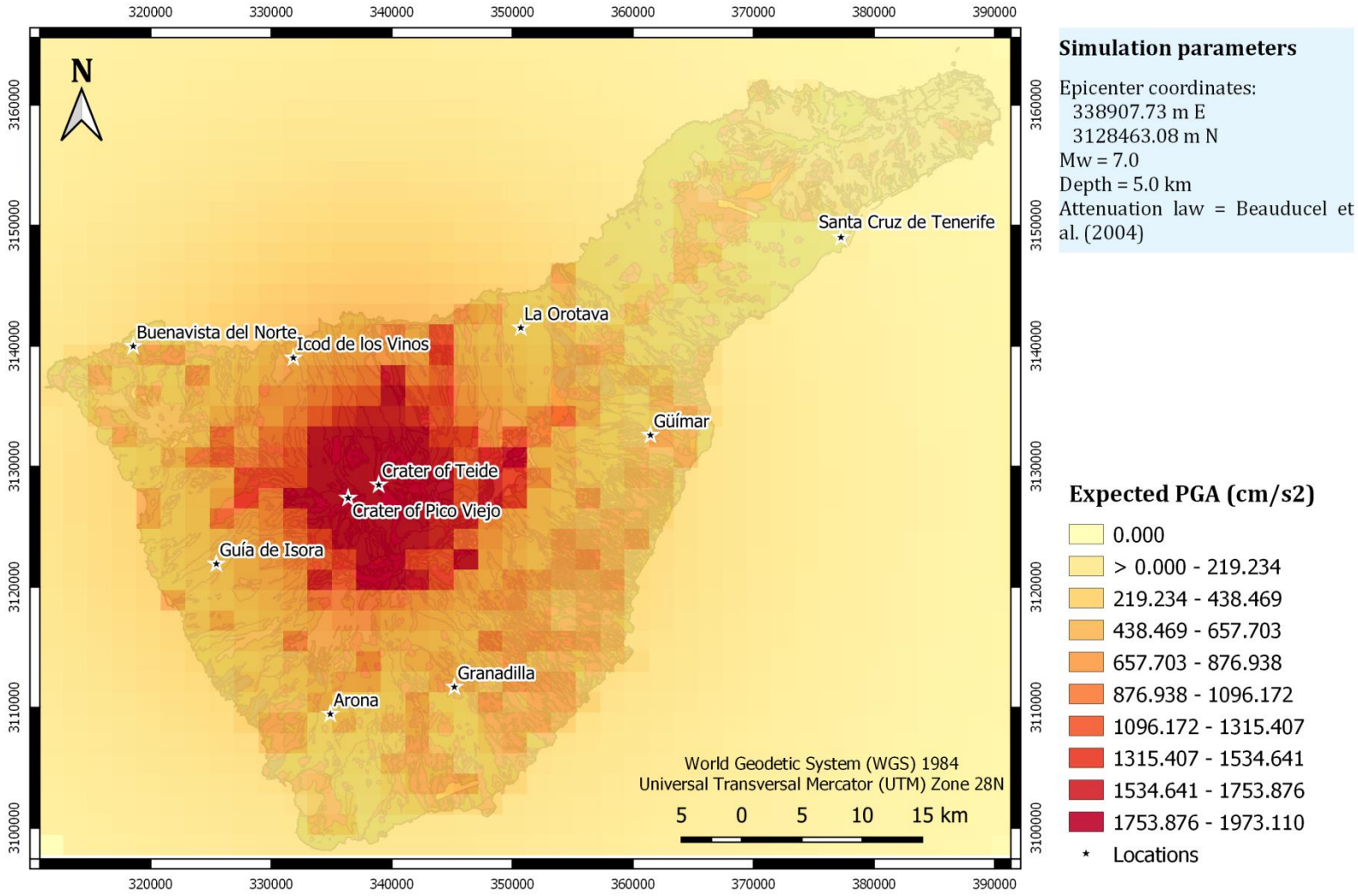

Figure S68. Expected PGA values for a M 7.0 synthetic earthquake located on the crater of Teide, Tenerife (Canary Islands), at a depth of 5.0 km, after applying the Beauducel et al. (2004) attenuation law.

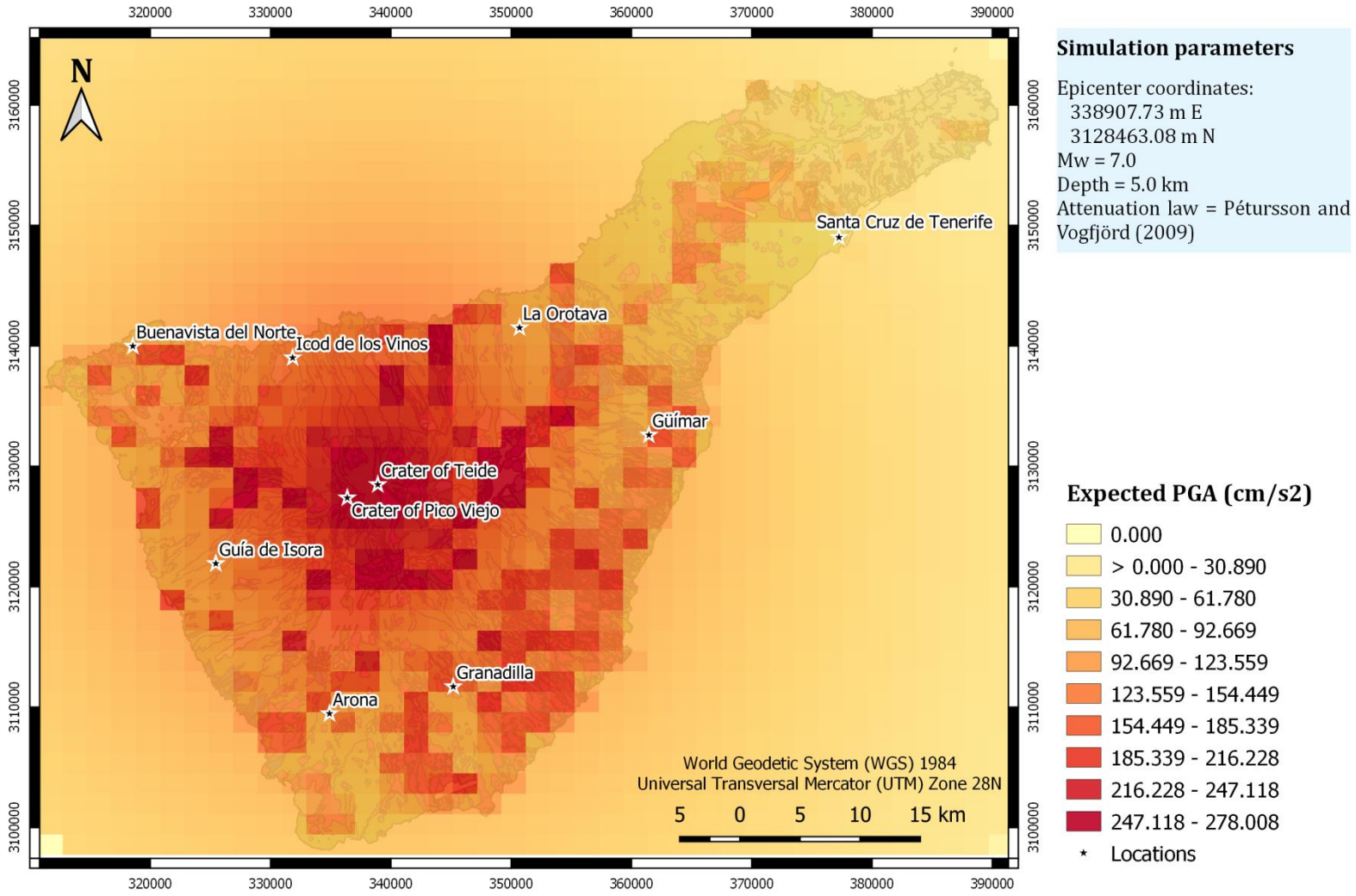

Figure S69. Expected PGA values for a M 7.0 synthetic earthquake located on the crater of Teide, Tenerife (Canary Islands), at a depth of 5.0 km, after applying the Pétursson and Vogfjörd (2009) attenuation law.

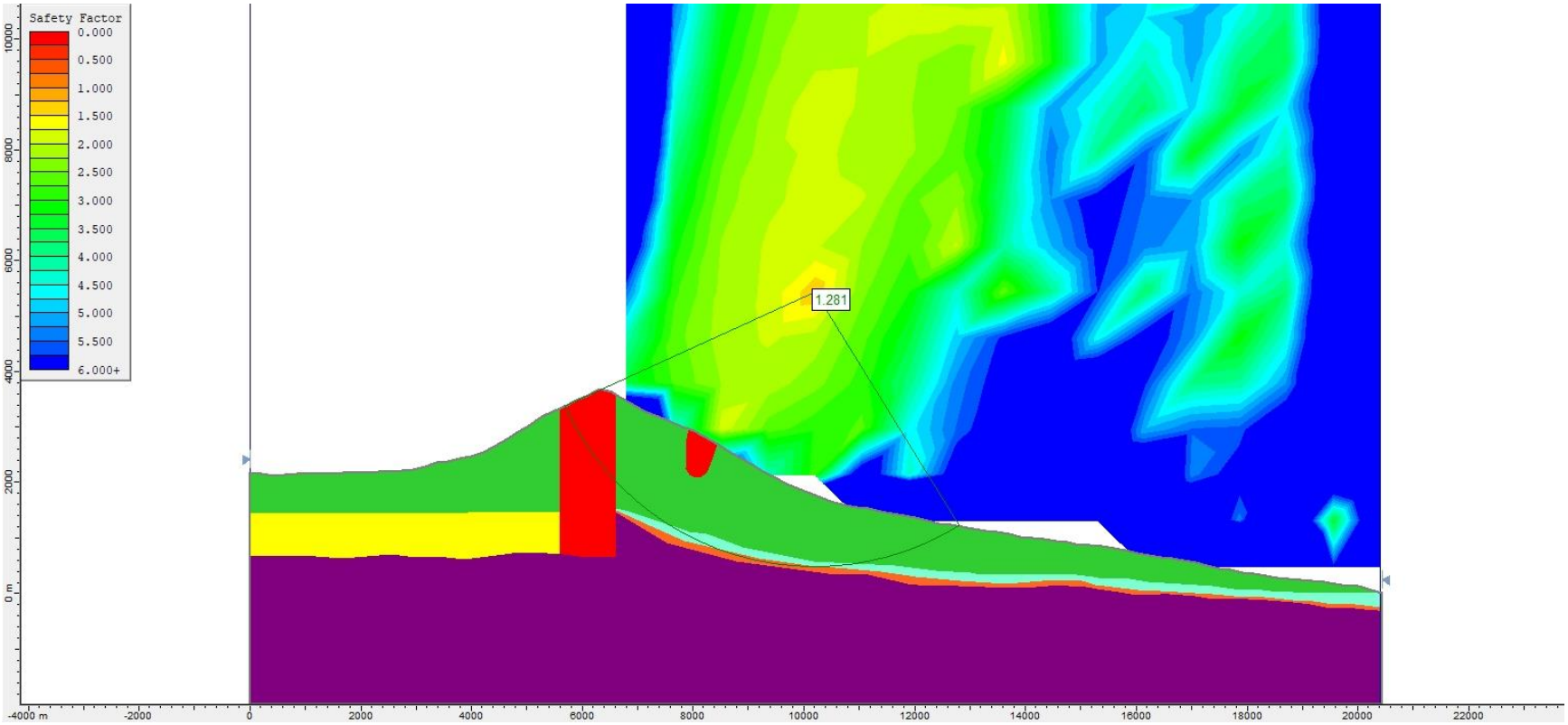

Figure S70. Slope stability static analysis for Model 1 (with alteration zones, Figure 4a), using the Bishop simplified method.

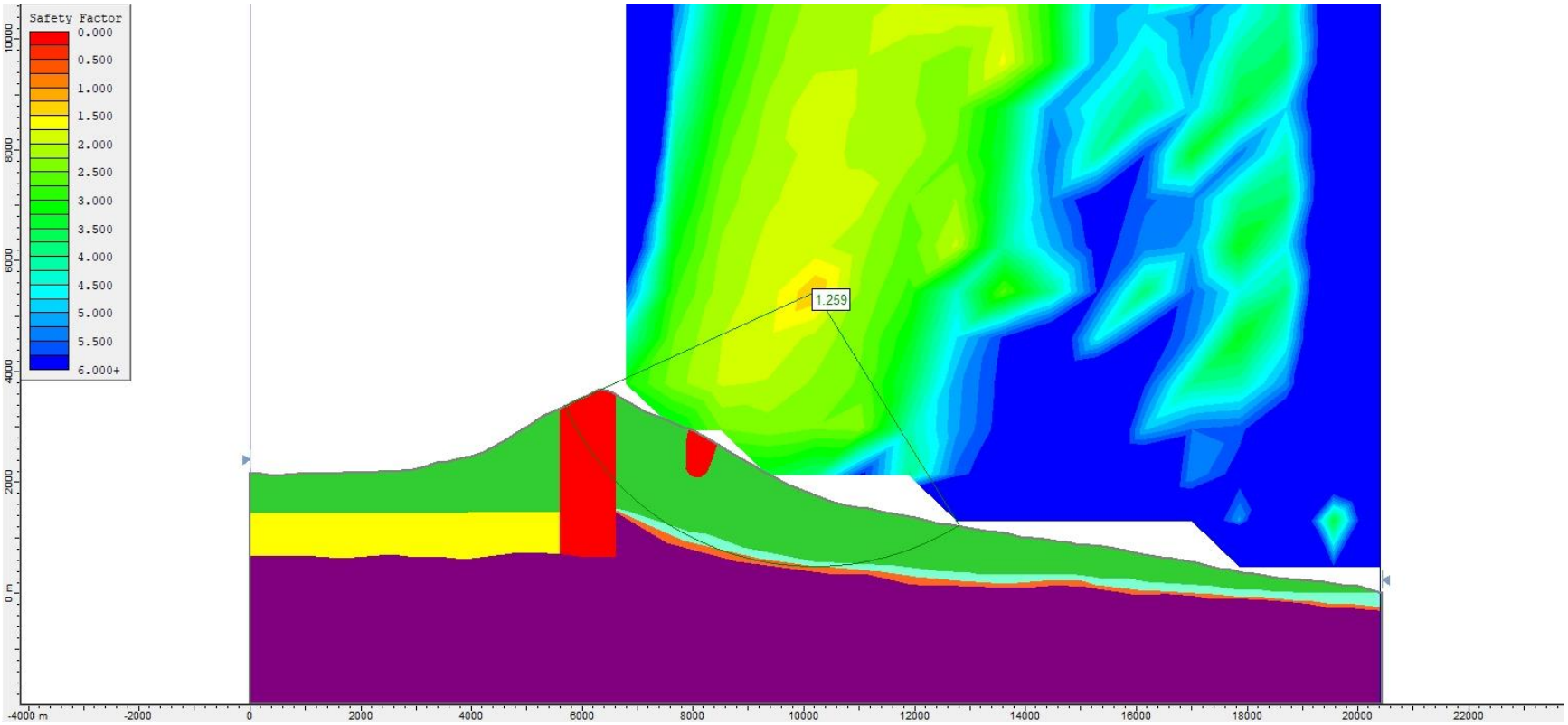

Figure S71. Slope stability static analysis for Model 1 (with alteration zones, Figure 4a), using the Janbu Generalised method.

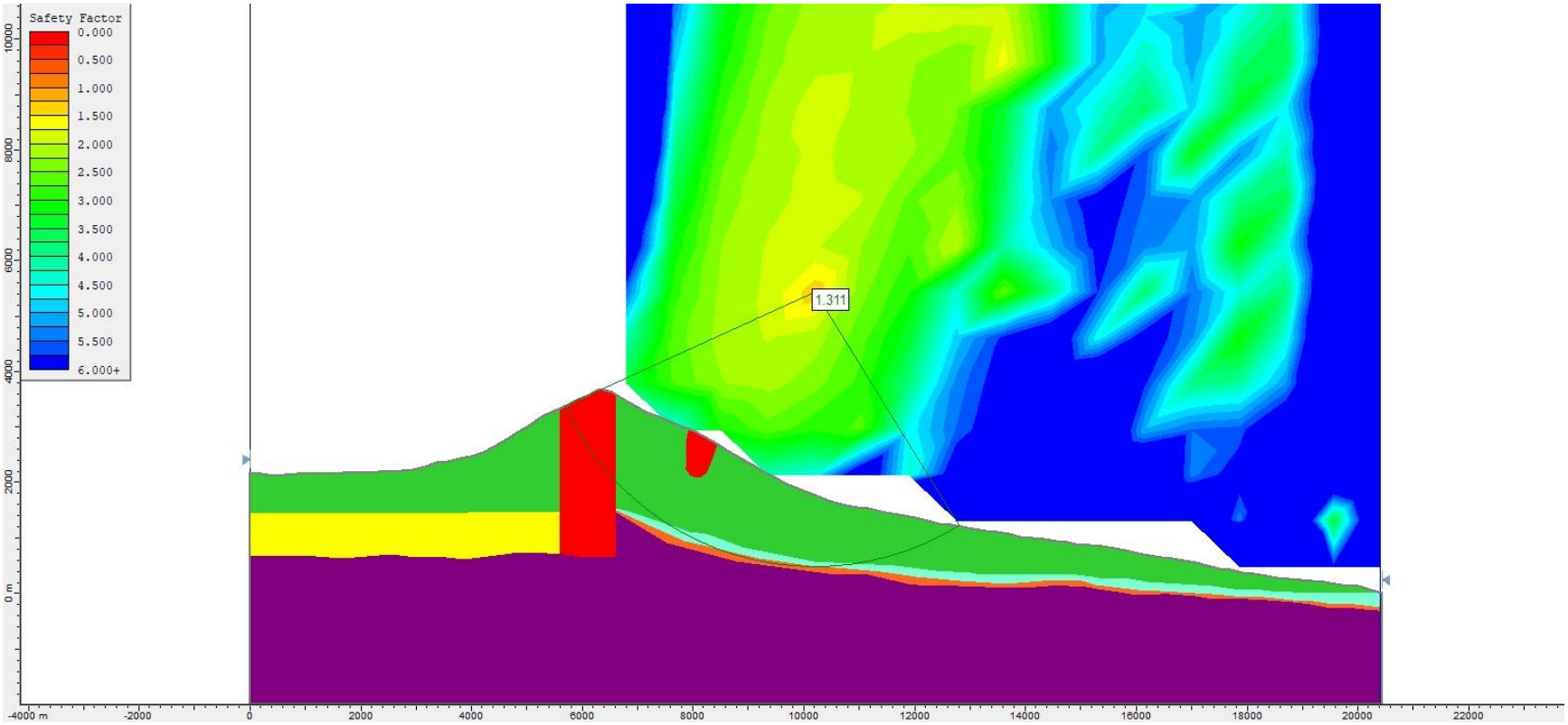

Figure S72. Slope stability static analysis for Model 1 (with alteration zones, Figure 4a), using the Morgenstern-Price method.

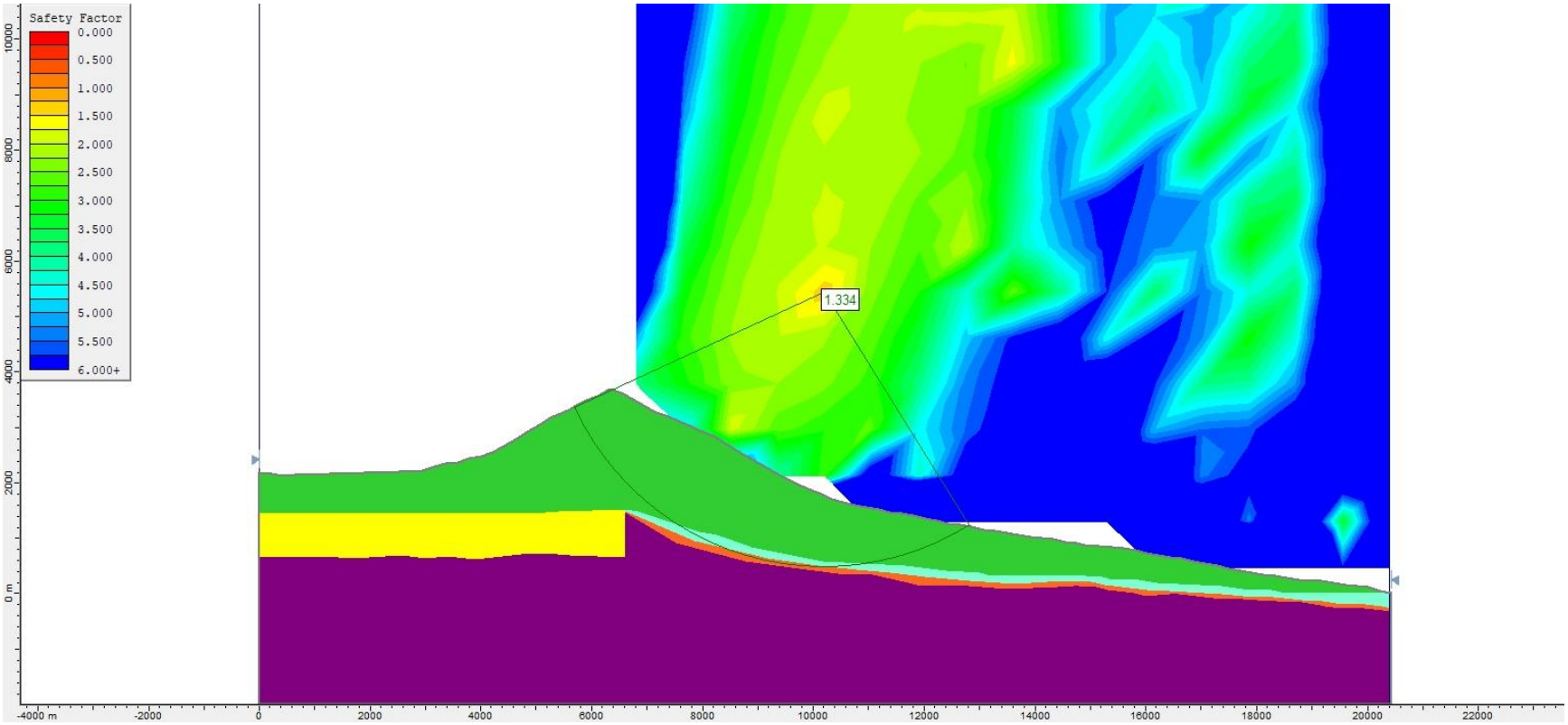

Figure S73. Slope stability static analysis for Model 2 (without alteration zones, Figure 4b), using the Bishop simplified method.

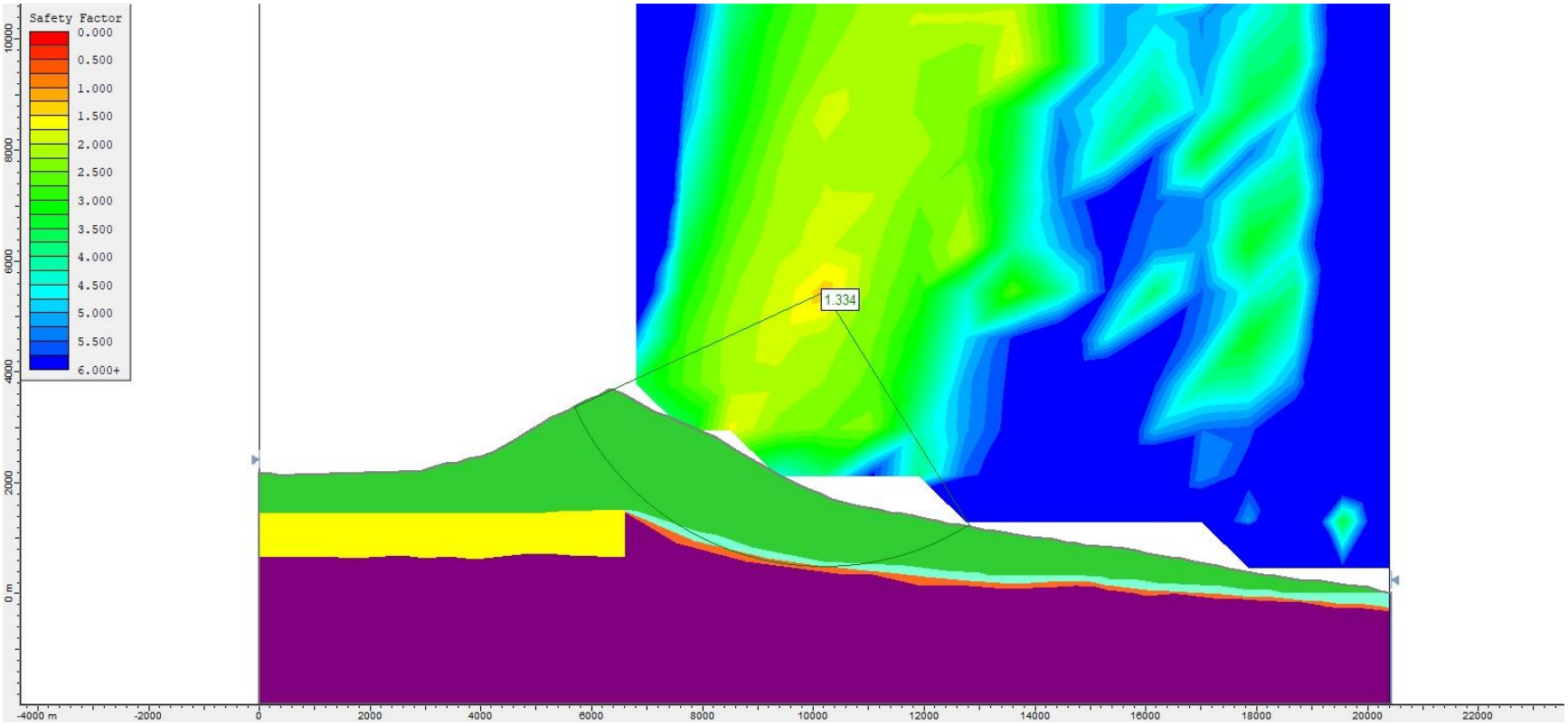

Figure S74. Slope stability static analysis for Model 2 (without alteration zones, Figure 4b), using the Janbu Generalised method.

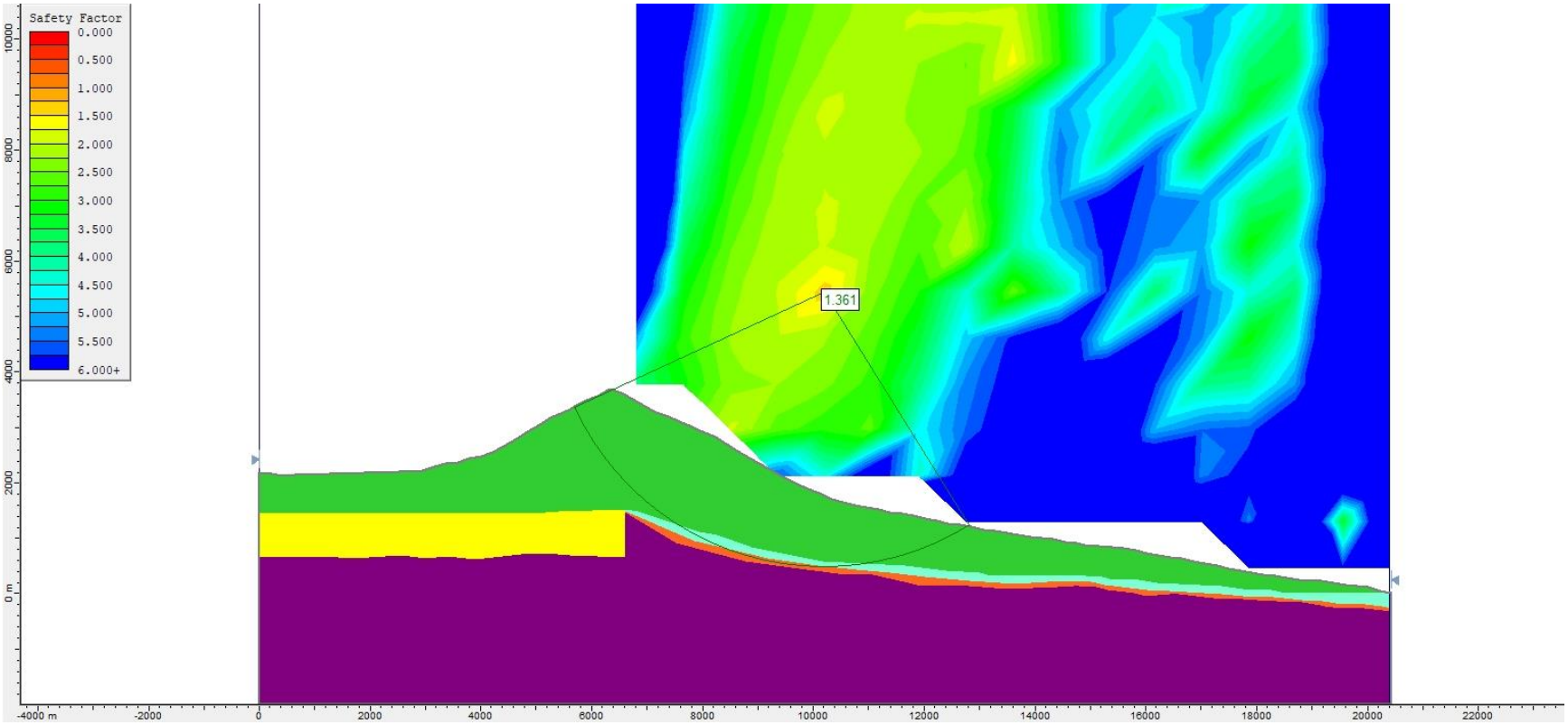

Figure S75. Slope stability static analysis for Model 2 (without alteration zones, Figure 4b), using the Morgenstern-Price method.

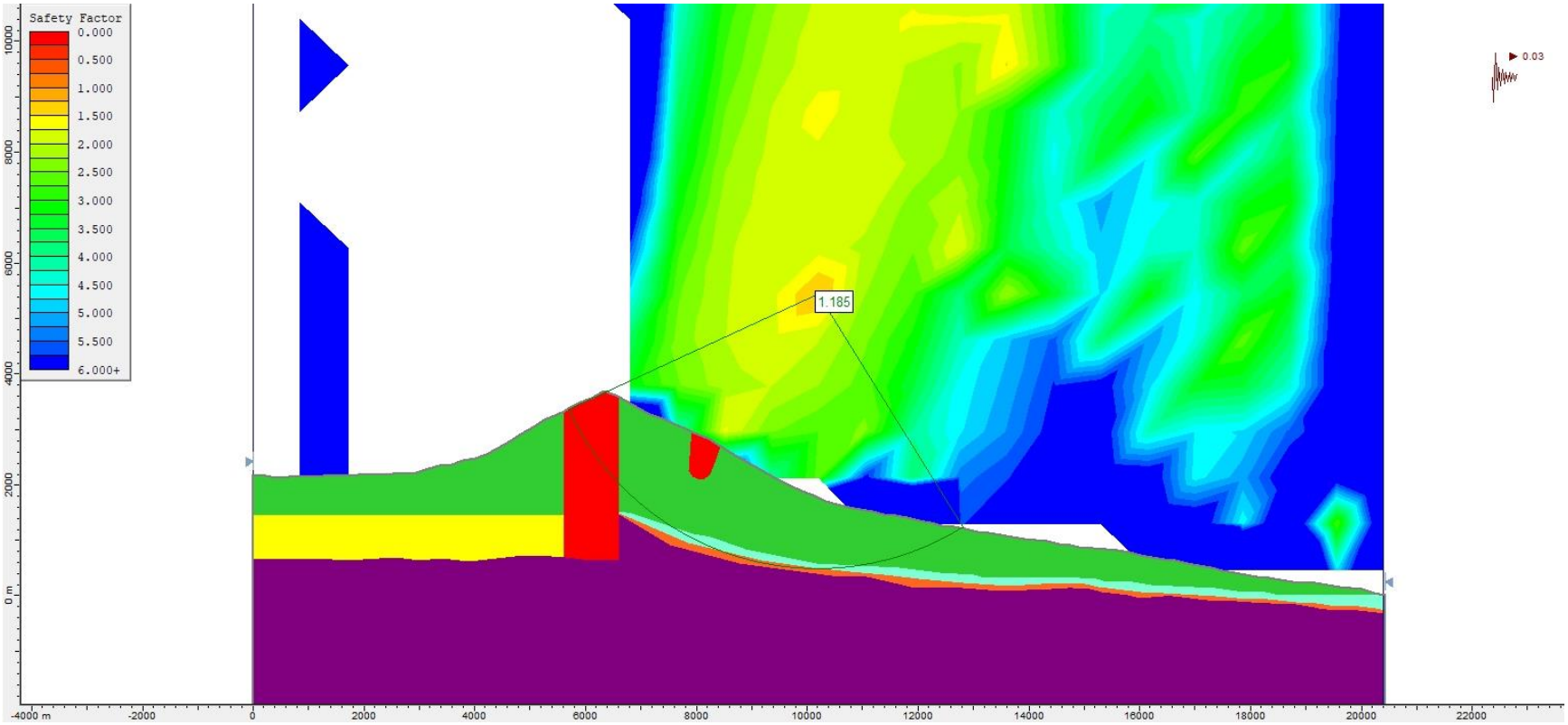

Figure S76. Slope stability pseudo-static analysis for Model 1 (with alteration zones, Figure 4a), using the Bishop simplified method and a k_h = 0.03.

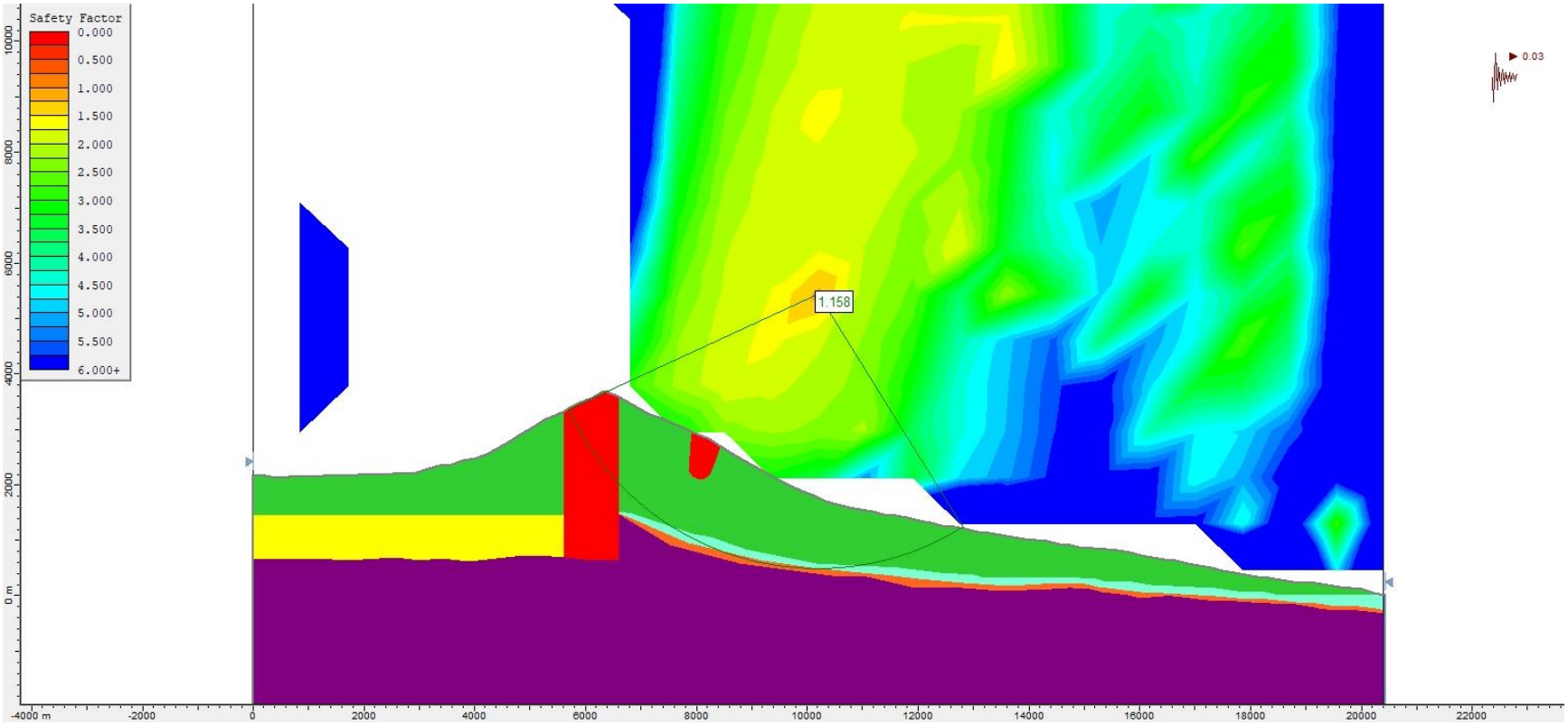

Figure S77. Slope stability pseudo-static analysis for Model 1 (with alteration zones, Figure 4a), using the Janbu Generalised method and a k_h = 0.03.

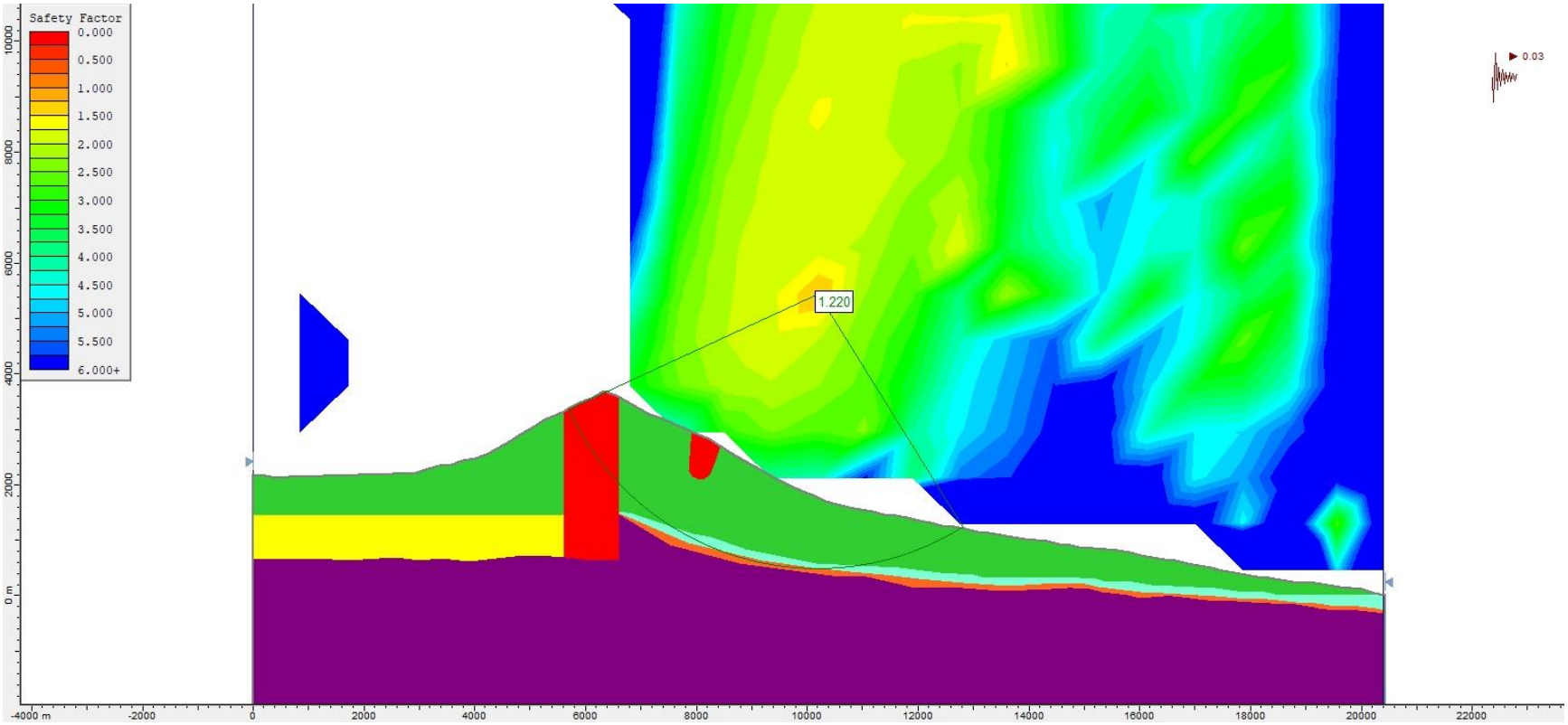

Figure S78. Slope stability pseudo-static analysis for Model 1 (with alteration zones, Figure 4a), using the Morgenstern-Price method and a k_h = 0.03.

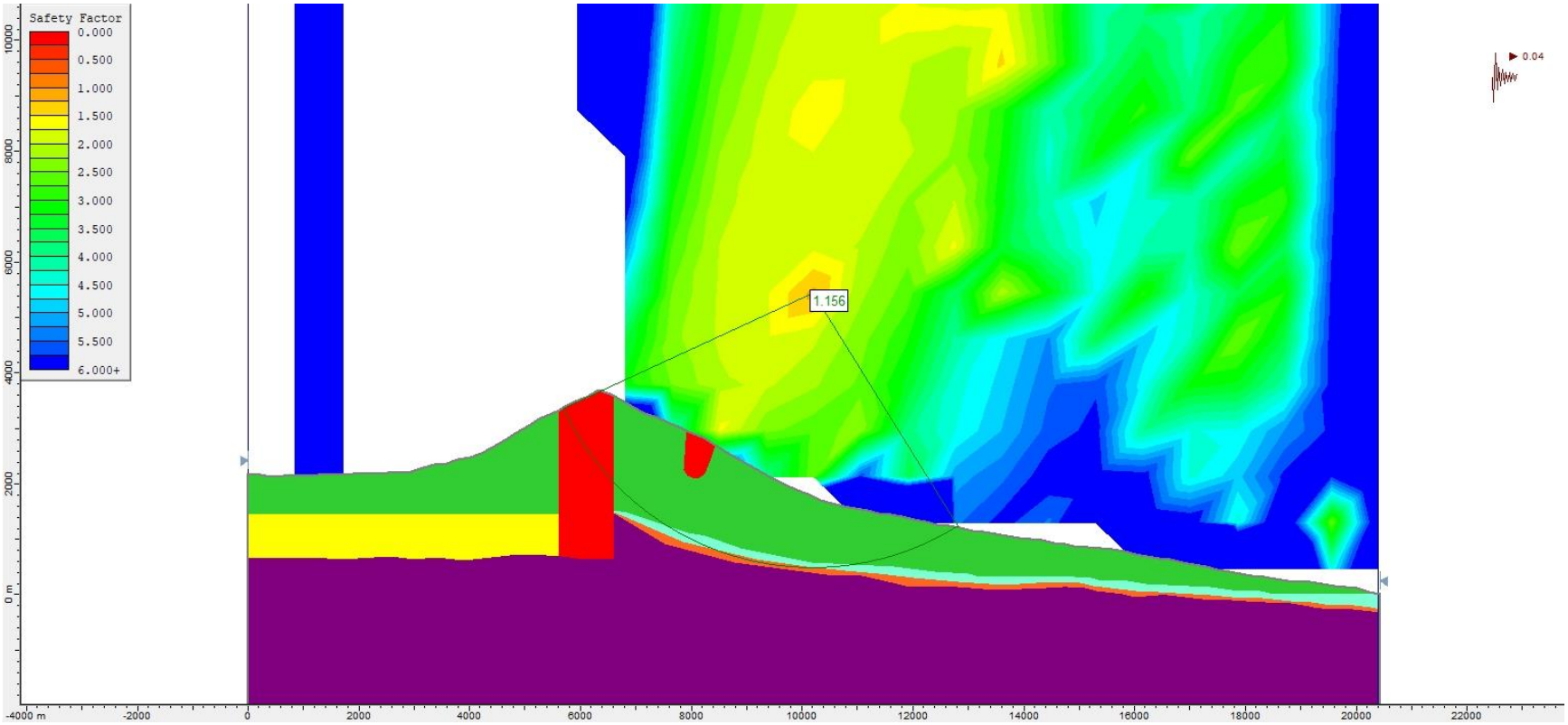

Figure S79. Slope stability pseudo-static analysis for Model 1 (with alteration zones, Figure 4a), using the Bishop simplified method and a k_h = 0.04.

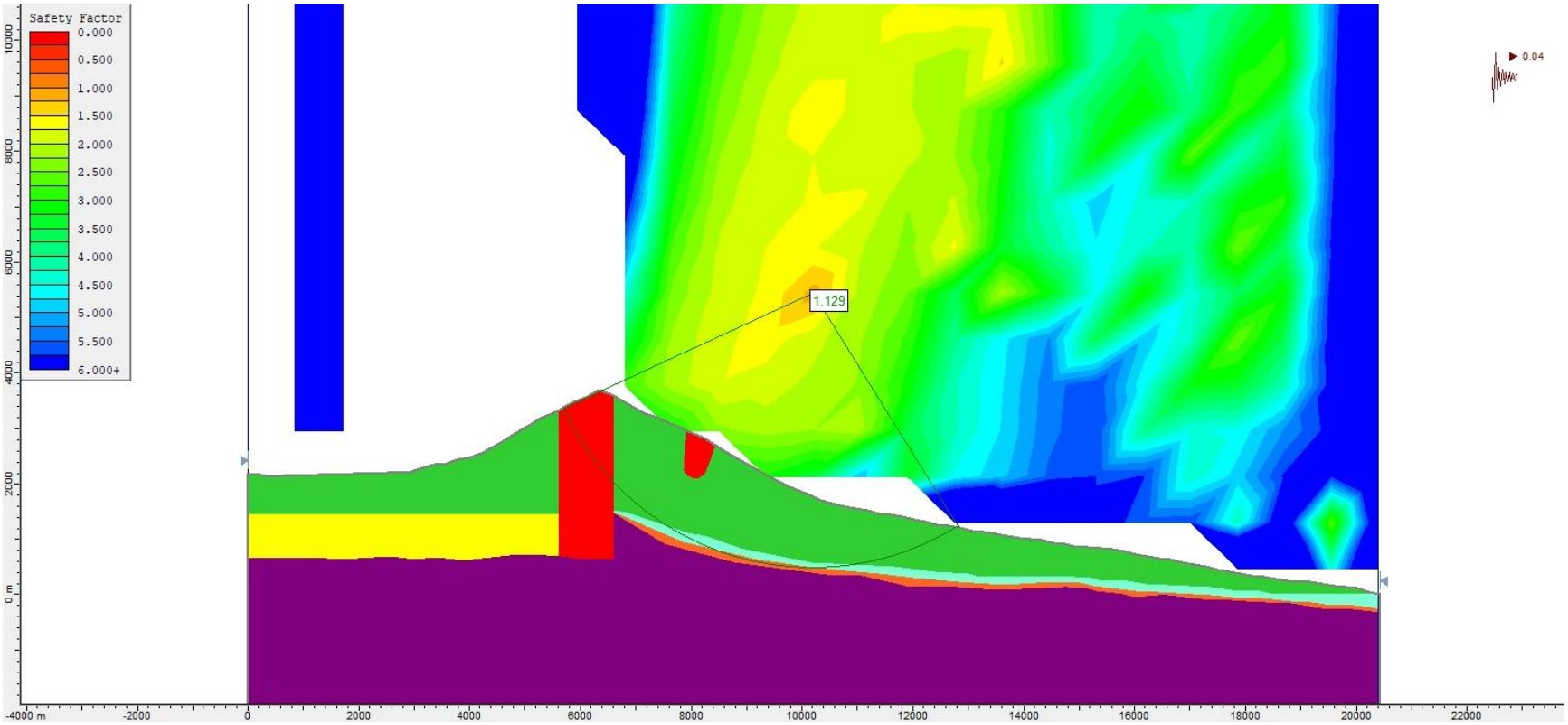

Figure S8o. Slope stability pseudo-static analysis for Model 1 (with alteration zones, Figure 4a), using the Janbu Generalised method and a k_h = 0.04.

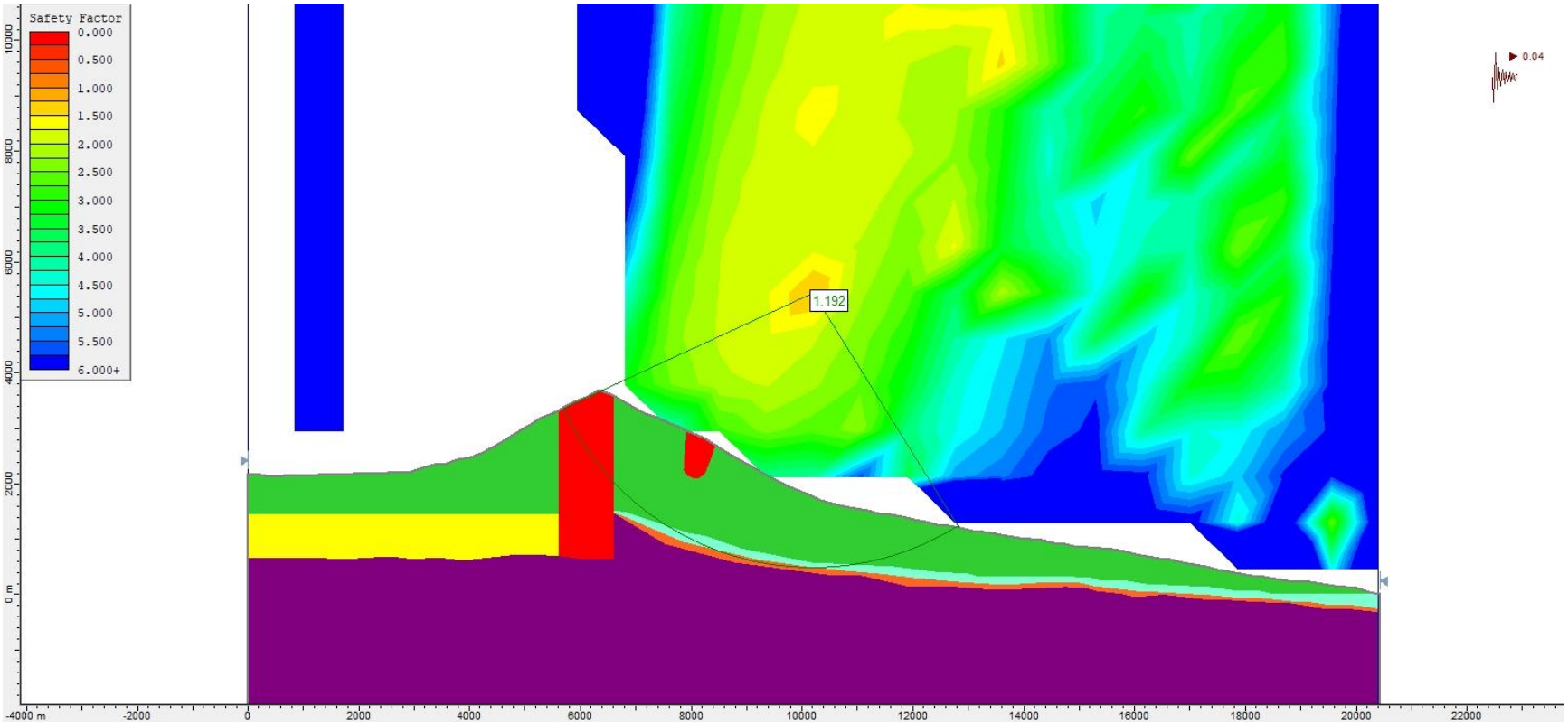

Figure S81. Slope stability pseudo-static analysis for Model 1 (with alteration zones, Figure 4a), using the Morgenstern-Price method and a k_h = 0.04.

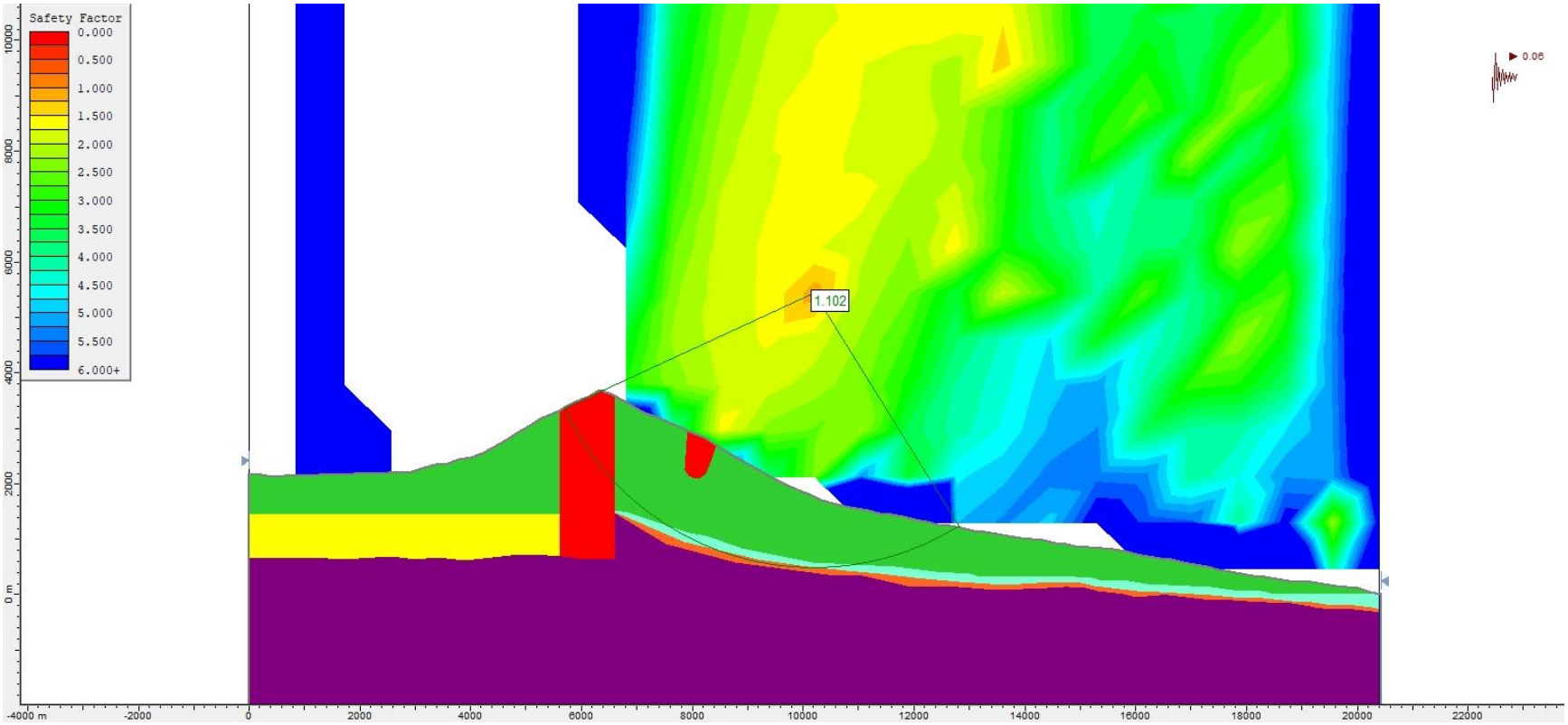

Figure S82. Slope stability pseudo-static analysis for Model 1 (with alteration zones, Figure 4a), using the Bishop simplified method and a k_h = 0.06.

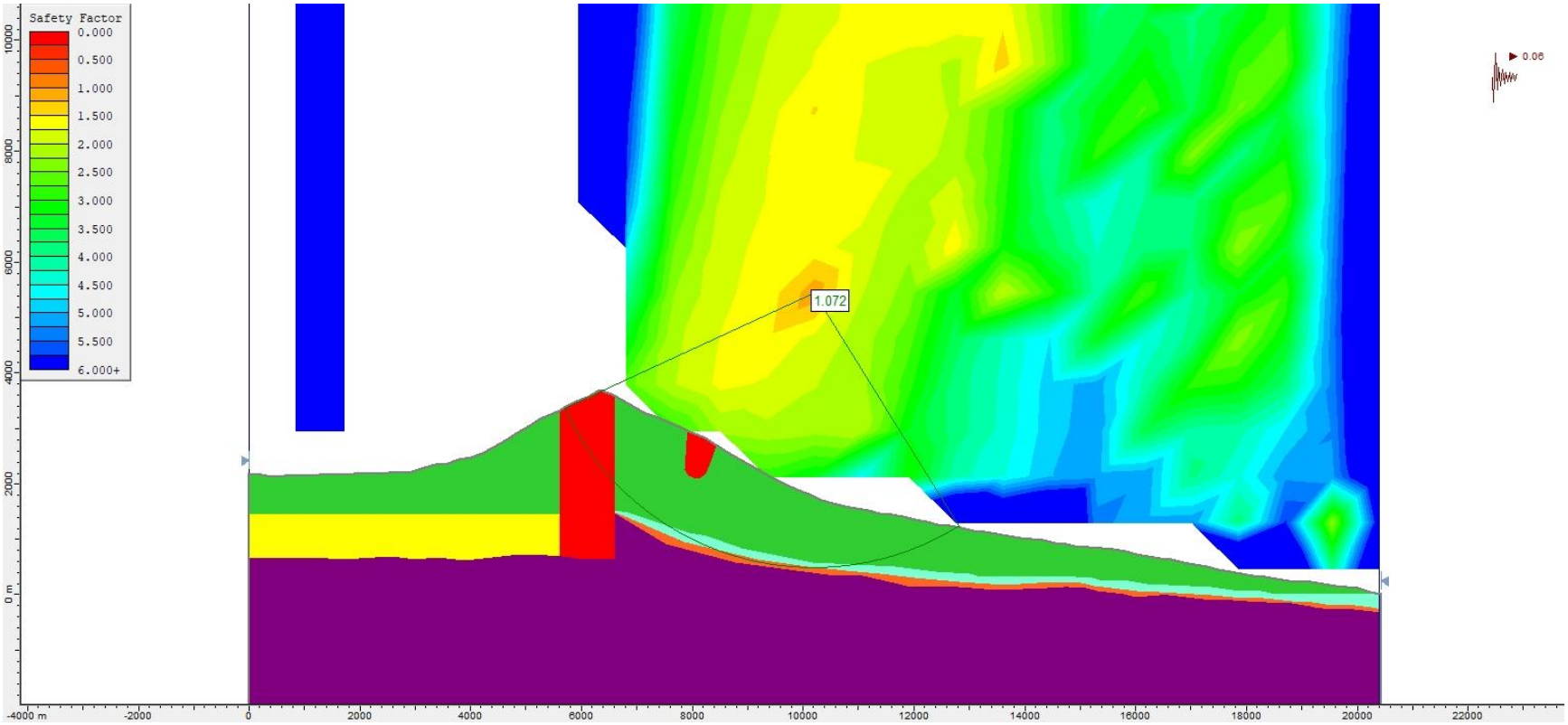

Figure S83. Slope stability pseudo-static analysis for Model 1 (with alteration zones, Figure 4a), using the Janbu Generalised method and a k_h = 0.06.

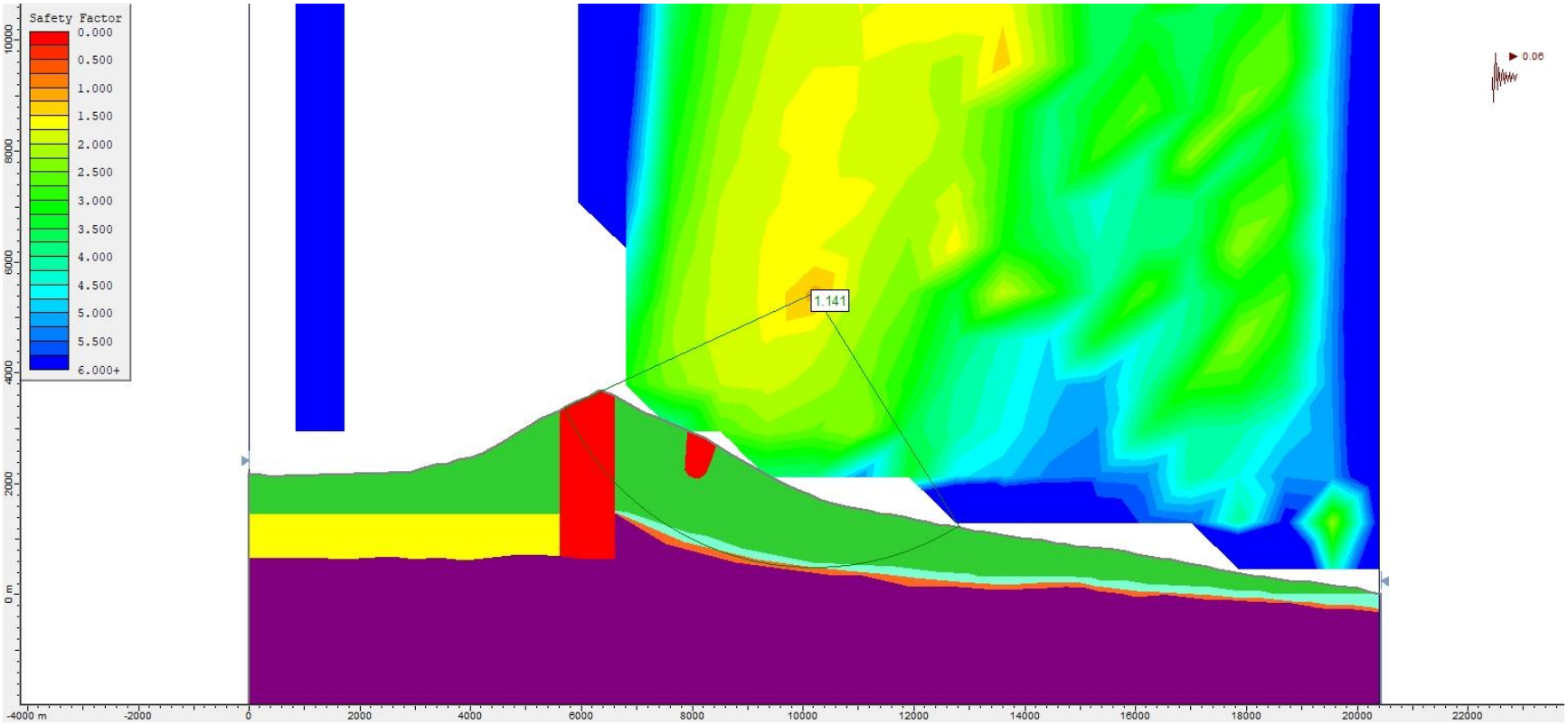

Figure S84. Slope stability pseudo-static analysis for Model 1 (with alteration zones, Figure 4a), using the Morgenstern-Price method and a k_h = 0.06.

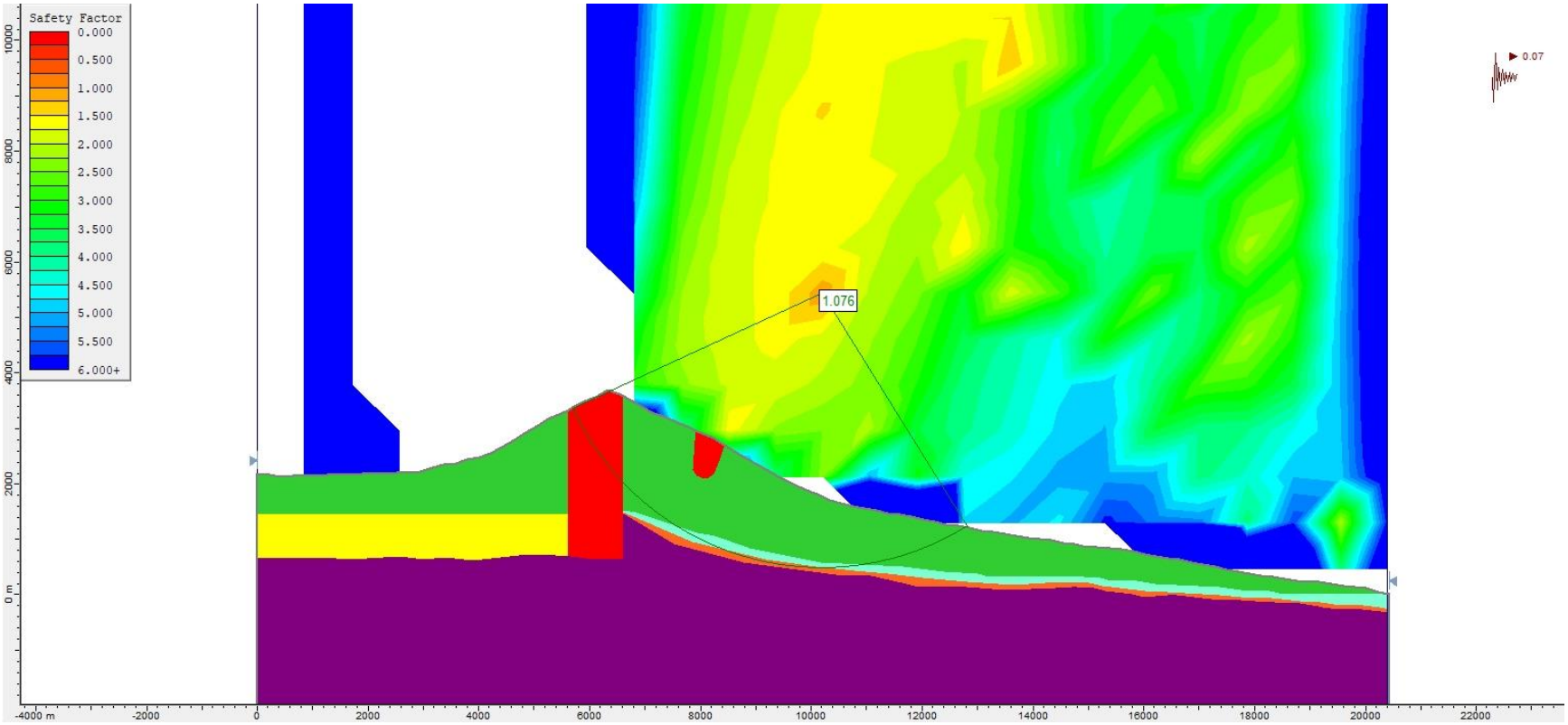

Figure S85. Slope stability pseudo-static analysis for Model 1 (with alteration zones, Figure 4a), using the Bishop simplified method and a k_h = 0.07.

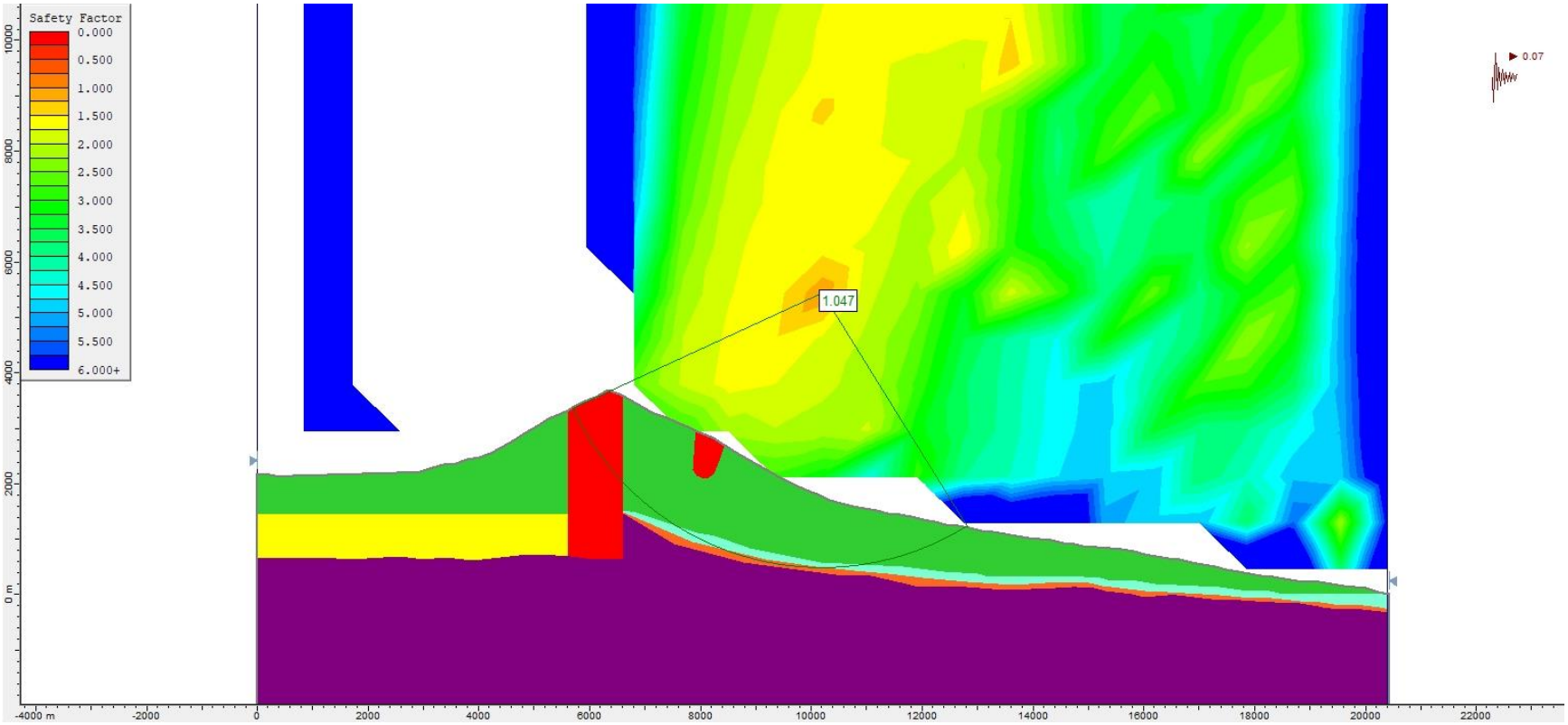

Figure S86. Slope stability pseudo-static analysis for Model 1 (with alteration zones, Figure 4a), using the Janbu Generalised method and a k_h = 0.07.

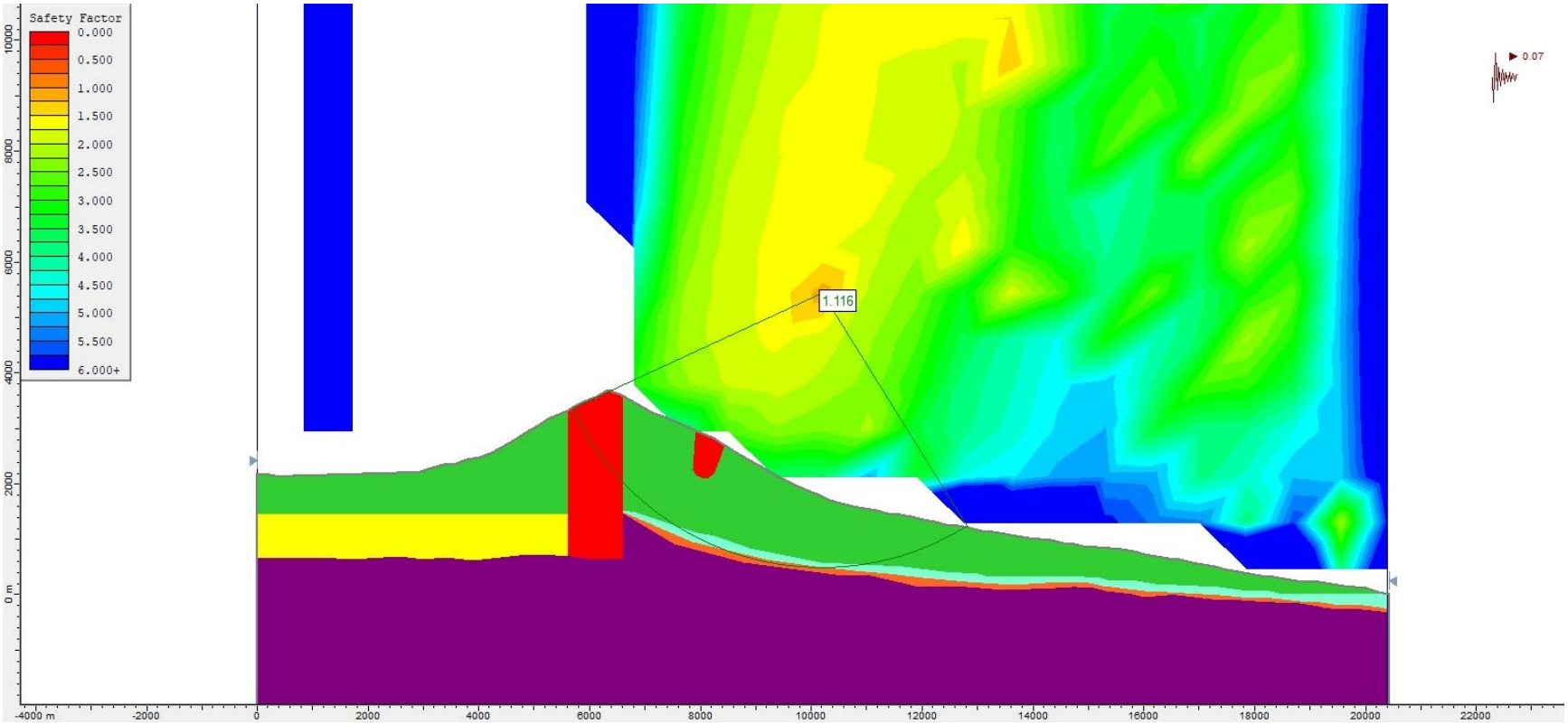

Figure S87. Slope stability pseudo-static analysis for Model 1 (with alteration zones, Figure 4a), using the Morgenstern-Price method and a k_h = 0.07.

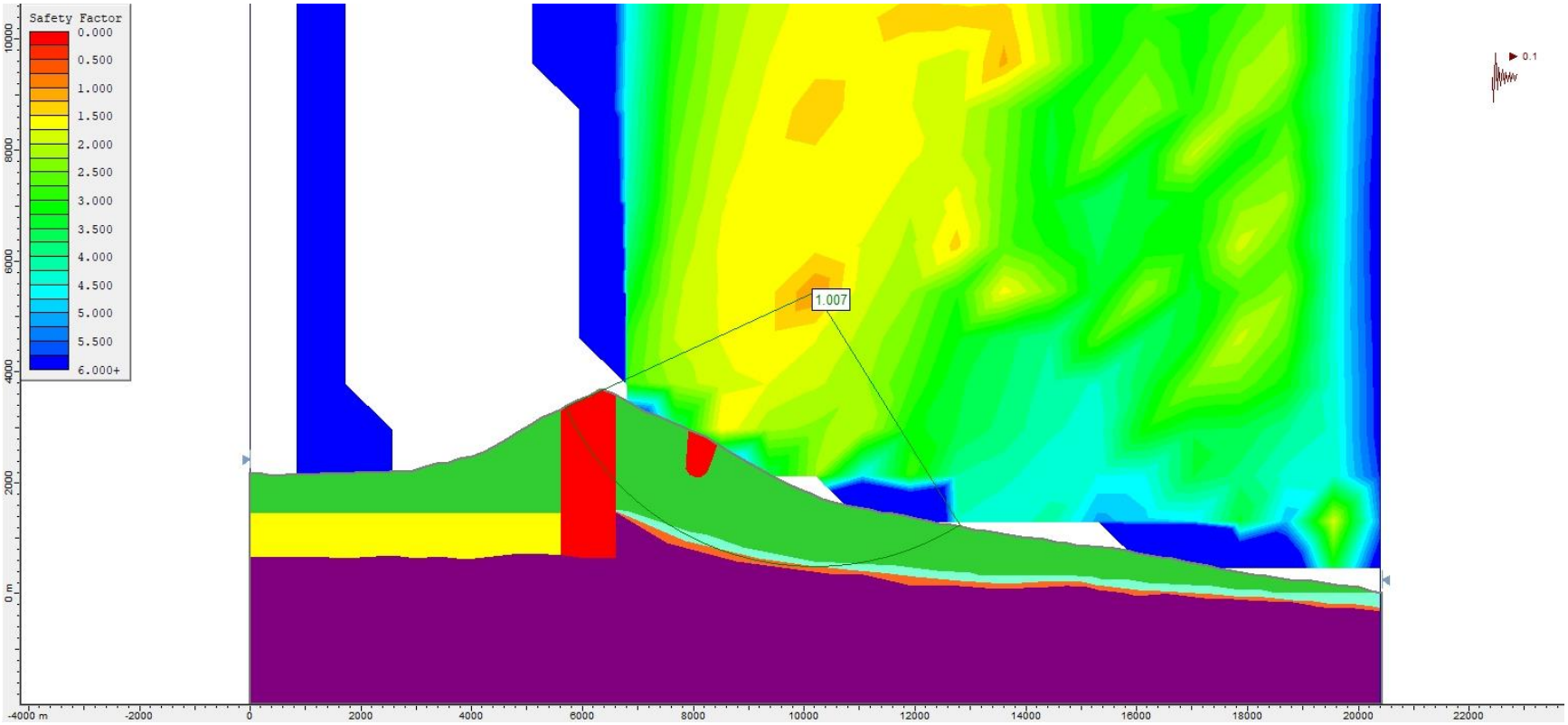

Figure S88. Slope stability pseudo-static analysis for Model 1 (with alteration zones, Figure 4a), using the Bishop simplified method and a k_h = 0.10.

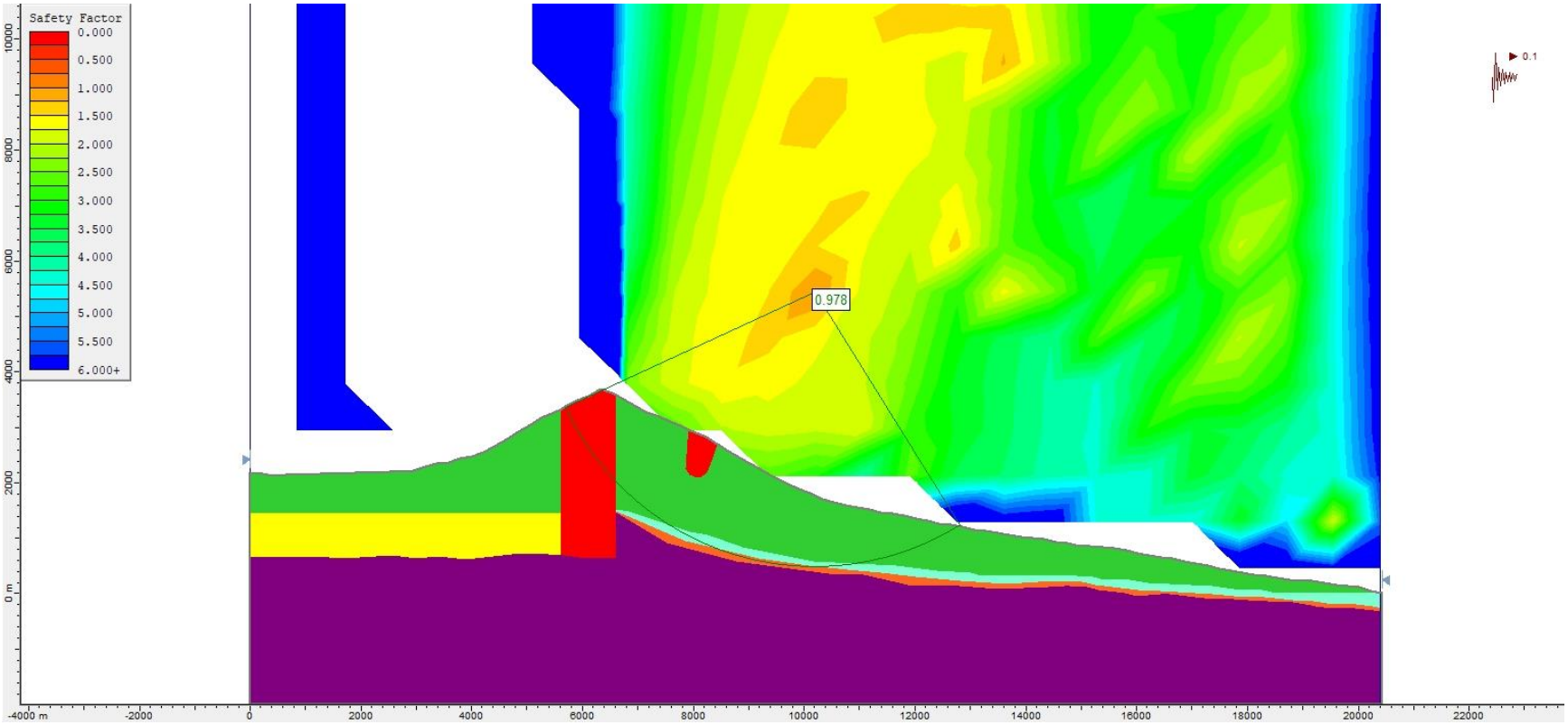

Figure S89. Slope stability pseudo-static analysis for Model 1 (with alteration zones, Figure 4a), using the Janbu Generalised method and a k_h = 0.10.

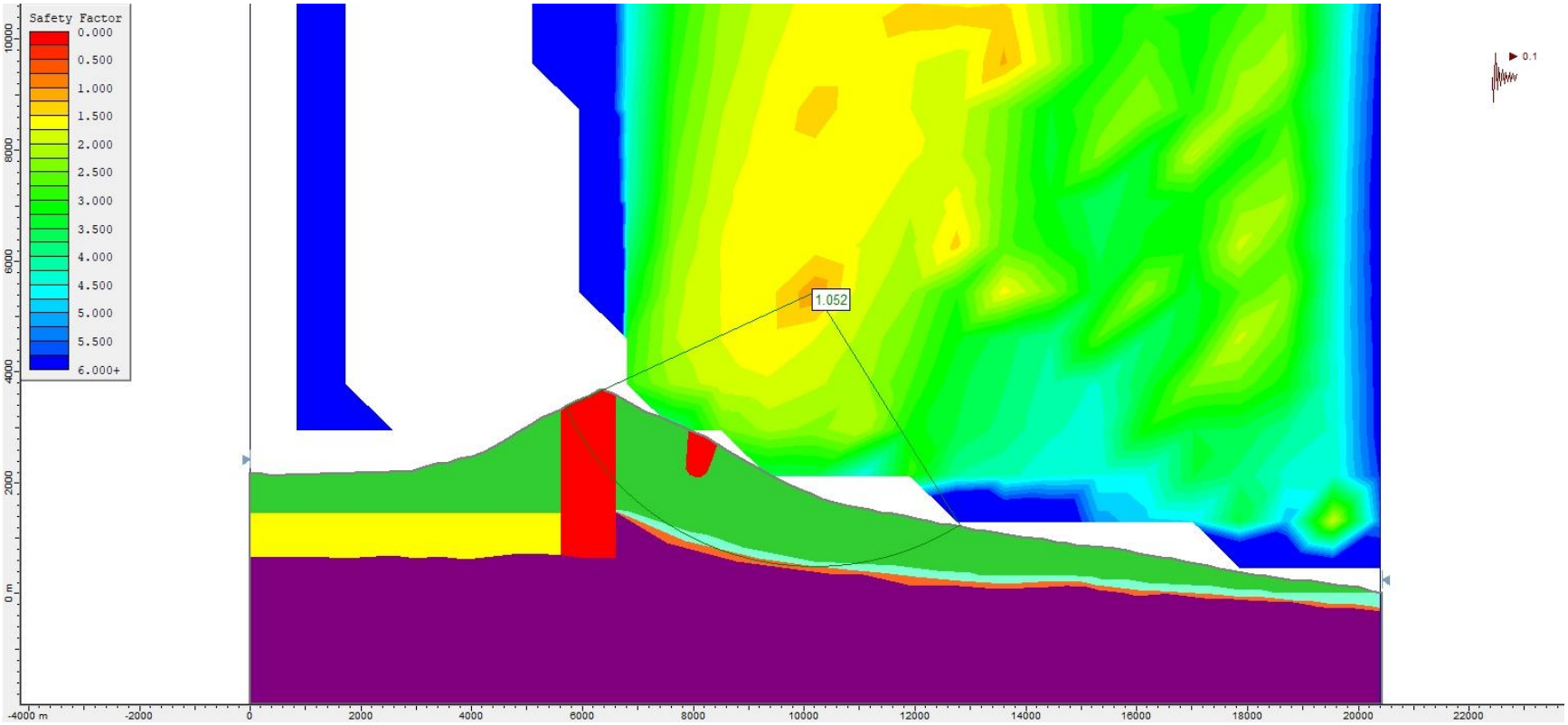

Figure S90. Slope stability pseudo-static analysis for Model 1 (with alteration zones, Figure 4a), using the Morgenstern-Price method and a k_h = 0.10.

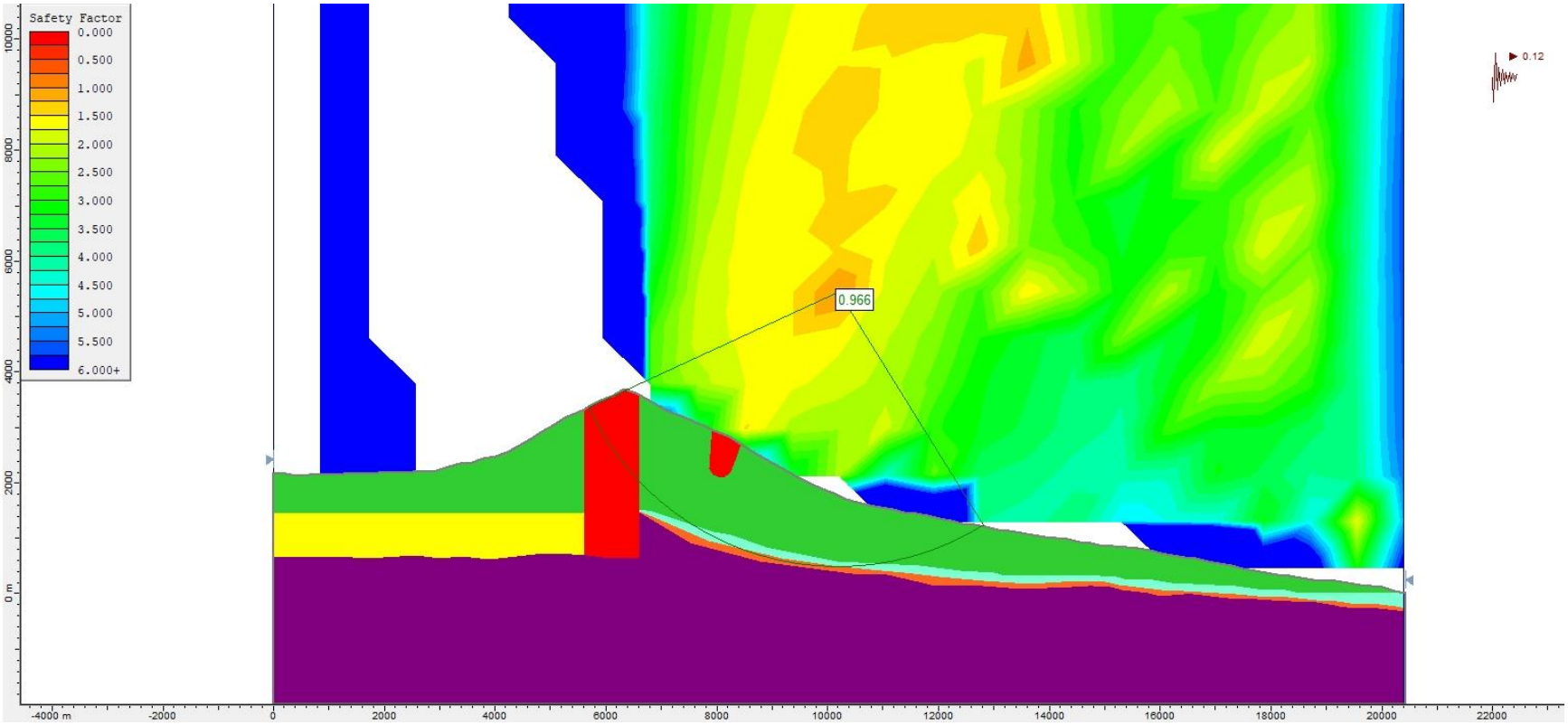

Figure S91. Slope stability pseudo-static analysis for Model 1 (with alteration zones, Figure 4a), using the Bishop simplified method and a k_h = 0.12.

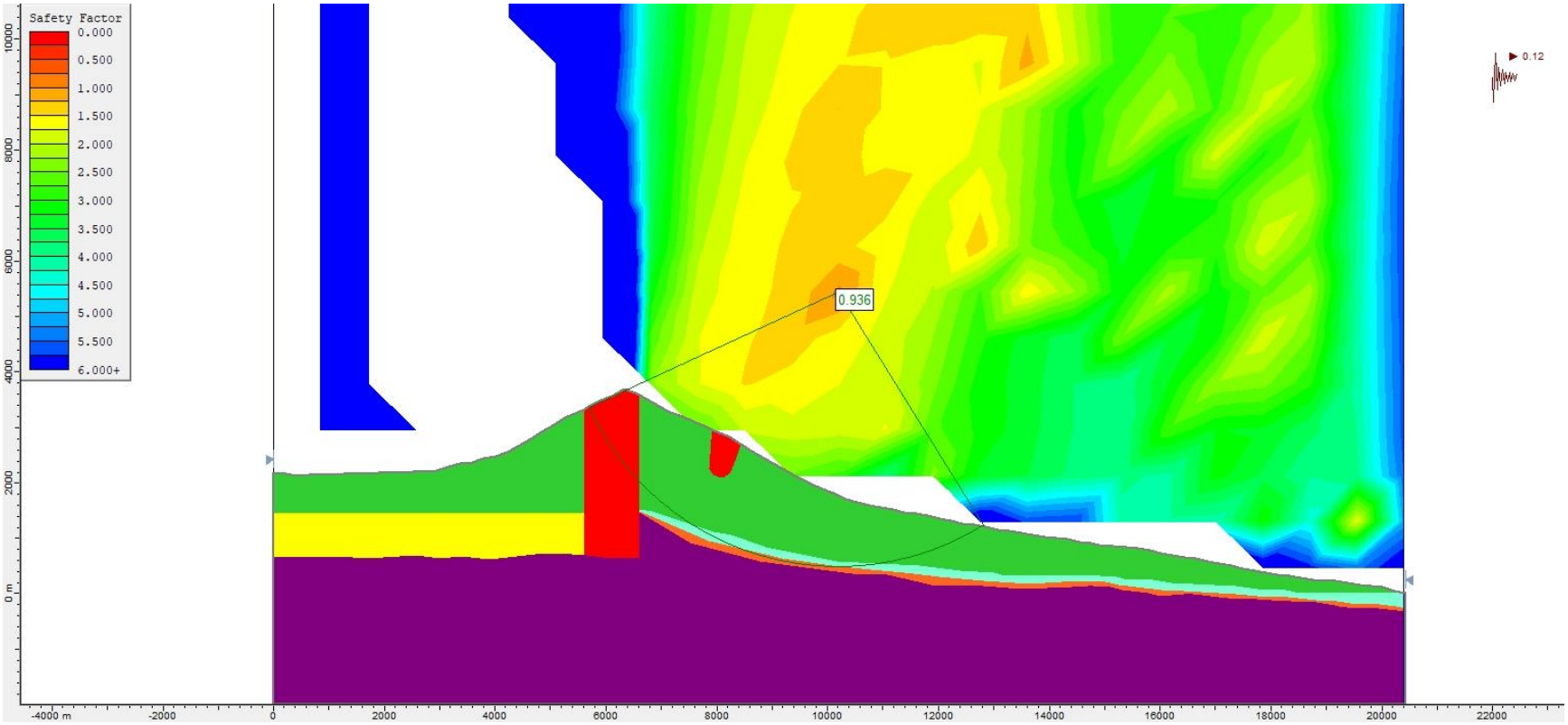

Figure S92. Slope stability pseudo-static analysis for Model 1 (with alteration zones, Figure 4a), using the Janbu Generalised method and a k_h = 0.12.

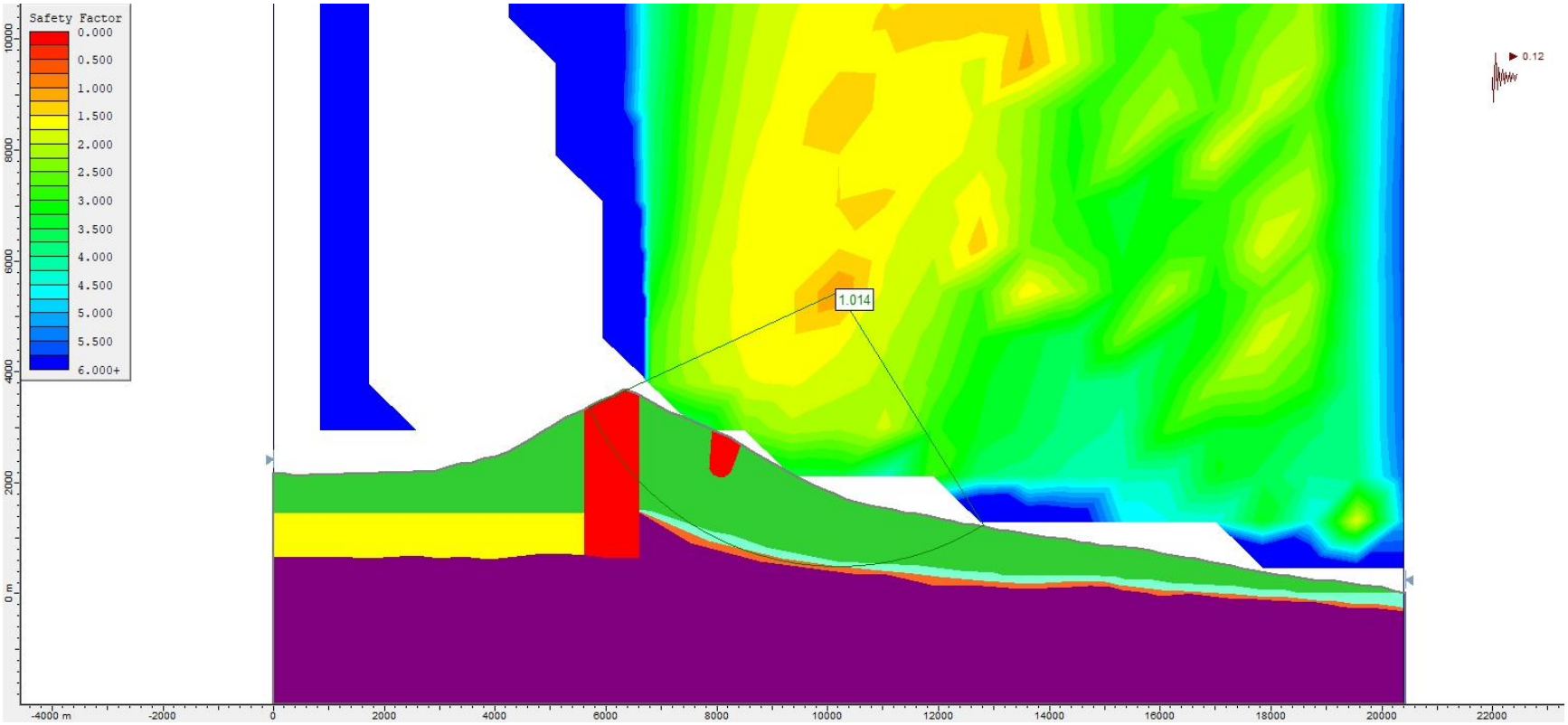

Figure S93. Slope stability pseudo-static analysis for Model 1 (with alteration zones, Figure 4a), using the Morgenstern-Price method and a k_h = 0.12.

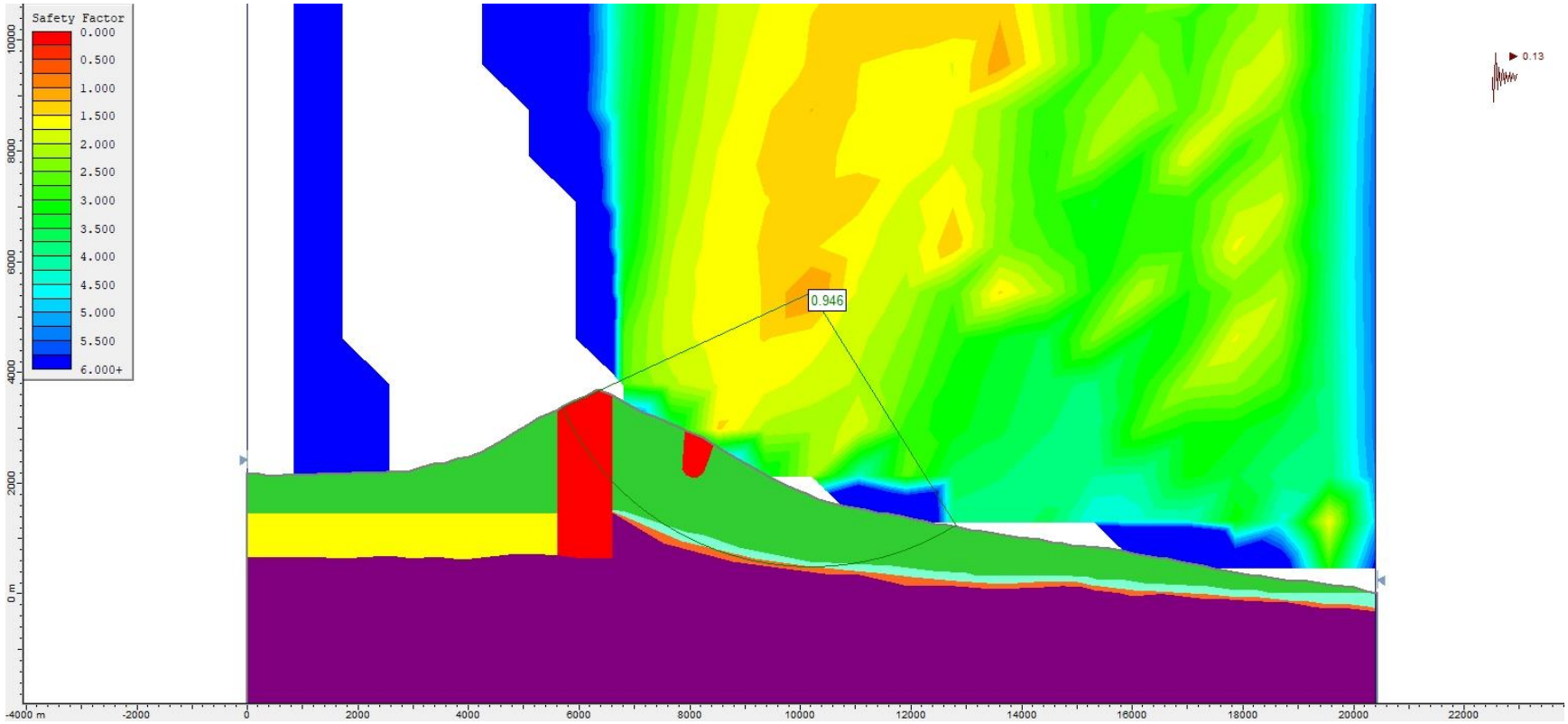

Figure S94. Slope stability pseudo-static analysis for Model 1 (with alteration zones, Figure 4a), using the Bishop simplified method and a k_h = 0.13.

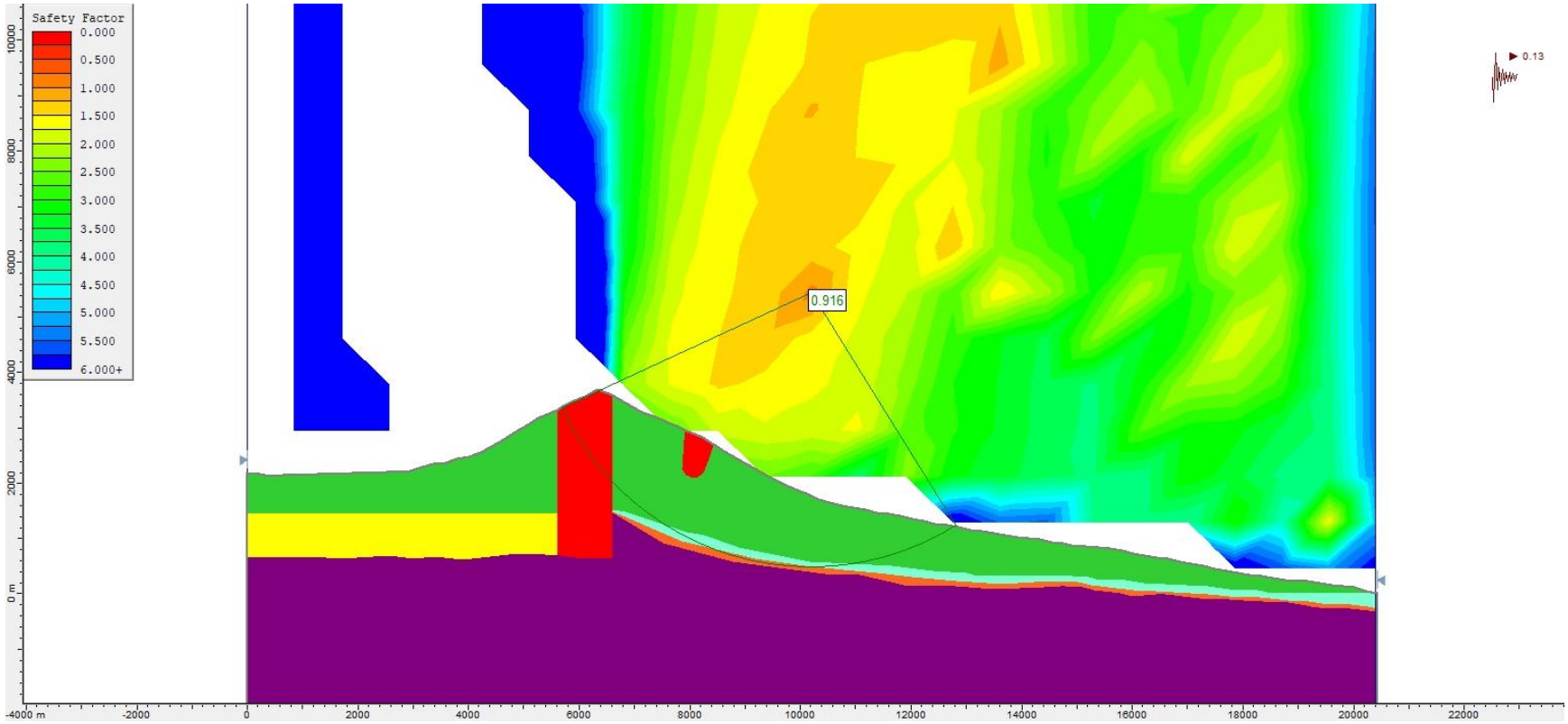

Figure S95. Slope stability pseudo-static analysis for Model 1 (with alteration zones, Figure 4a), using the Janbu Generalised method and a k_h = 0.13.

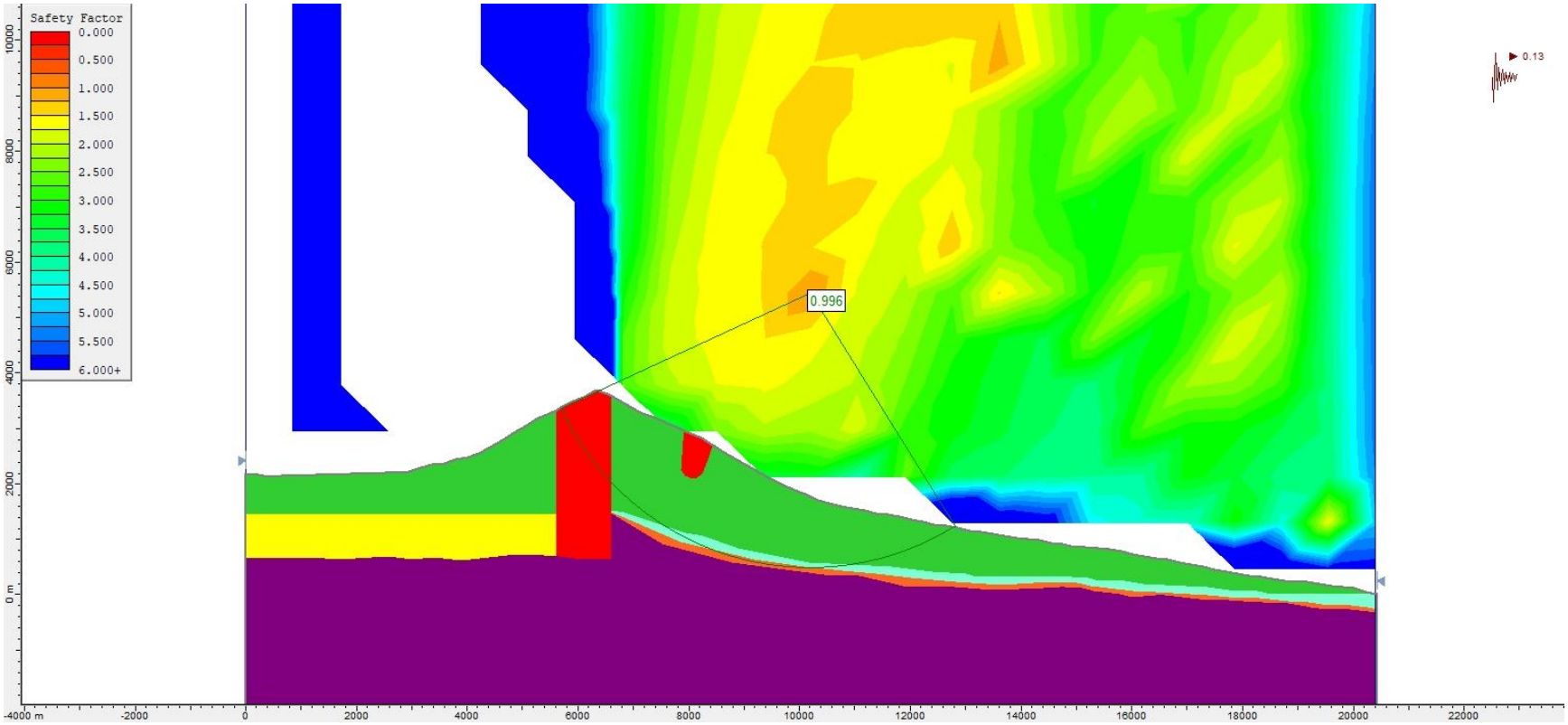

Figure S96. Slope stability pseudo-static analysis for Model 1 (with alteration zones, Figure 4a), using the Morgenstern-Price method and a k_h = 0.13.

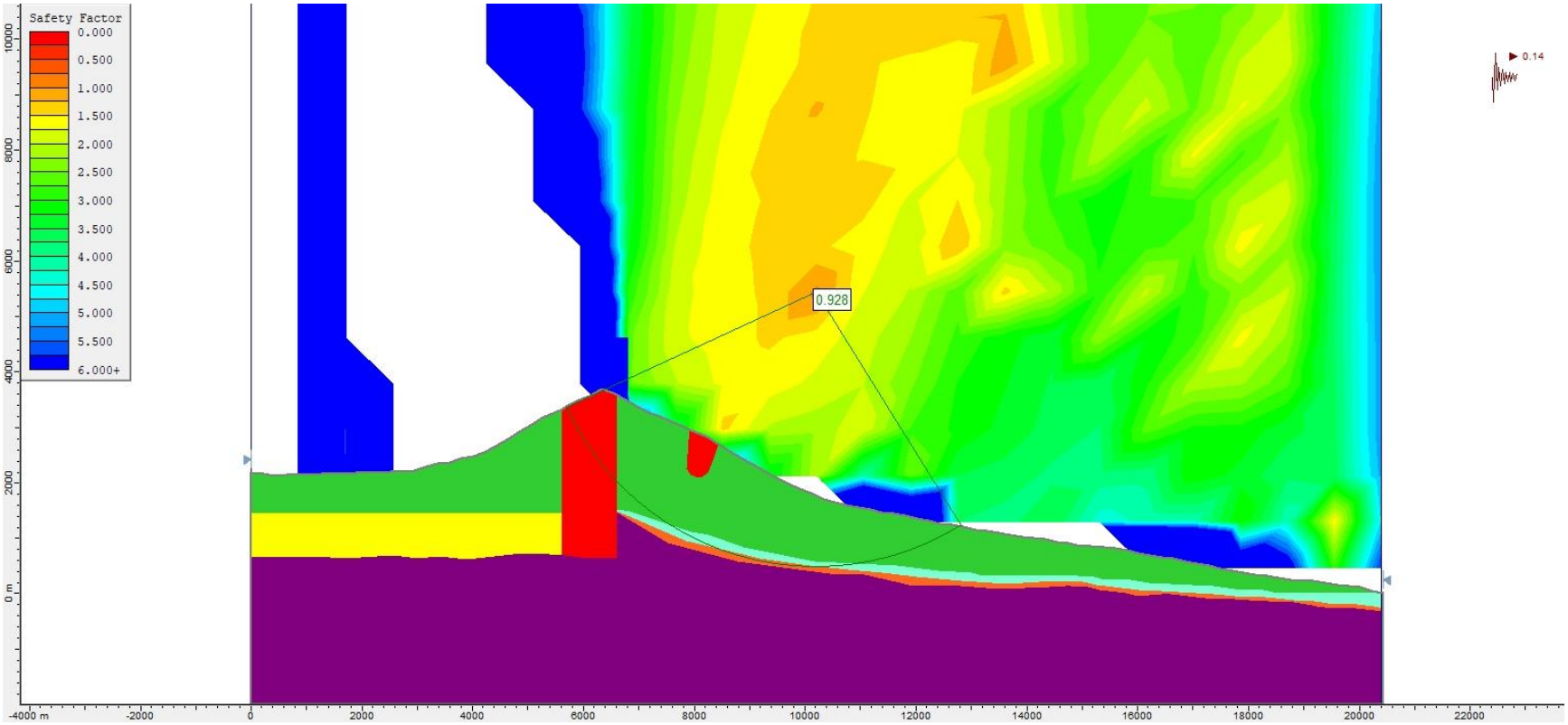

Figure S97. Slope stability pseudo-static analysis for Model 1 (with alteration zones, Figure 4a), using the Bishop simplified method and a k_h = 0.14.

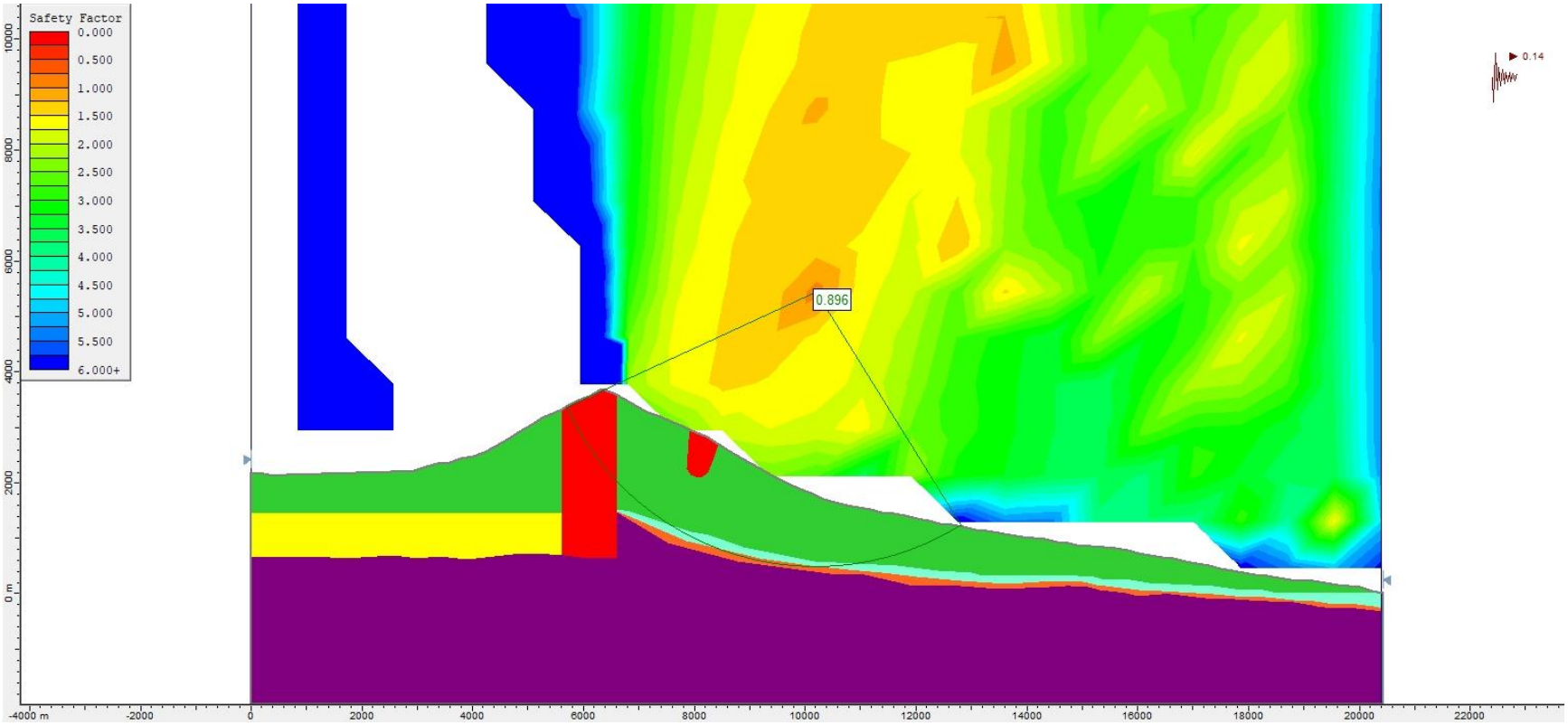

Figure S98. Slope stability pseudo-static analysis for Model 1 (with alteration zones, Figure 4a), using the Janbu Generalised method and a k_h = 0.14.

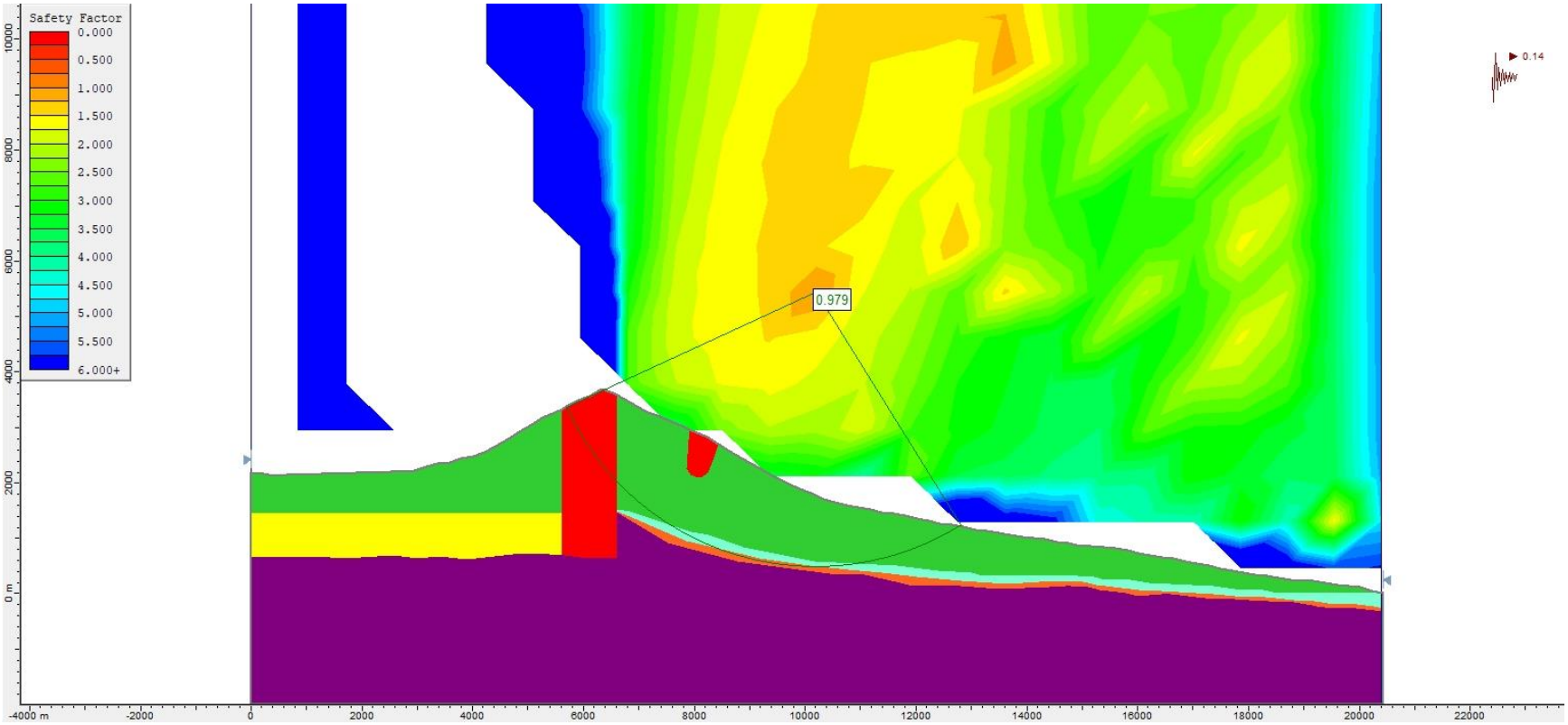

Figure S99. Slope stability pseudo-static analysis for Model 1 (with alteration zones, Figure 4a), using the Morgenstern-Price method and a k_h = 0.14.

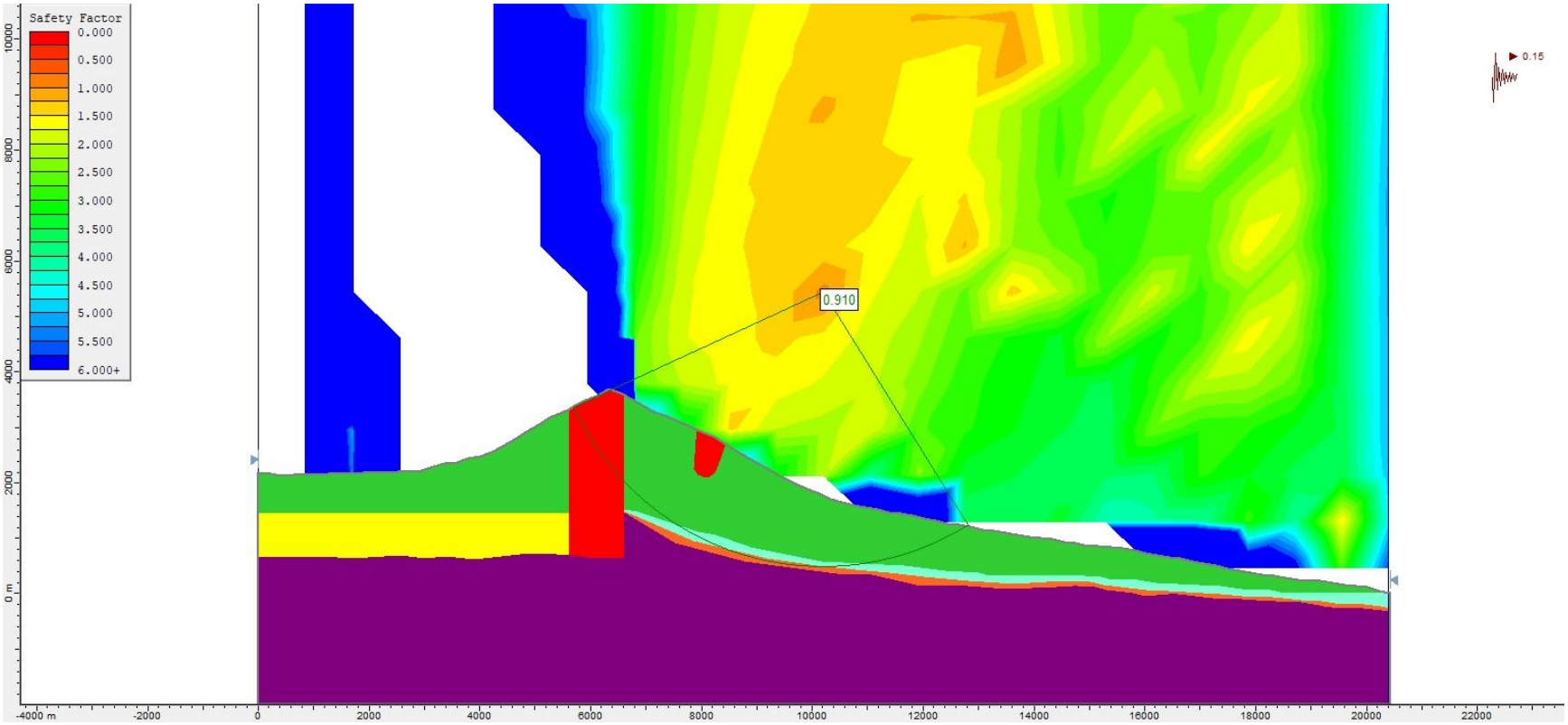

Figure S100. Slope stability pseudo-static analysis for Model 1 (with alteration zones, Figure 4a), using the Bishop simplified method and a k_h = 0.15.

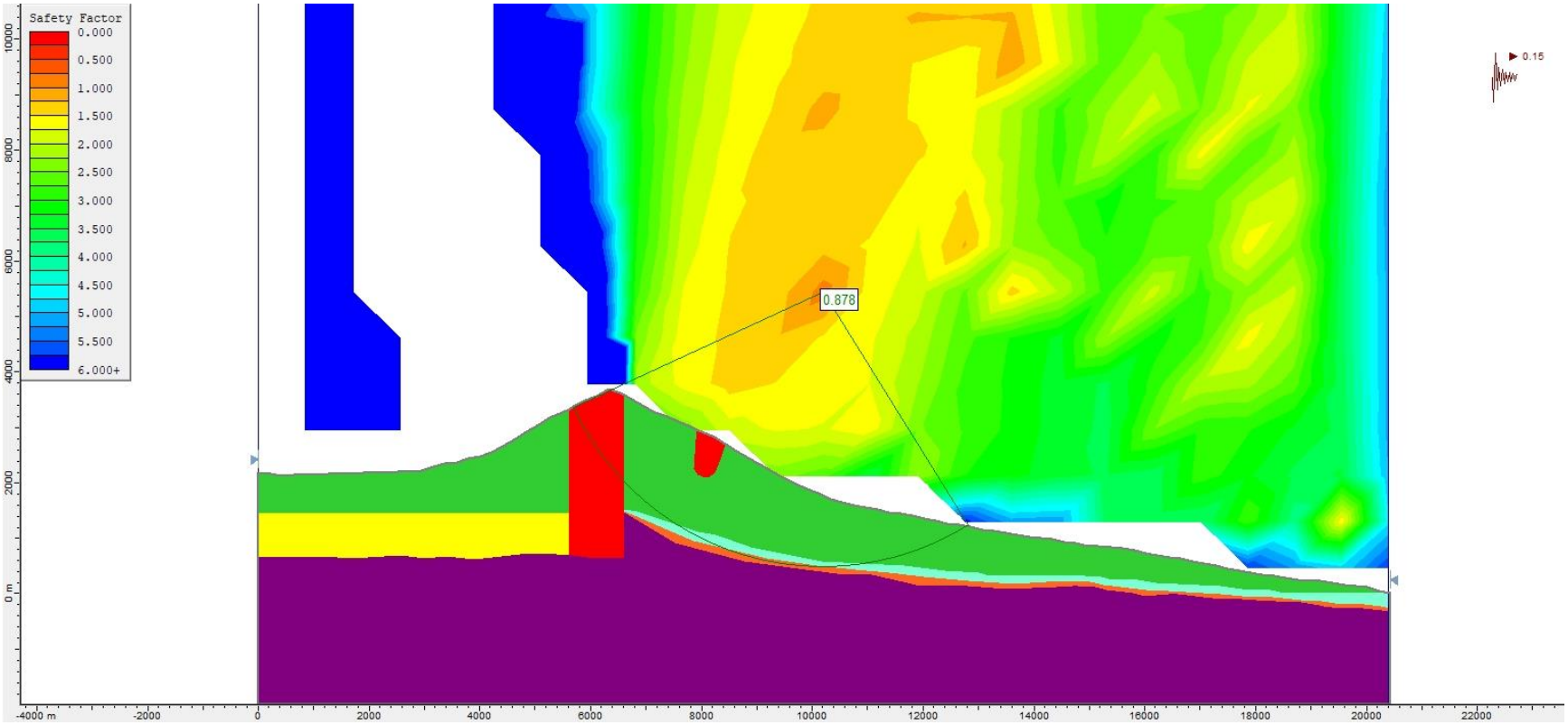

Figure S101. Slope stability pseudo-static analysis for Model 1 (with alteration zones, Figure 4a), using the Janbu Generalised method and a k_h = 0.15.

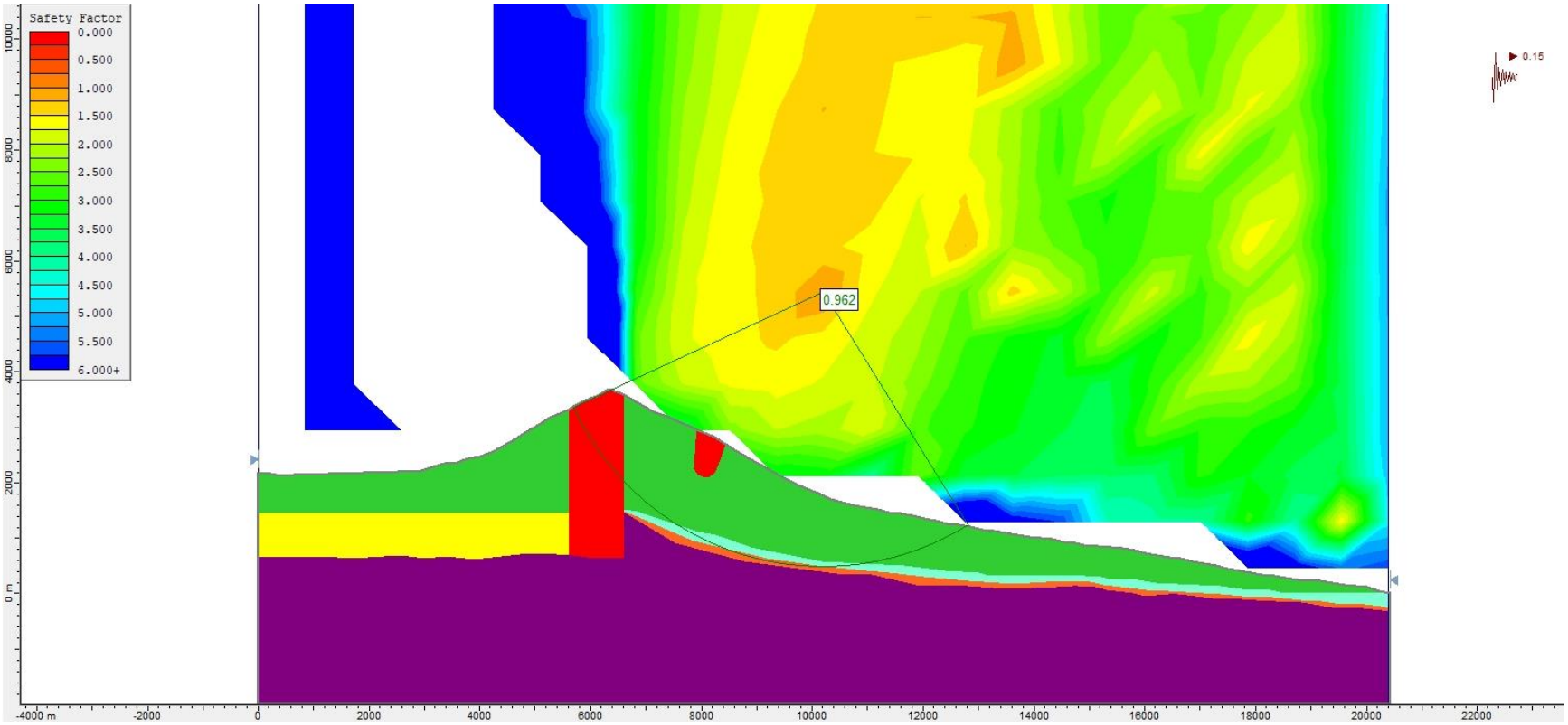

Figure S102. Slope stability pseudo-static analysis for Model 1 (with alteration zones, Figure 4a), using the Morgenstern-Price method and a k_h = 0.15.

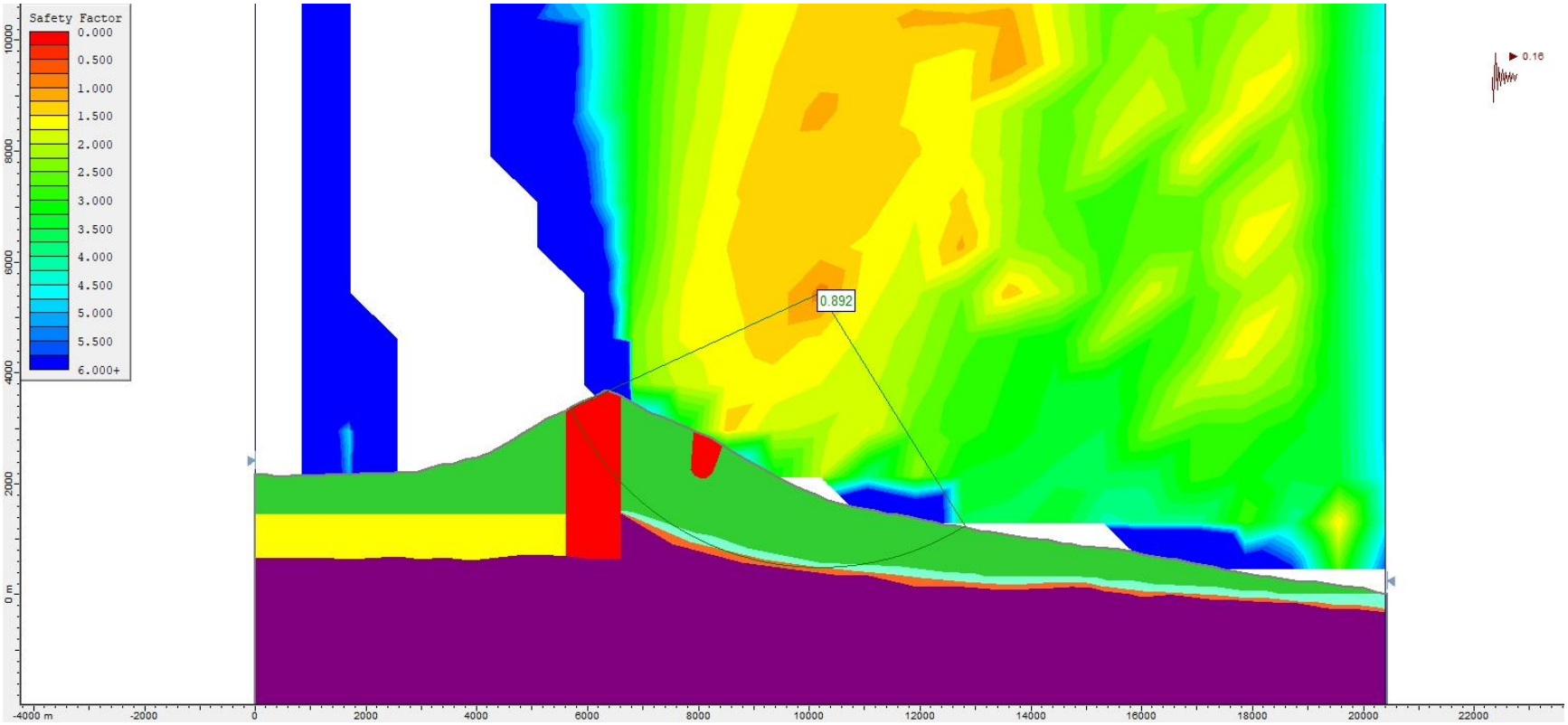

Figure S103. Slope stability pseudo-static analysis for Model 1 (with alteration zones, Figure 4a), using the Bishop simplified method and a k_h = 0.16.

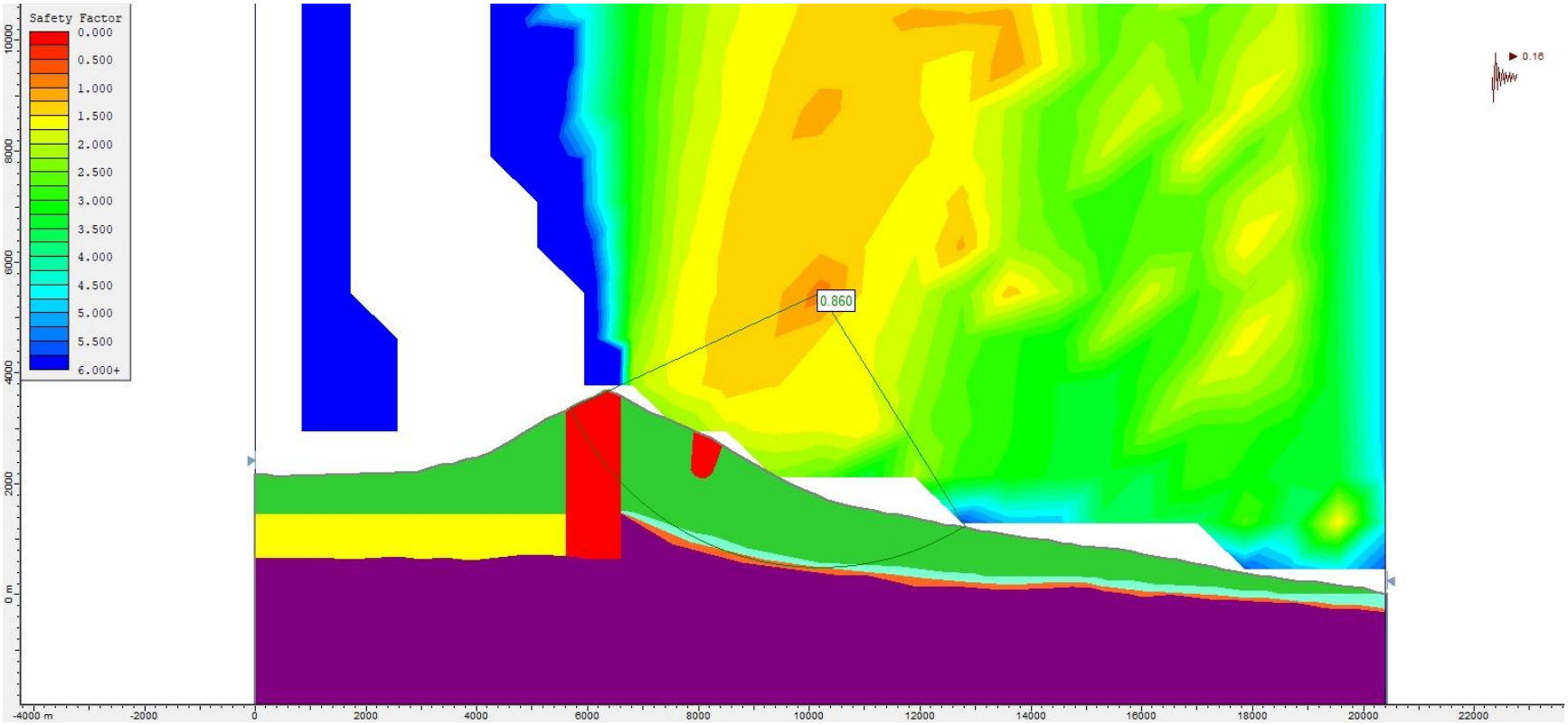

Figure S104. Slope stability pseudo-static analysis for Model 1 (with alteration zones, Figure 4a), using the Janbu Generalised method and a k_h = 0.16.

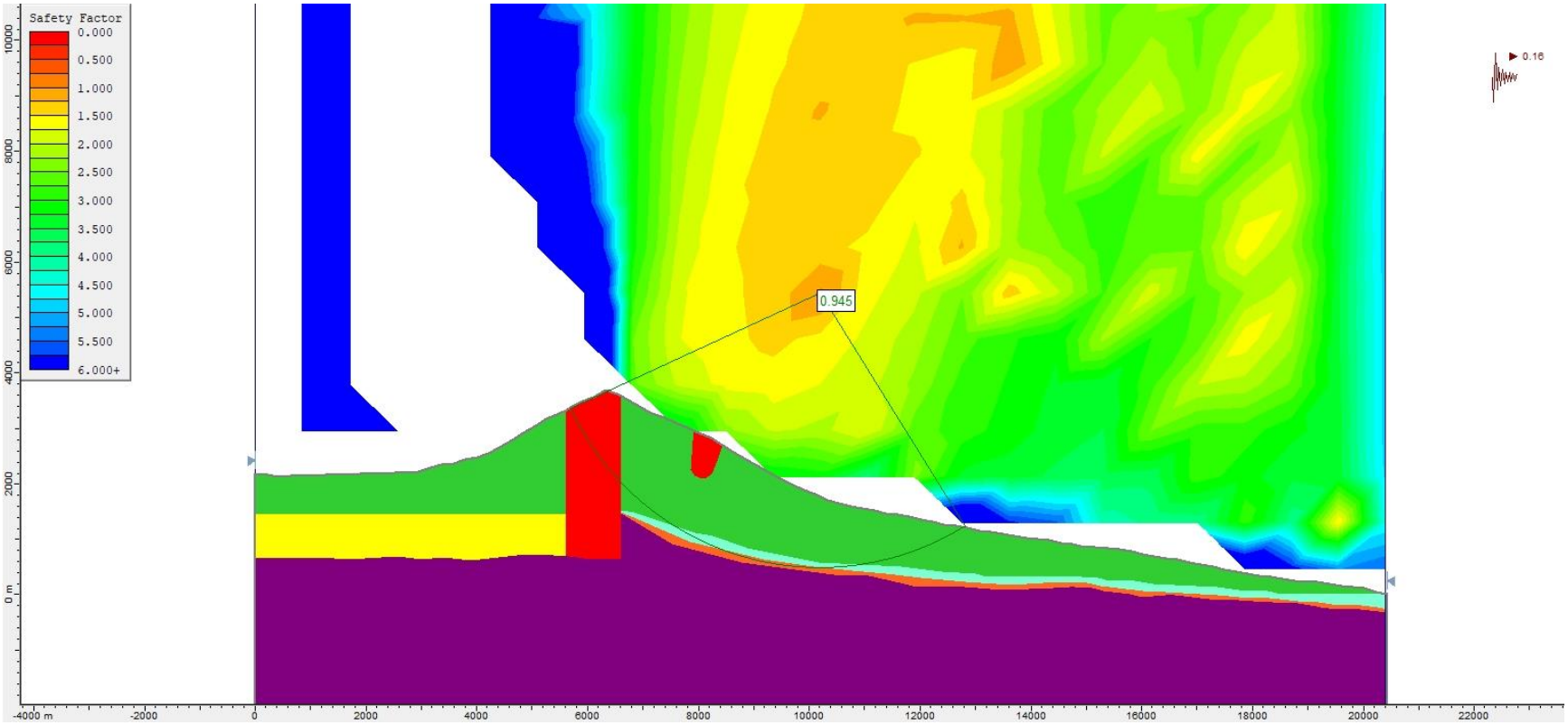

Figure S105. Slope stability pseudo-static analysis for Model 1 (with alteration zones, Figure 4a), using the Morgenstern-Price method and a k_h = 0.16.

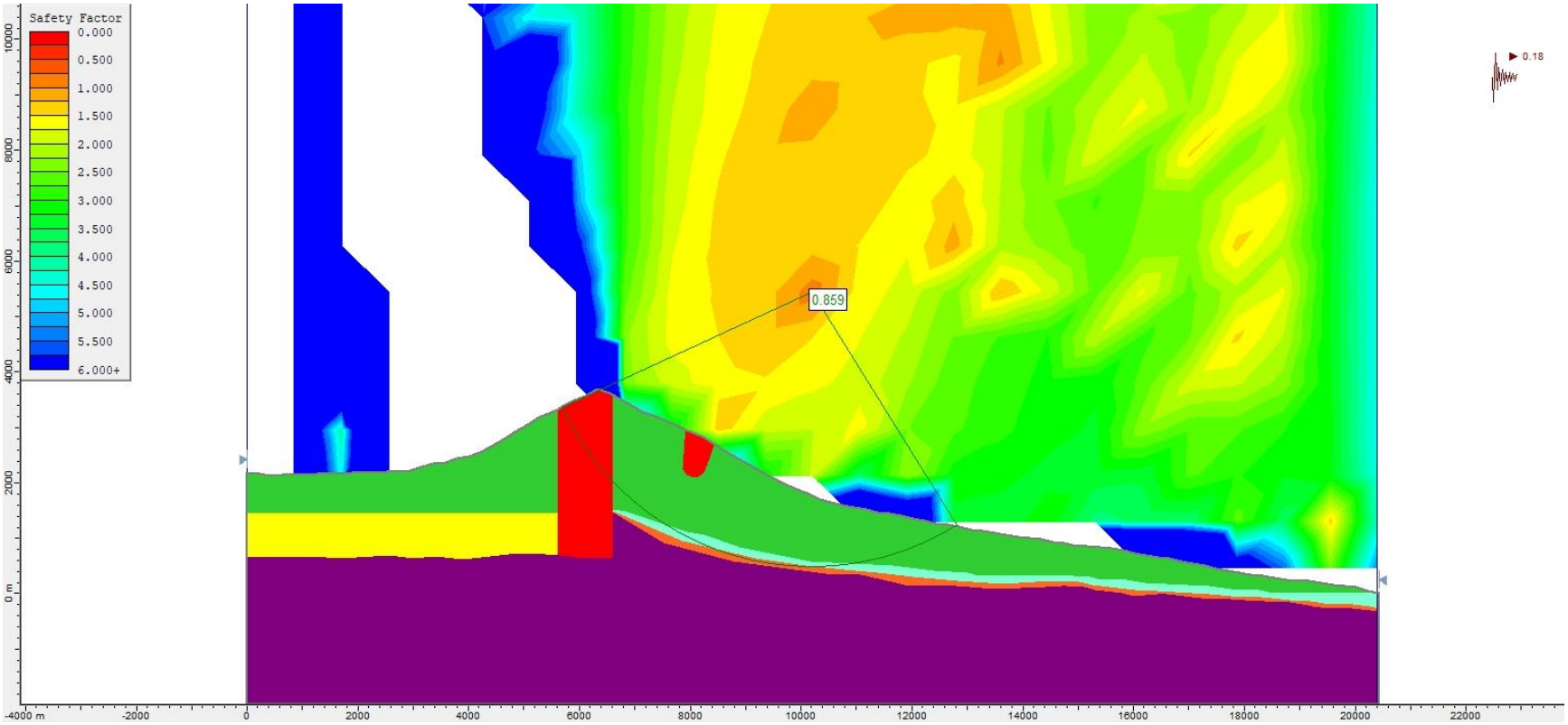

Figure S106. Slope stability pseudo-static analysis for Model 1 (with alteration zones, Figure 4a), using the Bishop simplified method and a k_h = 0.18.

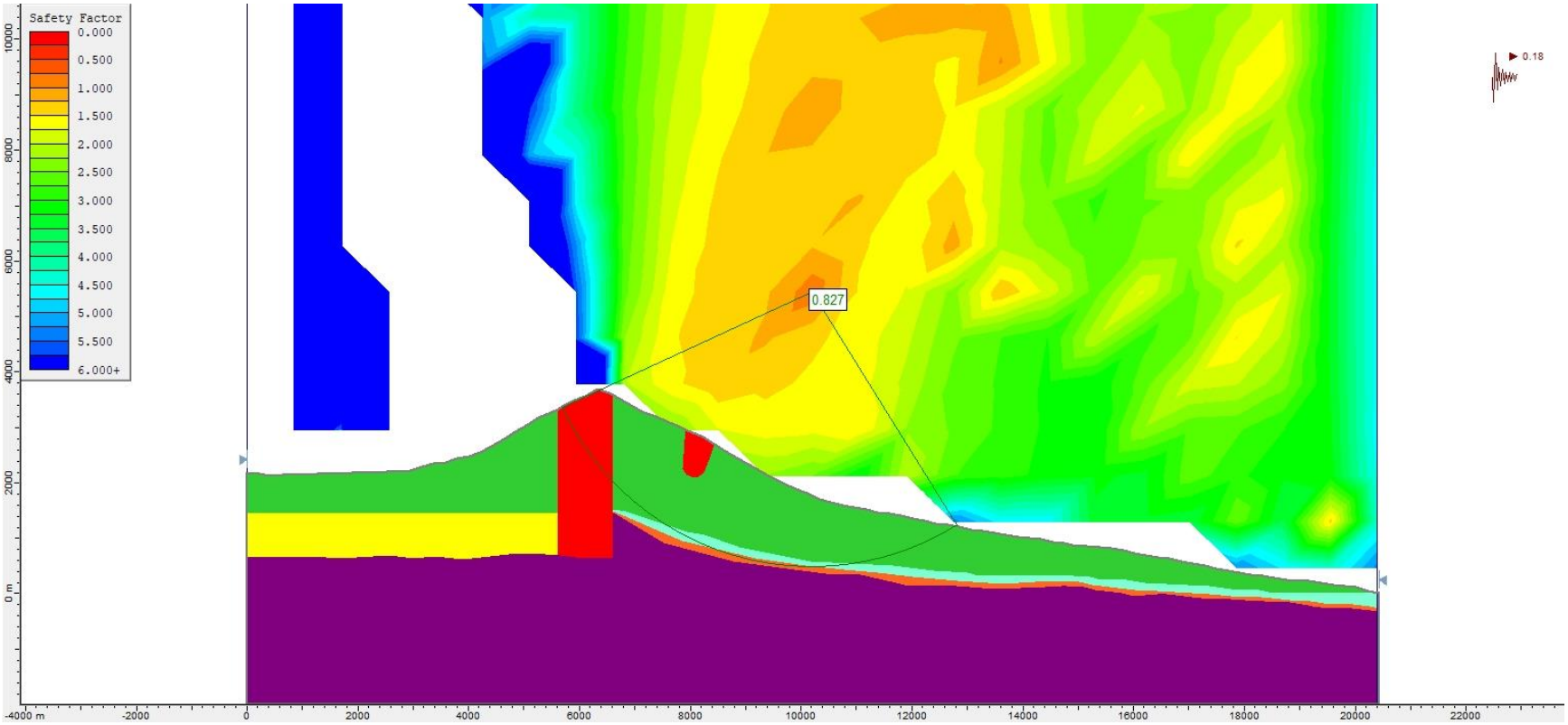

Figure S107. Slope stability pseudo-static analysis for Model 1 (with alteration zones, Figure 4a), using the Janbu Generalised method and a k_h = 0.18.

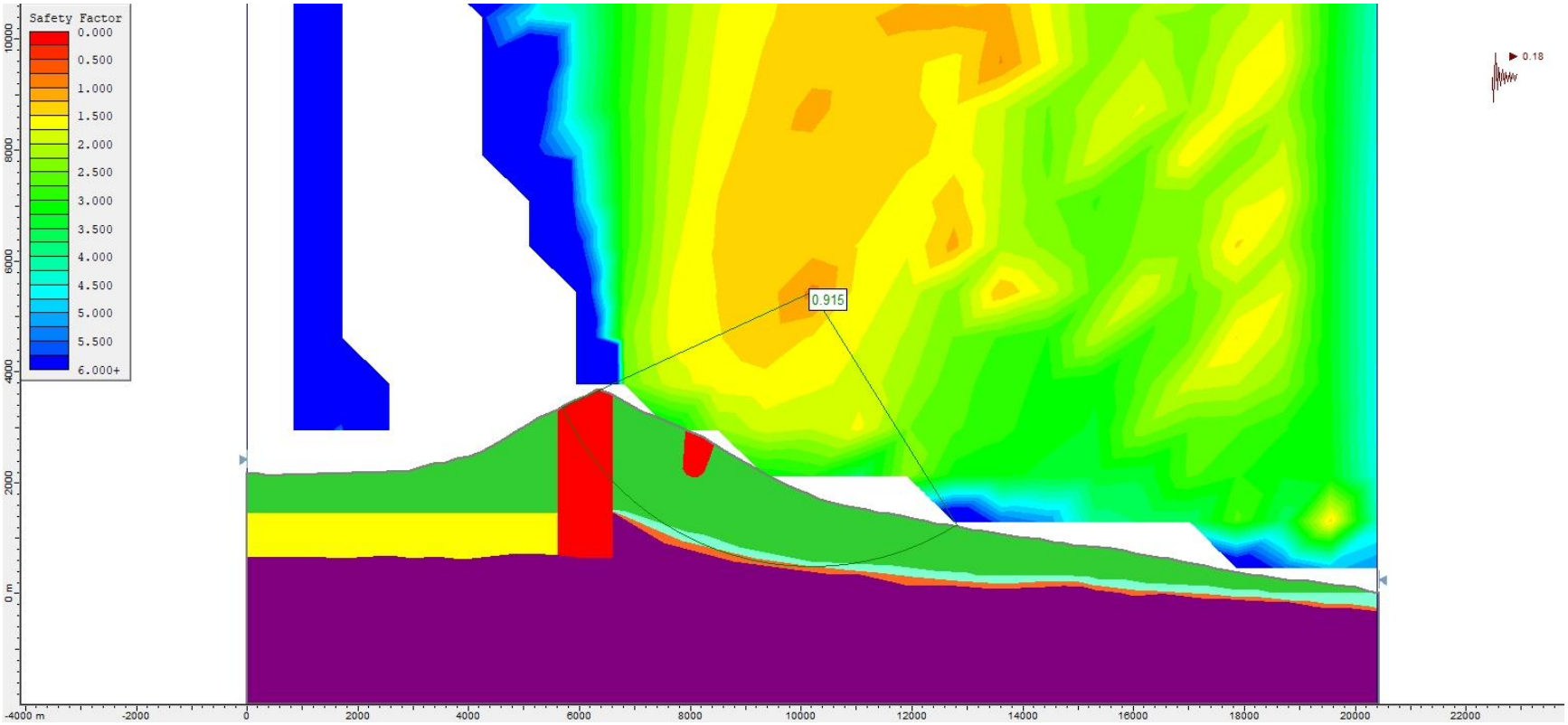

Figure S108. Slope stability pseudo-static analysis for Model 1 (with alteration zones, Figure 4a), using the Morgenstern-Price method and a k_h = 0.18.

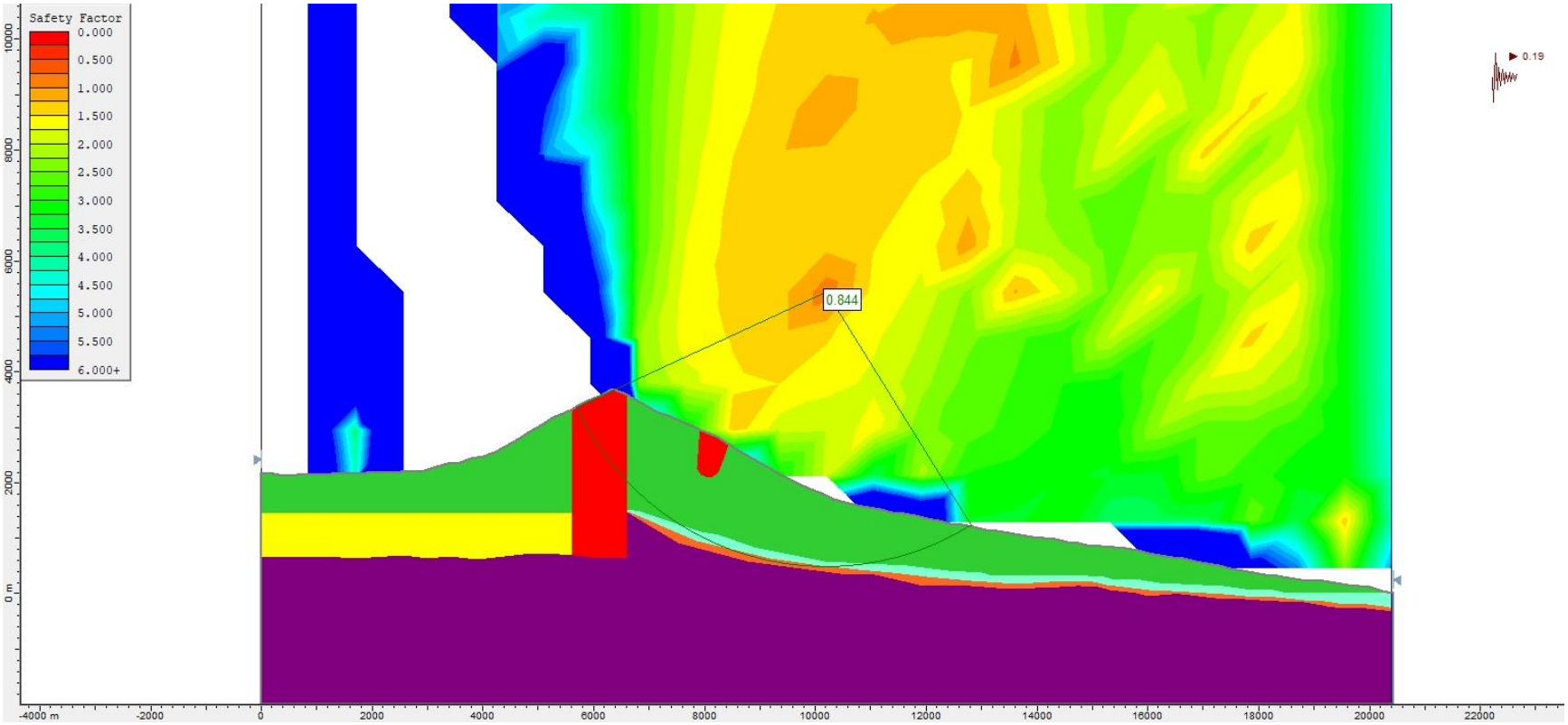

Figure S109. Slope stability pseudo-static analysis for Model 1 (with alteration zones, Figure 4a), using the Bishop simplified method and a k_h = 0.19.

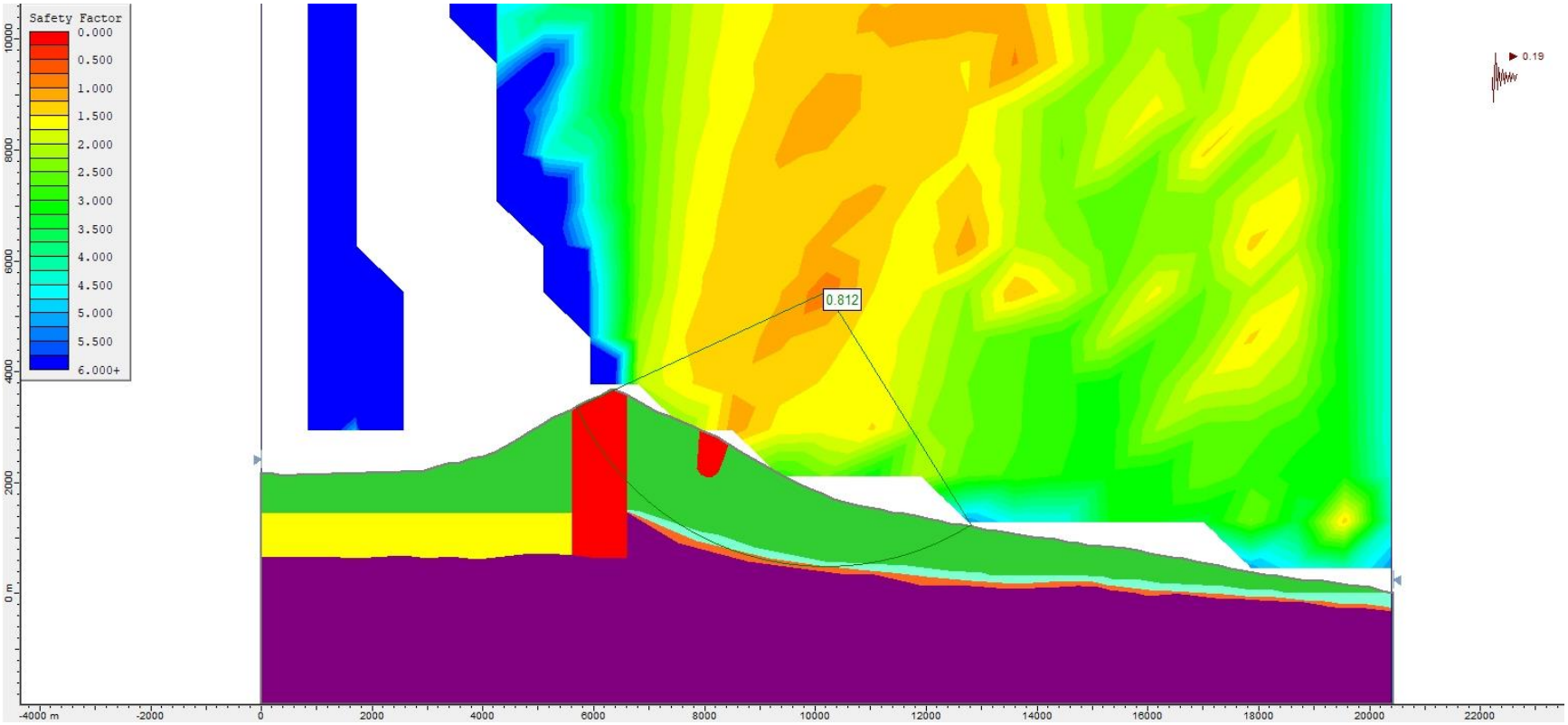

Figure S110. Slope stability pseudo-static analysis for Model 1 (with alteration zones, Figure 4a), using the Janbu Generalised method and a k_h = 0.19.

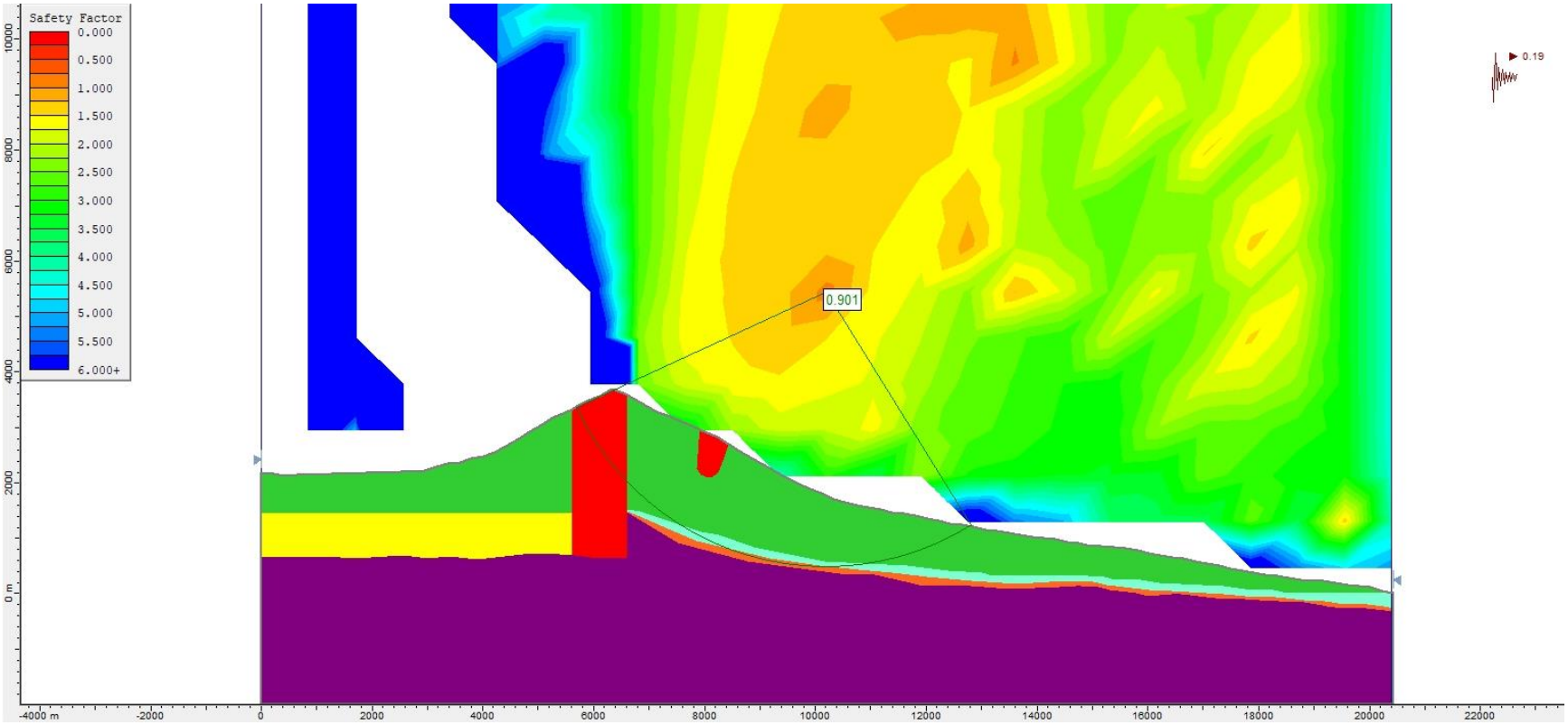

Figure S111. Slope stability pseudo-static analysis for Model 1 (with alteration zones, Figure 4a), using the Morgenstern-Price method and a k_h = 0.19.

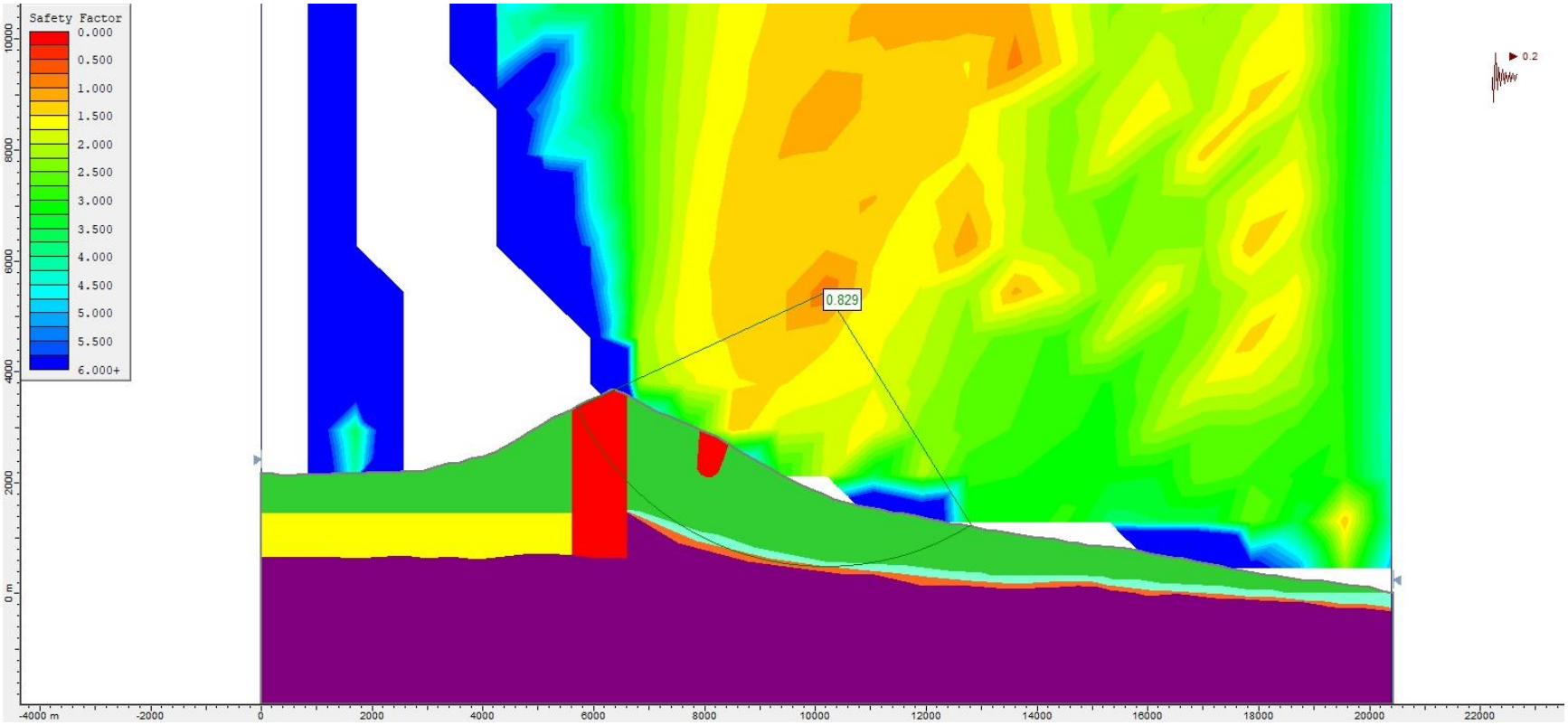

Figure S112. Slope stability pseudo-static analysis for Model 1 (with alteration zones, Figure 4a), using the Bishop simplified method and a k_h = 0.20.

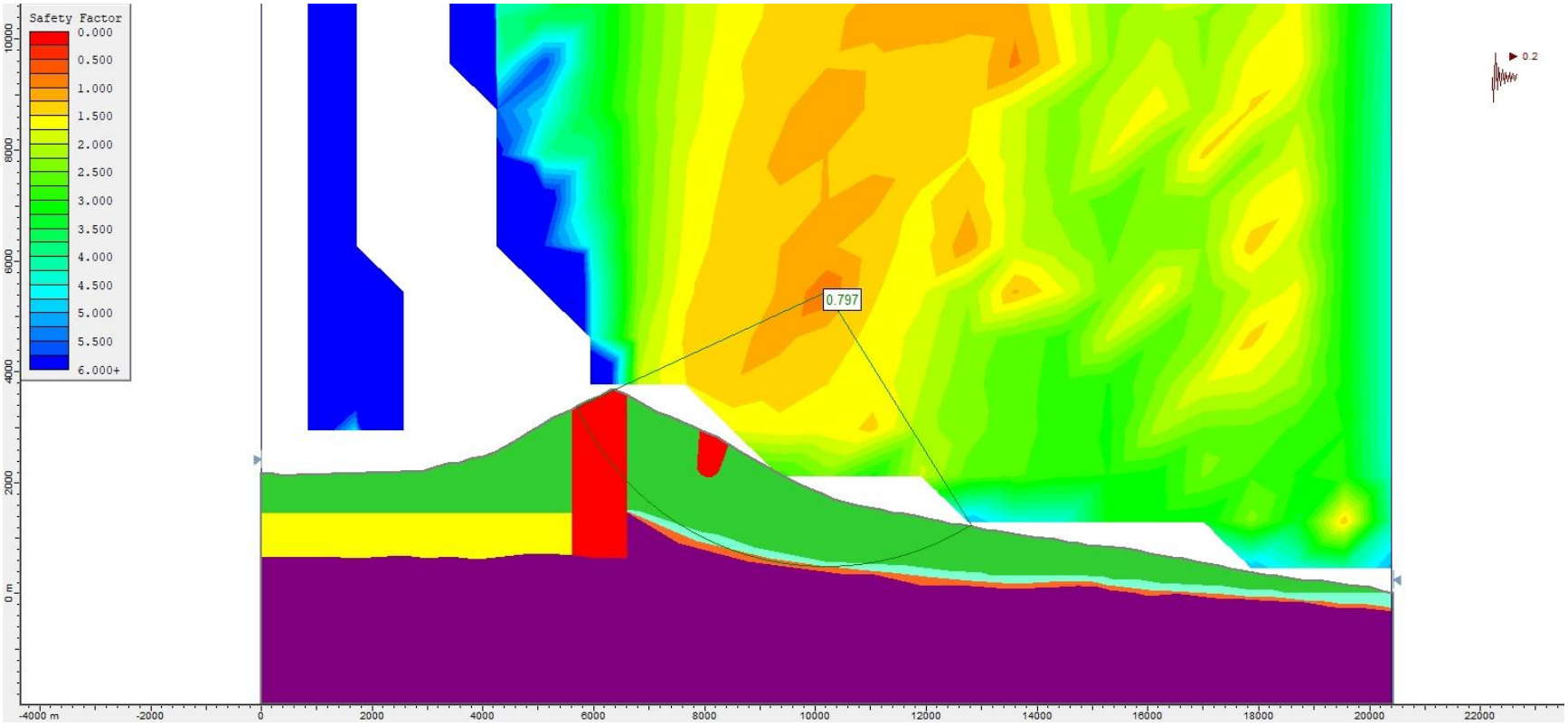

Figure S113. Slope stability pseudo-static analysis for Model 1 (with alteration zones, Figure 4a), using the Janbu Generalised method and a k_h = 0.20.

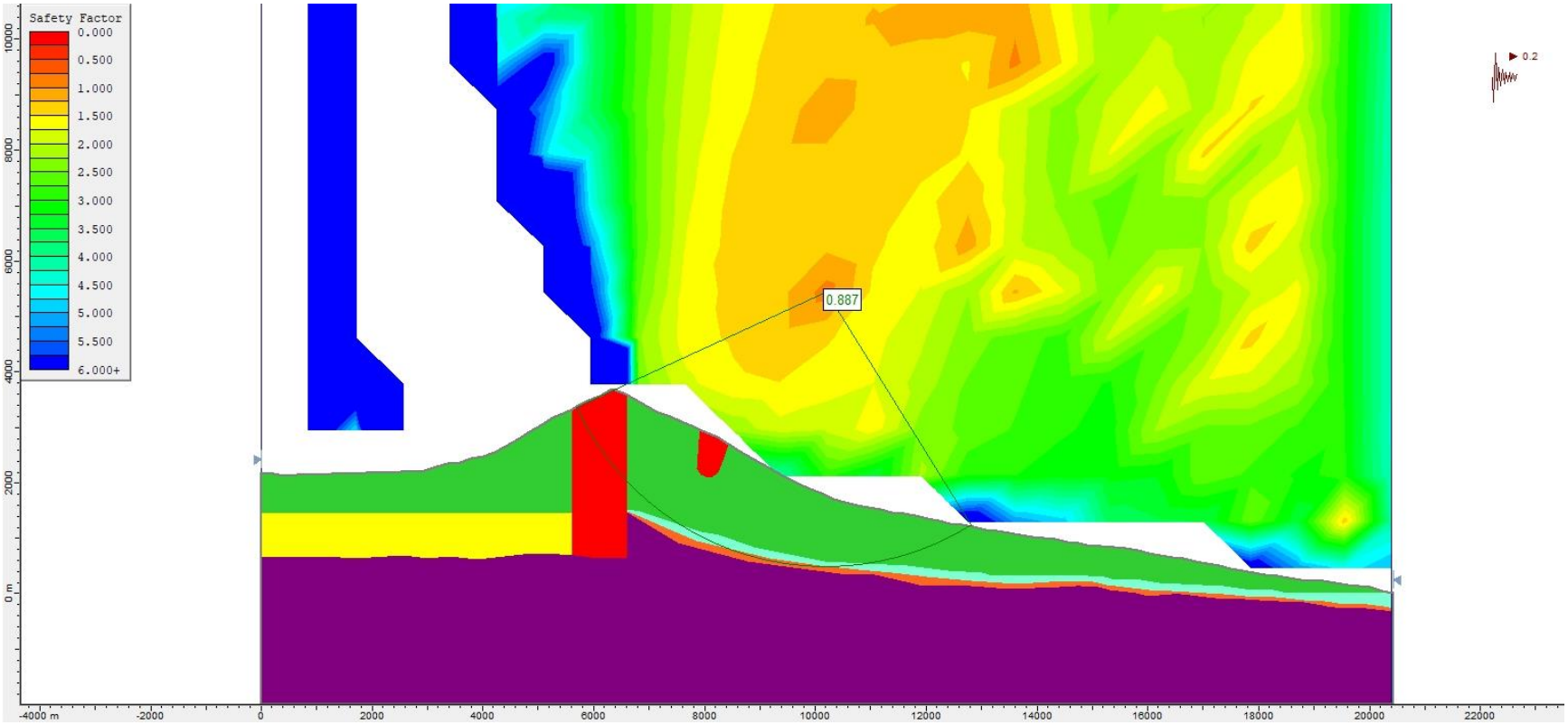

Figure S114. Slope stability pseudo-static analysis for Model 1 (with alteration zones, Figure 4a), using the Morgenstern-Price method and a k_h = 0.20.

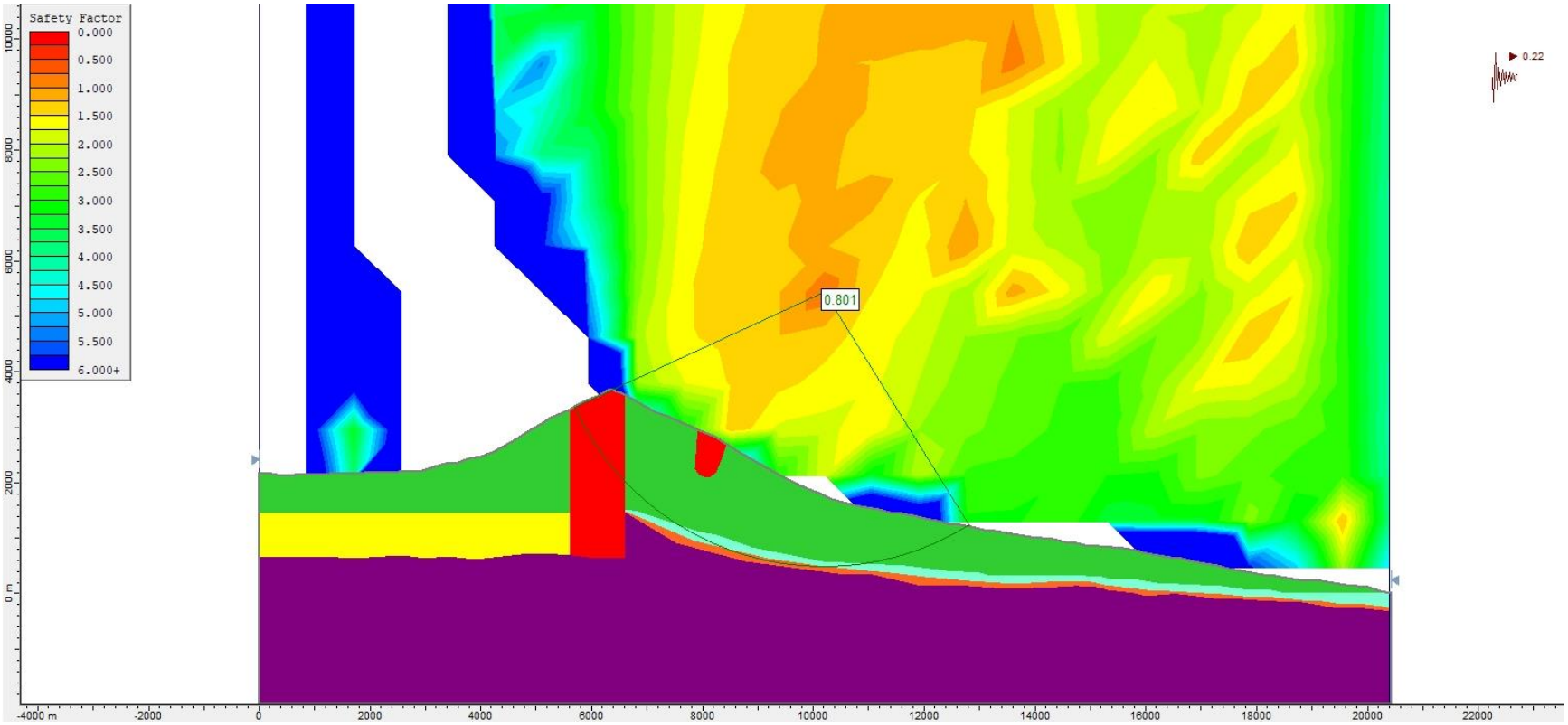

Figure S115. Slope stability pseudo-static analysis for Model 1 (with alteration zones, Figure 4a), using the Bishop simplified method and a k_h = 0.22.

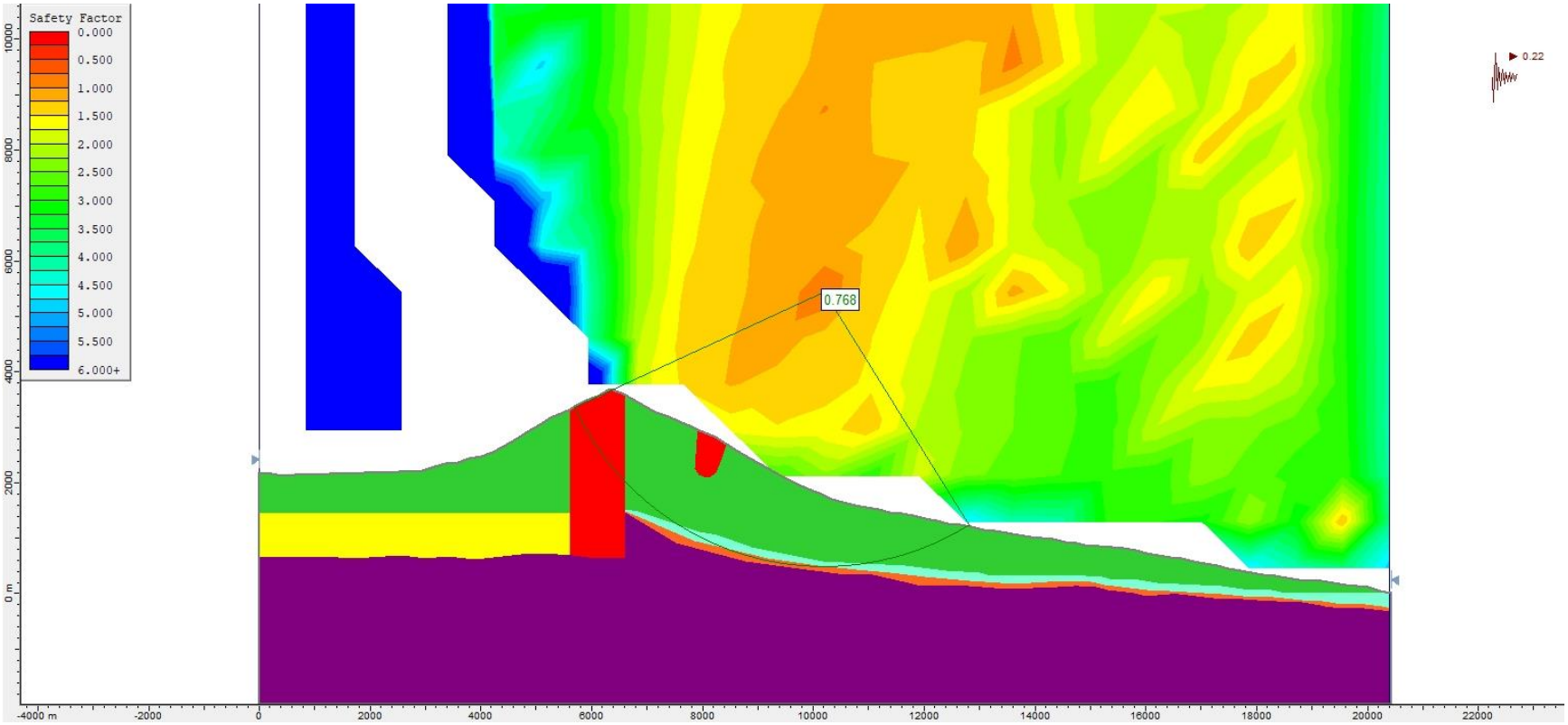

Figure S116. Slope stability pseudo-static analysis for Model 1 (with alteration zones, Figure 4a), using the Janbu Generalised method and a k_h = 0.22.

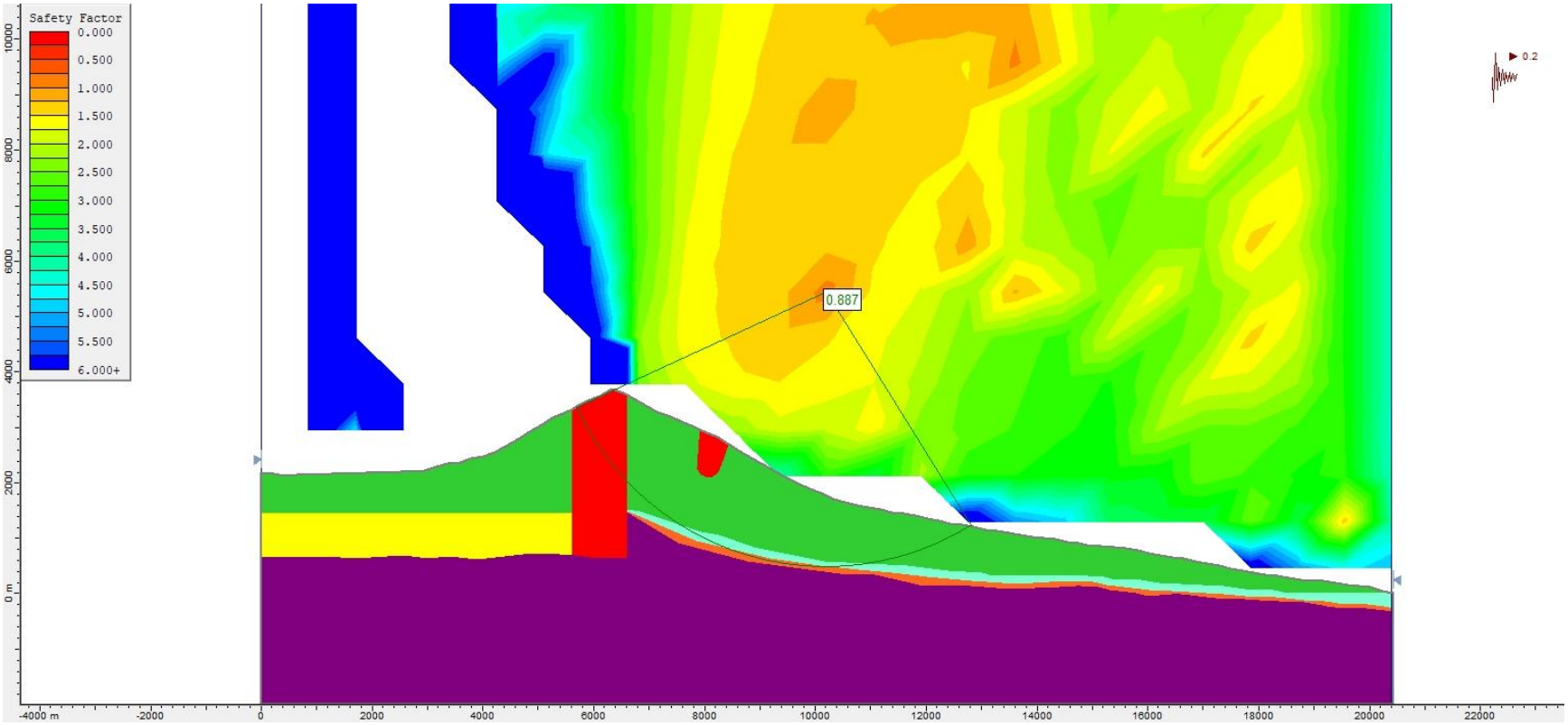

Figure S117. Slope stability pseudo-static analysis for Model 1 (with alteration zones, Figure 4a), using the Morgenstern-Price method and a k_h = 0.22.

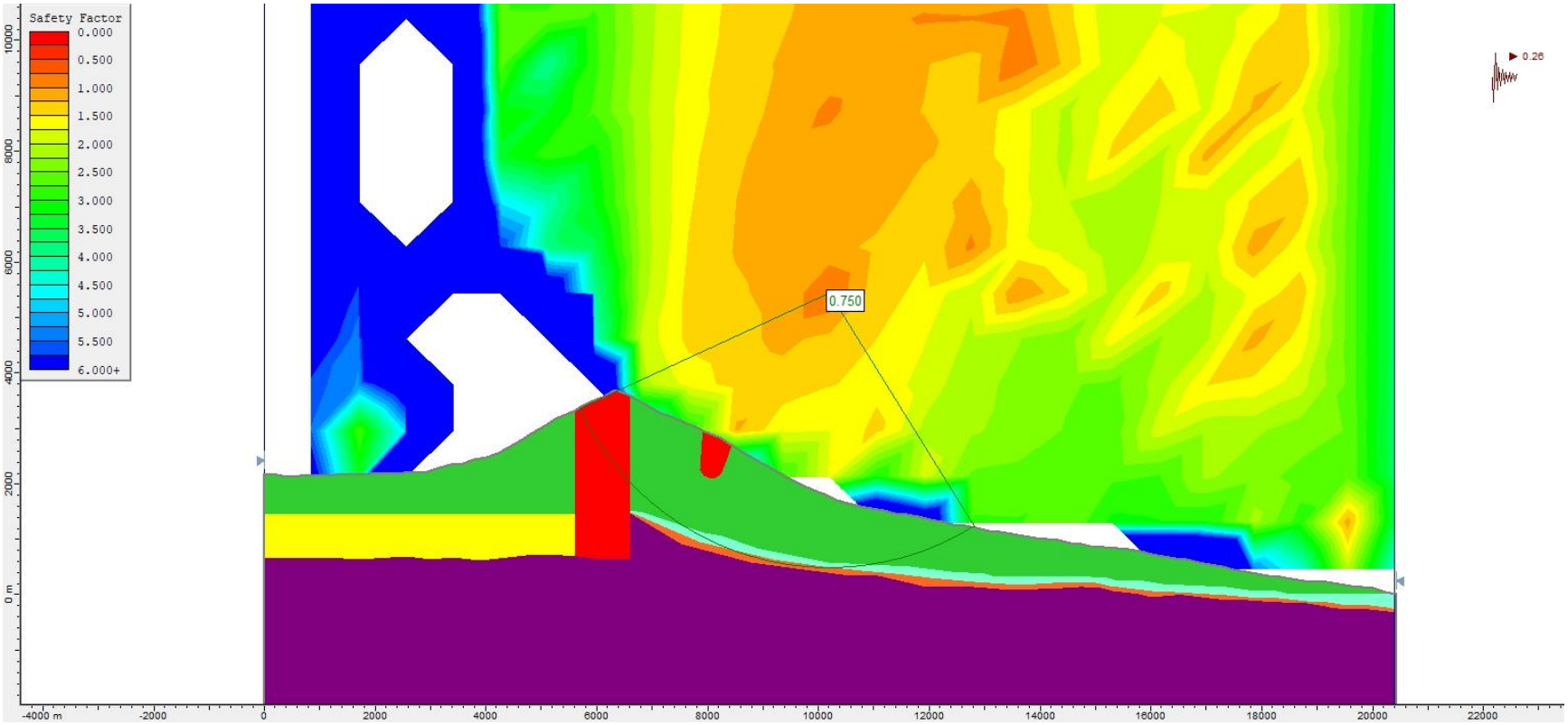

Figure S118. Slope stability pseudo-static analysis for Model 1 (with alteration zones, Figure 4a), using the Bishop simplified method and a k_h = 0.26.

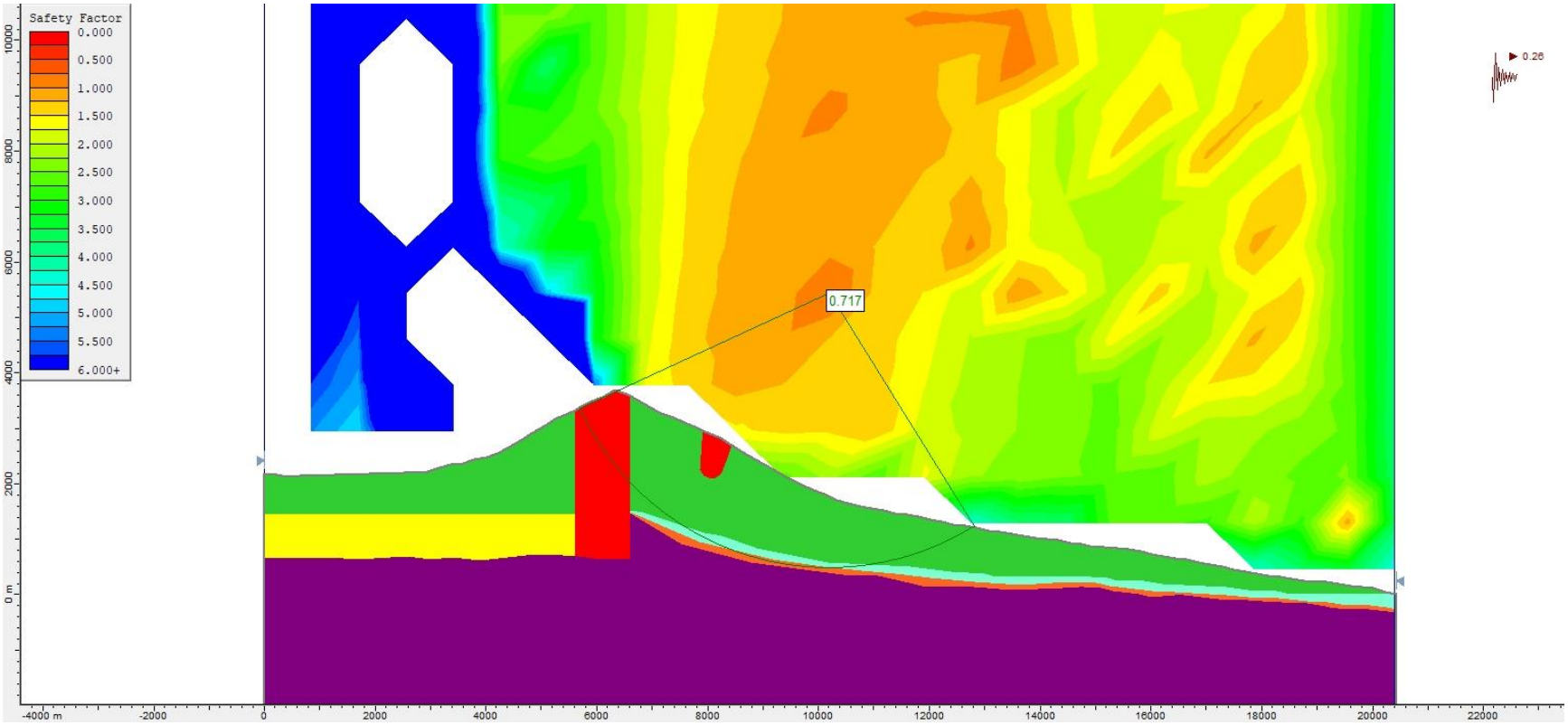

Figure S119. Slope stability pseudo-static analysis for Model 1 (with alteration zones, Figure 4a), using the Janbu Generalised method and a k_h = 0.26.

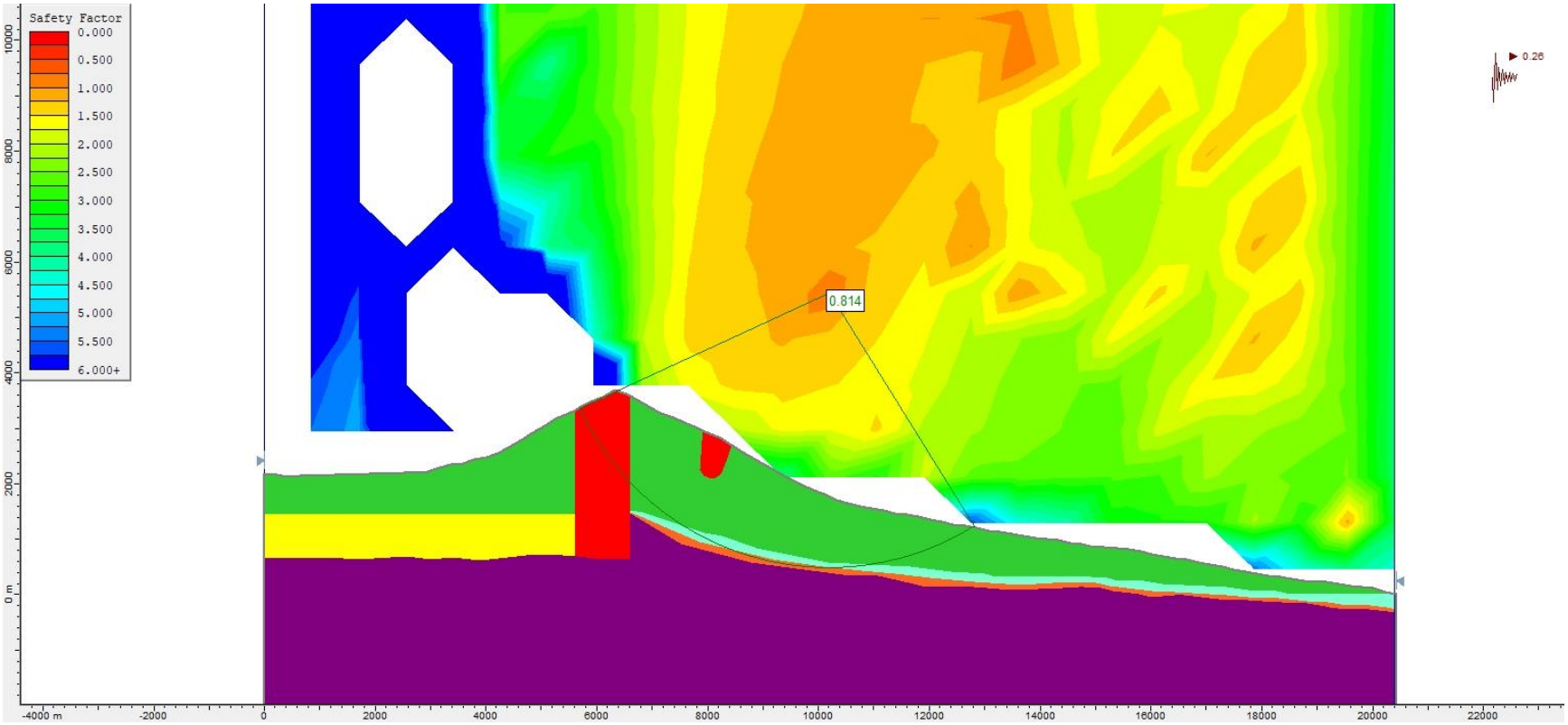

Figure S120. Slope stability pseudo-static analysis for Model 1 (with alteration zones, Figure 4a), using the Morgenstern-Price method and a k_h = 0.26.

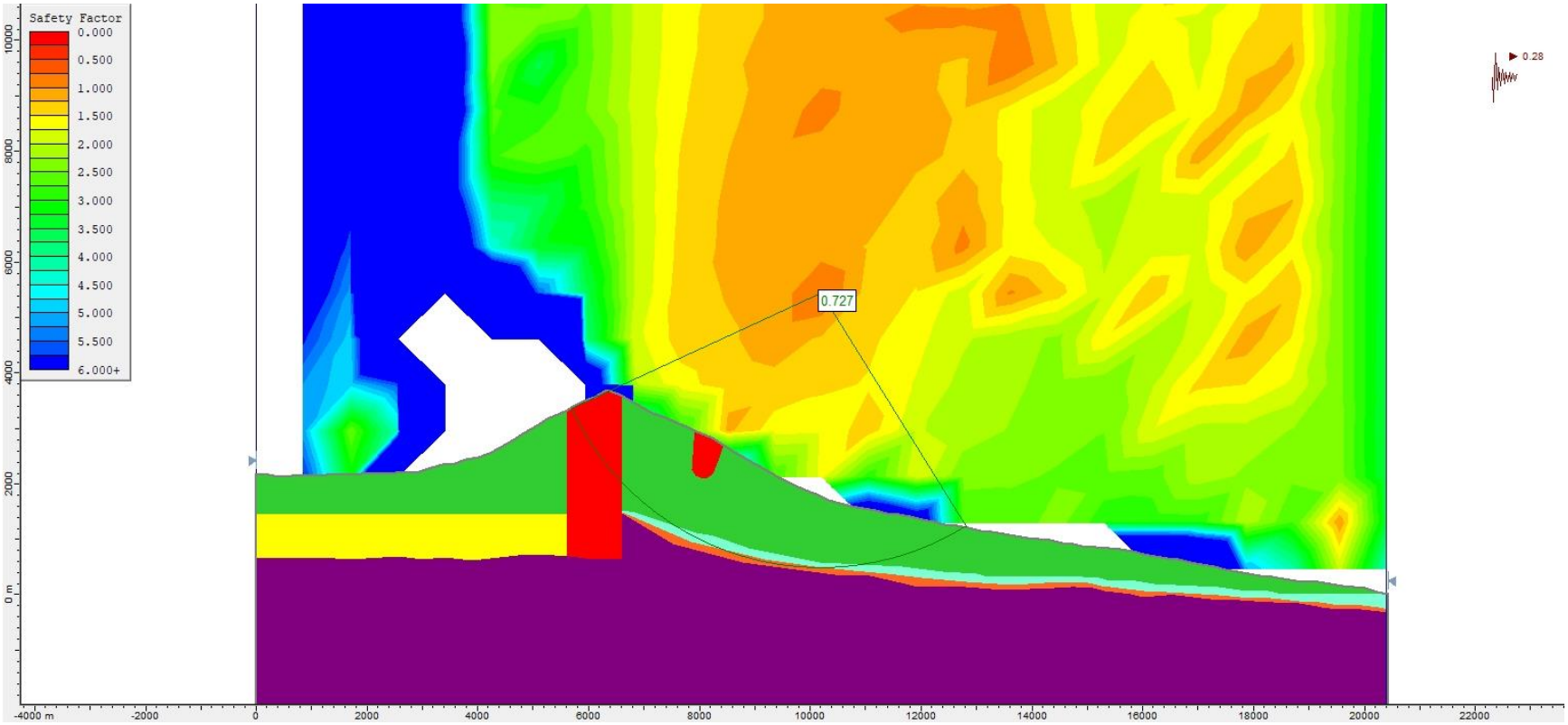

Figure S121. Slope stability pseudo-static analysis for Model 1 (with alteration zones, Figure 4a), using the Bishop simplified method and a k_h = 0.28.

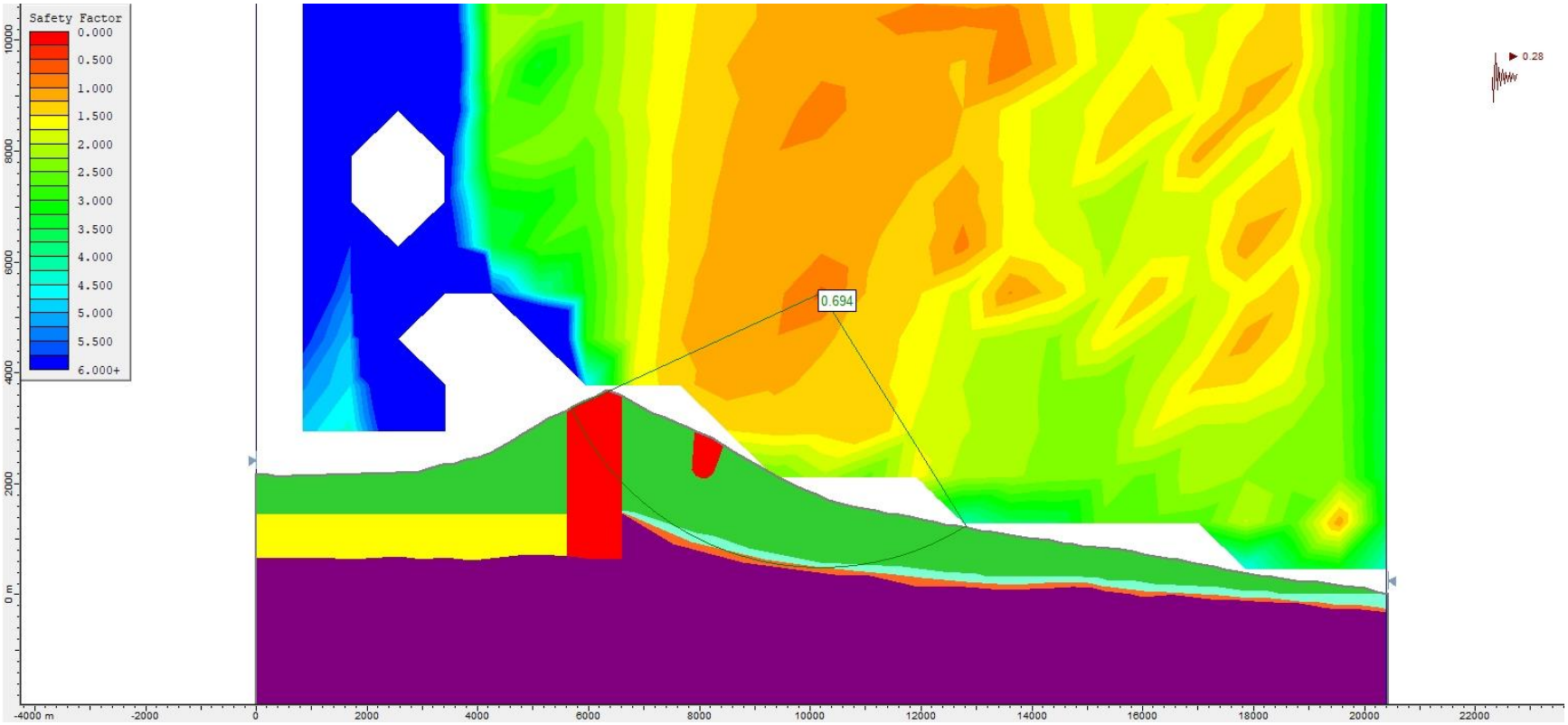

Figure S122. Slope stability pseudo-static analysis for Model 1 (with alteration zones, Figure 4a), using the Janbu Generalised method and a k_h = 0.28.

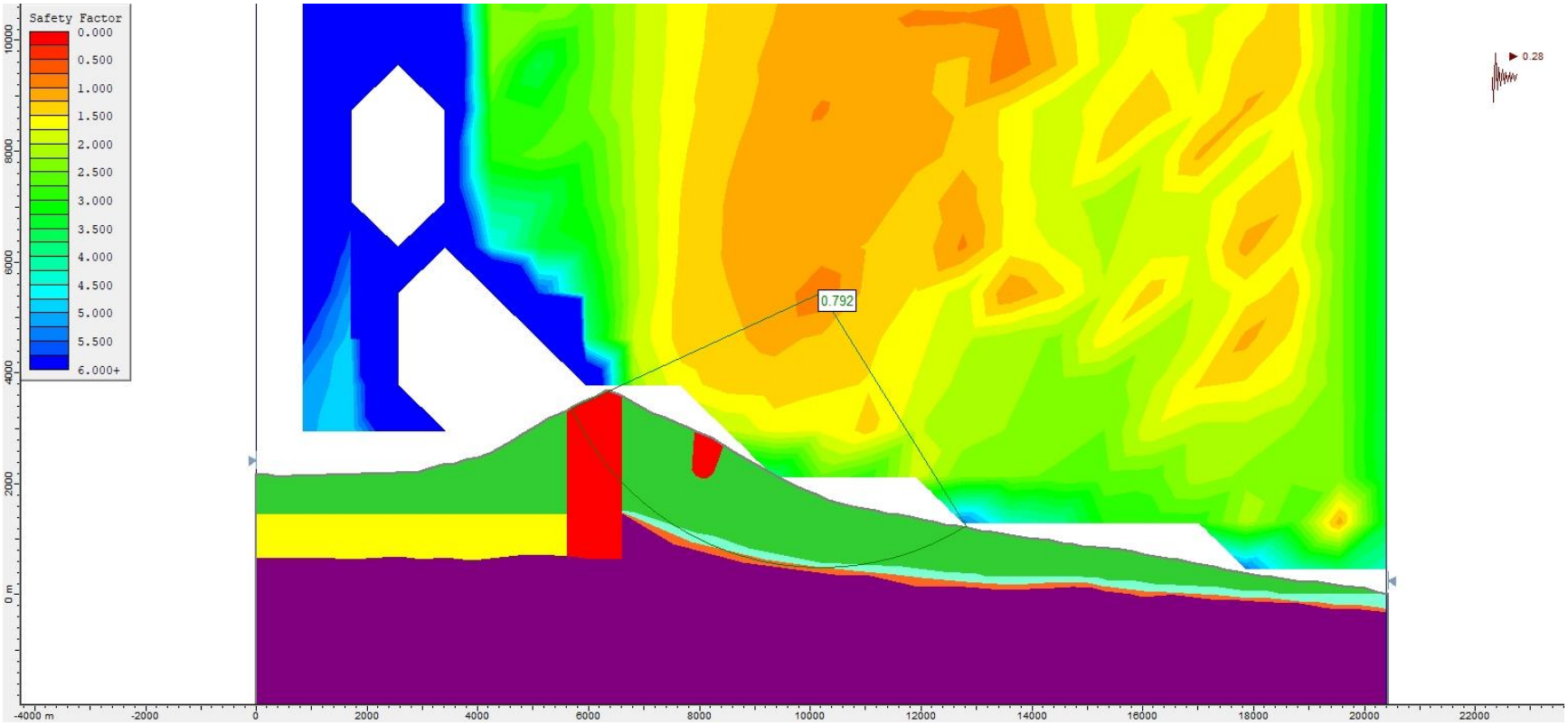

Figure S123. Slope stability pseudo-static analysis for Model 1 (with alteration zones, Figure 4a), using the Morgenstern-Price method and a k_h = 0.28.

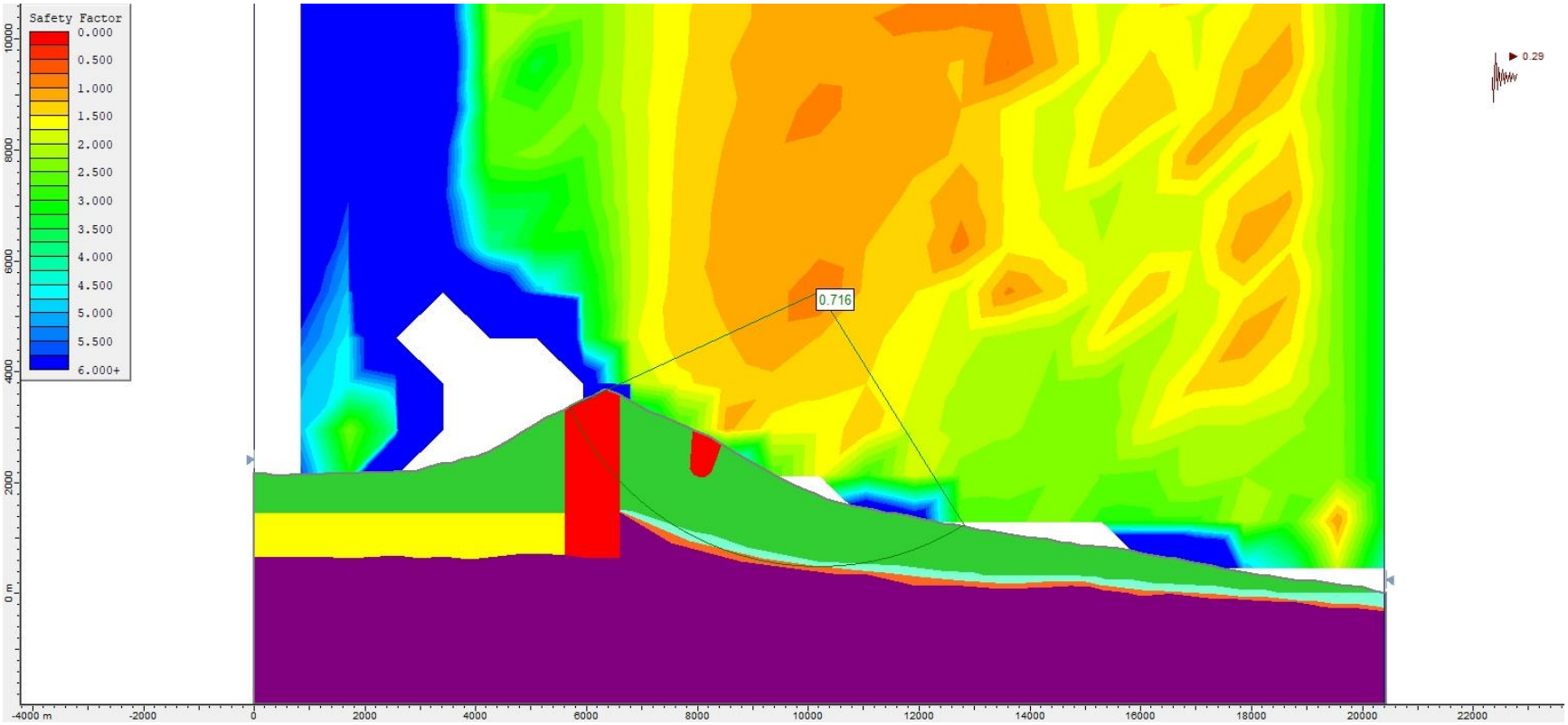

Figure S124. Slope stability pseudo-static analysis for Model 1 (with alteration zones, Figure 4a), using the Bishop simplified method and a k_h = 0.29.

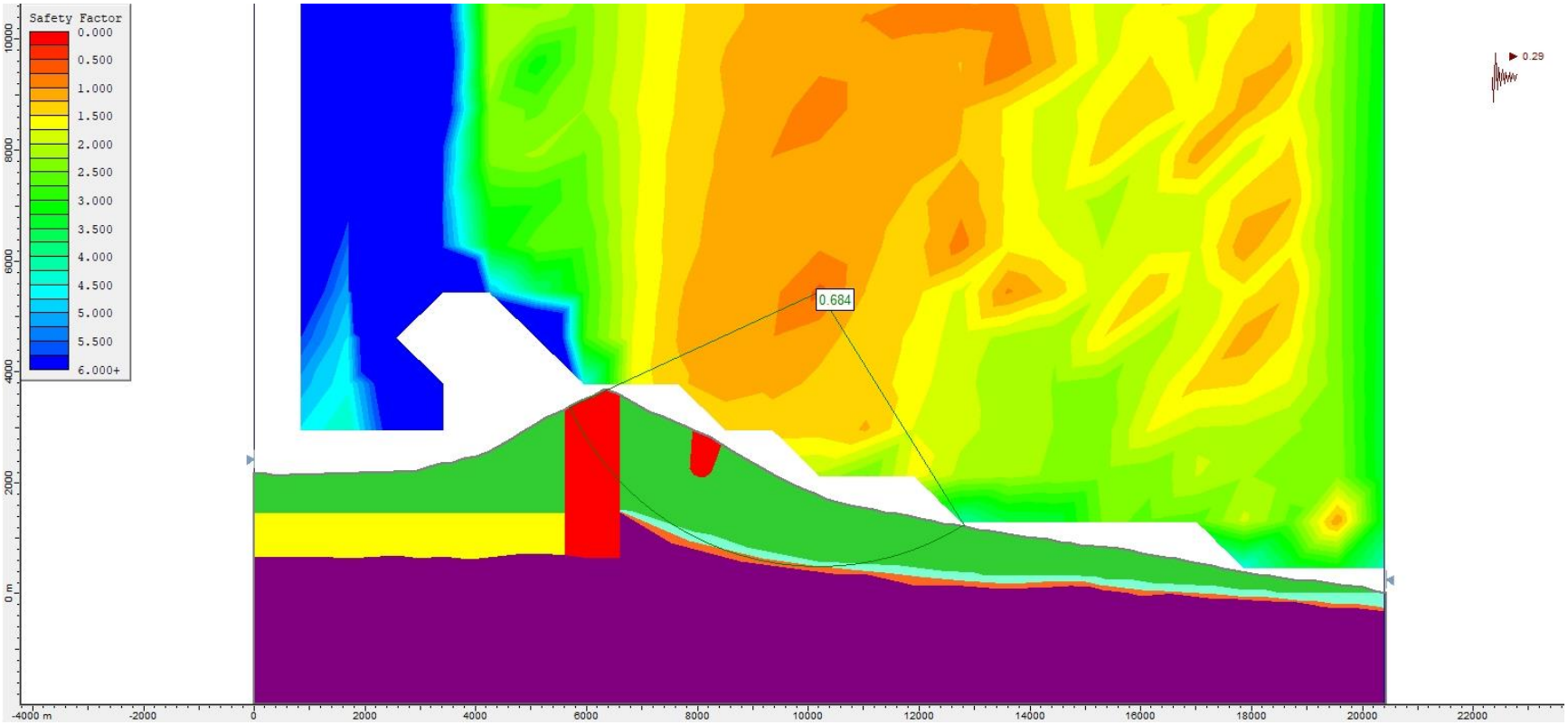

Figure S125. Slope stability pseudo-static analysis for Model 1 (with alteration zones, Figure 4a), using the Janbu Generalised method and a k_h = 0.29.

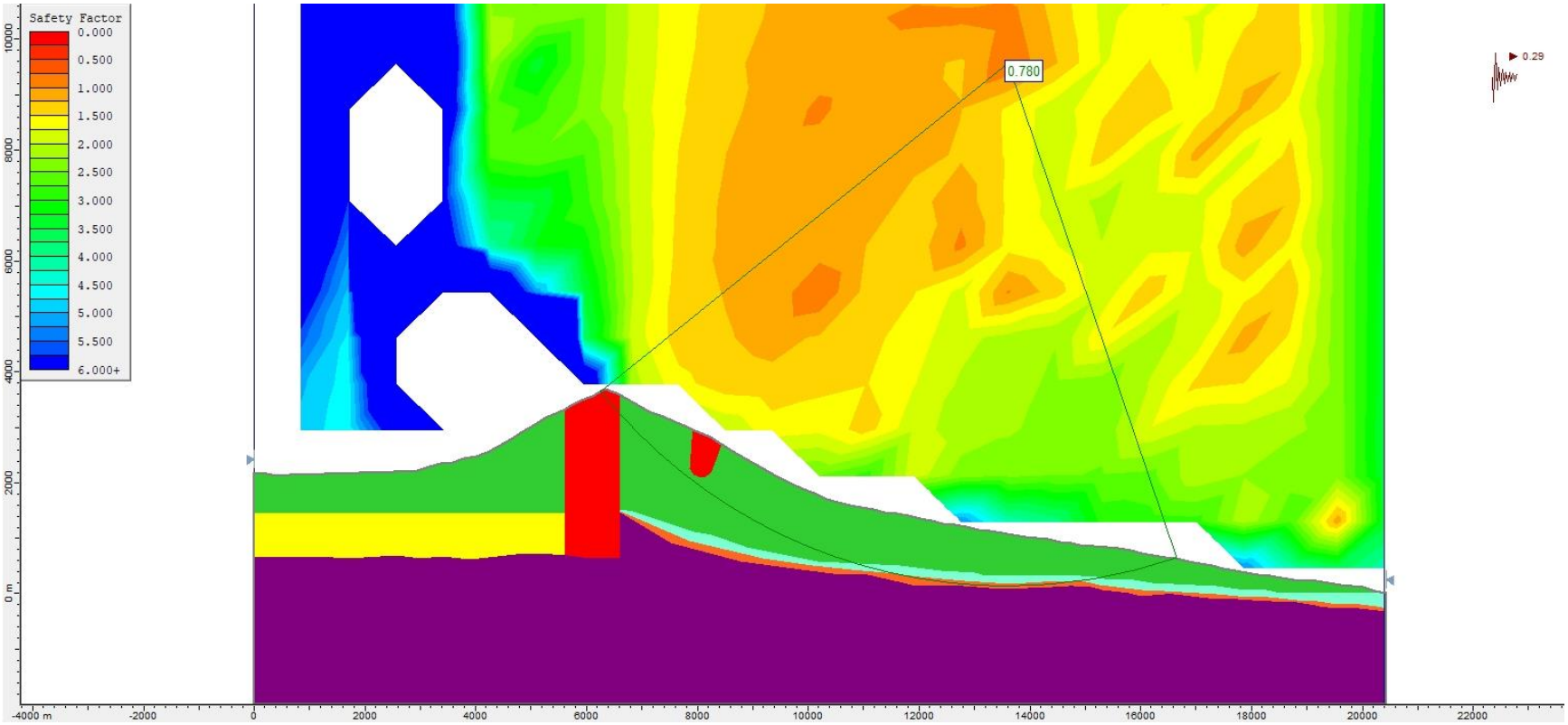

Figure S126. Slope stability pseudo-static analysis for Model 1 (with alteration zones, Figure 4a), using the Morgenstern-Price method and a k_h = 0.29.

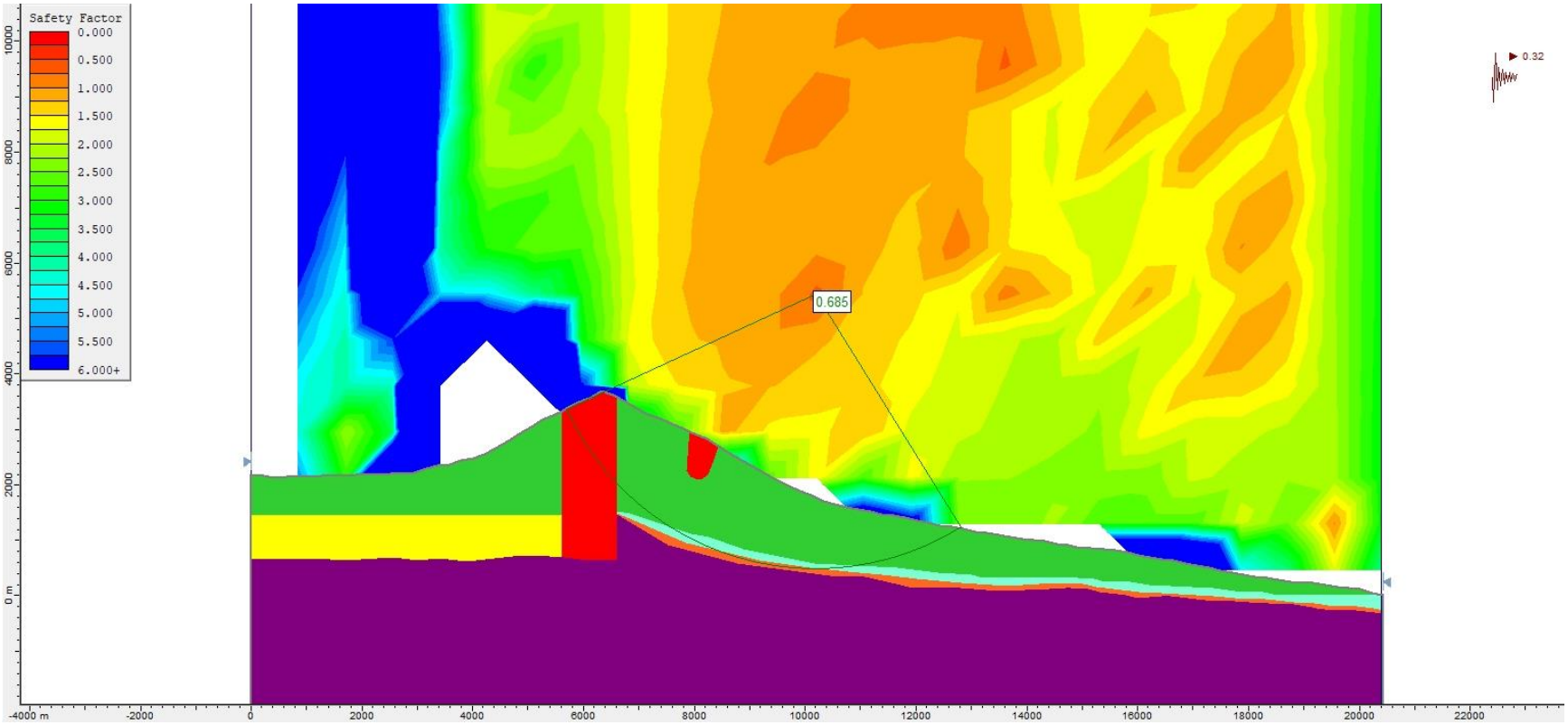

Figure S127. Slope stability pseudo-static analysis for Model 1 (with alteration zones, Figure 4a), using the Bishop simplified method and a k_h = 0.32.

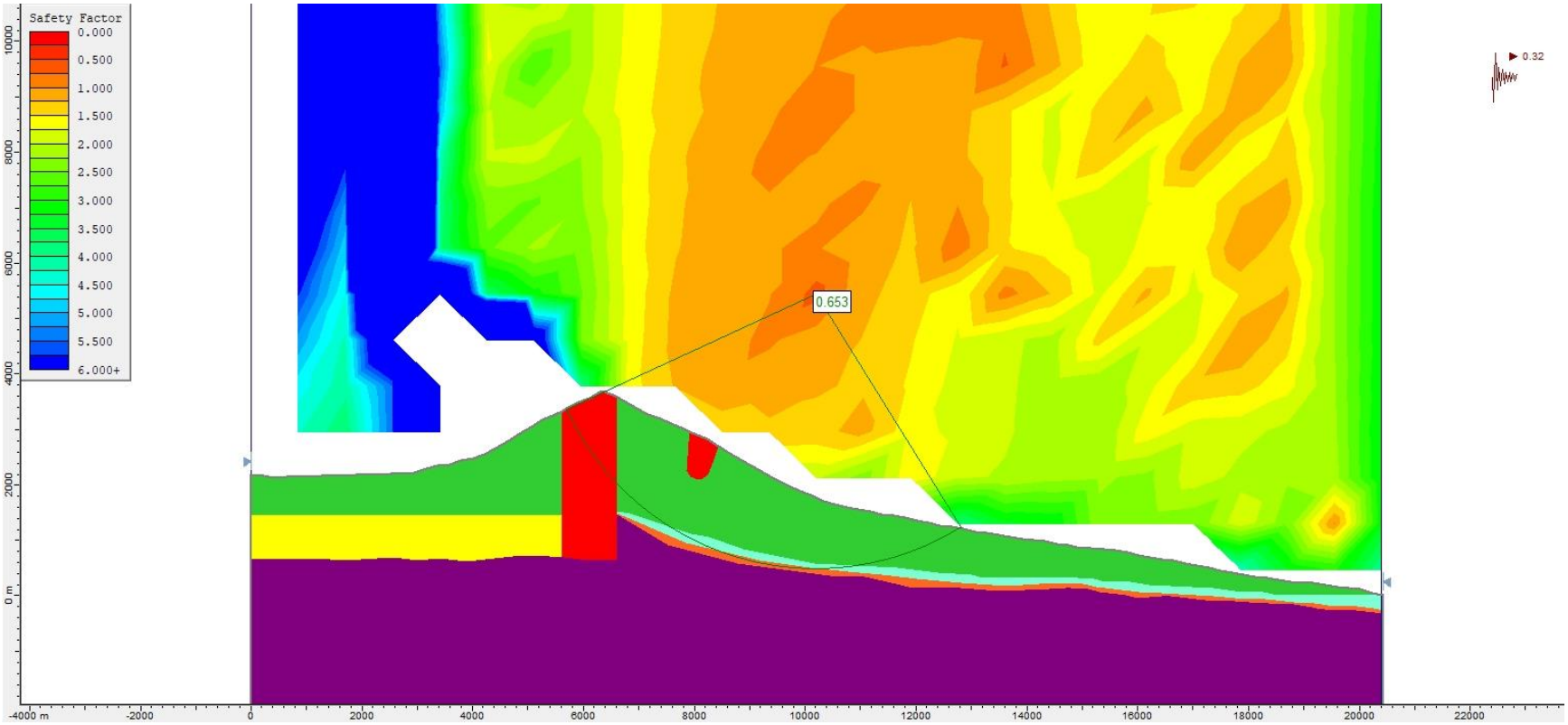

Figure S128. Slope stability pseudo-static analysis for Model 1 (with alteration zones, Figure 4a), using the Janbu Generalised method and a k_h = 0.32.

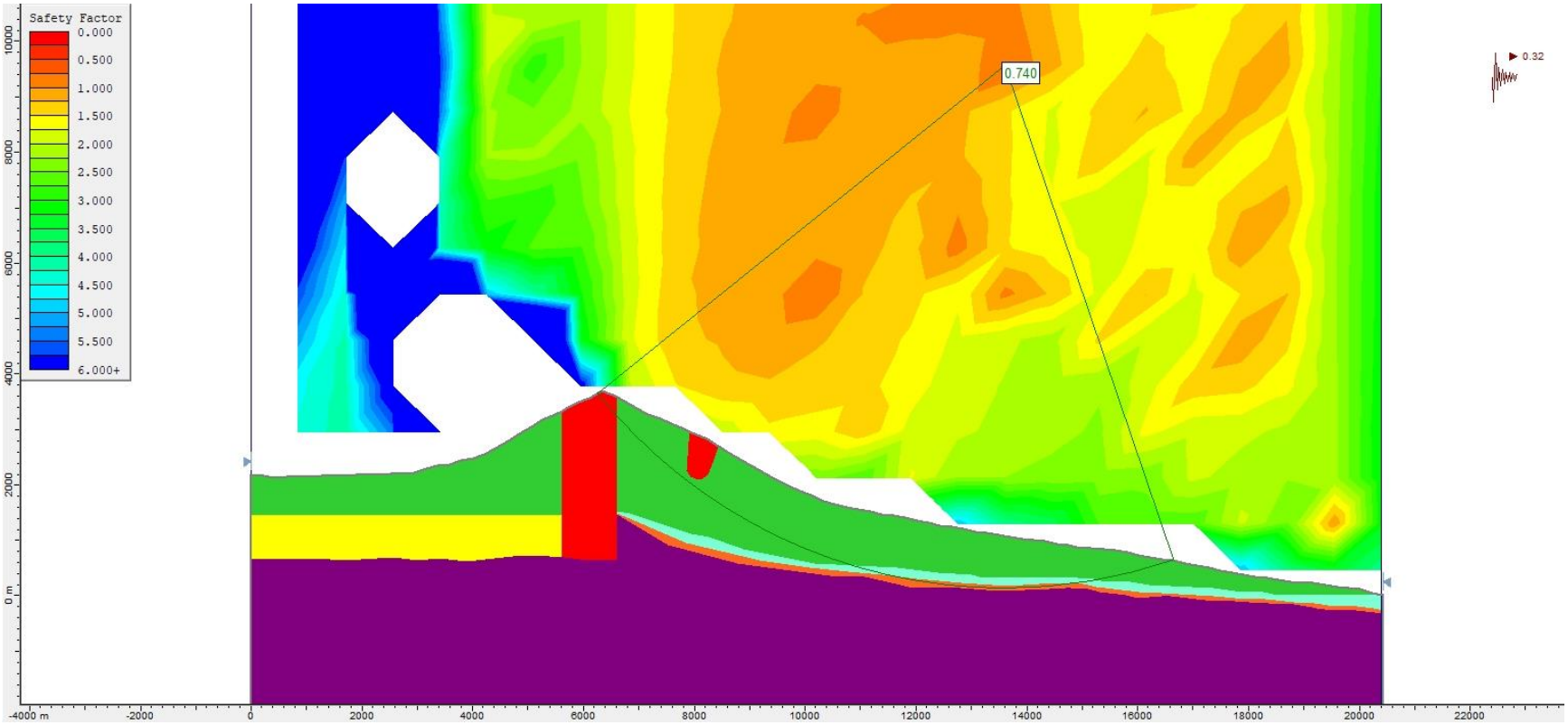

Figure S129. Slope stability pseudo-static analysis for Model 1 (with alteration zones, Figure 4a), using the Morgenstern-Price method and a k_h = 0.32.

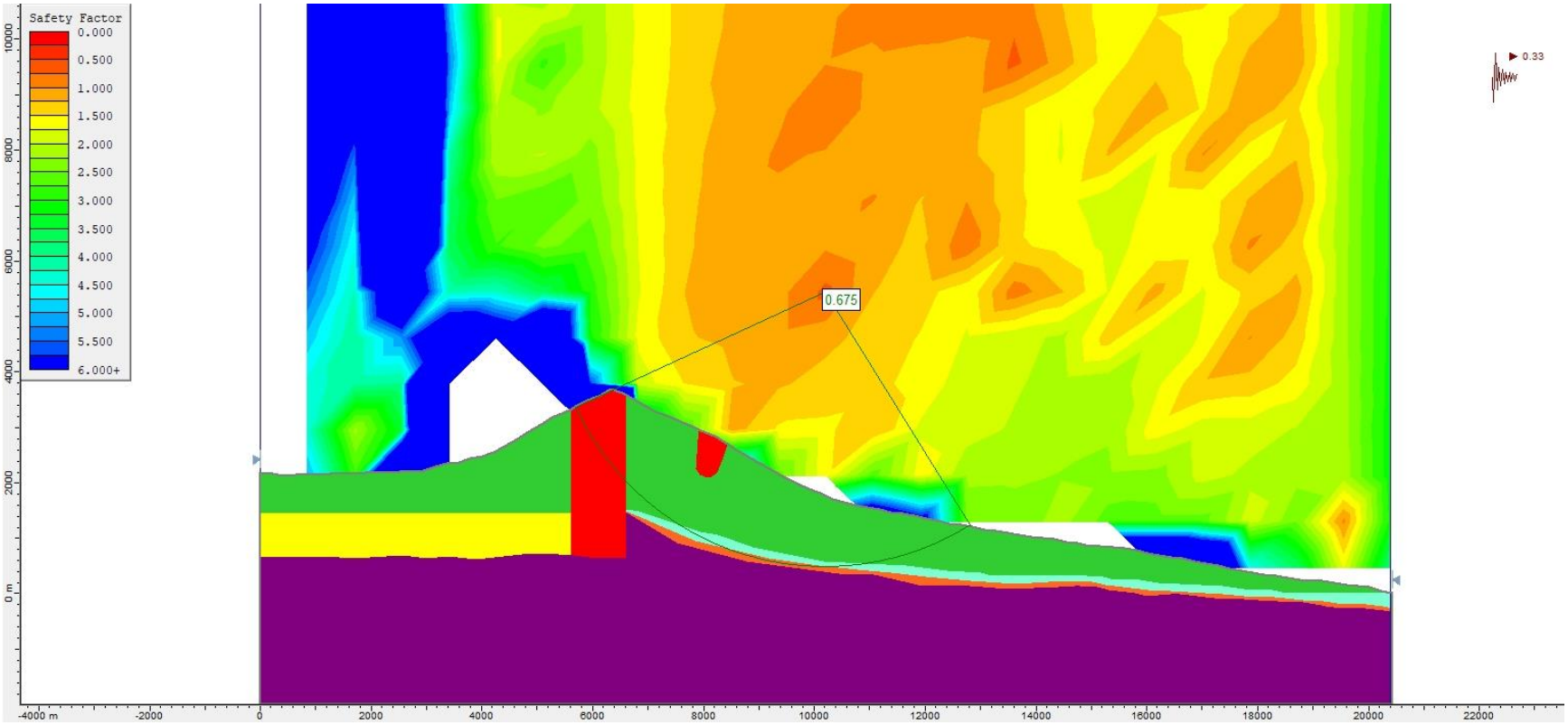

Figure S130. Slope stability pseudo-static analysis for Model 1 (with alteration zones, Figure 4a), using the Bishop simplified method and a k_h = 0.33.

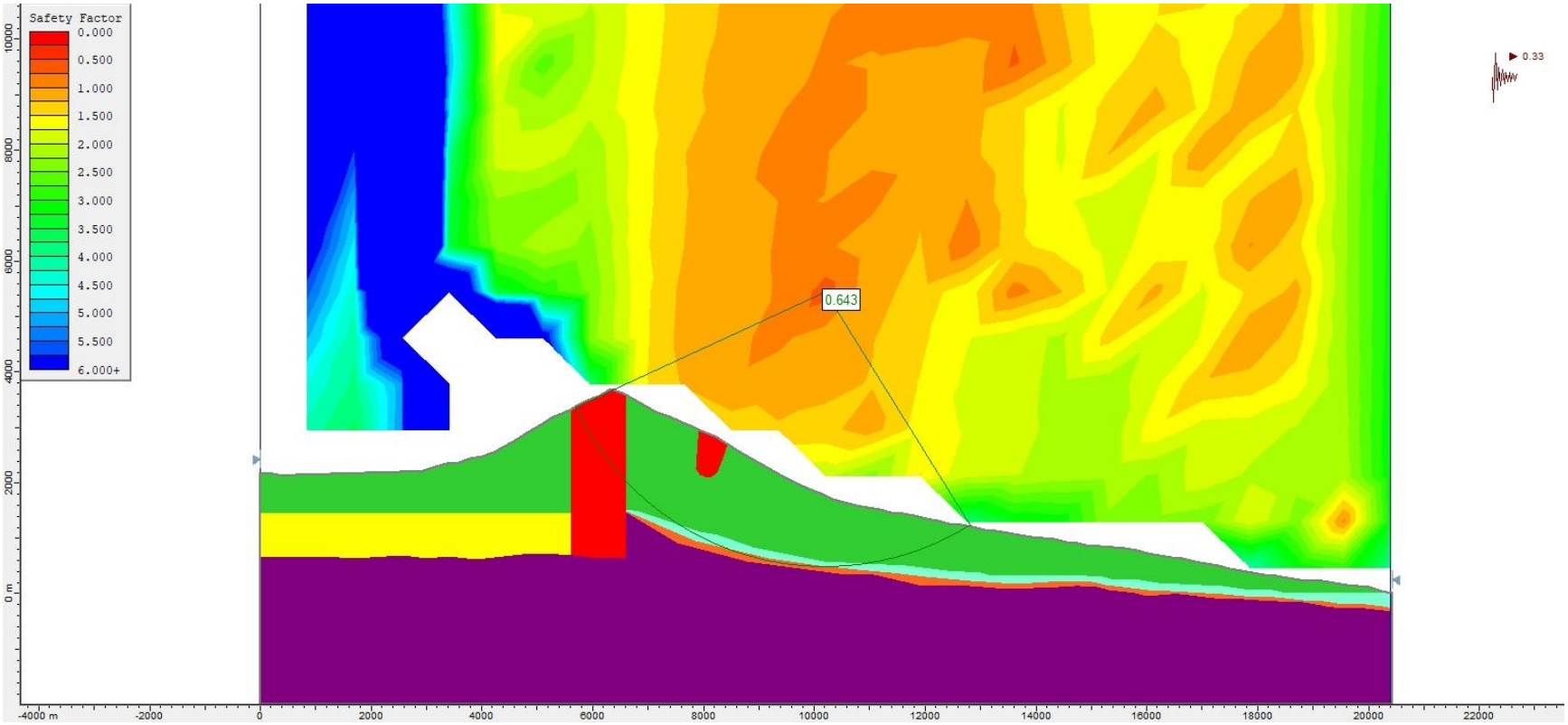

Figure S131. Slope stability pseudo-static analysis for Model 1 (with alteration zones, Figure 4a), using the Janbu Generalised method and a k_h = 0.33.

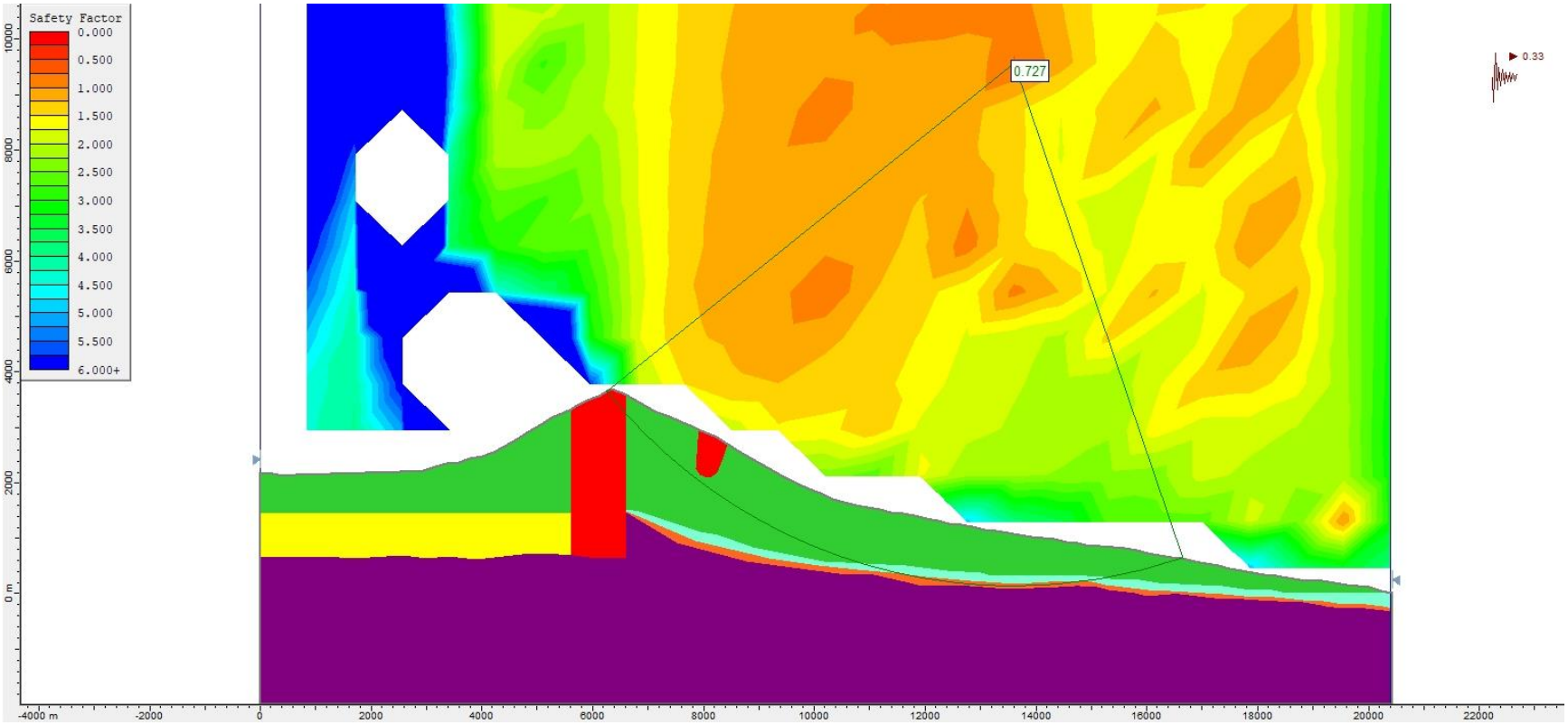

Figure S132. Slope stability pseudo-static analysis for Model 1 (with alteration zones, Figure 4a), using the Morgenstern-Price method and a k_h = 0.33.

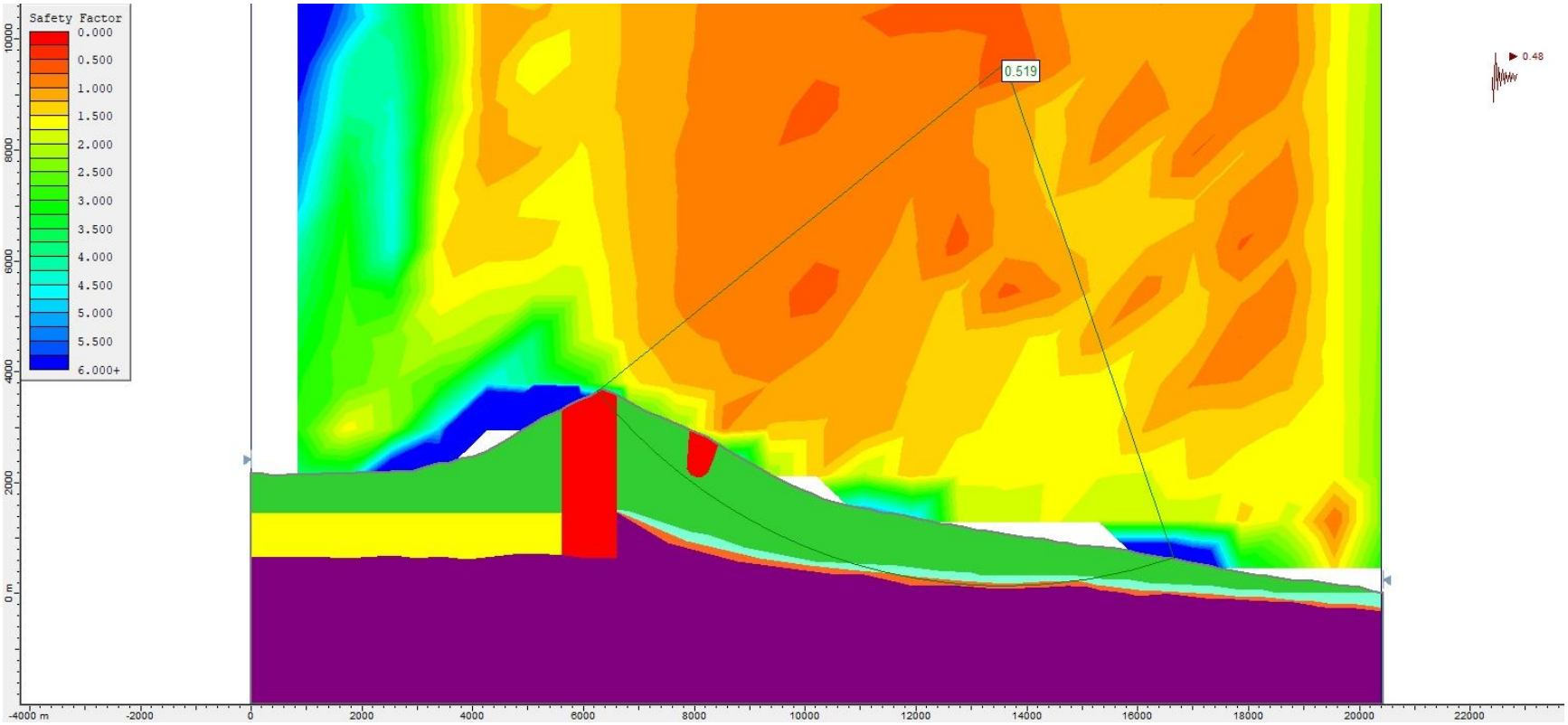

Figure S133. Slope stability pseudo-static analysis for Model 1 (with alteration zones, Figure 4a), using the Bishop simplified method and a k_h = 0.48.

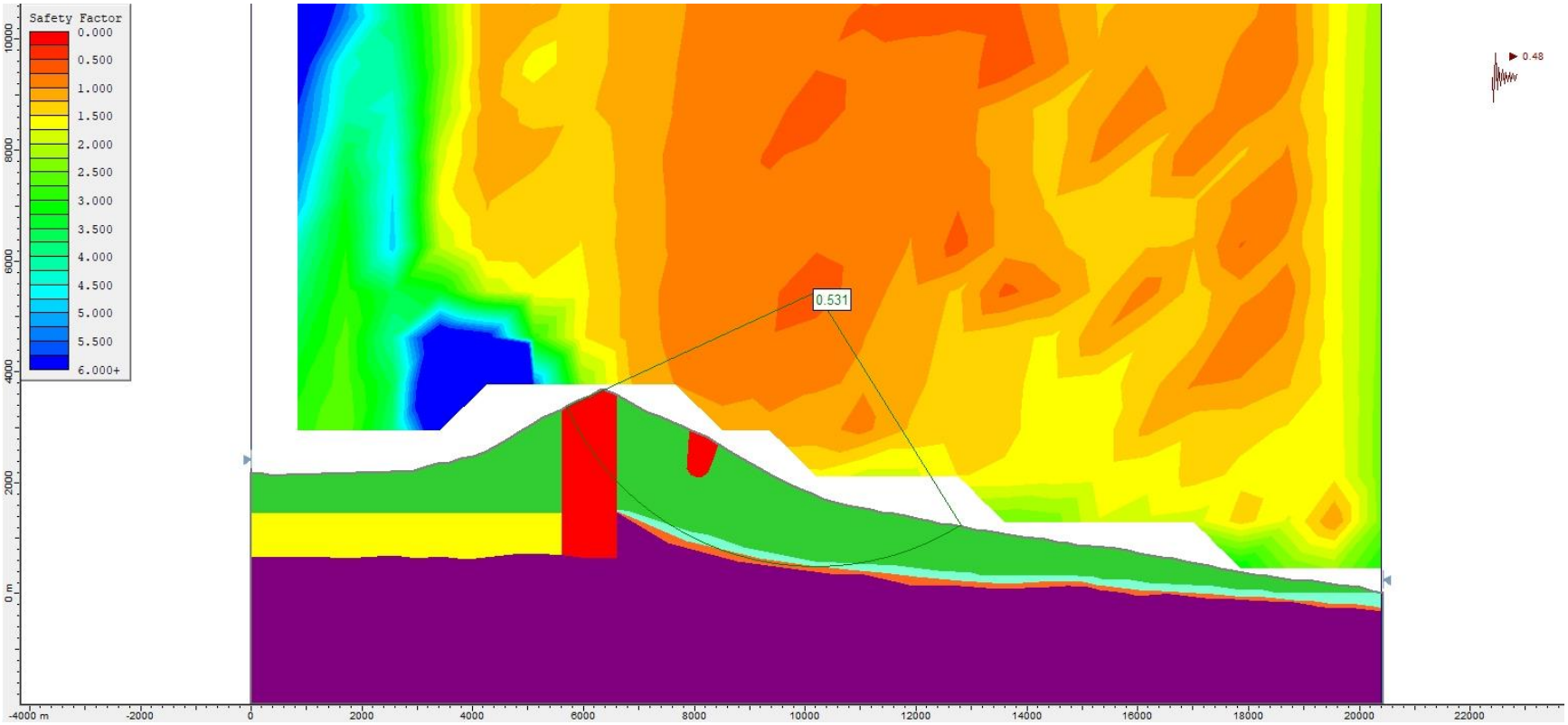

Figure S134. Slope stability pseudo-static analysis for Model 1 (with alteration zones, Figure 4a), using the Janbu Generalised method and a k_h = 0.48.

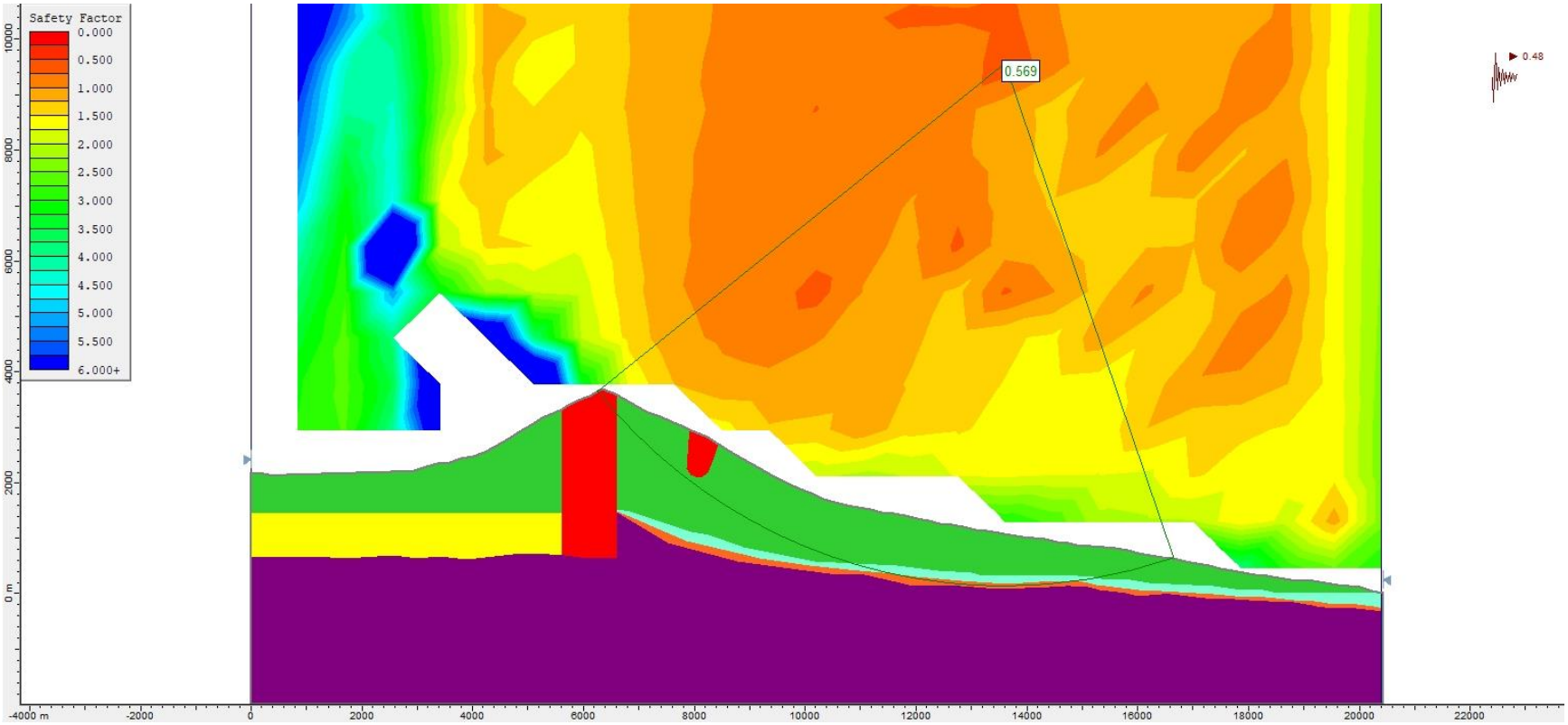

Figure S135. Slope stability pseudo-static analysis for Model 1 (with alteration zones, Figure 4a), using the Morgenstern-Price method and a k_h = 0.48.

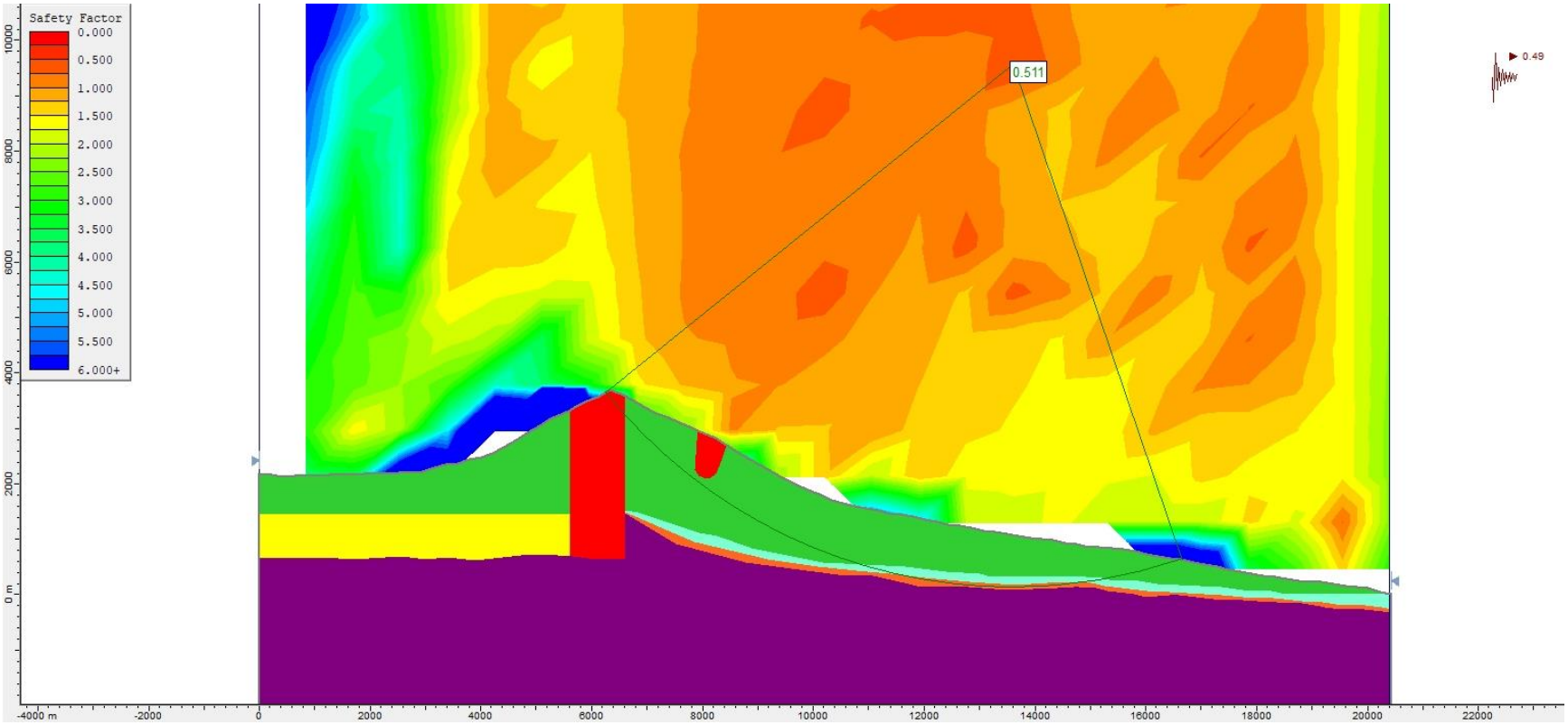

Figure S136. Slope stability pseudo-static analysis for Model 1 (with alteration zones, Figure 4a), using the Bishop simplified method and a k_h = 0.49.

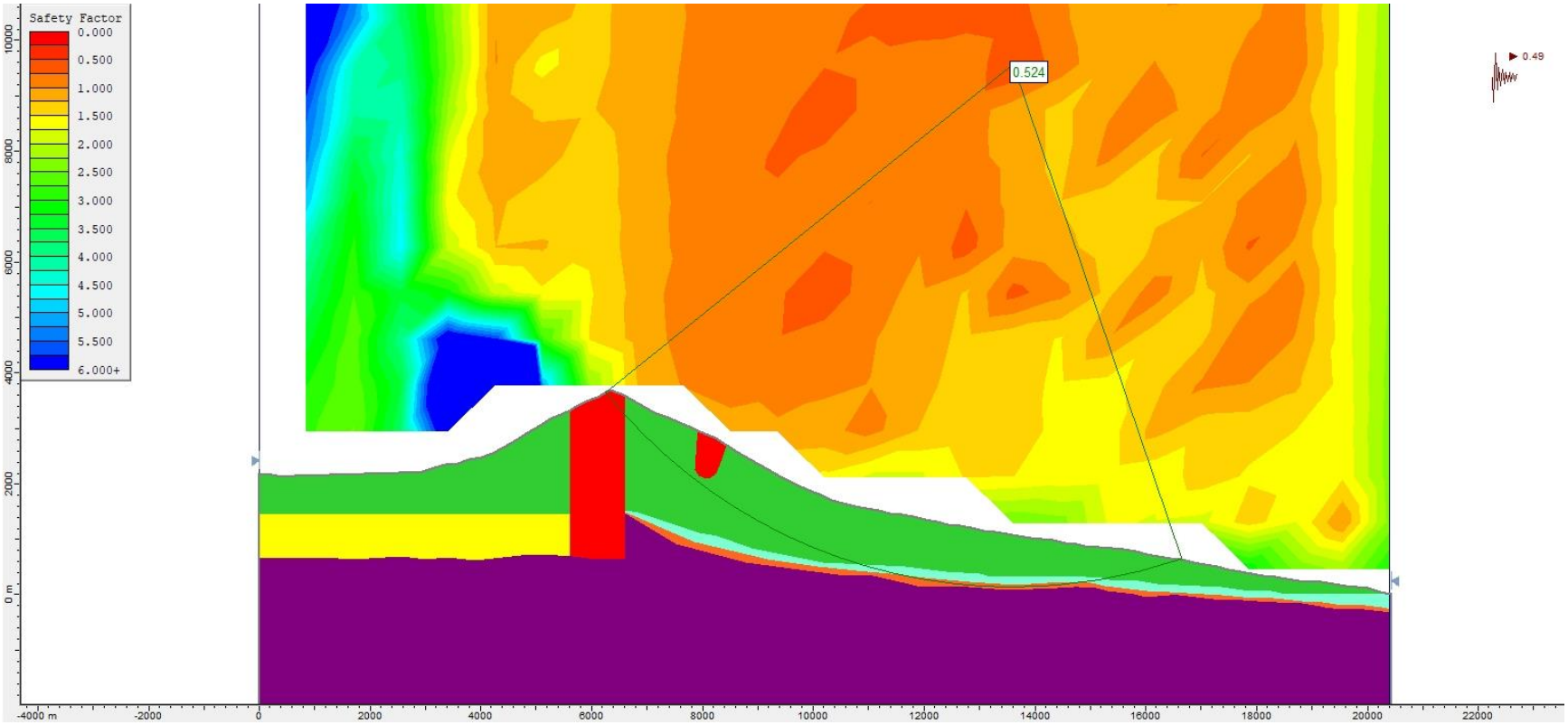

Figure S137. Slope stability pseudo-static analysis for Model 1 (with alteration zones, Figure 4a), using the Janbu Generalised method and a k_h = 0.49.

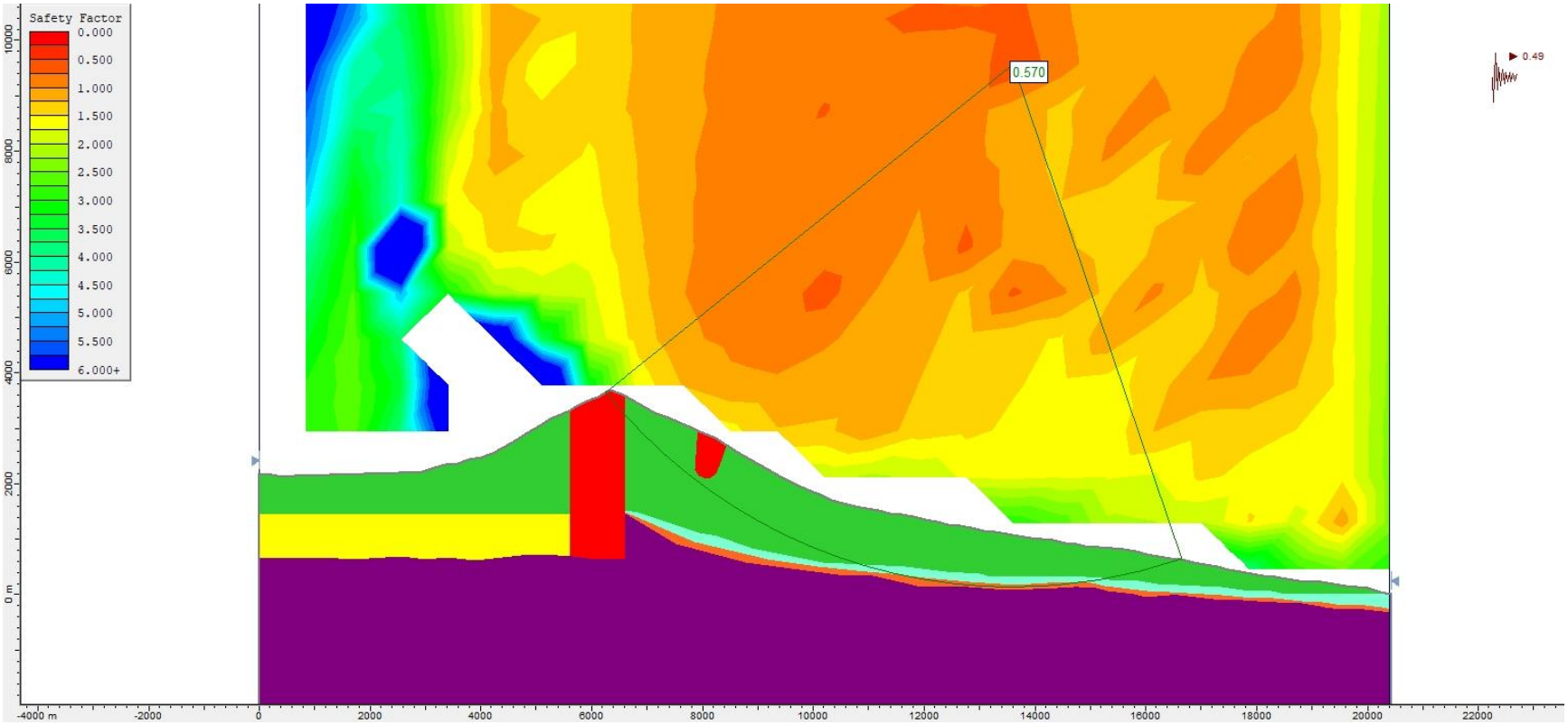

Figure S138. Slope stability pseudo-static analysis for Model 1 (with alteration zones, Figure 4a), using the Morgenstern-Price method and a k_h = 0.49.

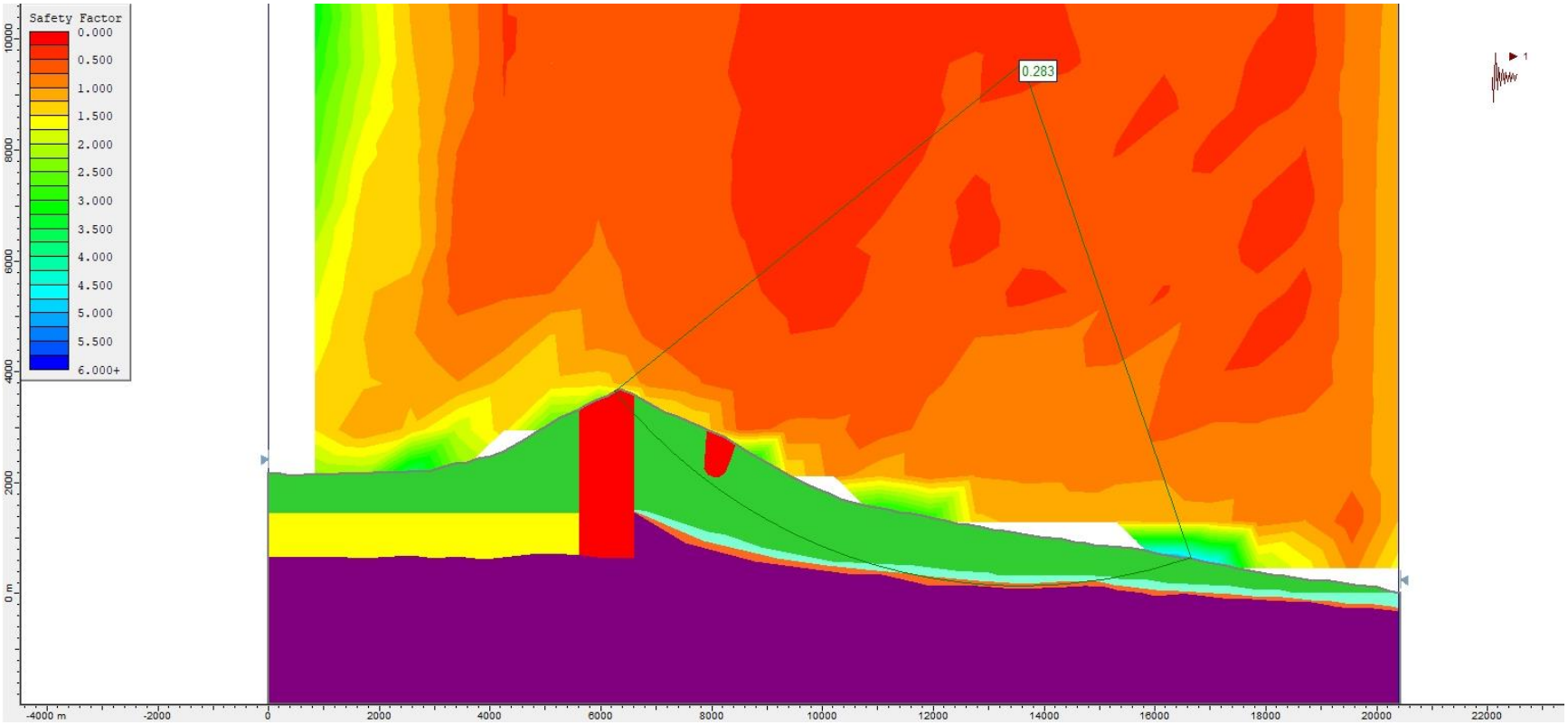

Figure S139. Slope stability pseudo-static analysis for Model 1 (with alteration zones, Figure 4a), using the Bishop simplified method and a k_h = 1.00.

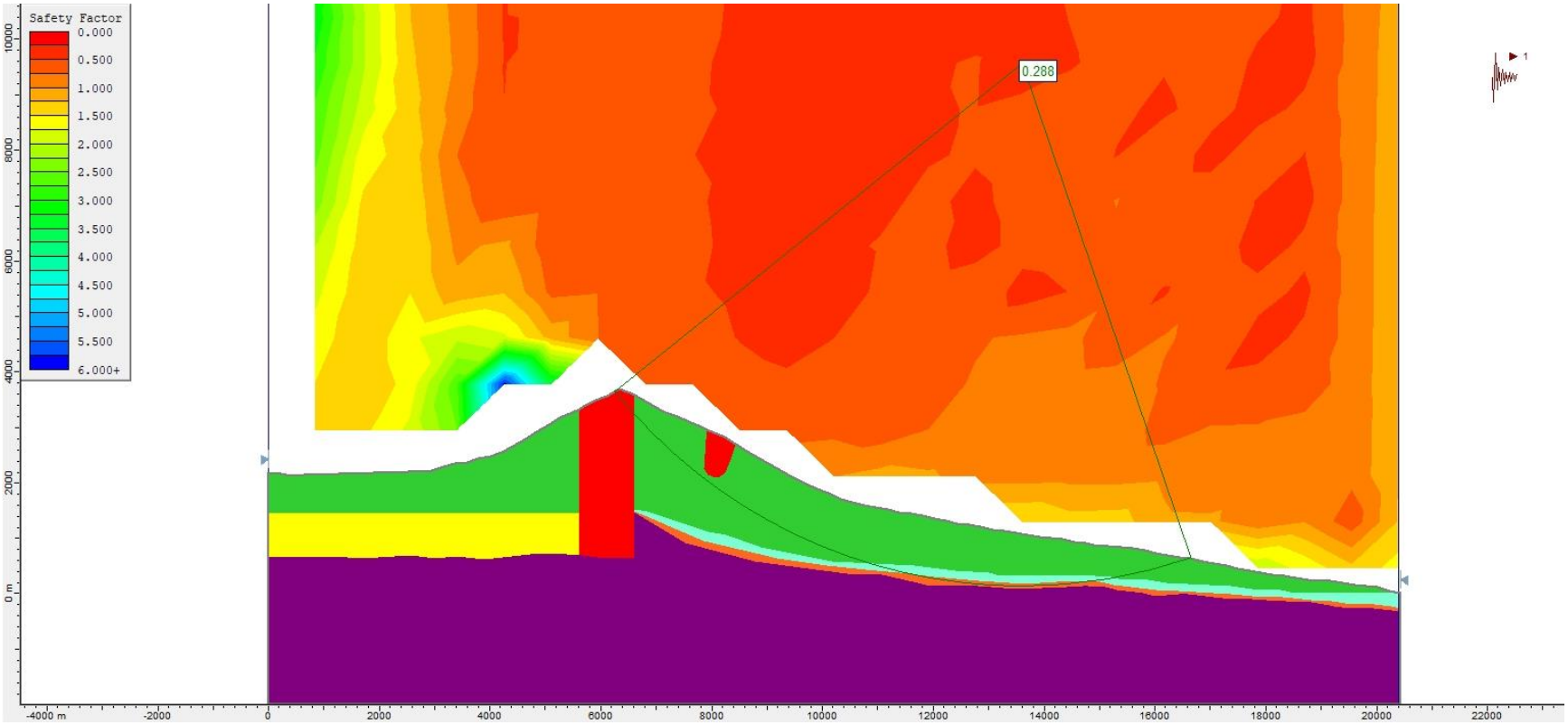

Figure S140. Slope stability pseudo-static analysis for Model 1 (with alteration zones, Figure 4a), using the Janbu Generalised method and a k_h = 1.00.

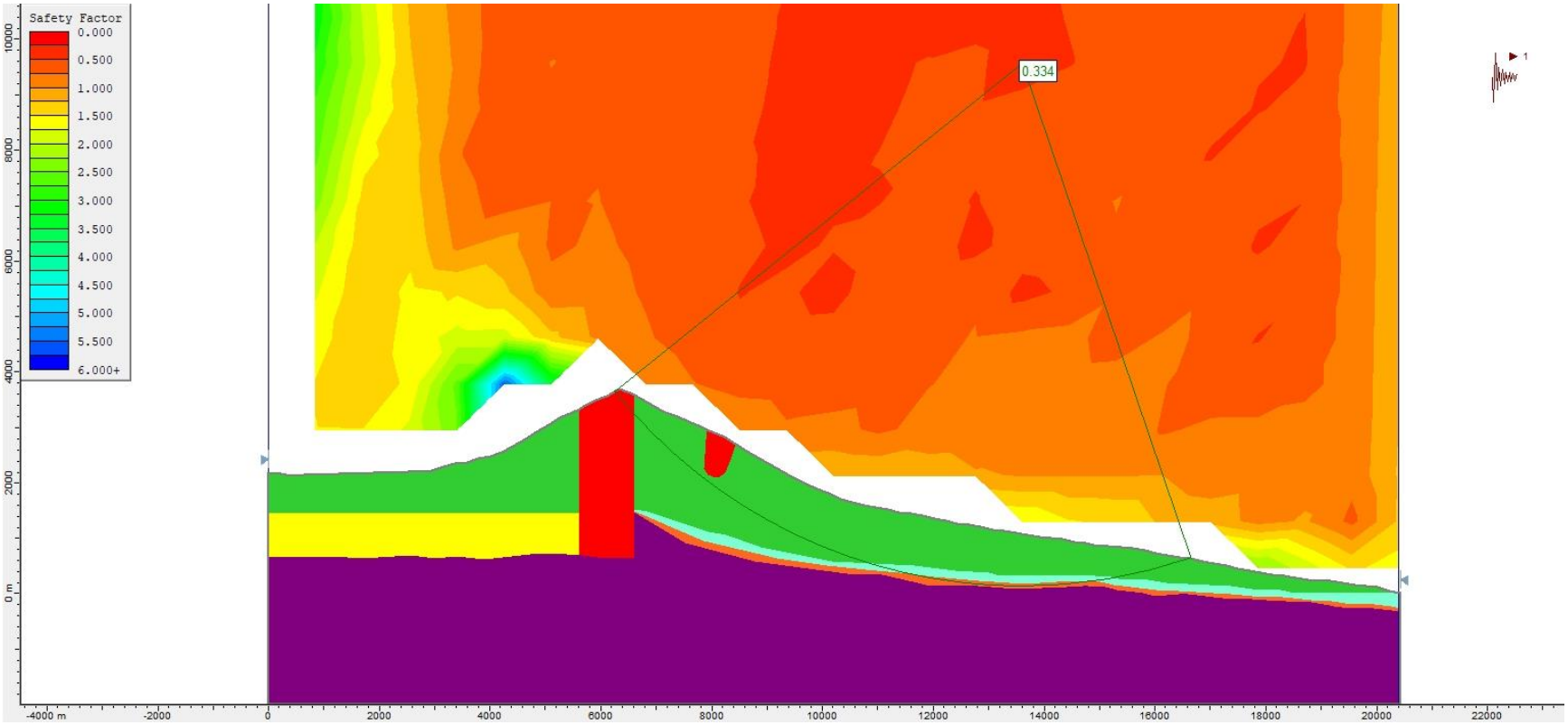

Figure S141. Slope stability pseudo-static analysis for Model 1 (with alteration zones, Figure 4a), using the Morgenstern-Price method and a k_h = 1.00.

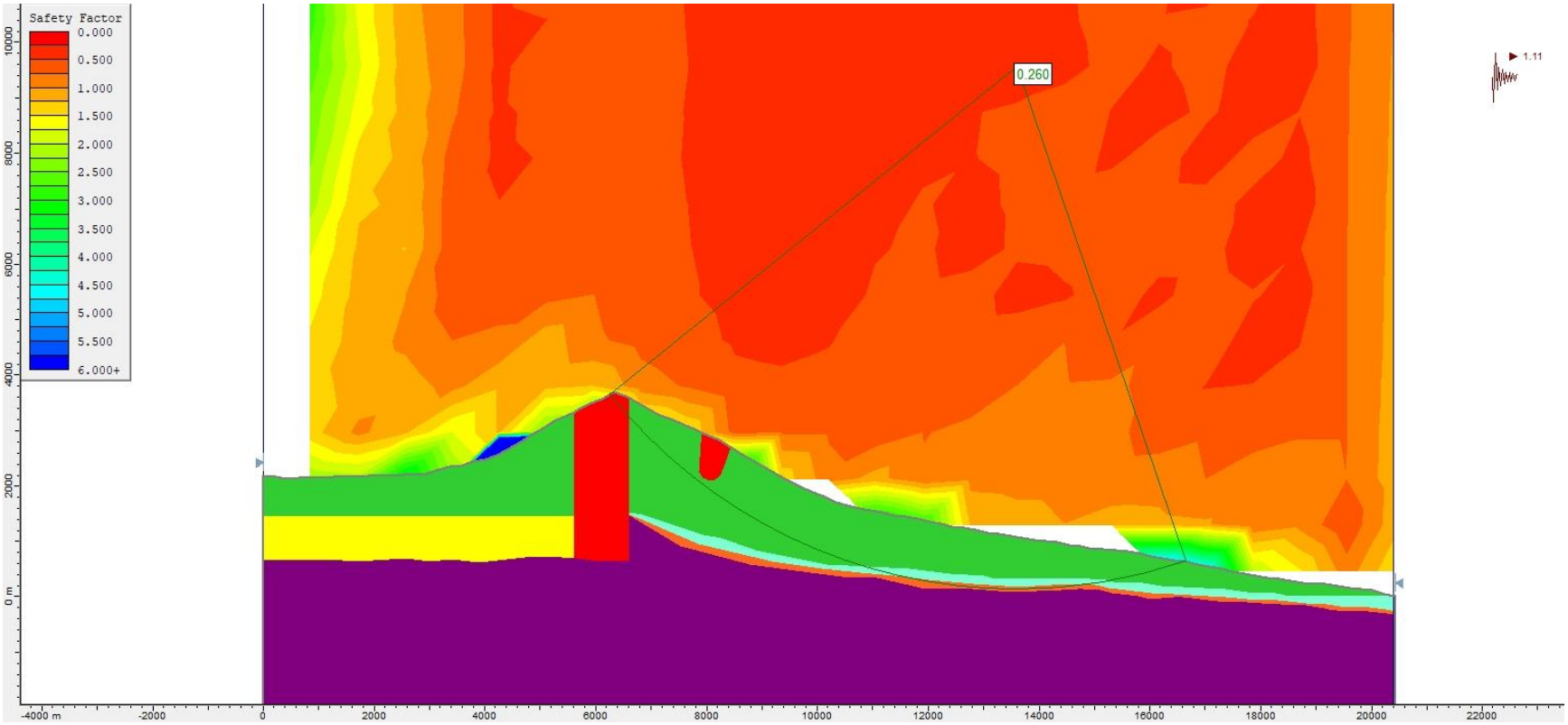

Figure S142. Slope stability pseudo-static analysis for Model 1 (with alteration zones, Figure 4a), using the Bishop simplified method and a k_h = 1.11.

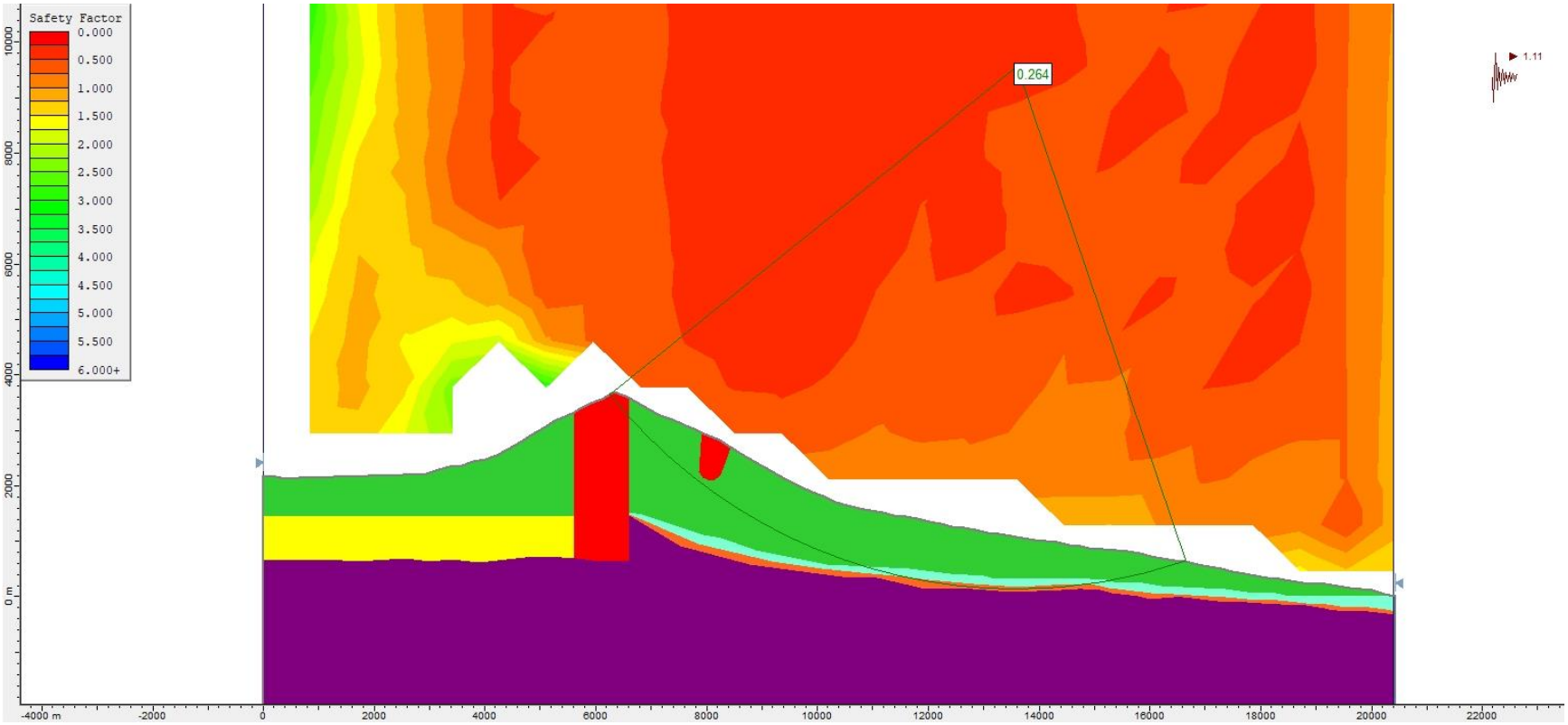

Figure S143. Slope stability pseudo-static analysis for Model 1 (with alteration zones, Figure 4a), using the Janbu Generalised method and a k_h = 1.11.

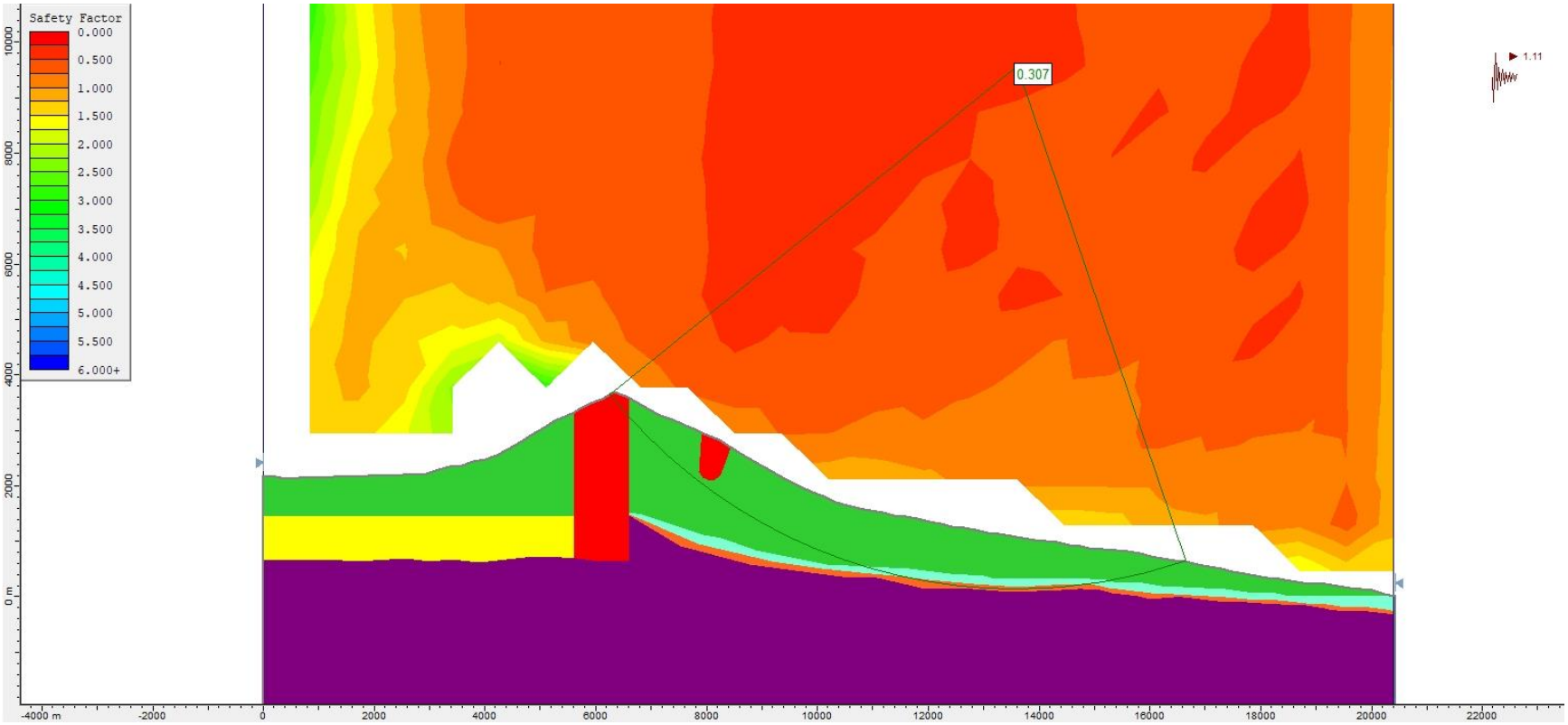

Figure S144. Slope stability pseudo-static analysis for Model 1 (with alteration zones, Figure 4a), using the Morgenstern-Price method and a k_h = 1.11.

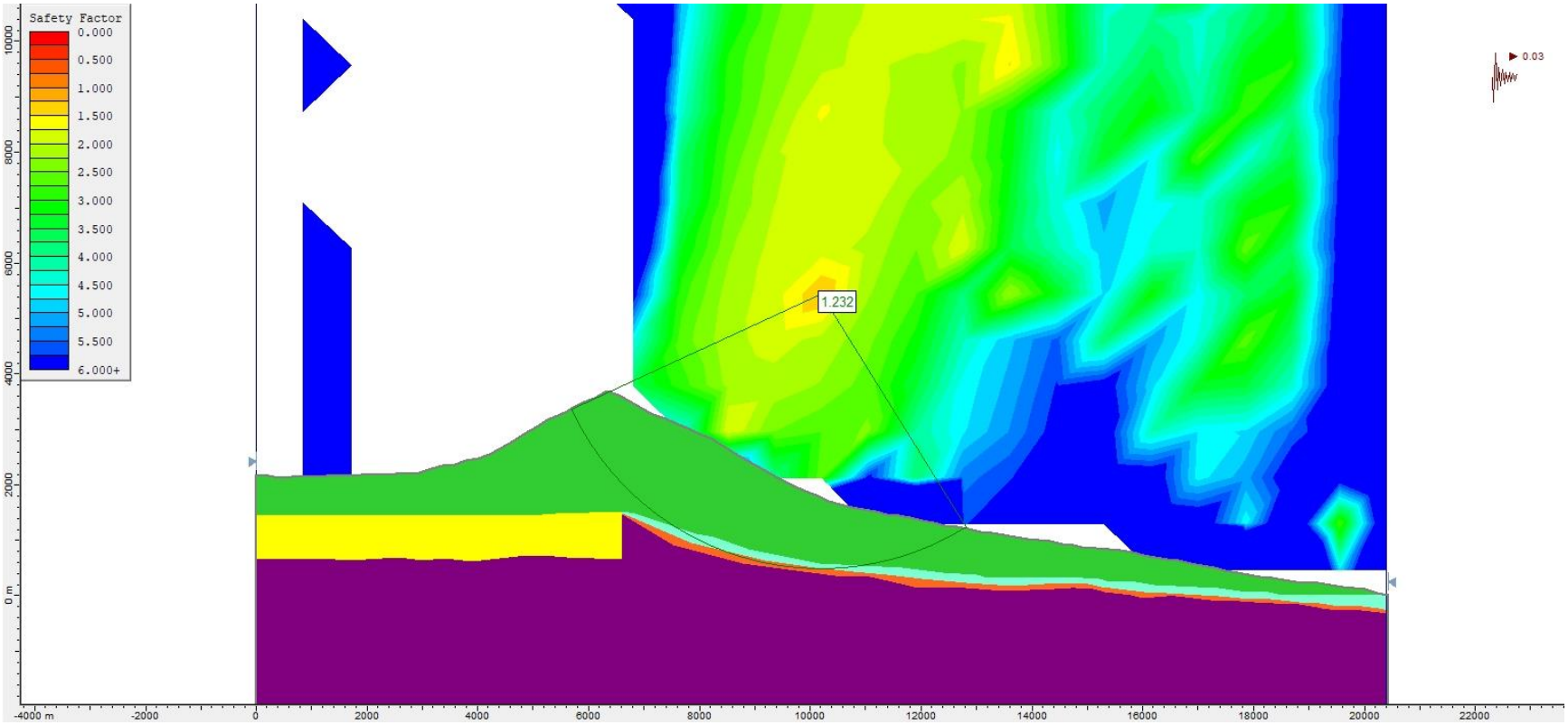

Figure S145. Slope stability pseudo-static analysis for Model 2 (without alteration zones, Figure 4b), using the Bishop simplified method and a k_h = 0.03.

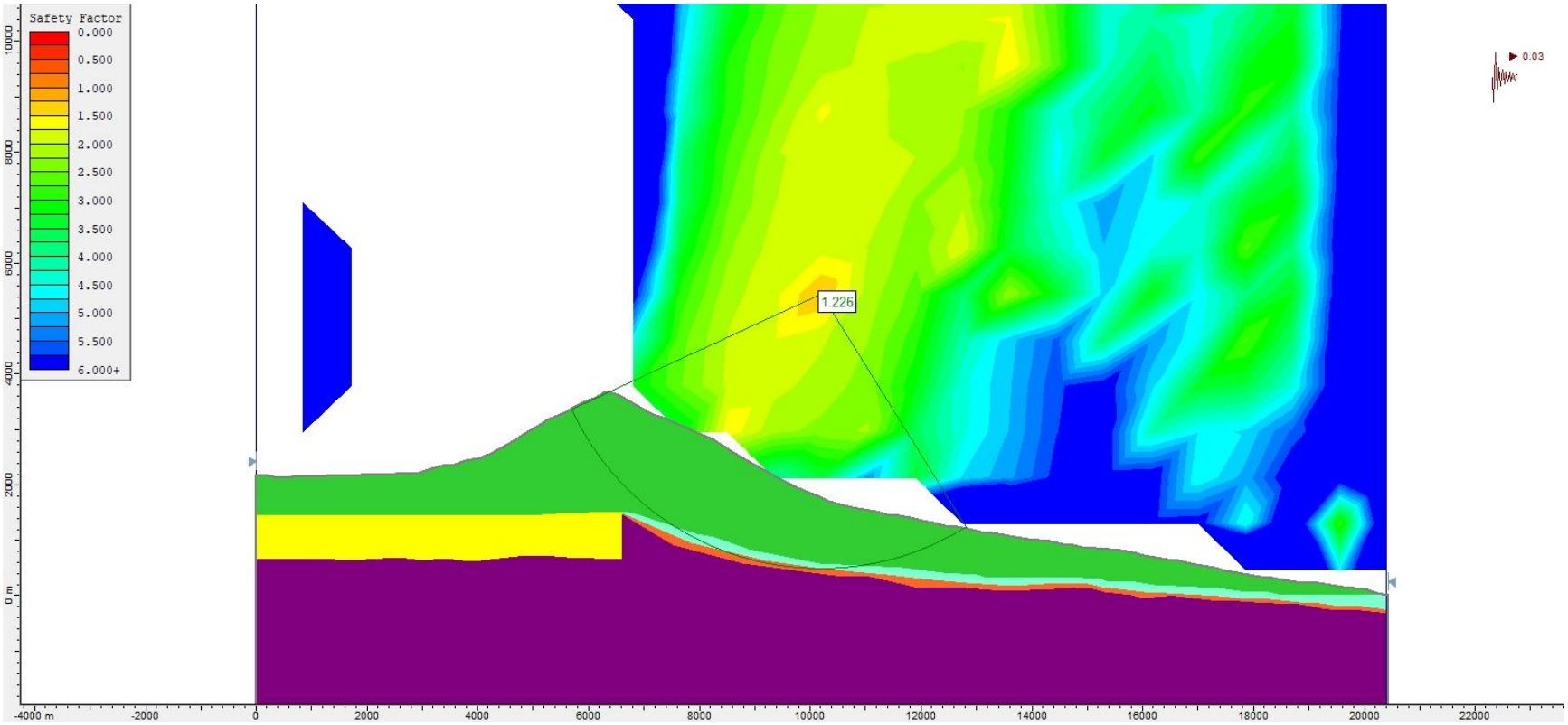

Figure S146. Slope stability pseudo-static analysis for Model 2 (without alteration zones, Figure 4b), using the Janbu Generalised method and a k_h = 0.03.

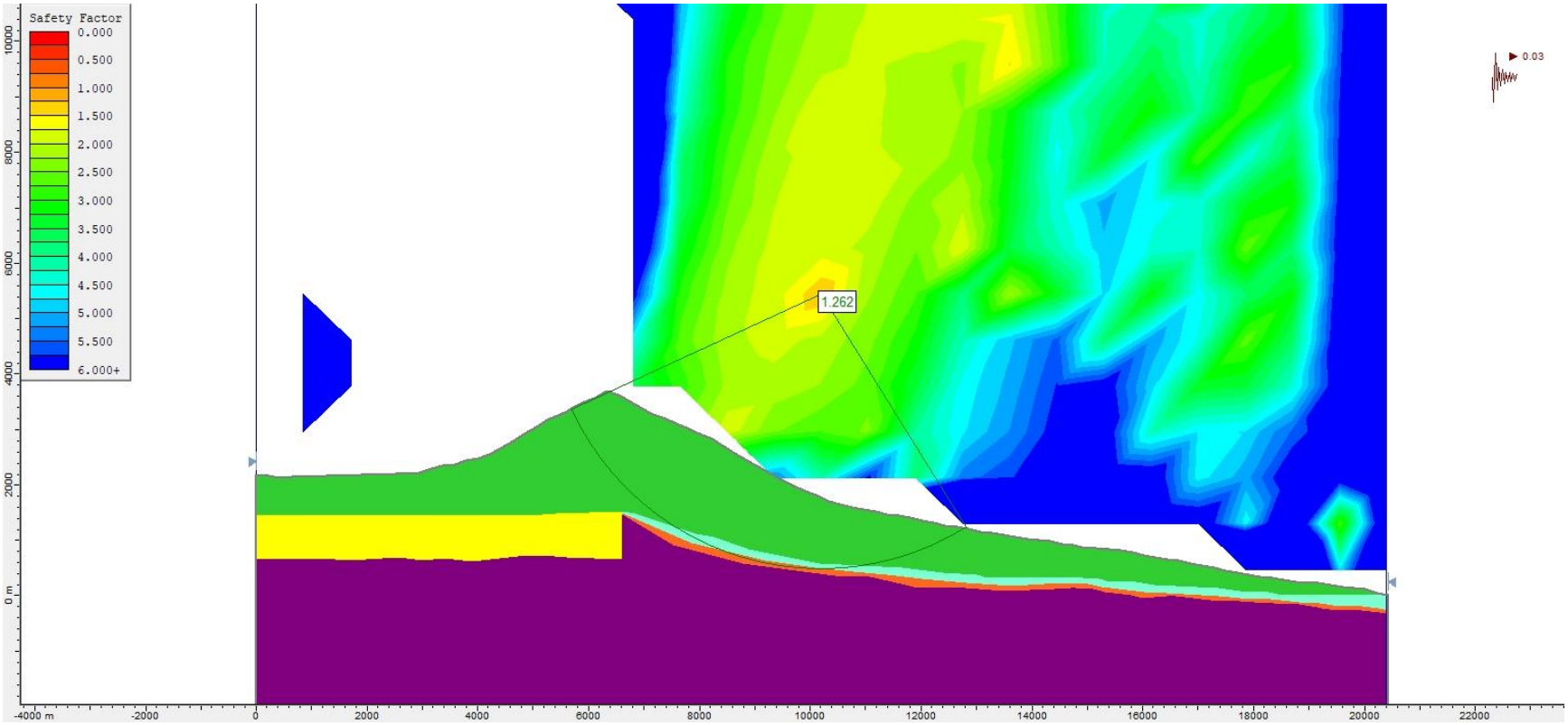

Figure S147. Slope stability pseudo-static analysis for Model 2 (without alteration zones, Figure 4b), using the Morgenstern-Price method and a k_h = 0.03.

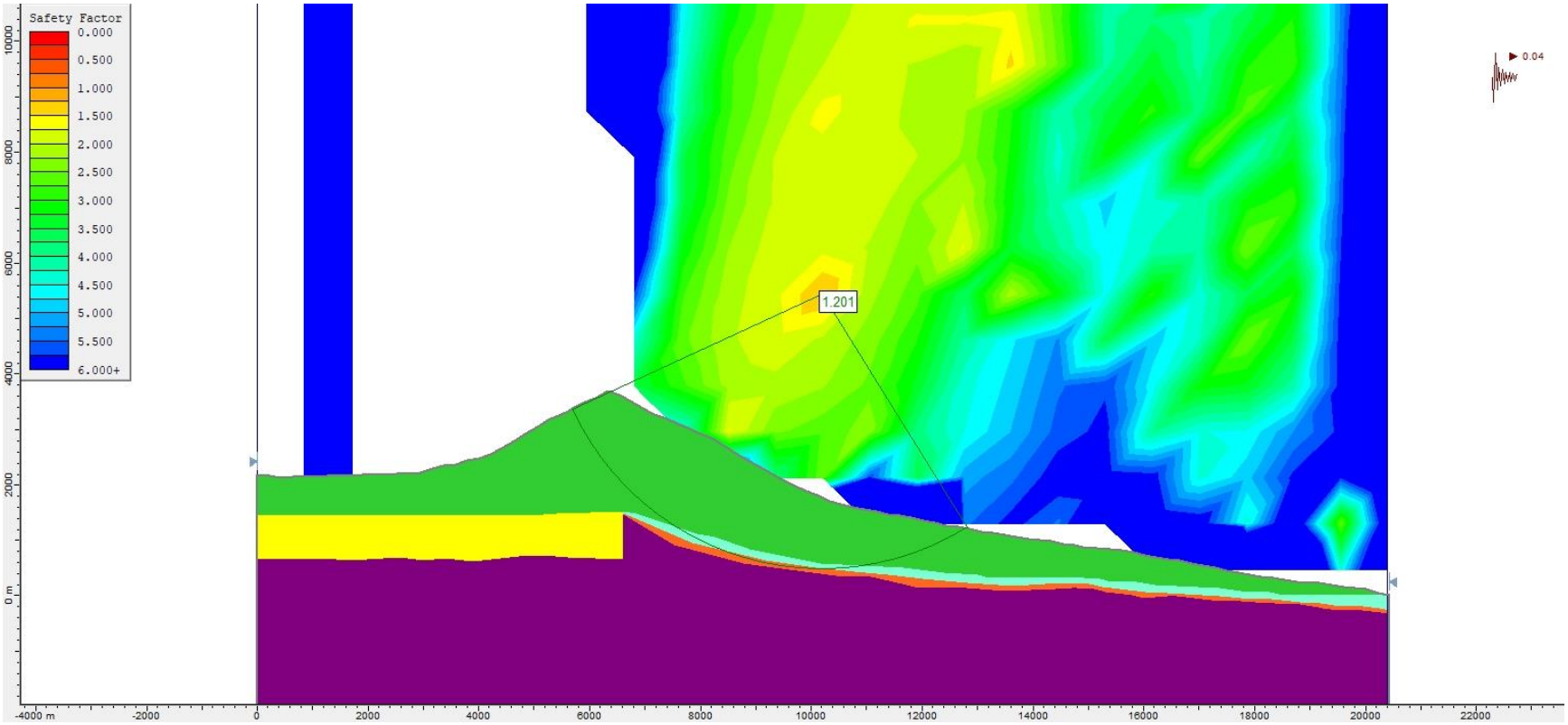

Figure S148. Slope stability pseudo-static analysis for Model 2 (without alteration zones, Figure 4b), using the Bishop simplified method and a k_h = 0.04.

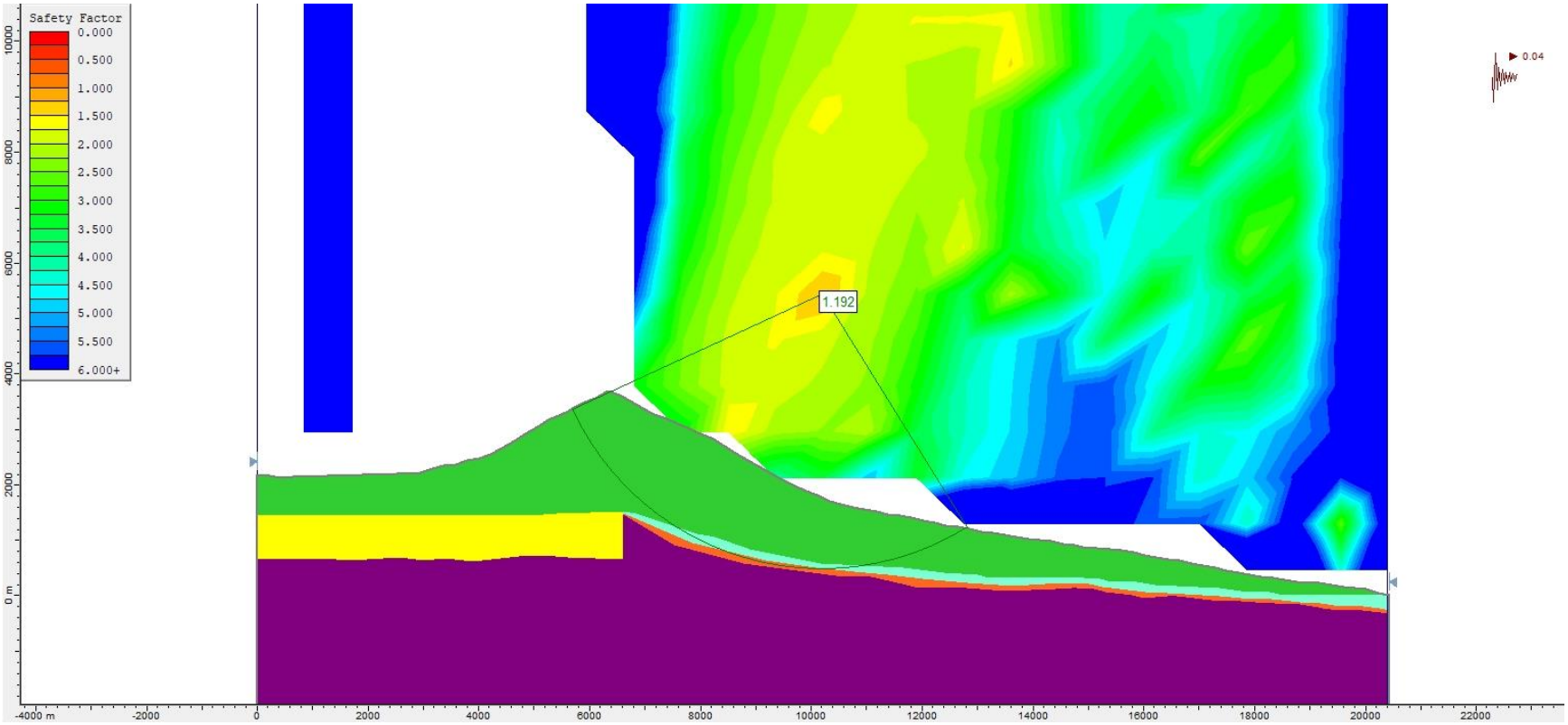

Figure S149. Slope stability pseudo-static analysis for Model 2 (without alteration zones, Figure 4b), using the Janbu Generalised method and a k_h = 0.04.

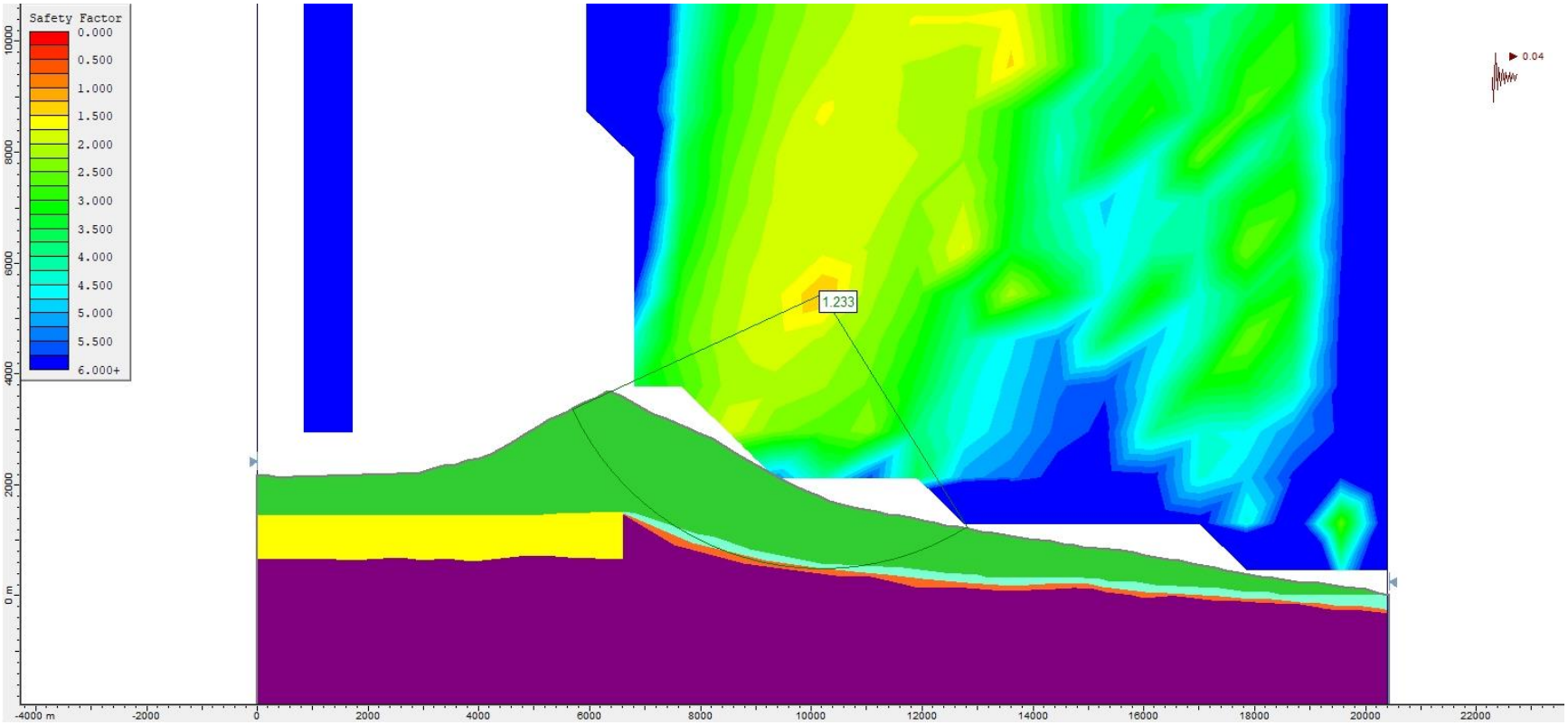

Figure S150. Slope stability pseudo-static analysis for Model 2 (without alteration zones, Figure 4b), using the Morgenstern-Price method and a k_h = 0.04.

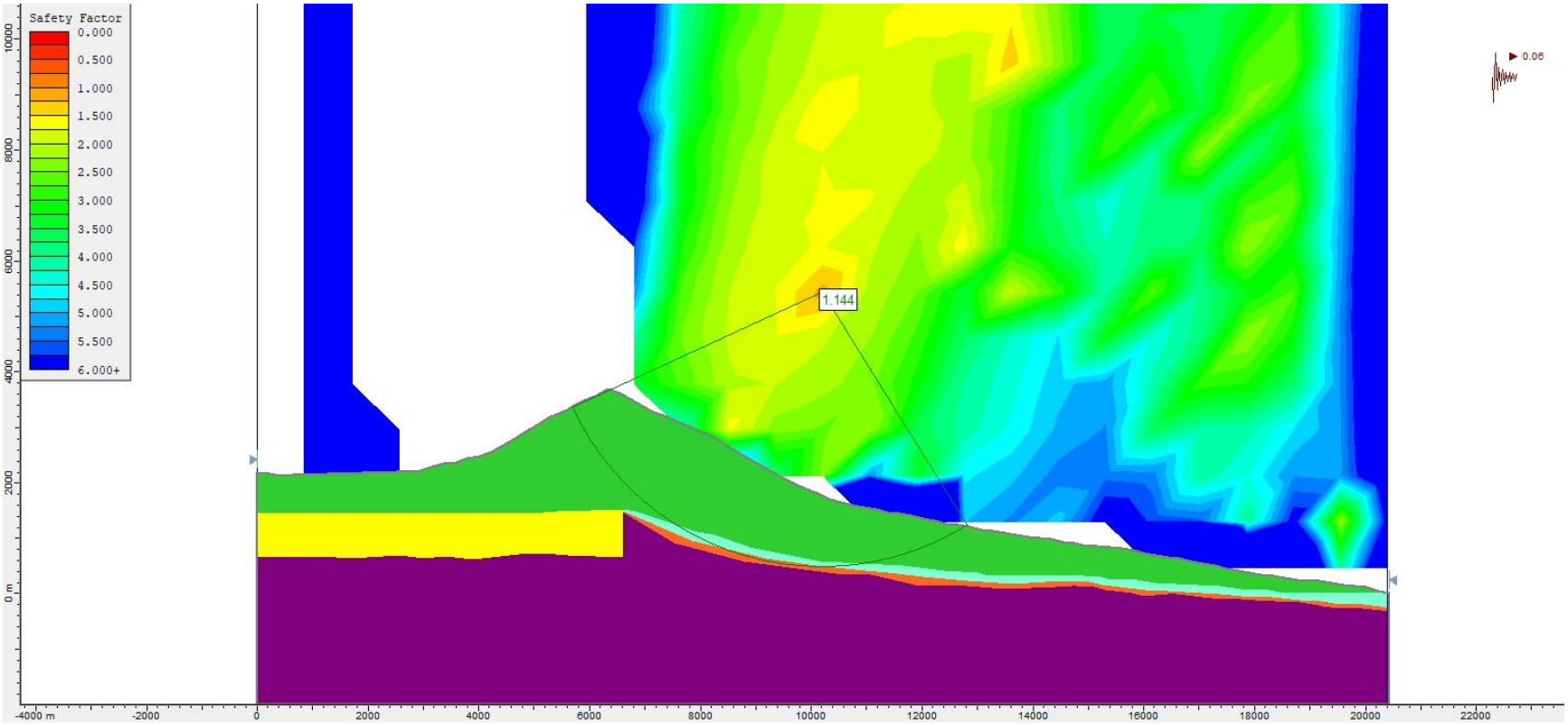

Figure S151. Slope stability pseudo-static analysis for Model 2 (without alteration zones, Figure 4b), using the Bishop simplified method and a k_h = 0.06.

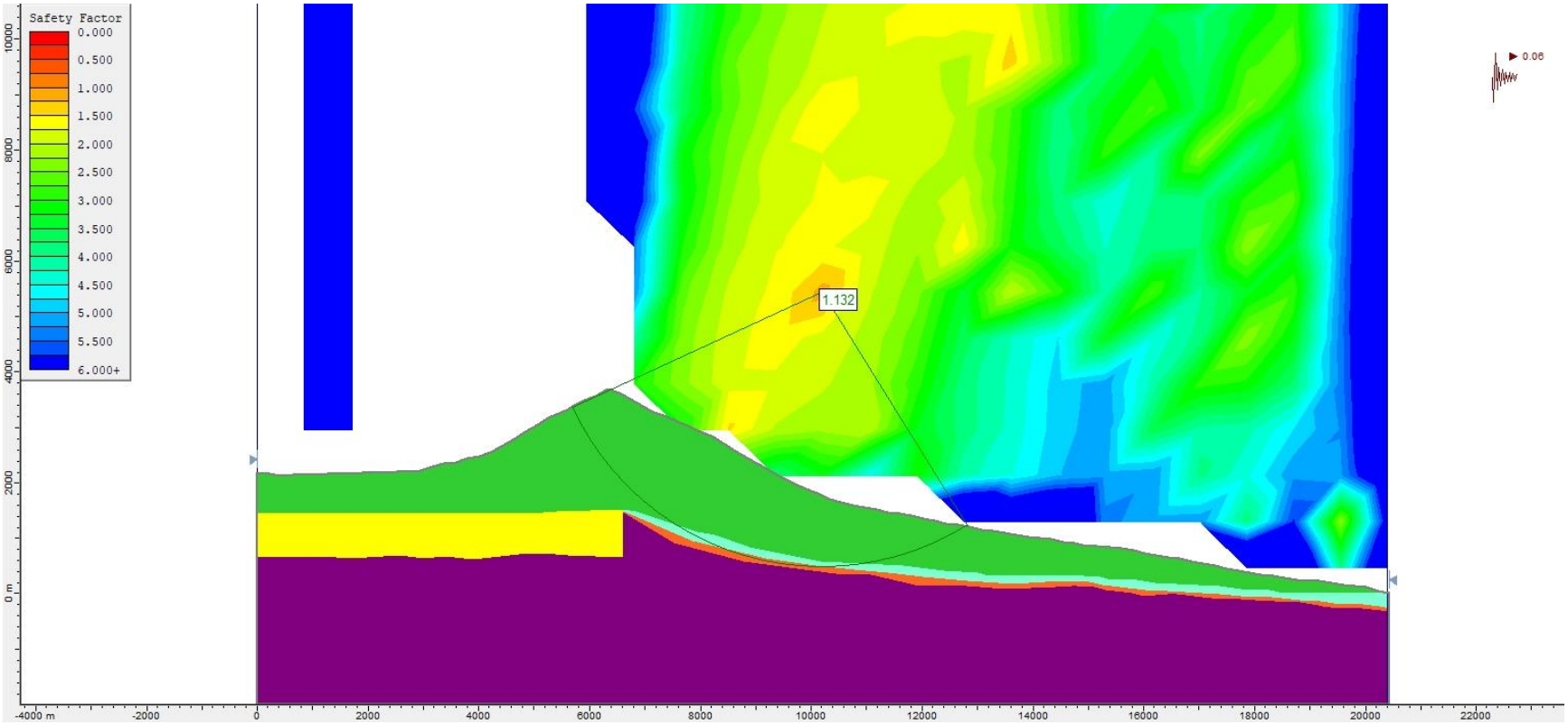

Figure S152. Slope stability pseudo-static analysis for Model 2 (without alteration zones, Figure 4b), using the Janbu Generalised method and a k_h = 0.06.

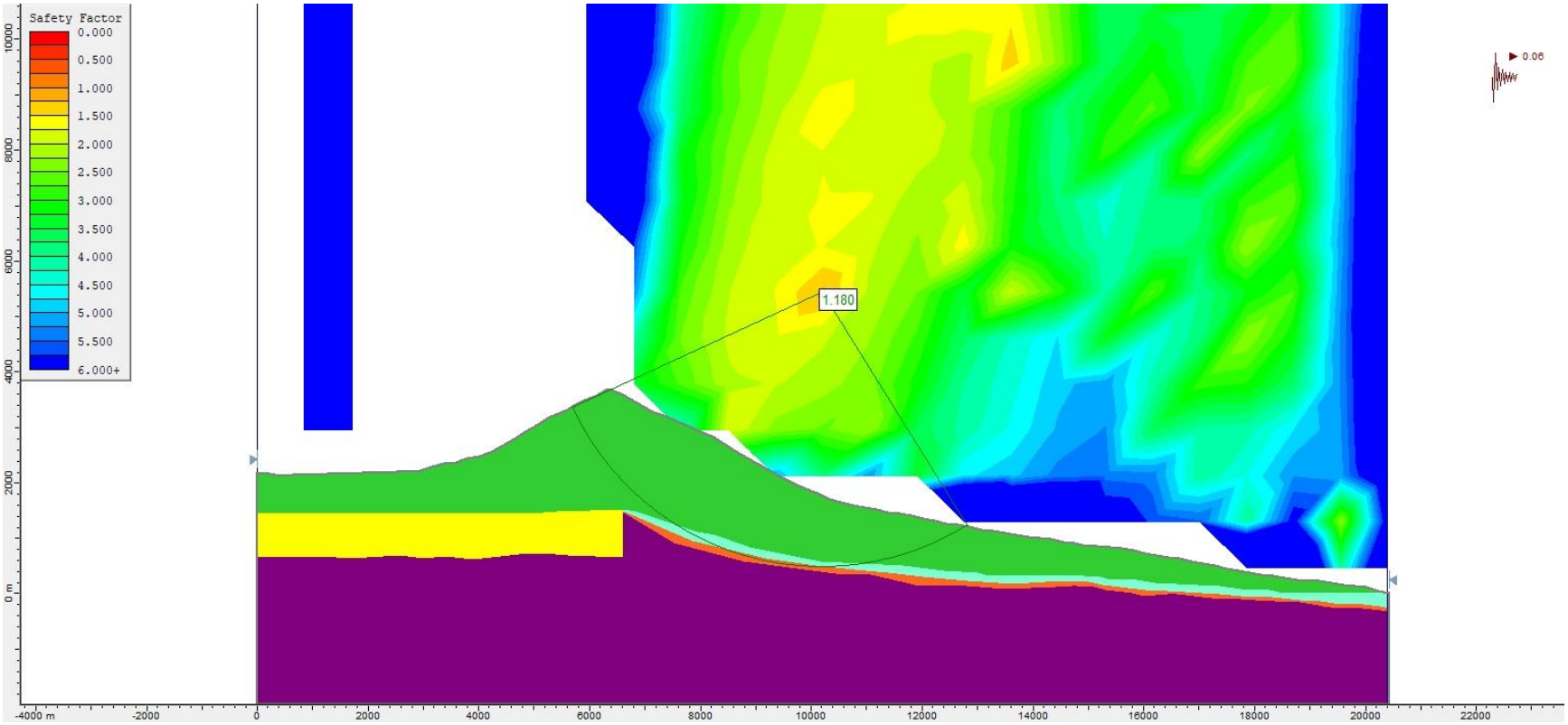

Figure S153. Slope stability pseudo-static analysis for Model 2 (without alteration zones, Figure 4b), using the Morgenstern-Price method and a k_h = 0.06.

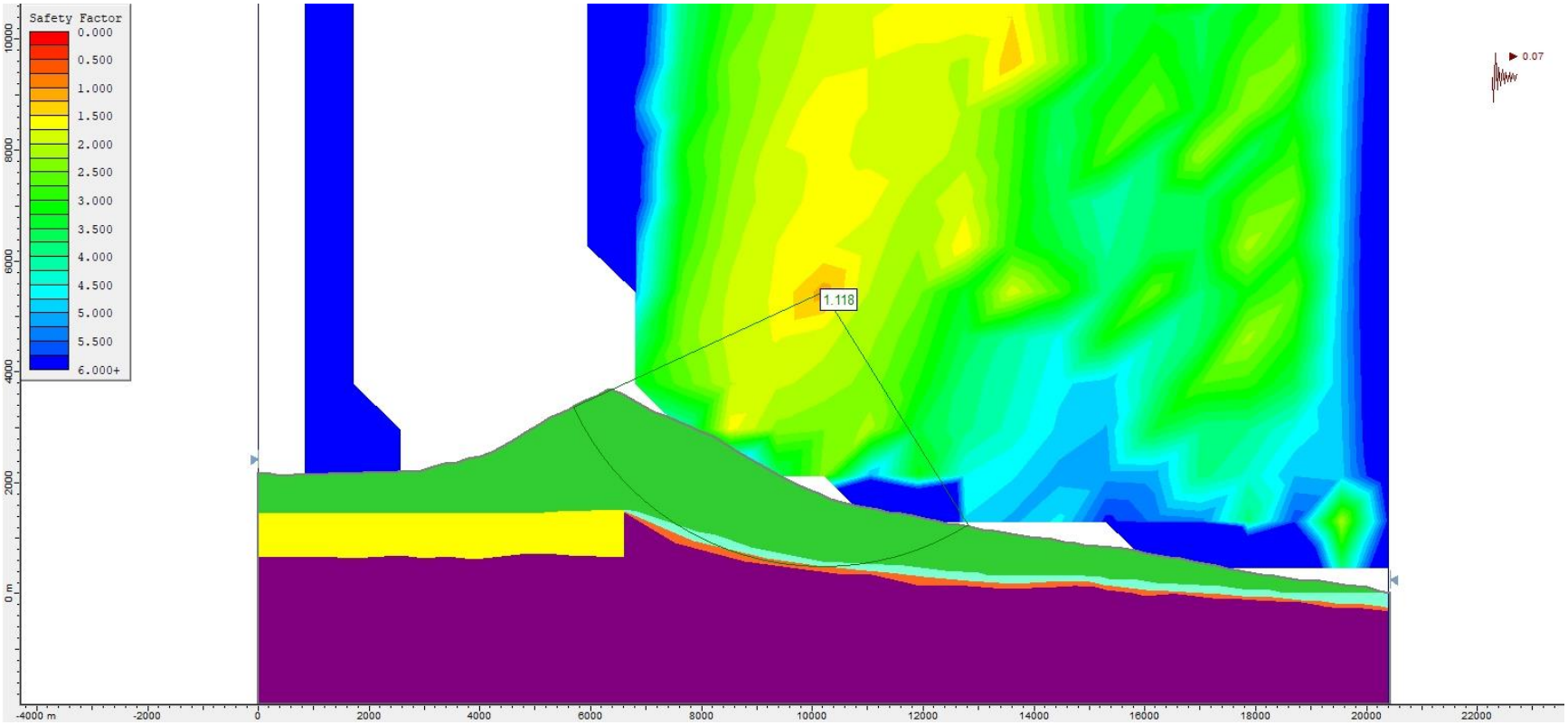

Figure S154. Slope stability pseudo-static analysis for Model 2 (without alteration zones, Figure 4b), using the Bishop simplified method and a k_h = 0.07.

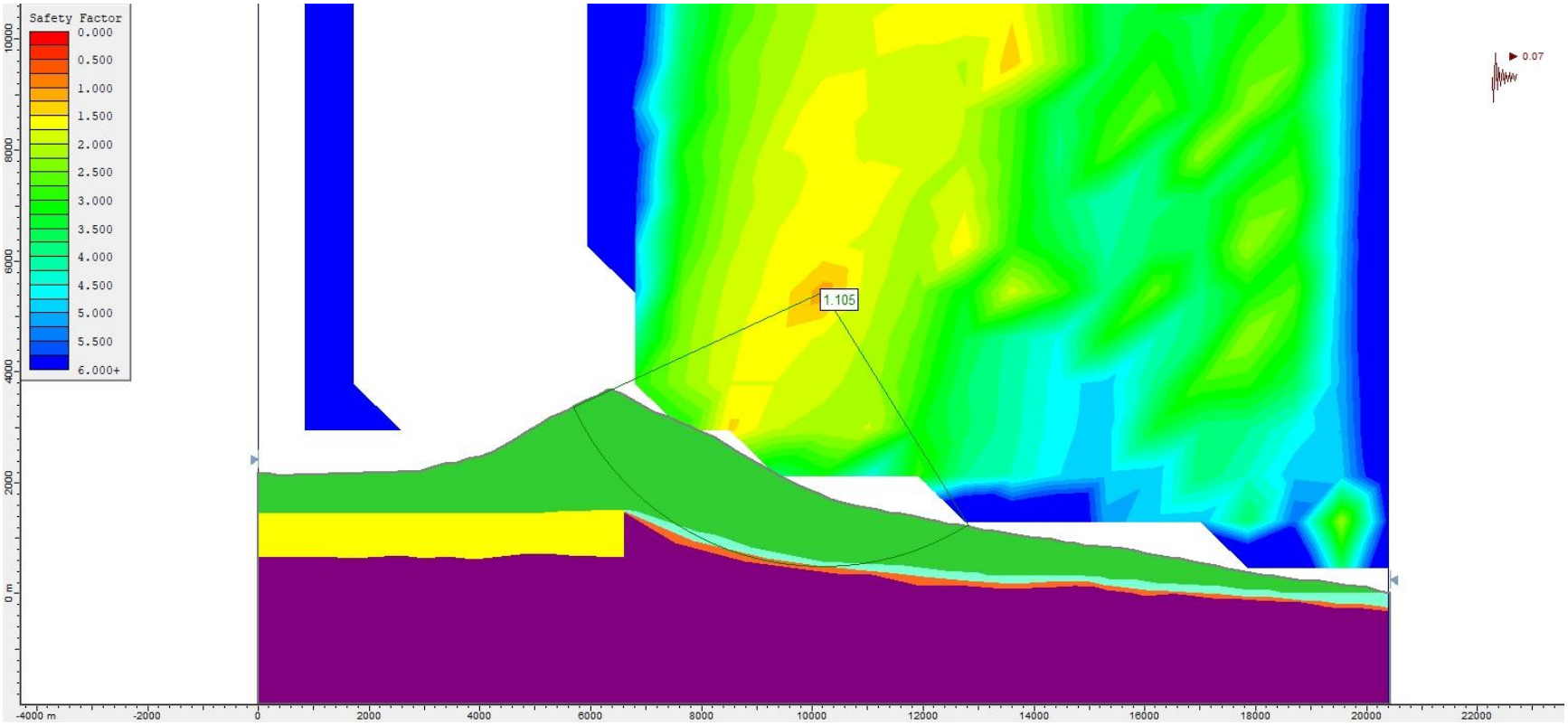

Figure S155. Slope stability pseudo-static analysis for Model 2 (without alteration zones, Figure 4b), using the Janbu Generalised method and a k_h = 0.07.

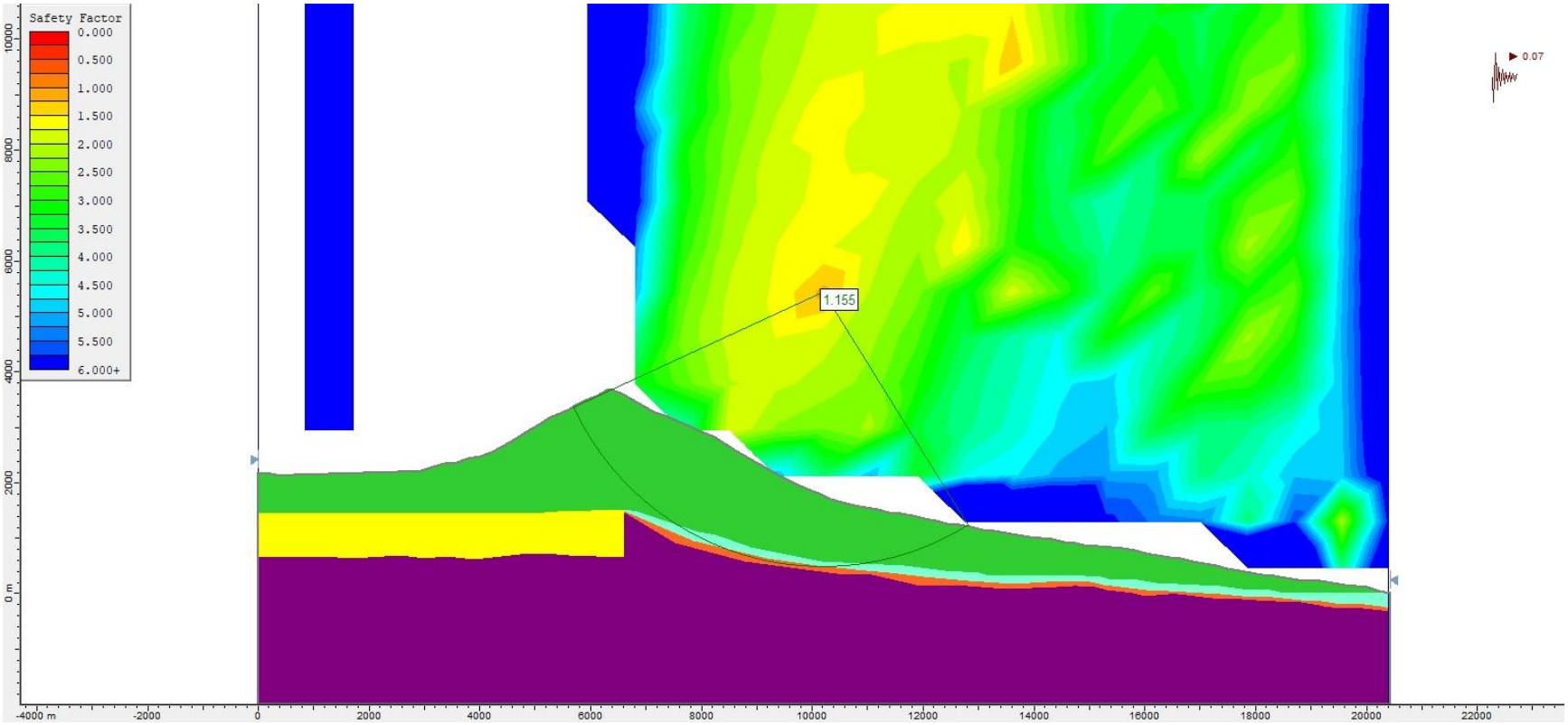

Figure S156. Slope stability pseudo-static analysis for Model 2 (without alteration zones, Figure 4b), using the Morgenstern-Price method and a k_h = 0.07.

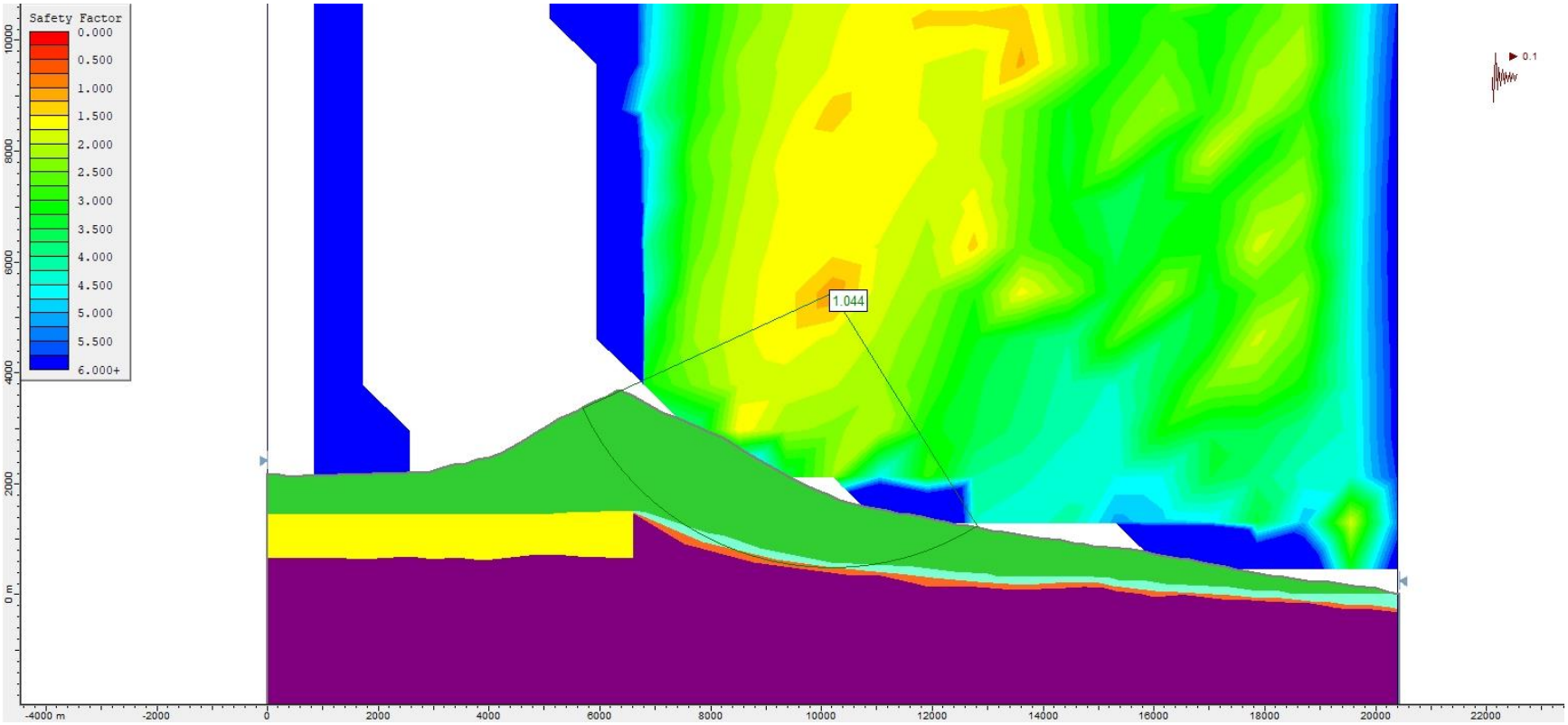

Figure S157. Slope stability pseudo-static analysis for Model 2 (without alteration zones, Figure 4b), using the Bishop simplified method and a k_h = 0.10.

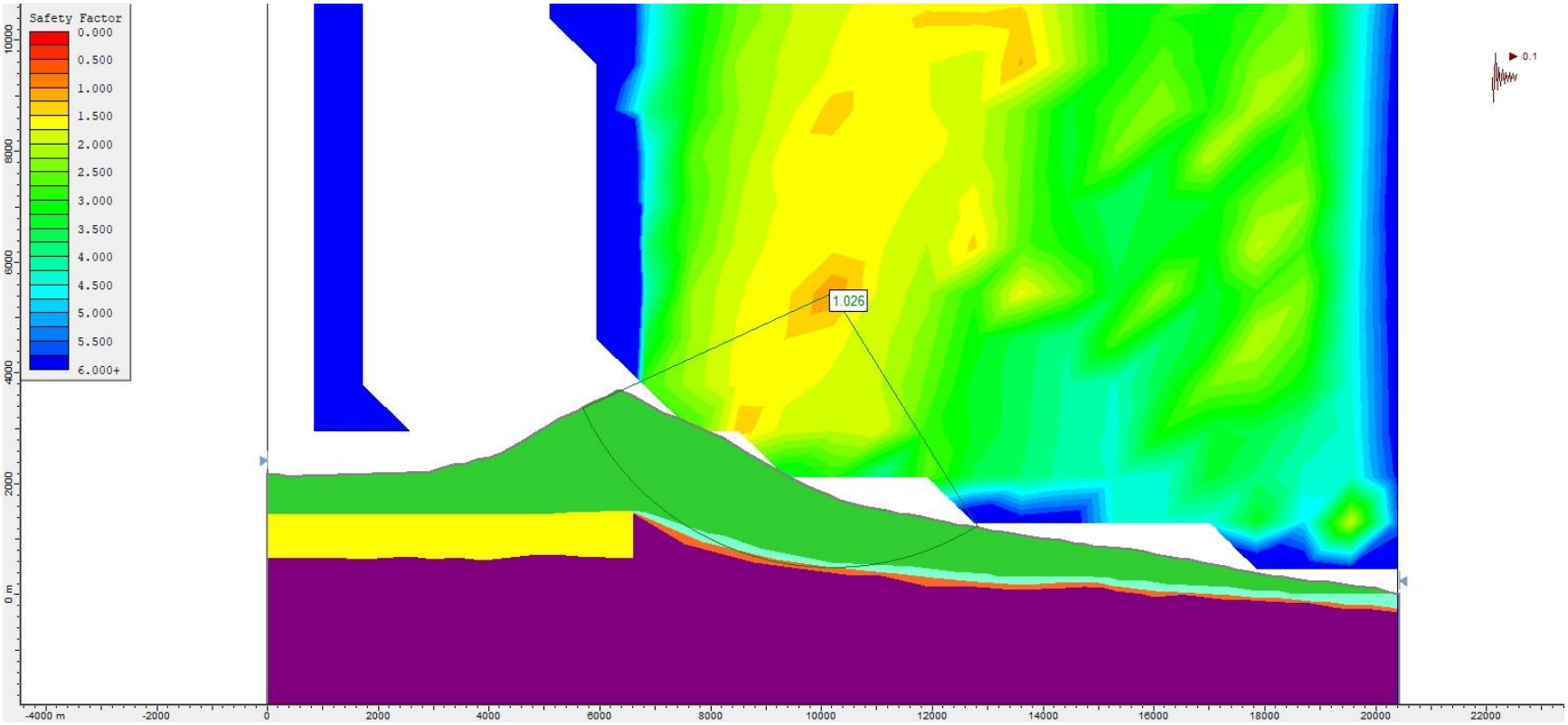

Figure S158. Slope stability pseudo-static analysis for Model 2 (without alteration zones, Figure 4b), using the Janbu Generalised method and a k_h = 0.10.

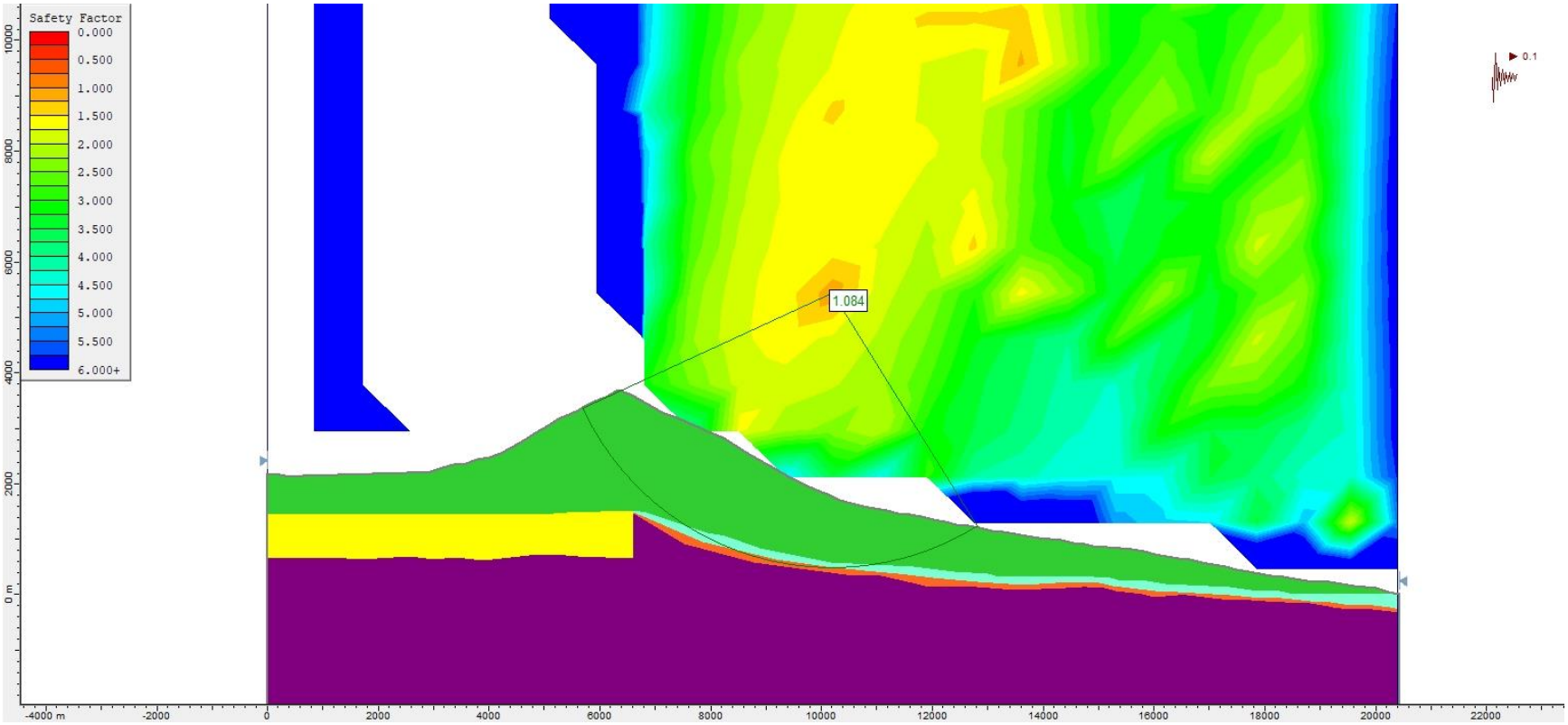

Figure S159. Slope stability pseudo-static analysis for Model 2 (without alteration zones, Figure 4b), using the Morgenstern-Price method and a k_h = 0.10.

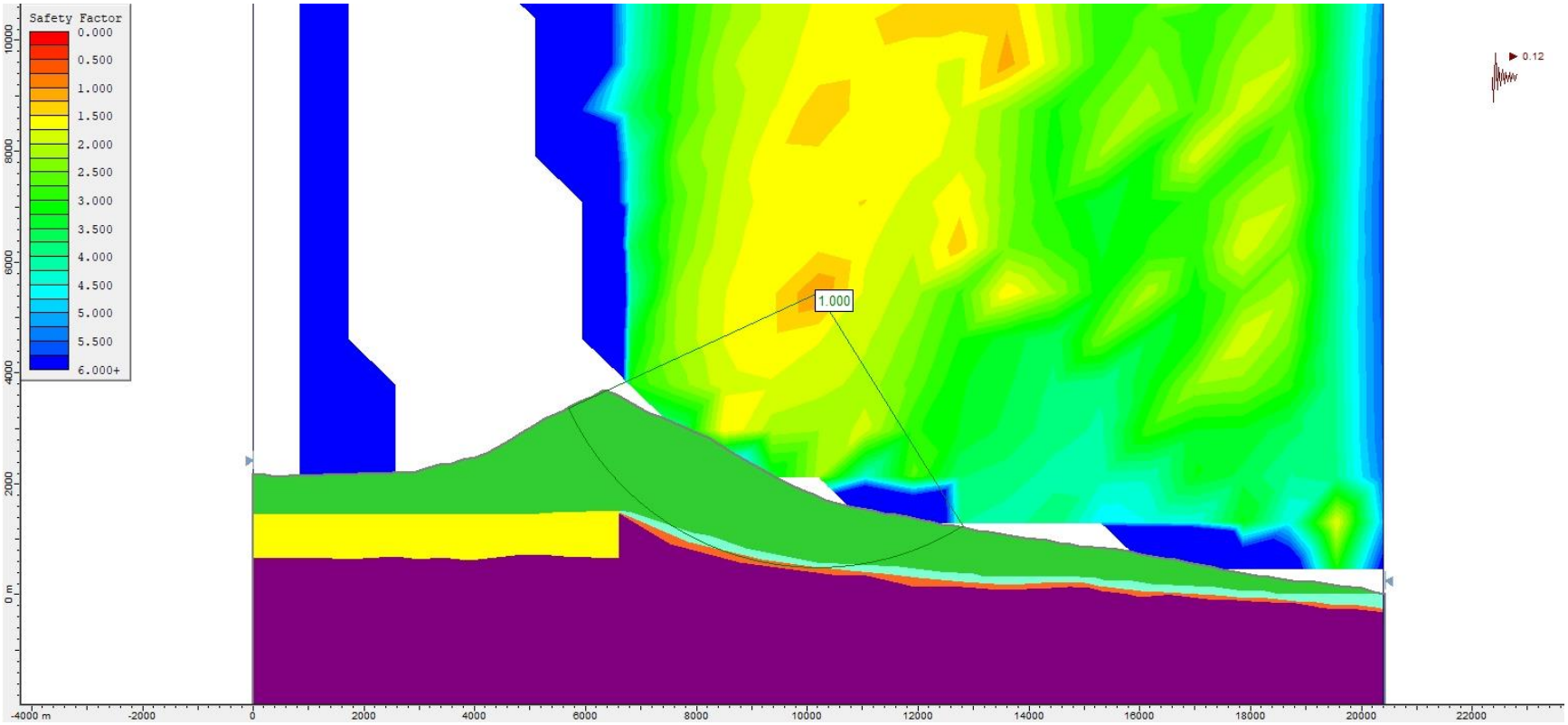

Figure S160. Slope stability pseudo-static analysis for Model 2 (without alteration zones, Figure 4b), using the Bishop simplified method and a k_h = 0.12.

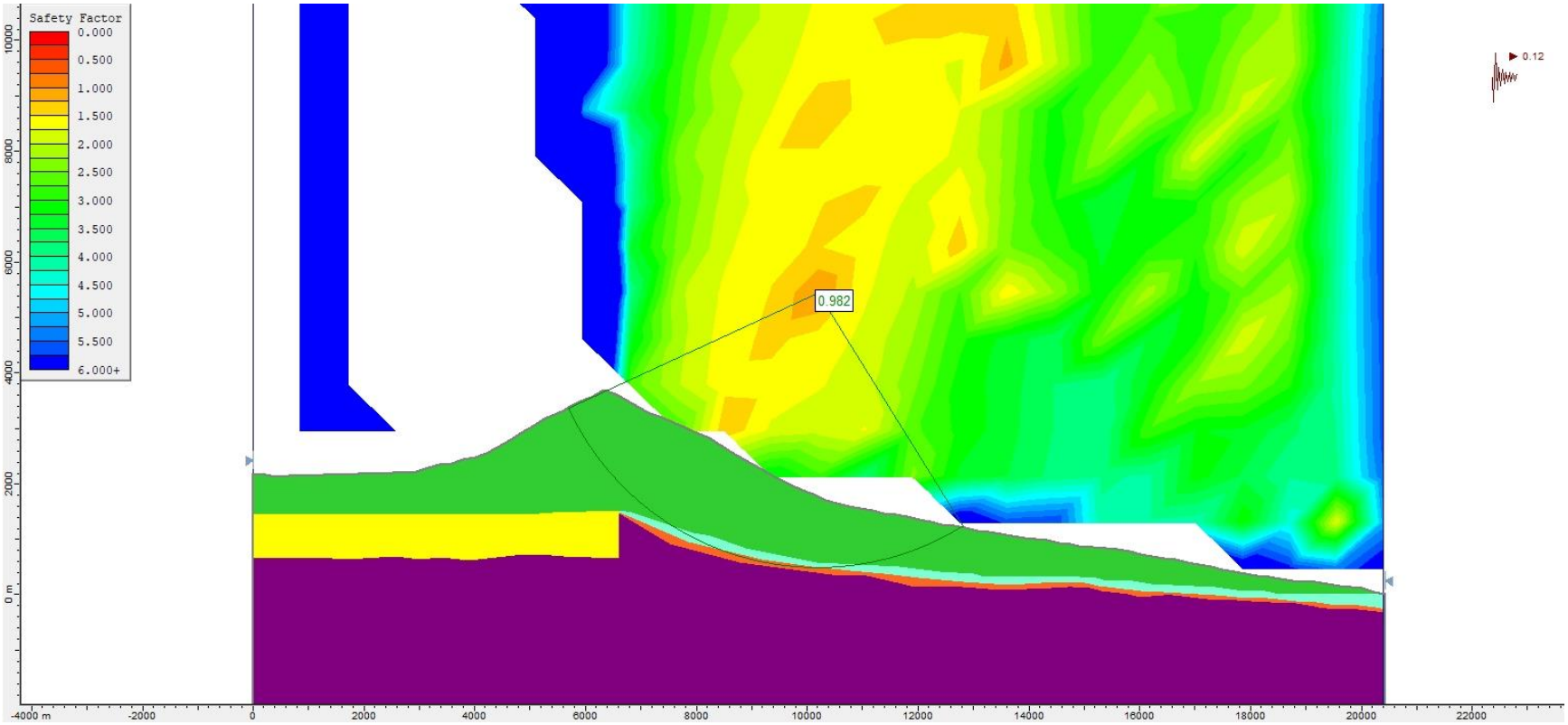

Figure S161. Slope stability pseudo-static analysis for Model 2 (without alteration zones, Figure 4b), using the Janbu Generalised method and a k_h = 0.12.

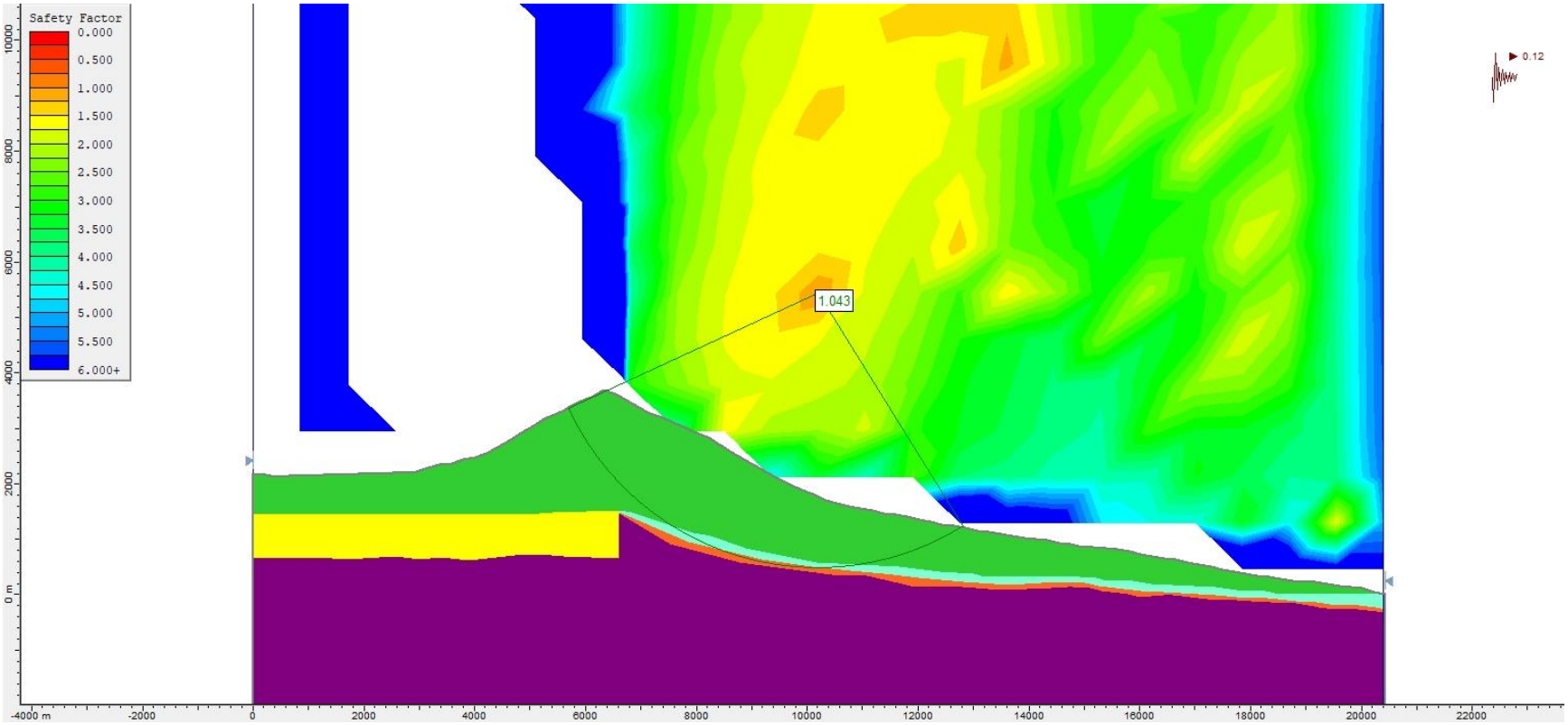

Figure S162. Slope stability pseudo-static analysis for Model 2 (without alteration zones, Figure 4b), using the Morgenstern-Price method and a k_h = 0.12.

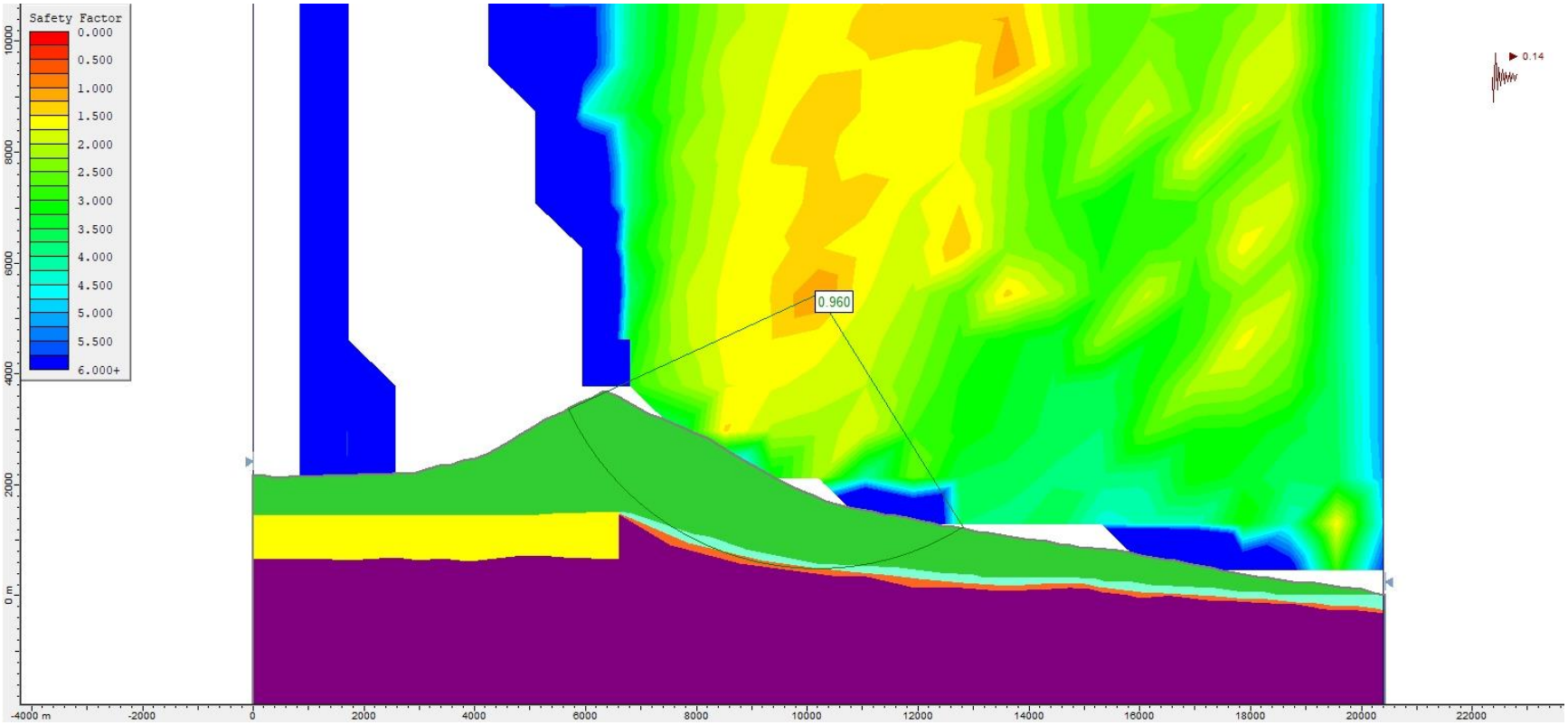

Figure S163. Slope stability pseudo-static analysis for Model 2 (without alteration zones, Figure 4b), using the Bishop simplified method and a $k_h = 0.14$.

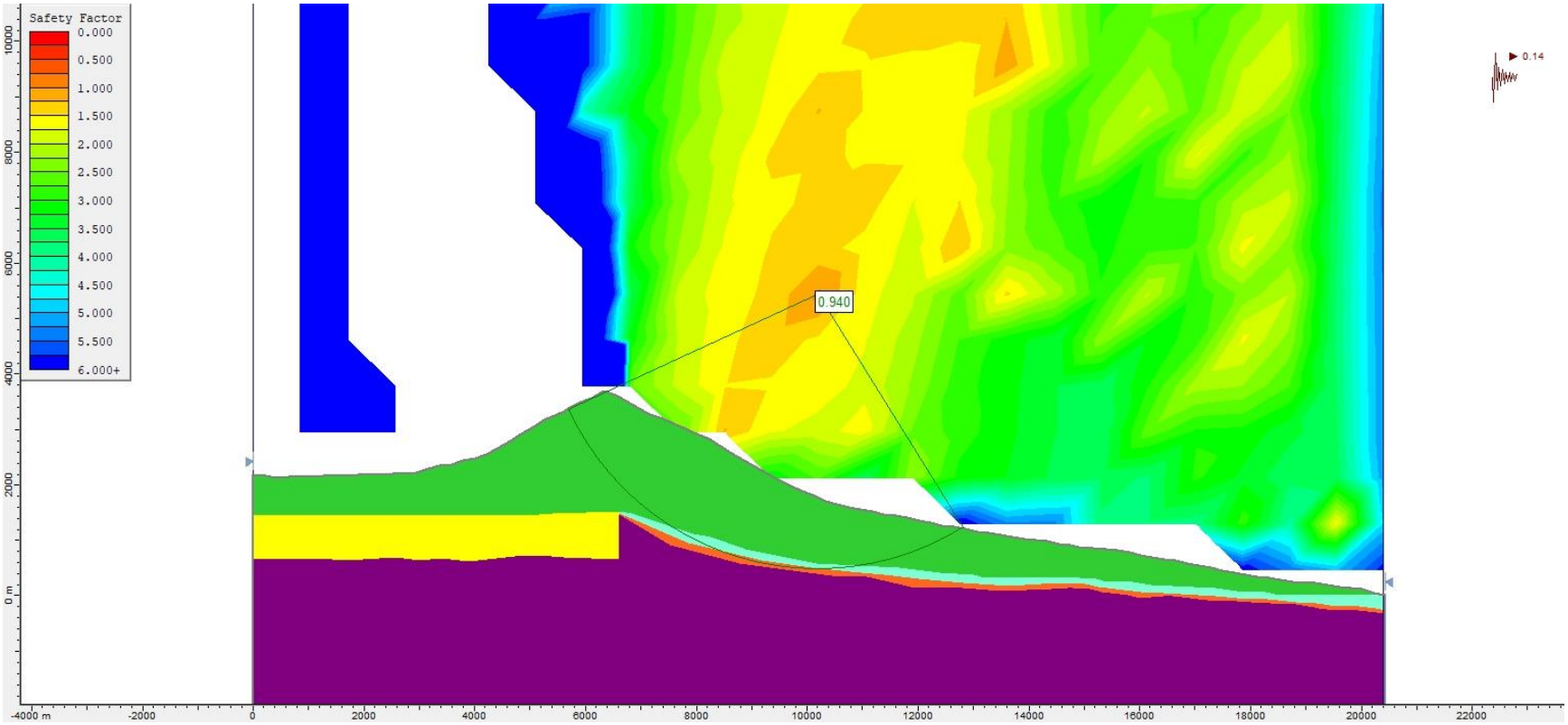

Figure S164. Slope stability pseudo-static analysis for Model 2 (without alteration zones, Figure 4b), using the Janbu Generalised method and a k_h = 0.14.

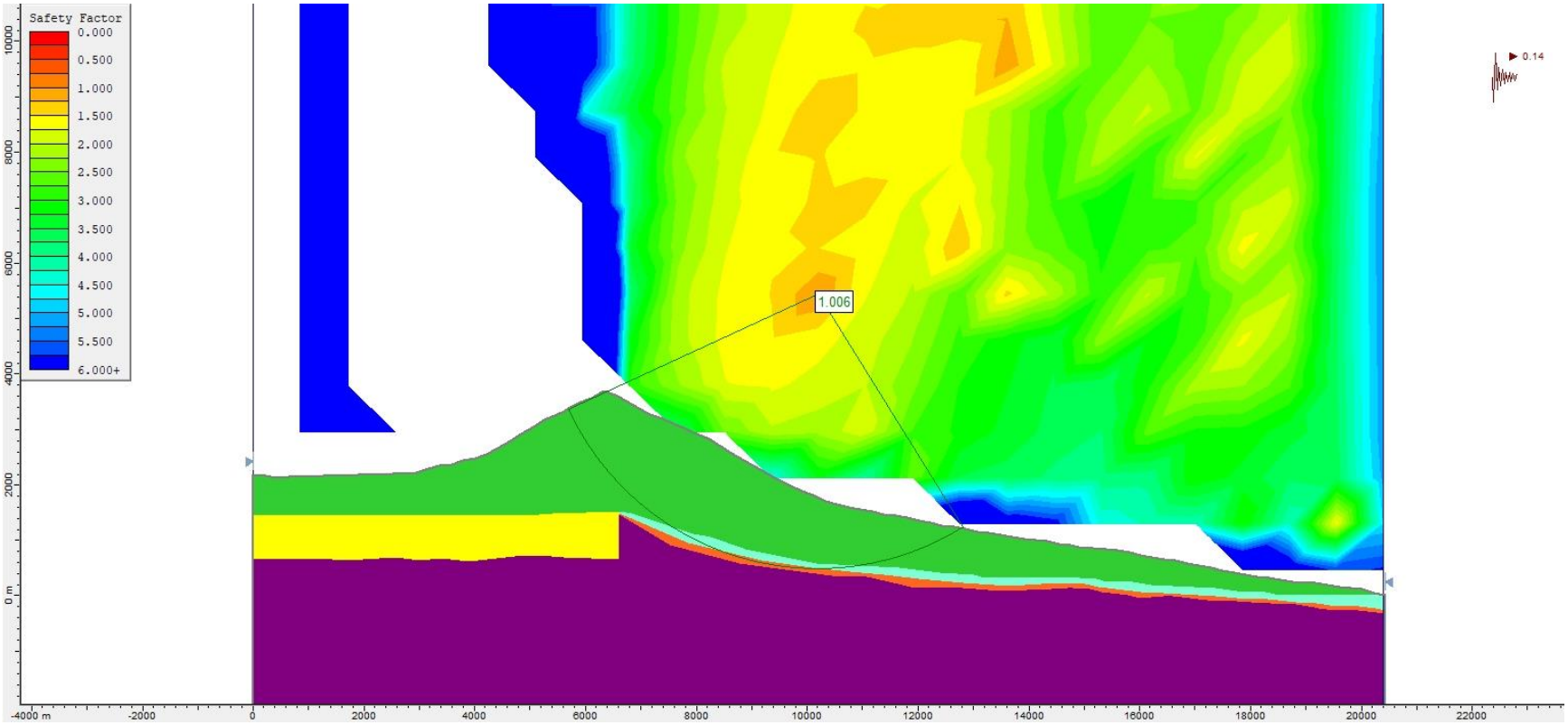

Figure S165. Slope stability pseudo-static analysis for Model 2 (without alteration zones, Figure 4b), using the Morgenstern-Price method and a k_h = 0.14.

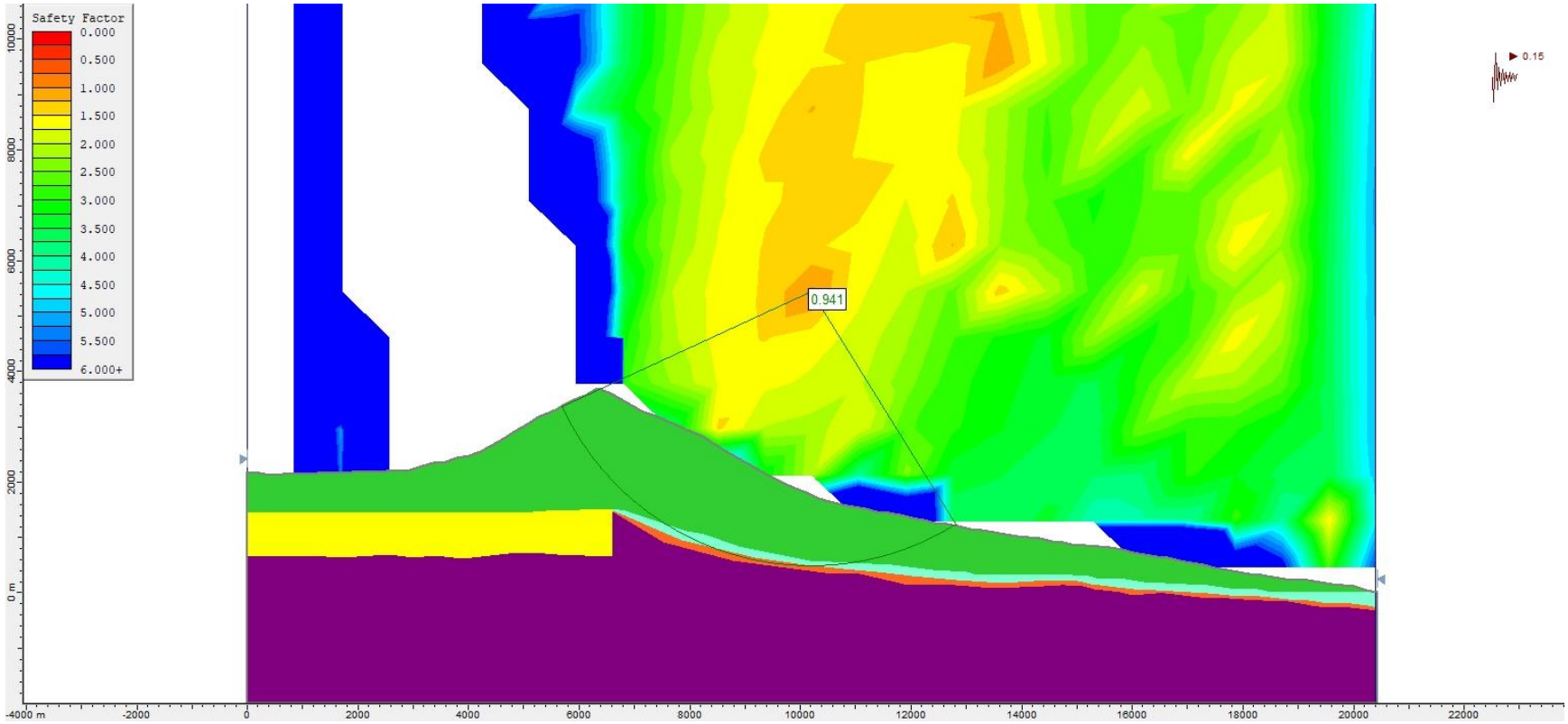

Figure S166. Slope stability pseudo-static analysis for Model 2 (without alteration zones, Figure 4b), using the Bishop simplified method and a $k_h = 0.15$.

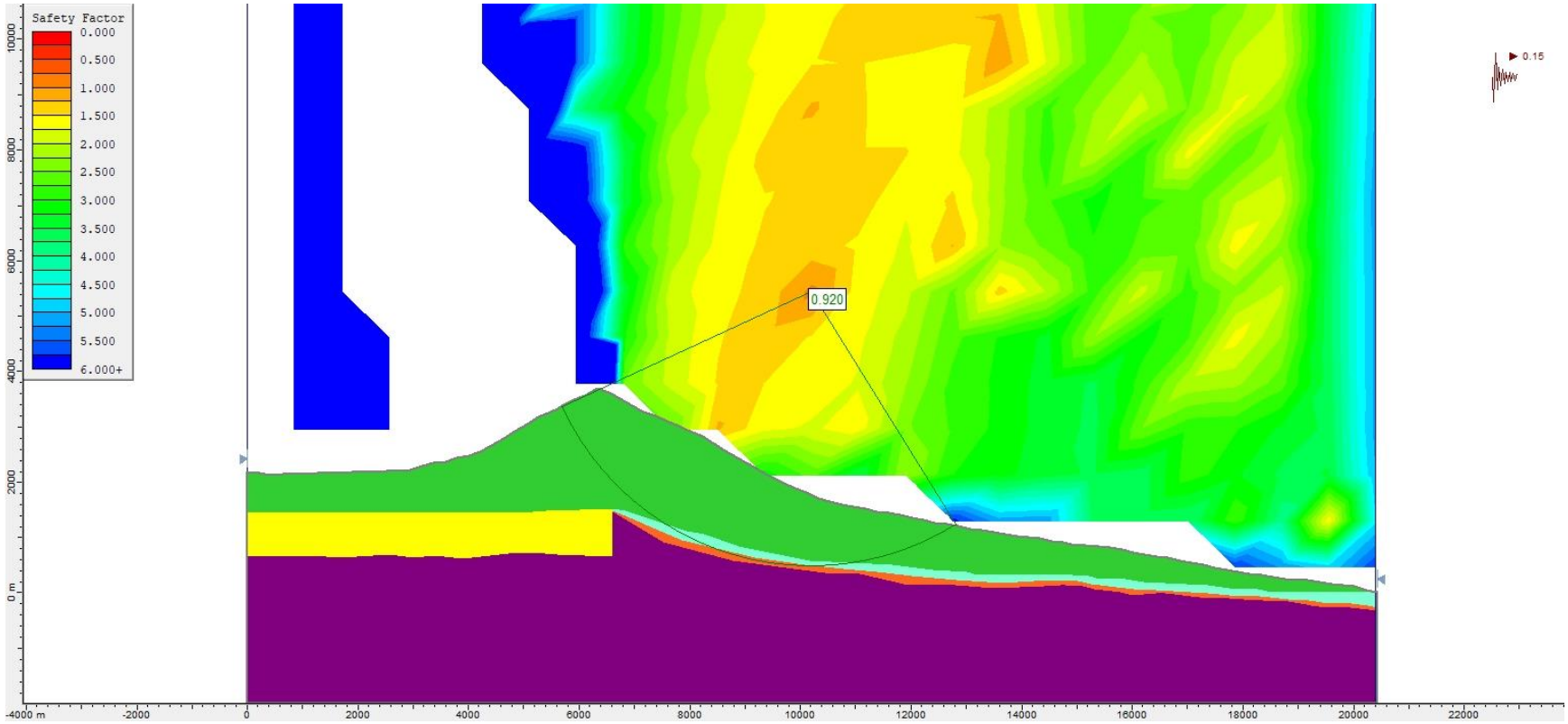

Figure S167. Slope stability pseudo-static analysis for Model 2 (without alteration zones, Figure 4b), using the Janbu Generalised method and a $k_h = 0.15$.

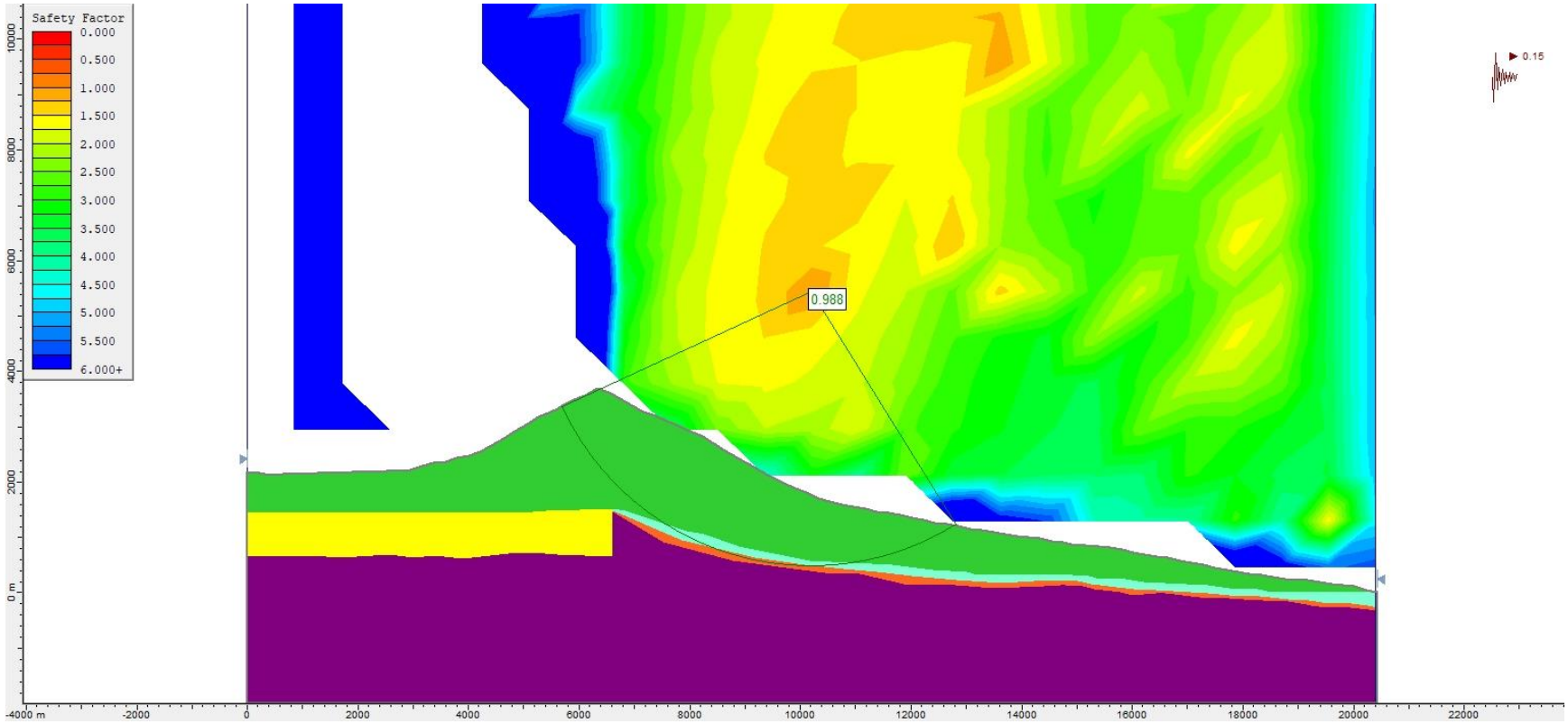

Figure S168. Slope stability pseudo-static analysis for Model 2 (without alteration zones, Figure 4b), using the Morgenstern-Price method and a k_h = 0.15.

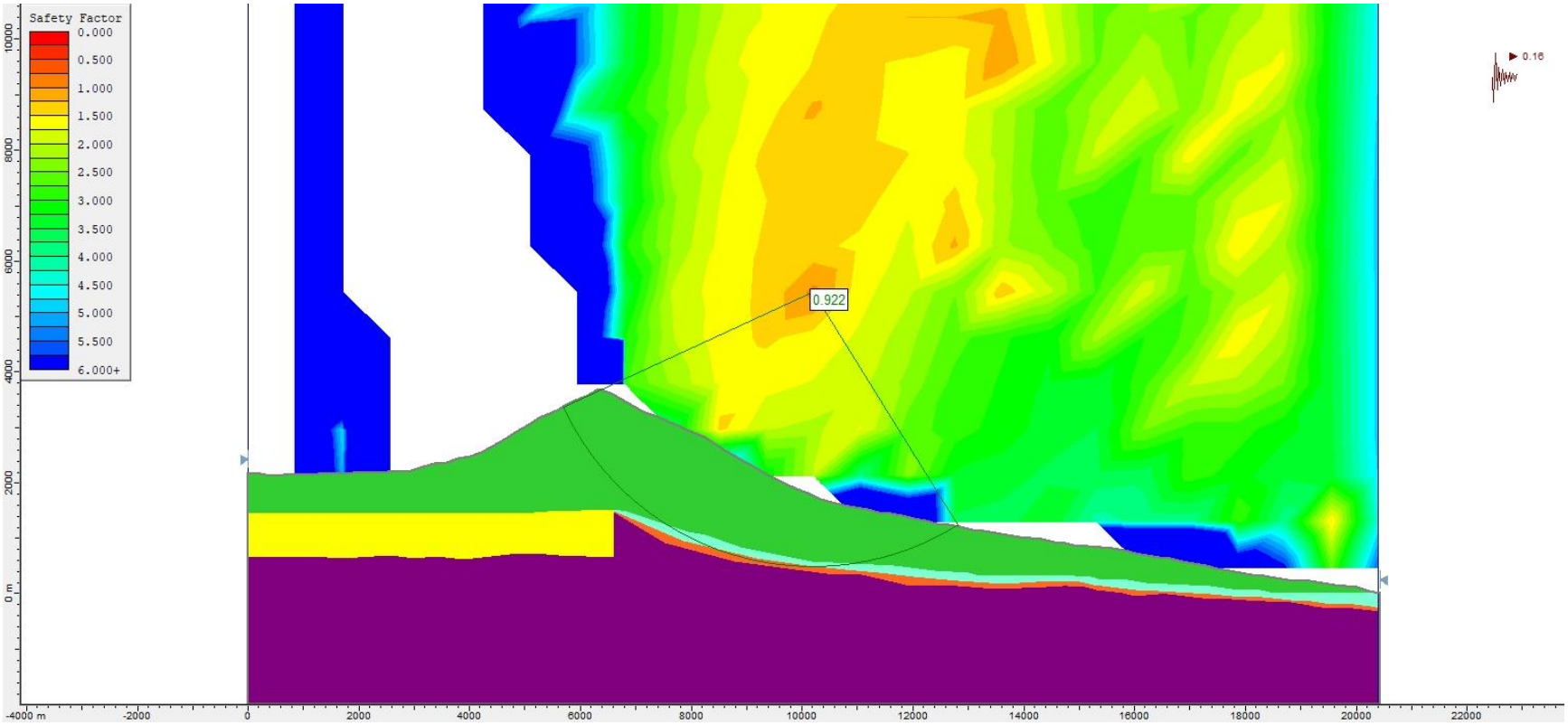

Figure S169. Slope stability pseudo-static analysis for Model 2 (without alteration zones, Figure 4b), using the Bishop simplified method and a k_h = 0.16.

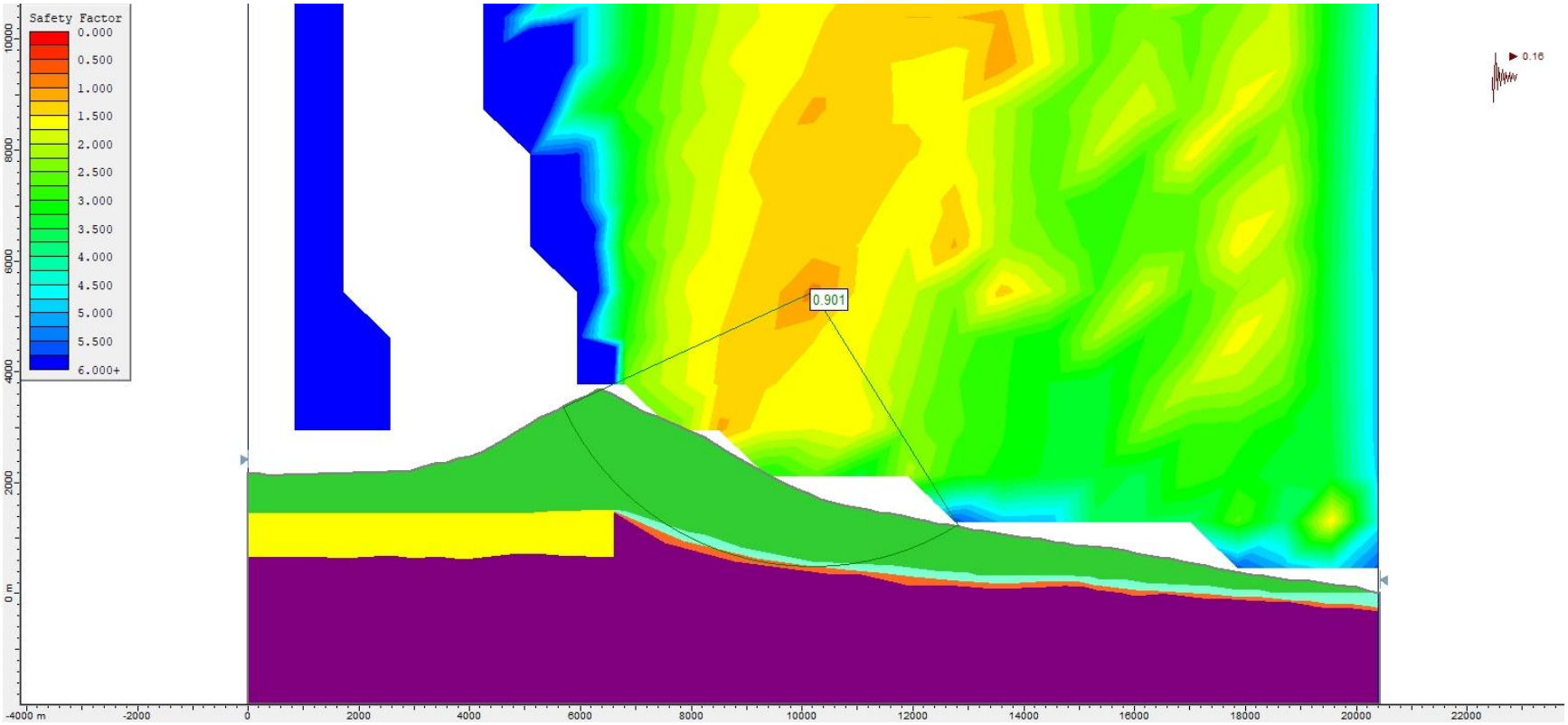

Figure S170. Slope stability pseudo-static analysis for Model 2 (without alteration zones, Figure 4b), using the Janbu Generalised method and a k_h = 0.16.

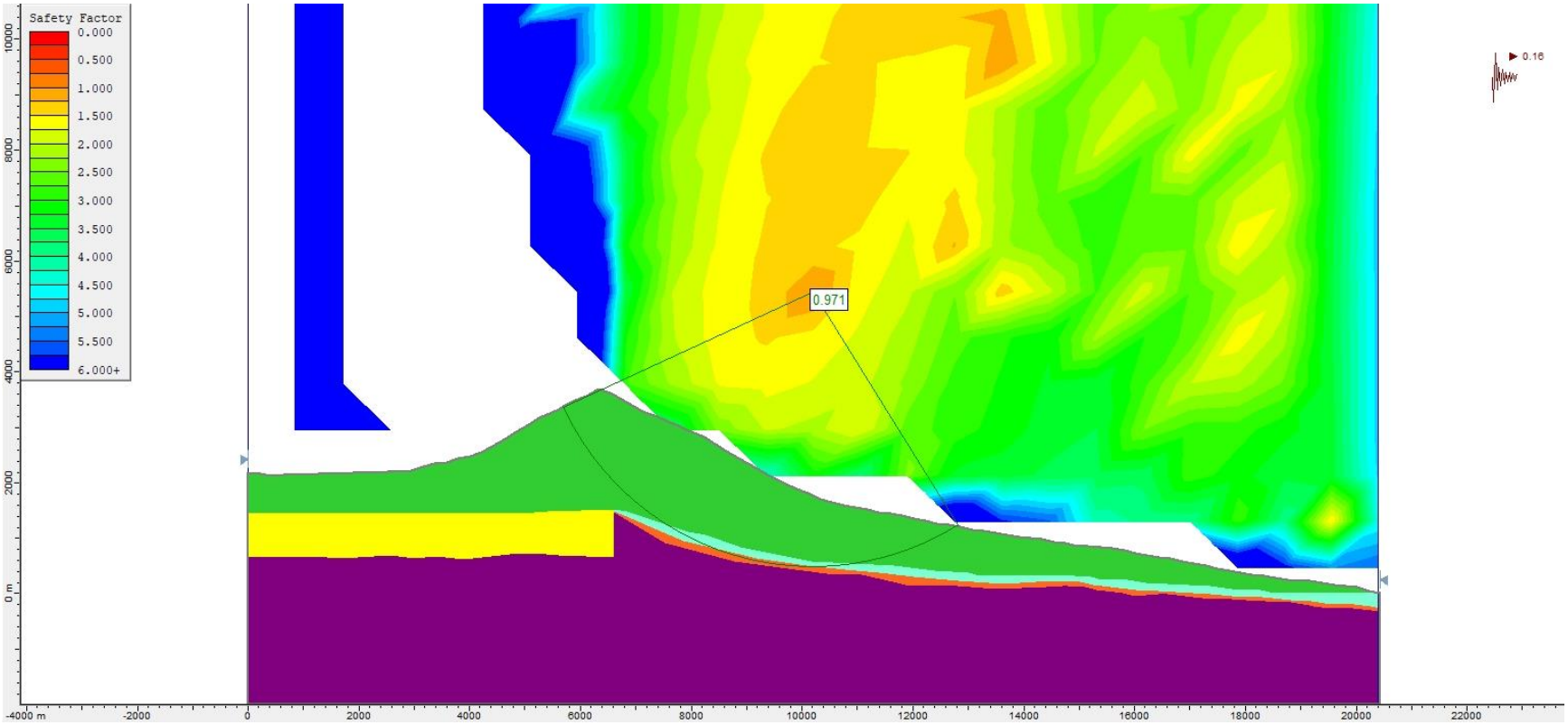

Figure S171. Slope stability pseudo-static analysis for Model 2 (without alteration zones, Figure 4b), using the Morgenstern-Price method and a k_h = 0.16.

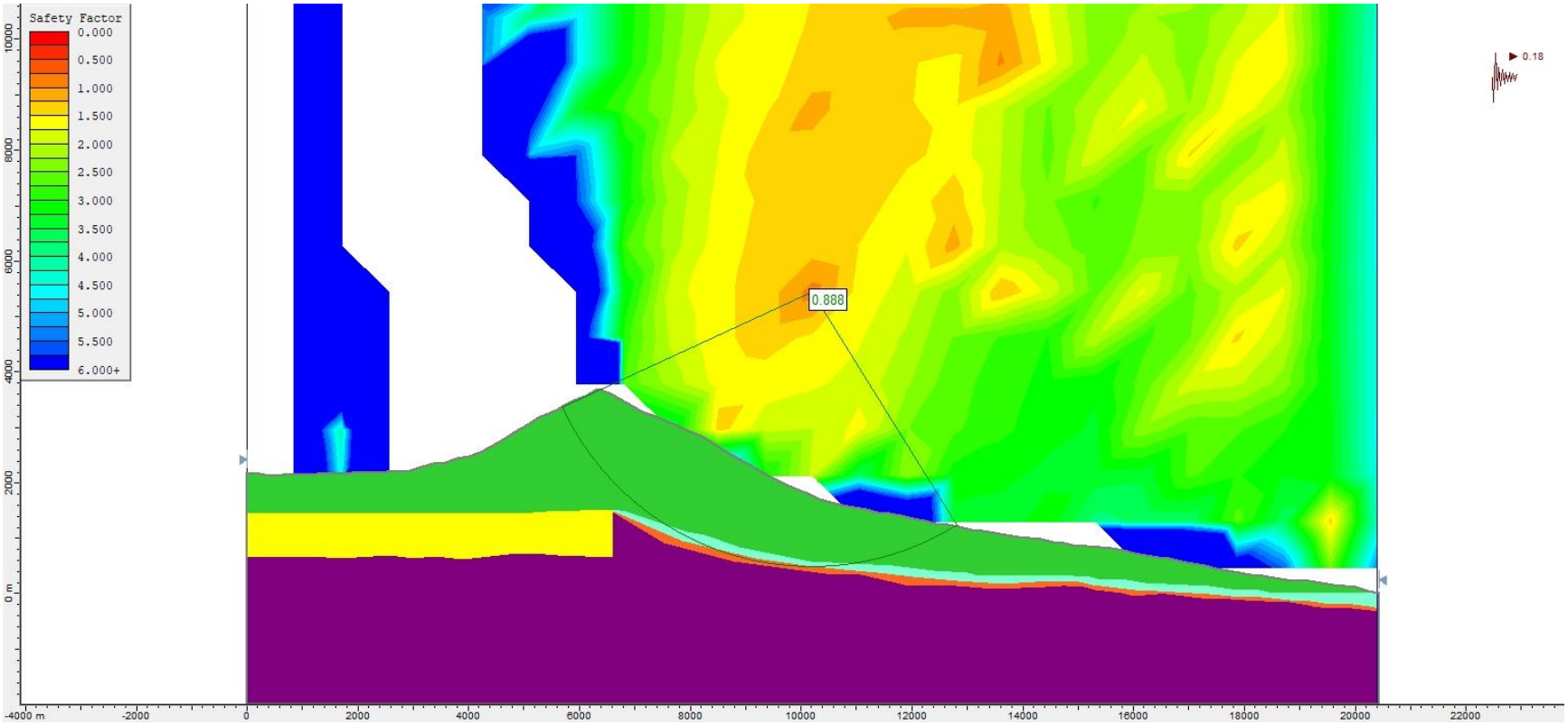

Figure S172. Slope stability pseudo-static analysis for Model 2 (without alteration zones, Figure 4b), using the Bishop simplified method and a k_h = 0.18.

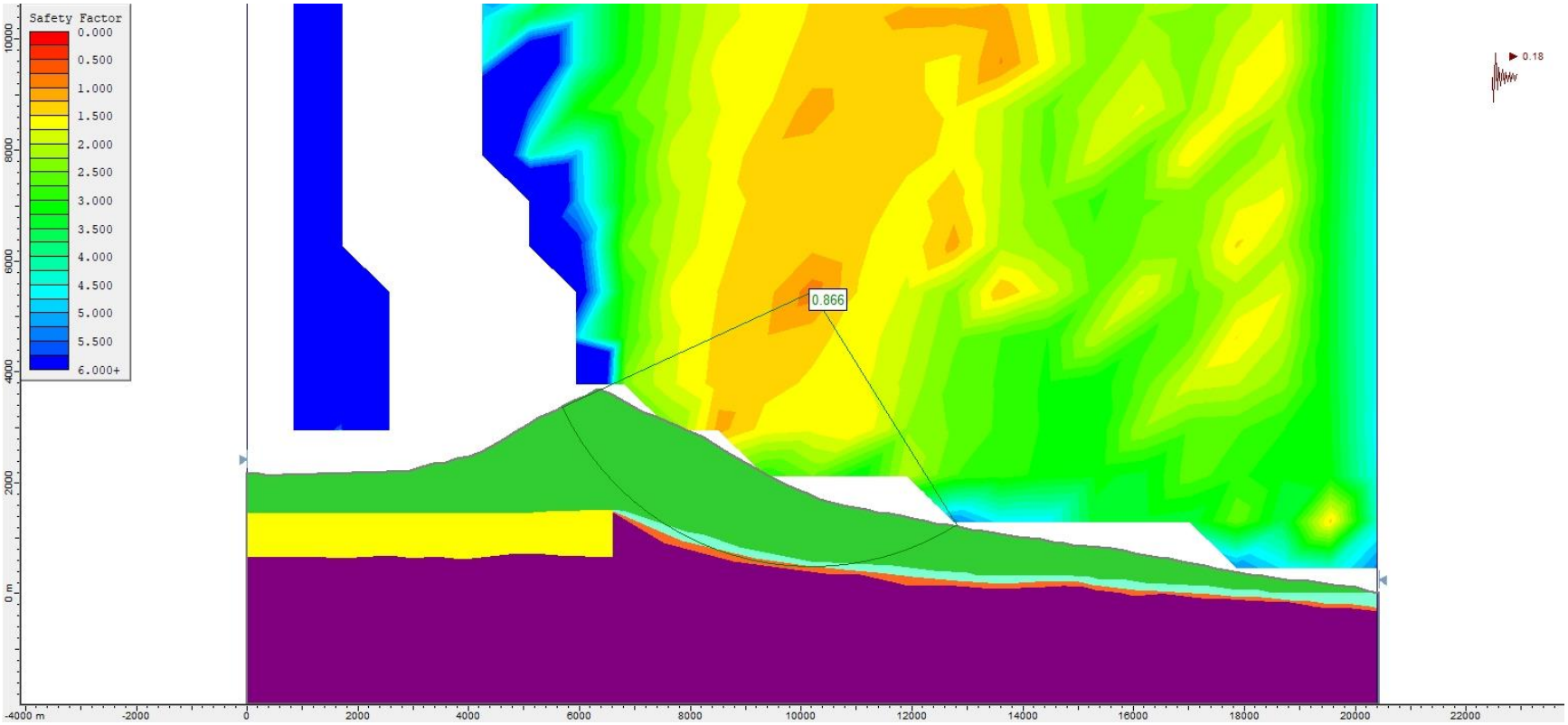

Figure S173. Slope stability pseudo-static analysis for Model 2 (without alteration zones, Figure 4b), using the Janbu Generalised method and a k_h = 0.18.

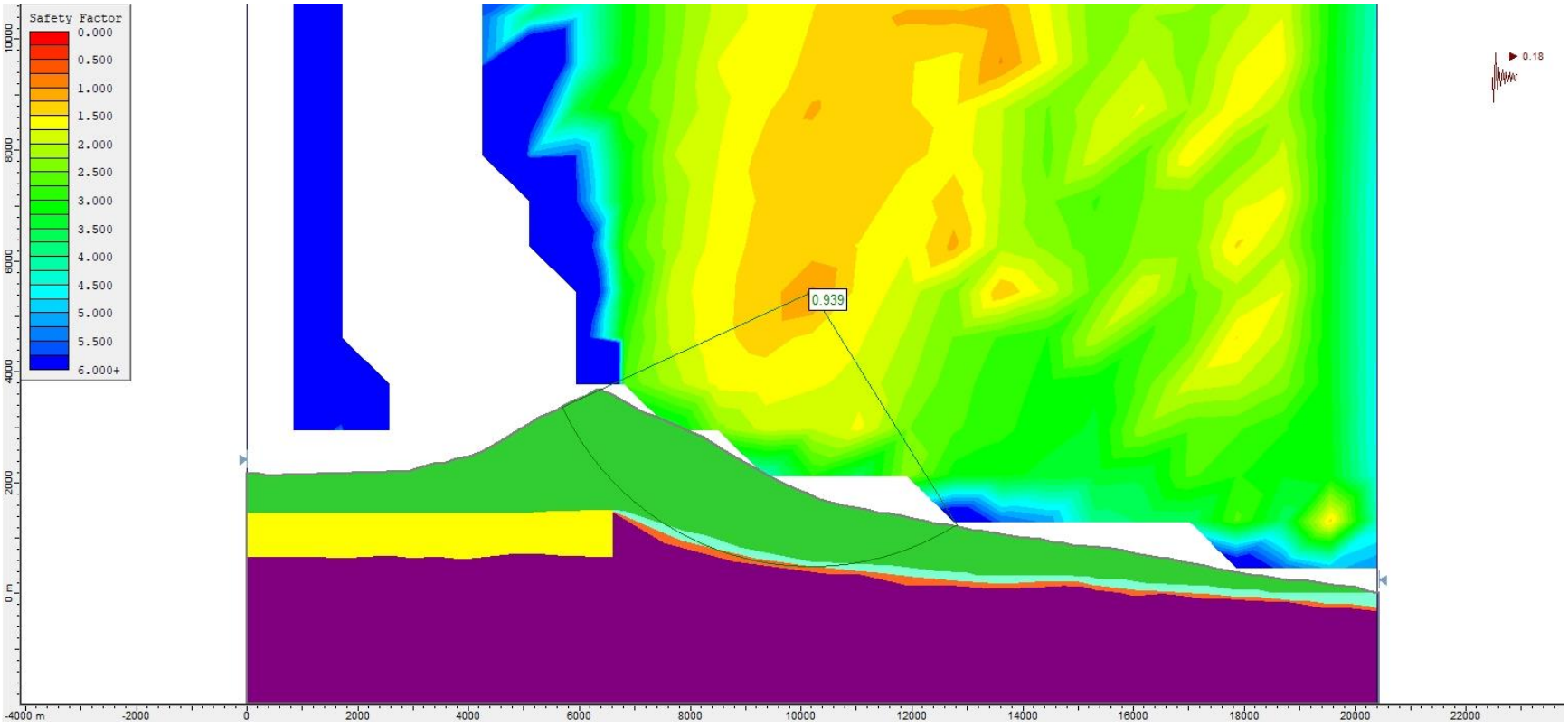

Figure S174. Slope stability pseudo-static analysis for Model 2 (without alteration zones, Figure 4b), using the Morgenstern-Price method and a k_h = 0.18.

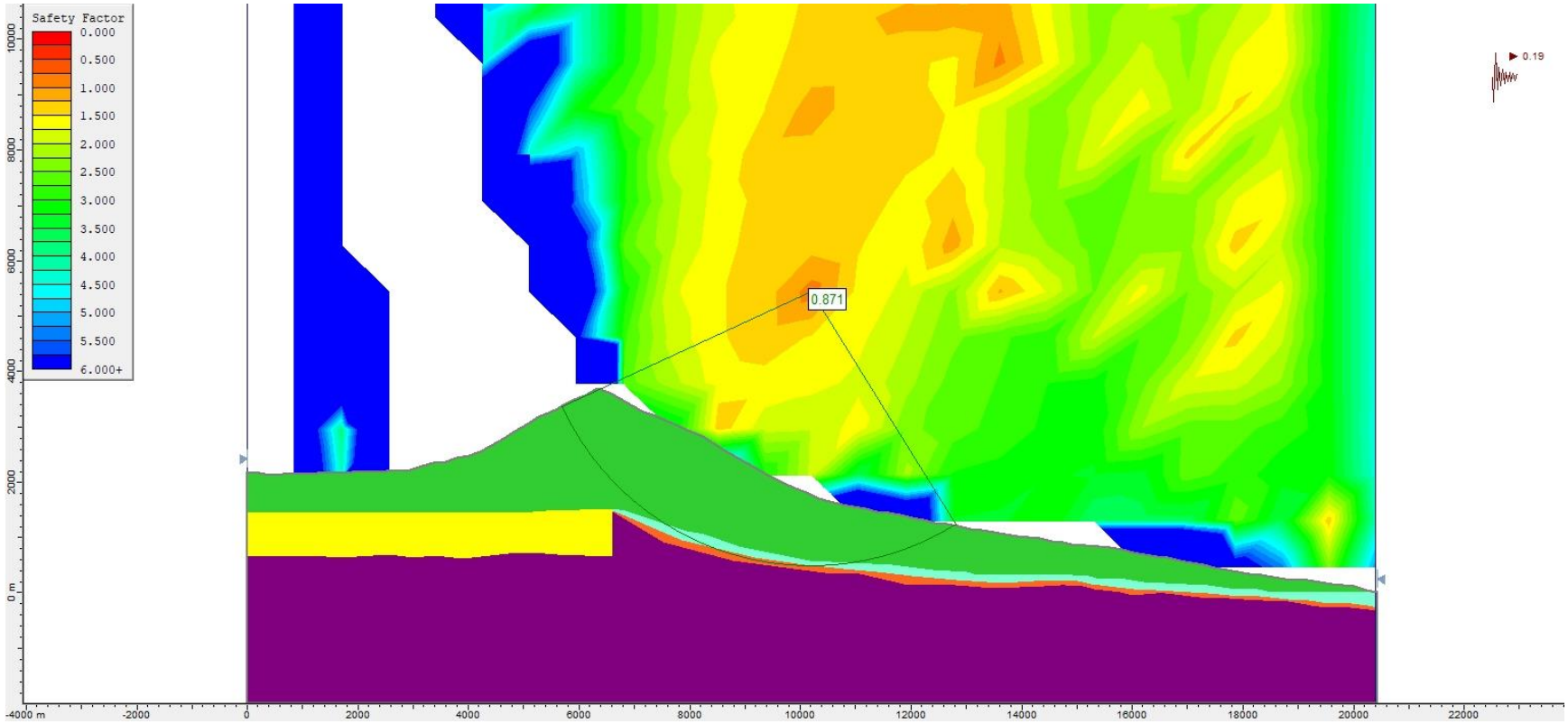

Figure S175. Slope stability pseudo-static analysis for Model 2 (without alteration zones, Figure 4b), using the Bishop simplified method and a k_h = 0.19.

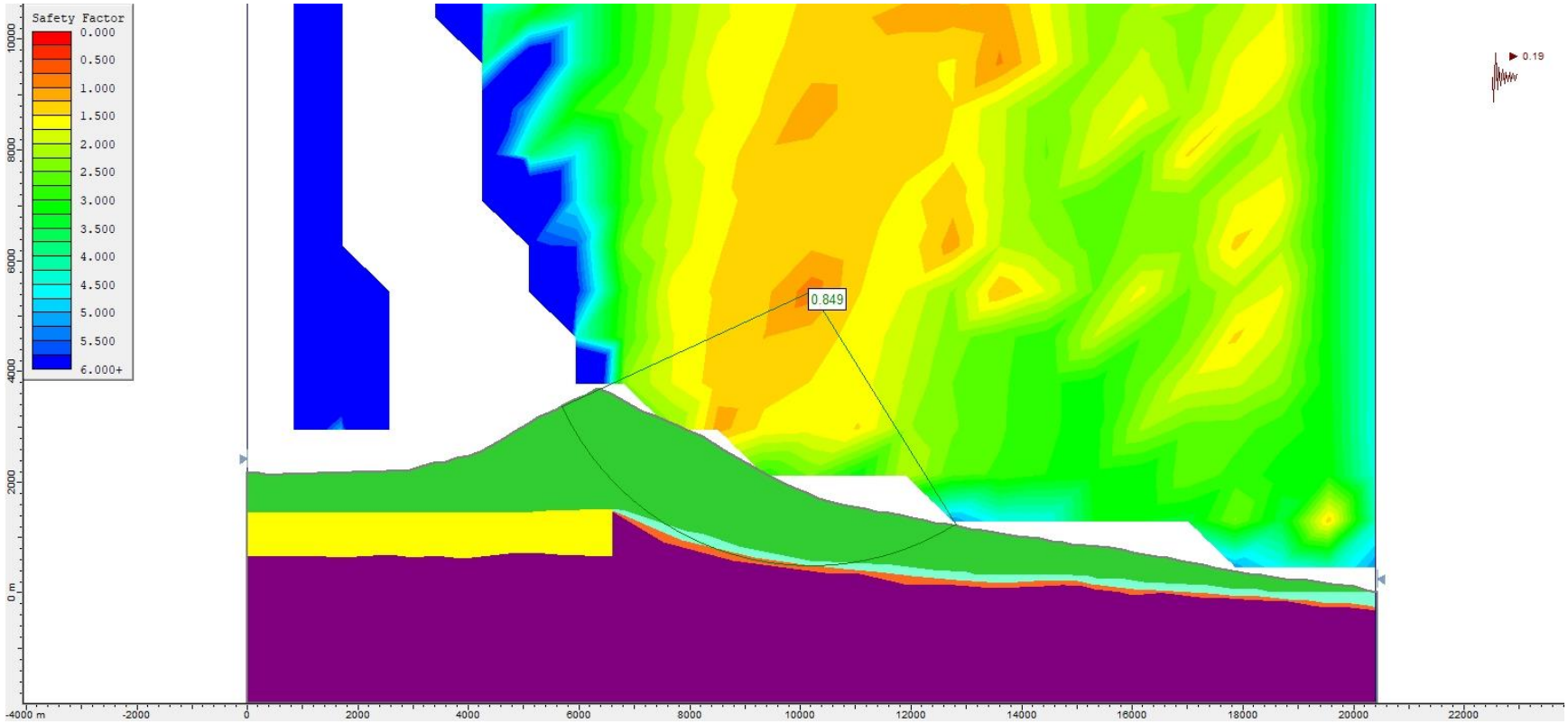

Figure S176. Slope stability pseudo-static analysis for Model 2 (without alteration zones, Figure 4b), using the Janbu Generalised method and a k_h = 0.19.

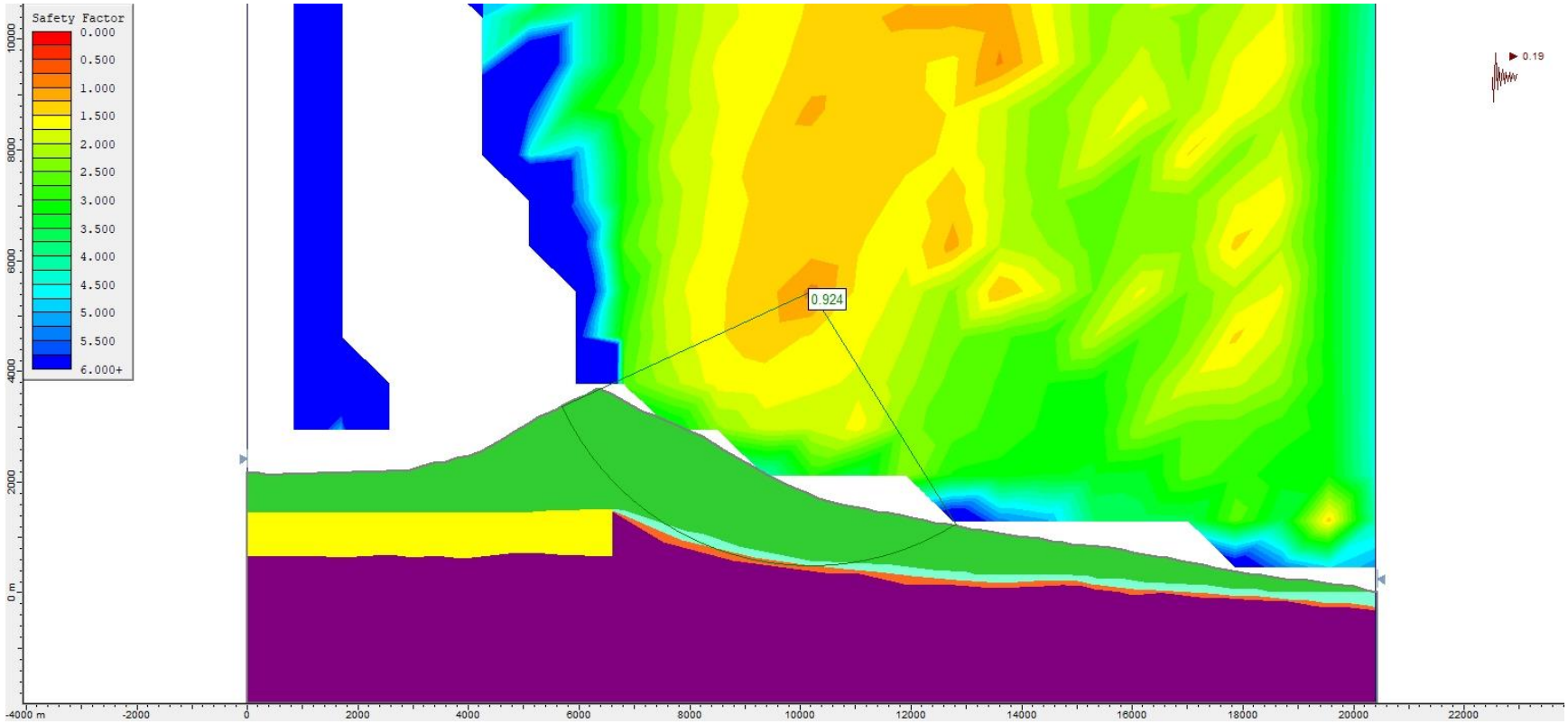

Figure S177. Slope stability pseudo-static analysis for Model 2 (without alteration zones, Figure 4b), using the Morgenstern-Price method and a k_h = 0.19.

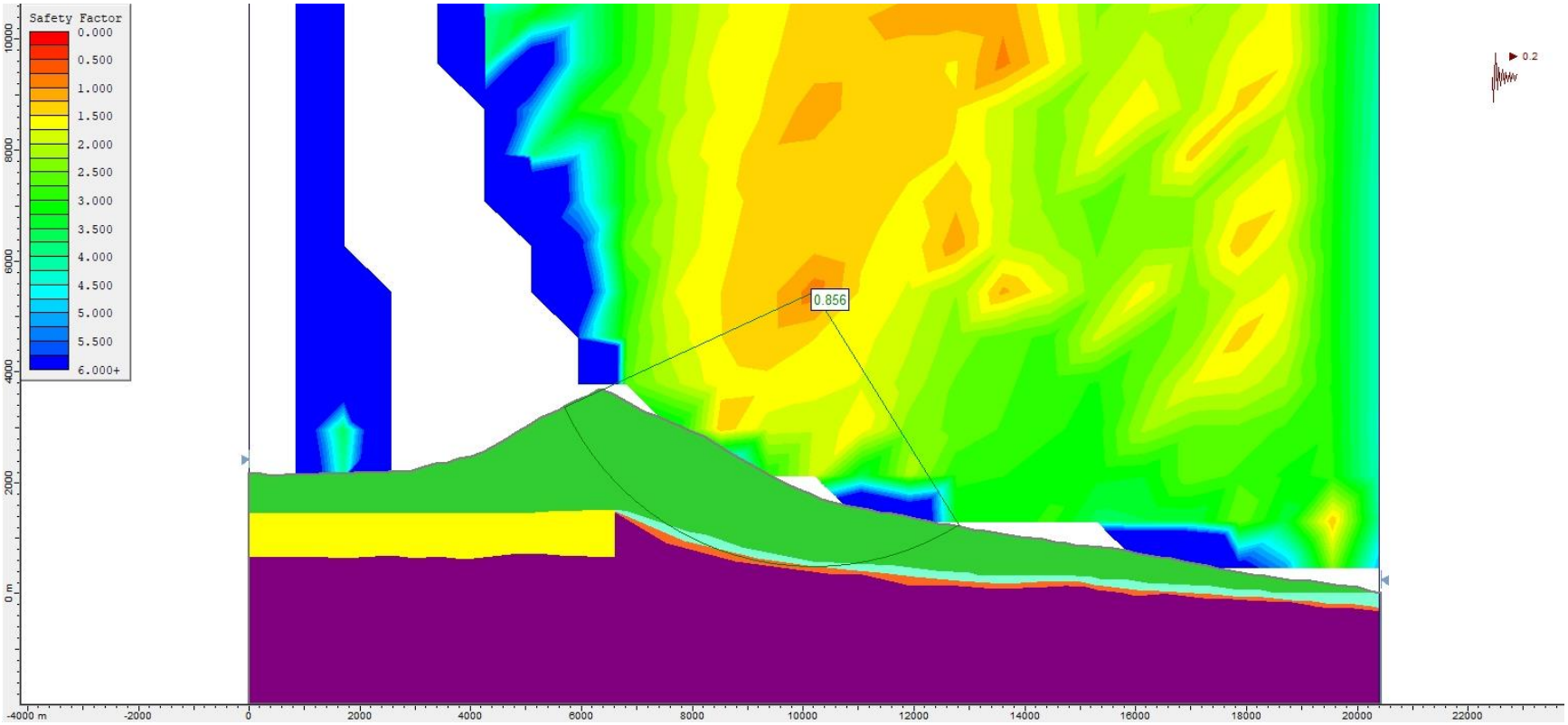

Figure S178. Slope stability pseudo-static analysis for Model 2 (without alteration zones, Figure 4b), using the Bishop simplified method and a k_h = 0.20.

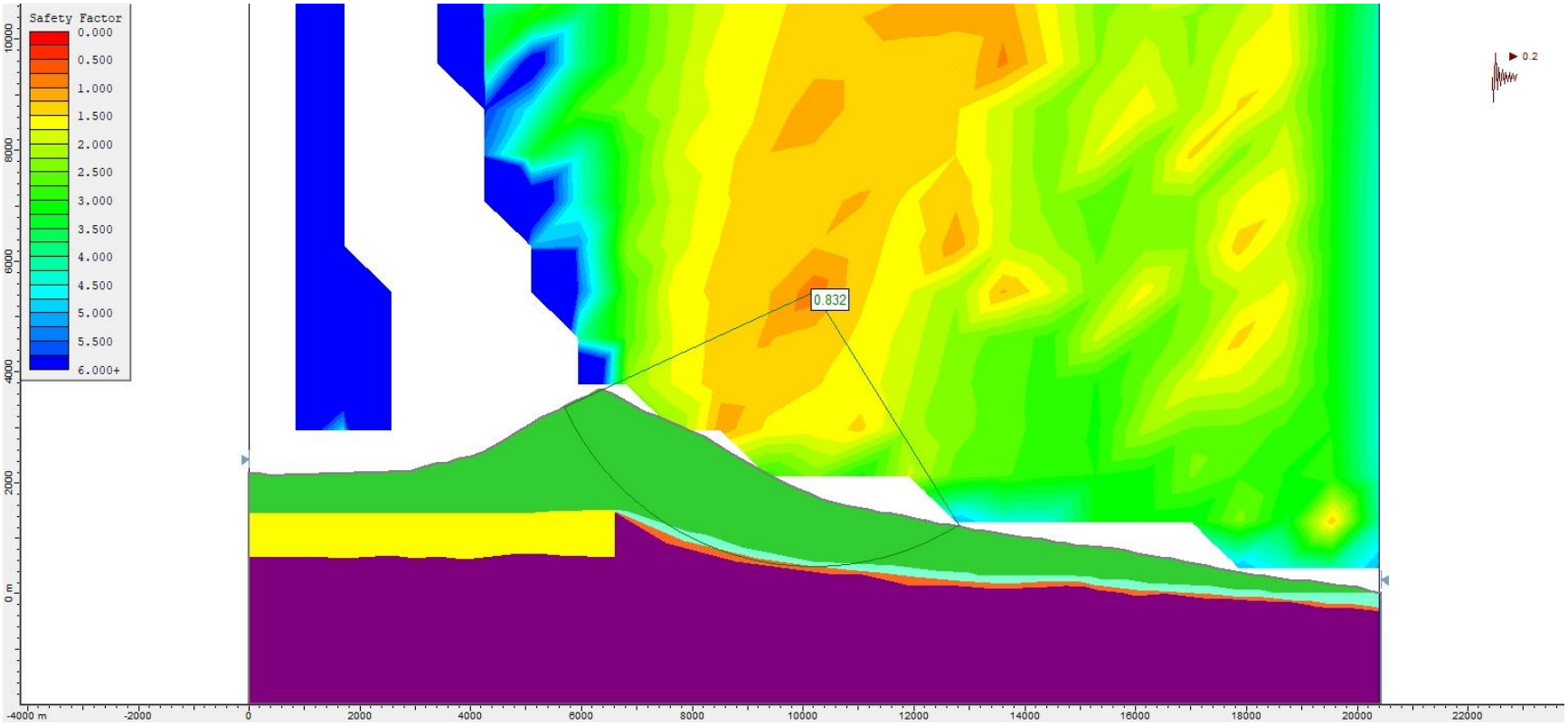

Figure S179. Slope stability pseudo-static analysis for Model 2 (without alteration zones, Figure 4b), using the Janbu Generalised method and a k_h = 0.20.

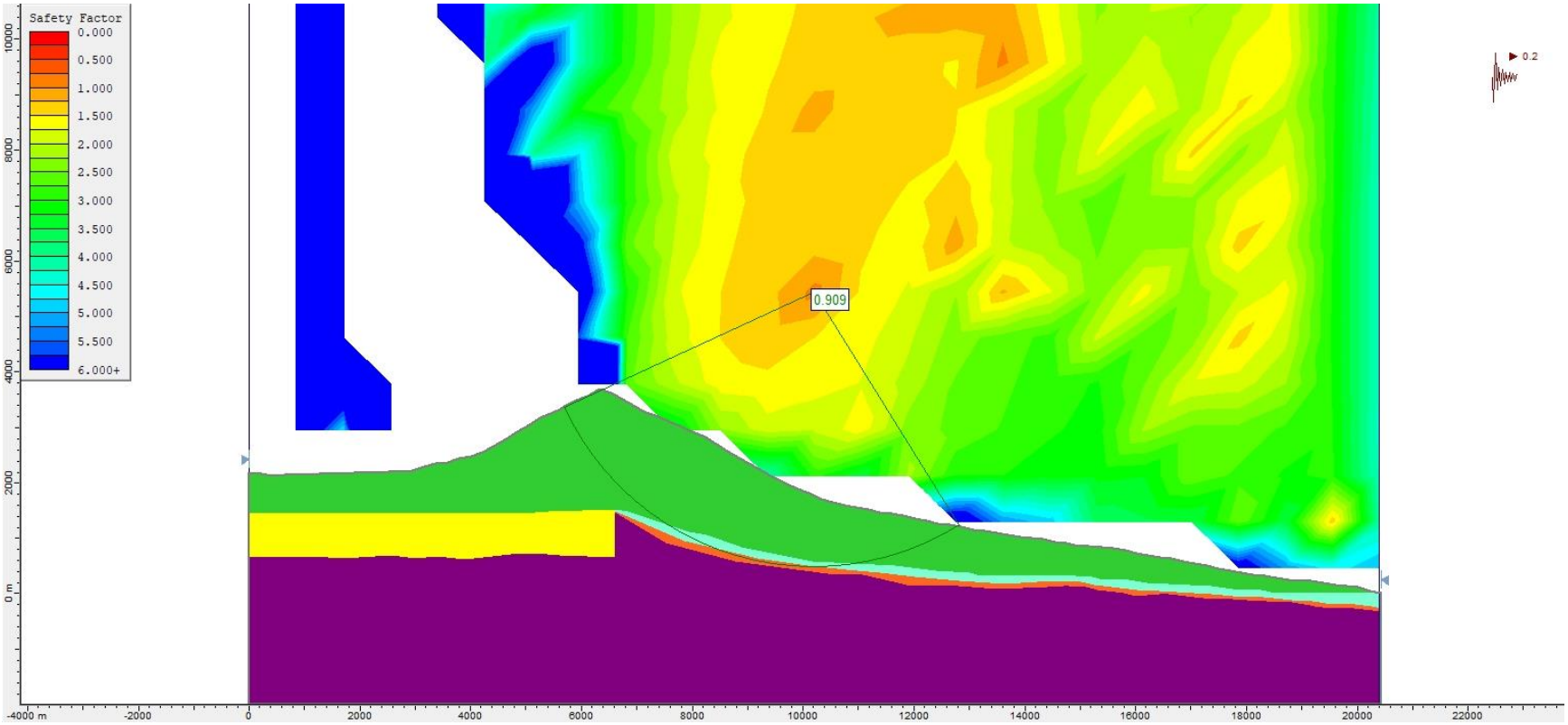

Figure S180. Slope stability pseudo-static analysis for Model 2 (without alteration zones, Figure 4b), using the Morgenstern-Price method and a k_h = 0.20.

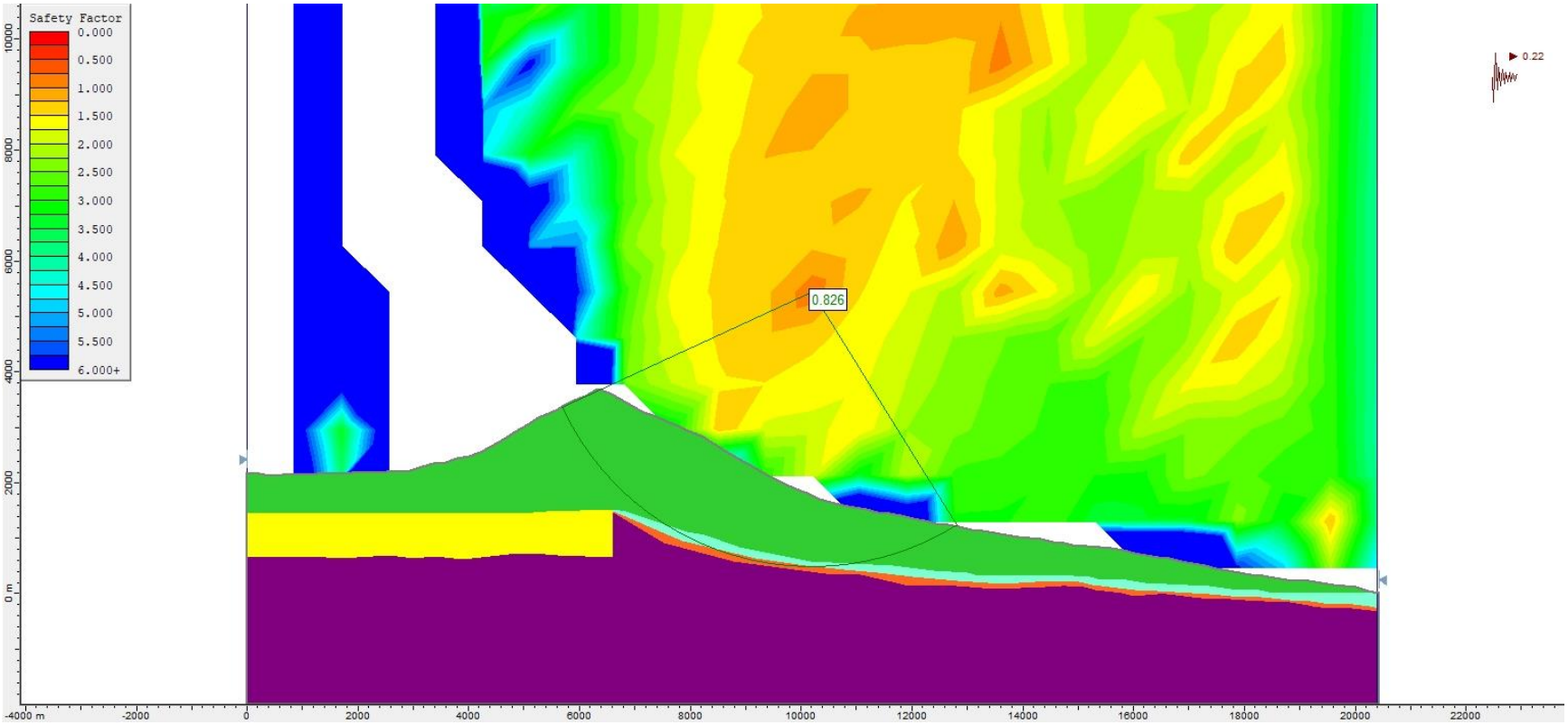

Figure S181. Slope stability pseudo-static analysis for Model 2 (without alteration zones, Figure 4b), using the Bishop simplified method and a k_h = 0.22.

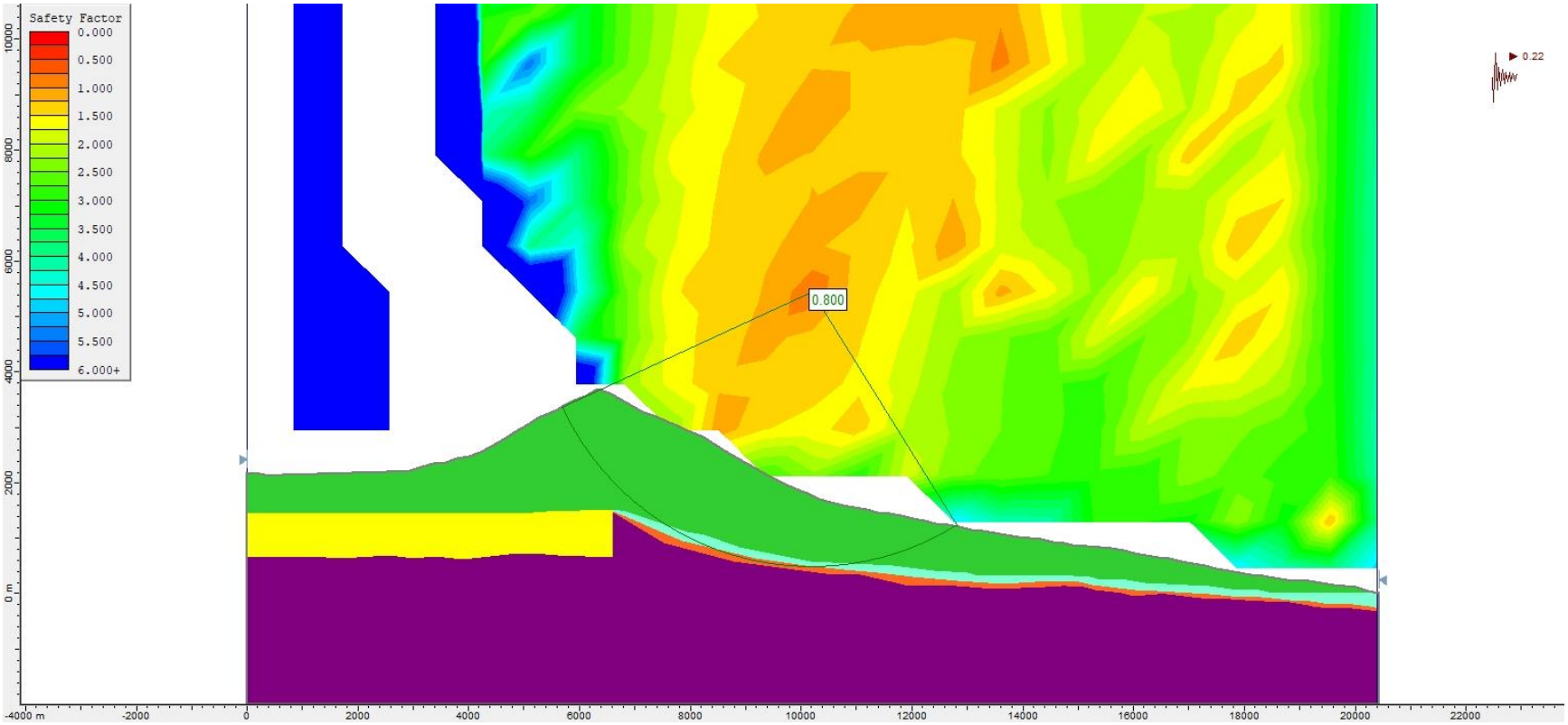

Figure S182. Slope stability pseudo-static analysis for Model 2 (without alteration zones, Figure 4b), using the Janbu Generalised method and a k_h = 0.22.

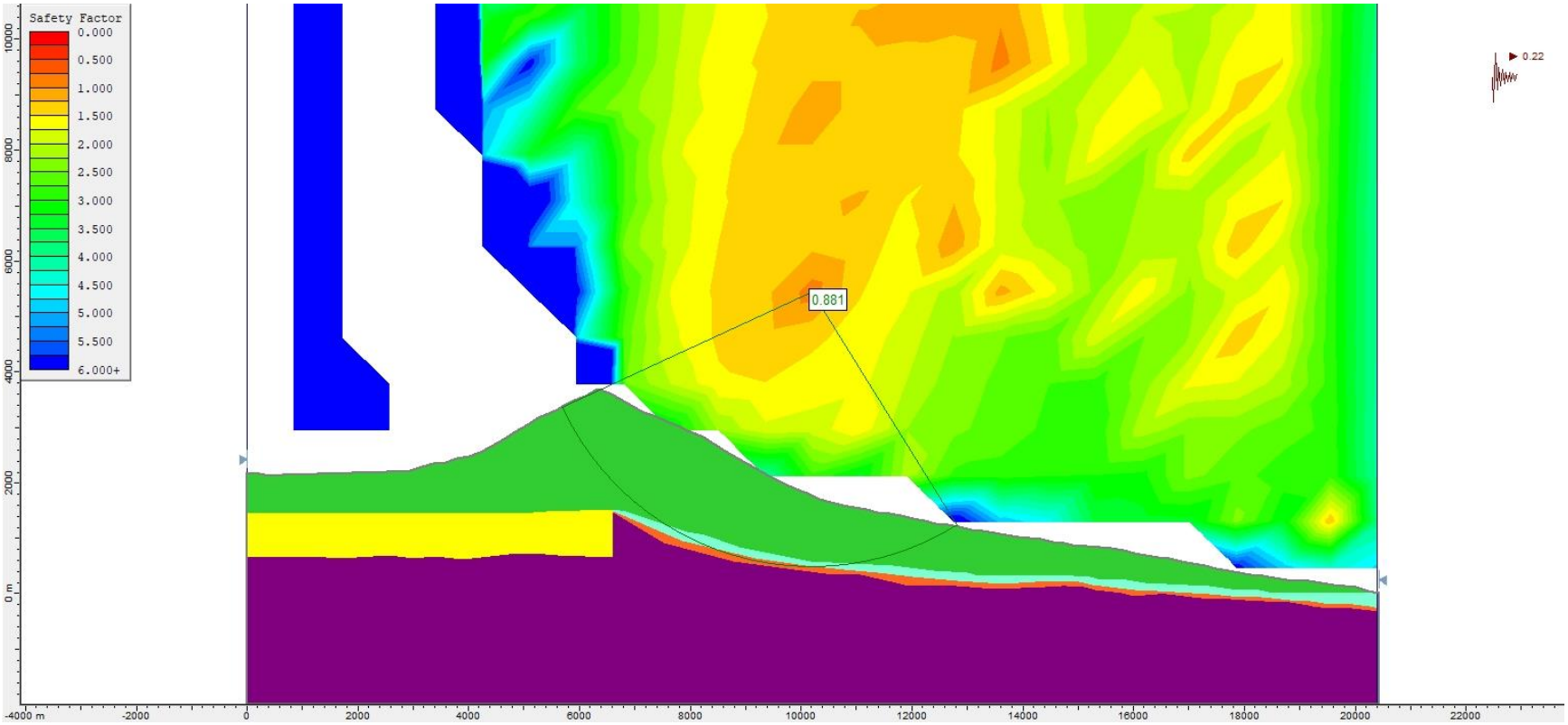

Figure S183. Slope stability pseudo-static analysis for Model 2 (without alteration zones, Figure 4b), using the Morgenstern-Price method and a k_h = 0.22.

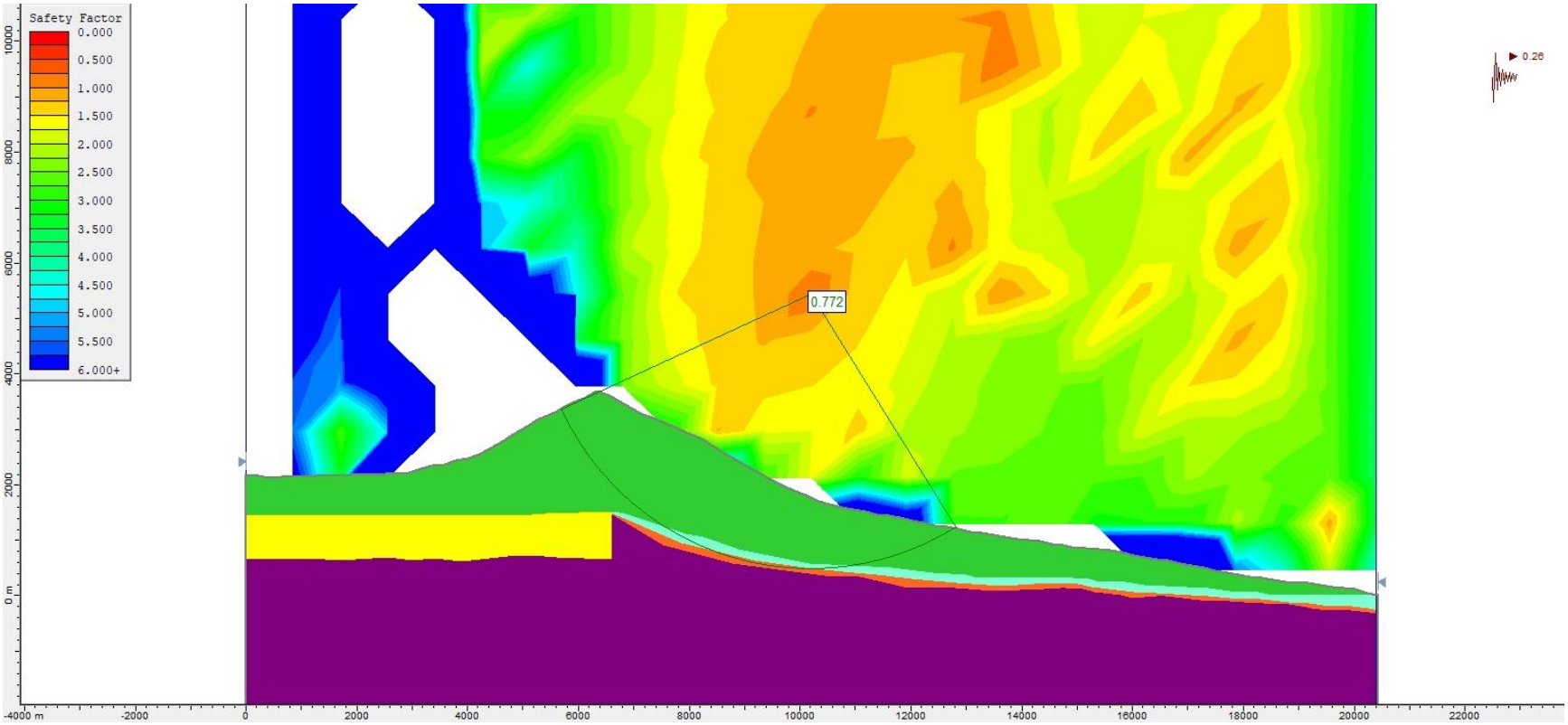

Figure S184. Slope stability pseudo-static analysis for Model 2 (without alteration zones, Figure 4b), using Bishop simplified method and a k_h = 0.26.

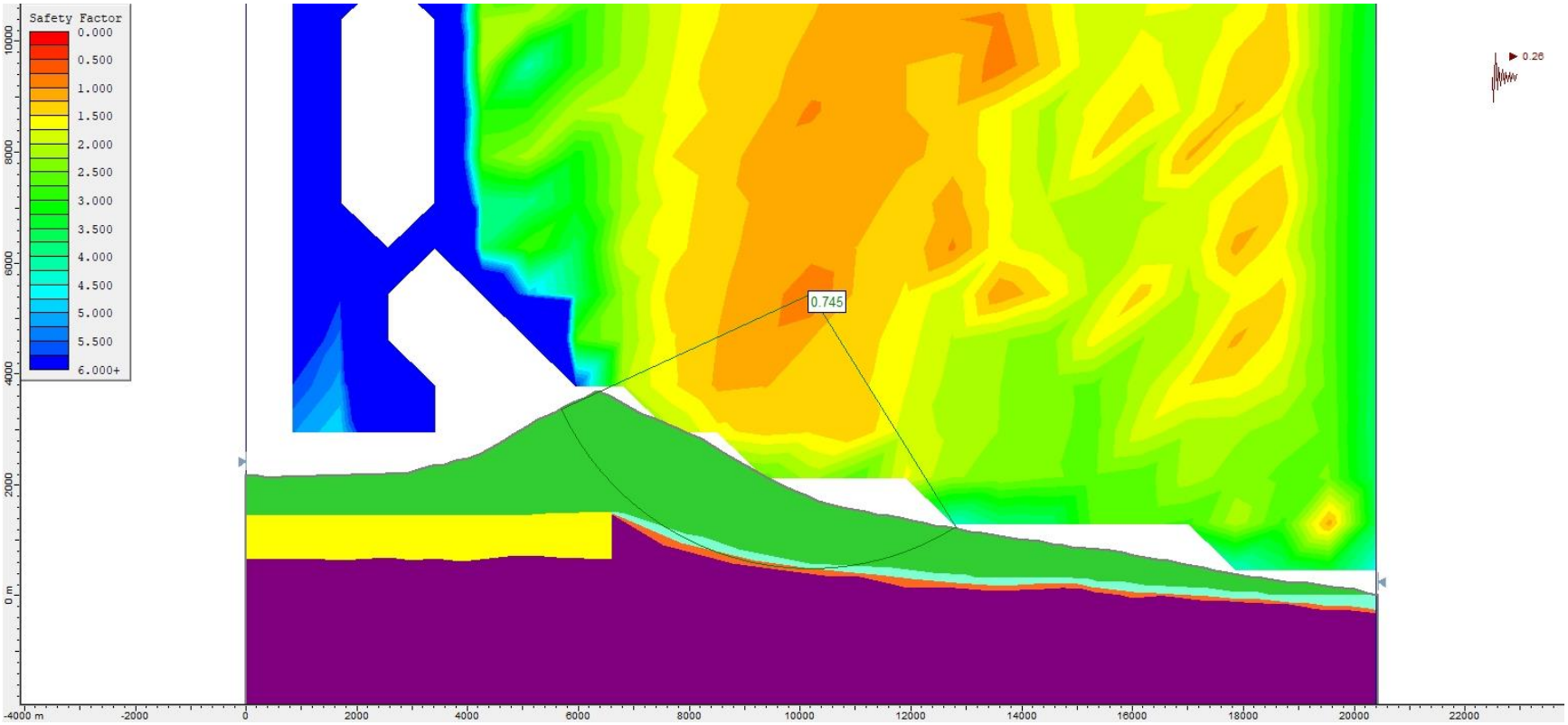

Figure S185. Slope stability pseudo-static analysis for Model 2 (without alteration zones, Figure 4b), using the Janbu Generalised method and a k_h = 0.26.

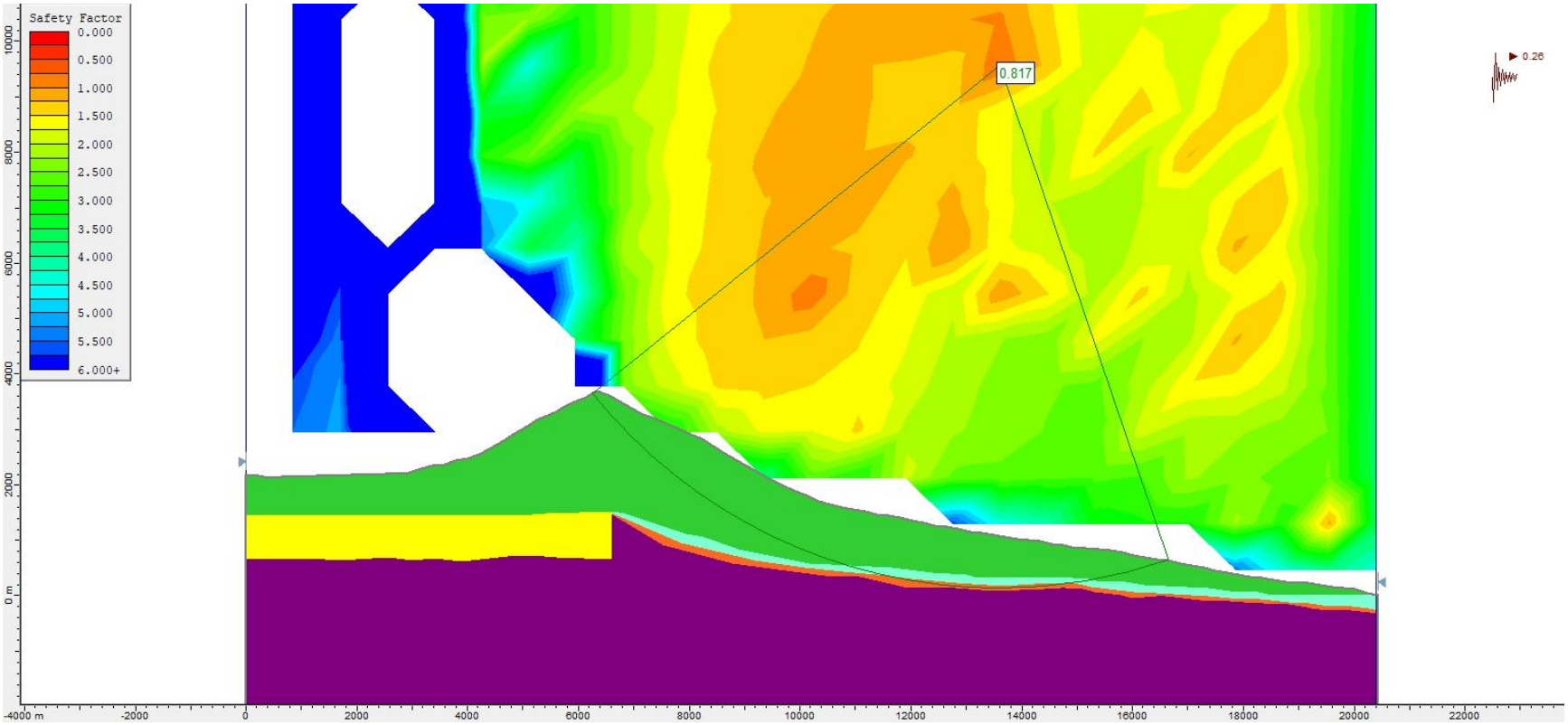

Figure S186. Slope stability pseudo-static analysis for Model 2 (without alteration zones, Figure 4b), using the Morgenstern-Price method and a k_h = 0.26.

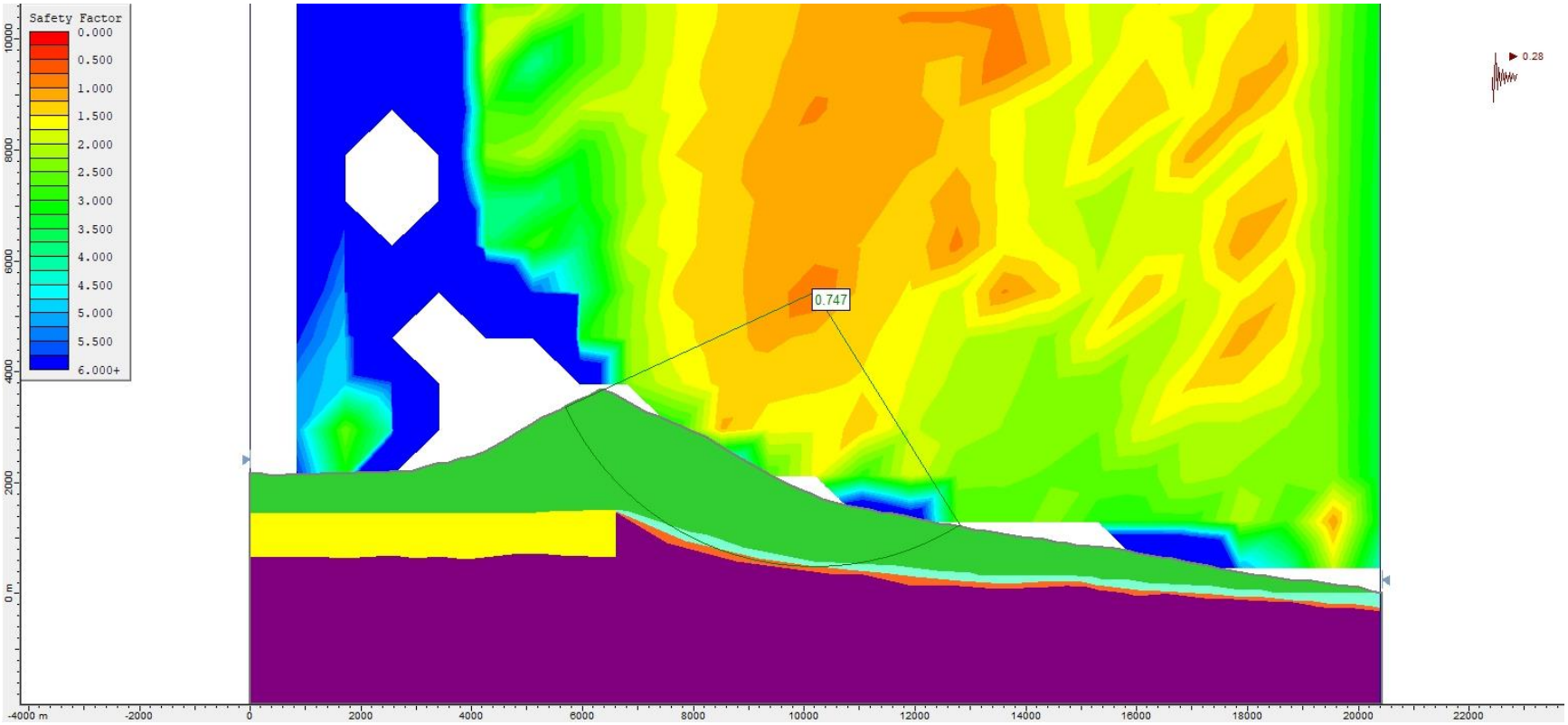

Figure S187. Slope stability pseudo-static analysis for Model 2 (without alteration zones, Figure 4b), using the Bishop simplified method and a k_h = 0.28.

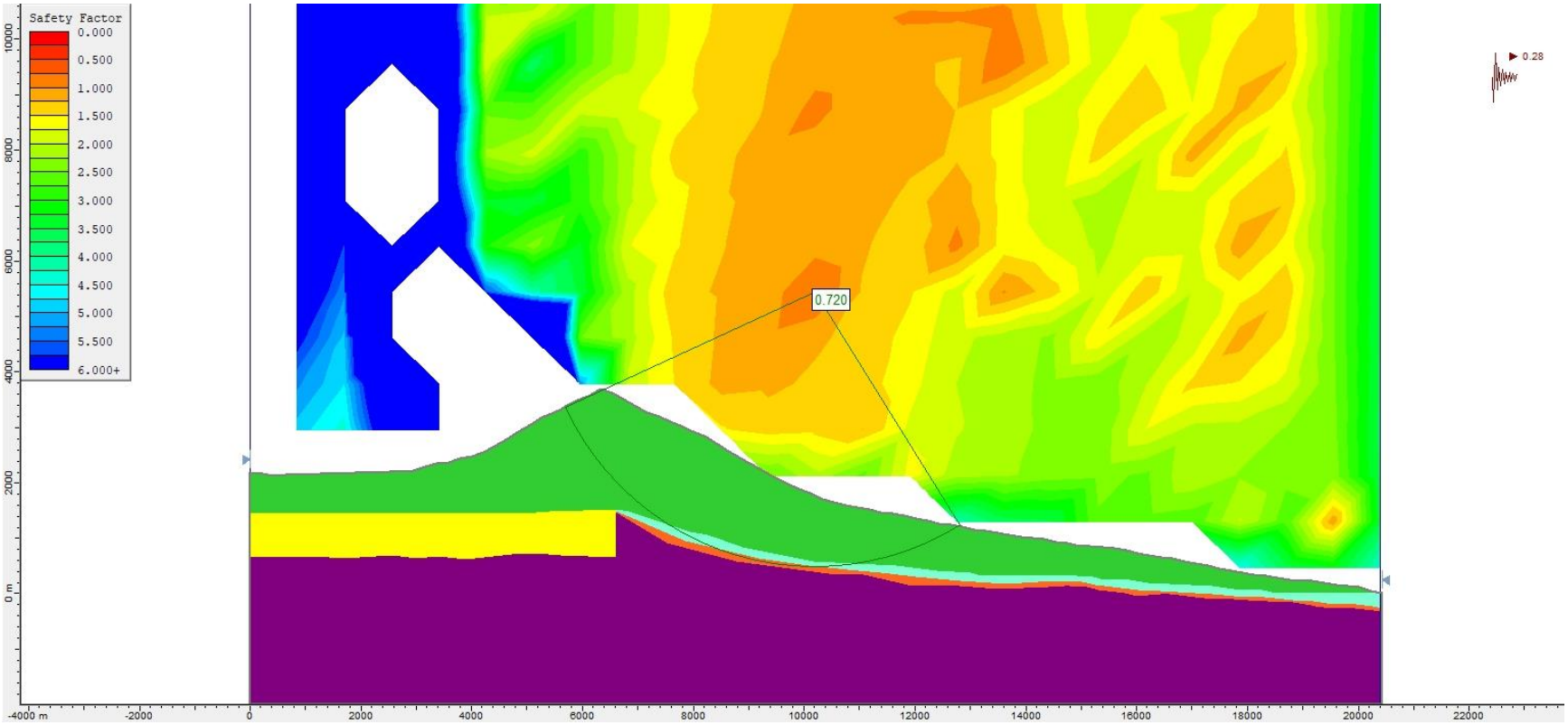

Figure S188. Slope stability pseudo-static analysis for Model 2 (without alteration zones, Figure 4b), using the Janbu Generalised method and a k_h = 0.28.

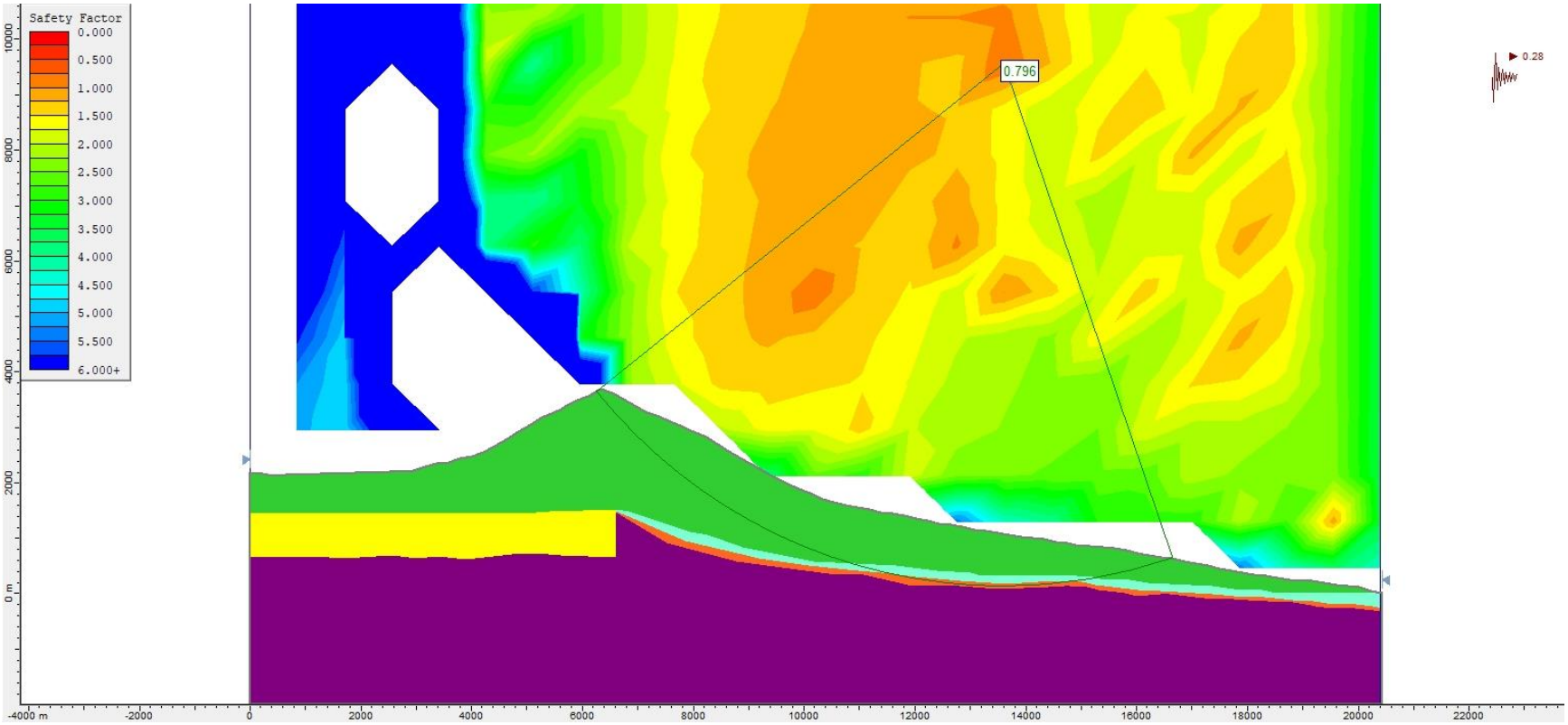

Figure S189. Slope stability pseudo-static analysis for Model 2 (without alteration zones, Figure 4b), using the Morgenstern-Price method and a k_h = 0.28.

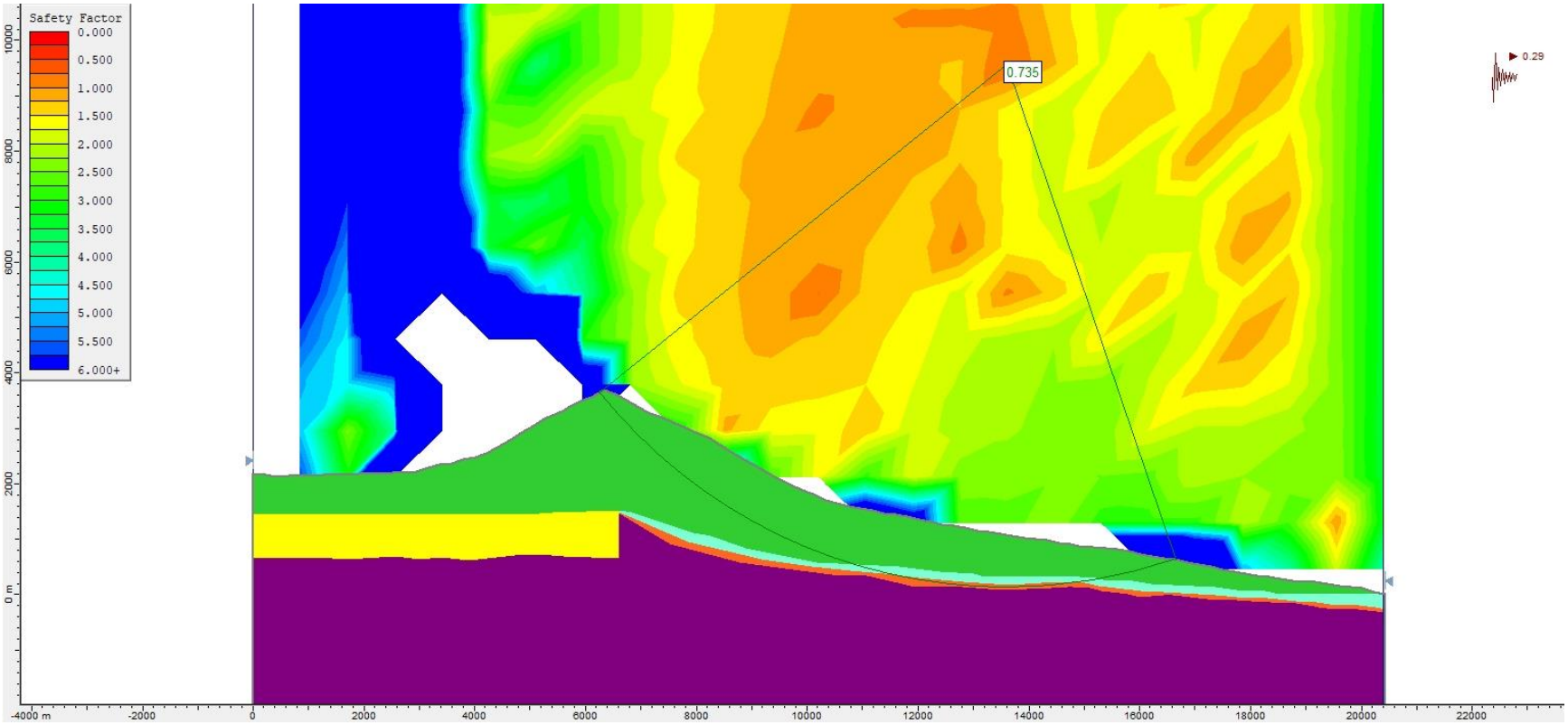

Figure S190. Slope stability pseudo-static analysis for Model 2 (without alteration zones, Figure 4b), using the Bishop simplified method and a k_h = 0.29.

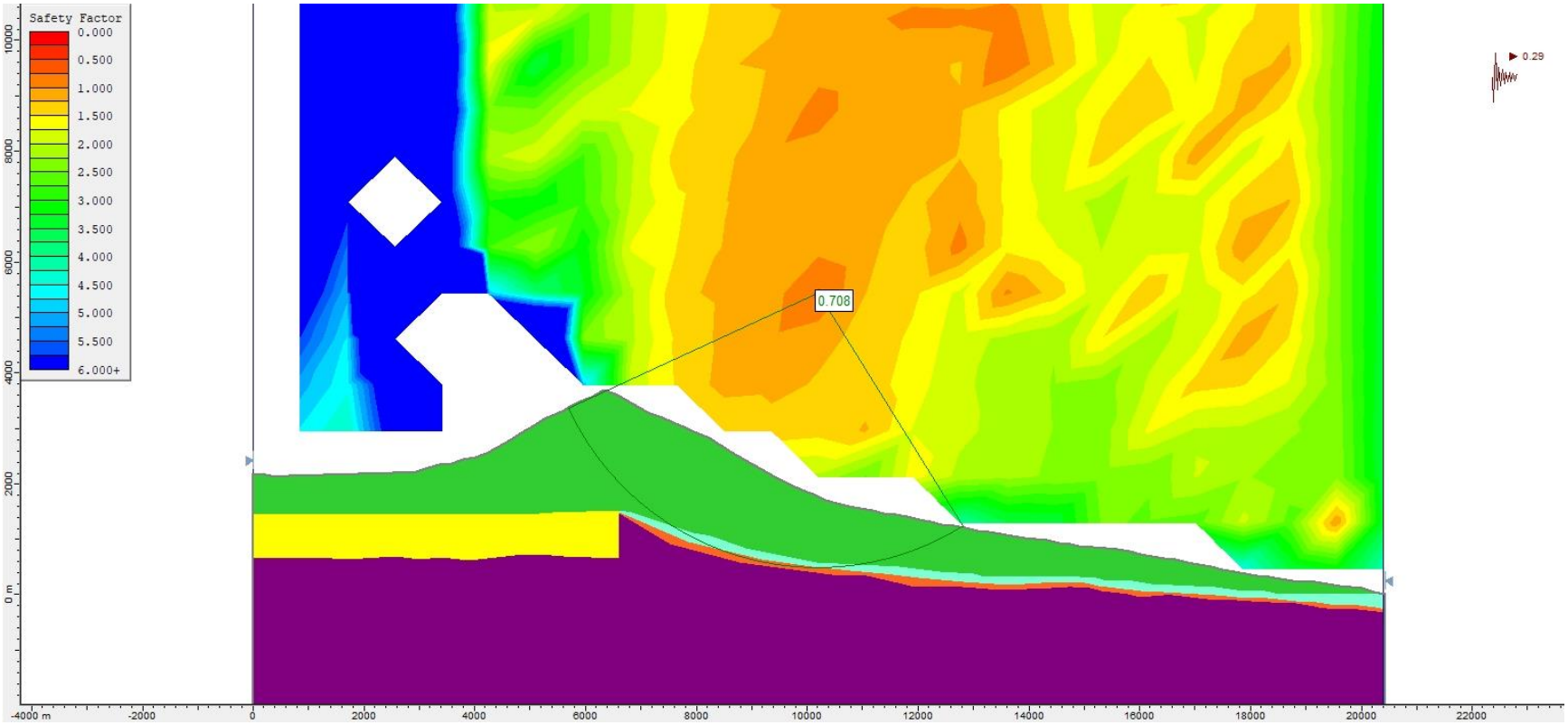

Figure S191. Slope stability pseudo-static analysis for Model 2 (without alteration zones, Figure 4b), using the Janbu Generalised method and a k_h = 0.29.

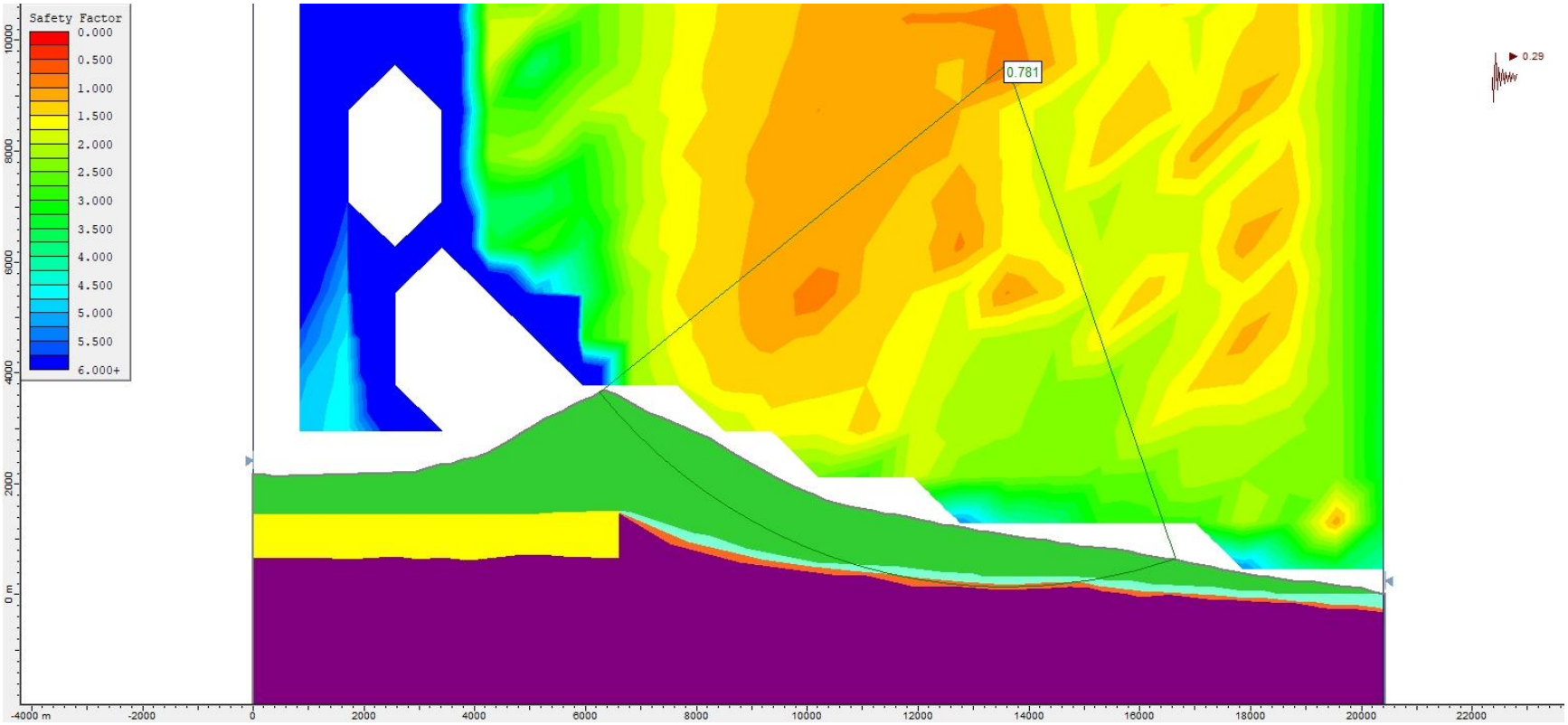

Figure S192. Slope stability pseudo-static analysis for Model 2 (without alteration zones, Figure 4b), using the Morgenstern-Price method and a k_h = 0.29.

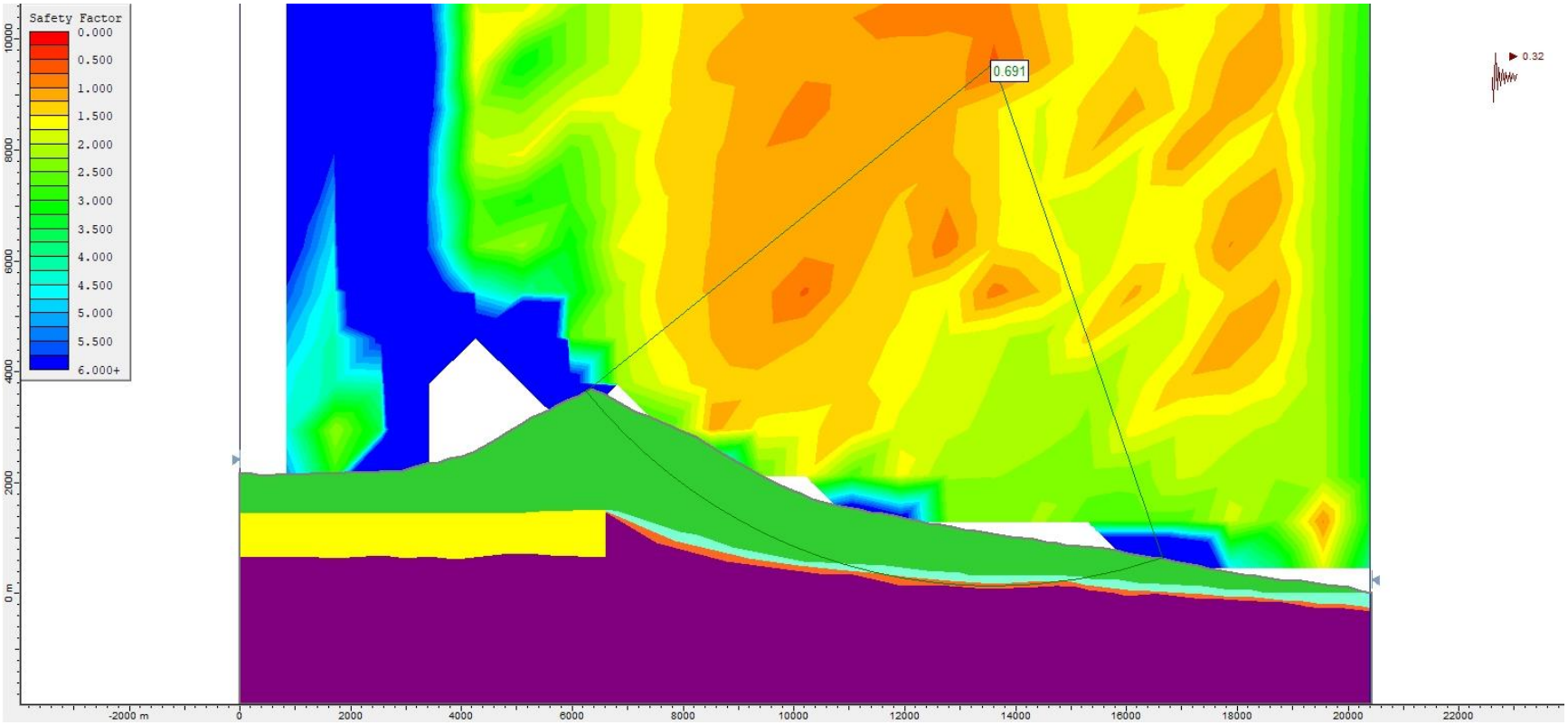

Figure S193. Slope stability pseudo-static analysis for Model 2 (without alteration zones, Figure 4b), using the Bishop simplified method and a k_h = 0.32.

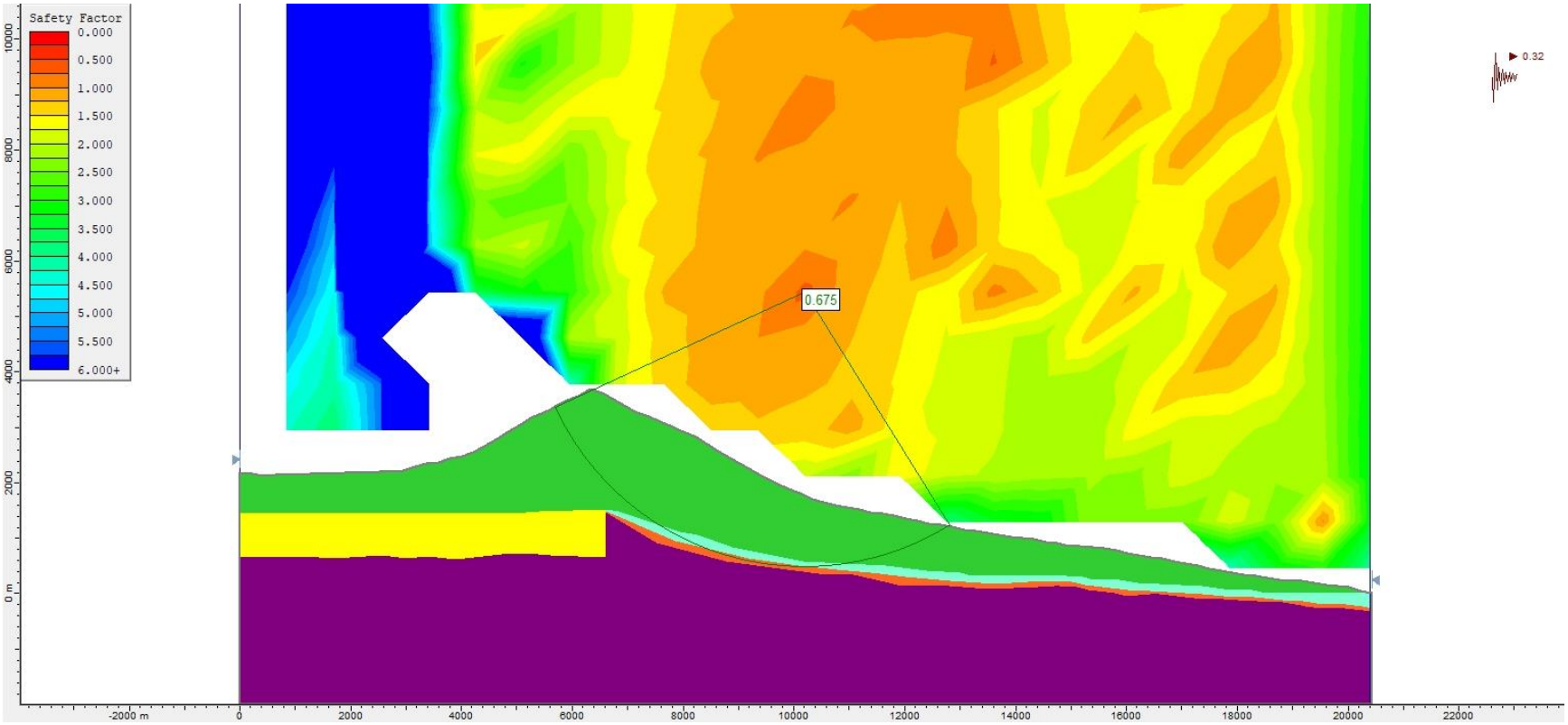

Figure S194. Slope stability pseudo-static analysis for Model 2 (without alteration zones, Figure 4b), using the Janbu Generalised method and a k_h = 0.32.

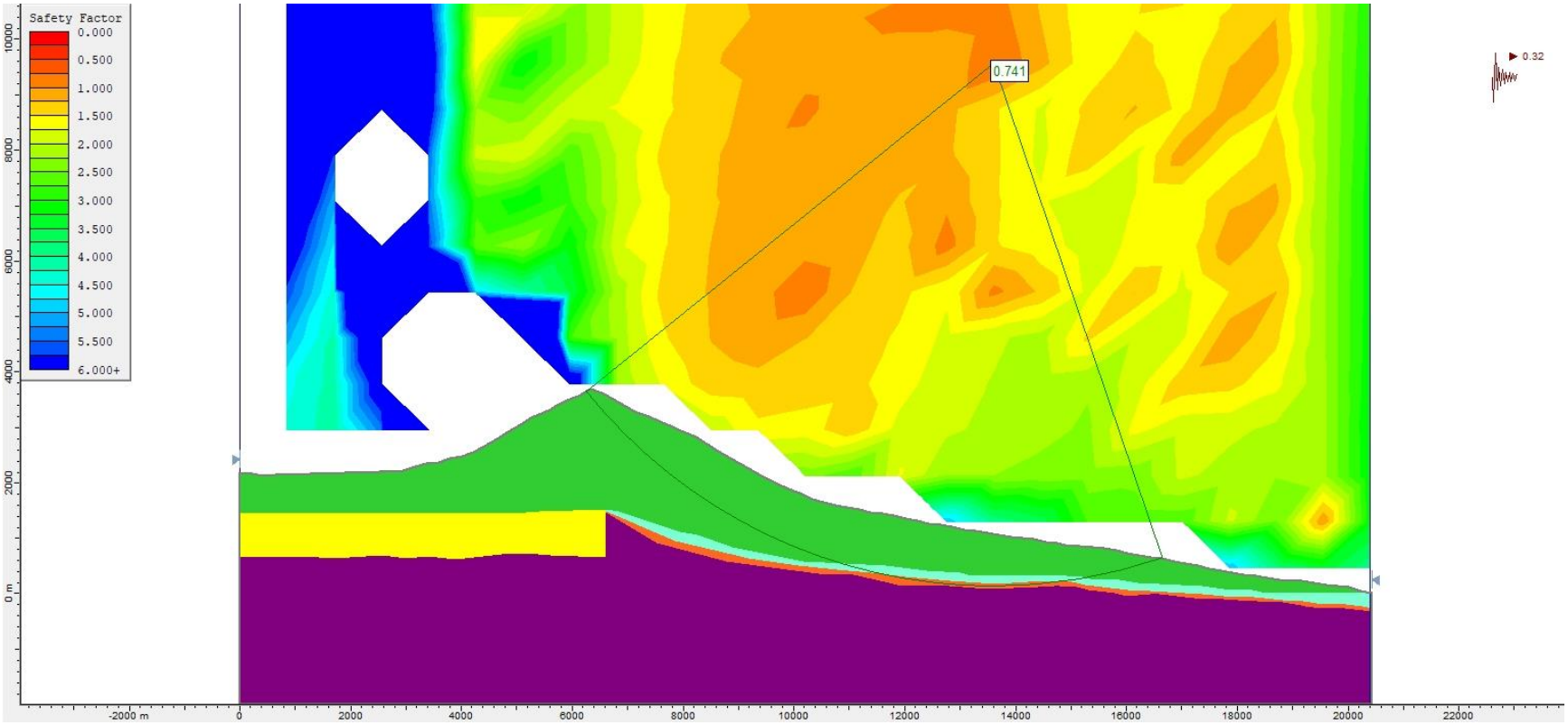

Figure S195. Slope stability pseudo-static analysis for Model 2 (without alteration zones, Figure 4b), using the Morgenstern-Price method and a $k_h = 0.32$.

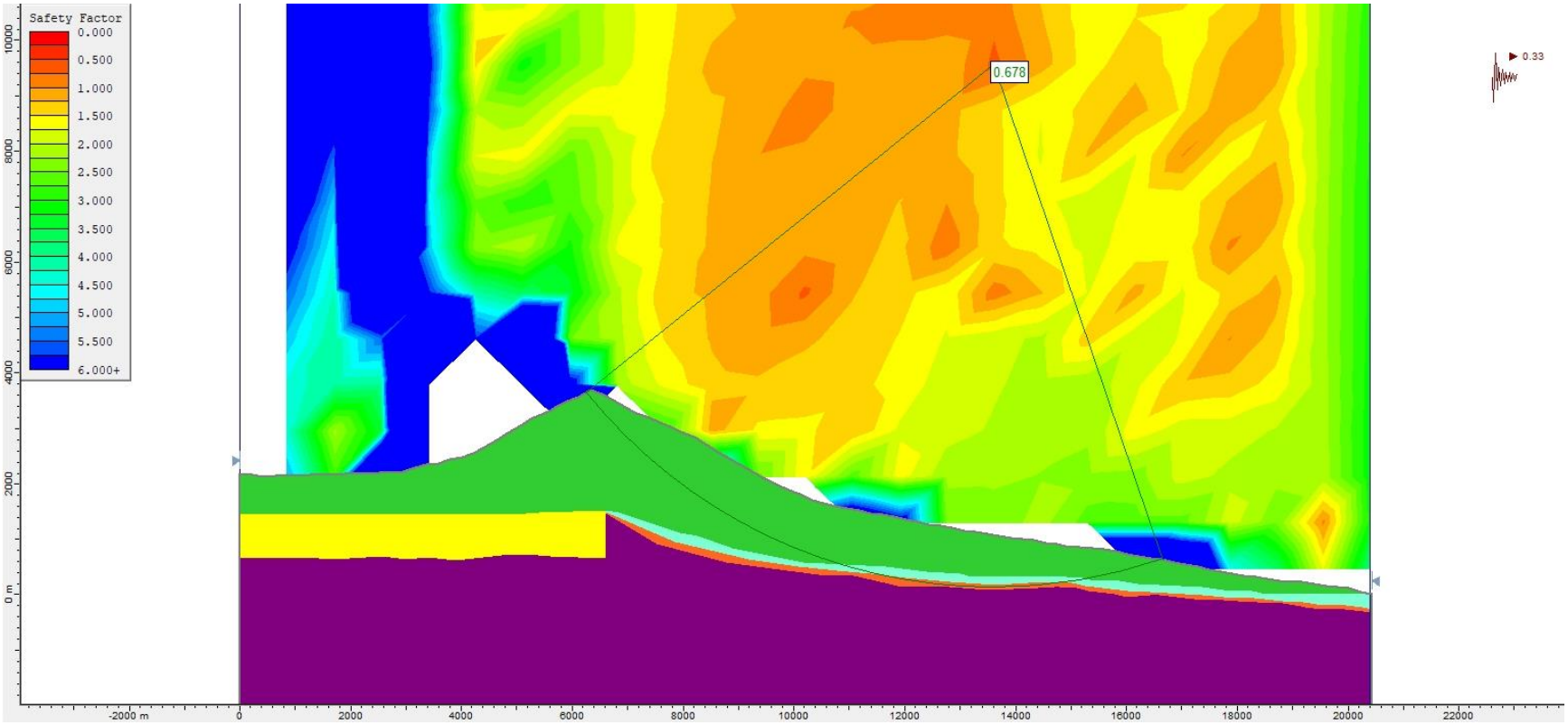

Figure S196. Slope stability pseudo-static analysis for Model 2 (without alteration zones, Figure 4b), using the Bishop simplified method and a k_h = 0.33.

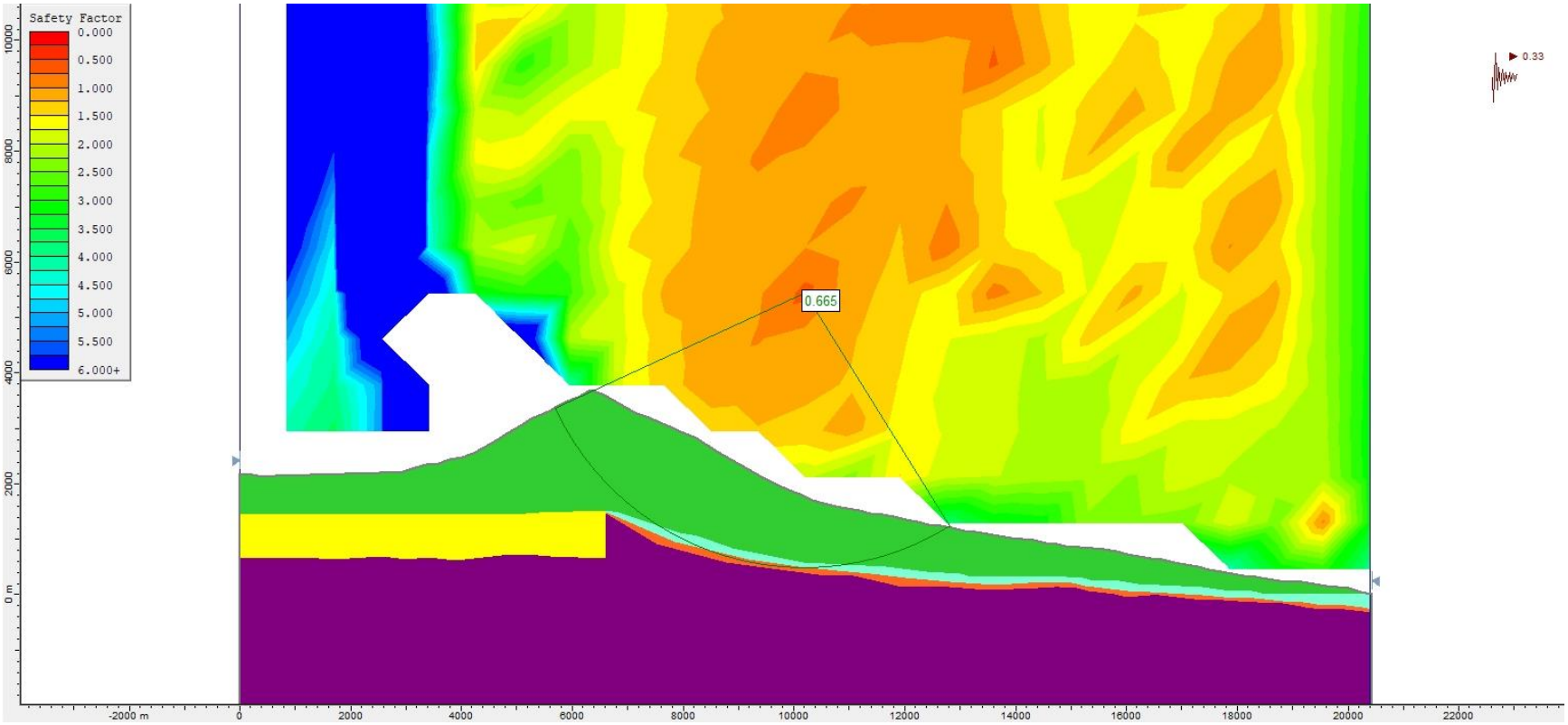

Figure S197. Slope stability pseudo-static analysis for Model 2 (without alteration zones, Figure 4b), using the Janbu Generalised method and a k_h = 0.33.

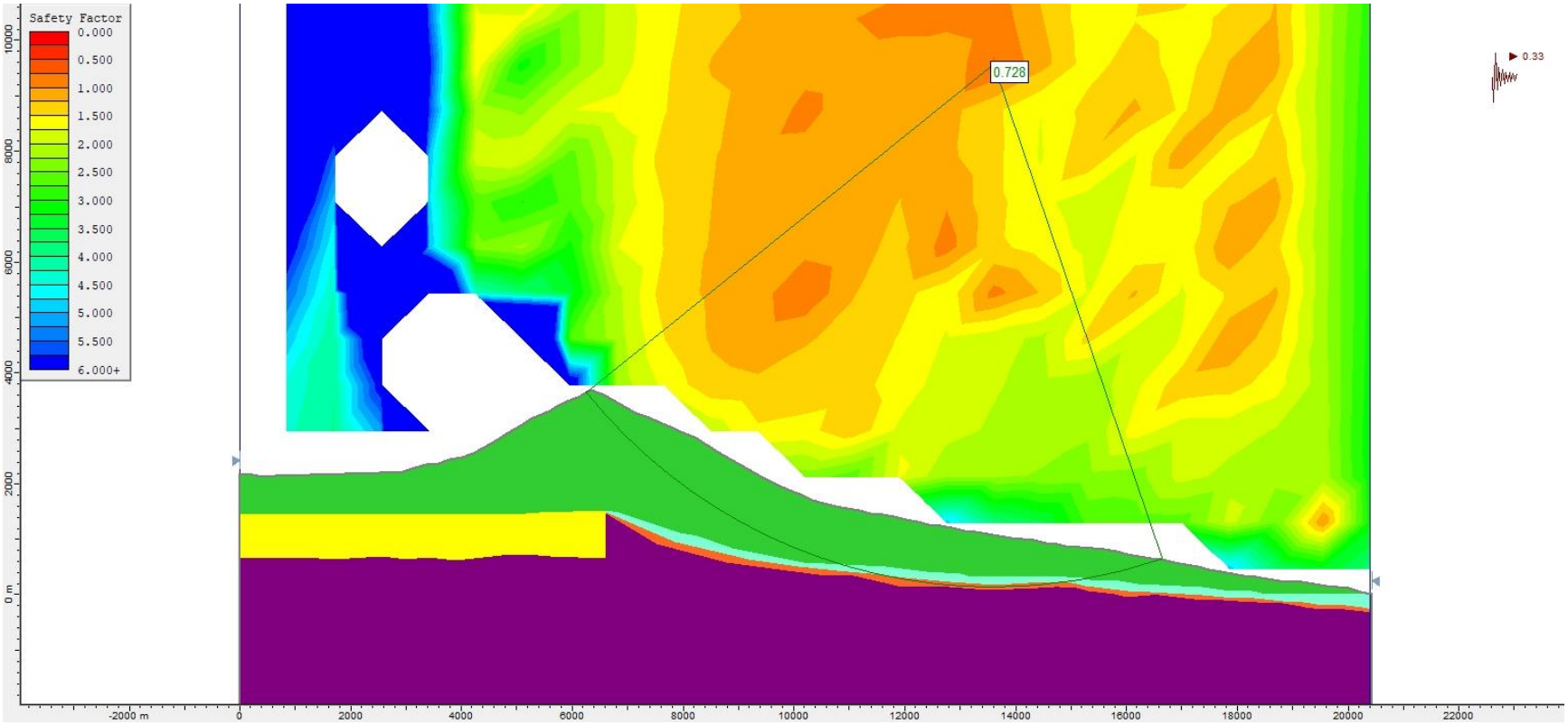

Figure S198. Slope stability pseudo-static analysis for Model 2 (without alteration zones, Figure 4b), using the Morgenstern-Price method and a k_h = 0.33.

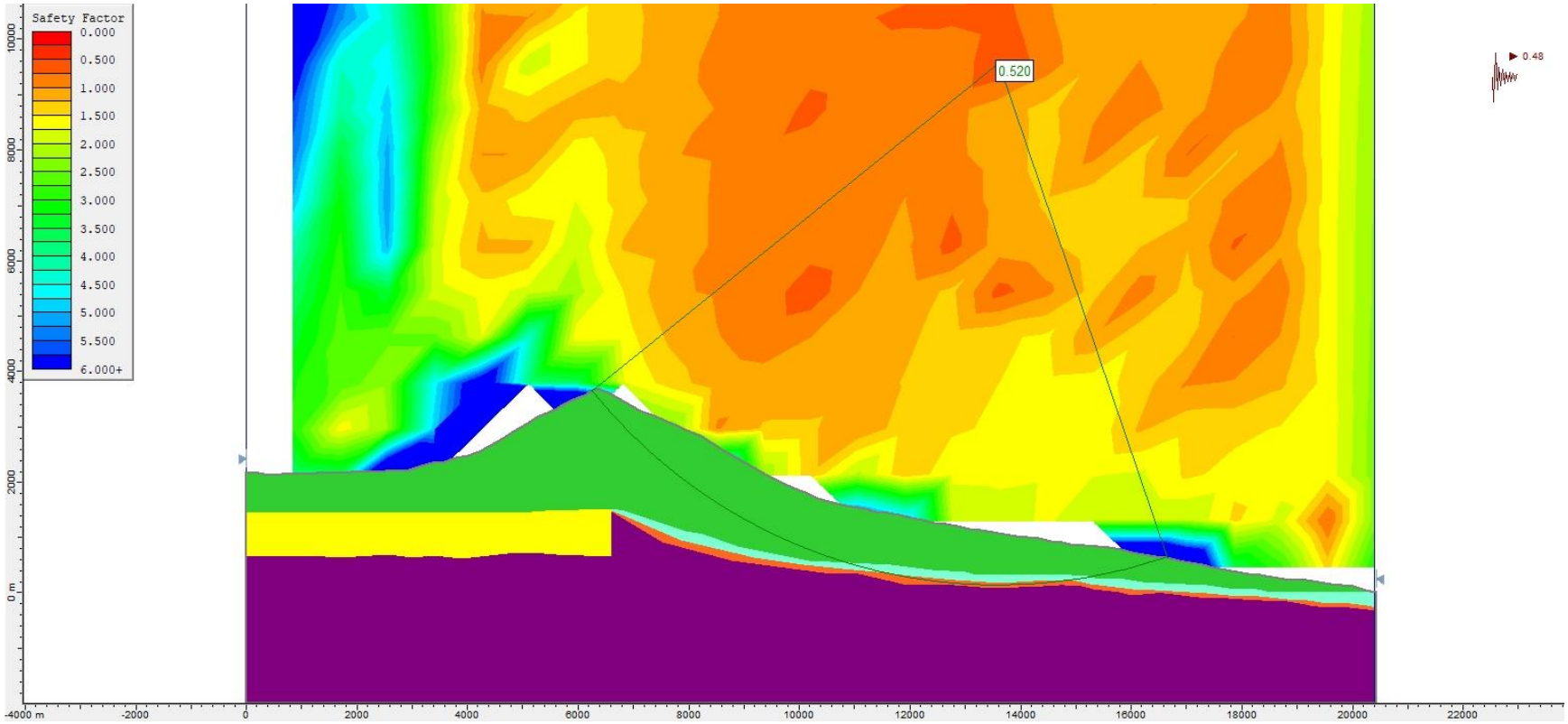

Figure S199. Slope stability pseudo-static analysis for Model 2 (without alteration zones, Figure 4b), using the Bishop simplified method and a $k_h = 0.48$.

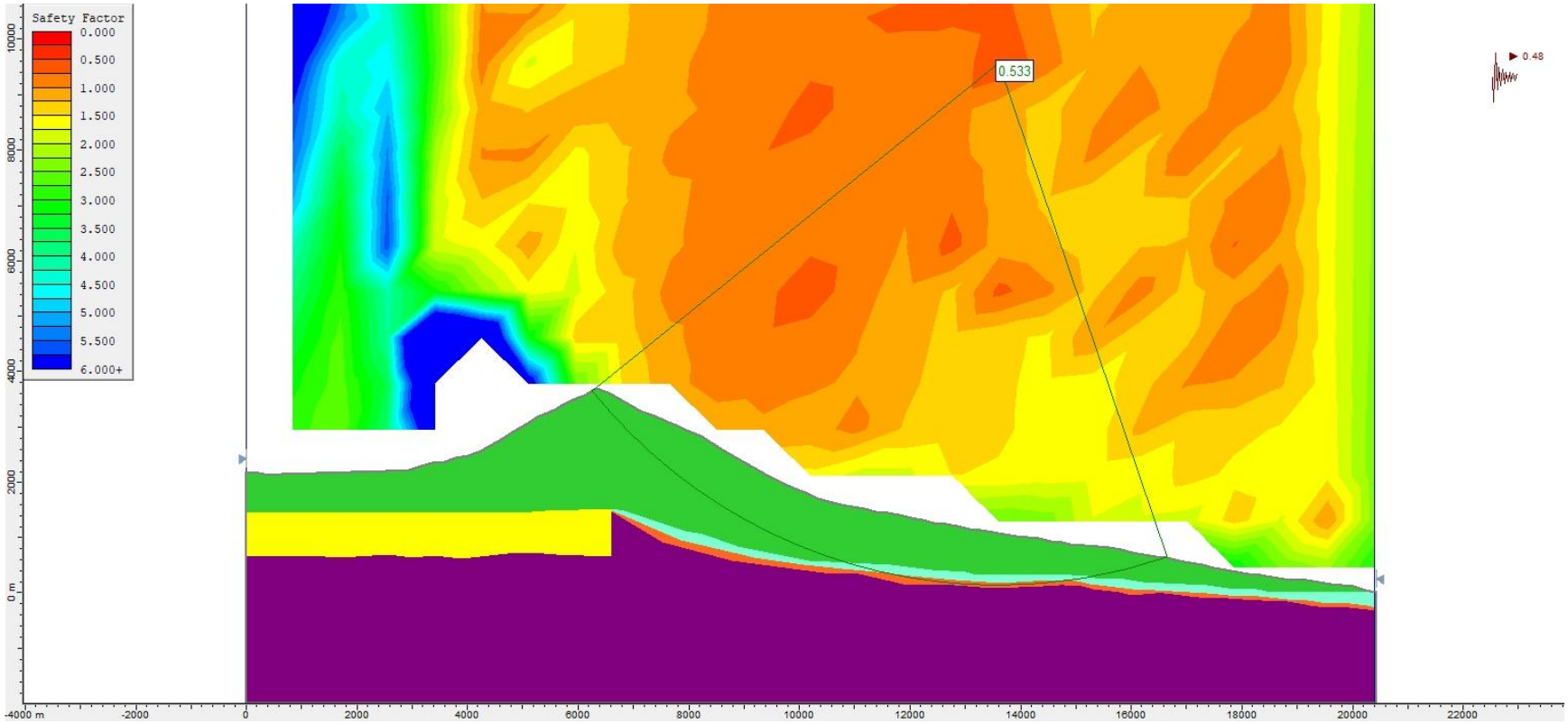

Figure S200. Slope stability pseudo-static analysis for Model 2 (without alteration zones, Figure 4b), using the Janbu Generalised method and a k_h = 0.48.

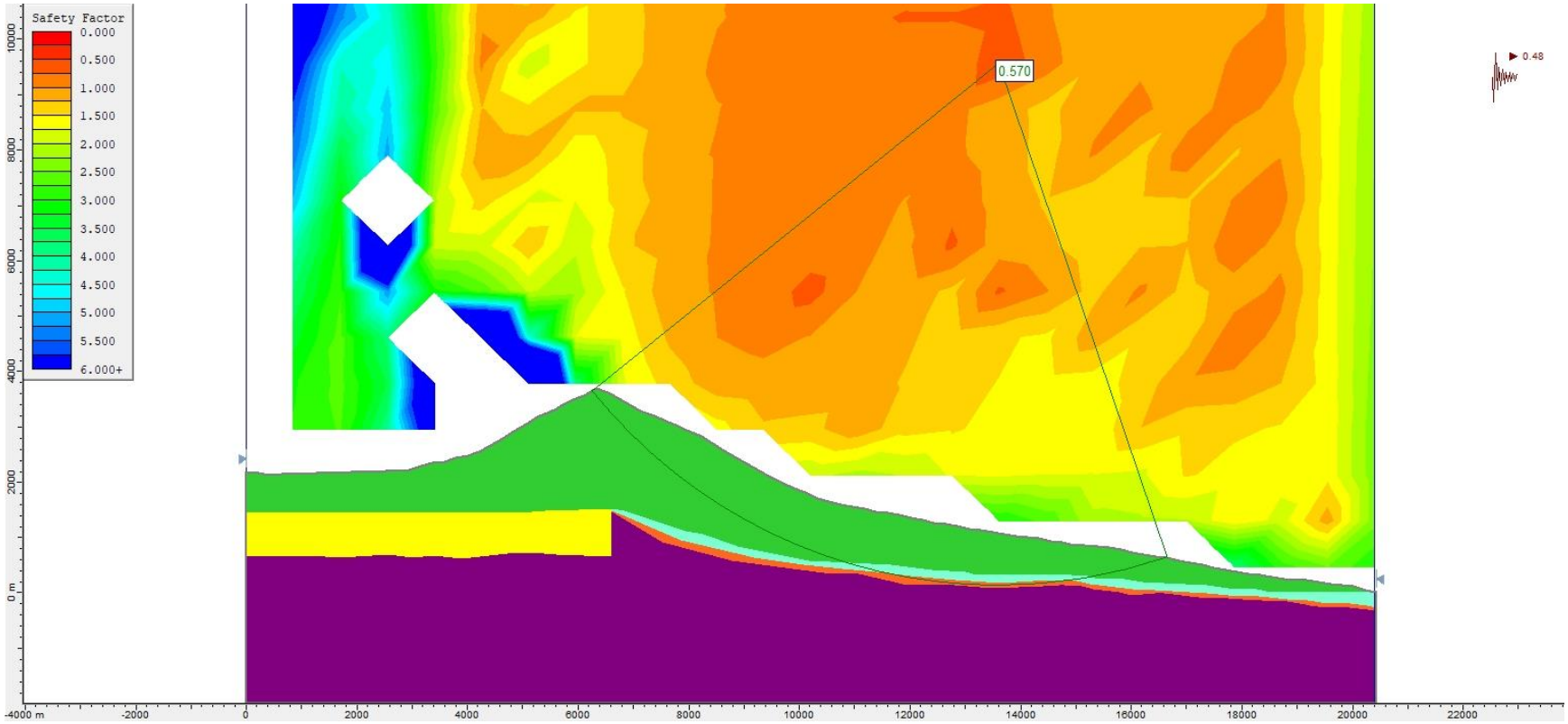

Figure S201. Slope stability pseudo-static analysis for Model 2 (without alteration zones, Figure 4b), using the Morgenstern-Price method and a k_h = 0.48.

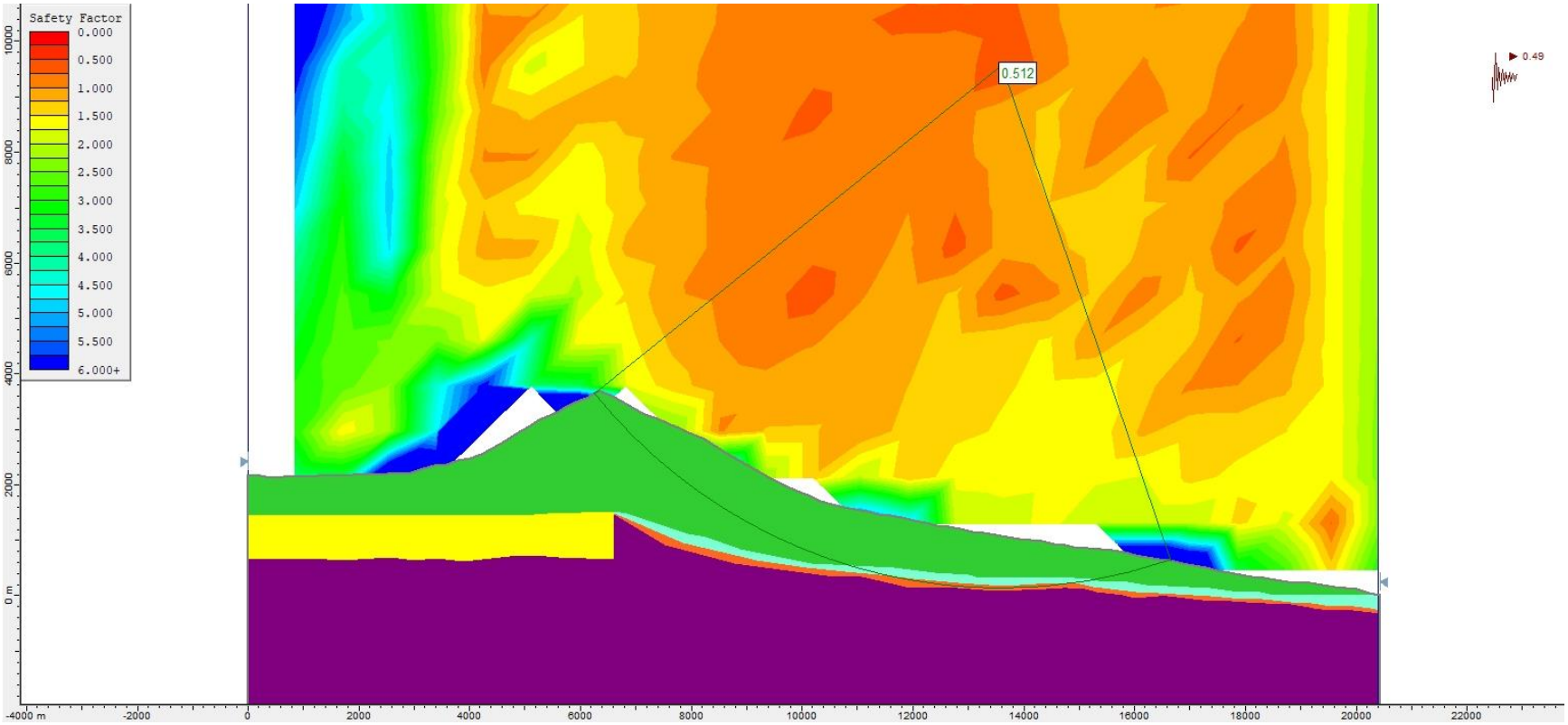

Figure S202. Slope stability pseudo-static analysis for Model 2 (without alteration zones, Figure 4b), using the Bishop simplified method and a k_h = 0.49.

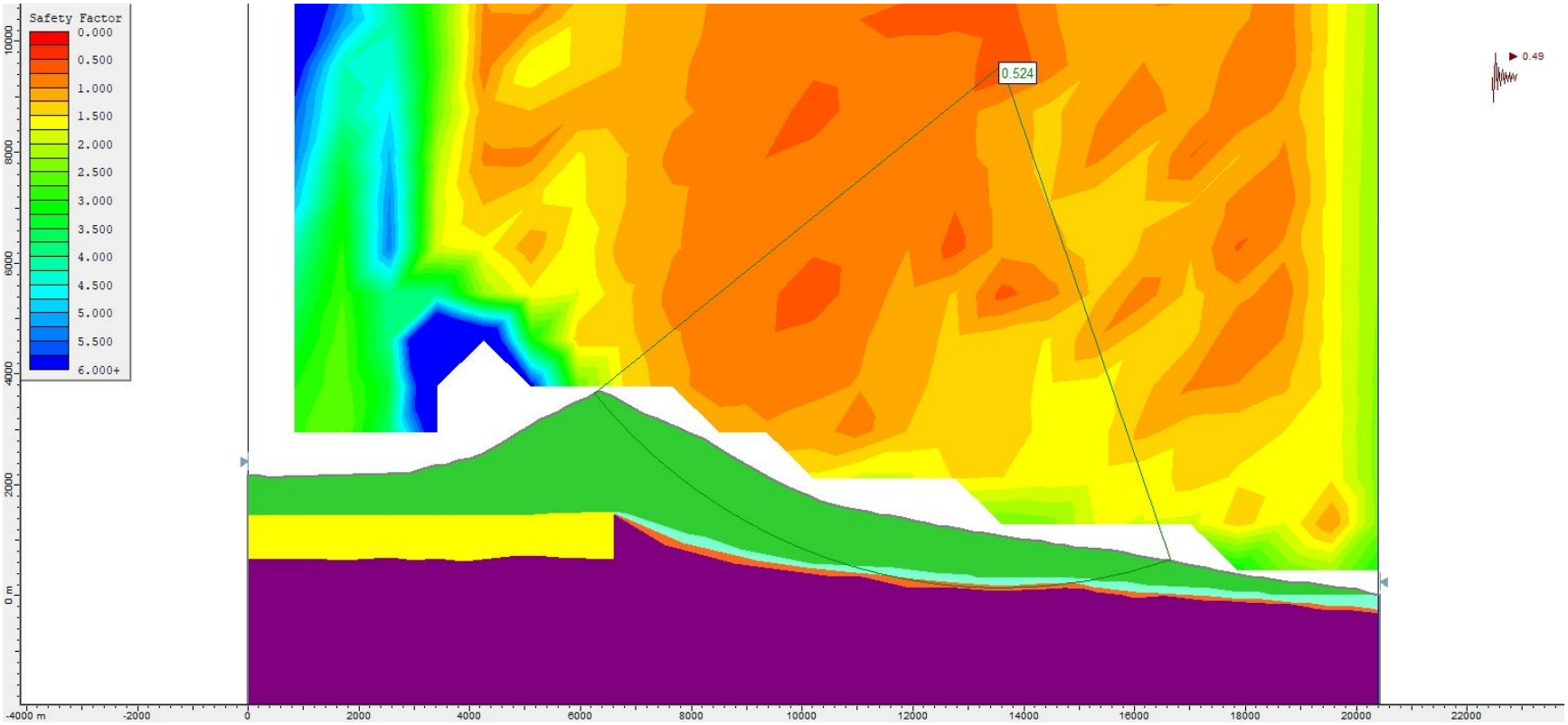

Figure S203. Slope stability pseudo-static analysis for Model 2 (without alteration zones, Figure 4b), using the Janbu Generalised method and a k_h = 0.49.

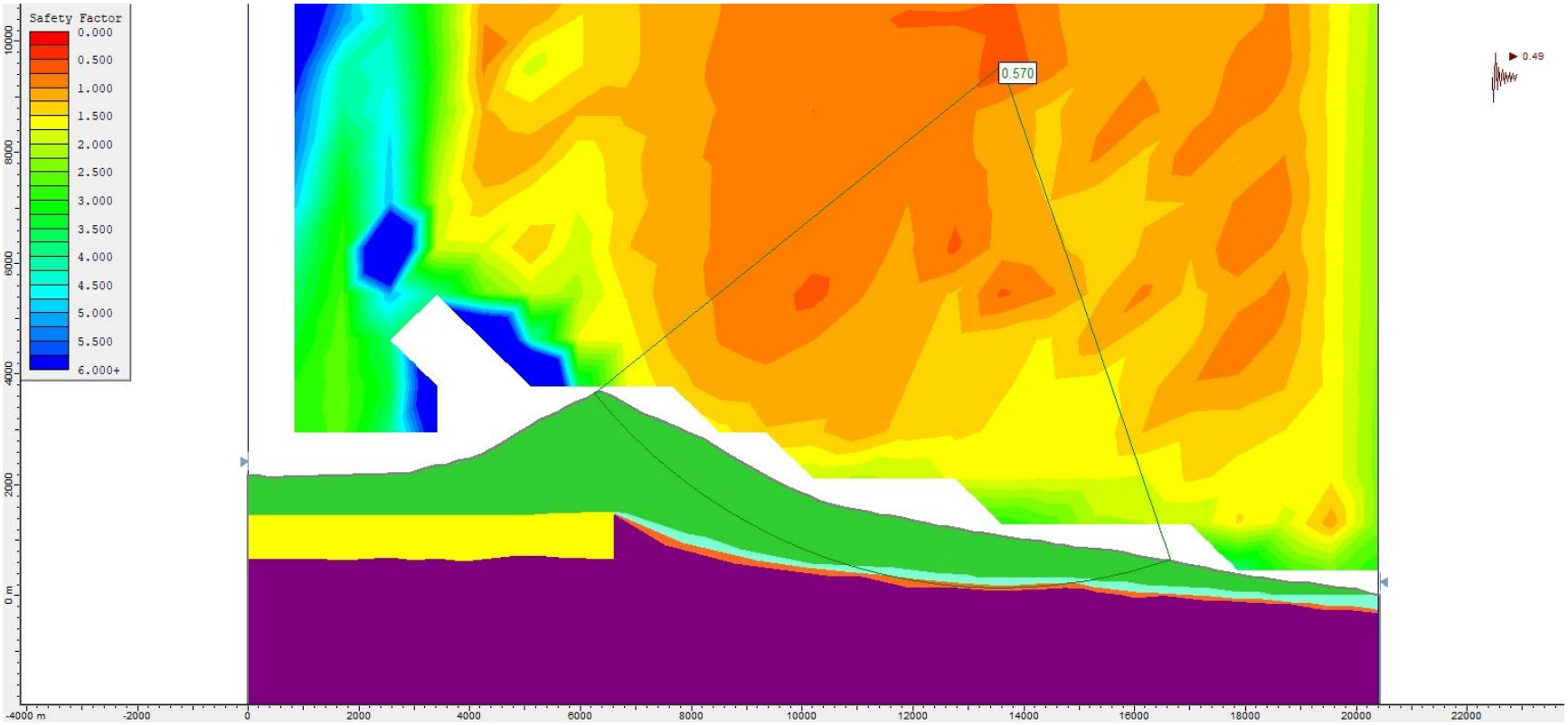

Figure S204. Slope stability pseudo-static analysis for Model 2 (without alteration zones, Figure 4b), using the Morgenstern-Price method and a k_h = 0.49.

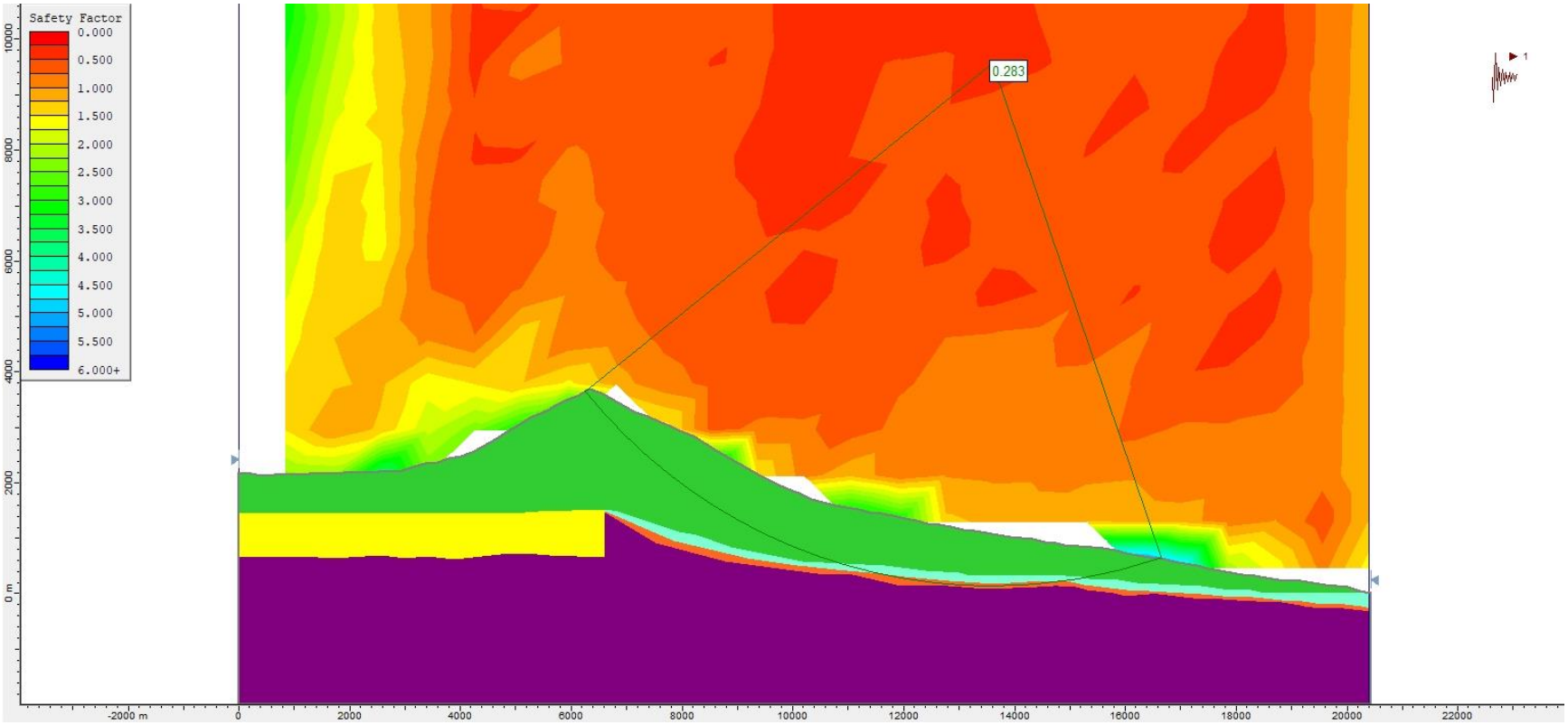

Figure S205. Slope stability pseudo-static analysis for Model 2 (without alteration zones, Figure 4b), using the Bishop simplified method and a k_h = 1.00.

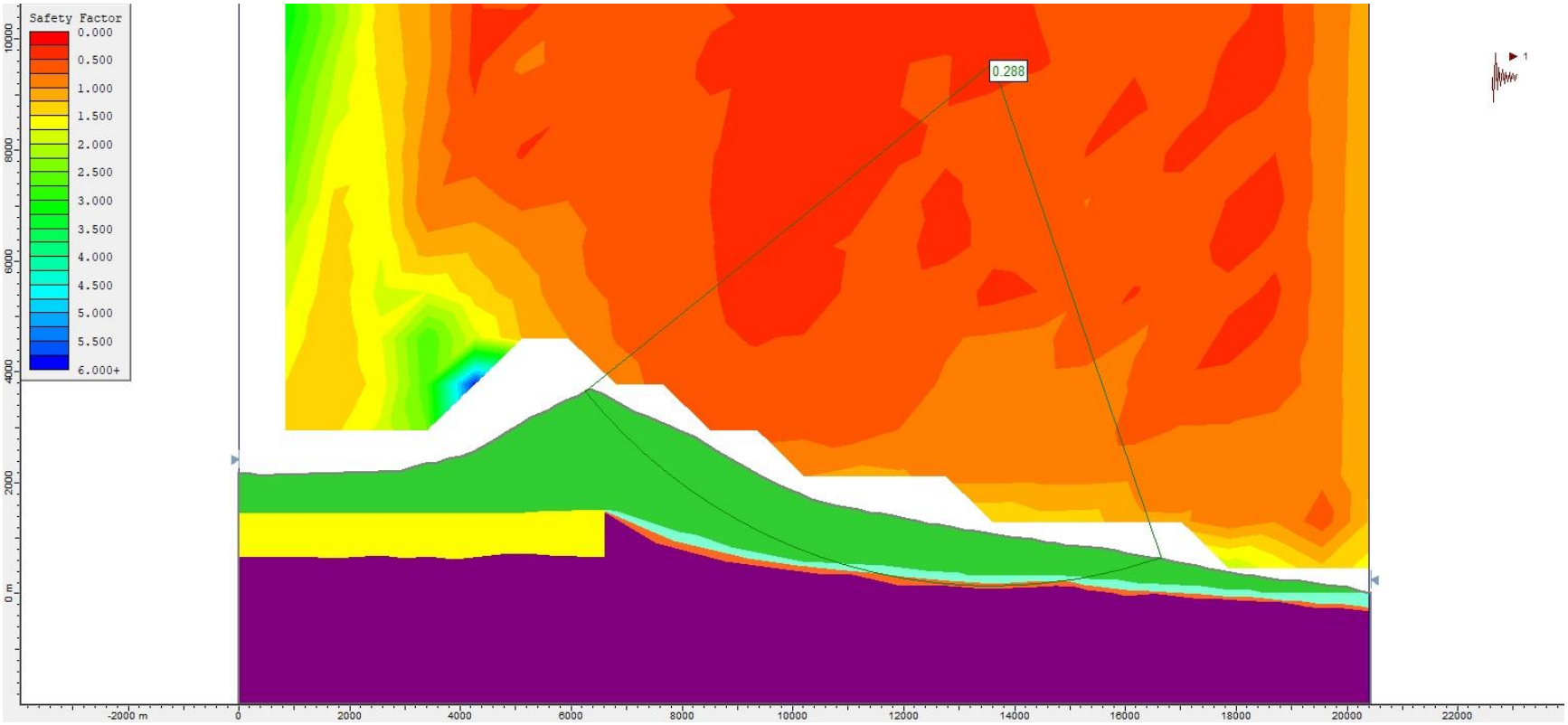

Figure S206. Slope stability pseudo-static analysis for Model 2 (without alteration zones, Figure 4b), using the Janbu Generalised method and a k_h = 1.00.

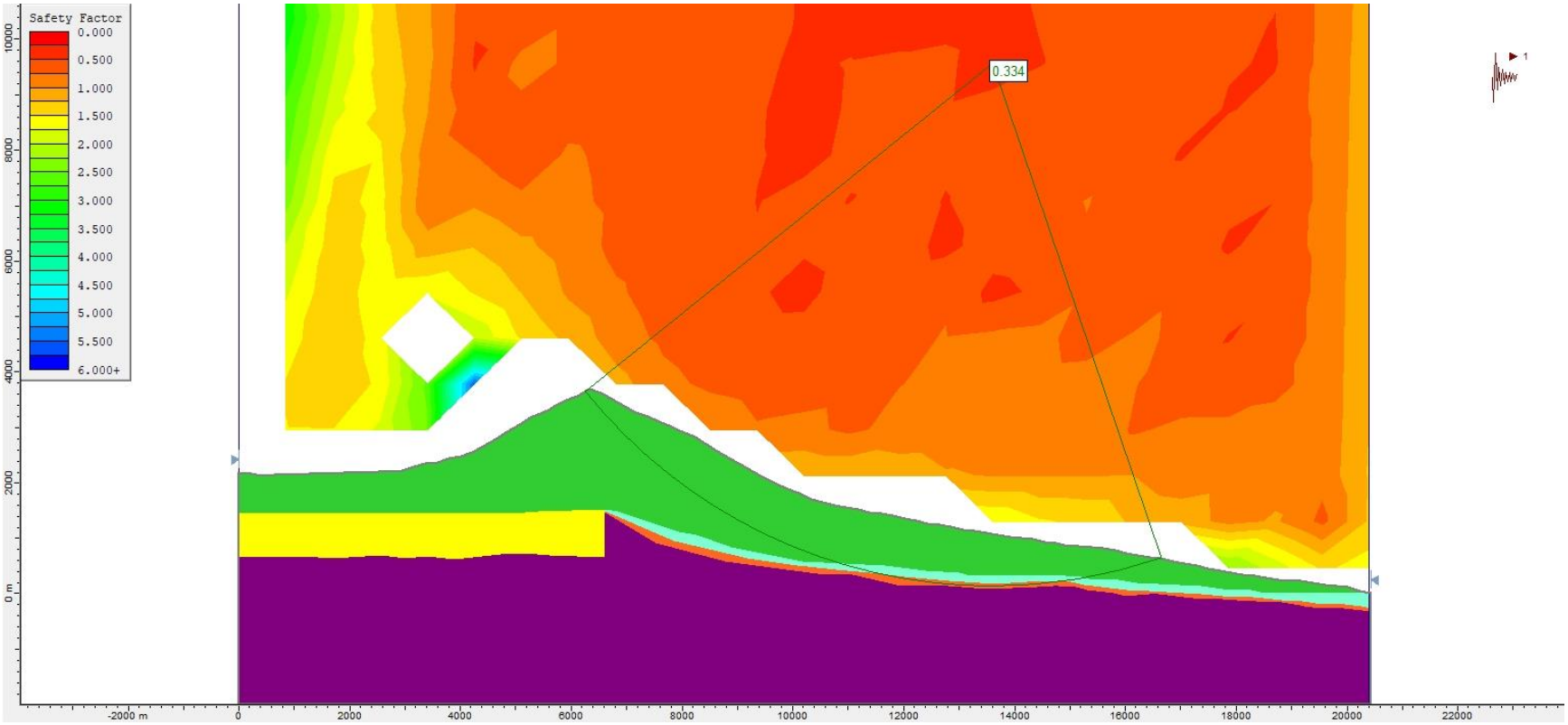

Figure S207. Slope stability pseudo-static analysis for Model 2 (without alteration zones, Figure 4b), using the Morgenstern-Price method and a k_h = 1.00.

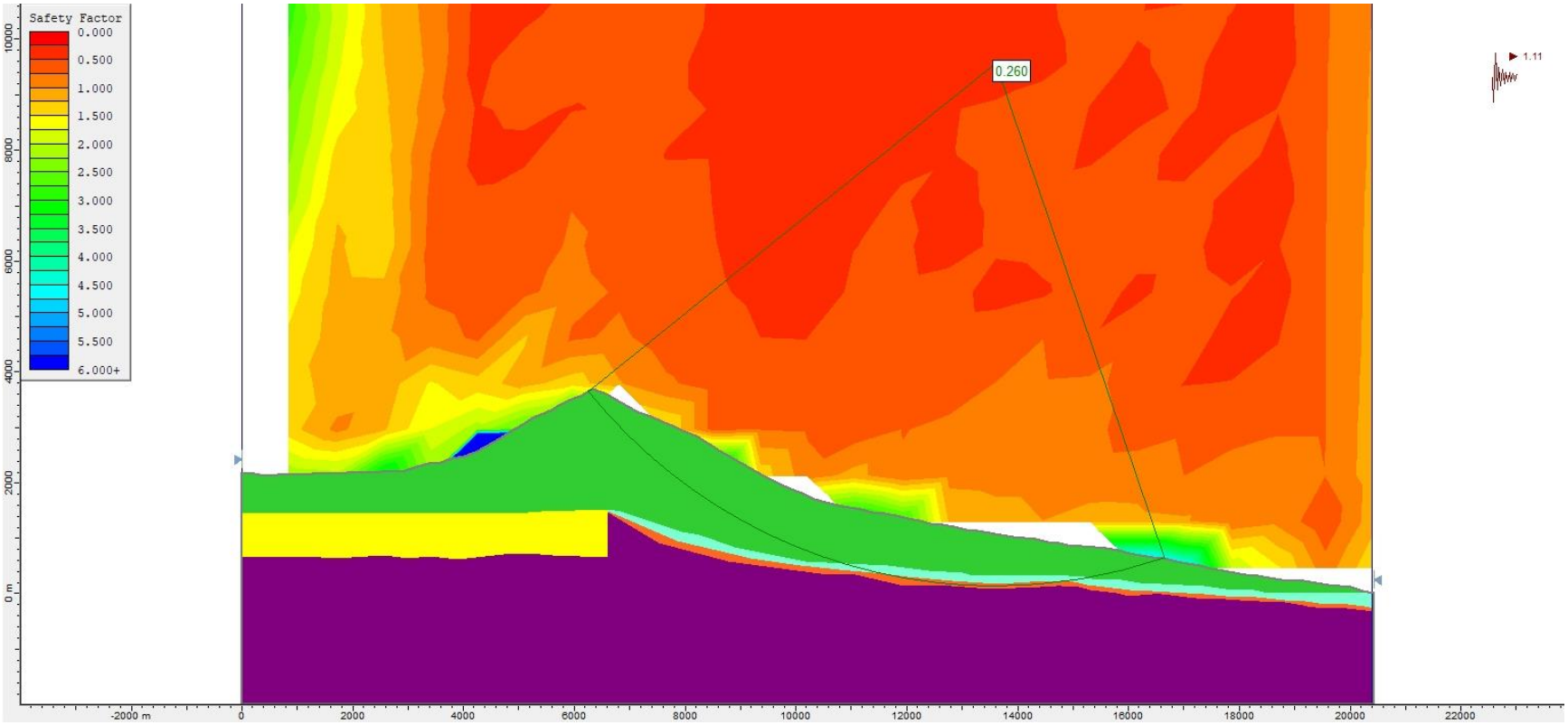

Figure S208. Slope stability pseudo-static analysis for Model 2 (without alteration zones, Figure 4b), using the Bishop simplified method and a k_h = 1.11.

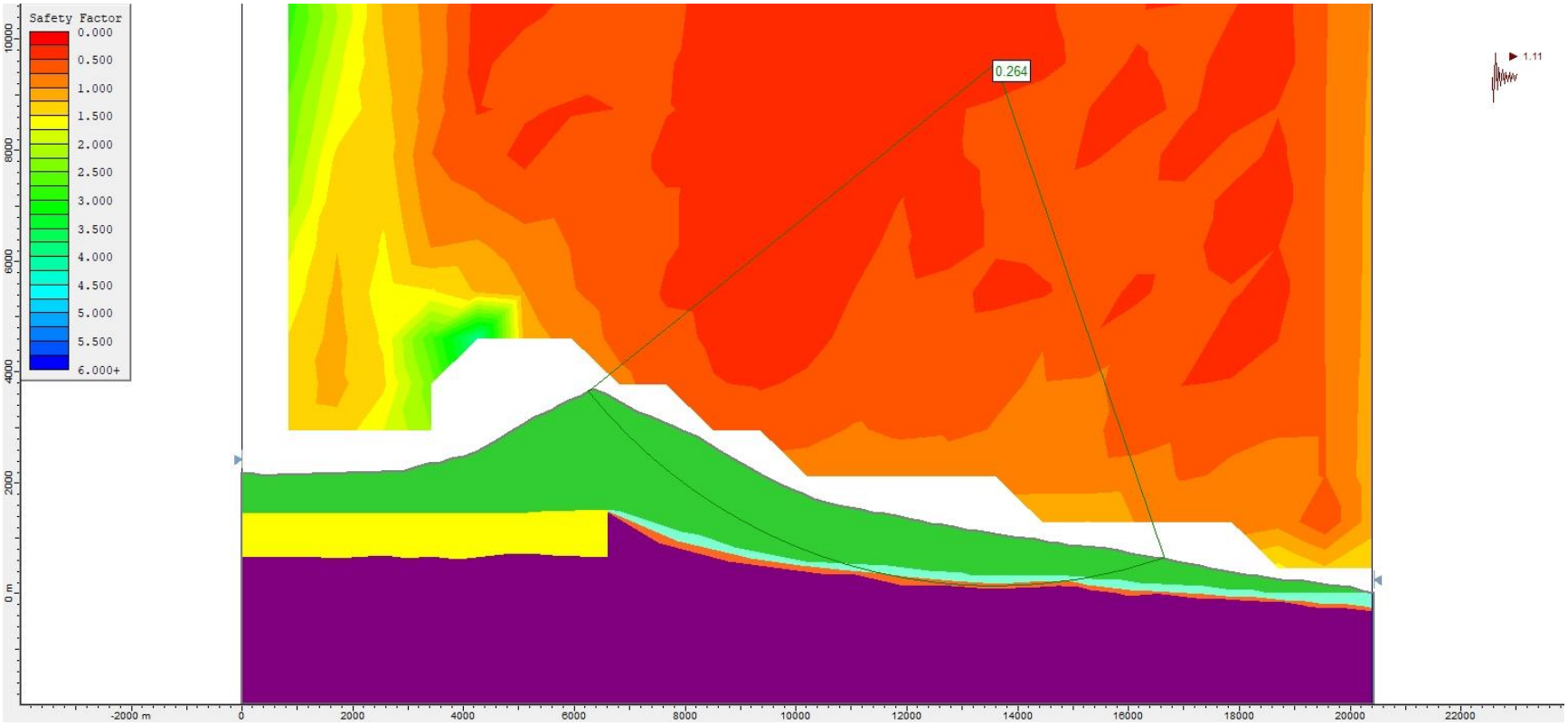

Figure S209. Slope stability pseudo-static analysis for Model 2 (without alteration zones, Figure 4b), using the Janbu Generalised method and a k_h = 1.11.

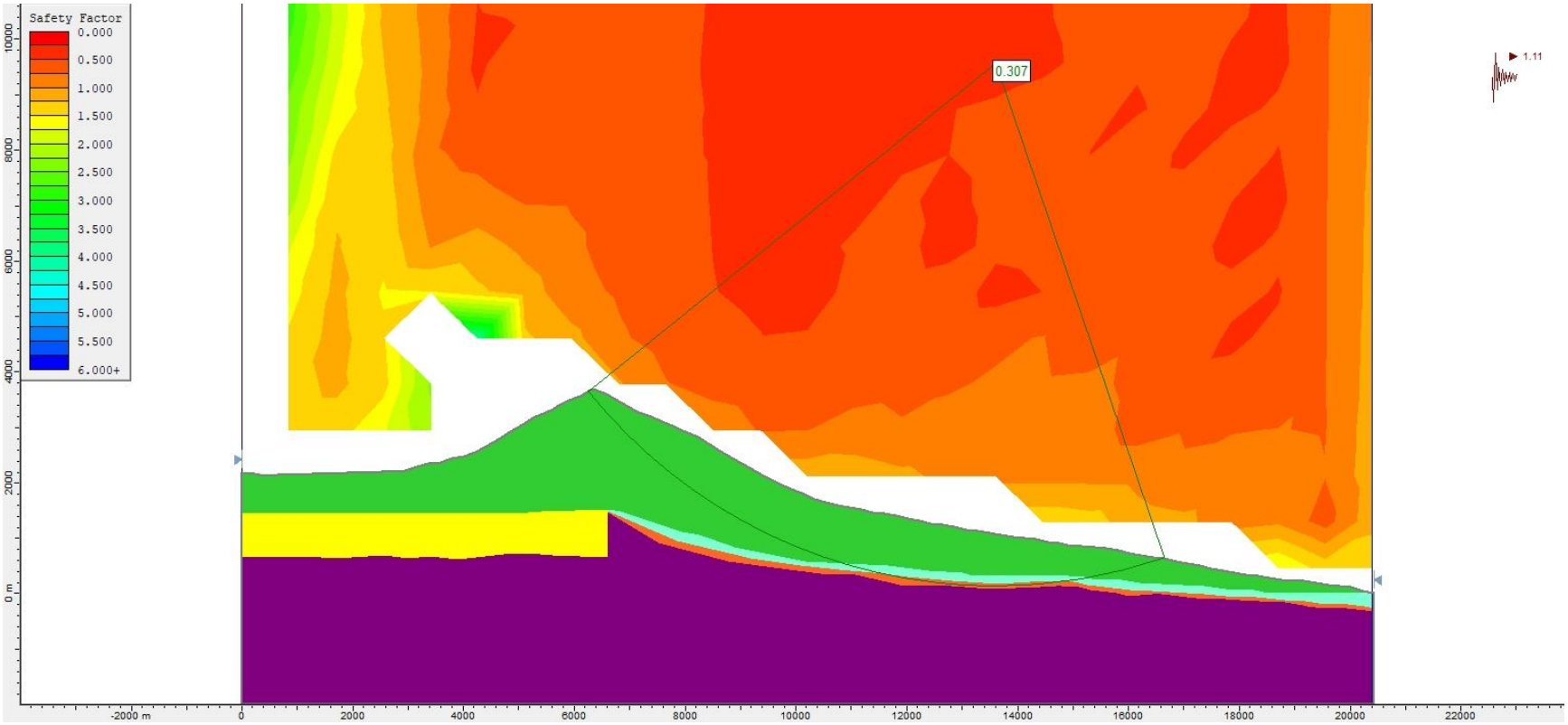

Figure S210. Slope stability pseudo-static analysis for Model 2 (without alteration zones, Figure 4b), using the Morgenstern-Price method and a k_h = 1.11.

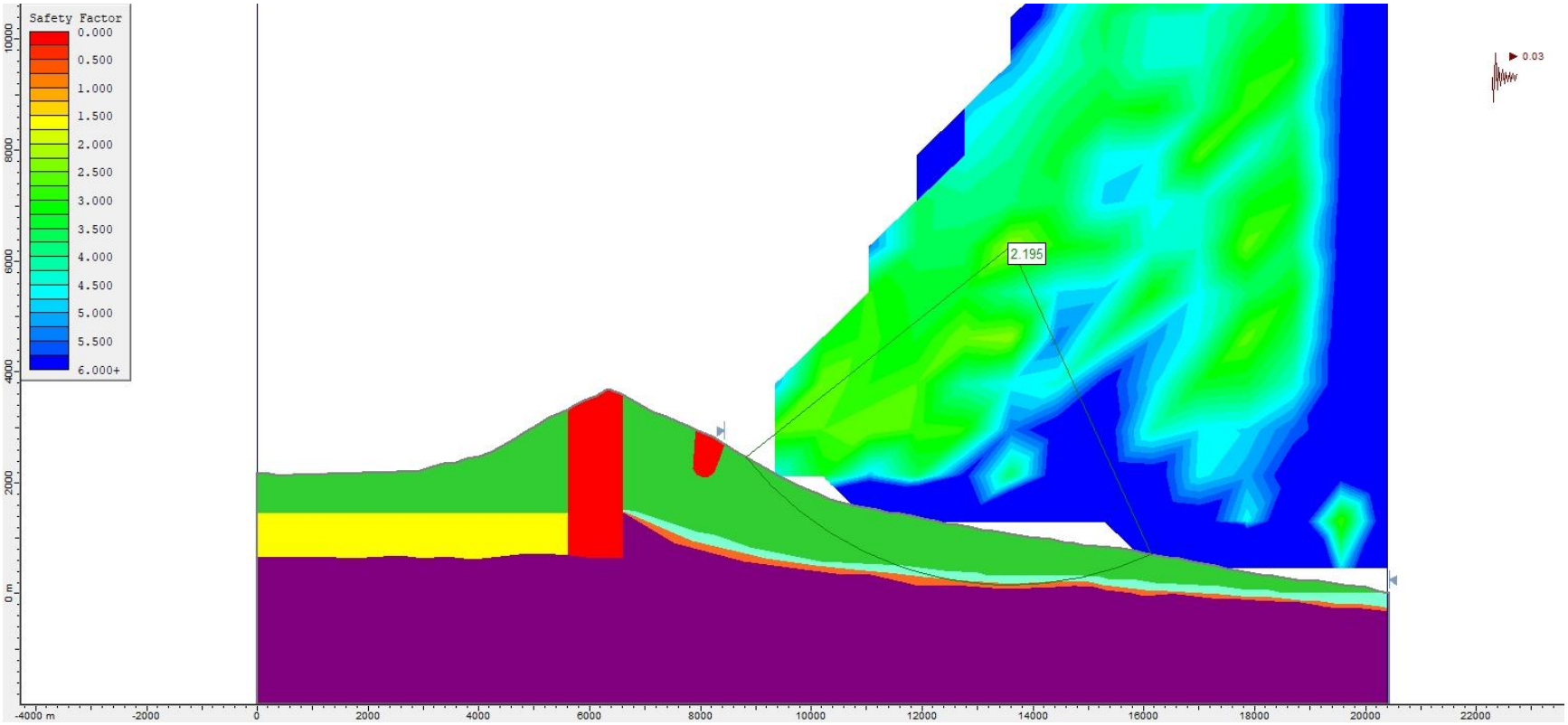

Figure S211. Slope stability pseudo-static analysis for Model 1 Bis (assuming a caldera collapse), using the Bishop simplified method and a k_h = 0.03.

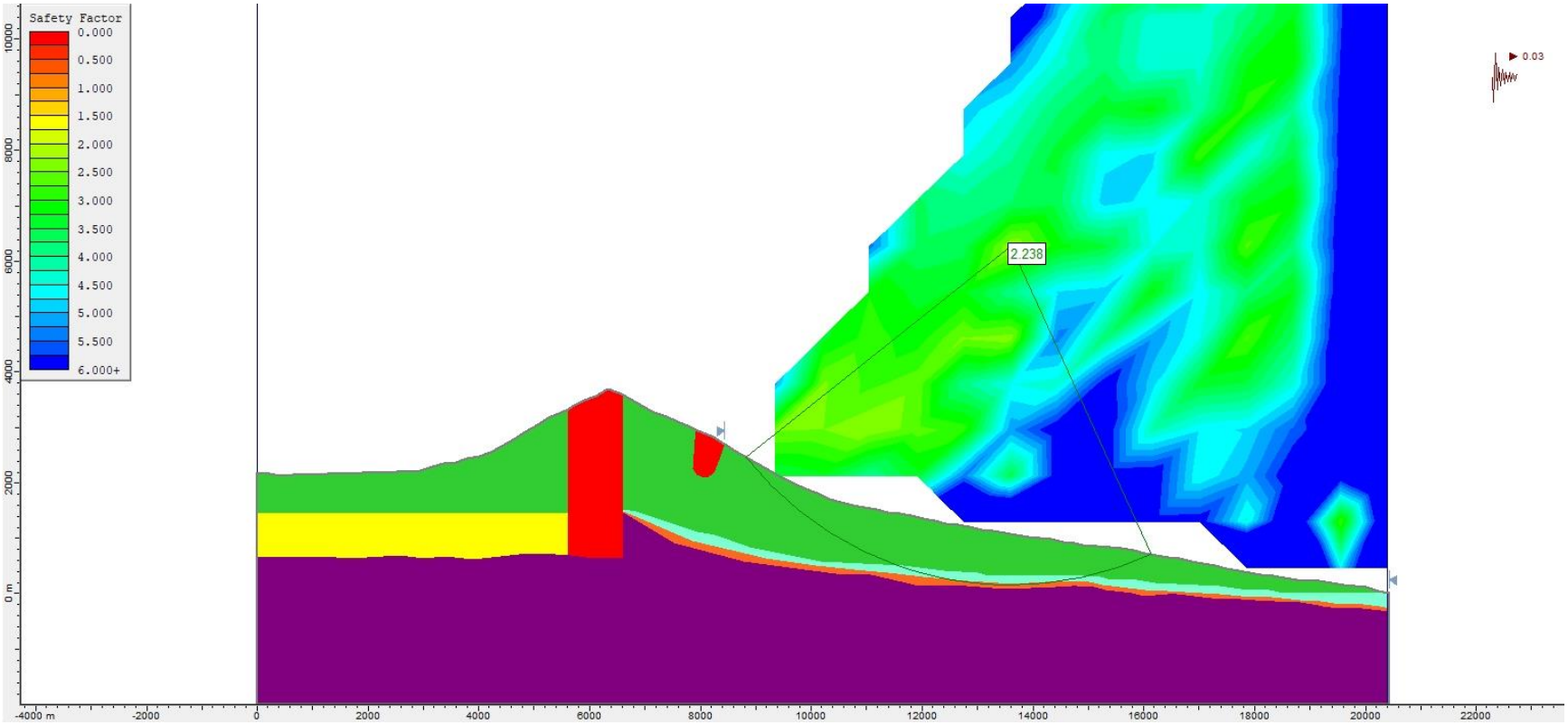

Figure S212. Slope stability pseudo-static analysis for Model 1 Bis (assuming a caldera collapse), using the Janbu Generalised method and a k_h = 0.03.

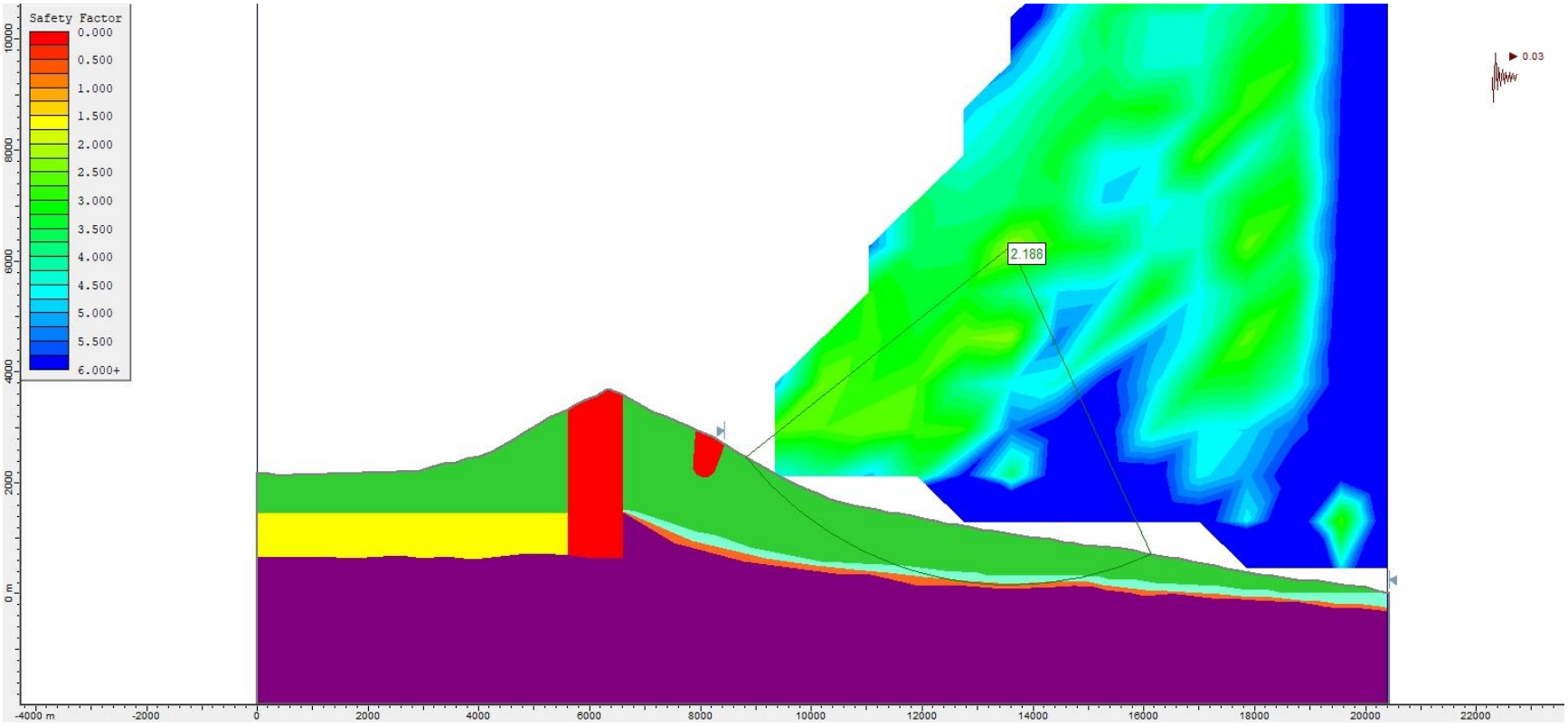

Figure S213. Slope stability pseudo-static analysis for Model 1 Bis (assuming a caldera collapse), using the Morgenstern-Price method and a k_h = 0.03.

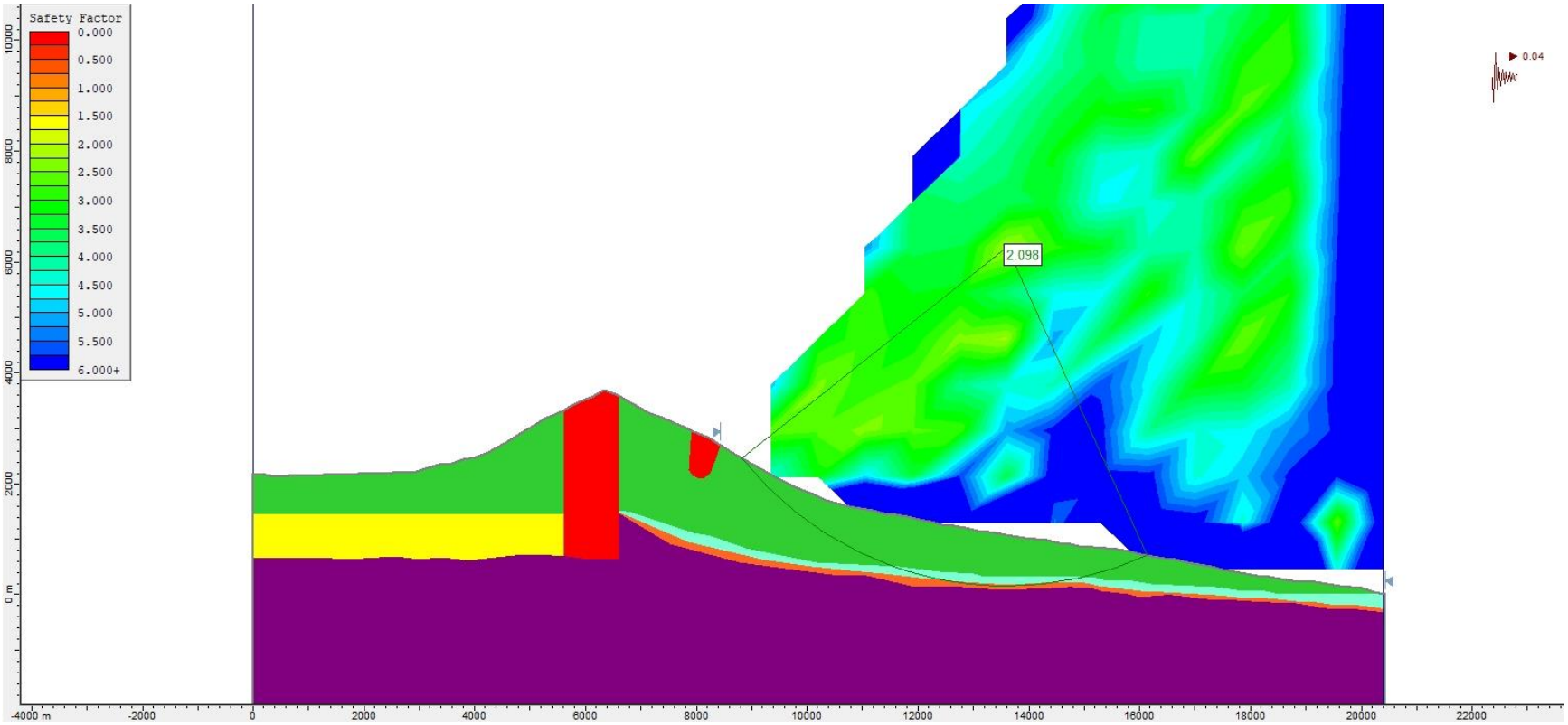

Figure S214. Slope stability pseudo-static analysis for Model 1 Bis (assuming a caldera collapse), using the Bishop simplified method and a k_h = 0.04.

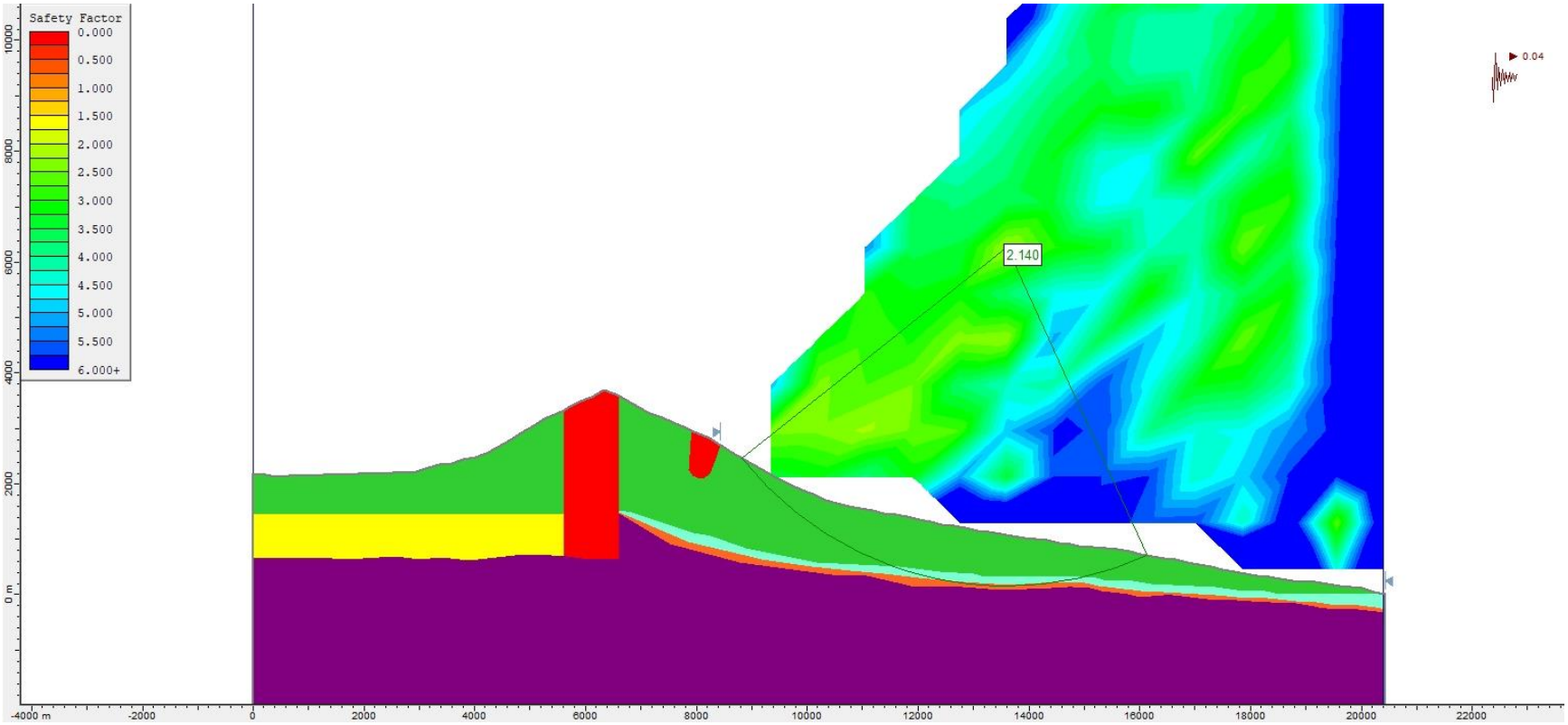

Figure S215. Slope stability pseudo-static analysis for Model 1 Bis (assuming a caldera collapse), using the Janbu Generalised method and a k_h = 0.04.

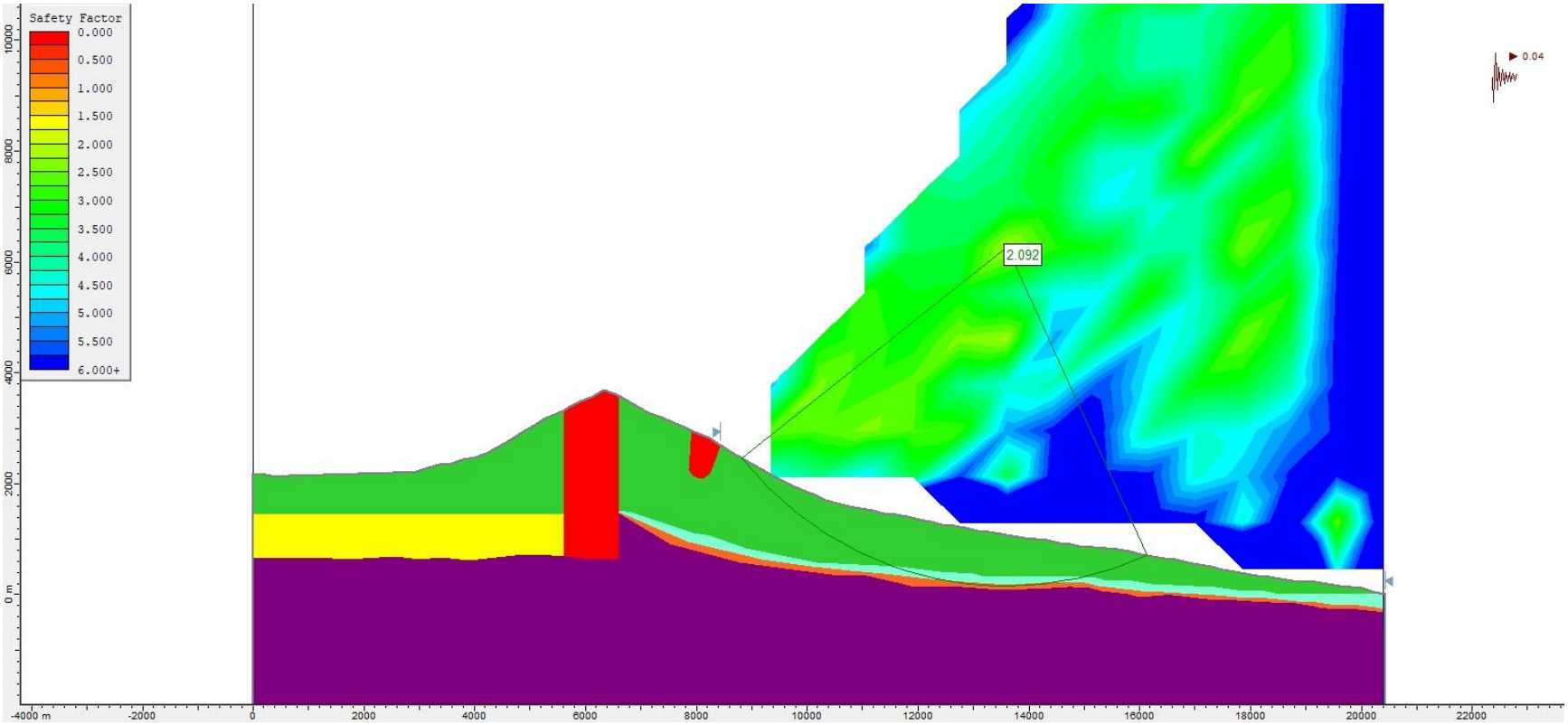

Figure S216. Slope stability pseudo-static analysis for Model 1 Bis (assuming a caldera collapse), using the Morgenstern-Price method and a k_h = 0.04.

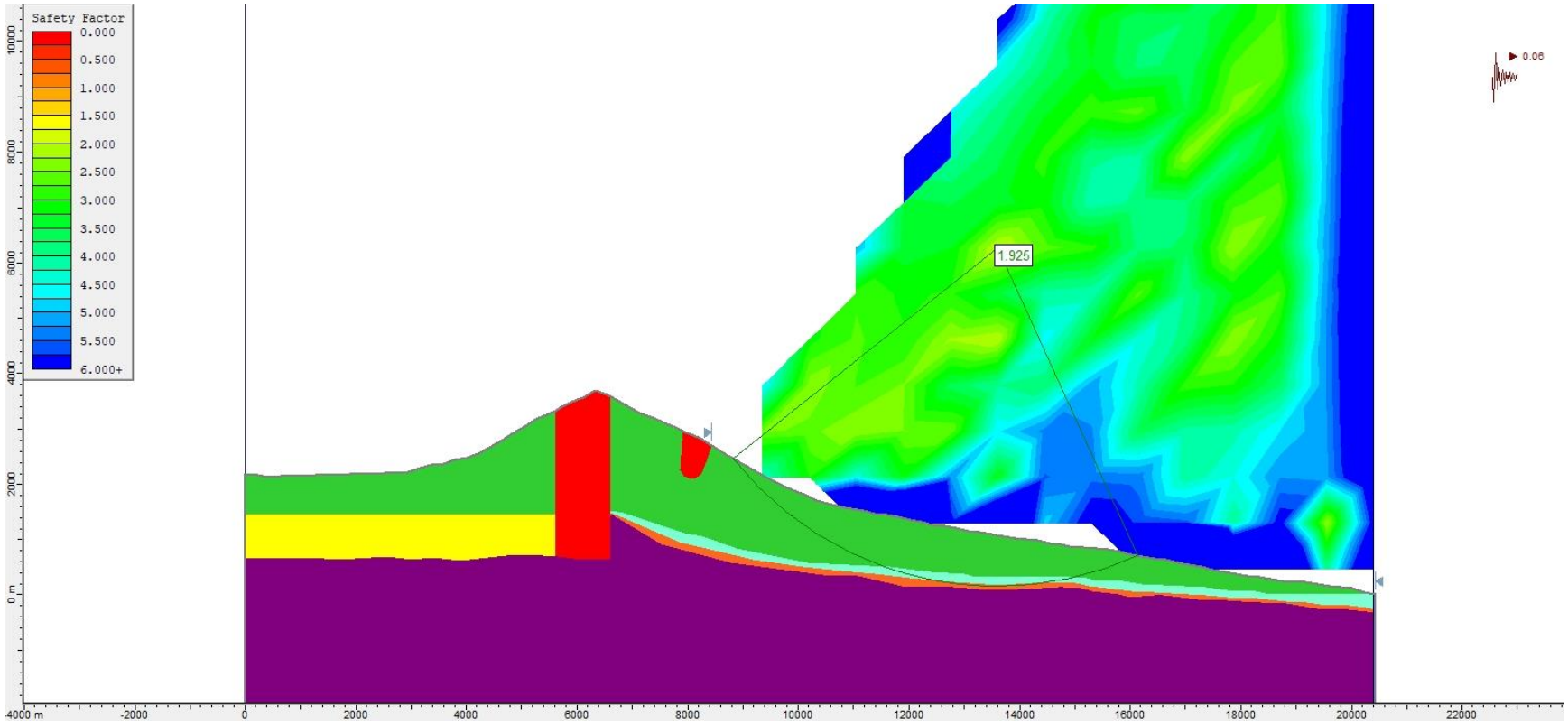

Figure S217. Slope stability pseudo-static analysis for Model 1 Bis (assuming a caldera collapse), using the Bishop simplified method and a k_h = 0.06.

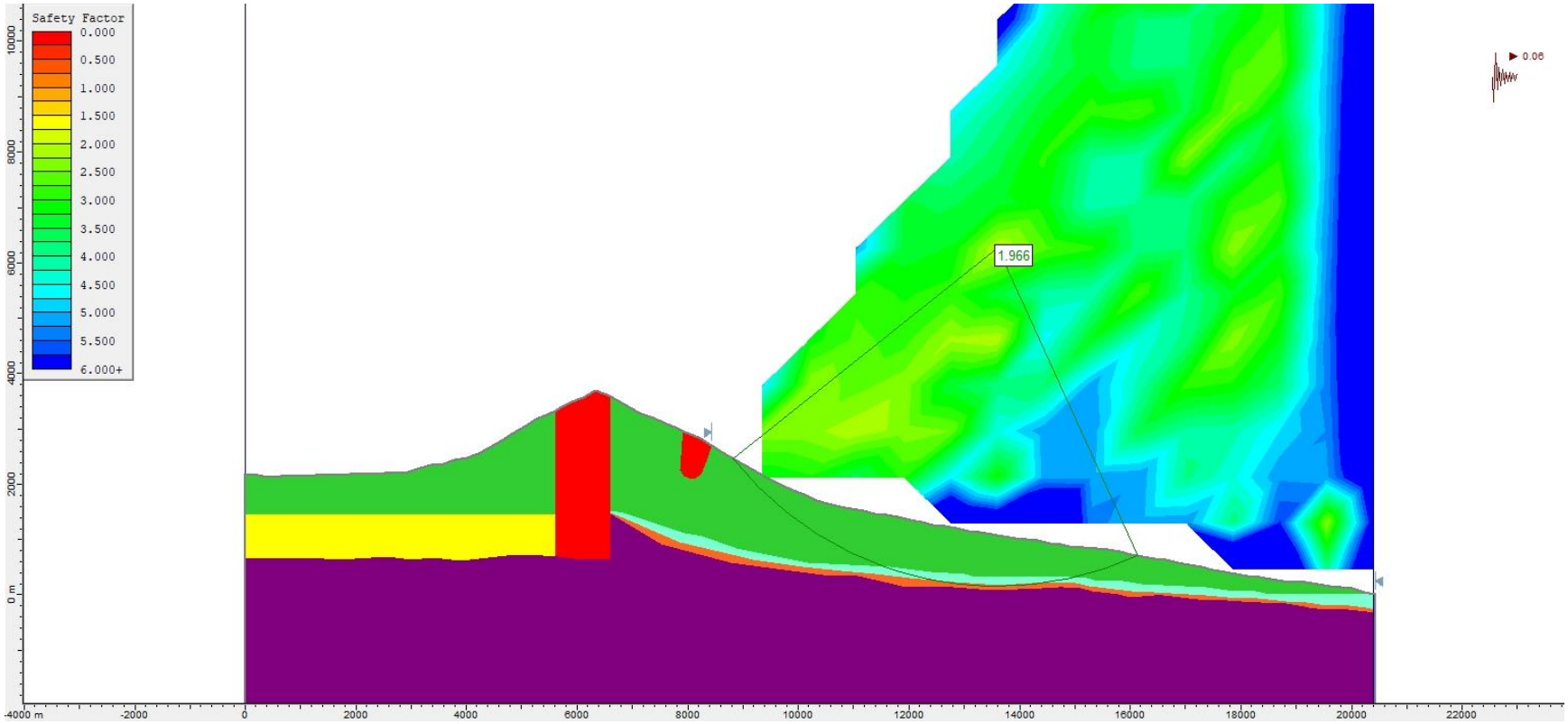

Figure S218. Slope stability pseudo-static analysis for Model 1 Bis (assuming a caldera collapse), using the Janbu Generalised method and a k_h = 0.06.

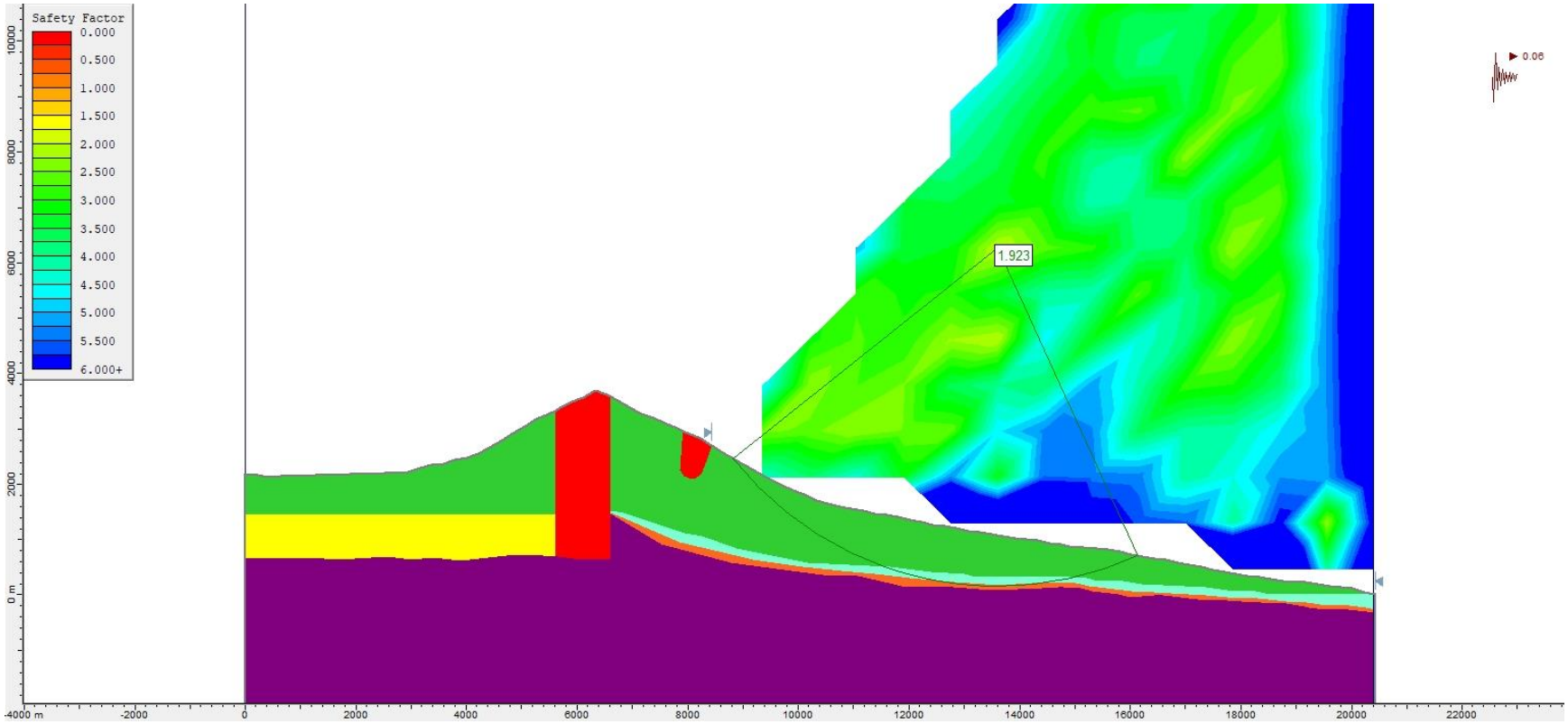

Figure S219. Slope stability pseudo-static analysis for Model 1 Bis (assuming a caldera collapse), using the Morgenstern-Price method and a k_h = 0.06.

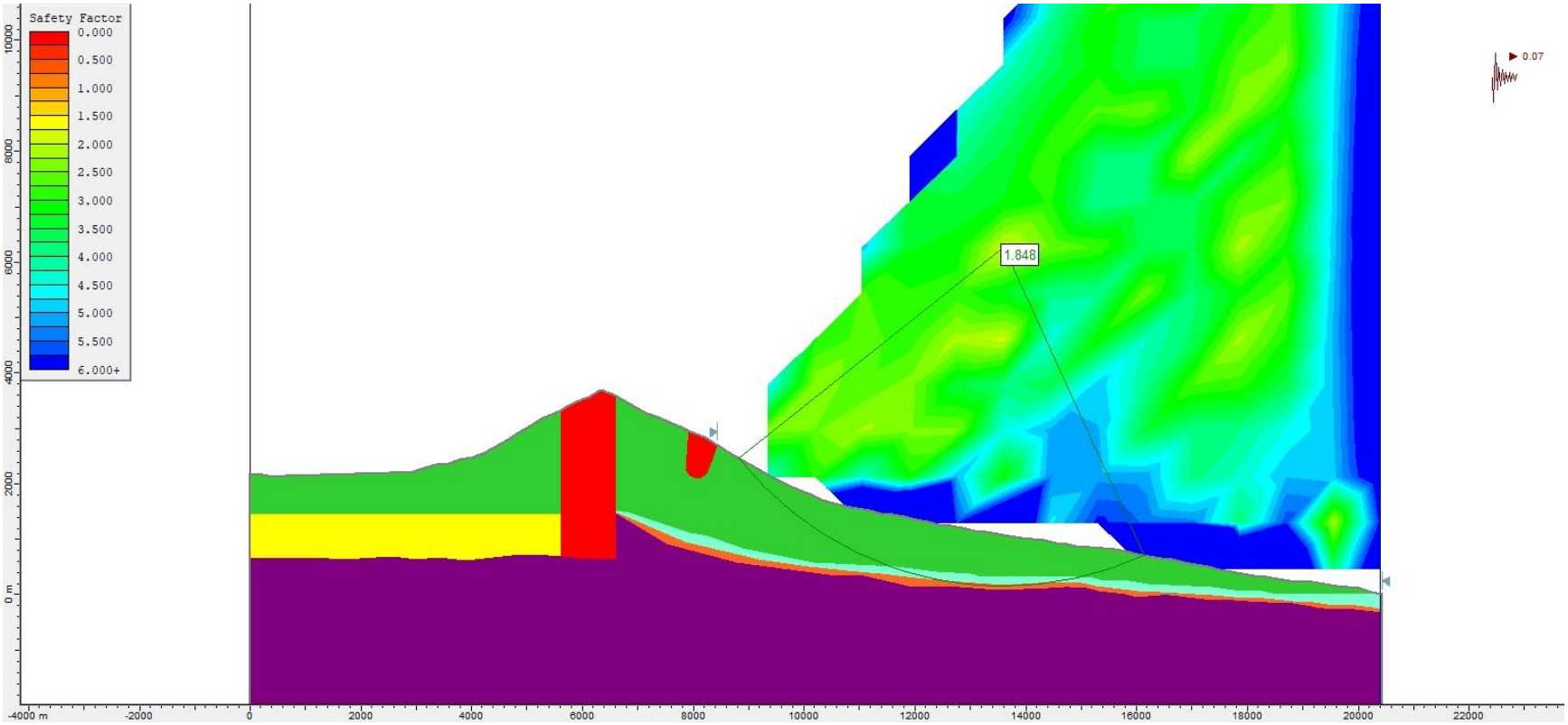

Figure S220. Slope stability pseudo-static analysis for Model 1 Bis (assuming a caldera collapse), using the Bishop simplified method and a k_h = 0.07.

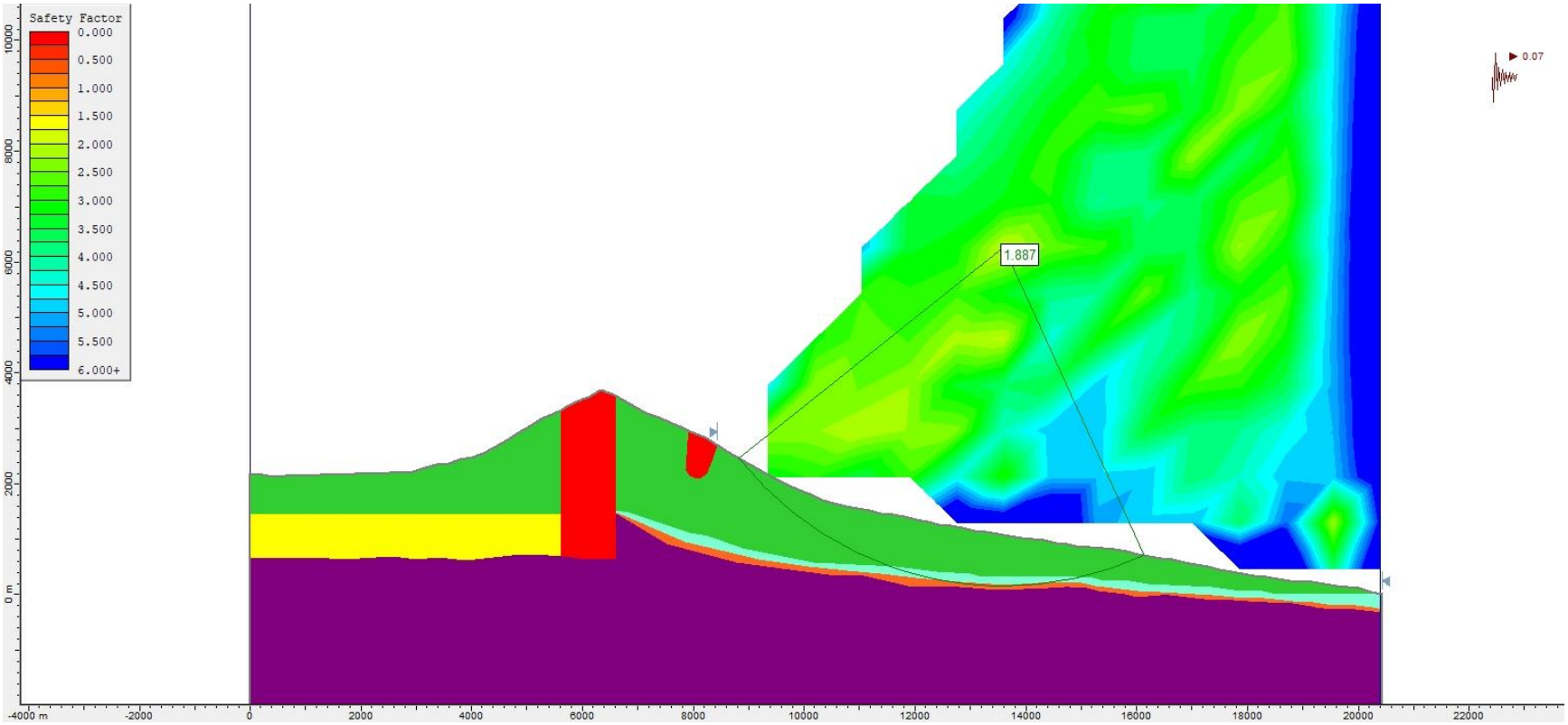

Figure S221. Slope stability pseudo-static analysis for Model 1 Bis (assuming a caldera collapse), using the Janbu Generalised method and a k_h = 0.07.

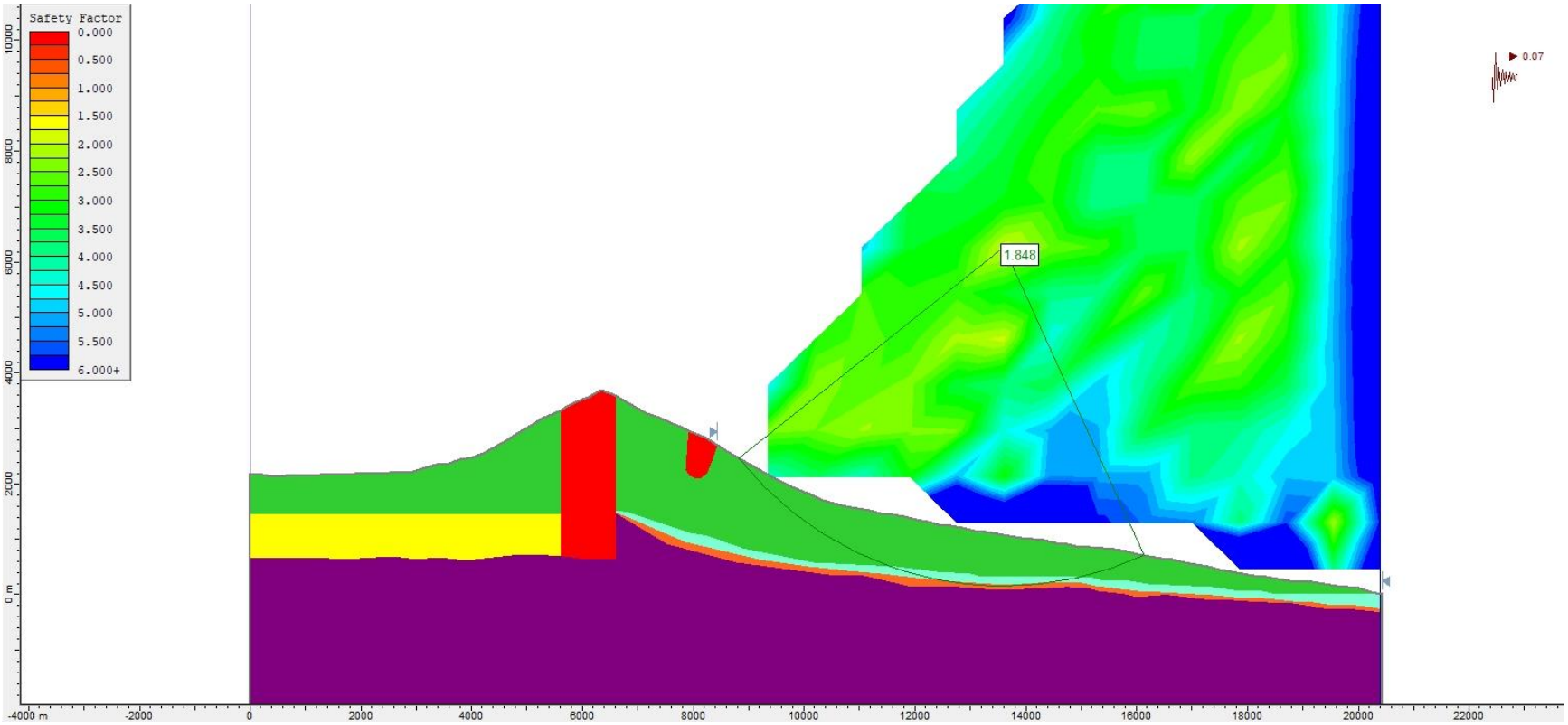

Figure S222. Slope stability pseudo-static analysis for Model 1 Bis (assuming a caldera collapse), using the Morgenstern-Price method and a k_h = 0.07.

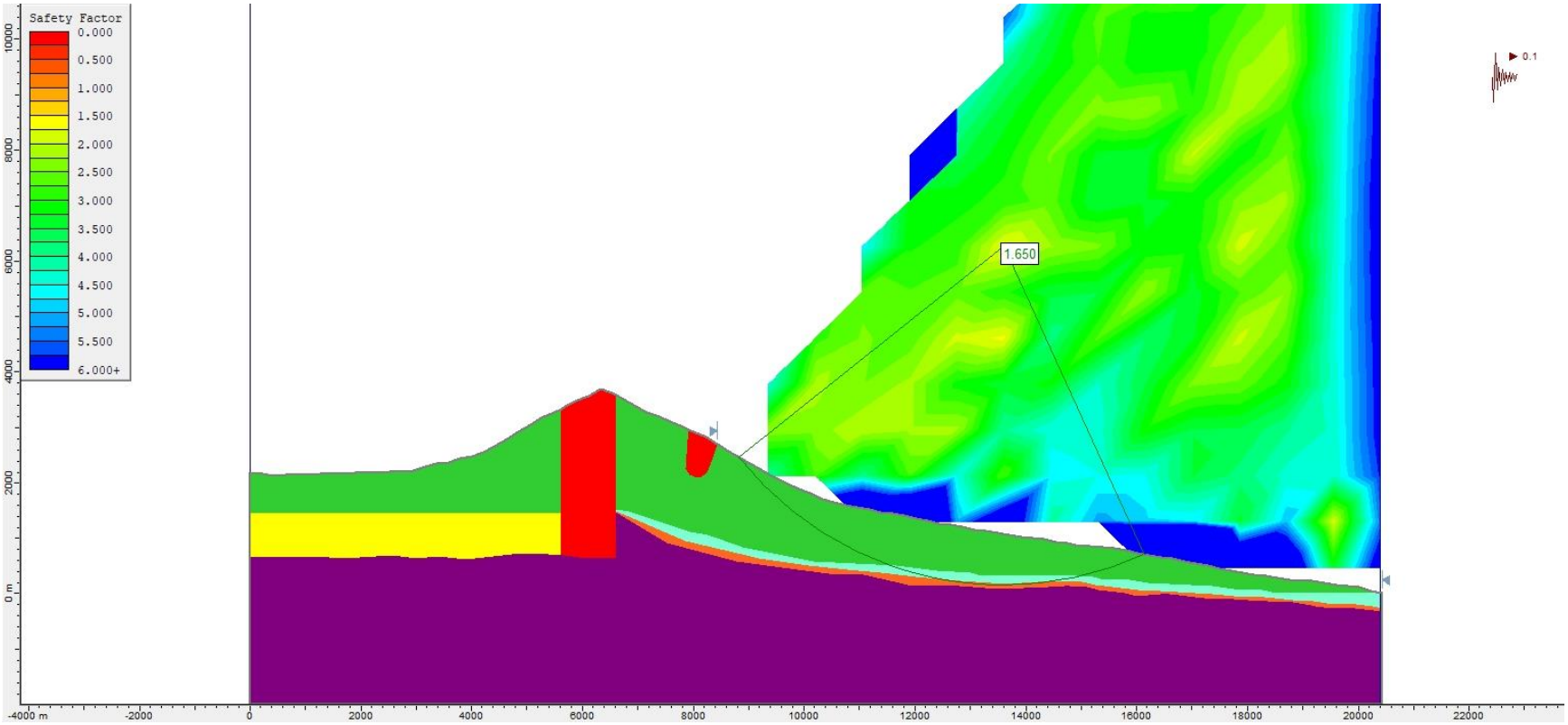

Figure S223. Slope stability pseudo-static analysis for Model 1 Bis (assuming a caldera collapse), using the Bishop simplified method and a k_h = 0.10.

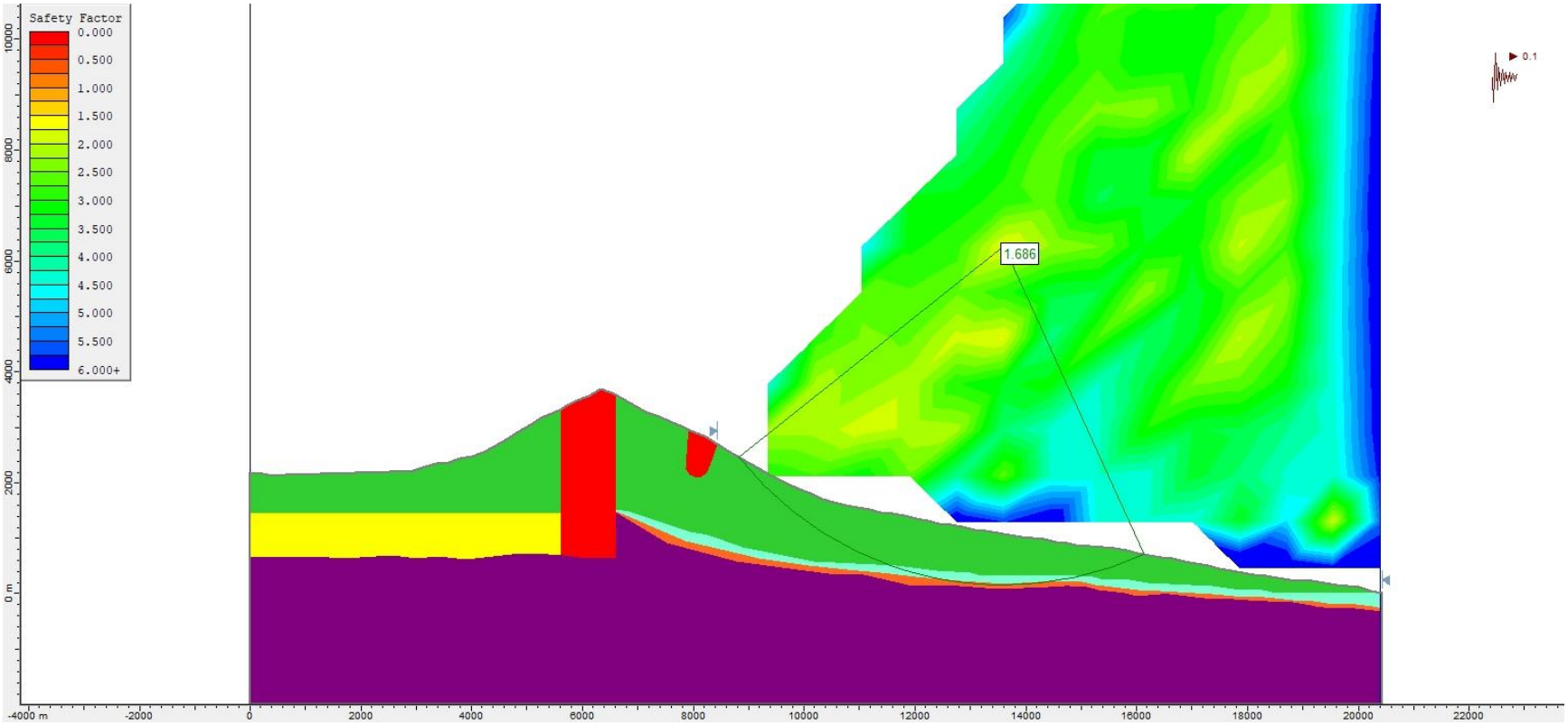

Figure S224. Slope stability pseudo-static analysis for Model 1 Bis (assuming a caldera collapse), using the Janbu Generalised method and a k_h = 0.10.

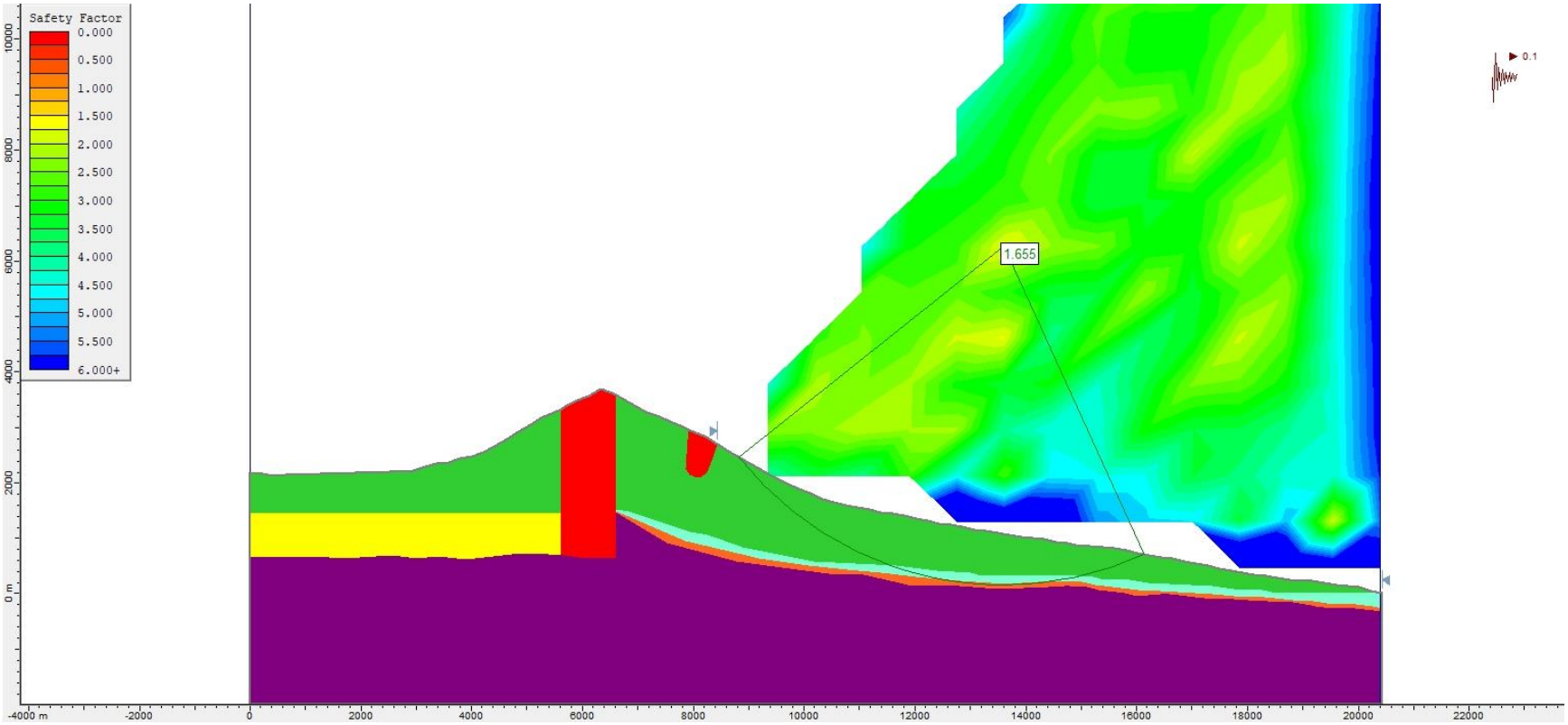

Figure S225. Slope stability pseudo-static analysis for Model 1 Bis (assuming a caldera collapse), using the Morgenstern-Price method and a k_h = 0.10.

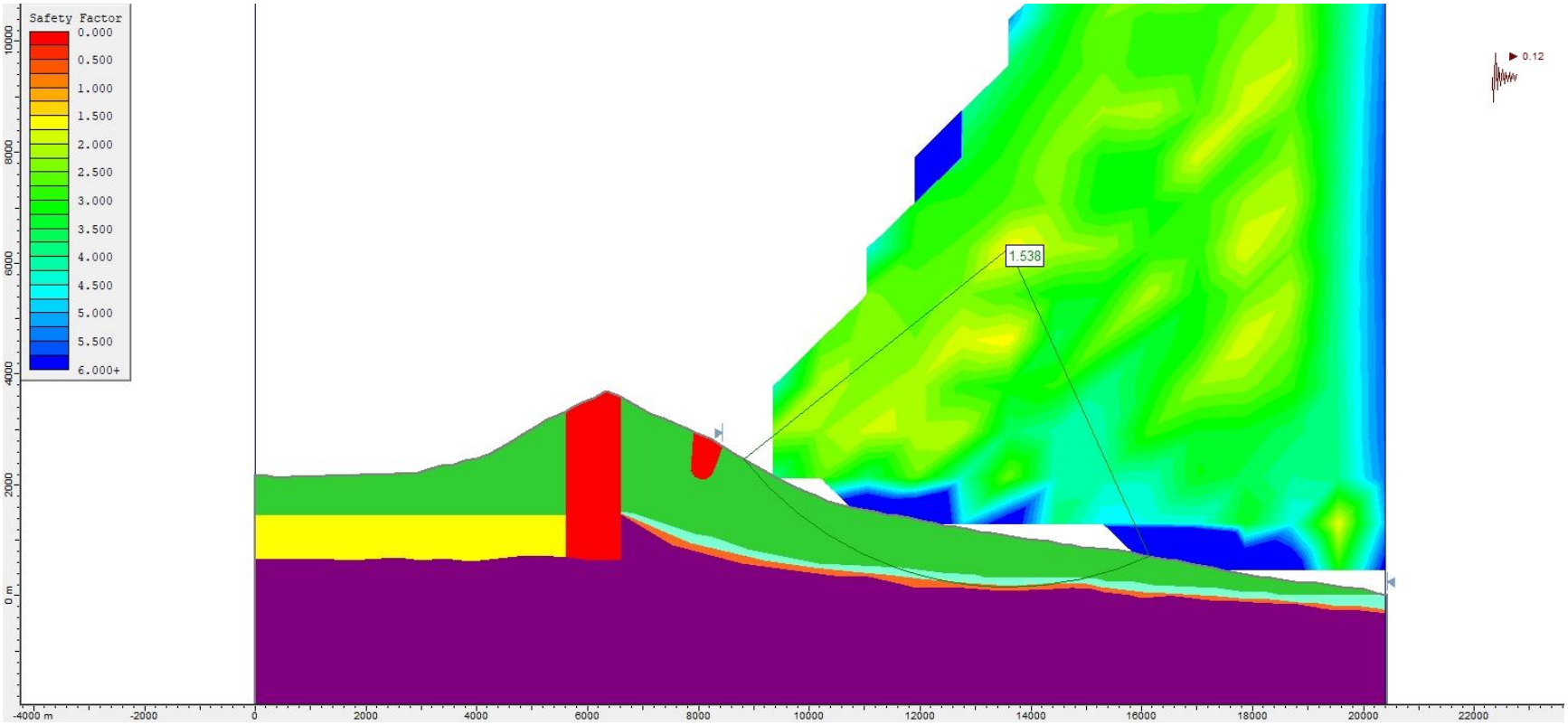

Figure S226. Slope stability pseudo-static analysis for Model 1 Bis (assuming a caldera collapse), using the Bishop simplified method and a k_h = 0.12.

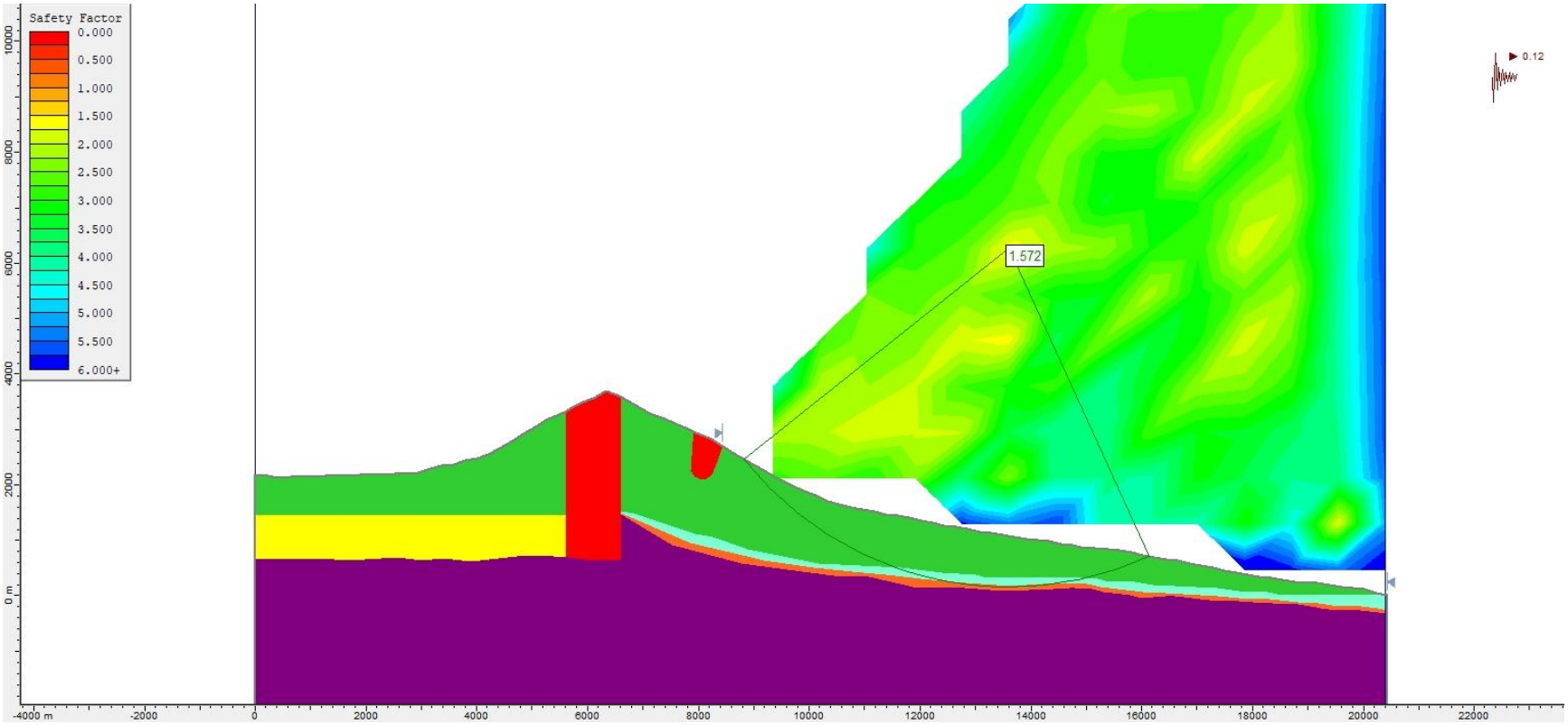

Figure S227. Slope stability pseudo-static analysis for Model 1 Bis (assuming a caldera collapse), using the Janbu Generalised method and a k_h = 0.12.

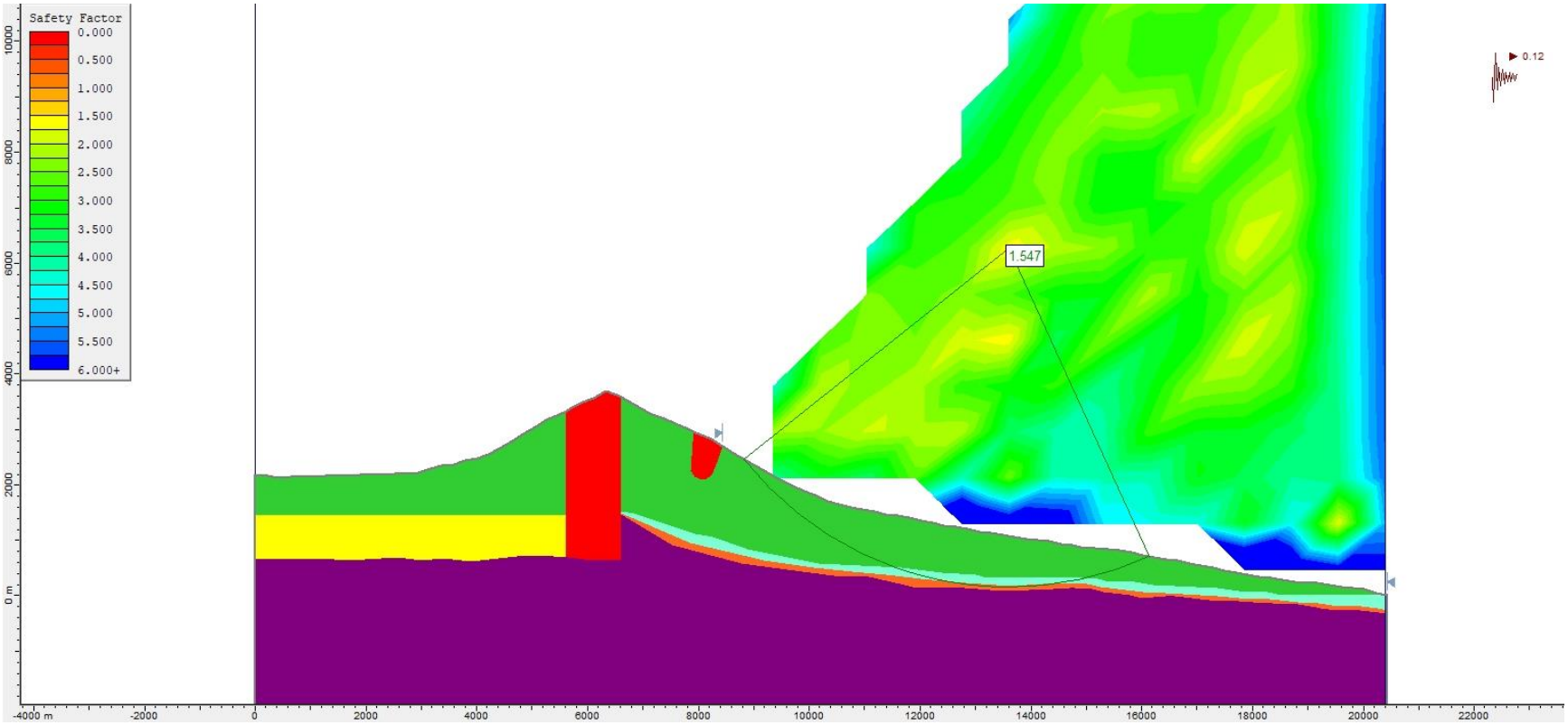

Figure S228. Slope stability pseudo-static analysis for Model 1 Bis (assuming a caldera collapse), using the Morgenstern-Price method and a k_h = 0.12.

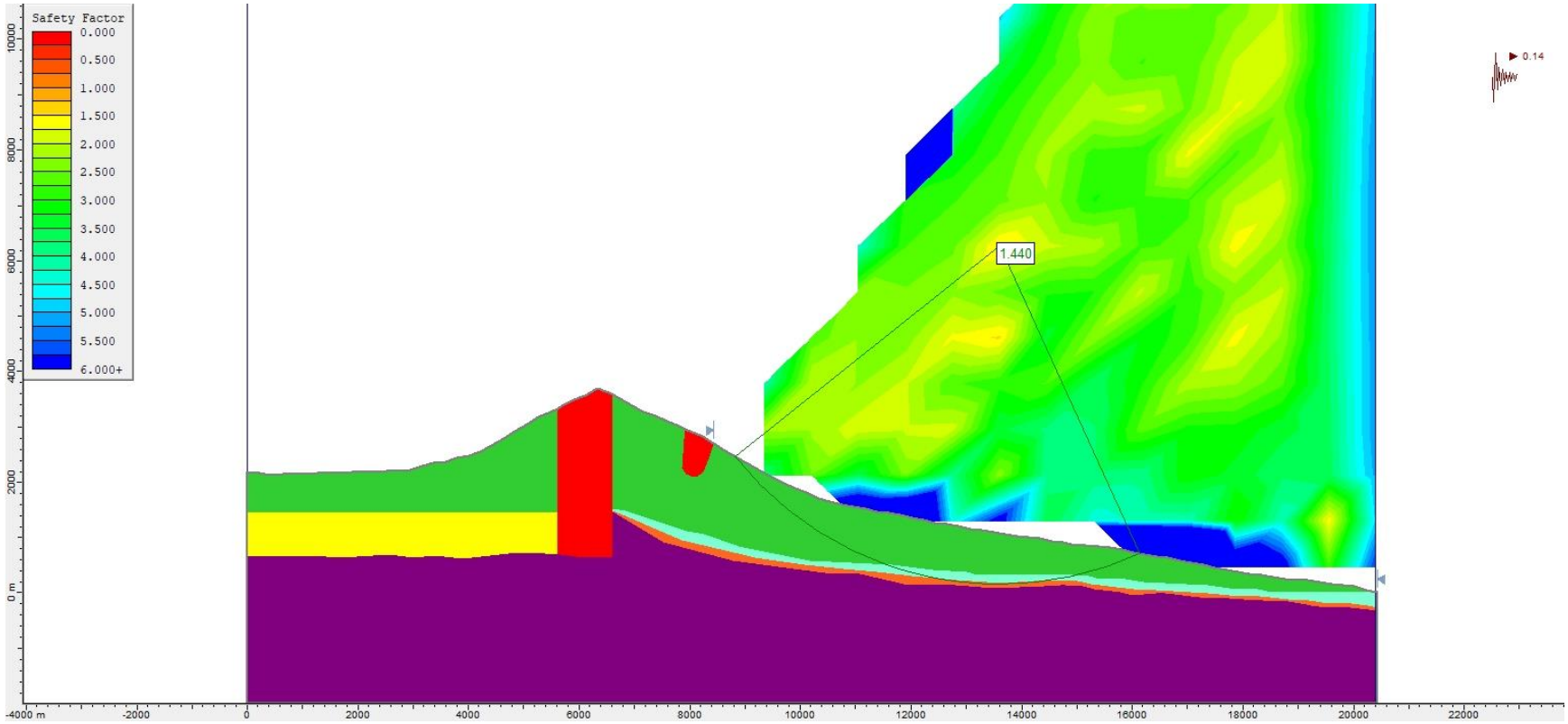

Figure S229. Slope stability pseudo-static analysis for Model 1 Bis (assuming a caldera collapse), using the Bishop simplified method and a k_h = 0.14.

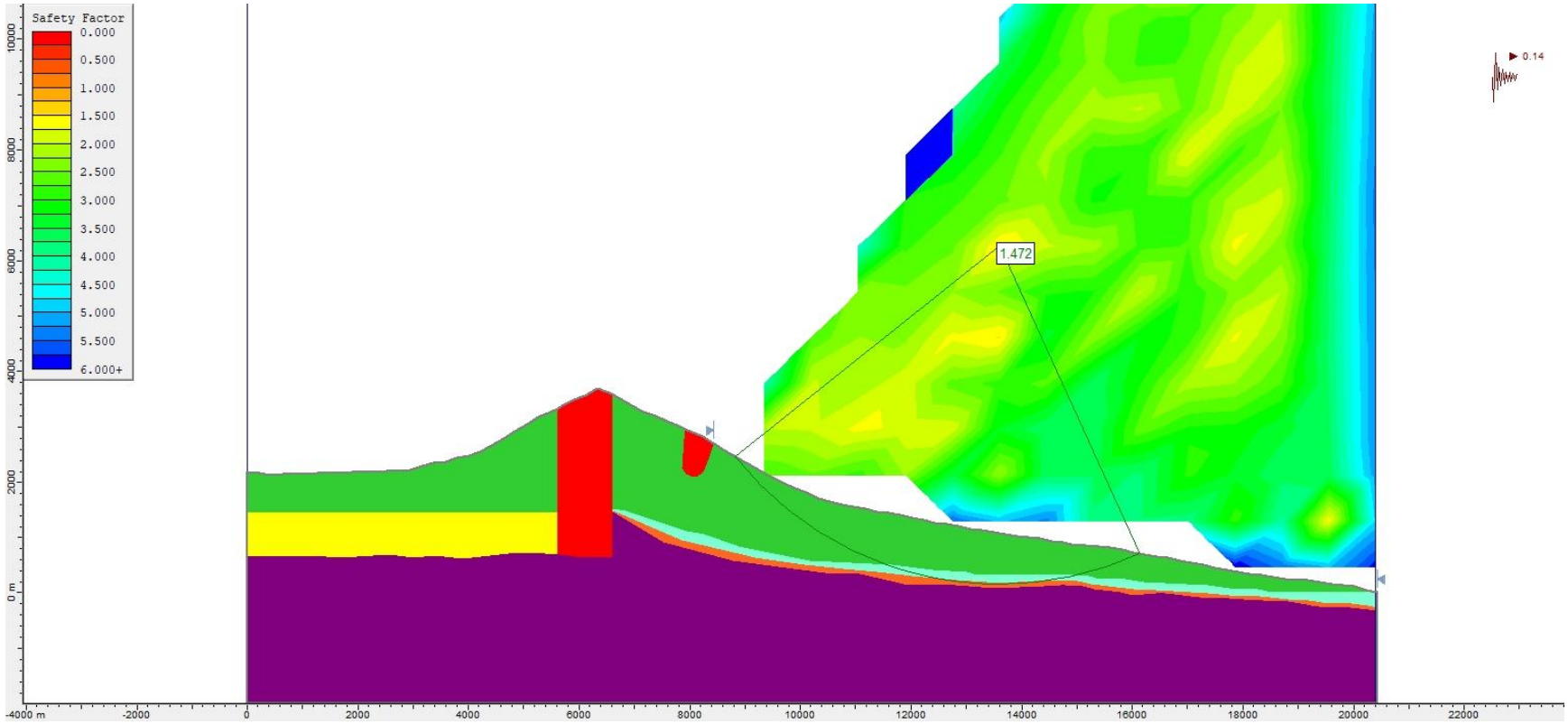

Figure S230. Slope stability pseudo-static analysis for Model 1 Bis (assuming a caldera collapse), using the Janbu Generalised method and a k_h = 0.14.

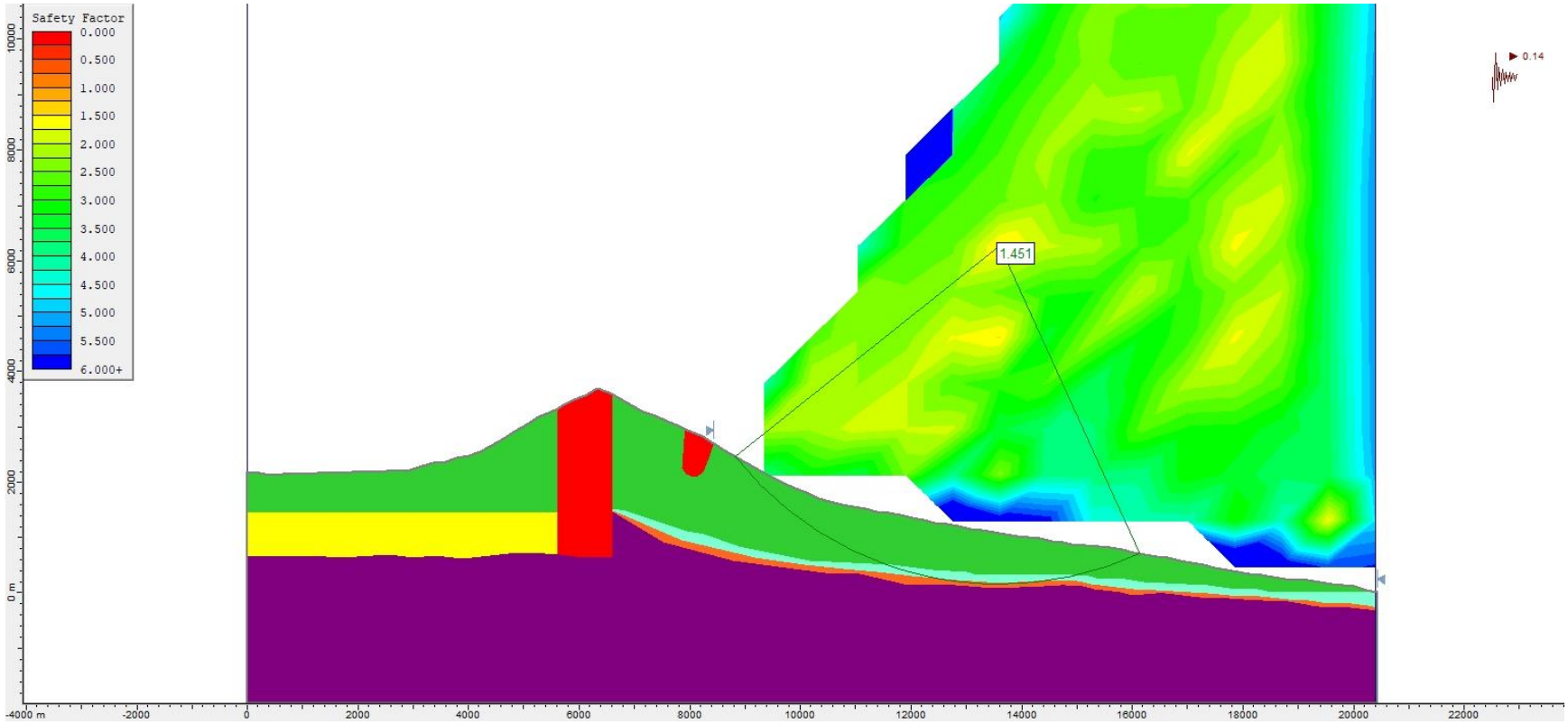

Figure S231. Slope stability pseudo-static analysis for Model 1 Bis (assuming a caldera collapse), using the Morgenstern-Price method and a k_h = 0.14.

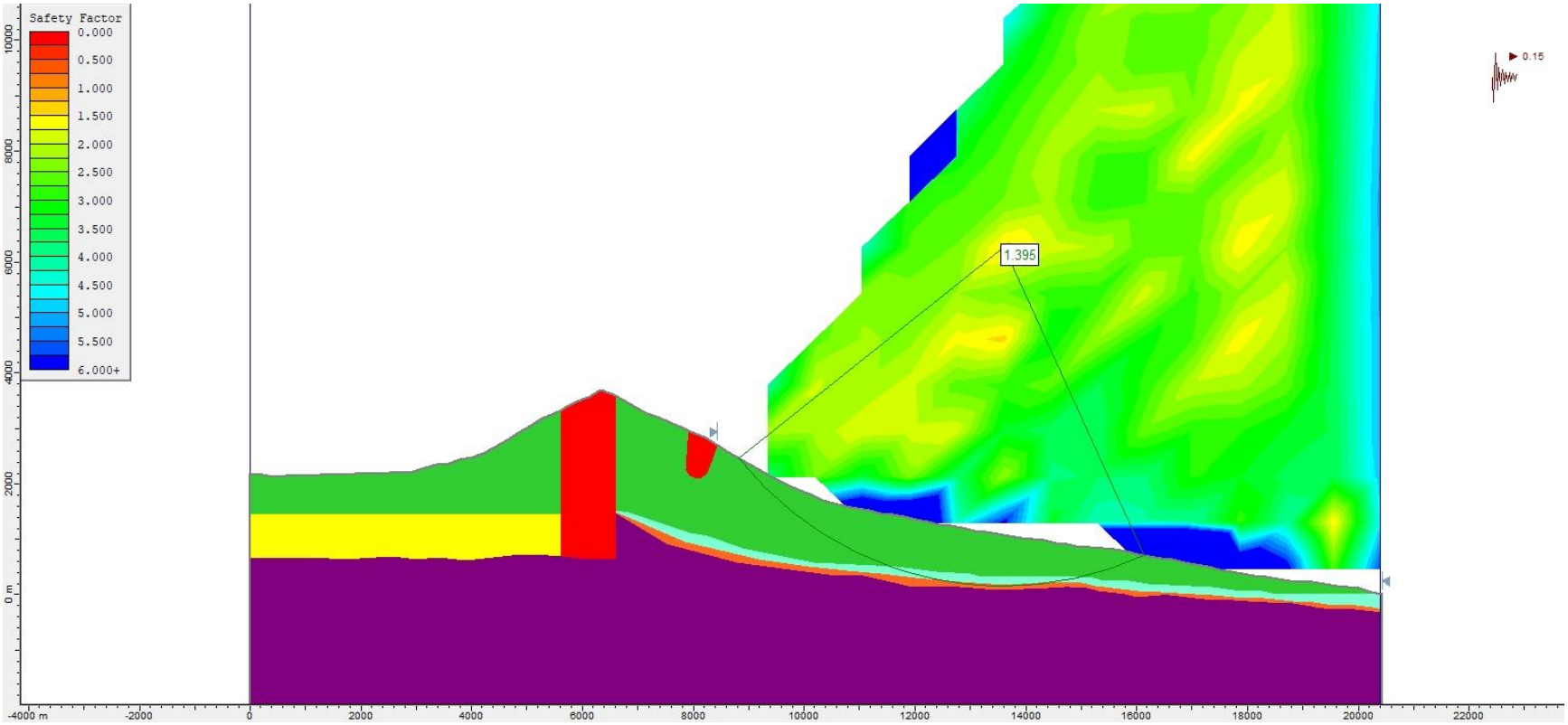

Figure S232. Slope stability pseudo-static analysis for Model 1 Bis (assuming a caldera collapse), using the Bishop simplified method and a k_h = 0.15.

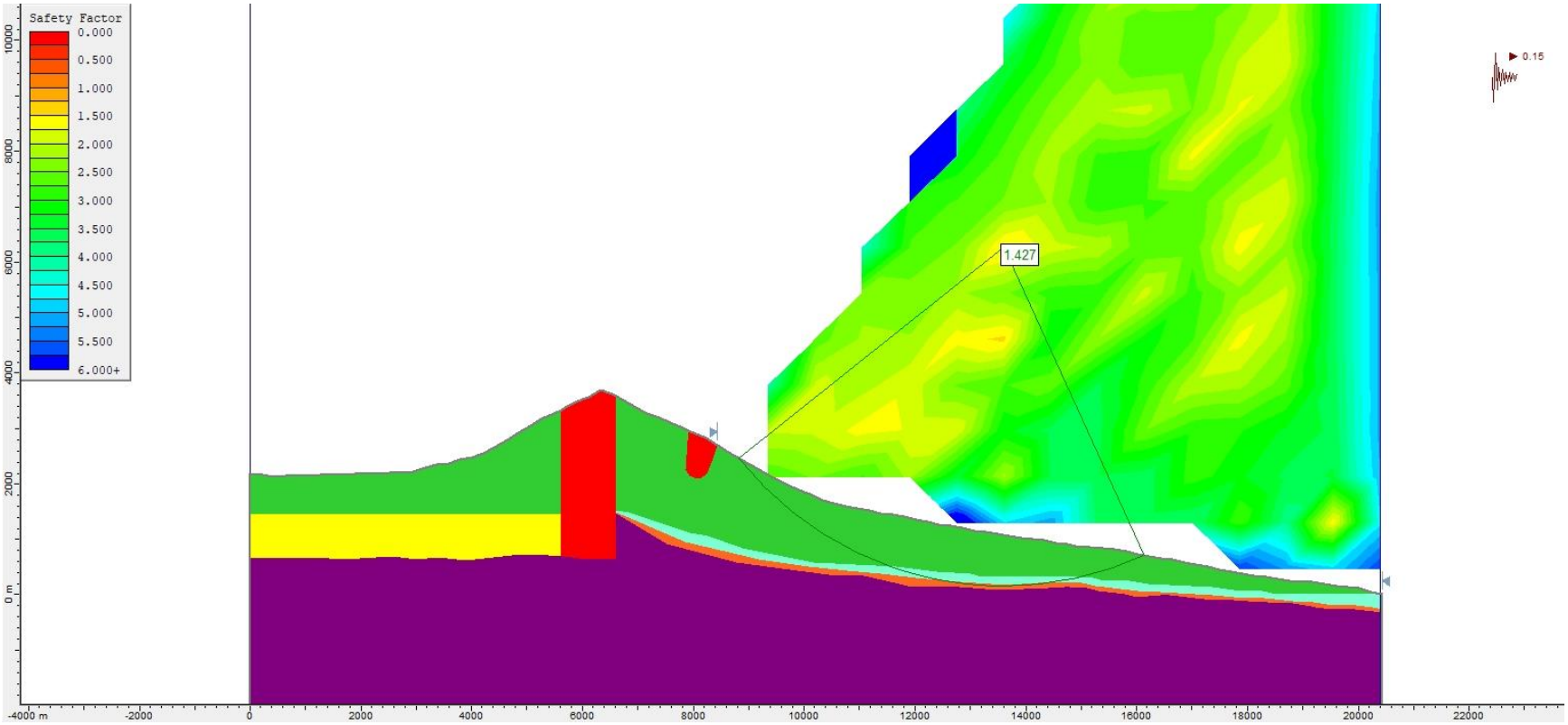

Figure S233. Slope stability pseudo-static analysis for Model 1 Bis (assuming a caldera collapse), using the Janbu Generalised method and a k_h = 0.15.

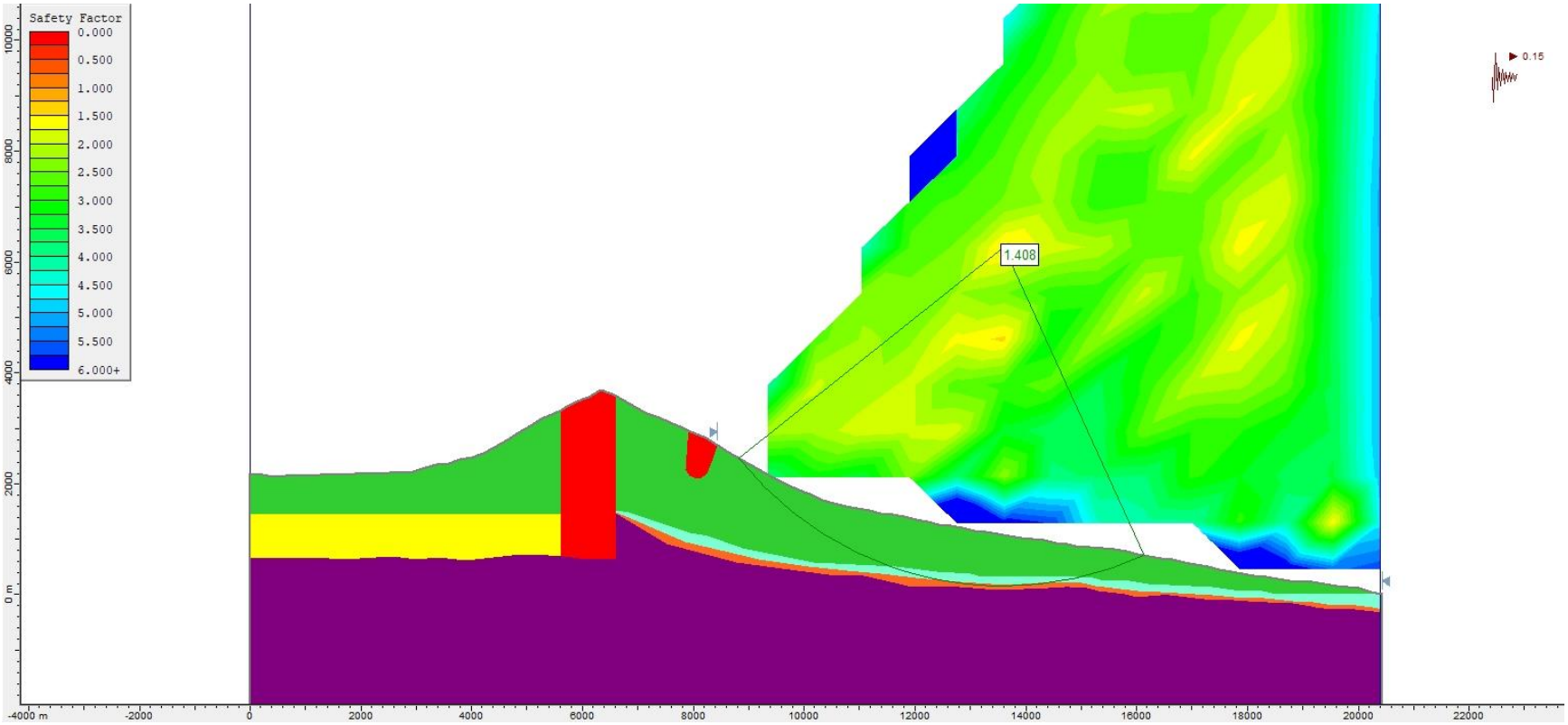

Figure S234. Slope stability pseudo-static analysis for Model 1 Bis (assuming a caldera collapse), using the Morgenstern-Price method and a k_h = 0.15.

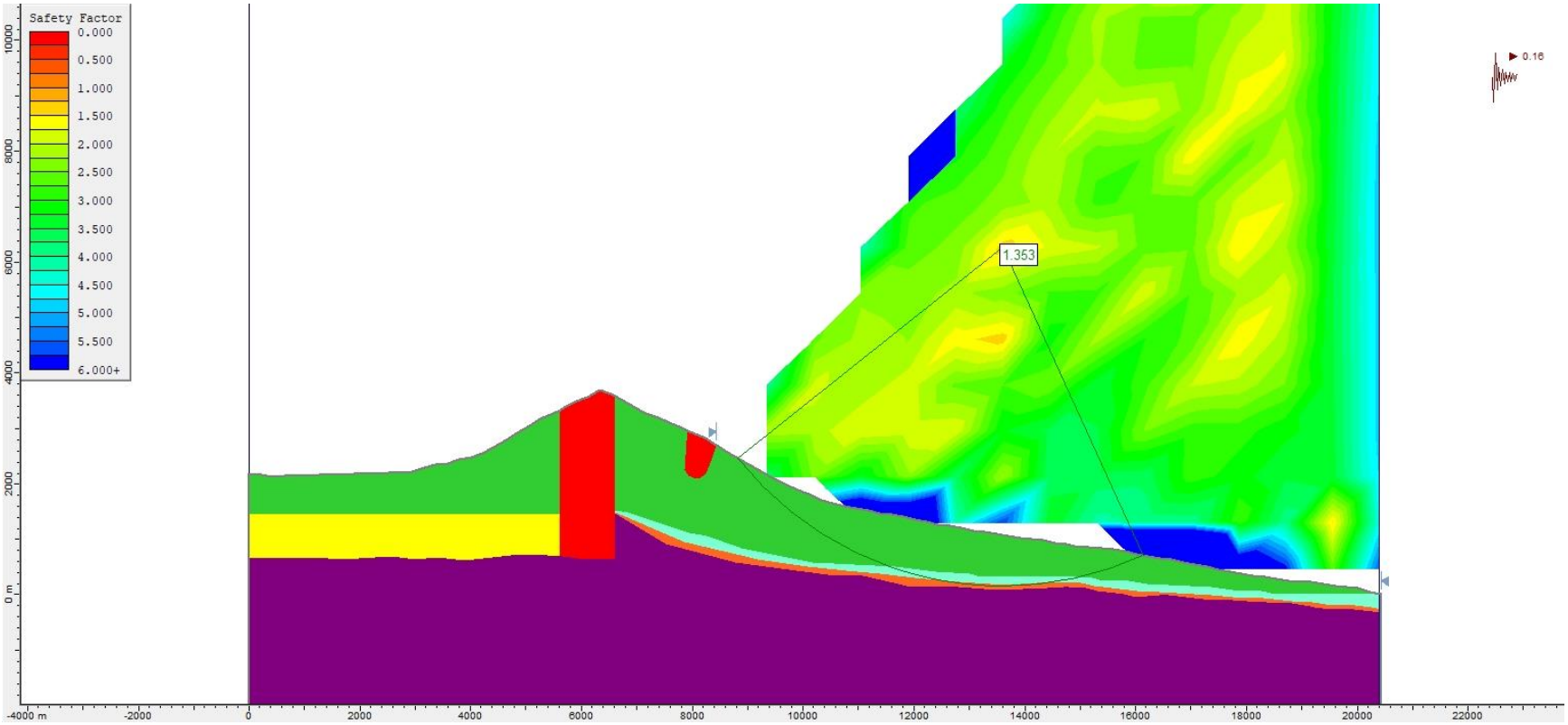

Figure S235. Slope stability pseudo-static analysis for Model 1 Bis (assuming a caldera collapse), using the Bishop simplified method and a k_h = 0.16.

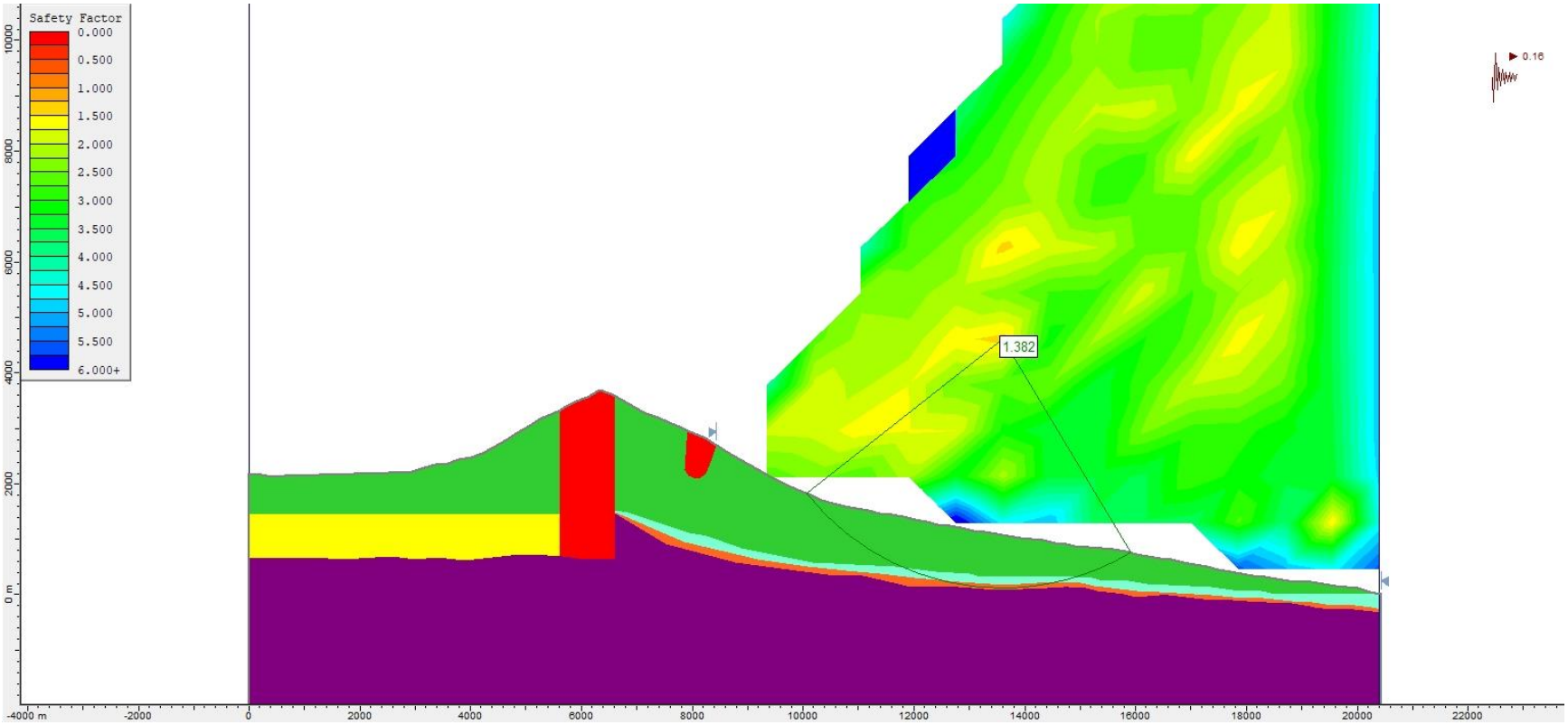

Figure S236. Slope stability pseudo-static analysis for Model 1 Bis (assuming a caldera collapse), using the Janbu Generalised method and a k_h = 0.16.

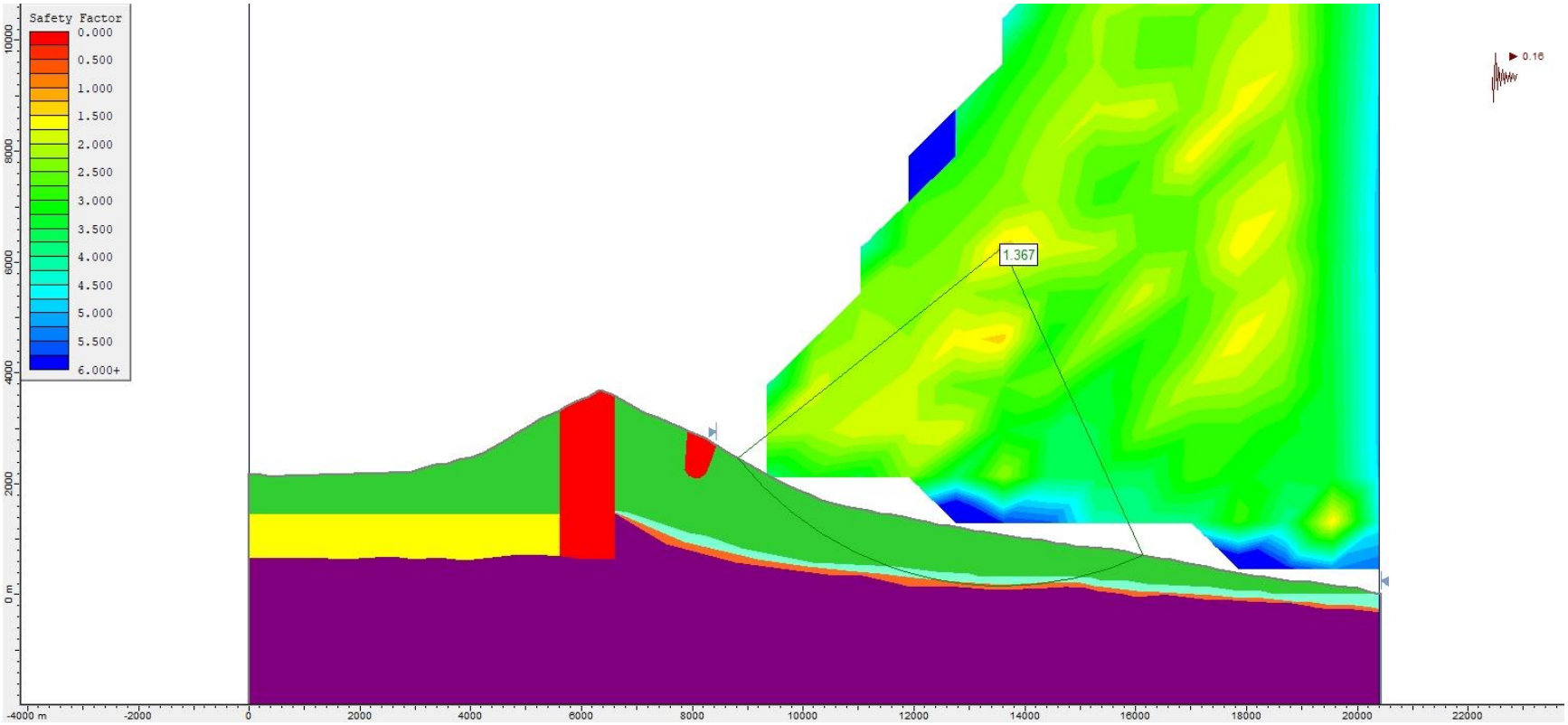

Figure S237. Slope stability pseudo-static analysis for Model 1 Bis (assuming a caldera collapse), using the Morgenstern-Price method and a k_h = 0.16.

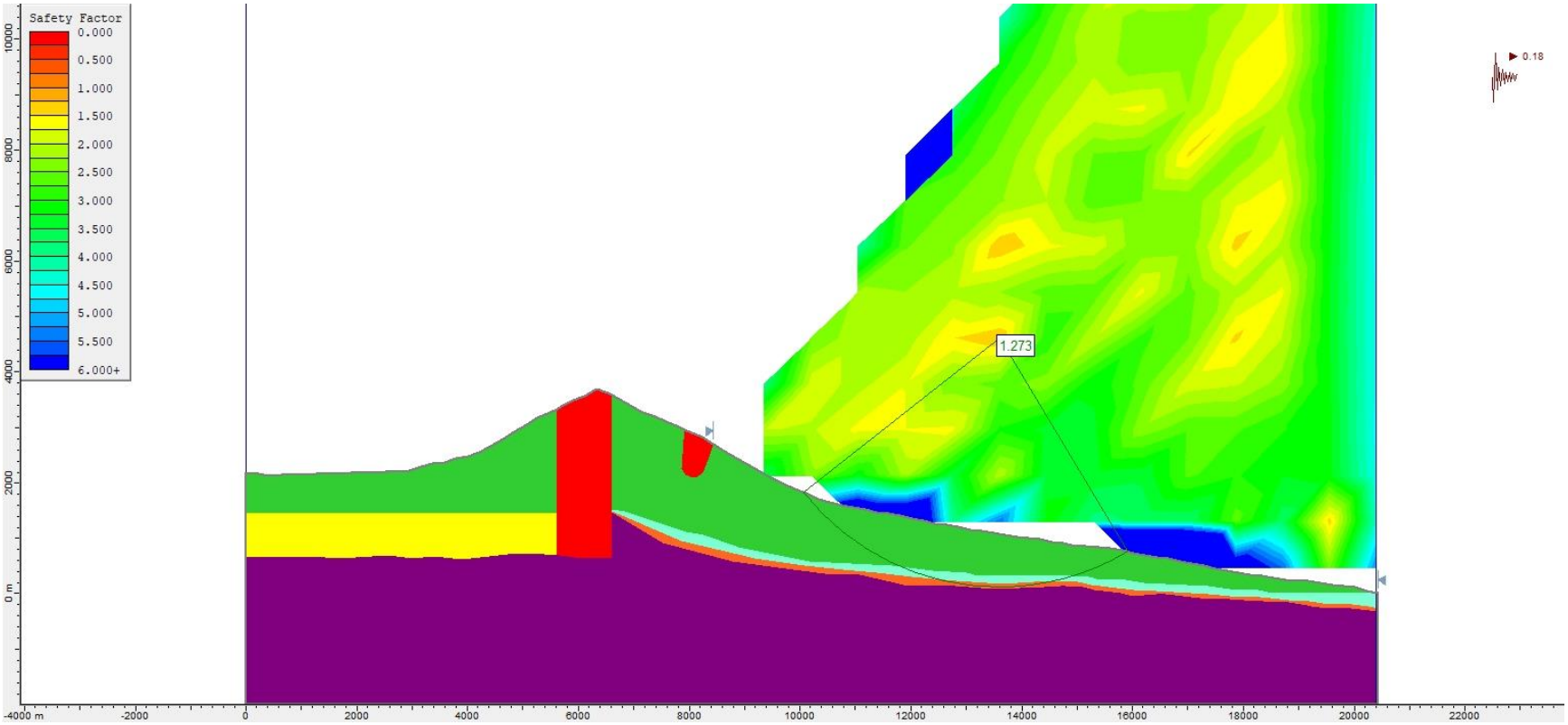

Figure S238. Slope stability pseudo-static analysis for Model 1 Bis (assuming a caldera collapse), using the Bishop simplified method and a k_h = 0.18.

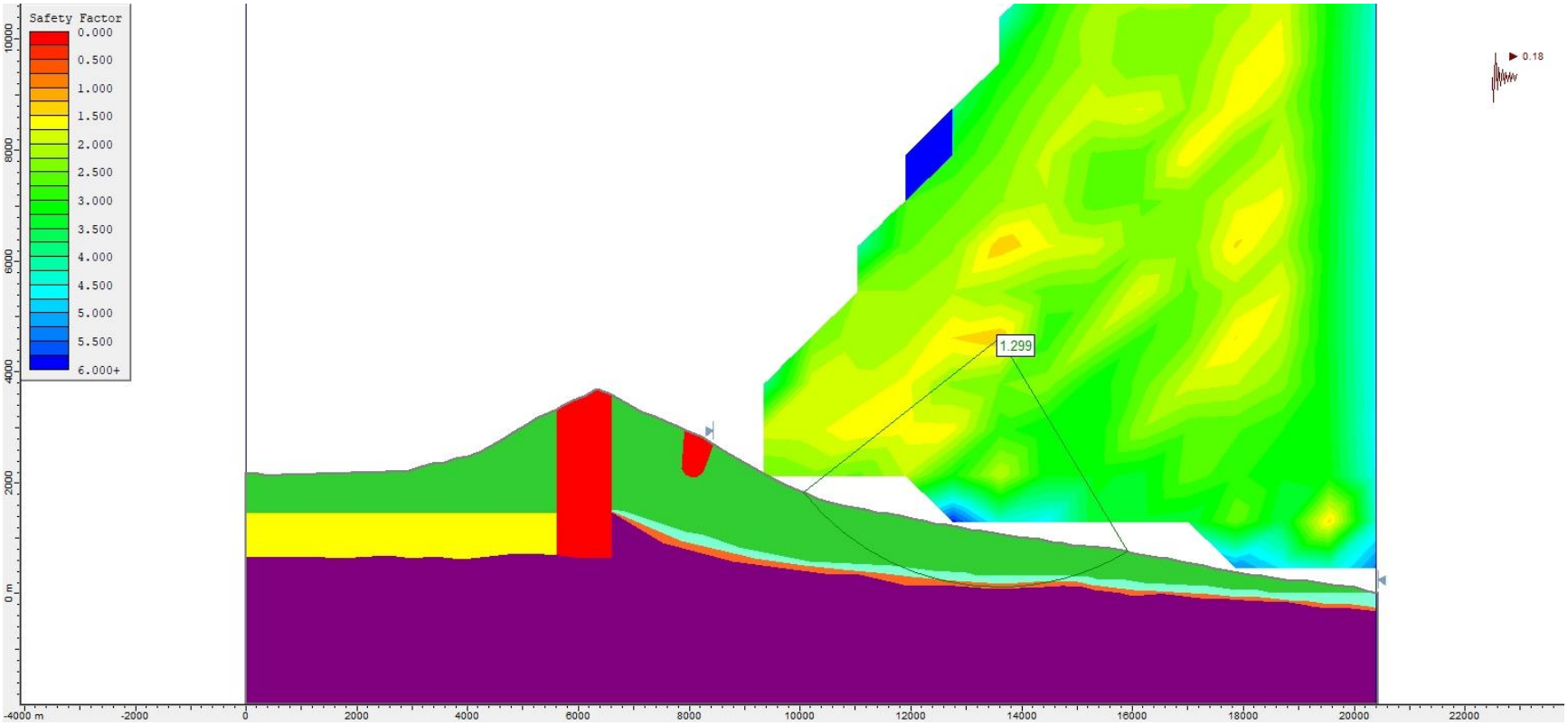

Figure S239. Slope stability pseudo-static analysis for Model 1 Bis (assuming a caldera collapse), using the Janbu Generalised method and a k_h = 0.18.

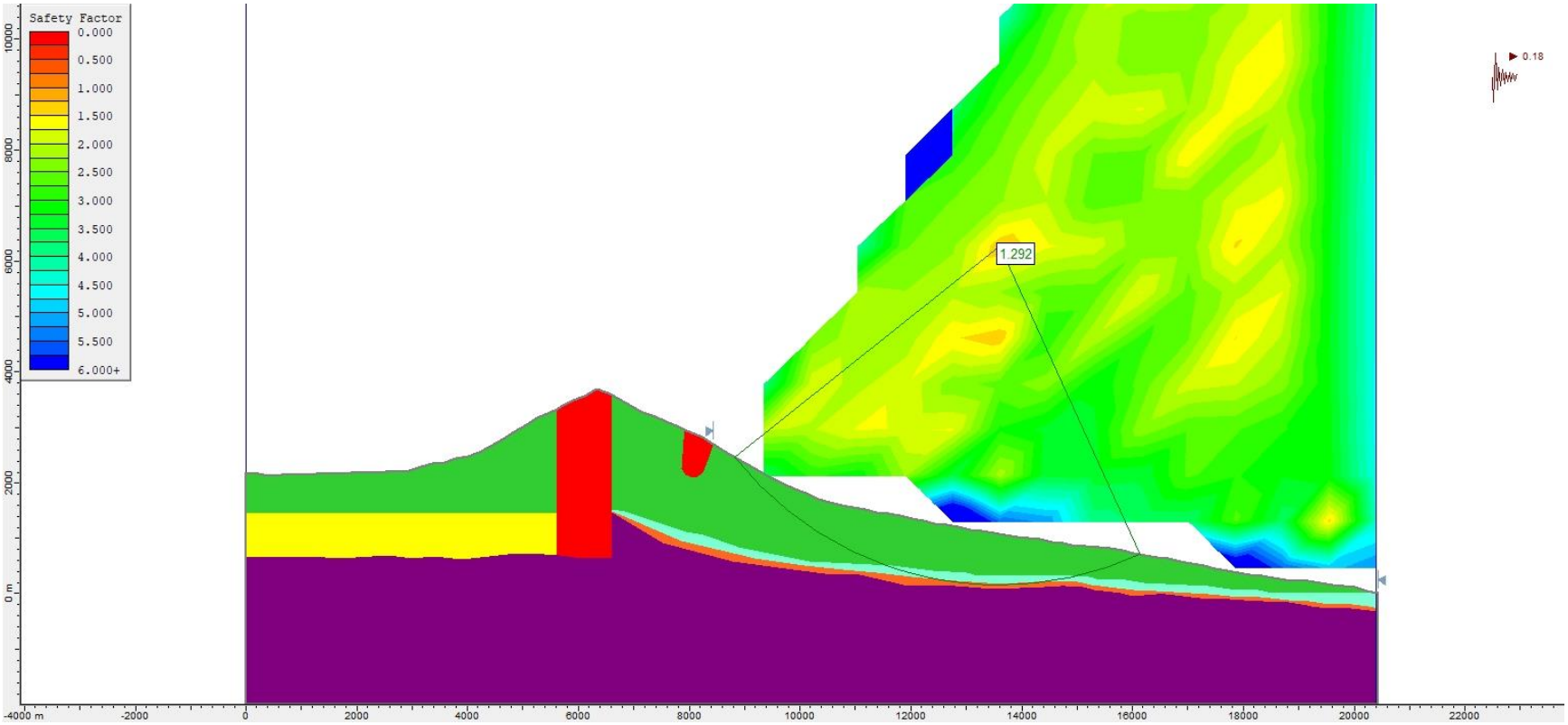

Figure S240. Slope stability pseudo-static analysis for Model 1 Bis (assuming a caldera collapse), using the Morgenstern-Price method and a k_h = 0.18.

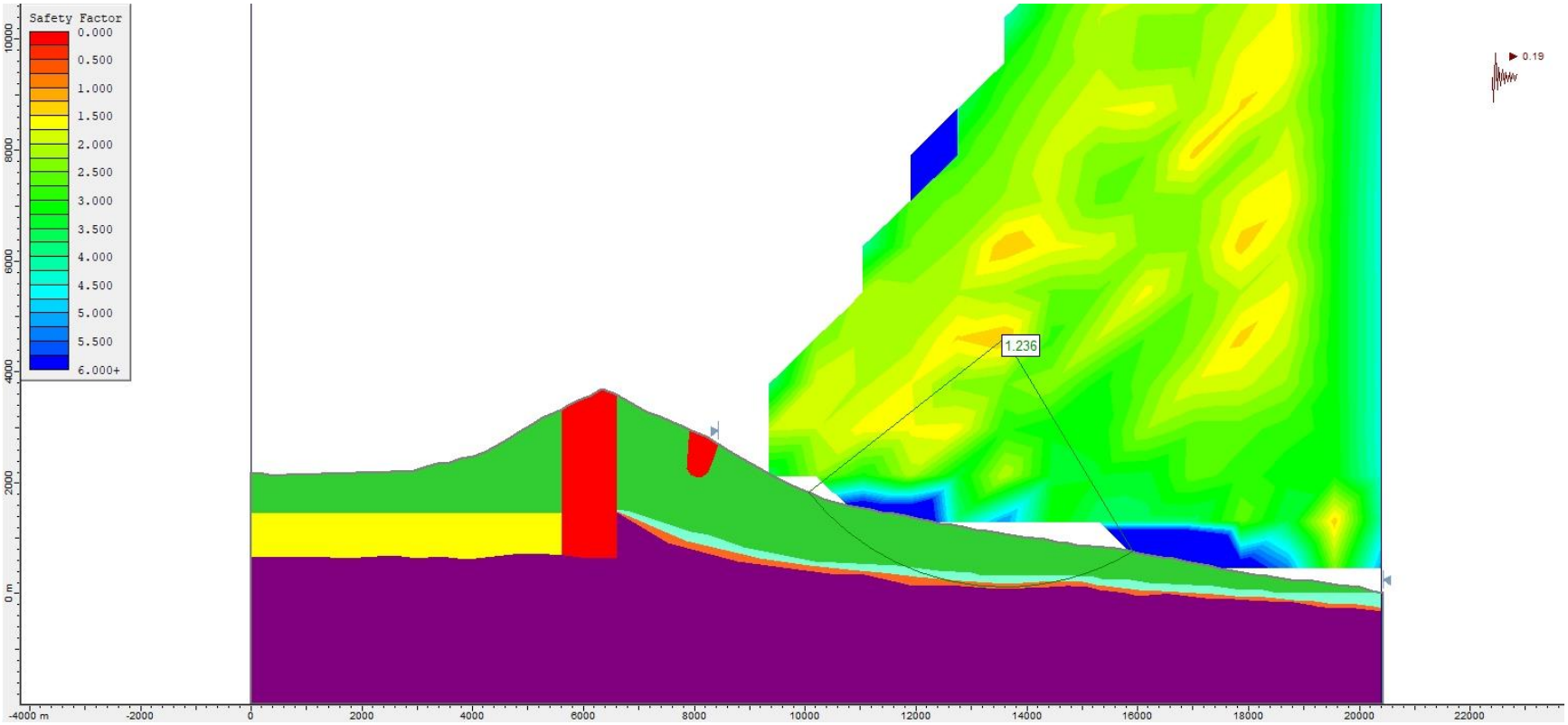

Figure S241. Slope stability pseudo-static analysis for Model 1 Bis (assuming a caldera collapse), using the Bishop simplified method and a k_h = 0.19.

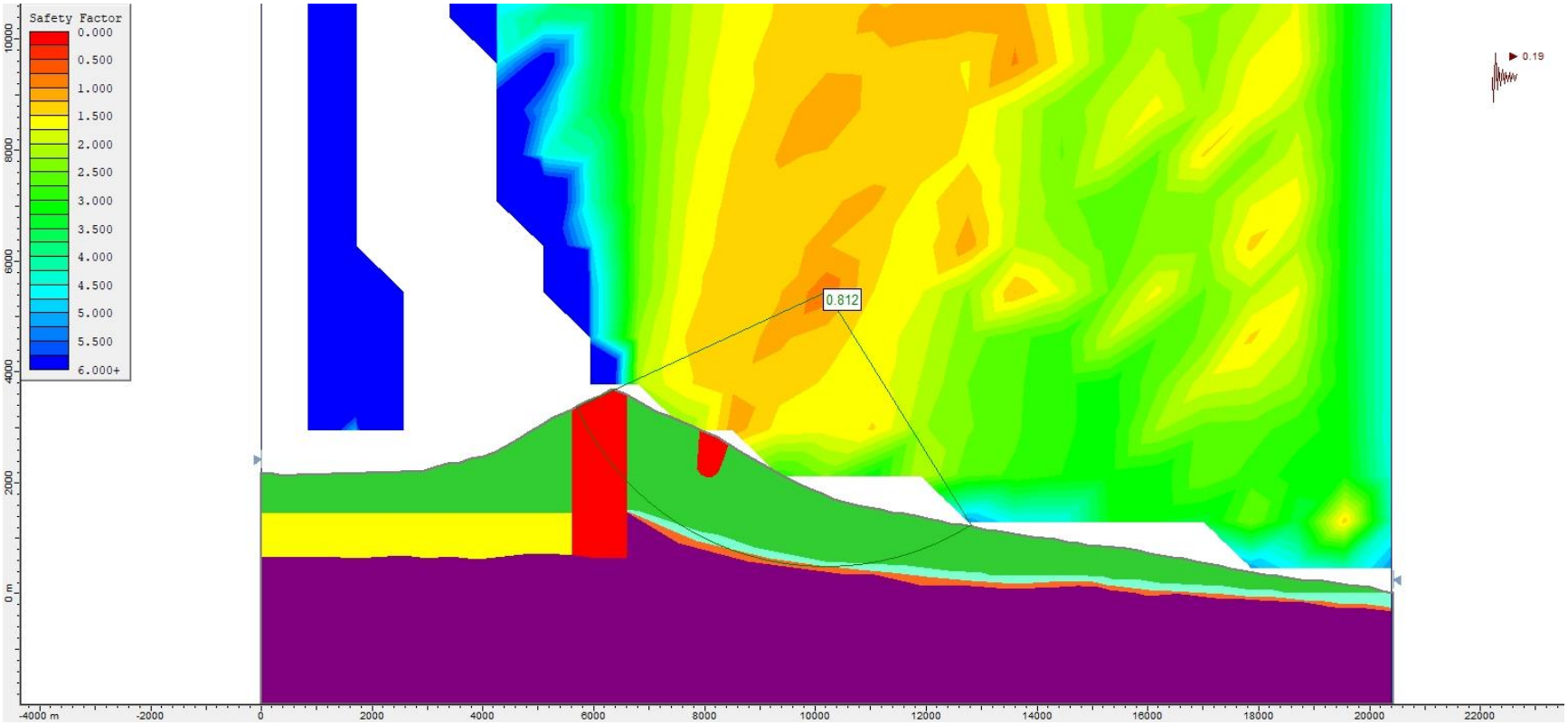

Figure S242. Slope stability pseudo-static analysis for Model 1 Bis (assuming a caldera collapse), using the Janbu Generalised method and a k_h = 0.19.

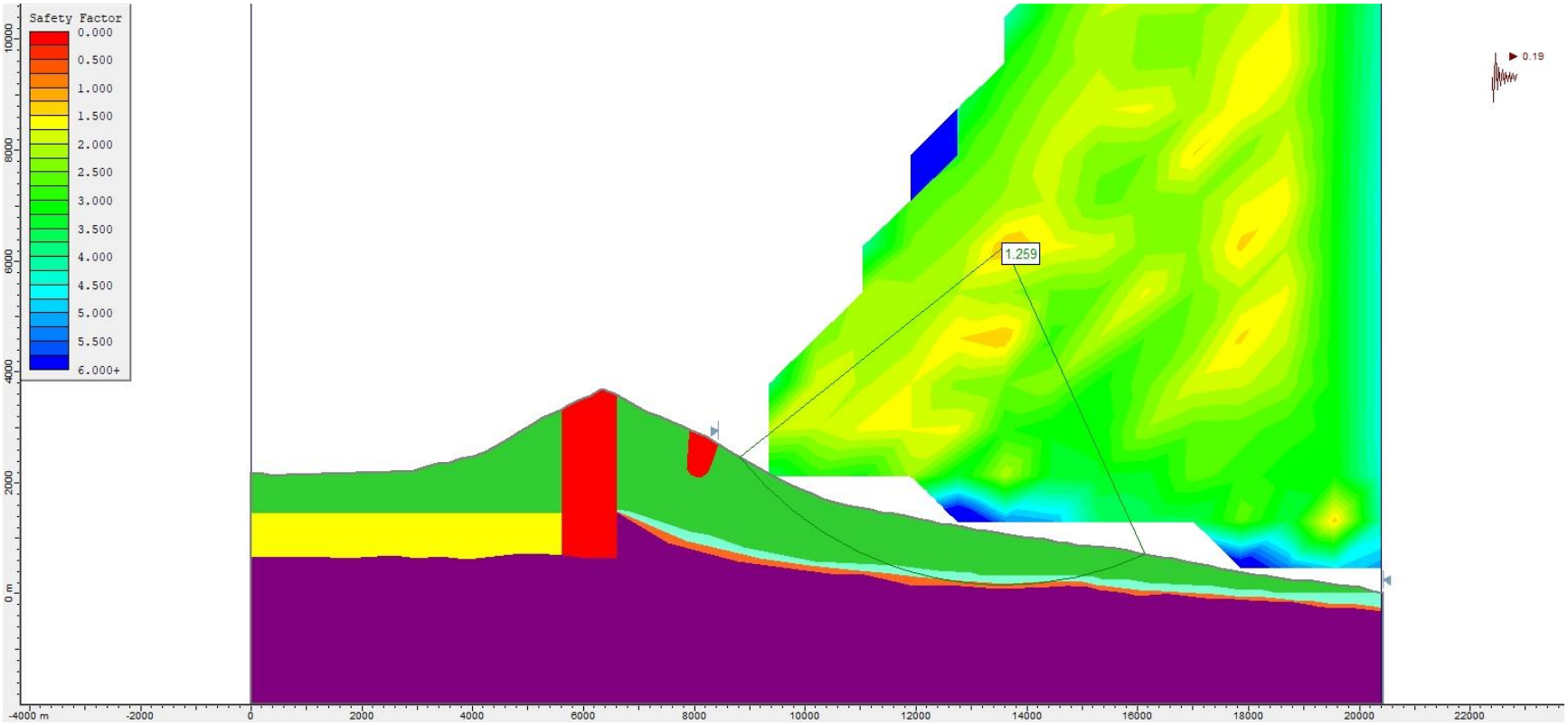

Figure S243. Slope stability pseudo-static analysis for Model 1 Bis (assuming a caldera collapse), using the Morgenstern-Price method and a k_h = 0.19.

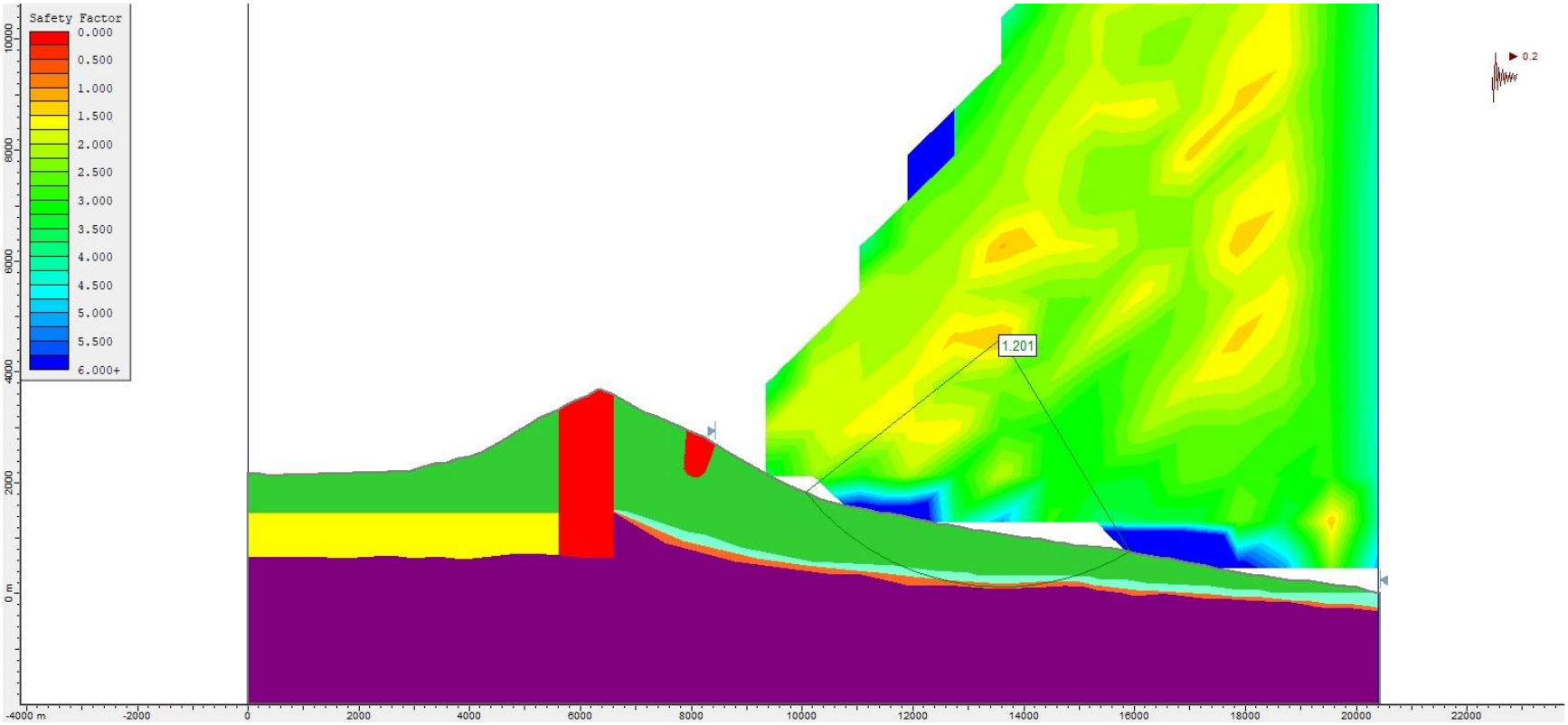

Figure S244. Slope stability pseudo-static analysis for Model 1 Bis (assuming a caldera collapse), using the Bishop simplified method and a k_h = 0.20.

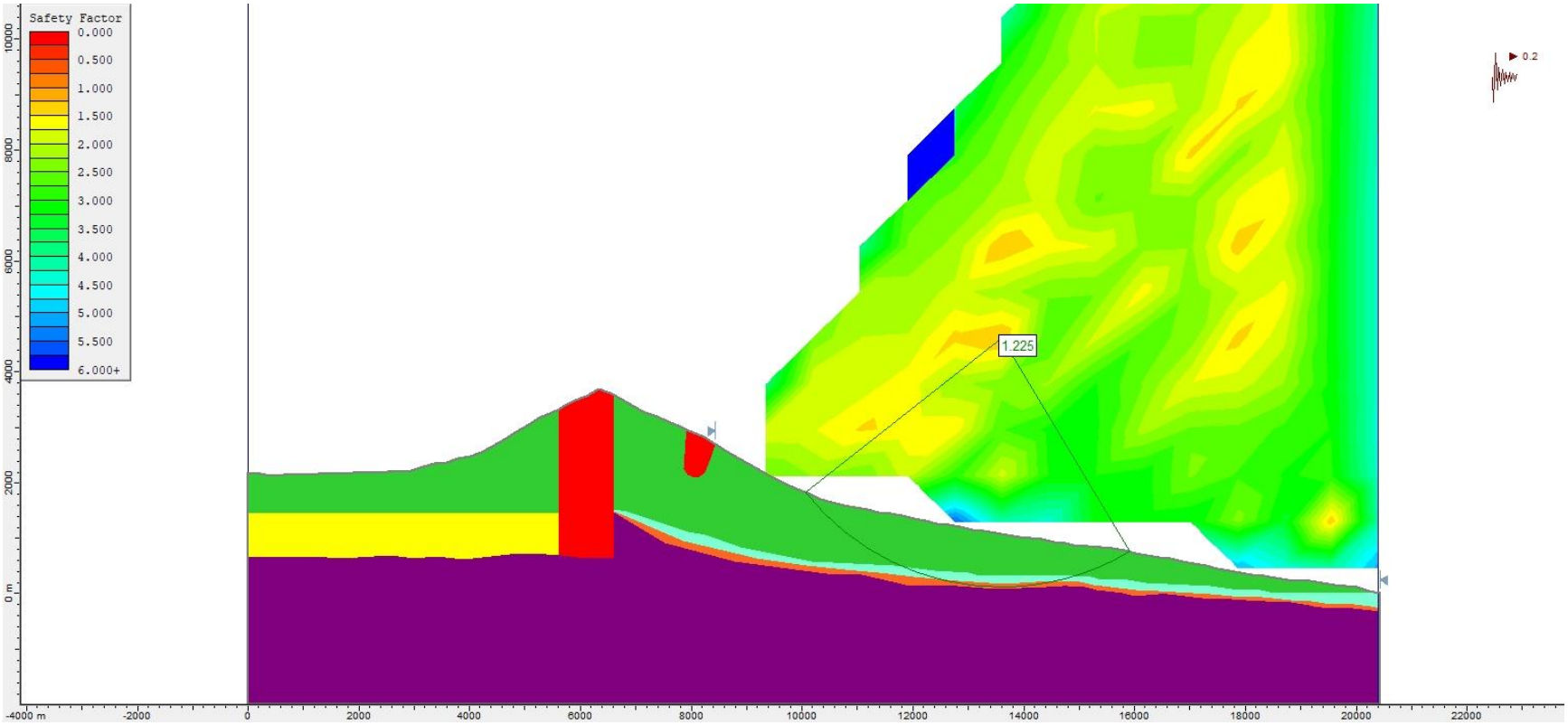

Figure S245. Slope stability pseudo-static analysis for Model 1 Bis (assuming a caldera collapse), using the Janbu Generalised method and a k_h = 0.20.

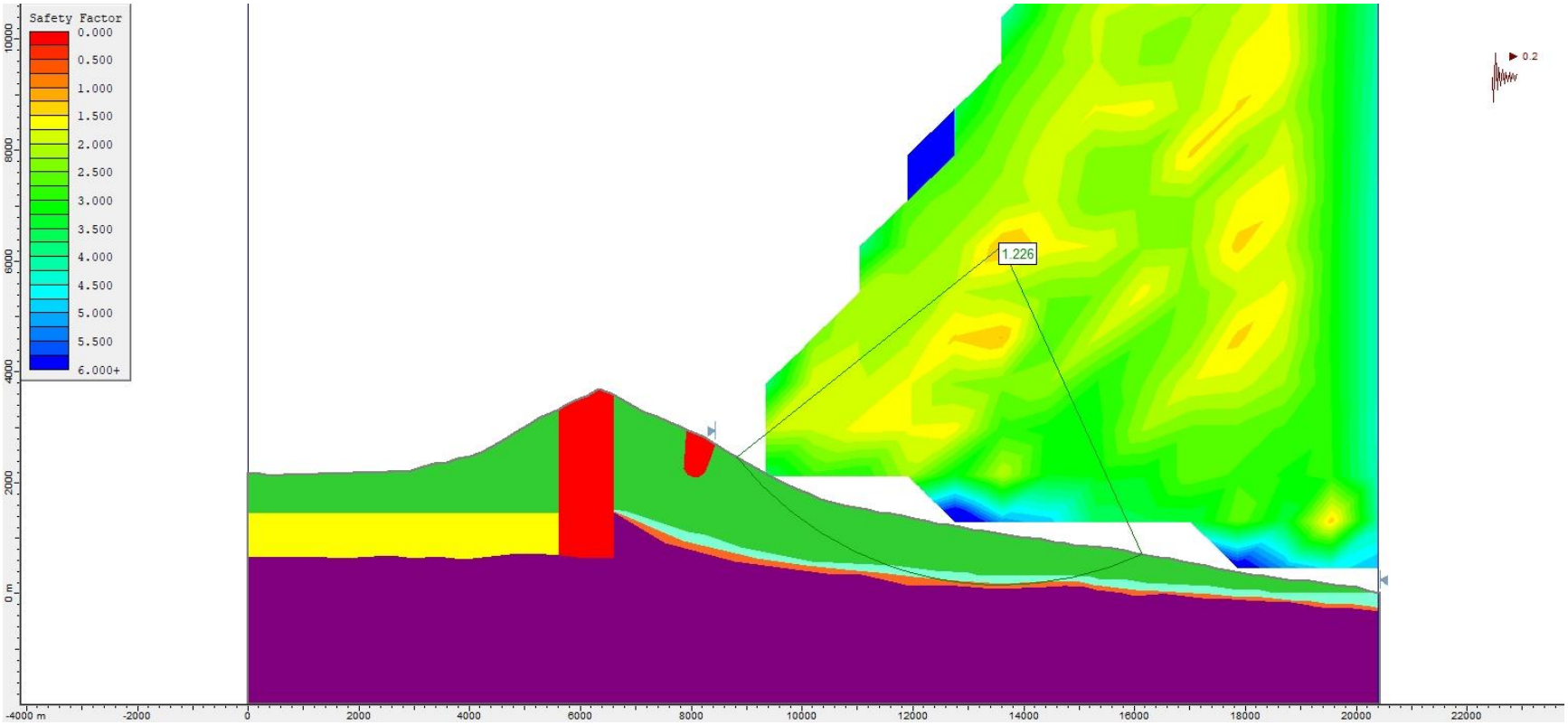

Figure S246. Slope stability pseudo-static analysis for Model 1 Bis (assuming a caldera collapse), using the Morgenstern-Price method and a k_h = 0.20.

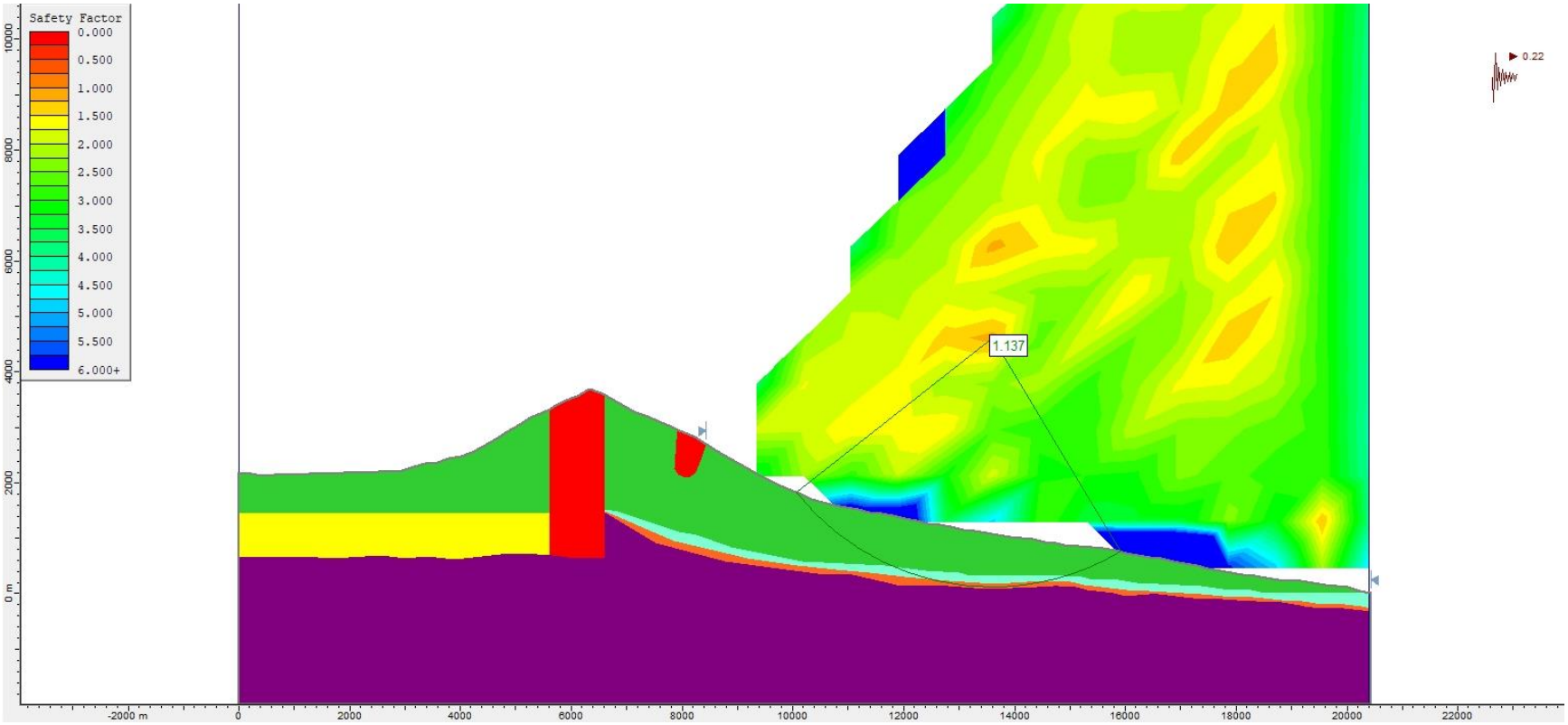

Figure S247. Slope stability pseudo-static analysis for Model 1 Bis (assuming a caldera collapse), using the Bishop simplified method and a k_h = 0.22.

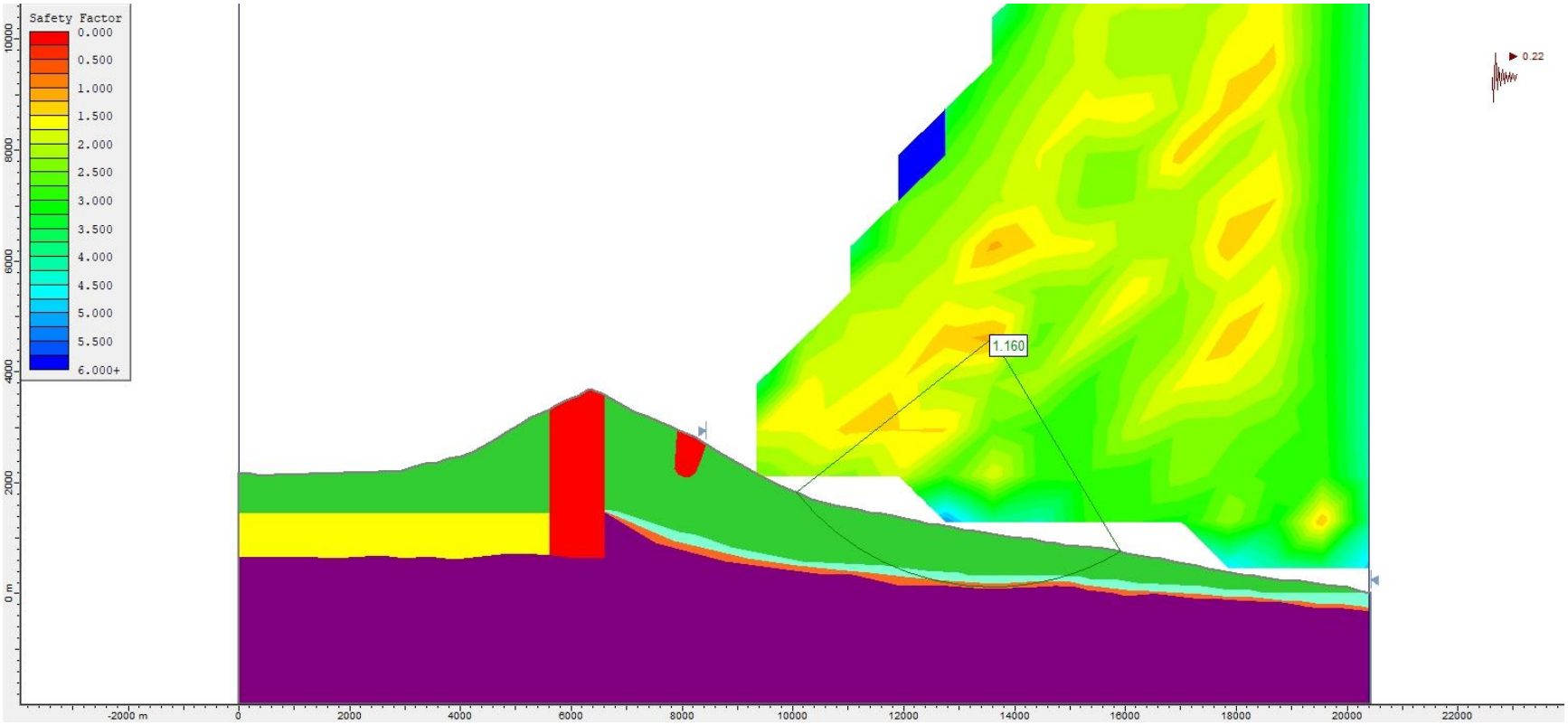

Figure S248. Slope stability pseudo-static analysis for Model 1 Bis (assuming a caldera collapse), using the Janbu Generalised method and a k_h = 0.22.

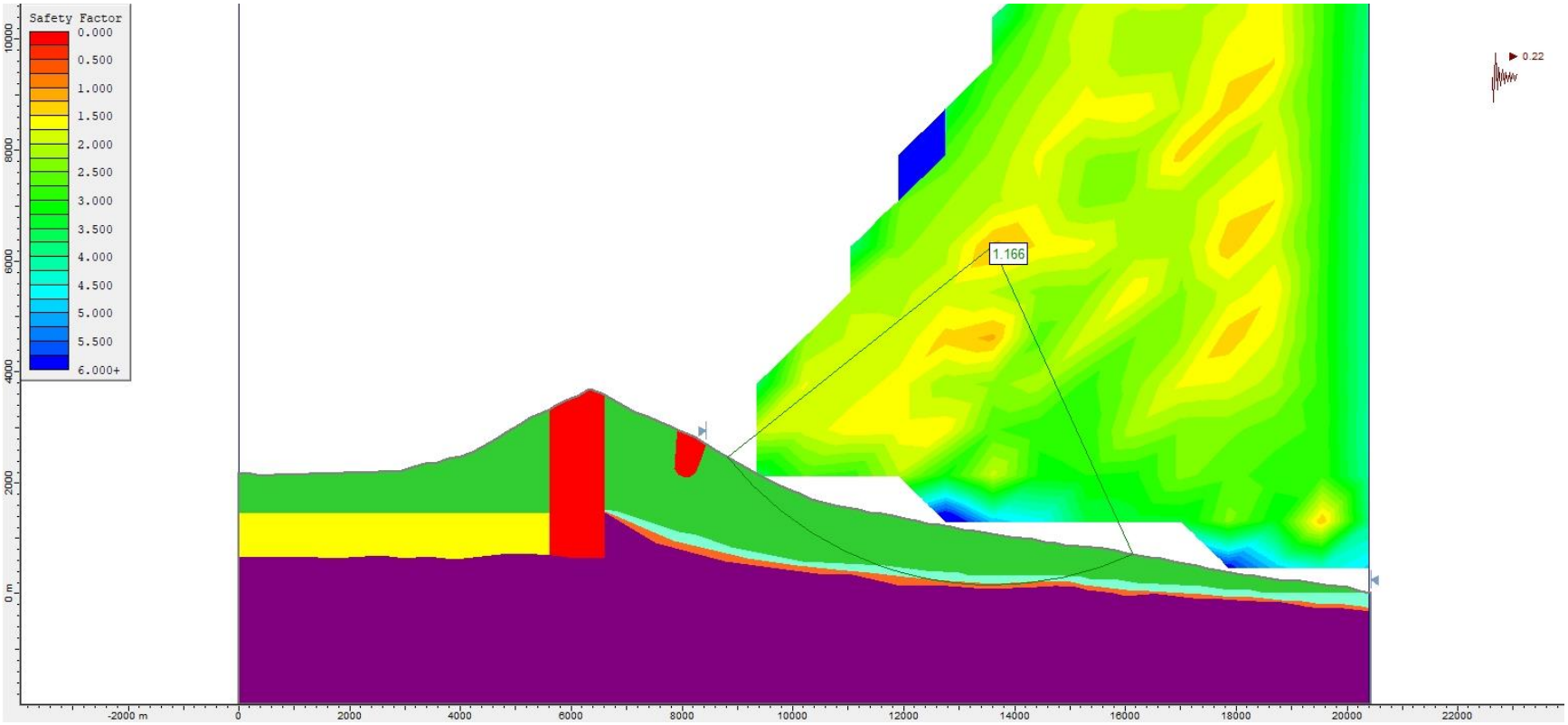

Figure S249. Slope stability pseudo-static analysis for Model 1 Bis (assuming a caldera collapse), using the Morgenstern-Price method and a k_h = 0.22.

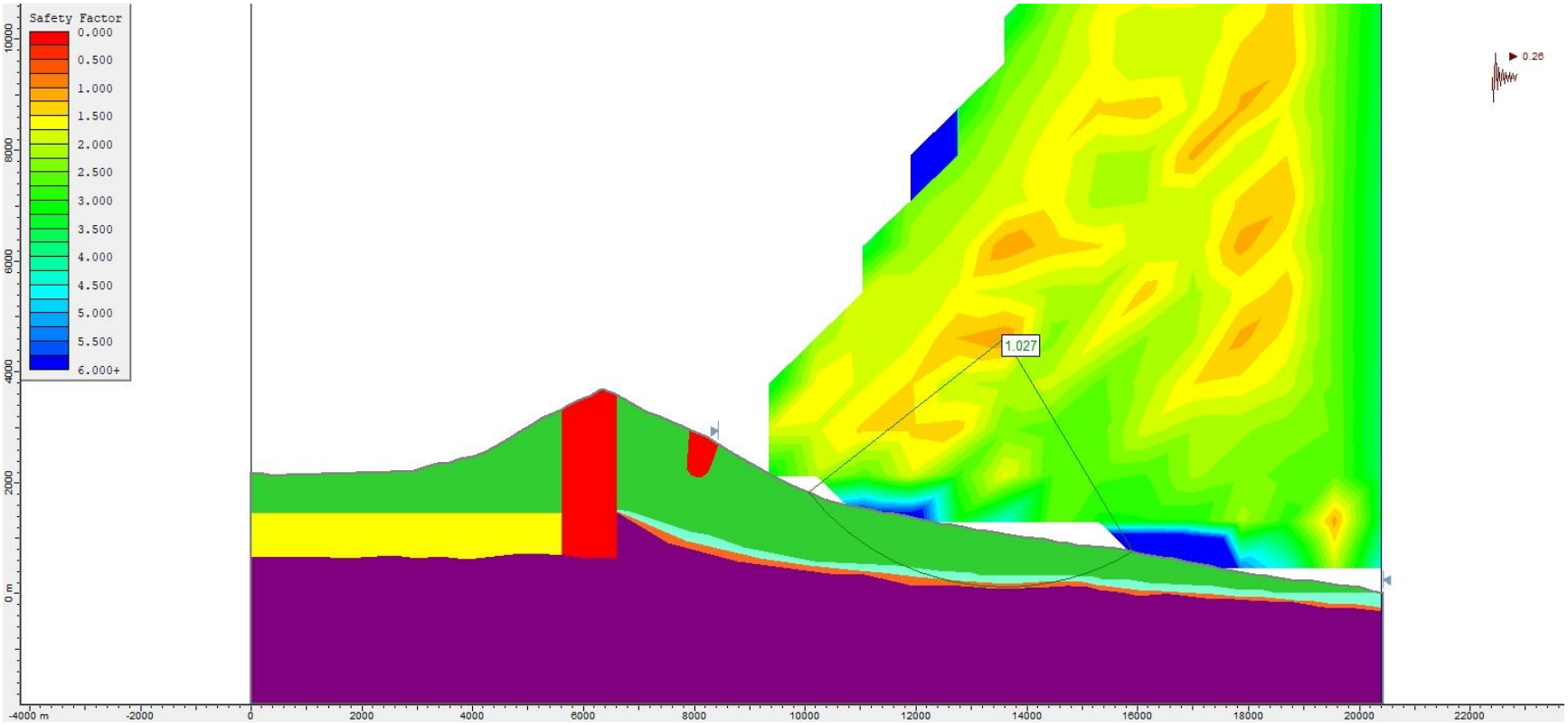

Figure S250. Slope stability pseudo-static analysis for Model 1 Bis (assuming a caldera collapse), using the Bishop simplified method and a k_h = 0.26.

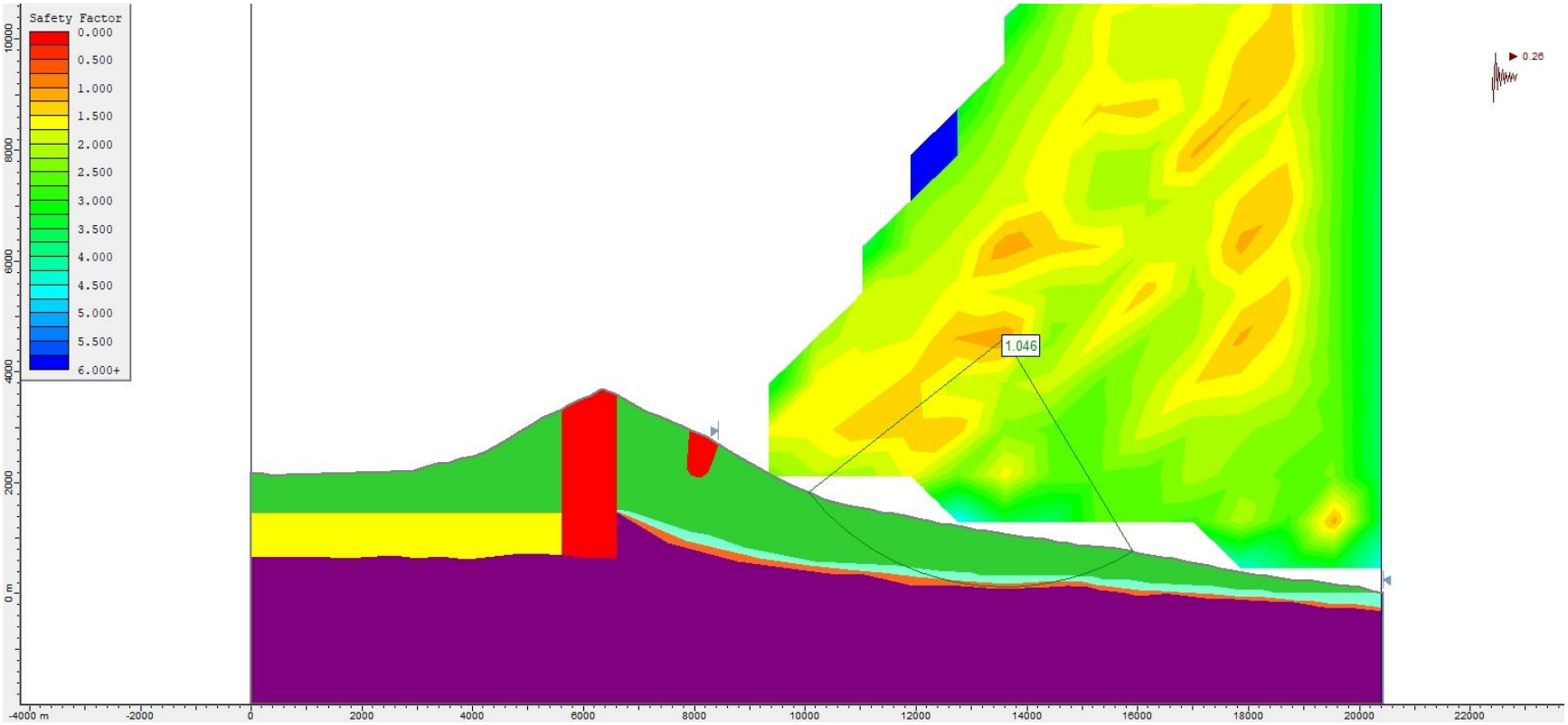

Figure S251. Slope stability pseudo-static analysis for Model 1 Bis (assuming a caldera collapse), using the Janbu Generalised method and a k_h = 0.26.

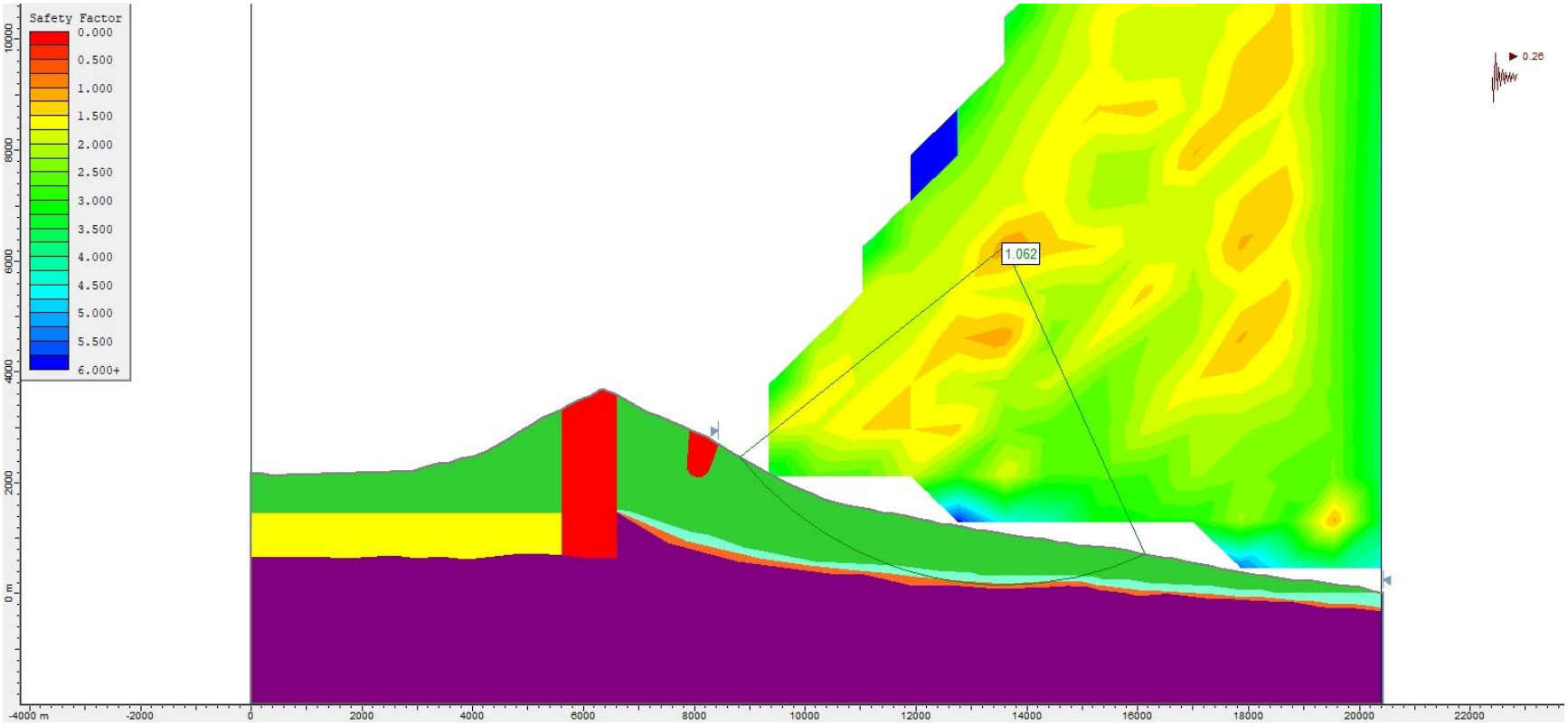

Figure S252. Slope stability pseudo-static analysis for Model 1 Bis (assuming a caldera collapse), using the Morgenstern-Price method and a k_h = 0.26.

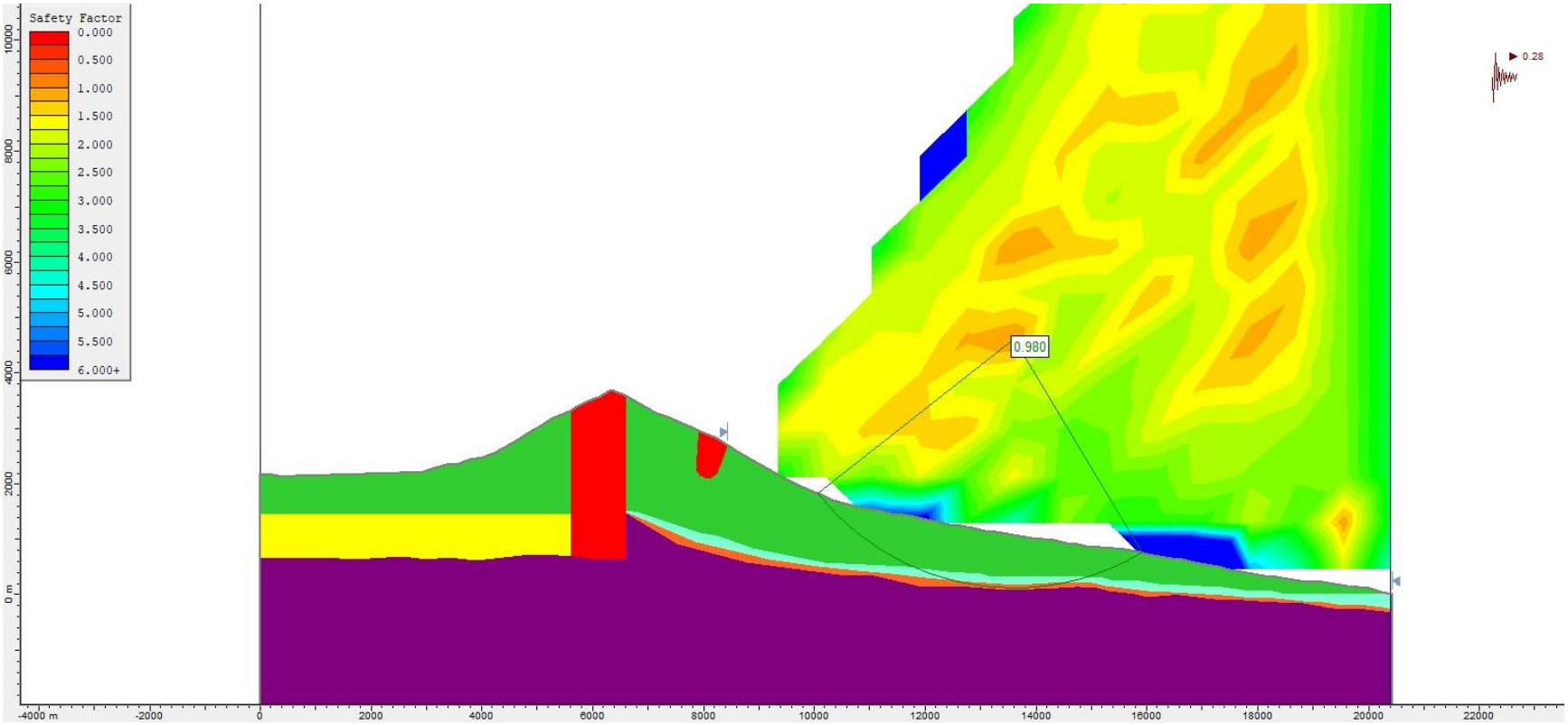

Figure S253. Slope stability pseudo-static analysis for Model 1 Bis (assuming a caldera collapse), using the Bishop simplified method and a k_h = 0.28.

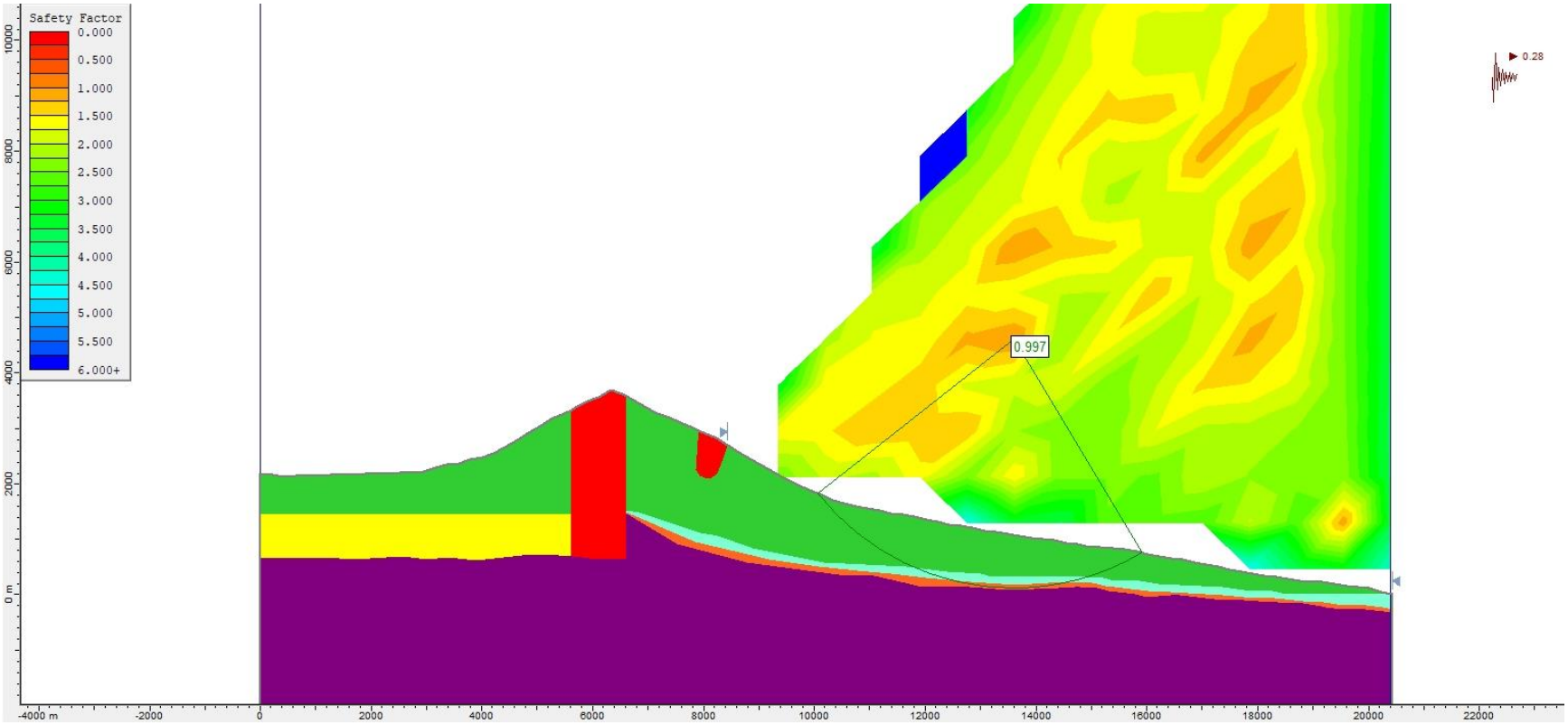

Figure S254. Slope stability pseudo-static analysis for Model 1 Bis (assuming a caldera collapse), using the Janbu Generalised method and a k_h = 0.28.

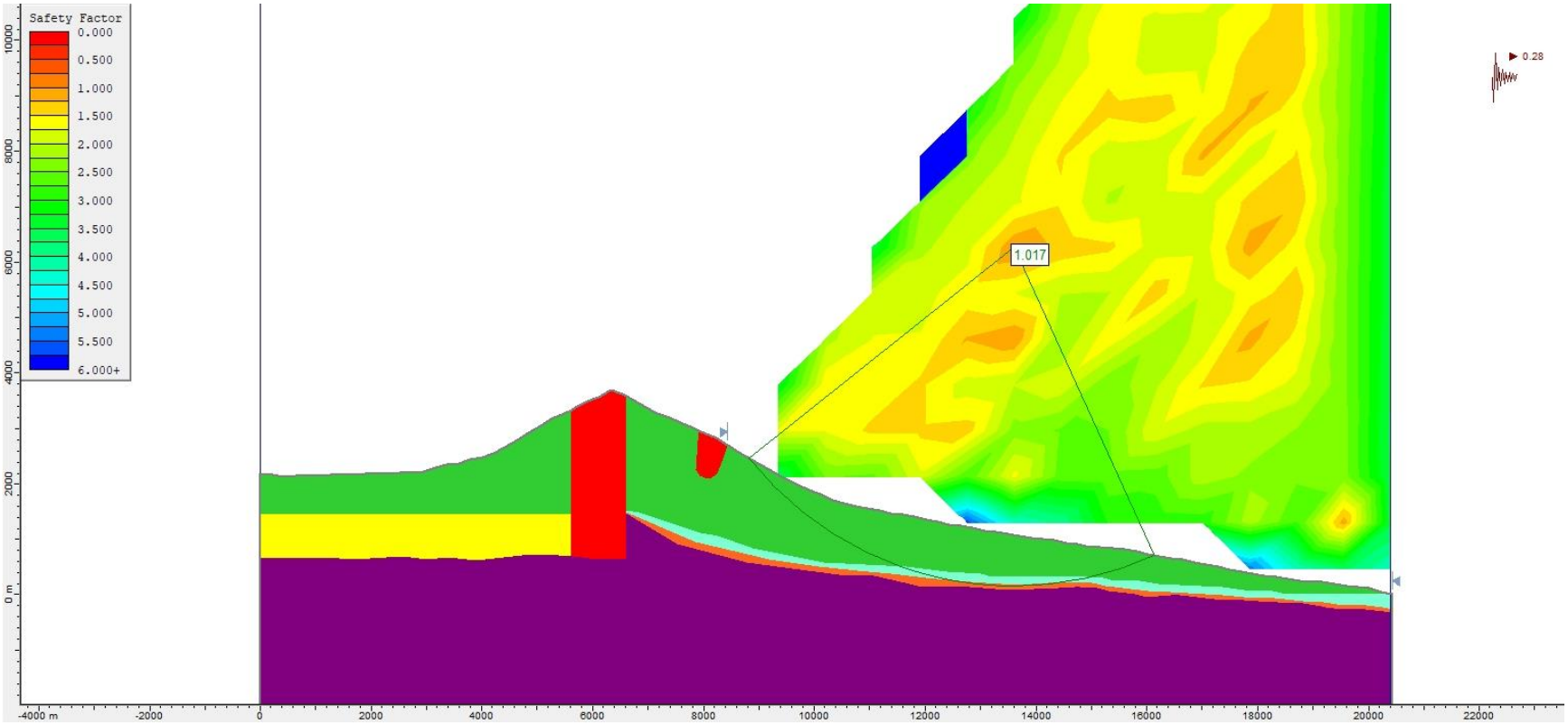

Figure S255. Slope stability pseudo-static analysis for Model 1 Bis (assuming a caldera collapse), using the Morgenstern-Price method and a k_h = 0.28.

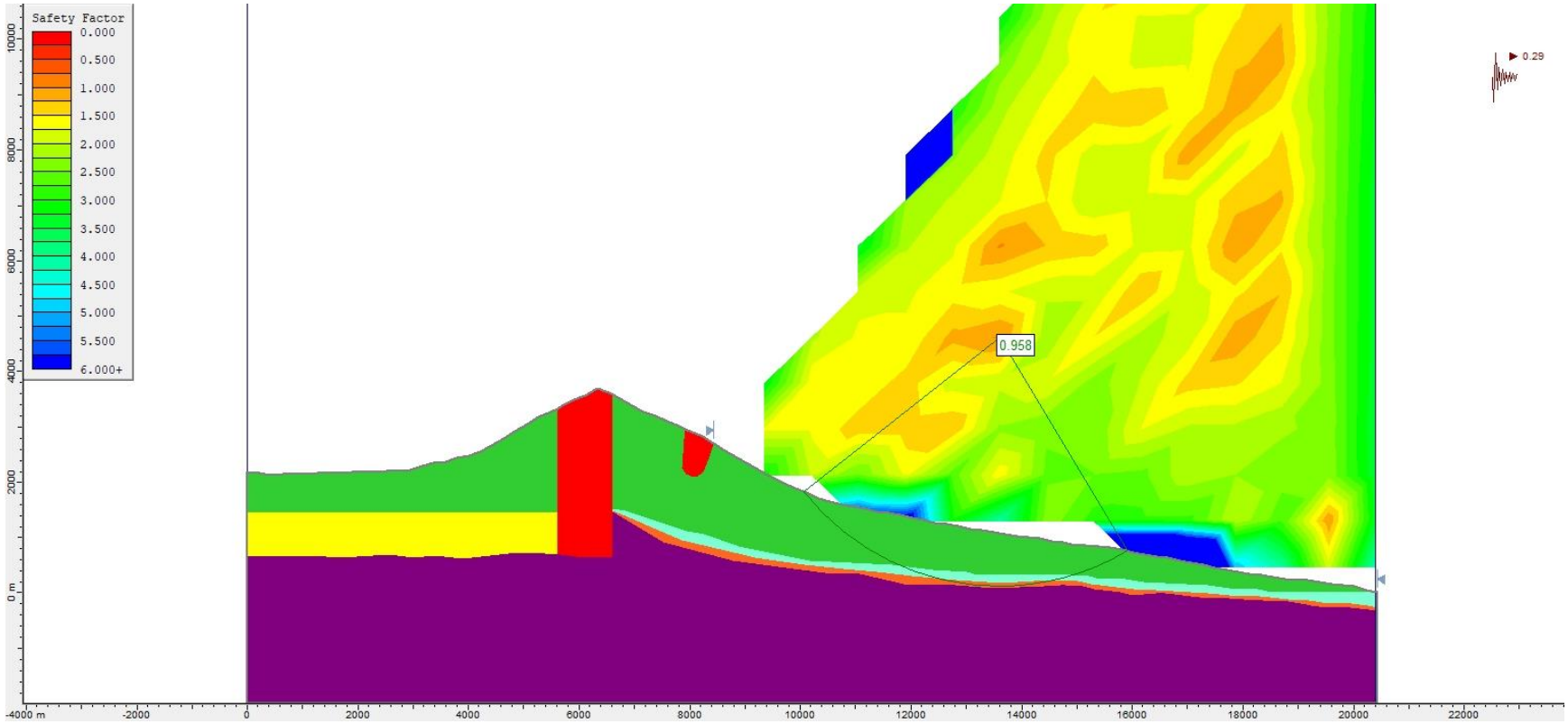

Figure S256. Slope stability pseudo-static analysis for Model 1 Bis (assuming a caldera collapse), using the Bishop simplified method and a k_h = 0.29.

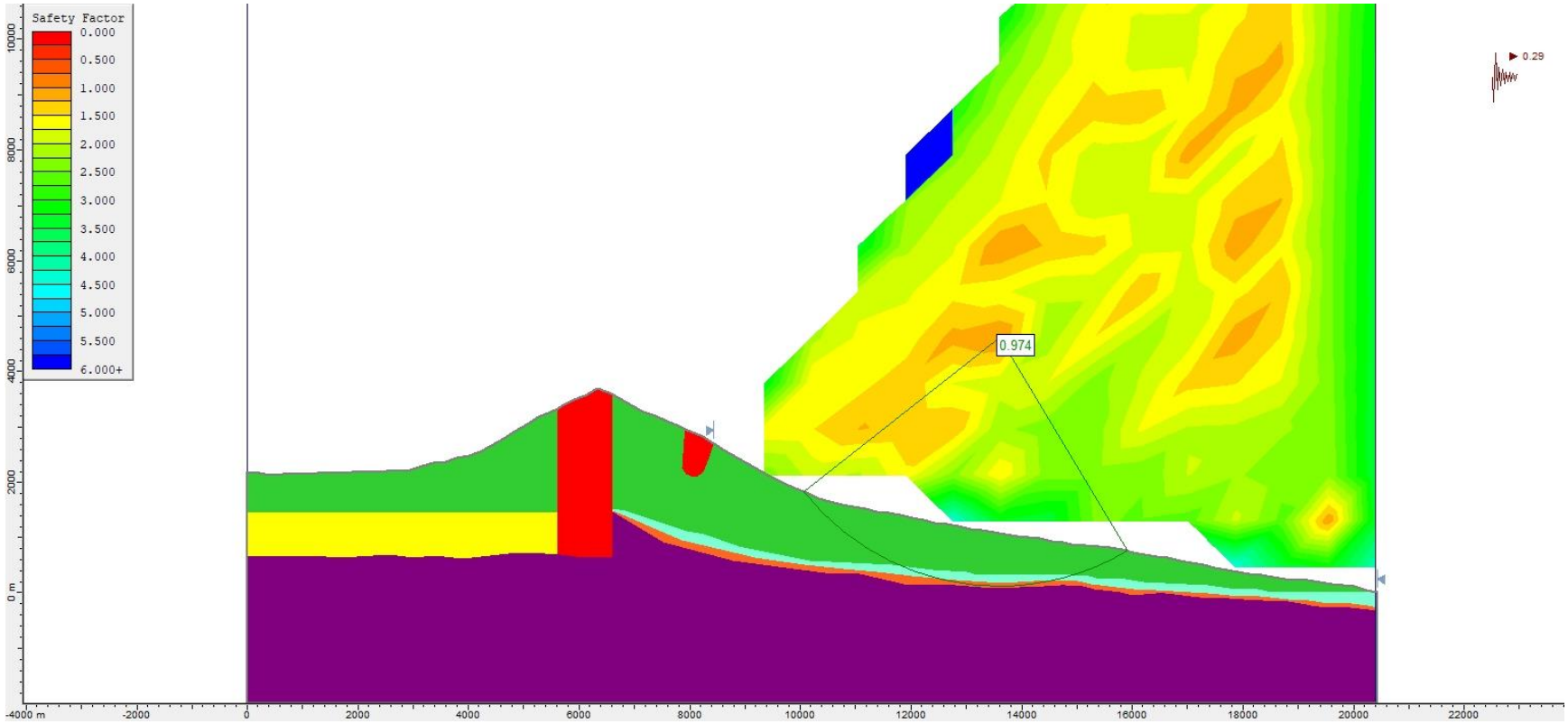

Figure S257. Slope stability pseudo-static analysis for Model 1 Bis (assuming a caldera collapse), using the Janbu Generalised method and a k_h = 0.29.

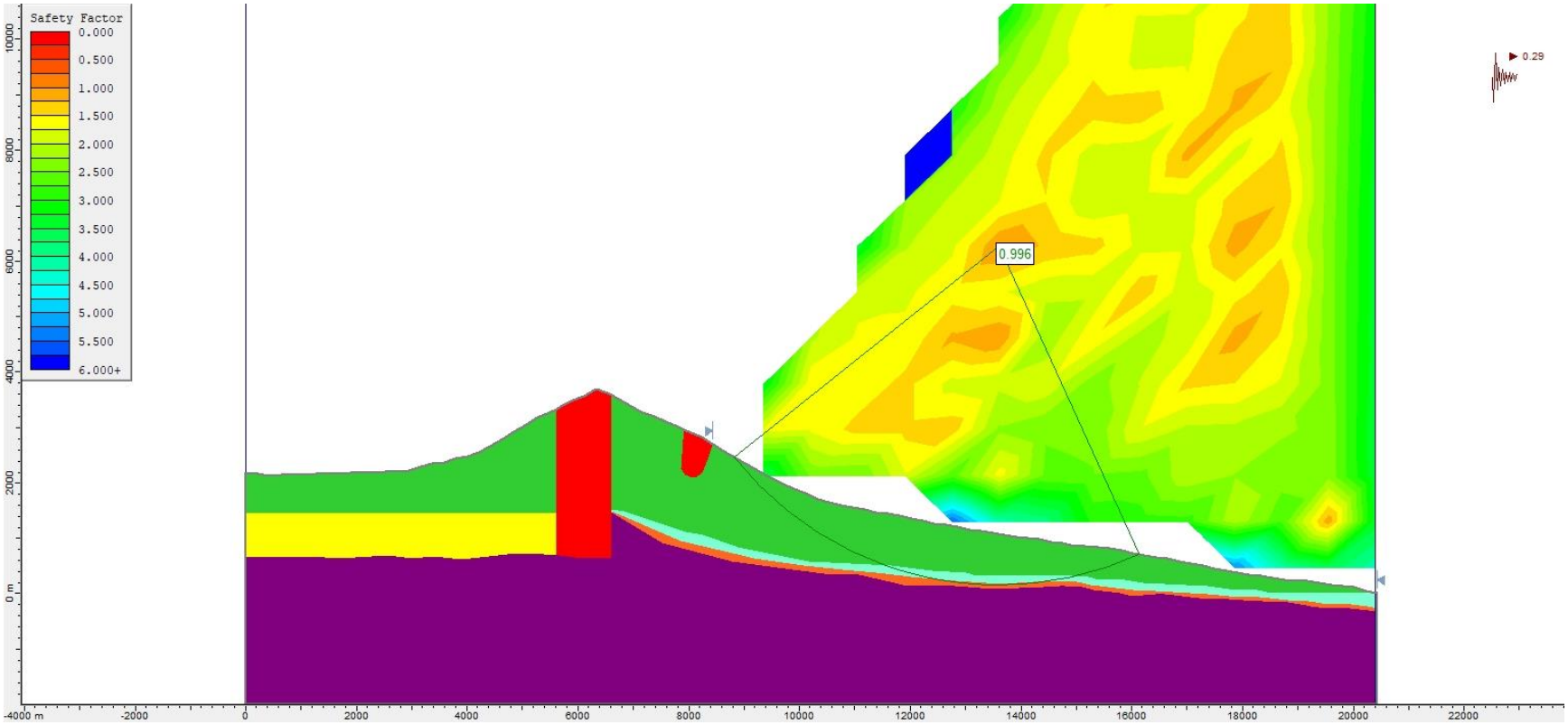

Figure S258. Slope stability pseudo-static analysis for Model 1 Bis (assuming a caldera collapse), using the Morgenstern-Price method and a k_h = 0.29.

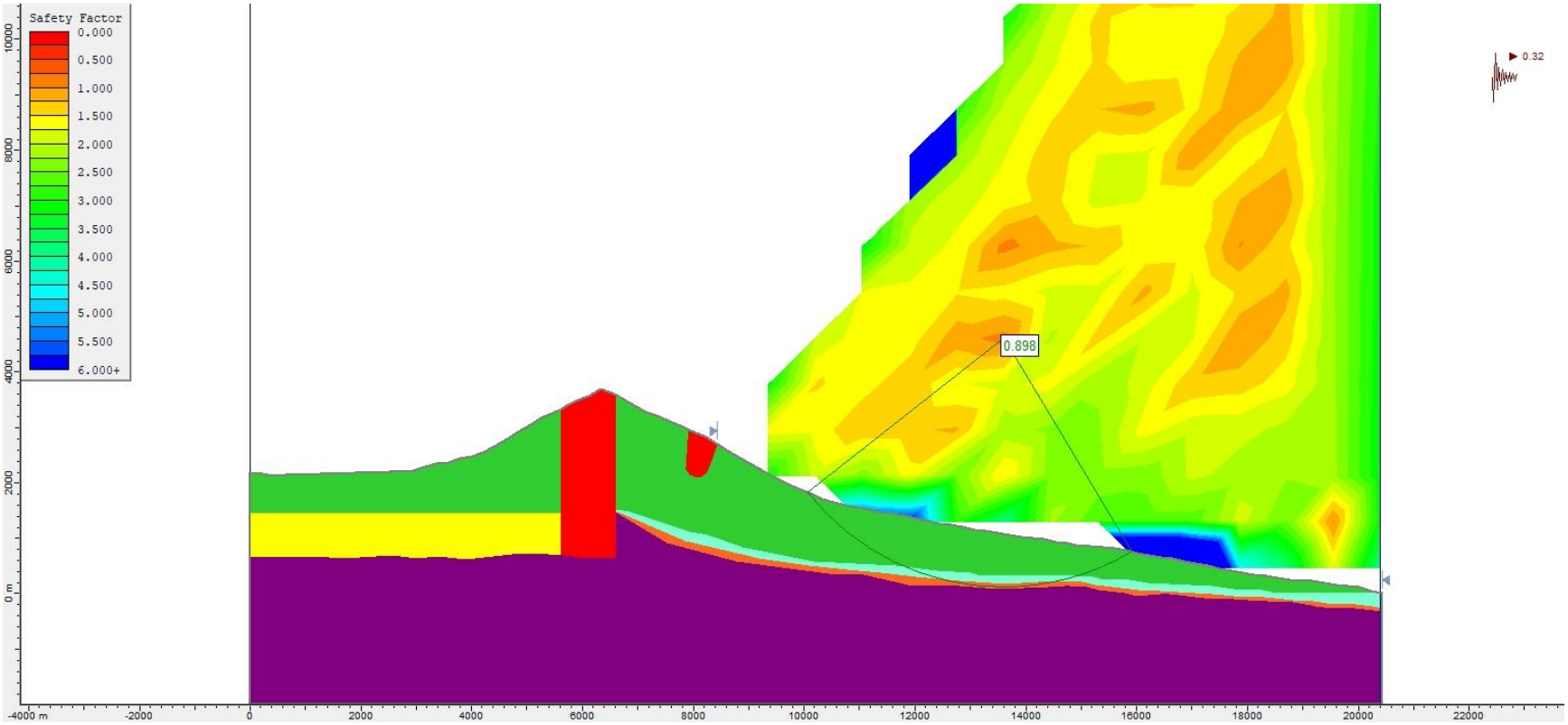

Figure S259. Slope stability pseudo-static analysis for Model 1 Bis (assuming a caldera collapse), using the Bishop simplified method and a k_h = 0.32.

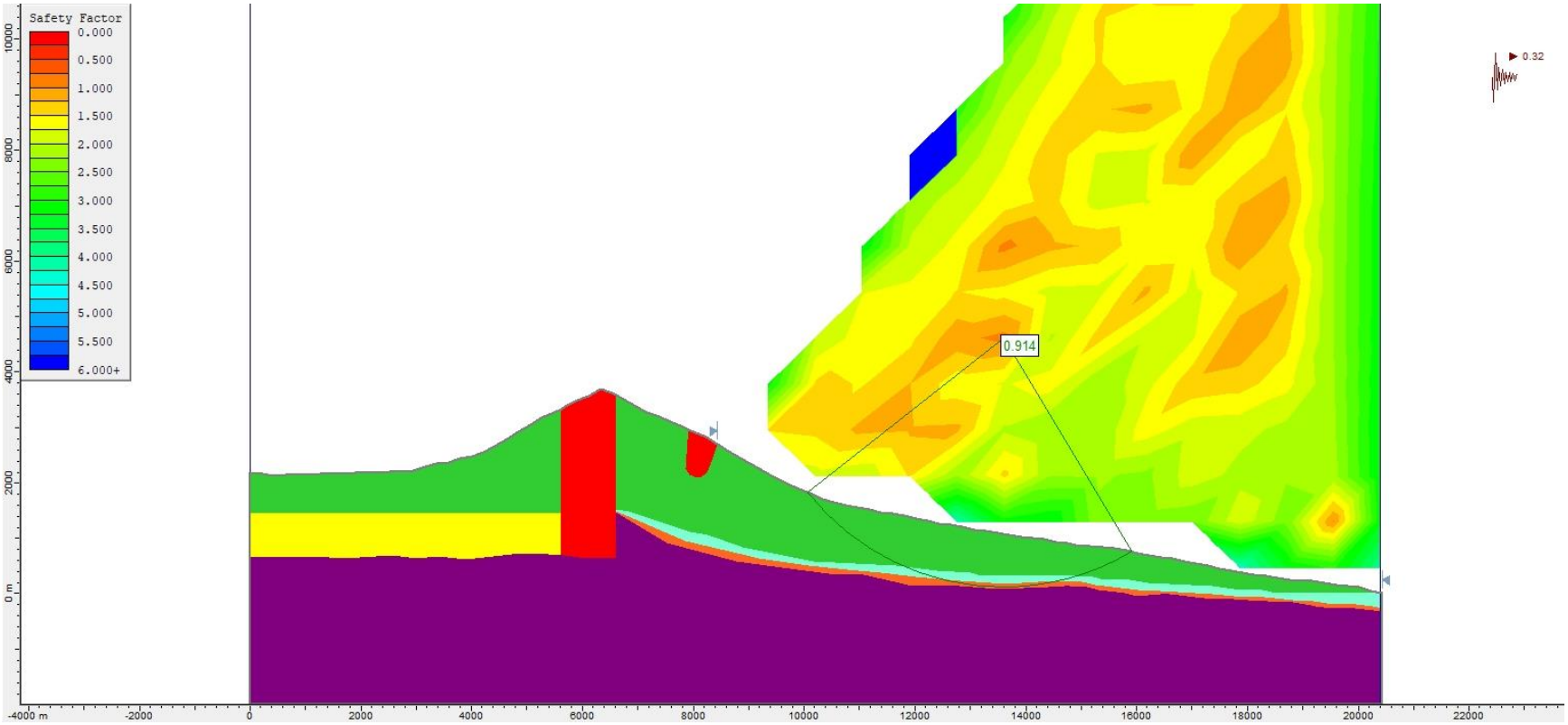

Figure S260. Slope stability pseudo-static analysis for Model 1 Bis (assuming a caldera collapse), using the Janbu Generalised method and a k_h = 0.32.

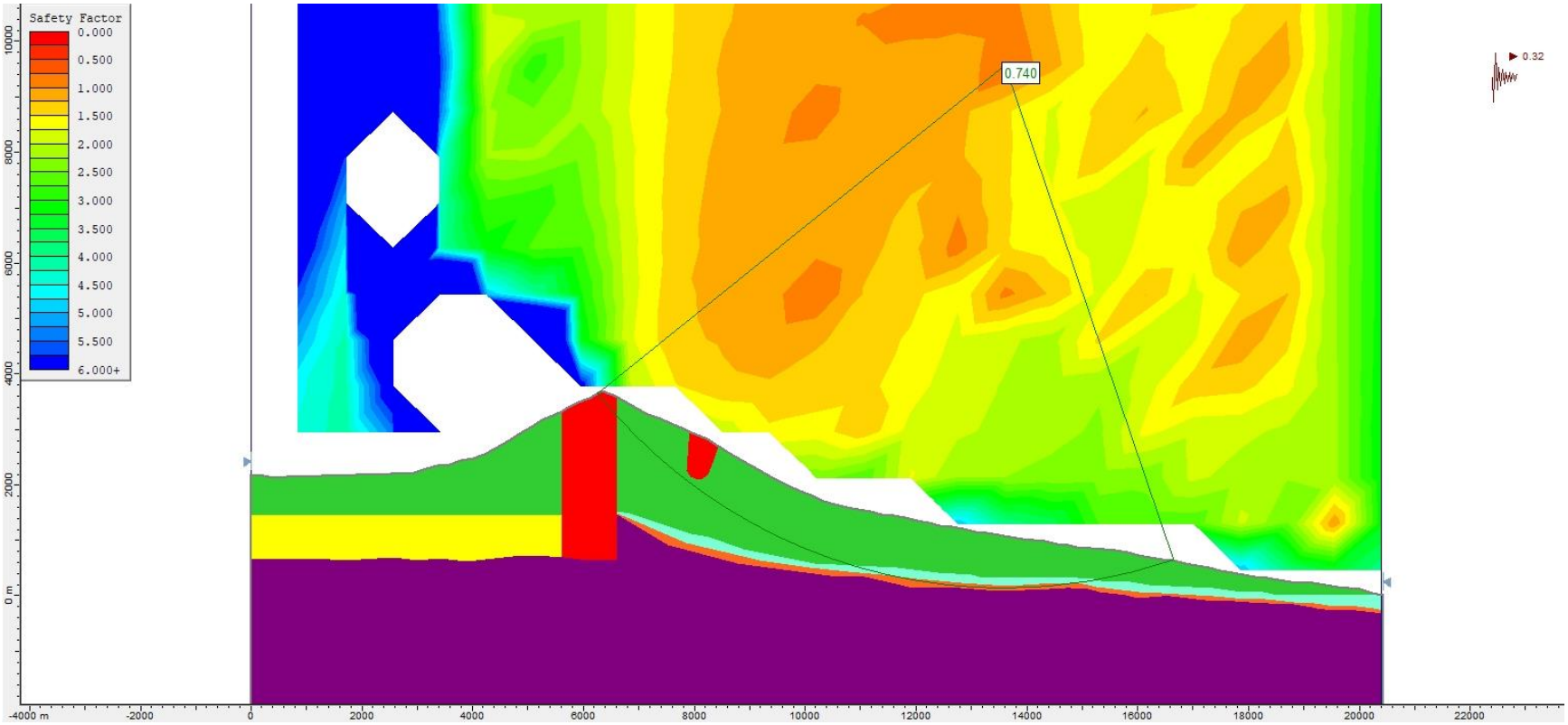

Figure S261. Slope stability pseudo-static analysis for Model 1 Bis (assuming a caldera collapse), using the Morgenstern-Price method and a k_h = 0.32.

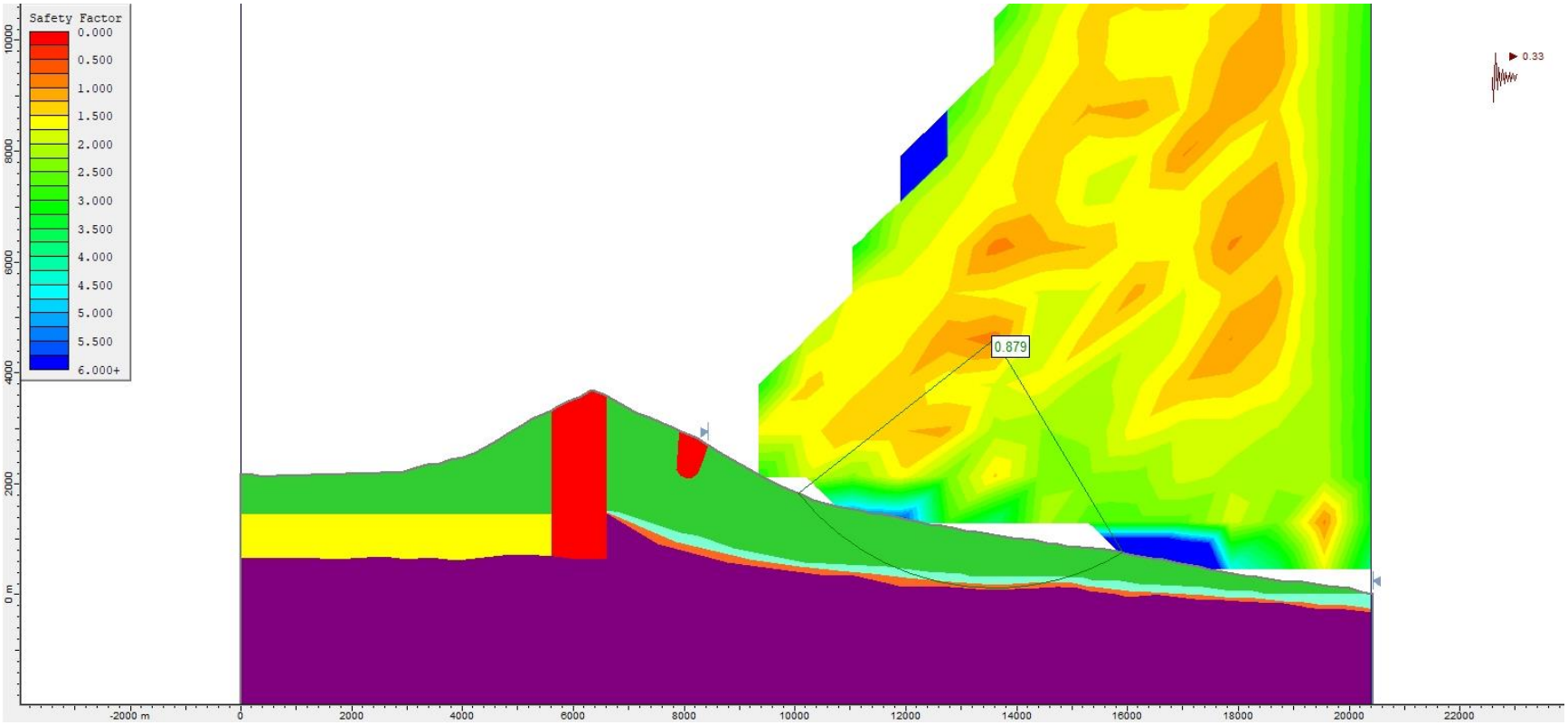

Figure S262. Slope stability pseudo-static analysis for Model 1 Bis (assuming a caldera collapse), using the Bishop simplified method and a k_h = 0.33.

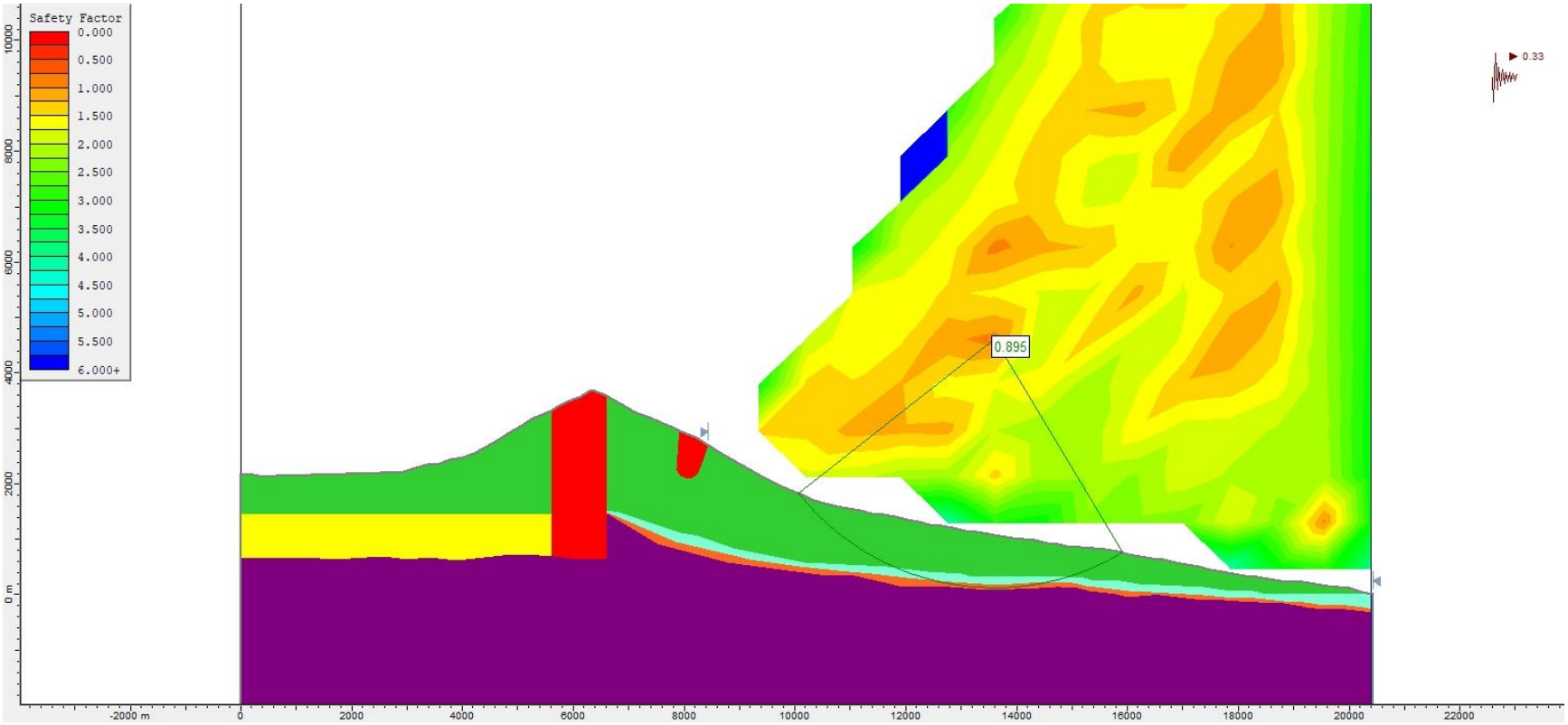

Figure S263. Slope stability pseudo-static analysis for Model 1 Bis (assuming a caldera collapse), using the Janbu Generalised method and a k_h = 0.33.

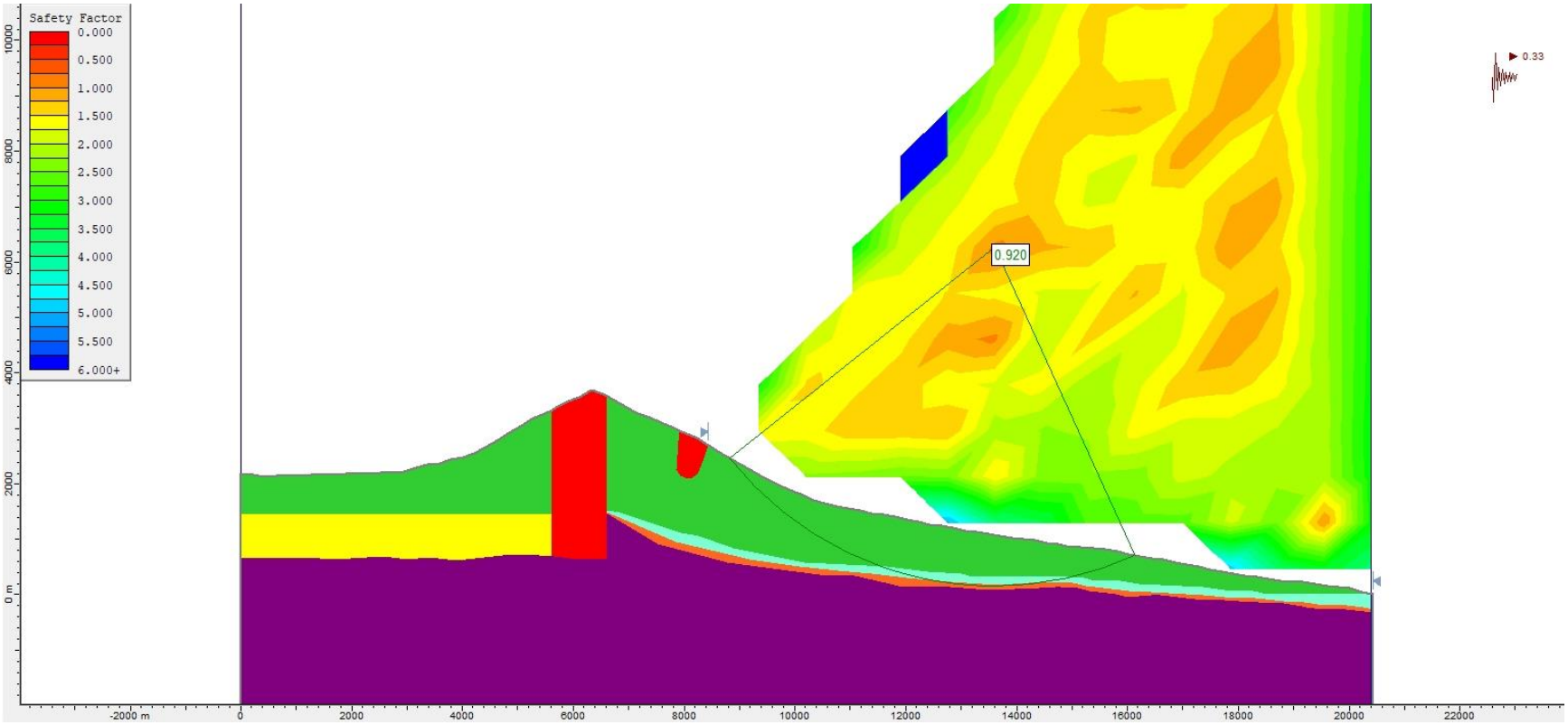

Figure S264. Slope stability pseudo-static analysis for Model 1 Bis (assuming a caldera collapse), using the Morgenstern-Price method and a k_h = 0.33.

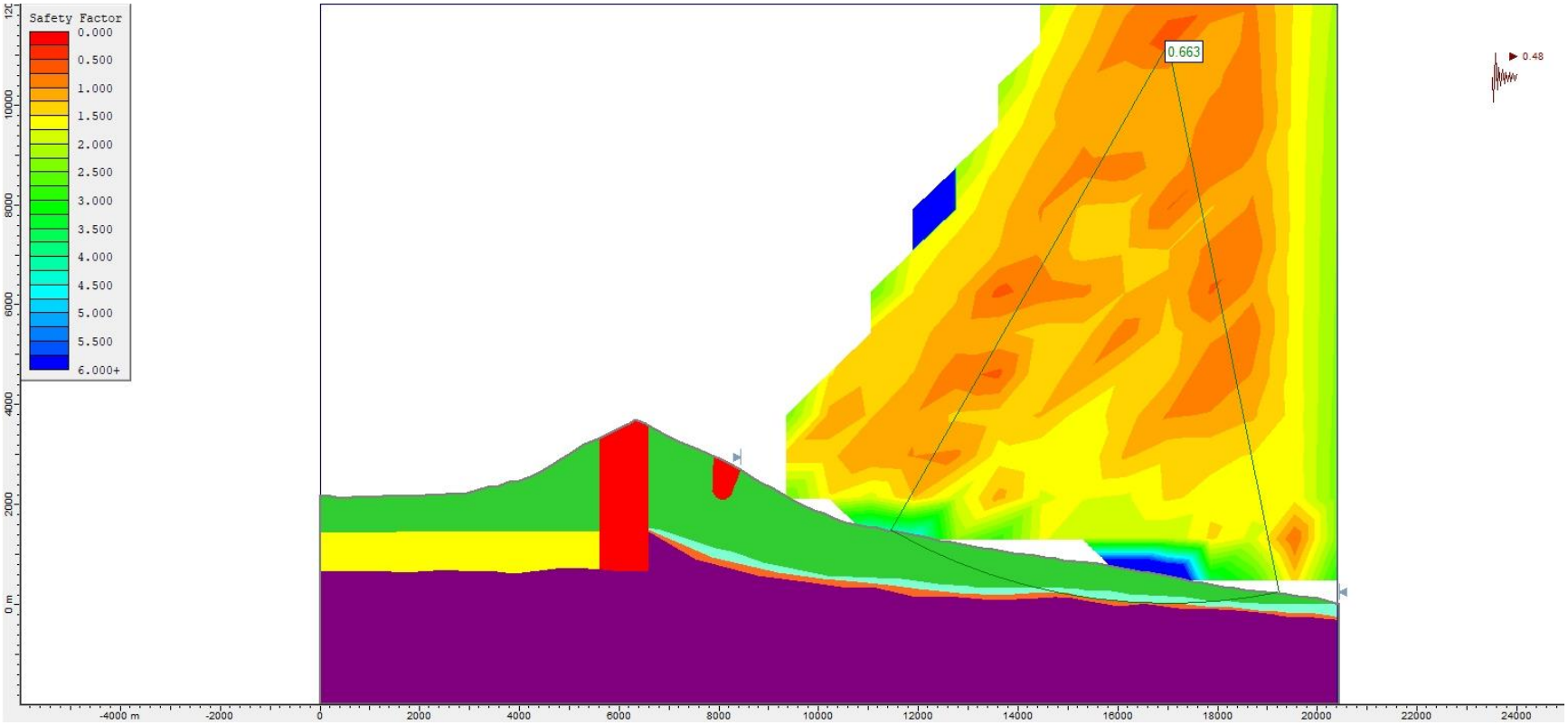

Figure S265. Slope stability pseudo-static analysis for Model 1 Bis (assuming a caldera collapse), using the Bishop simplified method and a k_h = 0.48.

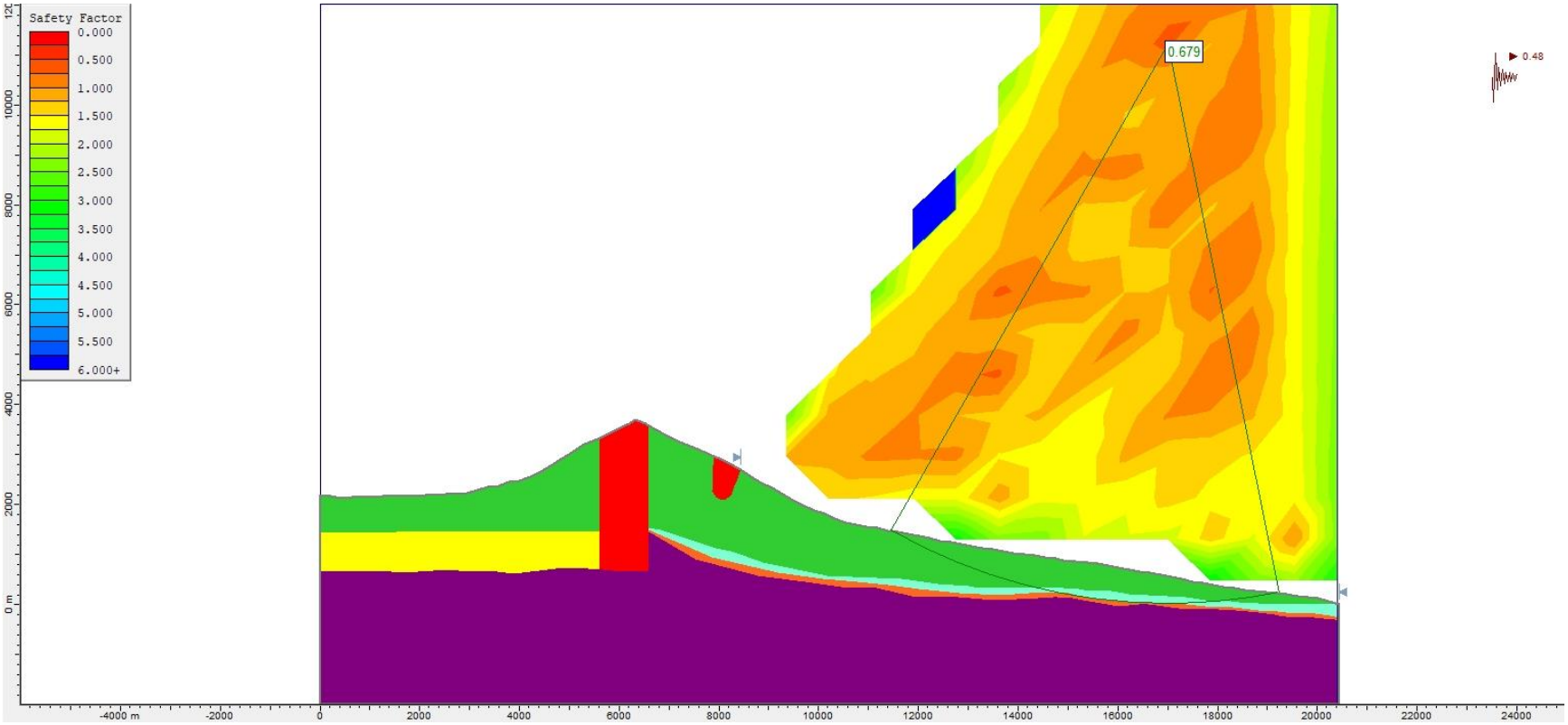

Figure S266. Slope stability pseudo-static analysis for Model 1 Bis (assuming a caldera collapse), using the Janbu Generalised method and a k_h = 0.48.

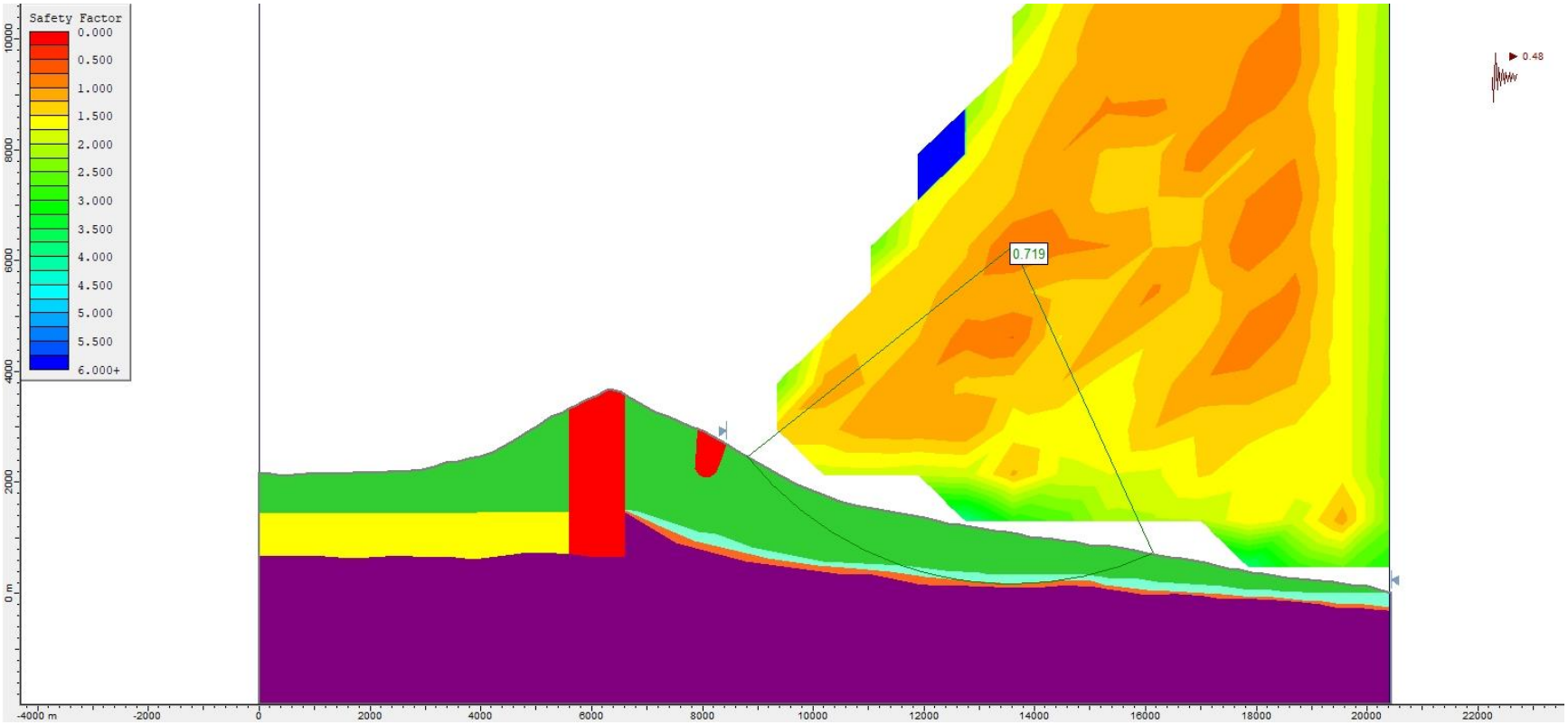

Figure S267. Slope stability pseudo-static analysis for Model 1 Bis (assuming a caldera collapse), using the Morgenstern-Price method and a k_h = 0.48.

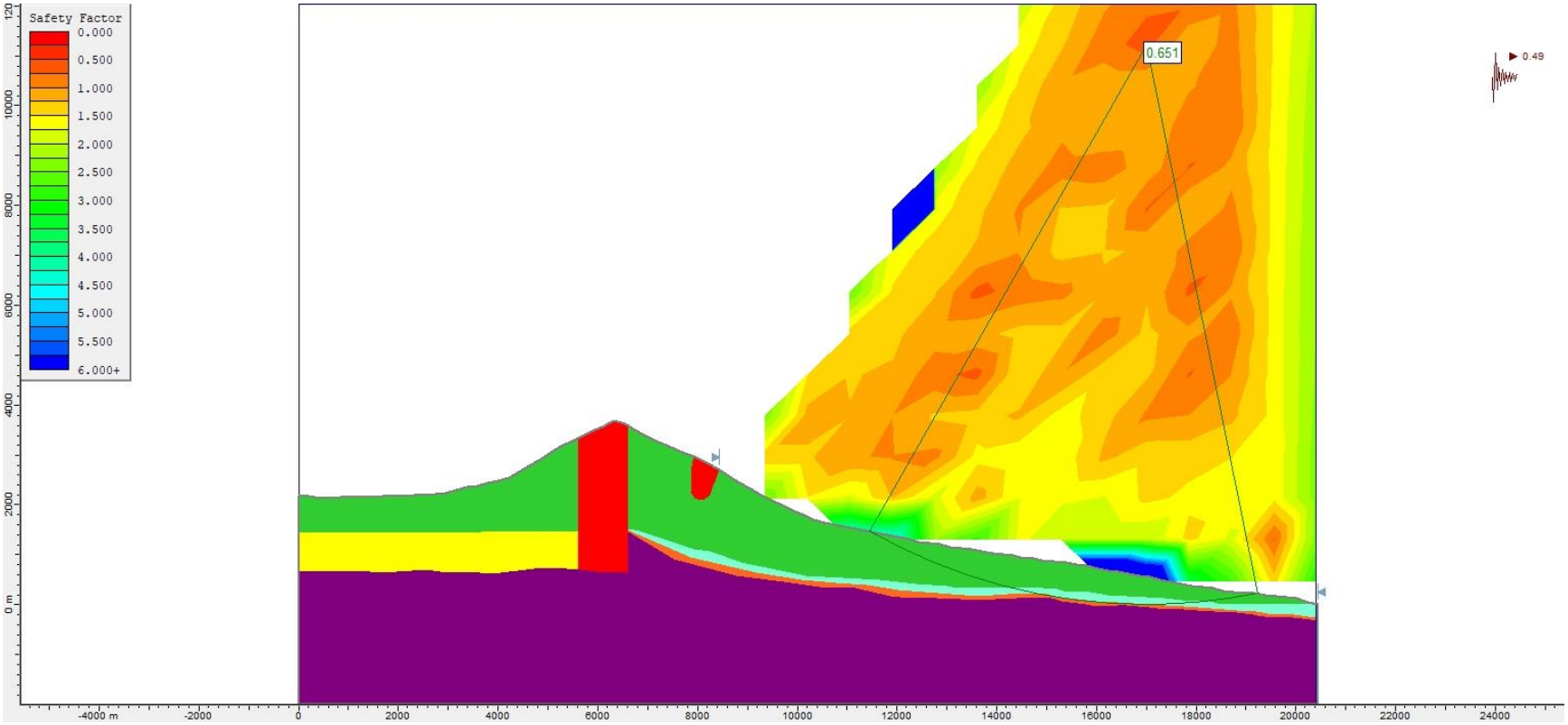

Figure S268. Slope stability pseudo-static analysis for Model 1 Bis (assuming a caldera collapse), using the Bishop simplified method and a k_h = 0.49.

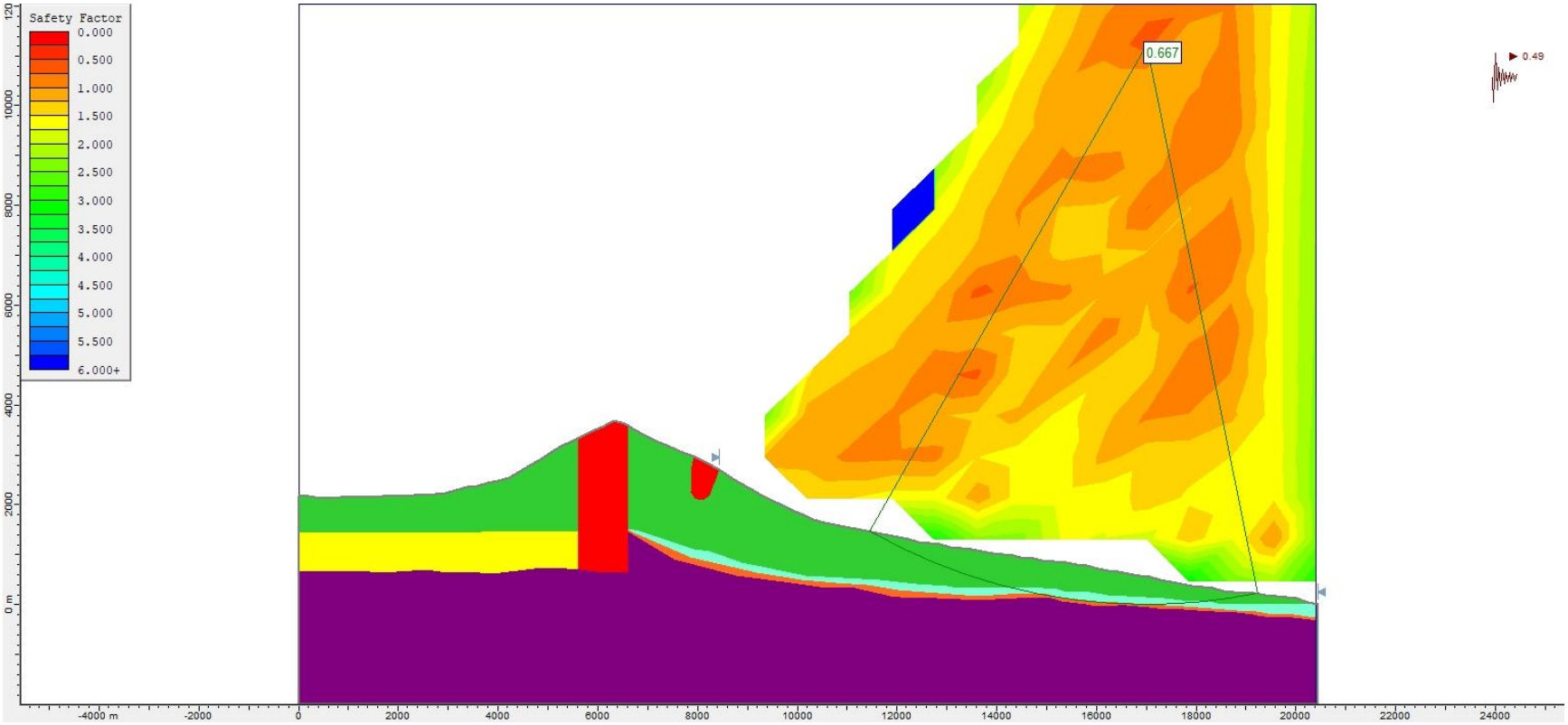

Figure S269. Slope stability pseudo-static analysis for Model 1 Bis (assuming a caldera collapse), using the Janbu Generalised method and a k_h = 0.49.

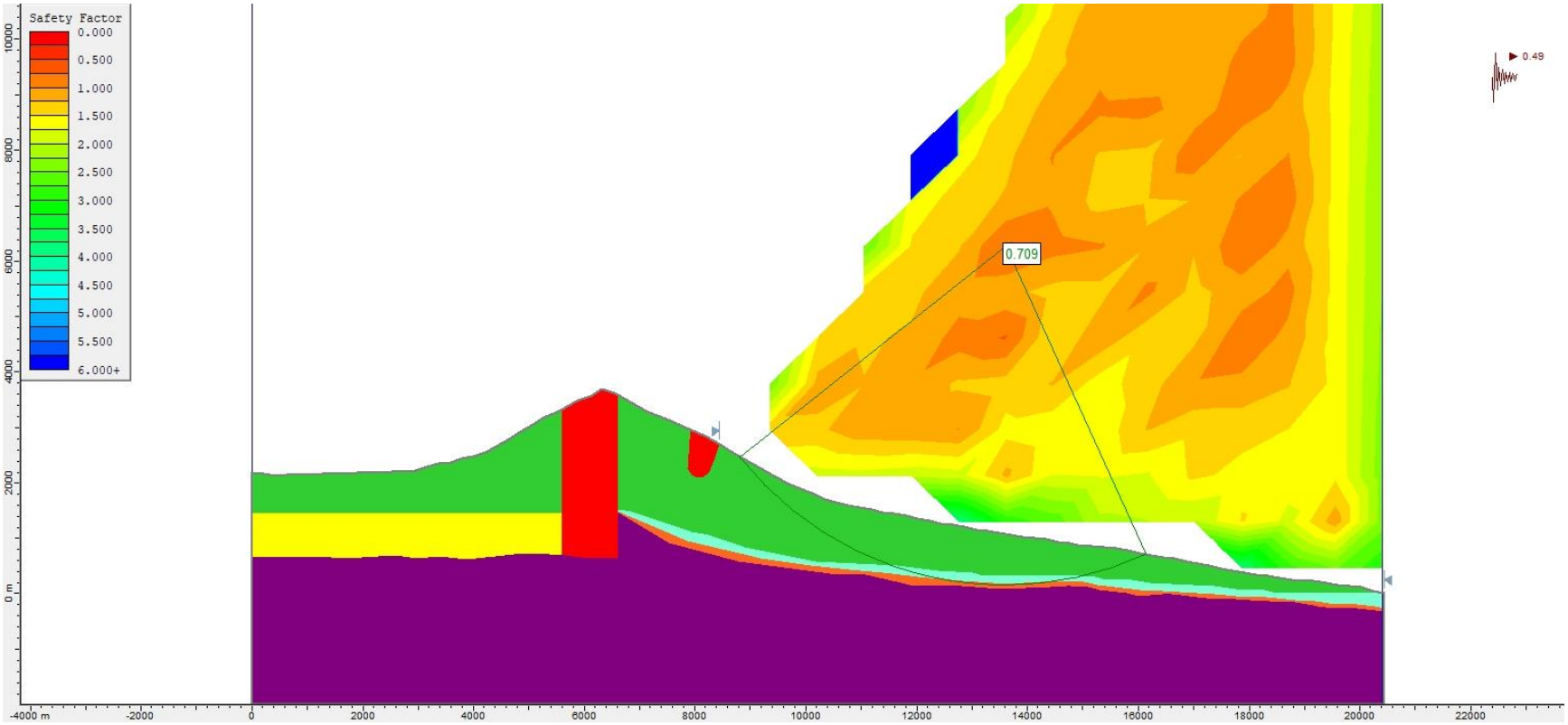

Figure S270. Slope stability pseudo-static analysis for Model 1 Bis (assuming a caldera collapse), using the Morgenstern-Price method and a k_h = 0.49.

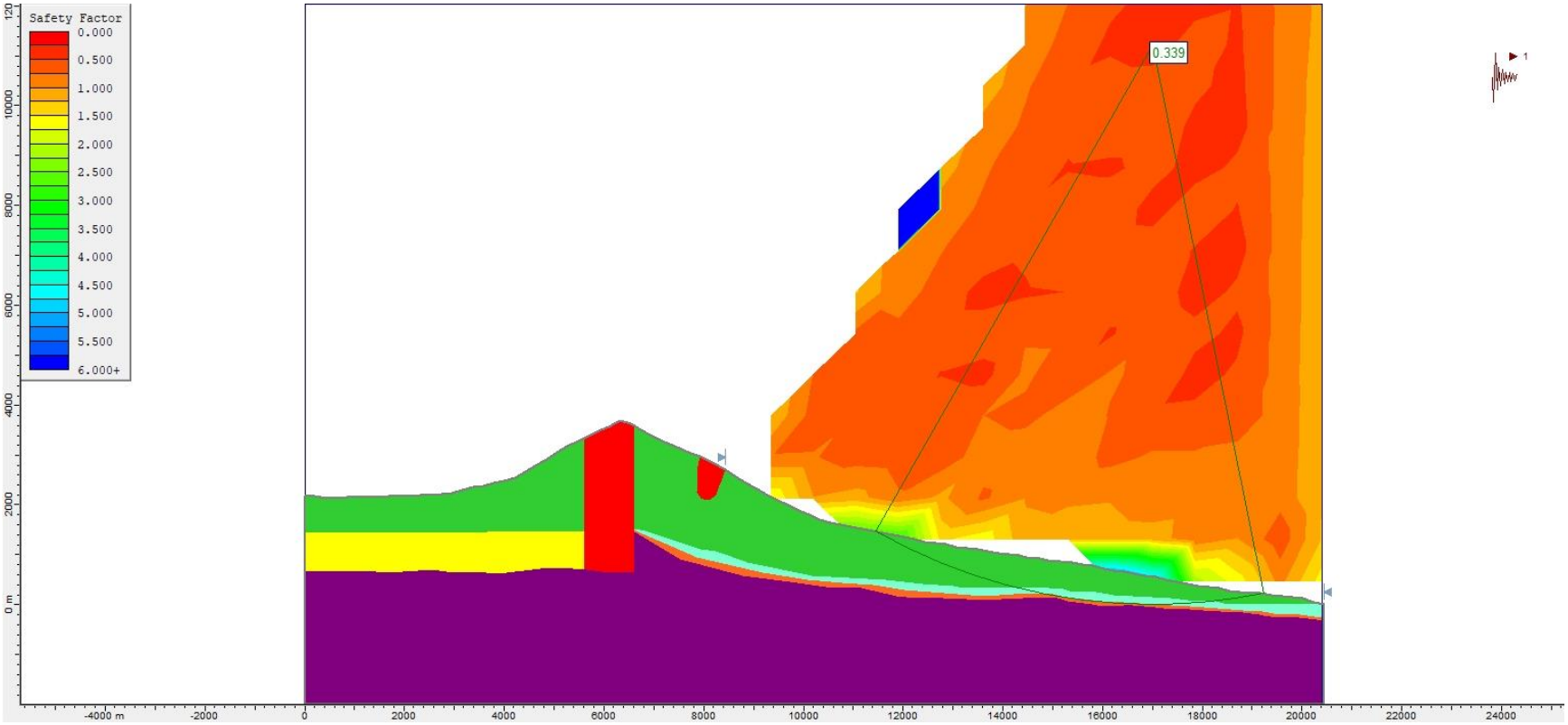

Figure S271. Slope stability pseudo-static analysis for Model 1 Bis (assuming a caldera collapse), using the Bishop simplified method and a k_h = 1.00.

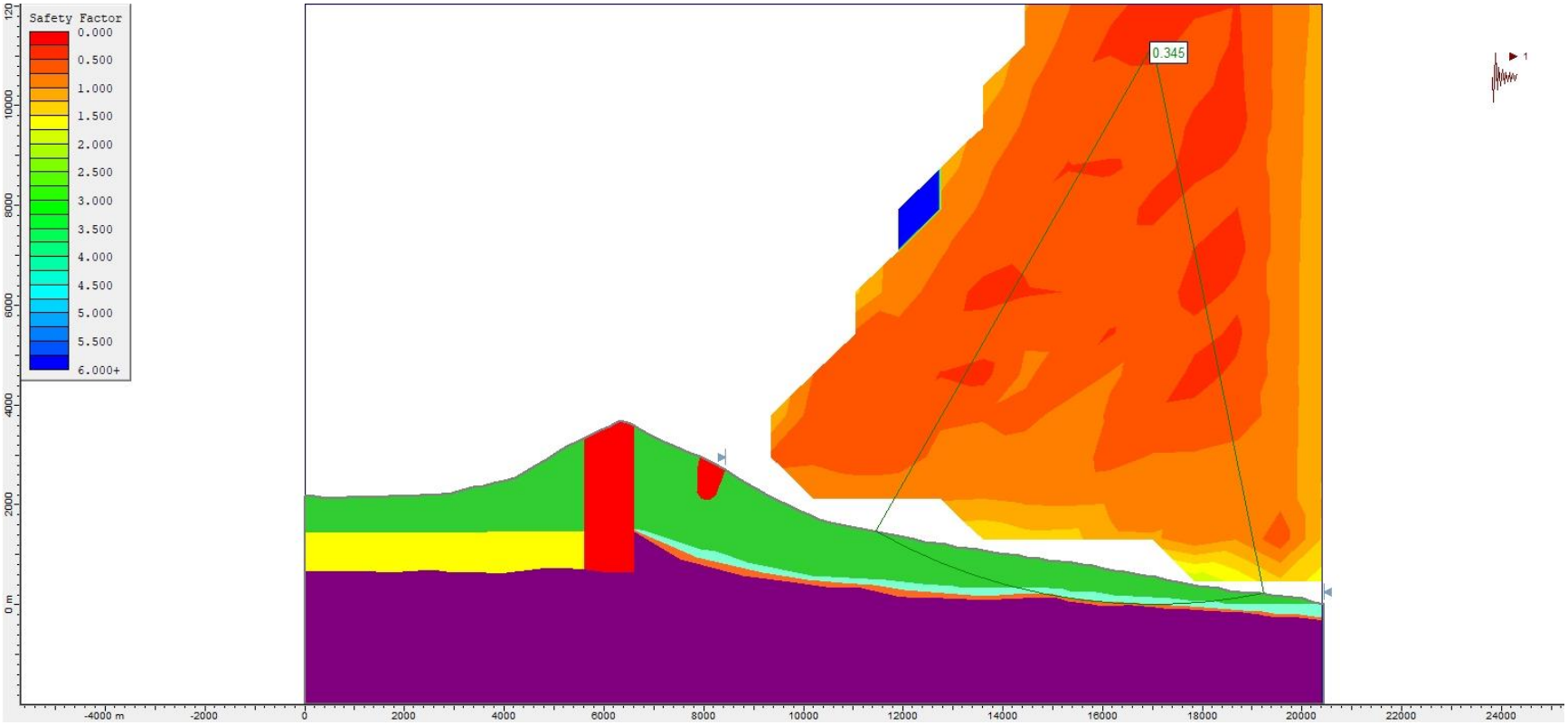

Figure S272. Slope stability pseudo-static analysis for Model 1 Bis (assuming a caldera collapse), using the Janbu Generalised method and a k_h = 1.00.

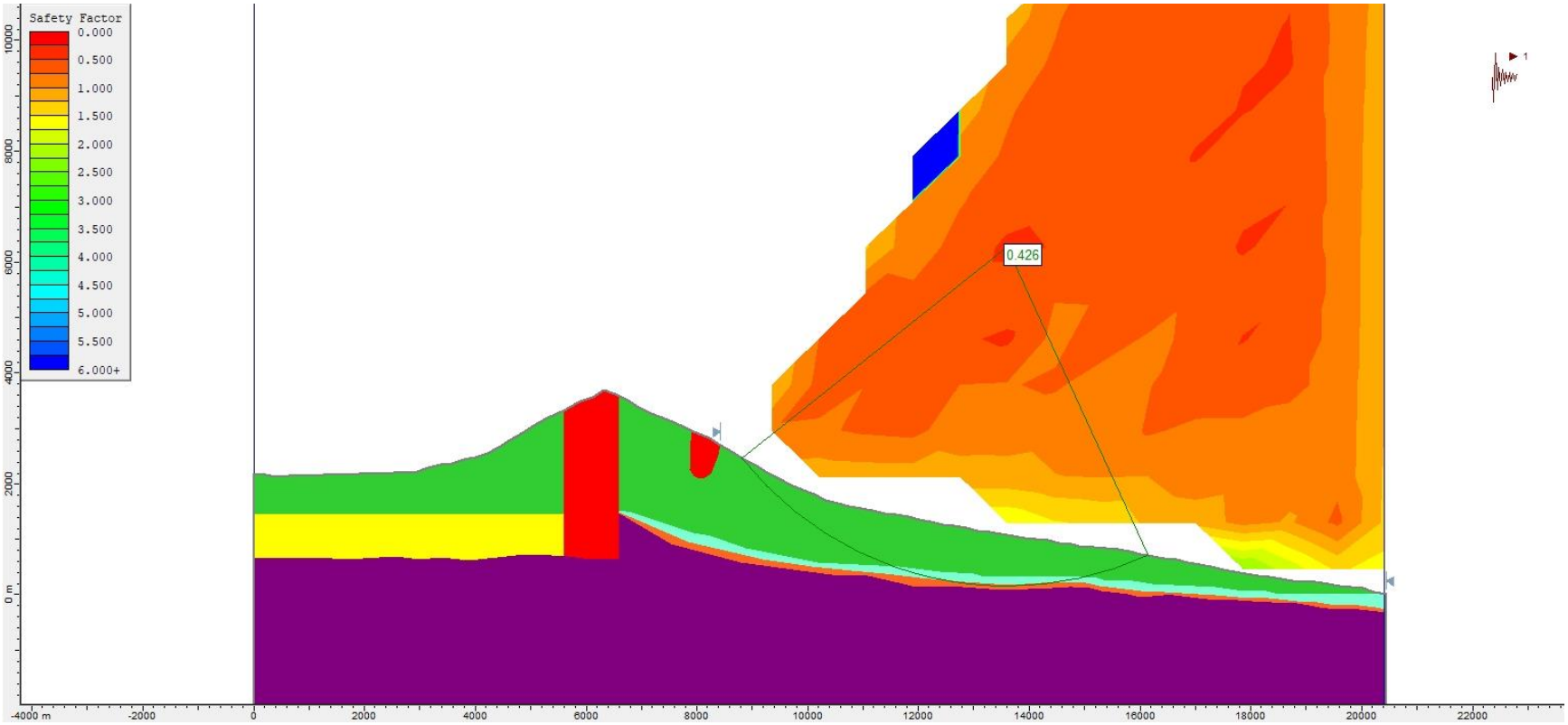

Figure S273. Slope stability pseudo-static analysis for Model 1 Bis (assuming a caldera collapse), using the Morgenstern-Price method and a k_h = 1.00.

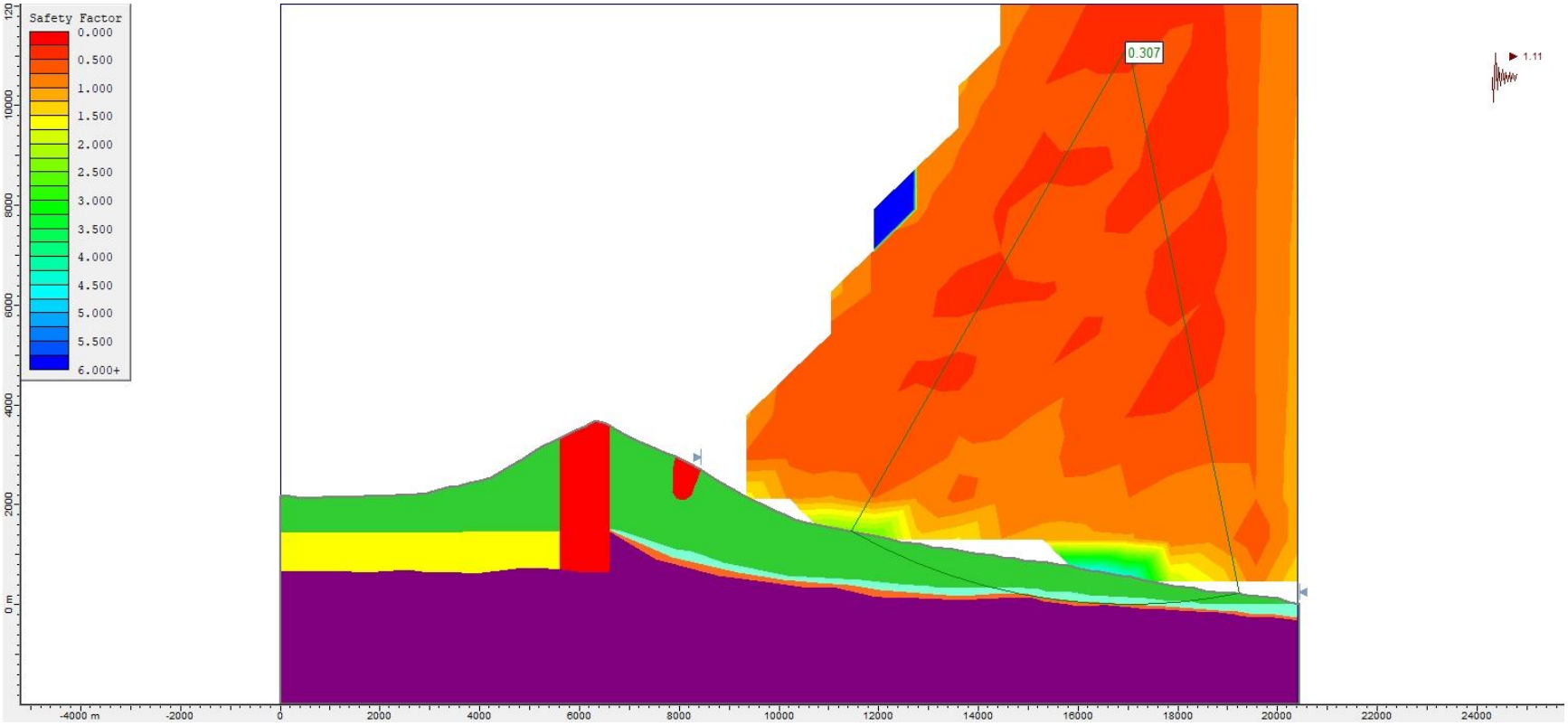

Figure S274. Slope stability pseudo-static analysis for Model 1 Bis (assuming a caldera collapse), using the Bishop simplified method and a k_h = 1.11.

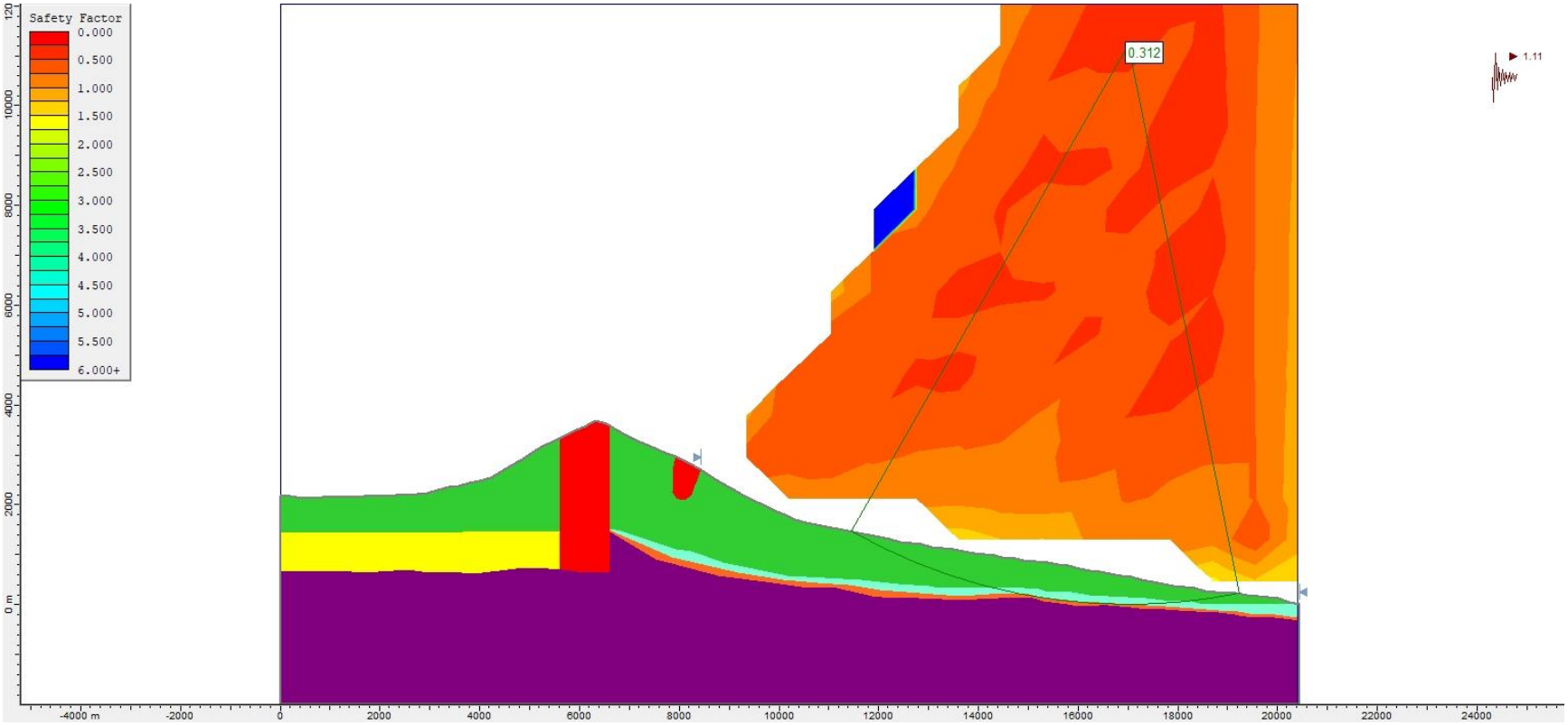

Figure S275. Slope stability pseudo-static analysis for Model 1 Bis (assuming a caldera collapse), using the Janbu Generalised method and a k_h = 1.11.

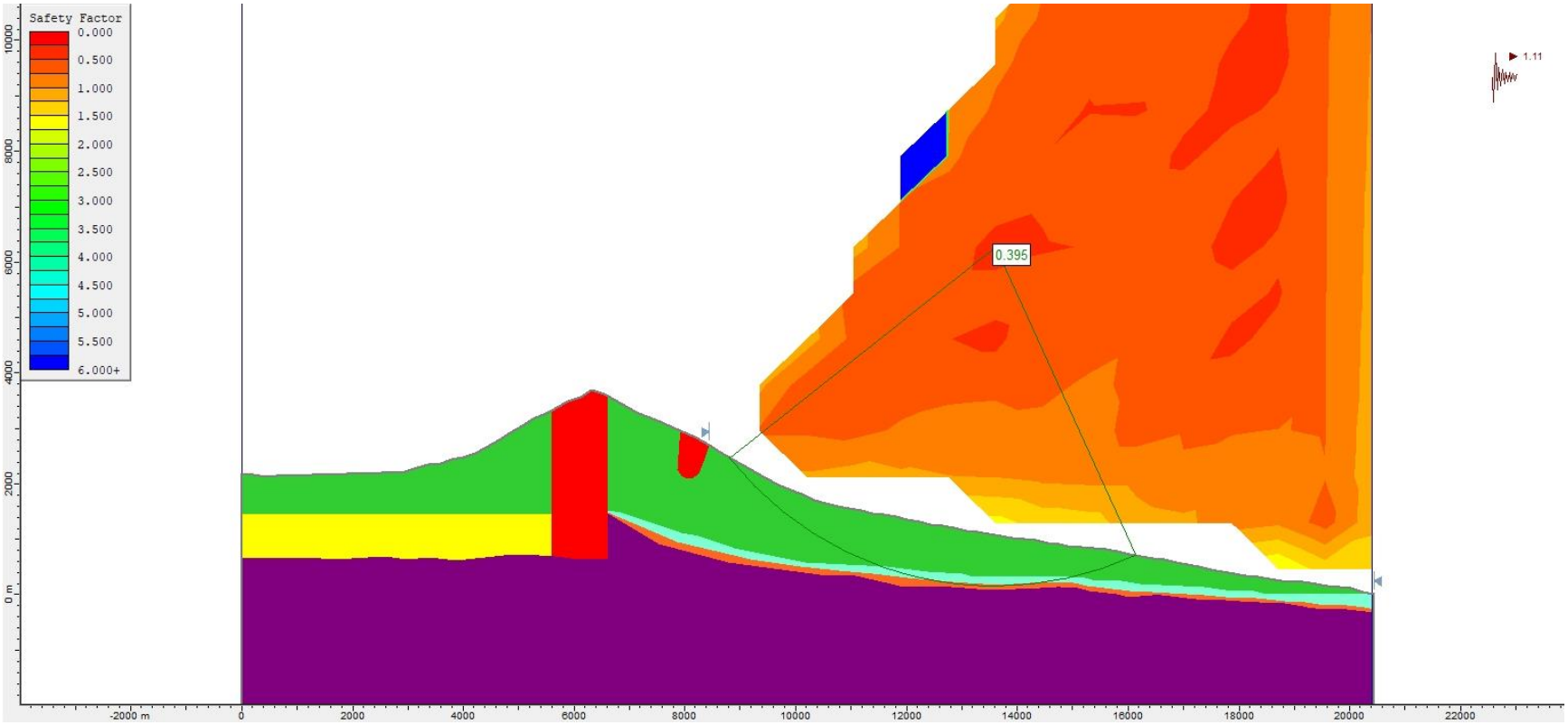

Figure S276. Slope stability pseudo-static analysis for Model 1 Bis (assuming a caldera collapse), using the Morgenstern-Price method and a k_h = 1.11.

PDC simulations

Collapse equivalent angle	Collapse equivalent height	Maximum length reached on land (km)	Direction of maximum length	Extension (km^2)	Affected areas
4º	**2,000 m**	60.4	NE	2,034.38	The whole island of Tenerife
	3,000 m	60.4	NE	2,034.38	The whole island of Tenerife
7º	**2,000 m**	46.30	NE	1,876.39	The whole island of Tenerife except the north of Santa Cruz de Tenerife, Tegueste and San Cristóbal de la Laguna municipalities.
	3,000 m	54.40	NE	1,975.61	The whole island of Tenerife except the north of Santa Cruz de Tenerife municipality.
11º	**2,000 m**	29.30	NE, S	1,597.51	The whole island of Tenerife except the northeastern municipalities and two small regions in the southern coast of Arona and in the west of Buenavista del Norte.
	3,000 m	34.40	NE	1,682.93	The whole island of Tenerife except the northeastern municipalities.
15º	**2,000 m**	21.20	NE, SW, NW	1,025.51	The northern municipalities of Tenerife, from Los Silos to La Orotava, the western municipalities, and the north of the southern and eastern municipalities.
	3,000 m	25.00	E, SE, SW	1,406.19	The northern municipalities of Tenerife, from the east of Buenavista del Norte to Santa Úrsula, the western and eastern municipalities and the northern half of the southern municipalities.
19º	**2,000 m**	16.50	NE, NW	533.22	The northern municipalities of Tenerife, from Garachico to Los Realejos, and the central part of the island, covering the north of the western, southern and eastern municipalities.
	3,000 m	19.40	NE, SW, NW	880.52	The northern municipalities of Tenerife, from the east of Los Silos to La Orotava, almost all the western municiaplities and the north of the southern and eastern municipalities.
23º	**2,000 m**	13.20	N	300.97	Just beyond the limits of Las Cañadas caldera and almost all the extension of the northern municipalities from Icod de los Vinos to Los Realejos.
	3,000 m	15.70	NE, NW	526.69	The northern municipalities of Tenerife, from Garachico to Los Realejos, and the central part of the island, covering the north of the western, southern and eastern municipalities.
27º	**2,000 m**	9.90	N, NW	185.62	Las Cañadas caldera and the north of the northern municipalities from Icod de los Vinos to Los Realejos.
	3,000 m	12.80	N	327.54	Just beyond the limits of Las Cañadas caldera and almost all the extension of the northern municipalities from Icod de los Vinos to Los Realejos.

Table S1. Summary table with results obtained from the Pyroclastic Density Current (PDC) simulations. Data is extracted from and should be complemented with map scenarios shown in Figures S2 to S15.

Epicentre 1 (northern slope of Teide)				
		Pétursson and Vogfjörd (2009)	**Ágústsson et al. (2008)**	**Beauducel et al. (2004)**
Depth = 0 km	**Mw = 5**	0,10 g	0,61 g	0,12 g
	Mw = 6	0,19 g	3,04 g	0,48 g
	Mw = 7	0,29 g	11,99 g	1,95 g
Depth = 1,8 km	**Mw = 5**	0,10 g	0,61 g	0,12 g
	Mw = 6	0,19 g	3,04 g	0,48 g
	Mw = 7	0,29 g	11,99 g	1,95 g
Depth = 3,6 km	**Mw = 5**	0,10 g	0,61 g	0,12 g
	Mw = 6	0,19 g	3,04 g	0,48 g
	Mw = 7	0,29 g	11,99 g	1,95 g

Table S2. Summary table with maximum expected Peak Ground Acceleration (PGA) values obtained from seismic simulations for an epicentre located north of the Mt Teide summit.

Epicentre 2 (crater of Teide)				
		Pétursson and Vogfjörd (2009)	**Ágústsson et al. (2008)**	**Beauducel et al. (2004)**
Depth = 0 km	**Mw = 5**	0,10 g	0,67 g	0,12 g
	Mw = 6	0,20 g	3,35 g	0,49 g
	Mw = 7	0,28 g	13,21g	2,01g
Depth = 2,5 km	**Mw = 5**	0,10 g	0,67 g	0,12 g
	Mw = 6	0,20 g	3,35 g	0,49 g
	Mw = 7	0,28 g	13,21 g	2,01 g
Depth = 5 km	**Mw = 5**	0,10 g	0,67 g	0,12 g
	Mw = 6	0,20 g	3,35 g	0,49 g
	Mw = 7	0,28 g	13,21 g	2,01 g

Table S3. Summary table with maximum expected Peak Ground Acceleration (PGA) values obtained from seismic simulations for an epicentre located at the crater of Teide.

Model 1 (with alteration zones)	
Analysis method	**Factor of Safety**
Bishop simplified	1.281
Janbu Generalised	1.259
Morgenstern-Price	1.311

Table S4. Summary table with the Factors of Safety (FS) obtained from the slope stability static analysis for Model 1.

Model 2 (without alteration zones)	
Analysis method	**Factor of Safety**
Bishop simplified	1.334
Janbu Generalised	1.334
Morgenstern-Price	1.361

Table S5. Summary table with the Factors of Safety (FS) obtained from the slope stability static analysis for Model 2.

Model 1 (with alteration zones)																								
Analysis method	k_h																							
	0.03	**0.04**	**0.06**	**0.07**	**0.1**	**0.12**	**0.13**	**0.14**	**0.15**	**0.16**	**0.18**	**0.19**	**0.2**	**0.22**	**0.26**	**0.28**	**0.29**	**0.32**	**0.33**	**0.48**	**0.49**	**1.00**	**1.11**
Bishop simplified	1.185	1.156	1.102	1.076	1.007	0.966	0.946	0.928	0.910	0.892	0.859	0.844	0.829	0.801	0.750	0.727	0.716	0.685	0.675	0.519	0.511	0.283	0.260
Janbu Generalised	1.158	1.129	1.072	1.047	0.978	0.936	0.916	0.896	0.878	0.860	0.827	0.812	0.797	0.768	0.717	0.694	0.684	0.653	0.643	0.531	0.524	0.288	0.264
Morgenstern-Price	1.220	1.192	1.141	1.116	1.052	1.014	0.996	0.979	0.962	0.945	0.915	0.901	0.887	0.861	0.814	0.792	0.780	0.740	0.727	0.569	0.570	0.334	0.307

Table S6. Summary table with the Factors of Safety (FS) obtained for each value of k_h tested during the slope stability pseudo-static analysis for Model 1.

Model 2 (without alteration zones)																							
Analysis method	k_h																						
	0.03	**0.04**	**0.06**	**0.07**	**0.1**	**0.12**	**0.14**	**0.15**	**0.16**	**0.18**	**0.19**	**0.2**	**0.22**	**0.26**	**0.28**	**0.29**	**0.32**	**0.33**	**0.48**	**0.49**	**1.00**	**1.11**
Bishop simplified	1.232	1.201	1.144	1.118	1.044	1.000	0.960	0.941	0.922	0.888	0.871	0.856	0.826	0.772	0.747	0.735	0.691	0.678	0.520	0.512	0.283	0.260
Janbu Generalised	1.226	1.192	1.132	1.105	1.026	0.982	0.940	0.920	0.901	0.866	0.849	0.832	0.800	0.745	0.720	0.708	0.675	0.665	0.533	0.524	0.288	0.264
Morgenstern-Price	1.262	1.233	1.180	1.155	1.084	1.043	1.006	0.988	0.971	0.939	0.924	0.909	0.881	0.817	0.796	0.781	0.741	0.728	0.570	0.570	0.334	0.307

Table S7. Summary table with the Factors of Safety (FS) obtained for each value of k_h tested during the slope stability pseudo-static analysis for Model 2.

Model 1 Bis																							
Analysis method	k_h																						
	0.03	**0.04**	**0.06**	**0.07**	**0.1**	**0.12**	**0.14**	**0.15**	**0.16**	**0.18**	**0.19**	**0.2**	**0.22**	**0.26**	**0.28**	**0.29**	**0.32**	**0.33**	**0.48**	**0.49**	**1.00**	**1.11**
Bishop simplified	2.195	2.098	1.925	1.848	1.650	1.538	1.440	1.395	1.353	1.273	1.236	1.201	1.137	1.027	0.980	0.958	0.898	0.879	0.663	0.651	0.339	0.307
Janbu Generalised	2.238	2.140	1.966	1.887	1.686	1.572	1.472	1.427	1.382	1.299	1.261	1.225	1.160	1.046	0.997	0.974	0.914	0.895	0.679	0.667	0.345	0.312
Morgenstern-Price	2.188	2.092	1.923	1.848	1.655	1.547	1.451	1.408	1.367	1.292	1.259	1.226	1.166	1.062	1.017	0.996	0.938	0.920	0.719	0.709	0.426	0.395

Table S8. Summary table with the Factors of Safety (FS) obtained for each value of k_h tested during the slope stability pseudo-static analysis for Model 1 Bis.

Movie S1. Propagation over time across the Canary Islands of the tsunami caused by the impact of a landslide originating in the Icod valley, Tenerife, on the ocean, with a yield strength of the sliding block of 50,000 Pa.

Movie S2. Propagation over time across the Canary Islands of the tsunami caused by the impact of a landslide originating in the Icod valley, Tenerife, on the ocean, with a yield strength of the sliding block of 100,000 Pa.